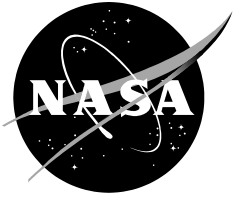


NASA/TM-20210019043



NASA Ground-Based Layered Pressure Vessels Materials Report

*R. Levi Shelton
Marshall Space Flight Center, Huntsville, Alabama*

National Aeronautics and
Space Administration

*Marshall Space Flight Center
Huntsville, AL 35805*

September 2021

NASA STI Program Report Series

The NASA STI Program collects, organizes, provides for archiving, and disseminates NASA's STI. The NASA STI program provides access to the NTRS Registered and its public interface, the NASA Technical Reports Server, thus providing one of the largest collections of aeronautical and space science STI in the world. Results are published in both non-NASA channels and by NASA in the NASA STI Report Series, which includes the following report types:

- **TECHNICAL PUBLICATION.** Reports of completed research or a major significant phase of research that present the results of NASA Programs and include extensive data or theoretical analysis. Includes compilations of significant scientific and technical data and information deemed to be of continuing reference value. NASA counterpart of peer-reviewed formal professional papers but has less stringent limitations on manuscript length and extent of graphic presentations.
- **TECHNICAL MEMORANDUM.** Scientific and technical findings that are preliminary or of specialized interest, e.g., quick release reports, working papers, and bibliographies that contain minimal annotation. Does not contain extensive analysis.
- **CONTRACTOR REPORT.** Scientific and technical findings by NASA-sponsored contractors and grantees.
- **CONFERENCE PUBLICATION.** Collected papers from scientific and technical conferences, symposia, seminars, or other meetings sponsored or co-sponsored by NASA.
- **SPECIAL PUBLICATION.** Scientific, technical, or historical information from NASA programs, projects, and missions, often concerned with subjects having substantial public interest.
- **TECHNICAL TRANSLATION.** English-language translations of foreign scientific and technical material pertinent to NASA's mission.

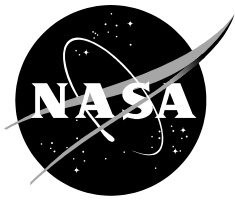
Specialized services also include organizing and publishing research results, distributing specialized research announcements and feeds, providing information desk and personal search support, and enabling data exchange services.

For more information about the NASA STI program, see the following:

- Access the NASA STI program home page at <http://www.sti.nasa.gov>
- Help desk contact information:

<https://www.sti.nasa.gov/sti-contact-form/> and select the "General" help request type.

NASA/TM–20210019043



NASA Ground-Based Layered Pressure Vessels Materials Report

*R. Levi Shelton
Marshall Space Flight Center, Huntsville, Alabama*

National Aeronautics and
Space Administration

*Marshall Space Flight Center
Huntsville, AL 35805*

September 2021

Acknowledgments

The findings documented here are the result of years of testing, analysis, and investigation, spanning multiple leads and significant participants. Without the contributions of countless individuals, this data collection would not be possible. I would like to recognize as many as possible here who have directly contributed to the construction of this technical memorandum, to the best of my knowledge.

Matthew Adler
Cameron Bosley
Clinton Canaday
Joseph Cardinal
Robert Dodds Jr.
Owen Greulich
Preston Jacobs
Maan Jawad
James A. Joyce
Benjamin Melia
William Prosser
David Riha
Brian Stoltz
Douglas Wells
MSFC EM22 Mechanical Test Lab and Machine Shop

And to the many others unnamed, thank you for your consistent efforts and excellence.

Table of Contents

Executive Summary	32
1 NESC Report	33
1.1 Material Anisotropy	37
1.2 Lot Variability	41
1.3 Fracture Toughness Methods	42
1.4 Master Curve Testing Considerations.....	44
2 FFS Methodology	45
3 Materials Characterization Process	48
3.1 Hardness and Chemistry	49
3.2 Metallography.....	49
3.3 Tensile and Fracture Testing.....	50
3.4 Fatigue Crack Growth Testing.....	52
4 ASTM E1820 and E1921 Background	54
4.1 ASTM E1820 Background.....	54
4.2 ASTM E1921 Background.....	56
5 LPV Fleet Characterization	74
5.1 Database Summary.....	75
6 Reference Literature Materials.....	78
6.1 Code Materials	78
6.1.1 A350	79
6.1.1.1 Material Specification Properties	79
6.1.1.1.1 ASME BPVC Properties.....	79
6.1.1.1.2 ASTM Specification Properties	79
6.1.1.2 Mill Test Report (MTR) Properties	79
6.1.1.3 Fracture Results	80
6.1.2 A517 (T-1).....	80
6.1.2.1 Material Specification Properties	81

6.1.2.1.1	ASME BPVC Properties.....	81
6.1.2.1.2	ASTM Material Properties	81
6.1.2.2	Mill Test Report (MTR) Properties.....	81
6.1.2.3	Fracture Results	81
6.1.3	SA-724	85
6.1.3.1	Material Specification Properties	85
6.1.3.1.1	ASME BPVC Properties.....	85
6.1.3.1.2	ASTM Specification Properties	85
6.1.3.2	Mill Test Report (MTR) Properties.....	86
6.1.3.3	Fracture Results	86
6.1.4	A387	86
6.1.4.1	Material Specification Properties	86
6.1.4.1.1	ASME BPVC Materials	86
6.1.4.1.2	ASTM Specification Properties	86
6.1.4.1.3	Welding Research Council Technical Review.....	87
6.1.4.2	Mill Test Report (MTR) Properties.....	87
6.1.4.3	Fracture Results	87
6.1.5	SA-182	88
6.1.5.1	Material Specification Properties	88
6.1.5.1.1	ASME BPVC Properties.....	88
6.1.5.1.2	ASTM Specification Properties	88
6.1.5.2	Mill Test Report (MTR) Properties.....	88
6.1.5.3	Fracture Results	88
6.1.6	A312	89
6.1.6.1	General Material Properties	89
6.1.6.2	Material Specification Properties	89
6.1.6.2.1	ASME BPVC Materials	89
6.1.6.2.2	ASTM Specification Properties	89
6.1.6.3	Mill Test Reports (MTR)	89
6.1.6.4	Fracture Results	89
6.1.7	SA-516	90

6.1.7.1	Material Specification Properties	90
6.1.7.1.1	ASME BPVC Materials	90
6.1.7.1.2	ASTM Specification Properties	90
6.1.7.1.3	Welding Research Institute Supplement 311-S	91
6.1.7.2	Mill Test Report (MTR) Properties	91
6.1.7.3	Fracture Results	91
6.1.8	A302B Plates	91
6.1.8.1	General Material Information.....	91
6.1.8.2	Material Specification Properties	92
6.1.8.2.1	ASME BPVC Materials	92
6.1.8.2.2	ASTM Specification Properties	92
6.1.8.3	Mill Test Report (MTR) Properties	93
6.1.8.4	Fracture Data	93
6.2	Non-Code Materials with Reference Literature	114
6.2.1	AO Smith 1148B	114
6.2.1.1	General Material Information.....	114
6.2.1.2	Material Specification Properties	115
6.2.1.3	Mill Test Report (MTR) Properties	115
6.2.1.4	Fracture Data	116
6.2.2	AO Smith 1135	116
6.2.2.1	General Material Properties	116
6.2.2.2	Material Specification Properties	116
6.2.2.2.1	Manufacturer Specification Properties	116
6.2.2.3	Mill Test Report (MTR) Properties	117
6.2.2.4	Fracture Results	117
6.3	Non-Code Materials with No Reference.....	117
6.3.1	SWC 100302	117
6.3.1.1	General Material Properties	117
6.3.1.2	Material Specification Properties	118
6.3.1.2.1	SWC 100302 Mechanical Properties	118
6.3.1.2.2	ASTM SPECIFICATION PROPERTIES.....	119

6.3.1.3	Mill Test Report (MTR) Properties	119
6.3.1.4	Fracture Results	120
6.3.2	SWC 90336	120
6.3.2.1	General Material Properties	120
6.3.2.2	Material Specification Properties	120
6.3.2.3	Mill Test Report (MTR) Properties	120
6.3.2.4	Fracture Results	121
7	Material Test Data	122
7.1	Description of Test Types and Analysis Methods	122
7.2	Parent Head Materials	131
7.2.1	A225	132
7.2.1.1	Chemical Composition	132
7.2.1.2	Metallography.....	133
7.2.1.3	Mechanical Properties	147
7.2.1.3.1	Smooth Tensile Tests	148
7.2.1.3.2	Notch Tensile Test.....	150
7.2.1.3.3	Fracture Properties	152
7.2.1.3.4	Fatigue Crack Growth Testing.....	172
7.2.1.3.5	Charpy Impact.....	173
7.2.2	A212	177
7.2.2.1	Chemical Composition	177
7.2.2.2	Metallography.....	178
7.2.2.2.1	Carburization Layer Thickness Study	184
7.2.2.3	Mechanical Properties	189
7.2.2.3.1	Smooth Tensile Tests	190
7.2.2.3.2	Notch Tensile Tests	191
7.2.2.3.3	Fracture Properties	193
7.2.2.3.4	Fatigue Crack Growth	199
7.2.2.3.5	Charpy Impact.....	199
7.2.3	A302B Modified	200
7.2.3.1	Chemical Composition	200

7.2.3.2	Metallography.....	200
7.2.3.3	Mechanical Properties	204
7.2.3.3.1	Smooth Tensile Tests	204
7.2.3.3.2	Notch Tensile Tests	205
7.2.3.3.3	Fracture Properties	205
7.2.3.3.4	Fatigue Crack Growth	211
7.2.3.3.5	Charpy Impact.....	211
7.3	Parent Shell Course Materials.....	226
7.3.1	1146	226
7.3.1.1	Chemical Composition	227
7.3.1.2	Metallography.....	228
7.3.1.3	Mechanical Properties	235
7.3.1.3.1	Smooth Tensile Tests	236
7.3.1.3.2	Notch Tensile	240
7.3.1.3.3	Fracture Properties	240
7.3.1.3.4	Fatigue Crack Growth	263
7.3.1.3.5	Charpy Impact.....	276
7.3.2	1143	277
7.3.2.1	Chemical Composition	277
7.3.2.2	Metallography.....	278
7.3.2.3	Mechanical Properties	278
7.3.2.3.1	Smooth Tensile Tests	279
7.3.2.3.2	Notch Tensile Test.....	280
7.3.2.3.3	Fracture Properties	281
7.3.2.3.4	Fatigue Crack Growth	286
7.3.2.3.5	Charpy Impact.....	286
7.3.3	T-1/A517	290
7.3.3.1	Chemical Composition	290
7.3.3.2	Metallography.....	290
7.3.3.3	Mechanical Properties	293
7.3.3.3.1	Smooth Tensile Tests	293

7.3.3.3.2	Notch Tensile Tests	295
7.3.3.3.3	Fracture Properties	295
7.3.3.3.4	Fatigue Crack Growth	300
7.3.3.3.5	Charpy Impact.....	303
7.4	Parent Nozzle Materials.....	304
7.4.1	AOS A-5002-Mod	304
7.4.1.1	Chemical Composition	304
7.4.1.2	Metallography.....	304
7.4.1.3	Mechanical Properties	304
7.4.1.3.1	Smooth Tensile Tests	305
7.4.1.3.2	Notch Tensile	305
7.4.1.3.3	Fracture Properties	305
7.4.1.3.4	Fatigue Crack Growth	309
7.4.1.3.5	Charpy Impact.....	309
7.4.2	A105	309
7.4.2.1	Chemical Composition	309
7.4.2.2	Metallography.....	310
7.4.2.3	Mechanical Properties	313
7.4.2.3.1	Smooth Tensile Tests	313
7.4.2.3.2	Notch Tensile Tests	316
7.4.2.3.3	Fracture Properties	316
7.4.2.3.4	Fatigue Crack Growth	324
7.4.2.3.5	Charpy Impact.....	324
7.5	Weld Materials.....	325
7.5.1	Longitudinal Wrapper Weld.....	325
7.5.1.1	Chemical Composition	326
7.5.1.2	Metallography.....	326
7.5.1.3	Mechanical Properties	337
7.5.1.3.1	Smooth Tensile Tests	337
7.5.1.3.2	Notch Tensile	340
7.5.1.3.3	Fracture Properties	341

7.5.1.3.4	Fatigue Crack Growth	361
7.5.1.3.5	Charpy Impact.....	368
7.5.2	Inner Layer Weld.....	369
7.5.2.1	Chemical Composition	369
7.5.2.2	Metallography.....	369
7.5.2.3	Mechanical Properties	375
7.5.2.3.1	Smooth Tensile Tests	375
7.5.2.3.2	Notch Tensile	377
7.5.2.3.3	Fracture Properties	377
7.5.2.3.4	Fatigue Crack Growth	389
7.5.2.3.5	Charpy Impact.....	395
7.5.3	Full Thickness Circumferential Welds.....	396
7.5.3.1	Chemical Composition	396
7.5.3.2	Metallography.....	396
7.5.3.3	Mechanical Properties	409
7.5.3.3.1	Smooth Tensile Tests	409
7.5.3.3.2	Notch Tensile	412
7.5.3.3.3	Fracture Properties	412
7.5.3.3.4	Fatigue Crack Growth	426
7.5.3.3.5	Charpy Impact.....	428
7.5.4	Nozzle Welds.....	429
7.5.4.1	Chemical Composition	429
7.5.4.2	Metallography.....	429
7.5.4.3	Mechanical Properties	430
7.5.4.3.1	Smooth Tensile Tests	431
7.5.4.3.2	Notch Tensile	432
7.5.4.3.3	Fracture Properties	432
7.5.4.3.4	Fatigue Crack Growth	441
7.5.4.3.5	Charpy Impact.....	442
8	Conclusions	442
8.1	Summary Charts.....	443

8.1.1	Head Data Summary	443
8.1.2	Nozzle Data Summary	446
8.1.3	Wrapper Data Summary	449
8.1.4	Weld Data Summary	454
	Bibliography	460

List of Figures and Tables

Table 1-1:	Definition of Material Testing Terms	35
Table 1-2:	Table 1-1 Continued	36
Table 1-3:	Table 1-2 Continued	37
Table 3-1:	Materials Characterization Process Diagram	48
Figure 3.2-1:	Example A212 Material Macro Cube Specimen Orientation.....	50
Figure 3.3-1:	Example Down-Select Cut Plan	51
Figure 3.3-2:	Master Curve Example	52
Figure 3.4-1:	Example Fatigue Crack Growth Test Results	53
Equation 4.1	(10)	55
Figure 4.2-1:	Example Cleavage with Master Curve Superimposed	58
Figure 4.2-2:	Schematics Depicting Cracking Mechanisms	59
Equation 4.2	60
Figure 4.2-3:	Probability of Failure (P_f) as a Function of J_c in Weibull Space.....	60
Figure 4.2-4:	Determination of P and P_f by Weibull Distribution	61
Figure 4.2-5:	Round Robin Data Indicating Model Independence to Test Temperature.	61
Equation 4.3	(7)	61
Equation 4.4	(7)	62
Equation 4.5	(7)	62
Equation 4.6	(7)	62
Equation 4.7	(7)	62

Figure 4.2-6: Supporting Data Used to Validate Master Curve	63
Figure 4.2-7: Example of Variability and Data Scatter Around Typical Master Curve	63
Figure 4.2-8: Master Curve Plotted Against the 95 % and 5 % Tolerance Bounding Curves.....	64
Figure 4.2-9: Vessel V0032 Data Set, Master Curve, and Confidence Bounds for A225 Steel ...	66
Figure 4.2-10: Bimodal Analysis of A225 Steel from the Hemispherical Head of Vessel V0032. 66	
Figure 4.2-11: Nozzle Weld Data with Data Scatter Beyond E1921 Tolerance Bounds	67
Figure 4.2-12: Application of Bimodal and Multimodal Analysis Methods of E1921 Annex X5. 68	
Figure 4.2-13: A225 Data Multimodal Median T_m Curve and Corresponding Bounds	69
Figure 4.2-14: Example T0TEM Input Data	71
Figure 4.2-15: Example T0TEM Master Curve Plot	72
Figure 4.2-16: Example T0TEM Bimodal Master Curve Plot	72
Table 4.2-1: Comparison of T0TEM with ASTM Master Curve Results.....	73
Table 4.2-2: Comparison of T0TEM with ASTM Bimodal Master Curve Results.....	73
Table 4.2-3: Comparison of T0TEM with ASTM Multimodal Master Curve Results.....	74
Figure 5.1-1: Fleet Characterization, Head Materials	76
Figure 5.1-2: Fleet Characterization, Nozzle Materials (Head and Shell)	76
Figure 5.1-3: Fleet Characterization, Wrapper Materials	77
Figure 5.1-4: Fleet Characterization, Inner Layer Materials	77
Table 6.1.1.1.1-1: A350 ASME BPVC Material Properties (22)	79
Table 6.1.1.1.2-1: ASTM A350 Mechanical Properties (22)	79
Table 6.1.1.1.2-2: ASTM A350 Chemical Composition (22)	79
Figure 6.1.1.3-1: A350 Master Curve Results.....	80
Table 6.1.2.1.1-1: SA-517 ASME BPVC Material Properties.....	81
Table 6.1.2.1.2-1: ASTM A517 Mechanical Properties (24)	81
Table 6.1.2.1.2-2: ASTM A517 Chemical Composition (24)	81
Figure 6.1.2.3-1: A517F Original Plot and Curve Fit from Barsom and Rolfe (25)	82
Table 6.1.2.3-1: A517F Raw Test Data	83

Table 6.1.2.3-2: A517F Master Curve Results	84
Figure 6.1.2.3-2: A517F Master Curve ($T_0 = -66^{\circ}\text{C}$)	84
Table 6.1.3.1.1-1: ASME SA-724 BPVC Material Properties	85
Table 6.1.3.1.2-1: ASTM A724 Mechanical Properties (26)	85
Table 6.1.3.1.2-2: ASTM A724 Chemical Composition (26)	85
Table 6.1.4.1.1-1: SA-387 ASME BPVC Material Properties	86
Table 6.1.4.1.2-1: ASTM A387 Mechanical Properties (27)	86
Table 6.1.4.1.2-2: ASTM A387 Chemical Properties (27)	87
Table 6.1.4.1.3-1: Technical Paper/Review Material Mechanical Properties (28)	87
Table 6.1.4.1.3-2: Technical Paper/Review Chemical Composition (28)	87
Table 6.1.4.2-1: MARS Vessel U Package (29)	87
Table 6.1.5.1.1-1: ASME SA-182 ASME BPVC Material Properties	88
Table 6.1.5.1.2-1: ASTM A182 Mechanical Properties (30)	88
Table 6.1.5.1.2-2: ASTM A182 Chemical Composition (30)	88
Table 6.1.6.2.1-1: ASME SA-312 BPVC Material Properties	89
Table 6.1.6.2.2-1: ASTM A312 Mechanical Properties (31)	89
Table 6.1.6.2.2-2: ASTM A312 Chemical Composition (31)	89
Table 6.1.7.1.1-1: SA-516 ASME BPVC Material Properties	90
Table 6.1.7.1.2-1: ASTM A516 Mechanical Properties (32)	90
Table 6.1.7.1.2-2: ASTM A516 Chemical Composition (32)	91
Table 6.1.7.1.3-1: 516-70 Normalized Condition Mechanical Properties (28)	91
Table 6.1.7.1.3-2: 516-70 Chemical Composition (28)	91
Table 6.1.8.2.2-1: ASTM A302 Mechanical Properties (33)	92
Table 6.1.8.2.2-2: ASTM Specification Chemical Composition (33)	93
Table 6.1.8.3-1 MTR Mechanical Properties	93
Table 6.1.8.3-2: MTR Chemical Compositions	93
Table 6.1.8.4-1: Fracture Property Study Test Matrix from McCabe et al. (34)	95

Table 6.1.8.4-2: A302B-Modified Chemical Compositions from McCabe et al. (34) 96

Table 6.1.8.4-3: Modified Tensile Properties from McCabe et al. (34) 96

Table 6.1.8.4-5: A302B Charpy Toughness Results from McCabe et al. (34)..... 98

Figure 6.1.8.4-1: J-Integral Versus Crack Growth from McCabe et al (34) 99

Table 6.1.8.4-6: T-L Orientation Fracture Test Results from McCabe et al. (34) 100

Figure 6.1.8.4-2: Typical J-R Curve for A302B from McCabe et al. (34)..... 101

Figure 6.1.8.4-3: J-R Results from McCabe et al. (34)..... 102

Table 6.1.8.4-7: Tabulated Averaged Results from McCabe et al. (34) 103

Figure 6.1.8.4-4: Typical Analysis Plot from McCabe et al. (34)..... 104

Figure 6.1.8.4-5: Charpy Ductile-Brittle Characterization Plot for A302B Steel (34)..... 105

Figure 6.1.8.4-6: NDT Toughness Reported by Pellini and Puzak (39)..... 107

Figure 6.1.8.4-7: L-T Charpy V Transition Temperatures at 30 ft-lb 109

Figure 6.1.8.4-8: T_0 Versus 20 ft-lb (28J) Charpy Transition from Wallin (42) 110

Figure 6.1.8.4-9: Revised T_0 Versus 30 ft-lb Charpy Correlation from Sokolov and Nanstad (43) 111

Figure 6.1.8.4-10: T_0 Versus 30 ft-lb Charpy Correlation from Sattari-Far and Wallin (44)..... 112

Figure 6.1.8.4-11: Proposed Linear Correlation Frequency Results for A302 L-T..... 113

Figure 6.1.8.4-12: Proposed Linear Correlation Frequency Results for A302 T-L..... 113

Table 6.2.1.2-1: Material Specification Equivalentents (46) 115

Table 6.2.1.2-2: Manufacturer Specification Mechanical Properties (46)..... 115

Table 6.2.1.2-3: Manufacturer Specification Chemical Composition (46)..... 115

Table 6.2.1.2-4: ASTM A225 (Parent) Mechanical Properties (47) 115

Table 6.2.1.2-5: ASTM A225 (Parent) Chemical Composition (47) 115

Table 6.2.1.3-1: MTR Mechanical Properties (48) 116

Table 6.2.1.3-2: MTR Chemical Compositions (48)..... 116

Table 6.2.2.2-1: AOS 1135 Specification Mechanical Properties (46) 116

Table 6.2.2.2-2: AOS Specification Chemical Composition (46)..... 117

Table 6.2.2.3-1: V- AOS 1135 Mechanical Properties	117
Table 6.2.2.3-2: V- AOS 1135 Chemical Composition	117
Table 6.3.1.2.1-1: SWC100302 Mechanical Properties (49)	119
Table 6.3.1.2.2-1: ASTM A533 Chemical Composition (36)	119
Table 6.3.1.2.2-2: ASTM A533 Mechanical Properties (36)	119
Table 6.3.1.3-1: MTR SWC100302 Mechanical Properties	119
Table 6.3.1.3-2: MTR SWC100302 Mechanical Properties	120
Table 6.3.2.2-1: 90336 Mechanical Properties Requirements (49)	120
Table 6.3.2.2-2: 90336 Chemical Composition Requirements (49)	120
Table 6.3.2.3-1: 90336 MTR Mechanical Properties (49)	121
Table 6.3.2.3-2: 90336 MTR Chemical Composition (49)	121
Table 7.1-1: V0023 Test Matrix	124
Table 7.1-2: V0032 Test Matrix	125
Table 7.1-3: MV50466-8 Test Matrix	126
Table 7.1-4: V0125 Test Matrix	127
Table 7.1-5: PV0296 Test Matrix	128
Table 7.1-6: V0348 Test Matrix	129
Table 7.1-7: V0071 Test Matrix	130
Table 7.1-8: V066 Test Matrix	131
Table 7.2.1.1-1: Standard Chemical Composition for A225	132
Table 7.2.1.1-2: Manufacturer Mill Certification Chemistry	133
Table 7.2.1.1-3: A225 Collected Chemistry Data	133
Figure 7.2.1.2-1: V0032 Head Cut Plan Metallography Specimens	135
Table 7.2.1.2-1: A225 Microstructure Specimen List, Vessels V0032 and PV0296	136
Figure 7.2.1.2-2: Macro Specimen Drawing	137
Figure 7.2.1.2-3: V0032 Macro Specimen	137
Figure 7.2.1.2-4: Micrographs of V0032 CP-380 90 Degree Location, 50X	138

Figure 7.2.1.2-5: Micrographs of V0032 CP-380 at 45 Degree Location, 50X	138
Figure 7.2.1.2-6: Micrographs of V0032 CP-380 at 0 Degree Location, 50X.....	139
Figure 7.2.1.2-7: Micrographs of V0032 CP-380 at 90 Degree Location, 100X	140
Figure 7.2.1.2-8: Micrographs of V0032 CP-380 at 45 Degree Location, 100X	140
Figure 7.2.1.2-9: Micrographs of V0032 CP-380 at 0 Degree Location, 100X	141
Figure 7.2.1.2-10: PV0296 Cut Plan for Macro Specimens	141
Figure 7.2.1.2-11: Micrographs of PV0296 CP-280 at 90 Degree Location, 50X	142
Figure 7.2.1.2-12: Micrographs of PV0296 CP-279 at 45 Degree Location, 50X	142
Figure 7.2.1.2-13: Micrographs of PV0296 CP-275 at 0 Degree Location, 50X	143
Figure 7.2.1.2-14: Micrographs of PV0296 CP-280 at 90 Degree Location, 100X	143
Figure 7.2.1.2-15: Micrographs of PV0296 CP-279 at 45 Degree Location, 100X	144
Figure 7.2.1.2-16: Micrographs of PV0296 CP-275 at 0 Degree Location, 100X	144
Figure 7.2.1.2-17: Macro Cut Plan V0023 A225 Head Material.....	145
Table 7.2.1.2-2: Macro Analysis V0023 A225.....	145
Figure 7.2.1.2-18: Metallography Cube As-Polished V0023 A225 100X.....	146
Figure 7.2.1.2-19: Metallography Cube Nital Etched V0023 A225 100X	146
Table 7.2.1.3-1: A225 Minimum Material Specifications.....	147
Table 7.2.1.3-2: LPV Mill Certification Material Properties A225.....	147
Table 7.2.1.3.1-1: A225 Smooth Tensile Data, MV50466-8.....	148
Table 7.2.1.3.1-2: A225 Smooth Tensile Data, PV0296	148
Table 7.2.1.3.1-3: A225 Smooth Tensile Data, V0032.....	149
Table 7.2.1.3.1-4: A225 Smooth Tensile Data, V0023.....	149
Table 7.2.1.3.1-5: A225 Smooth Tensile Data, V0125.....	149
Figure 7.2.1.3.1-1: A225 Smooth Specimen Tensile Plot for Sample 519-245	150
Table 7.2.1.3.2-1: A225 Notch Tensile Data, MV50466-8.....	151
Figure 7.2.1.3.2-1: A225 Notch Tensile Plot, MV50466-8.....	151
Figure 7.2.1.3.3-1: A225 Load Versus COD Plot, Sample 440-16.....	152

Figure 7.2.1.3.3-2: A225 J_q Versus Δa Plot, Sample 440-16	153
Figure 7.2.1.3.3-3: V0032 Specimen Layout	153
Table 7.2.1.3.3-1: V0125 A225 Head Fracture Data	154
Table 7.2.1.3.3-2: MV50466-8 A225 Head Fracture Data.....	155
Figure 7.2.1.3.3-4: MV50466-8 A225 Head T_0 Plot ($T_0 = -43^\circ\text{C}$).....	156
Table 7.2.1.3.3-3: MV50466-8 A225 Head T_0 Individual Specimen Results.....	157
Table 7.2.1.3.3-4: MV50466-8 A225 Head T_0 Calculation Results	157
Table 7.2.1.3.3-5: V0023 A225 Head Fracture Data	158
Figure 7.2.1.3.3-5: V0023 A225 Head T_0 Plot ($T_0 = -2^\circ\text{C}$).....	159
Table 7.2.1.3.3-6: V0023 A225 Head T_0 Individual Specimen Results	160
Table 7.2.1.3.3-7 V0023 A225 Head T_0 Calculation Results	160
Table 7.2.1.3.3-8 V0032 A225 Head Fracture Data.....	161
Figure 7.2.1.3.3-6: V0032 A225 Head T_0 Plot ($T_0 = -104^\circ\text{C}$).....	162
Table 7.2.1.3.3-9: V0032 A225 Head T_0 Individual Specimen Results	163
Table 7.2.1.3.3-10: V0032 A225 Head T_0 Calculation Results.....	163
Figure 7.2.1.3.3-7: V0032 A225 Head Multimodal T_m Plot ($T_m = -89^\circ\text{C}$).....	164
Table 7.2.1.3.3-11: V0032 A225 Head Multimodal T_m Calculation Results	164
Table 7.2.1.3.3-12: PV0296 A225 Head Fracture Data	165
Figure 7.2.1.3.3-8: PV0296 A225 Head T_0 Plot ($T_0 = -75^\circ\text{C}$).....	166
Table 7.2.1.3.3-13: PV0296 A225 Head T_0 Individual Specimen Results	167
Table 7.2.1.3.3-14: PV0296 A225 Head T_0 Calculation Results.....	167
Figure 7.2.1.3.3-9: PV0296 A225 Head Multimodal T_m Plot ($T_m = -70^\circ\text{C}$).....	168
Table 7.2.1.3.3-15: PV0296 A225 Head Multimodal T_m Calculation Results	168
Figure 7.2.1.3.3-10: A225 Fracture Toughness Plot.....	169
Figure 7.2.1.3.3-11: A225 Combined Set T_0 Plot ($T_0 = -87^\circ\text{C}$).....	170
Table 7.2.1.3.3-16 A225 Combined Set T_0 Calculation Results.....	170
Figure 7.2.1.3.3-12: A225 Combined Set Multimodal T_m Plot ($T_m = -63^\circ\text{C}$).....	171

Table 7.2.1.3.3-17: A225 Combined Set Multimodal T_m Calculation Results	171
Figure 7.2.1.3.4-1: V0023 A225 Cut Plan for da/dN Specimen	172
Figure 7.2.1.3.4-2: A225 Fatigue Crack Growth Plot, V0023	173
Figure 7.2.1.3.5-1: Section of V0032 Showing Charpy Specimen Location	174
Table 7.2.1.3.5-1: V0032 A225 Charpy Test Results	175
Figure 7.2.1.3.5-2: Charpy Impact Energy as a Function of Circumferential Angle	176
Table 7.2.2.1-1: ASTM A212-64 Standard Chemistry Values (53).....	177
Table 7.2.2.1-2: Manufacturer Mill Certification Chemistry.....	178
Table 7.2.2.1-3: V0348 Collected Chemistry Data	178
Figure 7.2.2.2-1: Sample Cut Plan for Macros from V0348 Head	179
Figure 7.2.2.2-2: Macro from V0348 Head Material at 0 Degrees 10X Magnification	180
Figure 7.2.2.2-3: Macro from V0348 Head Material at 90 Degrees 10X Magnification	180
Figure 7.2.2.2-4: Through-Thickness Macro	181
Figure 7.2.2.2-5: Outside Surface Grain Size.....	182
Figure 7.2.2.2-6: Mid-Thickness Grain Size	182
Figure 7.2.2.2-7: Inside Surface Grain Size.....	183
Figure 7.2.2.2-8: V0348 Grain Count Head Material Center of Thickness 100X Magnification	184
Figure 7.2.2.2.1-1: V0348 Surface study Head Material Outer Surface (0.01 Inch Grind Depth)	185
Figure 7.2.2.2.1-2: V0348 Grain Analysis Head Material Outer Surface (0.01 Inch Grind Depth)	186
Figure 7.2.2.2.1-3: V0348 Surface study Head Material Outer Surface (0.035 Inch Grind Depth)	187
Figure 7.2.2.2.1-4: V0348 Grain Analysis Head Material Outer Surface (0.035 Inch Grind Depth)	188
Table 7.2.2.3-1: A212 Minimum Material Specifications.....	189
Table 7.2.2.3-2: LPV Mill Certification Material Properties A212B.....	190
Table 7.2.2.3.1-1: A212 Tensile Data V0348	191

*Note: C denotes circumferential orientation.....	191
Figure 7.2.2.3.1-1: A212 Smooth Specimen Tensile Plot for Sample 483-27	191
Table 7.2.2.3.2-1: A212 Notch Tensile Data, V0348	192
Figure 7.2.2.3.2-1: A212 Notch Tensile Plot, V0348	193
Figure 7.2.2.3.3-1: Cut Plan for V0348 Fracture Specimens (C-M Orientation)	194
Table 7.2.2.3.3-1: A212 Fracture Data V0348.....	195
Figure 7.2.2.3.3-2: A212 Load Versus COD Plot, Sample 483-2.....	196
Figure 7.2.2.3.3-3: A212 J_q Versus Δa Plot, Sample 483-2	197
Table 7.2.2.3.3-2: T_0 Individual Specimen Results	197
Table 7.2.2.3.3-3: T_0 Calculation Results.....	198
Figure 7.2.2.3.3-4: A212 T_0 Plot	199
Figure 7.2.3.1-1: ASTM A302/A302M-82 Standard Chemistry Values (33).....	200
Table 7.2.3.1-1: A302 Collected Chemistry Data, V0071	200
Figure 7.2.3.2-1: Cut Plan for Macros from V0071 Head.....	201
Table 7.2.3.2-1: A302 Macro Observations, V0071	201
Figure 7.2.3.2-2: A302 Macro 617-59	202
Figure 7.2.3.2-3: A302 Macro 617-60	202
Figure 7.2.3.2-4: A302 Macro 617-61	203
Figure 7.2.3.2-5: A302 Macro Cube, V0071	203
Figure 7.2.3.3-1: A302 Minimum Material Specifications (33).....	204
Table 7.2.3.3.1-1: A302 Tensile Data V0071	204
Figure 7.2.3.3.1-1: A302 Smooth Tensile Plot for Sample 617-23	205
Figure 7.2.3.3.3-1: Example Cut Plan for V0071 Fracture Specimens (C-M Orientation).....	206
Table 7.2.3.3.3-1: A302 Fracture Data V0071.....	207
Figure 7.2.3.3.3-2: A302 Load Versus COD Plot, Sample 617-7	208
Figure 7.2.3.3.3-3: A302 J_q Versus Δa Plot, Sample 617-7	209
Table 7.2.3.3.3-2: T_0 Individual Specimen Results	209

Table 7.2.3.3.3-3: T ₀ Calculation Results	210
Figure 7.2.3.3.3-4: A302 T ₀ Plot	211
Table 7.2.3.3.5-1: A302 Charpy Impact Results V0071	212
Table 7.2.3.3.5-2: A302 Chemistry ORNL (58).....	212
Table 7.2.3.3.5-3: A302 Chemistry V0071.....	213
Figure 7.2.3.3.5-1: Tensile Properties of V0071 A302B Modified and ORNL A302B	213
Figure 7.2.3.3.5-2: Typical Charpy Data Set (57).....	214
Figure 7.2.3.3.5-3: A302 30 ft-lb Transition Temperatures L-T Orientation (43)	215
Figure 7.2.3.3.5-4: A302 30 ft-lb Transition Temperatures T-L Orientation (43)	215
Figure 7.2.3.3.5-5: Wallin Correlation Between T ₀ and 20 ft-lb Charpy Transition (43), (21) ..	217
Figure 7.2.3.3.5-6: Revised T ₀ to 30 ft-lb Charpy Correlation (43), (21)	217
Figure 7.2.3.3.5-7: A302B T ₀ ORNL Correlation Wang (43), (21)	218
Figure 7.2.3.3.5-8: A302B T ₀ ORNL Correlation Wang (43), (21)	219
Figure 7.2.3.3.5-9: 30 ft-lb Transition ORNL Charpy, V0071 for A302B (43), (21)	219
Figure 7.2.3.3.5-10: Chaouadi (37) Master Curve for ORNL A302B.....	220
Figure 7.2.3.3.5-11: Upper Shelf J-R Curve; V0071 Versus ORNL (37) Average in L-T Orientation	221
Figure 7.2.3.3.5-12: Upper Shelf J-R Curve, V0071 Versus Average ORNL (37) in T-L Orientation	222
Figure 7.2.3.3.5-13: Upper Shelf Charpy Toughness, V0071 Versus ORNL (37)	223
Figure 7.2.3.3.5-14: Charpy Transition Evaluation for V0071 A302B Modified.....	224
Figure 7.2.3.3.5-15: ORNL T ₀ to Charpy T ₃₀ Correlation with V0071 Point Added	225
Table 7.3.1.1-1: 1146 Manufacturer Specifications (% Composition) (56), (58)	227
Figure 7.3.1.1-1: 1146 Material Chemistry Mill Certifications (Percent Composition) (56), (58)	227
Table 7.3.1.1-2: 1146 Material Chemistry Collected Data (Percent Composition)	228
Figure 7.3.1.2-1: V0023 Inner Layer Circumferential Weld Hardness Map.....	229
Table 7.3.1.2-1: Average Hardness Values.....	229

Figure 7.3.1.2-2: V0023 Inner Layer Weld	230
Figure 7.3.1.2-3: Hardness Data from Plates A and B, Oriented by Vessel Location.....	230
Figure 7.3.1.2-4: Hardness Data from Plates A, B, and C, Aligned by Original Plate Length	231
Figure 7.3.1.2-5: Cut Plan for Macros from V0023 Inner Layer	232
Figure 7.3.1.2-6: Macro Size and Face Orientation.....	233
Figure 7.3.1.2-7: C4-2 0B at 100x Magnification.....	233
Figure 7.3.1.2-8: C3-10B at 100x Magnification.....	234
Table 7.3.1.2-2: Analysis of Macros	234
Table 7.3.1.3-1: 1146 Standard Material Properties, Minimums and Ranges (58), (60).....	235
Table 7.3.1.3-2: 1146 Collected Mill Certification Values.....	235
Table 7.3.1.3.1-1: 1146 Smooth Tensile Data, Vessel MV50466-8.....	237
Table 7.3.1.3.1-2: 1146 Smooth Tensile Data, Vessel V0023.....	238
Table 7.3.1.3.1-3: 1146 Smooth Tensile Data, Vessel V0032.....	239
Table 7.3.1.3.1-4: 1146 Smooth Tensile Data, Vessel V0125.....	239
Figure 7.3.1.3.1-1: 1146 Smooth Specimen Tensile Plot for Sample 440-106.....	240
Figure 7.3.1.3.3-1: 1146 Load Versus COD Plot, Sample 440-87	241
Figure 7.3.1.3.3-2: 1146 J_q Versus Δa Plot, Sample 440-87	242
Figure 7.3.1.3.3-3: Cut Plan for MV50466-8 Fracture Specimens	243
Table 7.3.1.3.3-1: V0125 1146 Wrapper Fracture Data.....	244
Figure 7.3.1.3.3-4: V0125 1146 Wrapper Layer T_0 Plot ($T_0 = -13^\circ\text{C}$)	245
Table 7.3.1.3.3-2: V0125 1146 Wrapper Layer T_0 Individual Specimen Results.....	246
Table 7.3.1.3.3-3: V0125 1146 Wrapper Layer T_0 Calculation Results	246
Table 7.3.1.3.3-4: V0125 1146 Wrapper Layer T_0 Calculation Results	247
Table 7.3.1.3.3-5: V0032 Inner Layer 1146 Fracture Data	247
Figure 7.3.1.3.3-5: V0032 Inner Layer T_0 Plot ($T_0 = -52^\circ\text{C}$)	248
Table 7.3.1.3.3-6: V0032 Inner Layer T_0 Plot ($T_0 = -52^\circ\text{C}$)	249
Table 7.3.1.3.3-7: V0032 Inner Layer 1146 T_0 Calculation Results	249

Table 7.3.1.3.3-8: V50466-8 1146 Inner Layer Fracture Data.....	250
Figure 7.3.1.3.3-6: MV50466-8 1146 Inner Layer Fracture Data	251
Table 7.3.1.3.3-9: MV50466-8 1146 Inner Layer T_0 Individual Specimen Results	252
Table 7.3.1.3.3-10: MV50466-8 1146 Inner Layer T_0 Calculation Results.....	253
Figure 7.3.1.3.3-7: MV50466-8 1146 Inner Layer Multimodal T_m Plot ($T_m = -38\text{ }^\circ\text{C}$)	253
Table 7.3.1.3.3-11: MV50466-8 1146 Inner Layer Multimodal T_m Calculation Results	254
Table 7.3.1.3.3-12: MV50466-8 1146 Wrapper Layer Fracture Data	254
Figure 7.3.1.3.3-8: MV50466-8 1146 Wrapper Layer T_0 Plot ($T_0 = -9^\circ\text{C}$).....	255
Table 7.3.1.3.3-13: MV50466-8 1146 Wrapper Layer T_0 Individual Specimen Results	256
Table 7.3.1.3.3-14: MV50466-8 1146 Wrapper Layer T_0 Calculation Results.....	256
Table 7.3.1.3.3-15: V0023 1146 Inner Layer C4-1 0A and 0B Fracture Data	257
Table 7.3.1.3.3-16: V0023 1146 Inner Layer C3-1 0B Fracture Data	257
Figure 7.3.1.3.3-9: V0023 1146 Inner Layer C3-1 0B T_0 Plot ($T_0 = -100^\circ\text{C}$).....	258
Table 7.3.1.3.3-17: V0023 1146 Inner Layer C3-1 0B T_0 Individual Specimen Results	259
Table 7.3.1.3.3-18: V0023 1146 Inner Layer C3-1 0B T_0 Calculation Results.....	259
Table 7.3.1.3.3-19: V0023 1146 Inner Layer C4-2 0B Fracture Data	260
Figure 7.3.1.3.3-10: V0023 1146 Inner Layer C4-2 0B T_0 Plot ($T_0 = 61^\circ\text{C}$).....	260
Table 7.3.1.3.3-20: V0023 1146 Inner Layer C4-2 0B T_0 Individual Specimen Results	261
Table 7.3.1.3.3-21: V0023 1146 Inner Layer C4-2 0B T_0 Calculation Results.....	261
Table 7.3.1.3.3-22: V0023 1146 Wrapper Layer Fracture.....	262
Figure 7.3.1.3.3-11: 1146 Combined T_0 Plots.....	263
Table 7.3.1.3.4-1: V0023 da/dN Test Matrix.....	264
Table 7.3.1.3.4-2: V0023 da/dN Results.....	264
Figure 7.3.1.3.4-1: V0023-0A-1A/1B Plot $R = 0.1$	265
Figure 7.3.1.3.4-2: V0023-0A-2A/2B Plot $R = 0.1$	266
Figure 7.3.1.3.4-3: V0023-0A-3A/3B Plot $R = 0.7$	267
Figure 7.3.1.3.4-4: V0023-0A-4A/4B Plot $R = 0.7$	268

Figure 7.3.1.3.4-5: V0023-0B-1A/1B Plot R=0.1	269
Figure 7.3.1.3.4-6: V0023-0B-2A/2B Plot R =0.1	270
Figure 7.3.1.3.4-7: V0023-0B-3A/3B Plot R = 0.7	271
Figure 7.3.1.3.4-8: V0023-0B-4A/4B Plot R = 0.7	272
Figure 7.3.1.3.4-9: V0023-2A-1A/1B Plot R = 0.1	273
Figure 7.3.1.3.4-10: V0023-2A-2A/2B Plot R = 0.1	274
Figure 7.3.1.3.4-11: V0023-2A-3A/3B Plot R = 0.7	275
Figure 7.3.1.3.4-12: V0023-2A-4A/4B Plot R = 0.7	276
Table 7.3.2.1-1: CB&I 1143 Material Chemistry Specification (59)	277
Table 7.3.2.1-3: V0125 1143 Inner Layer Chemistry Data	278
Table 7.3.2.3-2: Mill Certification Mechanical Properties	279
Table 7.3.2.3.1-1: V0125 1143 Inner Layer Tensile Data	280
Figure 7.3.2.3.1-1: V0125 1143 Smooth Specimen Tensile Plot for Sample CP344-4-76.....	280
Figure 7.3.2.3.3-1: Cut Plan for V0125 Inner Specimens	281
Table 7.3.2.3.3-1: 1143 Fracture Data V03487	282
Figure 7.3.2.3.3-2: 1143 Load Versus COD Plot, Sample CP344-4-43.....	283
Figure 7.3.2.3.3-3: 1143 J_q Versus Δa Plot, Sample CP344-4-43.....	284
Table 7.3.2.3.3-2: V0125 1143 T_0 Individual Specimen Results	285
Table 7.3.2.3.3-3: V0125 1143 T_0 Calculation Results.....	285
Figure 7.3.2.3.3-4: V0125 1143 T_0 Plot	286
Figure 7.3.2.3.5-1: V0125 Charpy Cut Plan	287
Table 7.3.2.3.5-1: V0125 1143 Charpy Data	287
Figure 7.3.2.3.5-2: V0125 1143 V-Notch Charpy Fracture Surface 74°F.....	288
Figure 7.3.2.3.5-3: V0125 1143 V-Notch Charpy Fracture Surface -40°F	288
Figure 7.3.2.3.5-4: V0125 1143 Charpy Plot	289
Table 7.3.3.1-1: ASTM A517-84 Standard Chemistry Values (24).....	290
Table 7.3.3.1-2: T-1 Collected Chemistry Data Vessel V0066	290

Figure 7.3.3.2-1: Cut Plan for Macros from V066 Layer.....	291
Table 7.3.3.2-1: Macro Observations.....	292
Figure 7.3.3.2-2: Macro from V0066 as Polished.....	292
Figure 7.3.3.2-3: Macro from V0066 Etched.....	293
Table 7.3.3.3-1: A517 Minimum Material Specifications (24)	293
Table 7.3.3.3.1-1: T-1 Tensile Data V00667	294
Figure 7.3.3.3.1-1: T-1 Smooth Specimen Tensile Plot for Sample 629-7	294
Figure 7.3.3.3.3-1: Cut Plan for V0066 Fracture Specimens	295
Table 7.3.3.3.3-1: T-1 Fracture Data V0066	296
Figure 7.3.3.3.3-2: T-1 Load Versus COD Plot, Sample 629-3	297
Figure 7.3.3.3.3-3: T-1 J_q Versus Δa Plot, Sample 629-3	298
Table 7.3.3.3.3-2: T_0 Individual Specimen Results	298
Table 7.3.3.3.3-3: T_0 Calculation Results.....	299
Figure 7.3.3.3.3-4: T-1 T_0 Plot.....	300
Figure 7.3.3.3.4-1: T-1 Fatigue Crack Growth Plot, $R = 0.11$	301
Figure 7.3.3.3.4-2: T-1 Fatigue Crack Growth Plot, $R = 0.7$	302
Figure 7.3.3.3.4-3: T-1 Fatigue Crack Growth Plot, Combined	303
Table 7.4.1.1-1: AOS 5002 Chemistry Specification (60).....	304
Table 7.4.1.1-2: 5002 Collected Chemistry Data.....	304
Table 7.4.1.3-1: AO Smith 5002 Mechanical Specification (60).....	305
Figure 7.4.1.3.3-1: MV50466-8 Nozzle Fracture Cut Plan.....	305
Table 7.4.1.3.3-1: AOS 5002 Fracture Data MV50466-8.....	306
Figure 7.4.1.3.3-2: AOS 5002 Load Versus COD Plot, Sample 440-253	307
Figure 7.4.1.3.3-3: AOS 5002 J_q Versus Δa Plot, Sample 440-253.....	307
Table 7.4.1.3.3-2: T_0 Individual Specimen Results	308
Table 7.4.1.3.3-3: T_0 Calculation Results.....	308
Figure 7.4.1.3.3-4: AOS 5002 T_0 Plot	309

Table 7.4.2.1-1: A105 Chemistry Requirements (61).....	310
Table 7.4.2.1-2: A105 V0032 Mill Certification Values	310
Table 7.4.2.1-3: A105 Nozzle Collected Chemistry Data.....	310
Figure 7.4.2.2-1: Cut Plan for Macros from V0032 A105 Nozzle	311
Table 7.4.2.2-1: A105 Nozzle Macro Evaluations.....	311
Figure 7.4.2.2-2: A105 Nozzle Macro Cube As-Polished 100X.....	312
Figure 7.4.2.2-3: A105 Nozzle Macro Cube Nital Etch 50X	313
Table 7.4.2.3-1: A105 Standard Specification Value (61).....	313
Table 7.4.2.3-2: A105 Standard Specification Value.....	313
Table 7.4.2.3.1-1: A105 Nozzle Tensile Data V0032	315
Table 7.4.2.3.1-2: A105 Nozzle Tensile Data V0348	315
Figure 7.4.2.3.1-1: A105 Smooth Specimen Tensile Plot for Sample 380-196	316
Figure 7.4.2.3.3-1: Cut Plan for V0032 Nozzle Specimens	317
Figure 7.4.2.3.3-2: A105 Load Versus COD Plot, Sample 380-208.....	318
Figure 7.4.2.3.3-3: A105 J_q Versus Δa Plot, Sample 380-208	319
Table 7.4.2.3.3-1: A105 Nozzle Fracture Data V0032	320
Table 7.4.2.3.3-2: T_0 Individual Specimen Results V0032 A105 Nozzle	320
Table 7.4.2.3.3-3: T_0 Calculation Results V0032 A105 Nozzle.....	320
Figure 7.4.2.3.3-4: V0032 A105 Nozzle T_0 Plot ($T_0 = -92^\circ\text{C}$)	321
Table 7.4.2.3.3-4: A105 Nozzle Fracture Data V0348	322
Table 7.4.2.3.3-5 T_0 Individual Specimen Results V0348 A105 Nozzle	322
Table 7.4.2.3.3-6 T_0 Calculation Results V0348 A105 Nozzle.....	322
Figure 7.4.2.3.3-5: V0348 A105 Nozzle T_0 Plot ($T_0 = -111^\circ\text{C}$).....	323
Figure 7.4.2.3.3-6: A105 Nozzle T_0 Combined Master Curve Plot	324
Figure 7.5.1-1: Weld Offset Diagram	326
Table 7.5.1.1-1: Longitudinal Weld Collected Chemistry Data	326
Figure 7.5.1.2-1: Cut Plan for Macros from MV50466-8 Seam Weld	327

Figure 7.5.1.2-2: V0125 Seam Weld Macro	328
Figure 7.5.1.2-3: MV50466-8 Seam Weld Macro (Edge of wrapper plate unfused)	329
Figure 7.5.1.2-4: MV50466-8 Seam Weld Macro (Significant porosity)	329
Figure 7.5.1.2-5: MV50466-8 Seam Weld 440-163 Indent Locations	330
Figure 7.5.1.2-6: MV50466-8 Seam Weld 440-163 Hardness Trace	331
Figure 7.5.1.2-7: MV50466-8 Seam Weld 440-173 Indent Locations	331
Figure 7.5.1.2-8: MV50466-8 Seam Weld 440-173 Hardness Trace	332
Figure 7.5.1.2-9: MV50466-8 Seam Weld 440-183 Indent Locations	332
Figure 7.5.1.2-10: MV50466-8 Seam Weld 440-183 Hardness Trace	333
Figure 7.5.1.2-11: V0125 Seam Weld CP344-3-30 Indent Locations	334
Figure 7.5.1.2-12: V0125 Seam Weld CP344-3-30 Hardness Trace	334
Figure 7.5.1.2-13: V0125 Seam Weld CP344-3-43 Indent Locations	335
Figure 7.5.1.2-14: V0125 Seam Weld CP344-3-43 Hardness Trace	335
Figure 7.5.1.2-15: V0125 Seam Weld CP344-3-54 Indent Locations	336
Figure 7.5.1.2-16: V0125 Seam Weld CP344-3-54 Hardness Trace	337
Figure 7.5.1.3.1-1: Longitudinal Seam Weld Smooth Tensile Plot Sample 519-53.....	338
Table 7.5.1.3.1-1: Longitudinal Weld Smooth Tensile Data MV50466-8.....	338
Table 7.5.1.3.1-2 Longitudinal Weld Smooth Tensile Data V0023	339
Table 7.5.1.3.1-3: Longitudinal Weld Smooth Tensile Data V0032	339
Table 7.5.1.3.1-4: Longitudinal Weld Smooth Tensile Data V0125	340
Figure 7.5.1.3.1-1: Longitudinal Seam Weld Smooth Tensile Plot Sample 519-53.....	340
Figure 7.5.1.3.3-1: Longitudinal Seam Weld Load Versus COD Plot, Sample 519-103.....	341
Figure 7.5.1.3.3-2: Longitudinal Seam Weld Jq Versus Δa Plot, Sample 519-103	342
Figure 7.5.1.3.3-3: Cut Plan for Fracture Specimens from MV50466-8 Seam Weld	343
Table 7.5.1.3.3-1: Seam Weld Fracture Data V0125	343
Table 7.5.1.3.3-2: Seam Weld Fracture Data MV50466-8	344
Figure 7.5.1.3.3-4: MV50466-8 Seam Weld Center T_0 Plot.....	344

Table 7.5.1.3.3-3: Seam Weld Center T ₀ Individual Specimen Results, MV50466-8	345
Table 7.5.1.3.3-4: MV50466-8 Seam Weld Center T ₀ Calculation Results.....	345
Table 7.5.1.3.3-5: Seam Weld HAZ Fracture Data MV50466-8.....	346
Figure 7.5.1.3.3-5: MV50466-8 Seam Weld HAZ T ₀ Plot.....	347
Table 7.5.1.3.3-6: MV50466-8 Seam Weld HAZ T ₀ Individual Specimen Results	348
Table 7.5.1.3.3-7: MV50466-8 Seam Weld HAZ T ₀ Calculation Results	348
Figure 7.5.1.3.3-6: V0032 Seam Weld T ₀ Plot	350
Table 7.5.1.3.3-9: V0032 Seam Weld T ₀ Individual Specimen Results.....	350
Table 7.5.1.3.3-10: V0032 Seam Weld T ₀ Calculation Results	351
Table 7.5.1.3.3-11: Seam Weld HAZ Fracture Data V0032	352
Figure 7.5.1.3.3-7: V0032 Seam Weld HAZ T ₀ Plot.....	353
Table 7.5.1.3.3-12: V0032 Seam Weld HAZ T ₀ Individual Specimen Results	353
Table 7.5.1.3.3-13 V0032 Seam Weld HAZ T ₀ Calculation Results.....	354
Table 7.5.1.3.3-14: Seam Weld Fracture Data V0023	355
Figure 7.5.1.3.3-8: V0023 Seam Weld T ₀ Plot	356
Table 7.5.1.3.3-15: V0023 Seam Weld T ₀ Individual Specimen Results.....	357
Table 7.5.1.3.3-16: V0023 Seam Weld T ₀ Calculation Results	357
Table 7.5.1.3.3-17 Seam Weld HAZ Fracture Data V0023	358
Figure 7.5.1.3.3-9: V0023 Seam Weld HAZ T ₀ Plot.....	359
Table 7.5.1.3.3-18: : V0023 Seam Weld HAZ T ₀ Individual Specimen Results	359
Table 7.5.1.3.3-19: V0023 Seam Weld HAZ T ₀ Calculation Results.....	360
Figure 7.5.1.3.3-10: Longitudinal Wrapper Weld and HAZ T ₀ Plot Combined.....	361
Figure 7.5.1.3.4-1: Specimen Cut Plan da/dN V0023 Seam Weld	362
Figure 7.5.1.3.4-2: Specimen Cut Plan da/dN V0023 Seam Weld (Continued)	363
Table 7.5.1.3.4-1: V0023 Seam Weld da/dN Test Matrix	364
Table 7.5.1.3.4-2: V0023 Seam Weld da/dN Results	364
Figure 7.5.1.3.4-3: V0023-2AB-LW-1 Plot R = 0.1	365

Figure 7.5.1.3.4-4: V0023-2AB-LW-2 Plot R = 0.1	366
Figure 7.5.1.3.4-5: V0023-2AB-LW-3 Plot R = 0.7	367
Figure 7.5.1.3.4-6: V0023-2AB-LW-4 Plot R = 0.7	368
Table 7.5.2.1-1: Collected Chemistry Data.....	369
Figure 7.5.2.2-1: Cut Plan for Macros from MV50466-8 Seam Weld	370
Figure 7.5.2.2-2: MV50466-8 Inner Weld Macro	370
Figure 7.5.2.2-3: V0032 Inner Weld Macro.....	371
Figure 7.5.2.2-4: V0032 Inner Weld Macro.....	371
Figure 7.5.2.2-5: V0125 Inner Weld Macro.....	372
Figure 7.5.2.2-6: V0125 Inner Weld Indent Locations	373
Figure 7.5.2.2-7: V0125 Inner Weld Hardness Trace	373
Figure 7.5.2.2-8: V0023 Inner Weld Indent Locations	374
Figure 7.5.2.2-9: V0023 Inner Weld Hardness Map.....	374
Figure 7.5.2.2-10: V0023 Inner Weld Hardness Distribution.....	375
Table 7.5.2.3.1-1: Inner Weld Smooth Tensile Data, MV50466-8	376
Table 7.5.2.3.1-3: Inner Weld Smooth Tensile Data, V0032.....	376
Table 7.5.2.3.1-4: Inner Weld Smooth Tensile Data, V0125.....	376
Figure 7.5.2.3.1-1: Inner Layer Weld Smooth Tensile Plot for Sample 519-206.....	377
Figure 7.5.2.3.3-1: Inner Layer Weld Load Versus COD Plot, Sample 519-191	378
Figure 7.5.2.3.3-2: Inner Layer Weld Jq Versus Δa Plot, Sample 519-191	379
Figure 7.5.2.3.3-3: Cut Plan for Fracture Specimens from MV50466-8 Inner Weld.....	380
Table 7.5.2.3.3-1: Inner Layer Weld Fracture Toughness Data, V0125	380
Table 7.5.2.3.3-2: Inner Layer Weld T_0 Individual Specimen Results, V0125	381
Figure 7.5.2.3.3-4: Inner Layer Weld T_0 Plot, V0125.....	382
Table 7.5.2.3.3-4: Inner Layer Weld Fracture Toughness Data, V0032	383
Table 7.5.2.3.3-6: Inner Layer Weld T_0 Calculation Results, V0032.....	383
Figure 7.5.2.3.3-5: Inner Layer Weld T_0 Plot, V0032.....	384

Table 7.5.2.3.3-7: Inner Layer Weld Fracture Toughness Data, V0023	384
Table 7.5.2.3.3-8: Inner Layer Weld T_0 Individual Specimen Results, V0023	385
Table 7.5.2.3.3-9: Inner Layer Weld T_0 Calculation Results, V0023	385
Figure 7.5.2.3.3-6: Inner Layer Weld T_0 Plot, V0023	386
Table 7.5.2.3.3-10: Inner Layer Weld HAZ Fracture Toughness Data, V0023.....	386
Table 7.5.2.3.3-11: Inner Layer Weld HAZ T_0 Individual Specimen Results, V0023.....	387
Table 7.5.2.3.3-12: Inner Layer Weld HAZ T_0 Calculation Results, V0023	387
Figure 7.5.2.3.3-7: Inner Layer Weld HAZ T_0 Plot, V0023	388
Figure 7.5.2.3.3-8: Inner Weld Combined T_0 Plot	389
Figure 7.5.2.3.4-1: Specimen Cut Plan da/dN V0023 Inner Layer Weld	390
Figure 7.5.2.3.4-2: Specimen Cut Plan da/dN V0023 Inner Layer Weld (Continued).....	390
Table 7.5.2.3.4-1: V0023 Inner Layer Weld da/dN Test Matrix	391
Table 7.5.2.3.4-2: V0023 Inner Layer Weld da/dN Results.....	391
Figure 7.5.2.3.4-3: V0023-0AB-LW-1 Plot R = 0.1	392
Figure 7.5.2.3.4-4: V0023-0AB-LW-2 Plot R = 0.1	393
Figure 7.5.2.3.4-5: V0023-0AB-LW-3 Plot R = 0.7	394
Figure 7.5.2.3.4-6: V0023-0AB-LW-4 Plot R = 0.7	395
Table 7.5.3.1-1: Collected Chemistry Data.....	396
Figure 7.5.3.2-1: Cut Plan for Macros from V0023 Head-to-Shell Weld.....	397
Figure 7.5.3.2-2 MV50466-8 Head-to-Shell Weld Macro (with Longitudinal Weld Intersection)	398
Figure 7.5.3.2-3: V0125 Head-to-Shell Weld Macro	399
Figure 7.5.3.2-4: V0032 Head-to-Shell Weld Macro	399
Figure 7.5.3.2-5: V0023 Head-to-Shell Weld Macro	400
Figure 7.5.3.2-6: V0023 Shell-to-Shell Weld Macro.....	401
Figure 7.5.3.2-7: V0125 Head-to-Shell Weld Indent Locations.....	402
Figure 7.5.3.2-8: V0125 Head-to-Shell Weld Traces 1 and 2	403

Figure 7.5.3.2-9: V0125 Head-to-Shell Weld Traces 3,4, and 5	403
Figure 7.5.3.2-10: MV50466-8 Head-to-Shell Weld Indent Location	404
Figure 7.5.3.2-11: MV50466-8 Head-to-Shell Weld Section A.....	405
Figure 7.5.3.2-12: MV50466-8 Head-to-Shell Weld Section B.....	405
Figure 7.5.3.2-13: MV50466-8 Head-to-Shell Weld Section	406
Figure 7.5.3.2-14: MV50466-8 Head-to-Shell Weld Section D.....	407
Figure 7.5.3.2-15: MV50466-8 Head-to-Shell Weld Hardness Frequency Comparison	407
Figure 7.5.3.2-16: MV50466-8 Head-to-Shell Weld Full Hardness Map.....	408
Table 7.5.3.3.1-1: Head-to-Shell Weld Smooth Tensile Data MV50466-8.....	409
Table 7.5.3.3.1-3: Head-to-Shell Weld Smooth Tensile Data V0032	410
Table 7.5.3.3.1-4: Head-to-Shell Weld Smooth Tensile Data V0023	411
Table 7.5.3.3.1-5: Shell-to-Shell Weld Smooth Tensile Data V0066.....	411
Figure 7.5.3.3.1-1: Full Thickness Weld Smooth Tensile Plot for Sample 519-310	412
Figure 7.5.3.3.3-1: Shell-to-Shell Weld Load Versus COD Plot, Sample 629-18	413
Figure 7.5.3.3.3-2: Shell-to-Shell Weld J_q Versus Δa Plot, Sample 629-18.....	414
Figure 7.5.3.3.3-3: Cut Plan for Fracture Specimens from V0023 Head-to-Shell Weld.....	415
Table 7.5.3.3.3-1: Head-to-Shell Weld Fracture Data, V0125.....	416
Table 7.5.3.3.3-2 Head-to-shell Weld HAZ (Head Side) Fracture Data, V0125.....	416
Table 7.5.3.3.3-3: Head-to-shell Weld Inner Shell V0032.....	416
Table 7.5.3.3.3-4: Head-to-shell Weld (Inner Layer) T_0 Individual Specimen Results, V0032 ..	417
Table 7.5.3.3.3-5 Head-to-shell Weld (Inner Layer) T_0 Calculation Results, V0032.....	417
Figure 7.5.3.3.3-4: Head-to-Shell Weld (Inner Layer) T_0 Plot, V0032	418
Table 7.5.3.3.3-6: Head-to-Shell Weld Wrapper Layer V0032.....	419
Table 7.5.3.3.3-7: Head-to-Shell Weld (Wrapper Layer) T_0 Individual Specimen Results, V0032	419
Table 7.5.3.3.3-8: Head-to-Shell Weld (Wrapper Layer) T_0 Calculation Results, V0032.....	420
Figure 7.5.3.3.3-5: Head-to-Shell Weld (Wrapper Layer) T_0 Plot, V0032	421

Table 7.5.3.3.3-10 Head-to-Shell Weld T_0 Individual Specimen Results, V0023	422
Table 7.5.3.3.3-11 Head-to-shell Weld T_0 Calculation Results, V0023	423
Figure 7.5.3.3.3-6: Head-to-shell Weld T_0 Plot, V0023	424
Table 7.5.3.3.3-12: Head-to-Shell Weld V0023.....	425
Table 7.5.3.3.3-13: Head-to-Shell Weld T_0 Individual Specimen Results, V0023	425
Table 7.5.3.3.3-14: Head-to-Shell Weld T_0 Calculation Results, V0023	425
Figure 7.5.3.3.3-7: Head-to-Shell Weld T_0 Plot, V0023.....	426
Figure 7.5.3.3.4-1: Cut Plan for Fatigue Specimens from V0023 Head-to-Shell Weld	427
Figure 7.5.3.3.4-2: Fatigue Crack Growth Curves, V0023 Head-to-Shell Weld and HAZ.....	428
Table 7.5.4.1-1: Collected Nozzle Weld Chemistry.....	429
Figure 7.5.4.2-1: MV50466-8 Nozzle Weld Hardness Map.....	430
Table 7.5.4.3.1-1: MV50466-8 Nozzle Weld Tensile Data.....	432
Figure 7.5.4.3.1-1: Nozzle Weld Smooth Tensile Plot Sample 440-298.....	432
Figure 7.5.4.3.3-1: MV50466-8 Example Fracture Cut Plan.....	433
Table 7.5.4.3.3-1: MV50466-8 Nozzle-to-Head Weld HAZ Fracture Data	434
Figure 7.5.4.3.3-2: MV50466-8 Nozzle-to-Head Weld HAZ T_0 Plot ($T_0 = -90^\circ\text{C}$)	435
Table 7.5.4.3.3-2: MV50466-8 Nozzle-to-Head Weld HAZ T_0 Individual Specimen Results	436
Figure 7.5.4.3.3-3: MV50466-8 Nozzle to Head Weld HAZ Multimodal T_m Plot ($T_m = -95^\circ\text{C}$) ...	437
Table 7.5.4.3.3-4: MV50466-8 Nozzle-to-Head Weld HAZ Multimodal T_m Calculation Results 7	437
Table 7.5.4.3.3-5 MV50466-8 Nozzle-to-Head Weld Fracture Data	438
Figure 7.5.4.3.3-4: MV50466-8 Nozzle-to-Head Weld T_0 Plot ($T_0 = -83^\circ\text{C}$)	439
Table 7.5.4.3.3-6: MV50466-8 Nozzle-to-Head Weld T_0 Individual Specimen Results.....	440
Table 7.5.4.3.3-7: MV50466-8 Nozzle-to-Head Weld T_0 Calculation Results	440
Figure 7.5.4.3.3-5: MV50466-8 Nozzle-to-Head Weld Multimodal T_m Plot ($T_m = -78^\circ\text{C}$)	441
Table 7.5.4.3.3-8: MV50466-8 Nozzle to Head Weld Multimodal T_m Calculation Results	441
Table 8.1.1-1: Head Material Hardness and Chemistry Data Summary	443

Table 8.1.1-2: Head Material Mechanical Data Summary 443

Figure 8.1.1-1: Head Material Median T₀ Curves..... 444

Figure 8.1.1-3: Head Material ECF v. Temperature 445

Figure 8.1.1-4: Head Material ECF at -20F 446

Table 8.1.2-2: Nozzle Material Mechanical Data Summary..... 446

Figure 8.1.2-1: Nozzle Material Median T₀ Curves..... 447

Figure 8.1.2-2: Nozzle Material ECF v. Temperature 448

Figure 8.1.2-3: Nozzle Material ECF at -20F 448

Figure 8.1.2-4: Nozzle Material ECF at -20F 449

Table 8.1.3-1: Wrapper Material Hardness and Chemistry Data Summary 449

Table 8.1.3-2: Wrapper Material Mechanical Data Summary 450

Figure 8.1.3-1: Wrapper Material Median T₀ Curves..... 450

Figure 8.1.3-2: Wrapper Material T₀ Lower Tolerance Bound..... 451

Figure 8.1.3-3: Wrapper Material ECF v. Temperature 452

Figure 8.1.3-4: Wrapper Material ECF at -20F 453

Table 8.1.4-1: Weld Material Hardness and Chemistry Data Summary 454

Table 8.1.4-2: Weld Material Mechanical Data Summary 454

Figure 8.1.4-1: Layer Weld Material Median T₀ Curves 455

Figure 8.1.4-2: Layer Weld Material T₀ Lower Tolerance Bound..... 456

Figure 8.1.4-3: Full Thickness Weld Material Median T₀ Curves 456

Figure 8.1.4-4: Full Thickness Weld Material T₀ Lower Tolerance Bound 457

Figure 8.1.4-5: Nozzle Weld Material Median T₀ Curves 457

Figure 8.1.4-6: Nozzle Weld Material T₀ Lower Tolerance Bound..... 458

Figure 8.1.4-7: Weld Material ECF v. Temperature 458

Figure 8.1.4-8: Weld Material ECF at -20F 459

EXECUTIVE SUMMARY

A significant portion of Layered Pressure Vessels (LPVs) manufactured for NASA in the 1950s and '60s are of non-code construction. These vessels were constructed to the standards of individual manufacturers rather than an industry or consensus standard and often contain legacy or proprietary materials, which have poor or no characterization. Obtaining correct material properties is the first step in assuring vessel safety and predicting life and critical failure modes before they happen. This report details the efforts of the LPV Project related to material properties and characterization. The goal in testing materials from deconstructed vessels was to provide material characterization utilizing modern test methods that would give a strong probabilistic base as an option for future analysis. ASTM E1820, Standard Test Method for Measurement of Fracture Toughness was used for fracture toughness; ASTM E1921, Standard Test Method for Determination of Reference Temperature, T_0 , for Ferritic Steels in the Transition Range for transition temperature; and ASTM E647, Standard Test Method for Measurement of Fatigue Crack Growth Rates for fatigue crack growth. Particular focus was placed on determination of transition temperature through evaluation of the T_0 reference temperature in accordance with ASTM E1921. Transition temperature testing allows for a probabilistic analysis of vessel materials that may be operating at temperatures below the transition from ductile tearing to brittle cleavage failure. This test method was not available at the time of construction and has proved invaluable to the characterization of older ferritic steels. The values reported are specific to the largest body of materials found in the current NASA fleet, but do not claim to be all inclusive. As demonstrated in this report, some materials contain extreme lot-to-lot variability. In some cases, this can be comfortably bounded by worst case probabilistic methods, however it is always recommended that vessel specific data be collected in as much depth as possible to ensure correct assumptions and avoid unduly restricting vessel usage.

1 NESC REPORT

The NASA Engineering Safety Center (NESC) Report (1) encapsulates the initial effort to characterize LPVs and provides valuable background to the origination of test efforts. Test results and materials characterization given in Section 7 are the results of discoveries during the NESC effort. Relative to materials testing, the background provided in this section serves to give the logic and reasoning behind the types and number of tests conducted during the full materials testing effort.

Section VIII of the American Society of Mechanical Engineers (ASME) Boiler and Pressure Vessel Code (BPVC) 2011 (2) provides rules for the construction of new pressure vessels. Newly constructed pressure vessels that fully comply with and are stamped in accordance with ASME BPVC Section VIII are considered to be “code” vessels. When layered methods of construction were added into the BPVC, A. O. Smith (AOS) and its competitors Nooter Corporation and Hahn and Clay were heavily involved in the development of the rules. The different companies had different fabrication procedures, and ASME used a consensus process to develop the rules. Thus, the rules that resulted allowed for a number of fabrication techniques and did not reflect what any individual company had done for previously constructed vessels.

Any impact testing performed typically consisted of U-notch or keyhole-notch Charpy specimens, which have a 5 mm deep notch with a 1 mm radius at the base. These were not permitted in the BPVC after 1967, when Charpy V-notch specimens, which have a 2 mm deep notch with a 45-degree angle and a 0.25mm radius at the base, were required. The development of the Charpy V-notch specimen occurred as a result of World War II ship failures caused by high ductile-brittle transition temperature steels similar to ASTM A225B. Earlier Charpy notch geometries were not sensitive to this phenomenon. (The Department of Transportation (DOT) also made this change related to DOT requirements for gas storage bottles the same year.) One of the later significant revisions of the ASME BPVC in this area was in 1987. The 1987 Addenda to the 1986 ASME BPVC Section VIII, Division 1 (3) added the UCS-66 curves for determining minimum design metal temperature (MDMT). At the time these vessels were constructed, the MDMT was typically based only on material strength and did not take into account brittle fracture that may occur at lower temperatures, including the nameplate MDMT.

There is evidence that some AOS vessels were keyhole impact tested at -40 °F, consistent with code procedures of the day, but the keyhole method used was removed from the BPVC in the early 1967 and is not acceptable in current practice because it was shown beginning in the 1950s that brittle failure of ship plates could be correlated with Charpy V notch, but not with Charpy keyhole notch characteristics (4). Thus, operating at or above the nameplate MDMT for these vessels may not ensure safety with respect to the potential for brittle failure.

Proprietary shell and nozzle materials used were not BPVC listed (approved) materials. These proprietary materials also failed to comply with the BPVC requirements for unlisted

materials. Thus, complete material fracture characteristics are not readily available. The head material, ASTM A225B, while included in some prior editions of the BPVC, was deleted as an acceptable material in the Summer 1979 Addenda of the 1977 Section VIII, Division 1 Code (5) and is not currently included in ASME BPVC Section II Materials (2019) (6).

NASA Centers were asked to identify any special concerns they had with respect to LPVs. One response highlighted the variability that has been observed in previous testing to characterize the material properties of the A225 material used in LPV heads. The variability makes it difficult to use generic materials properties for this material in analyses and may lead to requirements to use either very low bounding properties or to the development of some methods to assess properties specific to individual vessels. The problems associated with the unknown relevance of past Charpy U-notch or keyhole data to current fracture toughness methodologies were also highlighted. Material testing objectives were to develop an initial understanding of material performance of LPVs, more specifically, the structurally significant material properties, including tensile and fracture mechanics behavior. Representative surplus vessels were identified to collect data to develop a materials database.

Fracture toughness as a function of temperature was identified as the most influential material property for vessel assessment. The fully ductile fracture toughness (upper shelf) and the temperature at which the steel transitions to cleavage fracture (lower shelf) were determined to be of critical interest in the assessment of LPVs. The use of the T_0 reference temperature methodology from ASTM E1921, Standard Test Method for Determination of Reference Temperature, T_0 , for Ferritic Steels in the Transition Range (7) was chosen as a method to evaluate fracture mechanics toughness data relative to ductile-brittle transition effects as a function of temperature. Cleavage versus ductile in terms of ASTM E1921 refers to the fracture mechanism, (i.e., cleavage of crystal planes versus ductile crack-growth crack mechanism). A brittle structural failure can occur either by cleavage or ductile cracking, but implies a failure controlled by low toughness rather than net section yielding.

The E1921 approach was expected to minimize the number of test samples required to define the ductile-brittle transition curve. The E1921 method was considered especially advantageous because it uses a fracture-mechanics-based weakest link theory in the evaluation to maximize the information gained from testing from a limited number of tests and because E1921, as a statistical method, allows failure probability levels (confidence levels) to be statistically determined. The fact that it is a fracture-mechanics-based method rather than a correlation means that it gives an accurate, rather than conservative, measurement of the temperature above which cleavage fracture is not to be expected, compared with Nil-Ductility-Temperature (NDT)-based approaches. This method was applied to generate confidence curves for several LPV materials (see Section 7, Material Test Data).

Table 1-1: Definition of Material Testing Terms

Term	Definition
1T	Syntax used to represent fracture toughness specimen dimensions; general form is nT , where the specimen thickness is n inches
a	Crack size (length), a linear measure of the principal planar dimension of a crack
ASTM E 399-12	“Standard Test Method for Linear-Elastic Plane-Strain Fracture Toughness K_{IC} of Metallic Materials”
ASTM E 1820-11	“Standard Test Method for Measurement of Fracture Toughness”
ASTM E 1921-13	“Standard Test Method for Determination of Reference Temperature, T_0 , for Ferritic Steels in the Transition Range;” referred to as the Master Curve method
b_0	The initial remaining ligament, the distance from the crack tip to the back face of the specimen; a critical parameter for determining crack tip constraint
B_0	Full thickness of a fracture toughness specimen, ignoring side grooves if present
C	Used to designate the orientation of the crack or applied load for a toughness test specimen, indicating the circumferential direction around a pressure vessel
Compliance	Used for measuring crack length during fracture toughness testing; the ratio of specimen displacement increment to applied force increment (the inverse of specimen stiffness)
$C(T)$	Compact-tension specimen, a single-edge notched and fatigue cracked plate loaded in tension and used for fracture toughness tests
Δa	Change in specimen crack length during test, in this context, due to stable tearing

Table 1-2: Table 1-1 Continued

Term	Definition
δ	Kronecker delta from ASTM E 1921-13 analysis, equal to 1 if the datum is valid or 0 if the datum is a substitute value related statistical censoring of invalid test results
E	Elastic modulus
FCC	Face-centered cubic crystal system, the only steel crystalline structure to which ASTM E 1921-13 is directly applicable
ICP	Inductively coupled plasma, a quantitative chemistry technique for determining chemical composition
J_C	Fracture toughness test result measuring the energy of fracture, taken as the point of cleavage instability prior to the onset of significant stable tearing crack extension, and meeting validity requirements of ASTM E1820-11
J_{IC}	Fracture toughness test result measuring the energy of fracture, defined at an average of 0.008 inches of stable, ductile crack extension, and meeting validity requirements of ASTM E1820-11
K_{JC}	Fracture toughness test result for linear-elastic measure of fracture toughness and meeting validity requirements of ASTM E399
K_{JC}	Fracture toughness test result obtained by converting a J_C value to a linear-elastic equivalent stress intensity factor
$K_{JC(1T)}$	Fracture toughness test result obtained by adjusting a K_{JC} value to an equivalent value from a specimen of size 1T, accounts for statistical size effects on cleavage and used as an input to the T_0 analysis
$K_{JC(Limit)}$	Maximum allowed K_{JC} capacity of a specimen that will maintain a condition of high crack-front constraint at fracture based on specimen size; test results exceeding this limit must be statistically censored in order to be included in the ASTM E 1921-13 T_0 analysis
$K_{J_{\Delta a}}$	Value of K_J at the crack extension limit; tests that terminate in cleavage in which slow stable crack growth exceeds the smaller crack extension limit of either $0.05b_0$ or 0.040 in. must be statistically censored to be used in the ASTM E 1921-13 T_0 analysis by substituting this value for K_{JC}
L	Used for designating the orientation of the crack or applied load for a toughness test specimen, indicating the material longitudinal direction or pressure vessel longitudinal axis
M	Used for designating the orientation of the crack or applied load for a toughness test specimen, indicating the pressure vessel meridional axis for hemispherical heads
R	Used for designating the orientation of the crack or applied load for a toughness test specimen, indicating the pressure vessel radial axis
RT_{NDT}	An index temperature determined from Charpy V-notch and nil-ductility temperature data that provides conservative bounding values of fracture toughness versus temperature

Table 1-3: Table 1-2 Continued

Term	Definition
RT_{T0}	A Master Curve-based index temperature determined from fracture toughness data used as an alternative to RT_{NDT} as permitted by ASME Code Cases N-629 and N-631 that establishes an RT_{NDT} – like quantity from a T_0 value via the relationship $RT_{T0} = T_0 + 35^\circ\text{F}$.
S	Used for designating the orientation of the crack or applied load for a toughness test specimen, indicating the material short-transverse direction
SE(B)	Single-edge notch bend specimens, see ASTM E1820
σ_{Yr}	Yield strength
T	Used for designating the orientation of the crack or applied load for a toughness test specimen, indicating the material long-transverse direction
T	temperature
T_0	Reference transition temperature determined from ASTM E 1921-13 that represents the temperature at which the statistical median of the K_{Jc} distribution from 1T size specimens equals $100 \text{ MPa}\sqrt{\text{m}}$ ($91.1 \text{ ksi}\sqrt{\text{in.}}$) and statistically locates the fracture toughness versus temperature curve
$T_{35,50}$	Transition temperature from Charpy V-notch specimens that exhibit at least 35 mils of lateral expansion and not less than 50 ft-lbs of absorbed energy per ASTM E 23-12c.
T_{NDT}	nil-ductility-temperature from drop weight testing from ASTM E 208-06
u_{TS}	Ultimate strength
ν	Poisson's ratio
W	Width dimension for fracture toughness specimens; other specimen dimensions are commonly expressed relative to this width

1.1 Material Anisotropy

The correlation between the structural and material orientations must be identified first to orient and extract appropriate test specimens. As a general rule for Fitness for Service (FFS) assessments, fracture mechanics material property data are generated on the plane within the material that provides the least capability. For most thin-plate materials, specimens are extracted such that the crack is oriented parallel to the direction of elongated material grains, usually the longitudinal rolling direction. This typically produces bounding material properties. This philosophy for generating material data on the least capable orientation is required if the material orientation in the vessel is not certain. The small selection of sacrificial vessels under consideration in this assessment has illustrated that material orientation cannot be assumed to be consistent. While this assessment has proceeded mindful of determining bounding fracture properties in-plane, the behavior of cracks growing radially through the thickness of the materials has not been evaluated. Tests for this behavior in the thin-shell materials would typically use a surface-crack geometry. These studies were beyond the scope of the current assessment but should be considered for future evaluation. Material orientations are specified relative to the original plate corresponding the material: Longitudinal (L), Transverse (T), and Short-Transverse (S) directions. The structural orientations of a vessel are described by the Circumferential (C), Longitudinal (L), Radial (R), and Meridional (M, spherical head) directions.

Due to this anisotropic behavior, the material orientation for each piece of material needed to be determined prior to orienting the final set of test specimens. The shell materials proved fairly easy to orient, given that they maintained distinct orthogonal rolling directions. The only question to be resolved was whether the shell material longitudinal direction was oriented circumferentially around the vessel or along the vessel axis. Fracture toughness tests were performed in these two orientations (C-L and L-C) to determine the material orientation, which was always made clear by a large reduction in toughness in the longitudinal direction of the shell material. (Note that in the two-letter fracture toughness orientation designations above and elsewhere in this report, the first letter indicates the direction of applied loading, and the second letter indicates the direction of crack extension.) Identifying the bounding toughness orientation in the A225 head material was considerably more complicated. Both selective microstructural investigation and instrumented Charpy impact testing were used to help identify the material orientation. The microstructural evaluations were inconclusive, but the Charpy impact testing proved informative.

The biggest challenge of the A225 material involved identifying the lowest toughness orientation in the head. The plan to determine microstructural orientation began with a traditional metallographic approach. When metallographic methods proved inconclusive, a series of Charpy impact tests were used to provide further quantitative insight.

Metallographic microstructural evaluations at 50× and 100× magnifications were performed on A225 material from NASA Marshall Space Flight Center (MSFC) vessel V0032 and Glenn Research Center (GRC) V0296 for determining material orientation. Nine total samples in three orthogonal planes (C-M, R-C, and M-R) were taken at three equidistant circumferential locations around each head with 45 ° spacing between samples. The 0 ° location was chosen arbitrarily since there was no unique feature on the axisymmetric head that would indicate how the head was fabricated with respect to the parent plate. Each dimension of the metallurgical blanks was unique to maintain traceability of the macro orientations. The macros revealed no discernable microstructural evidence of the plate orientation prior to forming. For V0032, the microstructure appeared to be independent of the circumferential location with a uniform grain structure generally following the shape of the head.

Although the same Nital etching process (3% nitric acid, balance methanol) was followed for the samples from both heads, the grain orientation for GRC V0296 was much less apparent in the microstructural samples and less useful in determining material orientation.

The V0032 microstructure was dominated by what appeared to be considerable banding of pearlite and ferrite, which is undesirable. The dark bands are pearlite, and the lighter bands are ferrite. This banding is possibly a result of micro-segregation of alloying metals during the solidification of the original ingot, which was not ideally homogenized during the subsequent heat treatment. Alloying elements always segregate to some extent during the solidification of steel. Elements that are especially prone to segregation are carbon, phosphorus, sulfur, silicon, and manganese. Manganese is especially problematic because it lowers the chemical activity of

carbon in austenite, from which pearlite is formed. The manganese-rich areas are, thus, the last to transform and are mostly pearlite. During the microstructural evaluations, the banding features were observed regardless of the sample orientation or angular location. These microstructural features likely obscured any visible anisotropy introduced into the material from the original plate production.

These inconclusive microstructures, showing either no orientation or spherical banding following the forming of the head, were not expected. There was an expectation that the prior plate microstructure would remain dominant. Although exact historical records are incomplete, information on the typical head fabrication process was obtained from an industry consultant. For forming a head such as V0032, the steel mill would start with a thick slab of commercial A225 and roll the plate at a temperature close to 1,000 °F between two rolls to reduce the thickness. In this process, one primary direction would be stretched the most and become dominant, becoming the plate L direction. The orthogonal direction in the flat plane of the plate is identified as the T direction. Based on the desired surface area of the hemisphere, the head manufacturer would cut an appropriately sized disk out of the plate. The head manufacturer would usually heat the blank disk to around 800 to 900 °F and press it between male and female dies in small increments in order to attain the desired head dimensions and form. Based on this manufacturing process, the head forming operations would not be expected to eliminate the prior plate microstructure, but rather the plate material orientation would be projected over the head while retaining much of the original orthogonality.

If the prior plate microstructure remains, then the microstructure would continuously change circumferentially around the head, lining up with a prior plate orientation every 90°. The lack of such structure implies that the head material may have experienced an intermediate thermal treatment to eliminate the plate microstructure or might have been formed at a higher than anticipated temperature. Determining grain orientation by macros is commonly difficult in steels, particularly when the macros are arbitrarily oriented, as in this case. Given the inconclusive nature of these microstructural studies, a more quantitative approach with Charpy specimens was undertaken.

Instrumented Charpy V-notch tests, according to ASTM E2298-13 (8), were performed as a quick, relatively inexpensive yet quantitative way to determine the material orientation in the A225 head material from V0032. Due to deciding to focus on one lot of material, impact tests on the GRC V0296 head were not performed under this assessment. Instrumented Charpy tests utilize strain gages to capture the load versus displacement record at specimen impact. It is a more robust method than traditional Charpy tests, even if the load versus displacement is used only qualitatively as an aid to evaluate whether the fracture mechanism is brittle or ductile. The instrumented test is also preferred for its precision in measuring fracture energy; it is more precise than monitoring pendulum height after impact. This precision also serves to lower the minimum range of impact energies that can be reliably measured, which can be important with cleavage. Given cost considerations, samples were limited to two at each of the three circumferential locations in two orthogonal orientations, M-C and C-M. Note that the

direction of loading and crack extension is the same for Charpy specimens; therefore, in the two letter orientation designation for the Charpy specimen, the first letter indicates the direction of the long axis of the specimen, and the second letter indicates the direction of crack extension.

All tests were conducted at 0°F. Regarding the test temperature, these tests were not intended to determine the transition temperature but were simply used to reveal the least tough microstructural orientation in the material for subsequent fracture testing. The prior work by the Southwest Research Institute (SwRI) indicated that 0°F would be a good choice for determining anisotropy for this material because orientation impact energy differences appeared to be largest at 0°F in their tests. This work is documented in Cardinal, J.W. and Popelar, C.F., Multilayer Pressure Vessel Materials Testing and Analysis (Phase 2) (9). More informative fracture toughness tests were considered for determining the material orientation, but due to the required quantity, the Charpy tests were more financially viable, while being deemed to provide an adequate assurance of grain and rolling direction.

The Charpy impact results showed that the C-M orientation produced significantly lower impact energies than the M-C orientation with invariance to the sample circumferential location. This matches the observed orientation of the microstructural banding in the V0032 head material. It is possible that the material anisotropy effects in the V0032 head are being dominated by this banding structure. Future tests on head material without the banded microstructure may yield different results. It is suggested that all future efforts to identify the material orientation for pressure vessel heads predominantly utilize Charpy impact testing. Having attempted microstructural orientation evaluation in the A225 head material in the SwRI work, the GRC PV0296 head material, and the V0032 head, none of these investigations has provided clarity equal to that obtained from the Charpy impact data. Despite this finding, as future A225 material is evaluated it is suggested that the basic microstructure of the head material be documented for features such as banding.

Prior to testing the shell materials, as with A225 head material, material orientation needed to be determined with respect to the vessels such that samples could be machined from the material in the lowest toughness orientation. Based on the assumption of logical manufacturing processes where the shells are rolled from thin sheets as well as on prior SwRI testing results (9), this task was inherently much more direct for the shells than the head because there were only two possible complementary layouts for the shell materials:

1. The L direction of the plate material was coincident with the L direction of the vessel. This would be evaluated with C-L fracture samples.
2. The L direction of the plate material was coincident with the C direction of the vessel. This would be evaluated with L-C fracture samples.

To determine the material orientation, two standard ASTM E1820 (10) fracture toughness tests were performed at room temperature in the C-L and L-C orientations for each material and vessel section tested. These data were used to determine the material orientation, which would allow for test samples to be produced for determining T_0 from the Master Curve method. For 1143, a proprietary AO Smith material, fracture toughness tests performed at room temperature on the inner shell of section 4 from V0125 showed that the initiation fracture toughness was approximately 40% lower for the C-L orientation than for L-C. Neither of these tests produced a fully valid J_{Ic} or K_J value, but the results were sufficiently advisory on material anisotropy. Given this outcome, all specimens for determining T_0 for 1143 V0125 section 4 materials using the Master Curve method were obtained in the C-L orientation.

Inspection of the fracture surfaces for the two orientations confirmed the results, as the L-C surfaces were much more ductile than the C-L surfaces. Since the C-L orientation represents that the specimen loading direction was in the vessel circumferential direction with a crack plane in the vessel longitudinal direction, then, given the observed anisotropy, this inner shell was oriented in the lowest fracture toughness orientation with respect to the hoop loading direction in the vessel. This suggests that material anisotropy was not a consideration in the original vessel design, further confirming the need to use the lowest toughness orientation throughout any FFS evaluations of the LPV fleet. However, the results from the current study may not apply universally to all vessels; thus, in conducting further fracture toughness testing on materials from different lots and different manufacturers, it will be necessary first to determine the weakest orientation.

For the 1146, material taken from the outer shells of section 4 from V0125 showed that the initiation fracture toughness was approximately 45% lower for the C-L orientation than L-C; thus, all 1146 specimens were also made in the C-L sample orientation. It is important to note that, to reduce material and labor costs, plates were sometimes rolled into cylinders with the plate transverse direction in the vessel longitudinal direction and sometimes in the vessel circumferential direction.

1.2 Lot Variability

Though the LPV fleet is comprised of nominally the same steels based on the AOS designations previously discussed, the LPV fleet contains vessels fabricated over a span of years and by different vendors, and the steels may have been processed by different mills using different rolling procedures. The LPV steels are expected to contain significant lot-to-lot variability; thus, one cannot assume the data obtained in this study are directly applicable to all LPVs without a further characterization of this variability.

The initial plan for this assessment was to test from as many different lots of material as possible to diversify the testing and characterize the lot-to-lot variability. This goal shifted primarily due to technical reasons and, to a lesser extent, schedule reasons. The technical reason for the shift to single material lot evaluation was that the E1921 Master Curve test

method used in this investigation is best applied to a macroscopically homogeneous material having uniform and isotropic strength and toughness properties. Therefore, the proper way to approach the transition toughness evaluation was to test a sufficient quantity of specimens to independently evaluate each lot. The result from each lot can then be compared to other lots for variability.

1.3 Fracture Toughness Methods

Fracture toughness testing was the focus of this effort because fracture toughness as a function of temperature is the most important material property for FFS assessment of the vessels. The fully ductile fracture toughness (upper shelf) and the temperature at the transition to cleavage fracture (transition range) were of interest. The Master Curve methodology from ASTM E1921 (7) was used to facilitate the assessment of the fracture toughness data and determine the fracture toughness versus temperature behavior for the LPV materials. The Master Curve method is a robust approach to characterizing the temperature dependent fracture toughness of ferritic steels with as few as six test samples. The following background information on the Master Curve method will provide a brief introduction to the concept and convey the rationale for choosing this method to evaluate the LPV materials instead of using the more traditional impact energy (Charpy) methods.

Other than obvious schedule and cost constraints, the choice of a fracture toughness test method is usually dictated by the expected failure mechanism of the material. The two primary mechanisms by which fracture occurs in ferritic steels are ductile rupture and cleavage. These are micro-mechanisms for fracture that describe the mechanism by which a material fails at the microstructural level. Care is needed not to confuse these mechanisms with terms such as “ductile” or “brittle,” which are often used to describe the failure behavior of structures or specimens. Note that a ductile rupture fracture may very well occur in an unstable, “brittle” manner. This is common in many alloys used in the aerospace industry, such as high-strength aluminum or titanium alloys. Ductile rupture occurs in metals that fail by the growth and coalescence of voids initiating from loosened or broken inclusions and second-phase particles.

Cracks extend through this void coalescence process, driven by plastic deformation, ultimately leading to fracture in either a stable or unstable manner. This is the typical failure mechanism for structural steels when they are kept sufficiently warm and not loaded in a highly dynamic manner. In contrast, cleavage fracture is a much lower energy process that progresses by the splitting of atomic planes with little associated plasticity, resulting in a flat and faceted fracture surface. The cleavage fracture process is of primary concern in structural steels at reduced temperatures or high loading rates.

For ferritic body-centered-cubic steels, the fracture mechanism undergoes a demonstrative transition from ductile rupture to cleavage as temperature decreases, which leads to a concomitant decrease in fracture toughness. This temperature dependency of fracture toughness is common to all ferritic steels. Therefore, the material property of most

importance to ferritic structural steels in LPV applications is the ductile-brittle transition temperature curve that quantifies the fracture toughness loss with decreasing temperature and identifies the probability that a cleavage fracture will occur. Despite the common use of the term “transition temperature” that implies a discrete temperature below which steels fail by cleavage fracture, the reality is more subtle and complicated. An “upper shelf” exists where temperatures are sufficiently warm to ensure fracture progresses by ductile rupture mechanisms. Fracture toughness is greatest on the upper shelf and is generally consistent and repeatable. As temperatures decrease (or loading rates increase), the steel enters into a “transition range” where ductile rupture and cleavage are competing fracture mechanisms. In this range, the fracture behavior becomes considerably more variable since both mechanisms are operative and fracture toughness values drop below those of the upper shelf.

Determining this temperature range where cleavage fracture becomes probable is critical to understanding the reliability of the LPVs. Cleavage fracture events often result in unexpected, catastrophic structural failures. Historically, brittle fracture has been characterized by a linear elastic fracture toughness test to determine K_{Ic} , which treats the material in front of the crack tip as a homogeneous and elastic continuum. This simplistic approach is insufficient to characterize cleavage where the fracture process is governed by the random distribution of cleavage initiators, such as carbide particles or inclusions, in the highly stressed zone of material just in front of the crack tip. This makes cleavage initiation a strongly stochastic process that follows a weakest link model. Therefore, a statistical approach is needed to adequately characterize cleavage fracture. ASTM Standard E1921 (7) couples modern fracture mechanics and statistical methods to define a statistically based curve of fracture toughness versus temperature that is derived using only fracture-mechanics-based test data. The statistical nature of the method allows confidence bounds to be determined. This elastic-plastic method utilizes the J-integral at the point of cleavage instability, J_c which is converted into a stress-intensity equivalent, K_{Jc} , and uses these data points to define a curve of median fracture toughness, K_{Jc} versus temperature.

Performing elastic-plastic J tests and deriving K from J, as opposed to conducting linearly elastic K tests directly, was necessitated by specimen size limitations imposed by the thin, cylindrical pressure vessel layers. Specimens for J test methods can be as small as 1/40th the size required for linear-elastic K tests and still maintain sufficient constraint to produce toughness data that are unaffected by sample size (11). It would not have been possible to perform linear-elastic fracture toughness tests per ASTM E399 due to the thin-layer material constraints in LPV shells. Test specimens could not be made large enough to obtain the linear-elastic fracture toughness, K_{Ic} .

Reference Temperature for Nil Ductility Transition (RTNDT) is considered conservative compared to the fracture toughness versus temperature relationship determined by T_0 . The two methods differ in their approach. T_0 is a statistically based fracture mechanics method that allows for a direct determination of the transition temperature, whereas Temperature for Nil

Ductility Transition (TNDT) is defined by a relatively simple bounding method where the impact energy for fracture of blunt-notched specimens drops below a given threshold.

Defining RTNDT from T_0 is straightforward as given by the ASME code cases. On the other hand, defining the proper MDMT for the LPV fleet from this value will require additional study. The use of a Master Curve derived T_0 to define the RTNDT (and subsequently an MDMT) rather than a TNDT based on an impact energy threshold is expected to reduce conservatism in that value. (Note: the Master Curve was born out of necessity to reduce known conservatisms in the traditional RTNDT method, so the nuclear power industry could demonstrate adequate safety in aging structures in use beyond their original design service objectives.) The key distinction to underscore is that the Master Curve is consistent with a risk-informed framework for decision-making that provides the best estimates of fracture toughness by means of an explicit description of uncertainty. The Master Curve provides two key features: a statistical description of fracture toughness at a single temperature and the relationship between fracture toughness and temperature.

1.4 Master Curve Testing Considerations

It is noteworthy to consider that because T_0 was not known before completing the first round of tests and analysis, it is not surprising that some tests did not fail due to cleavage before the ductile crack extension limit was reached as test temperatures were iteratively decreased. Historical testing of nuclear grade materials, which are much tougher than the materials tested for the LPV program, conventionally violate the plastic constraint data qualification limit. What was determined from this test program is that testing at colder temperatures and then testing warmer, as needed, is likely a more effective method than testing in a decreasing temperature pattern. The former method is likely to converge more quickly on the temperatures required for cleavage. One caveat to this is the cautionary note that testing at exceptionally cold temperatures is not recommended because the test temperature must be within 50 °C of T_0 for it to be useable in the T_0 analysis. It is noted that for both the 1143 and the 1146 material, the testing temperatures ultimately required to produce cleavage pushed close to the extent of this allowable testing window. Too much weight should not be placed on Charpy impact methods, which can be overly conservative.

The T_0 value must not be confused with the MDMT used to limit vessel temperature in use. The T_0 value should be considered only a convenient way to express the fracture toughness of the material as a function of temperature with a statistically substantiated model of the data. There are a number of ways future work may utilize these T_0 values to arrive at a MDMT for a given vessel. First, it is important to recognize that the fracture toughness testing performed is representative of only the single lot. Additional evaluation of T_0 across many lots representing the larger LPV fleet, including all alloys and welds, is needed before obtaining T_0 values that may be considered representative of the entire LPV population.

2 FFS METHODOLOGY

The tasks of the materials discipline as related to fitness-for-service involve taking stock of all base material and weld combinations that require characterization, determining the level of fidelity required in the data, then planning and executing that material property data development. The following vessel elements are expected to be worked individually: head-to-shell welds, shell-to-shell welds, shell longitudinal welds, shell sections, nozzle-to-shell welds, nozzle-to-head welds, head sections, and nozzles. Each of these elements has unique aspects to be assessed, primarily the material behavior and limitations of each.

The role of material performance within fitness-for-service is fundamental and, in the case of LPVs, the fracture toughness of the material and the corresponding fatigue crack growth rate are the governing material properties of concern. The fracture toughness dictates how the material behaves in the presence of sharp discontinuities at relevant temperatures, such as a lack of fusion in a weld or a service-generated fatigue crack in cold service. However, an understanding of a broad spectrum of material properties is important to fitness for service implementation. Strength, ductility, modulus, corrosion resistance, and even magnetic properties may influence the assessment or inspection process in some fashion. The material behavior of most interest in this project is the temperature dependent fracture toughness and the temperature range where the LPV steels transition from a predictable, stable tearing mode of fracture to a more variable, unstable cleavage mode of fracture. All the LPVs in question are constructed of ferritic steels that fail by cleavage at temperatures below a ductile-brittle transition characteristic of the steel or weldment.

A deterministic fitness-for-service analysis determines the safe operational conditions and an inspection interval for a vessel in the presence of detected or hypothetical defects. The analytical deterministic path to assessing structural fitness-for-service corresponds to the traditional way structural assessments are performed within the Agency. For example, bounding conditions are assumed for structural configurations, load environments, and residual stresses, and the resulting combined stresses compared against a lower-bound material property, while the difference between the applied stress and the material capability must be sufficient to accommodate the required factor of safety. This is the basic design philosophy applied to all LPVs.

The materials characterization of common LPV materials serves as the base for all fitness-for-service rational, deterministic or probabilistic. Thus, the goal of the Materials Sub-Team is to develop an understanding of LPV materials and all necessary data for use in the integrated FFS methodology. Most of the materials in the LPV fleet are poorly characterized by current standards and were produced before modern fracture mechanics methods were common; therefore, the focus is primarily on fracture toughness properties of period LPV steels and their welds, with some added effort to evaluate the tensile flow properties, material hardness, and chemistries.

The challenge comes not in characterizing any given piece of material, but in sufficiently sampling materials from dismantled vessels to deduce properties that are applicable across the LPV fleet. Sampling methods have practical limitations governed by testing cost and material availability. Limits in material availability usually stem from an insufficient number of distinct material lots. In this project, sampling limitations arise primarily because materials for testing generally must be extracted from decommissioned vessels. While an expensive proposition, this tends not to limit the quantity of specimen sampling, as vessels are comparatively large. Rather, it limits the number of materials that can be sampled and the number of repeated material lots that can be sampled for any given alloy. Given the primary focus in determining fracture toughness as a function of temperature, the sampling required for any given lot of material is well defined by the analysis methods of ASTM E1820 (10) and E1921 (7). For upper shelf J resistance curve tests, two or three repeats at each temperature is sufficient. The toughness versus temperature transition is determined with the E1921 Master Curve method, and for this project, 12 to 16 specimens are allotted to determine a T_o reference temperature value for the material lot. (T_o is the Master Curve's measure of ductile-brittle transition temperature.) In some cases, generally for welds, material inhomogeneity requires testing of additional specimens to characterize the transition and corresponding confidence bounds.

Due to limitations in material traceability within a vessel, and because of the typical large size of material lots, each vessel sacrificed for testing is assumed to provide only one material lot for any given alloy, unless distinct chemistries are measured that clearly distinguish unique material lots. Each sacrificed vessel provides samples of steel from the vessel head, head-to-shell welds, wrapper steel, inner-layer steel, wrapper layer longitudinal welds, nozzle steels, etc. Because of this selective availability in material lots, practicality requires the project to provide rationale for adequate lot sampling and make careful decisions regarding vessels chosen for test. For materials representing a significant portion of the LPV fleet, such as the AOS 1146 family and ASTM A225 head materials, a five-lot sampling was chosen as adequate. In this context, adequacy of five-lot sampling means that properties derived from the testing of those materials will be assumed to have sufficient lot variability incorporated to apply to the fleet as a whole in FFS assessments. As data become available, statistical evaluations will be employed to assist in substantiating, or refuting, this assumption. If there is evidence that the five-lot data pool is not describing the variability, the project may either choose to test further material lots or use engineering judgement to bound the variability and carry the material property as a risk item. Non-destructive methods of evaluation such as assessments of chemistry and hardness will be used to limit the associated risk by recognizing critical components that may be outside the range of the data lot samples.

Five lots was chosen as achievable with rationale for adequacy stemming from other code practice. For example, the ASME BPVC, Section II, Part D, Mandatory Appendix 5 "Guidelines on the Approval of New Materials Under the ASME Boiler and Pressure Vessel Code," sub-section 5-700 "Required Sampling," (6) requires three lots of material (and in some cases a fourth) to cover lot variability. In aerospace disciplines, where factors of safety are

much smaller, additional lots are typically required: the Metallic Materials Properties Development and Standardization Handbook (MMPDS) (12) has a 10-lot requirement for mature properties, and Composite Materials Handbook-17 (13) has a five-lot requirement for mature properties. Though the choice of five material lots for this effort exceeds the common lot diversity expectation for ASME materials, the two additional lots planned for predominant LPV alloys are considered prudent given the unknown standards by which much the heritage materials were produced and a tendency for less “clean” steel from the period. These steel standards were very loosely written in both chemistry requirements and tensile properties, with no limits relatable to present day fracture toughness. The high metric of 10 lots from the MMPDS is not appropriate here for two reasons: First, the LPV structures have a factor of safety larger than that of most aerospace structures, and second, the primary property of interest in the FFS assessment, fracture toughness, when determined with the Master Curve method, can be rigorously treated statistically to determine suitable lower-bound values to help manage risk. To account for lot variability, the ASTM E1921 T_0 values for multiple lots of material can be evaluated and combined based on non-homogeneity assumptions in the statistical methods.

There are alloys in the LPV fleet that occur only in a small quantity of vessels. Reaching lot maturity for properties for these materials is not feasible, and even testing single lots may not be feasible. Materials representing a small minority in the fleet that go without substantiation of their properties will carry added risk in the material’s discipline. Some of the minority materials in the LPV fleet have other industrial history. To the extent possible, the Materials Sub-Team will minimize unknown property risks in these materials through data mining in literature. For minority materials left without material property coverage through characterization or data mining, alternative means in the integrated FFS logic will need to be employed to manage risk in these vessels or the vessels will be recommended for decommissioning. Methods of managing risk at the integrated level could include such methods as lowering the pressure rating or moving the vessel to remote conditions with access controls.

Weld evaluations add significant complication to the issue of sampling. The current technical path has predominant LPV welds receiving characterization equivalent to the predominant base metals. The number of test conditions in the LPV welds is significant when all weld material combinations and potential flaw locations are considered. The current technical path makes use of similarity arguments, where possible, following experimental validation. For example, weld heat affected zone toughness in shell materials is expected to be consistent across the weld types. If confirmed with fracture testing and metallurgy, the test burden is reduced. In a similar fashion, if weld heat affected zone toughness is shown to consistently bound weld centerline toughness, efficiencies in these test locations are also realized. The current path forward allows for these initial evaluations but assumes that efficiencies through similarity and bounding will be available.

3 MATERIALS CHARACTERIZATION PROCESS

Material characterization is the basis of a sound fitness for service plan. The materials characterized in this report may not completely cover the range of materials found in some pressure vessel fleets. In the instance that one of these unknown materials is found, a material characterization is the first step in understanding the potential risks of the vessel. There are various levels to material characterization starting with Nondestructive Evaluations (NDEs) and moving on to full mechanical test methods. Each approach has its own value in producing a basis for confident vessel analysis, as well as associated costs in time and monetary allocation. Performing these tests in the proper order can limit the amount of time and money spent, as well as ensure an appropriate level of confidence in the material properties. Table 3-1 is an example of the test matrix used to plan out which tests are necessary for the vessel to be properly characterized.

Table 3-1: Materials Characterization Process Diagram

Material Conditions	V0023										
	Material	RT Fracture	To Fracture	da/dN	Tensiles	Notch Tensiles	HCF	Metallography	Chemistry	Hardness	Charpy
Parent Material											
Head (stress relieved)	A225										
Nozzle	A105										
Inner layer (stress relieved)	1146										
Wrapper shell	1146										
Weld Material, Center											
Head-to-shell circumferential weld (green)											
Shell-to-shell circumferential weld (green)											
Longitudinal welds (green)											
Inner layer welds (stress relieved)											
Nozzle-to-head weld (stress relieved)											
Nozzle-to-shell weld (green)											
Weld Material, HAZ											
Head-to-shell circumferential weld, shell side (green)											
Head-to-shell circumferential weld, head side (green)											
Shell-to-shell circumferential weld (green)											
Longitudinal welds (green)											
Inner layer welds (stress relieved)											
Nozzle-to-head weld, nozzle side (stress relieved)											
Nozzle-to-head weld, head side (stress relieved)											
Nozzle-to-shell weld, shell side (green)											
Nozzle-to-shell weld, nozzle side (green)											
Tested											
In-Work											
Planned											

3.1 Hardness and Chemistry

Hardness and chemistry measurements are two assessment methods that give significant insight into the material properties. They are also the two most cost effective. Hardness measurements may be taken in-situ with portable hardness testing equipment. The hardness values of pressure vessel steels are highly indicative of strength and fracture properties. Softer materials tend to be more crack resistant, harder materials tend to be stronger but less crack resistant.

Chemistry testing is not completely nondestructive, but the method used (portable optical emissive spectroscopy) to obtain the data in this report can often fit within the corrosion limits of an operational vessel. Chemistry is critical in accurately determining the type and grade of a pressure vessel steel. Accurately determining the material type and grade opens the possibility of using mechanical testing archival data based on work already performed on the same material. Use of such data can significantly reduce the amount of testing required. It can also prevent the use of incorrect data derived from poorly documented construction records. However, note that chemistry cannot be the sole method of identifying a material and its subsequent properties.

When conducting chemistry testing, it is important to be certain that the tests are of the “effective” chemistry of the material. In some heads, a process called decarburization has occurred, resulting in a thin, low carbon layer of material on the surface where chemistry checks commonly are performed. The best practice to ensure proper chemistry measurement is to grind a test location and then check the chemistry. If the numbers are substantially different from the material specification, the test location must be ground deeper and retested until the values become consistent. This will ensure that the values are sufficiently representative of the base material character.

Chemistry is most effective in conjunction with hardness testing. As discovered in this project, some materials that are exact chemical matches may have received vastly different heat treatments. This situation renders the material properties significantly different in both strength and fracture toughness. A hardness test is the simplest and most effective way to determine if there is a difference resulting from heat treatment of a material. If the hardness and chemistry are similar in tested materials, it is most likely that the materials have similar mechanical properties. If the chemistry or hardness differs significantly, then any data obtained in reference to one should not be considered useful for the other.

3.2 Metallography

Metallography samples are useful when investigating pressure vessel steels. They are often the easiest way of identifying the mill rolling direction of the plate, which usually corresponds with the strongest orientation. Also, metallography can be used to characterize the grain size and shape. This is somewhat indicative of the strength and fracture toughness of

the material. Inconsistencies with a given material lot may be quickly sorted out as the result of improper heat treatment or post processing simply by examining the microstructure.

When examining welds, metallography specimens are valuable in determining the number of weld passes used and the size of the heat affected zone. For complete microstructure characterization, it is recommended that three specimens be taken. One face of each specimen should correspond to each material orientation and when completed, a model of the overall microstructure can be created.

The example in Figure 3.2-1 comes from an A212 head material. As described, a face in each orientation (circumferential, radial, and meridional) was prepared and the result is a macro cube that provides excellent insight into the materials history. Lamellar grain boundaries running in the circumferential direction, indicate the direction of work put into the material. In many cases such as this, it is also necessary to complete a full thickness macro.

This A212 head showed a decarburization zone located on the inner and outer surface of the head. Knowing this allowed a more accurate chemistry measurement to be taken since it was necessary to test the chemistry below the decarburization layer to obtain correct values.

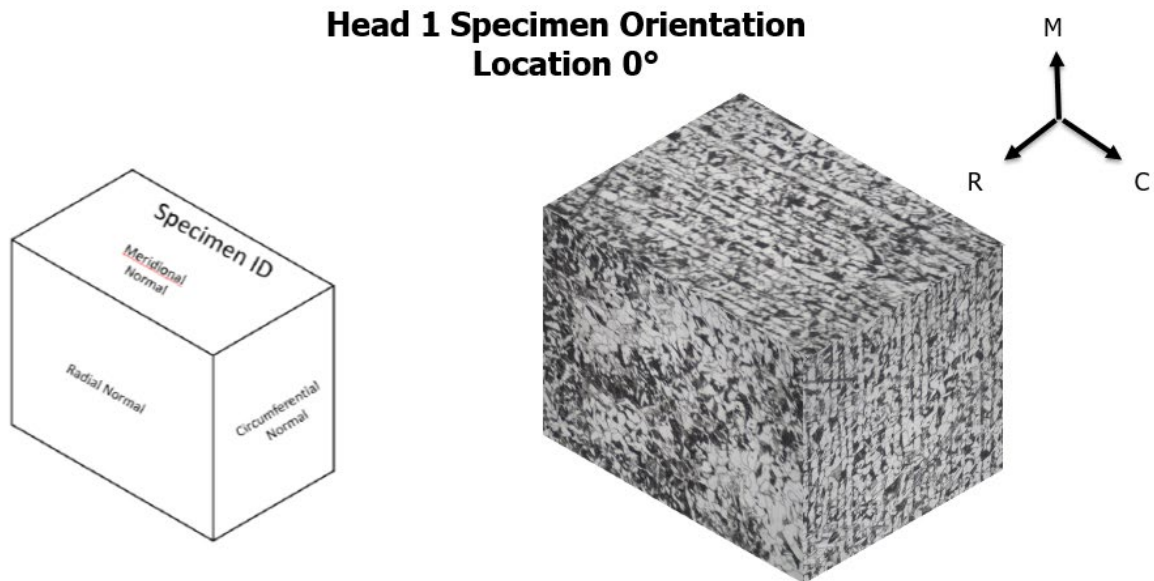


Figure 3.2-1: Example A212 Material Macro Cube Specimen Orientation

3.3 Tensile and Fracture Testing

Tensile tests are the most basic strength measurement for a material, indicating its yield and ultimate tensile strength. In determining tensile strength, it is important to test both orientations of the material in question, as strength will certainly vary with orientation. This will help give an accurate understanding of the material should a flaw be discovered in either

orientation. It is also useful for guiding fracture testing since different strength properties can affect fracture test parameters.

Figure 3.3-1 is an example of a down-select cut plan. Down-selecting is the method of testing tensile and fracture specimens in each orientation and guarantees identification of the weakest material orientation. For the project purposes, three tensile and three fracture specimens were tested in each orientation under ambient conditions. This was to quickly identify the weakest orientation, which will then become the targeted testing orientation. A significant difference in fracture toughness will be apparent at the conclusion of these tests. Whichever orientation has the lowest fracture toughness is most likely to be susceptible to flaws and the most likely to grow those flaws to a critical size. This is the value of concern as it represents the worst-case scenario of a flaw in the material. It is also possible to conduct a down-select using Charpy specimens, which are smaller and cheaper to run. These tests will give a quick determination of the material orientation, after which more thorough evaluation can be completed with compact tension specimens.

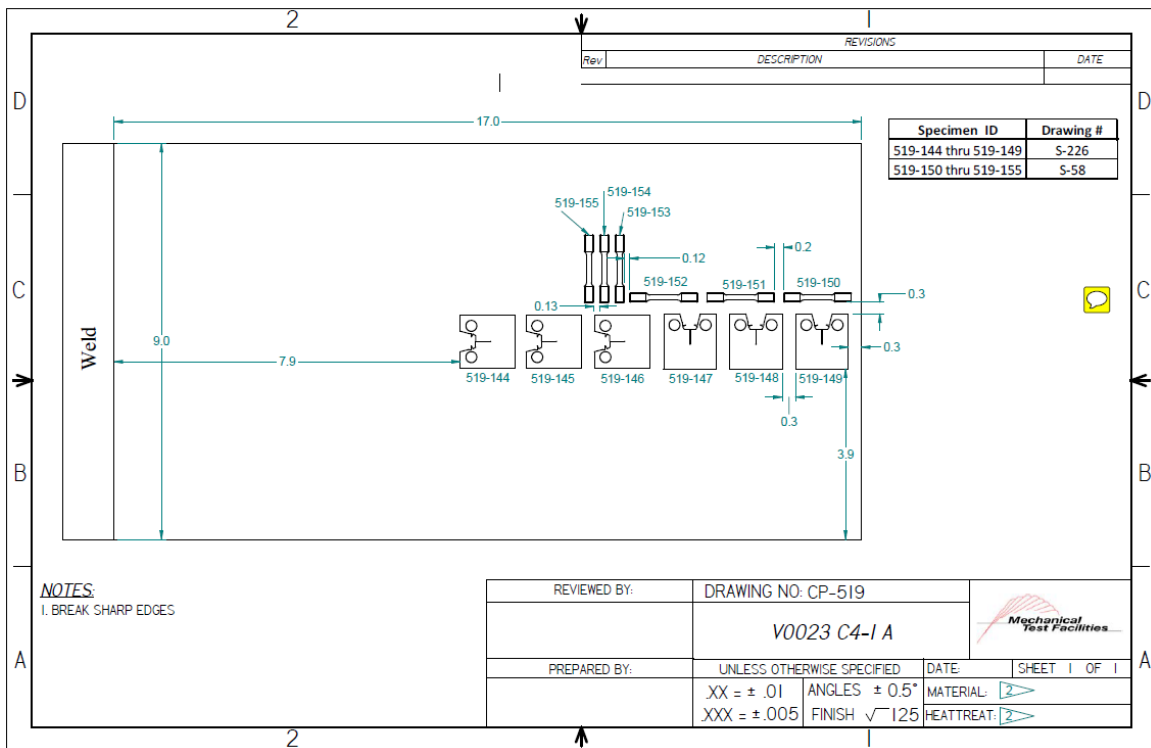


Figure 3.3-1: Example Down-Select Cut Plan

After determining the materials weakest orientation, the focus should be on accurately characterizing the material properties relative to the operating environment. To do this, more fracture tests should be conducted according to ASTM E1921 (7). The Master Curve method of E1921 gives a transition temperature, or T_0 , that is the temperature at which the material is likely to switch from a ductile tearing failure mode to uncontrolled crack extension. For older

pressure vessel steels, this temperature can often be within the range of commonly sustained outdoor temperatures. Knowledge of the transition temperature of the material allows understanding of the kind of crack growth that the material will experience under actual operating temperatures. This is critical information for determination of safe operating pressures and temperatures for LPVs.

The Master Curve in Figure 3.3-2 gives expected fracture toughness values at each temperature within calculated tolerance bounds. This curve can be used to determine the appropriate fracture toughness to use when conducting a fitness for service or safe life analysis.

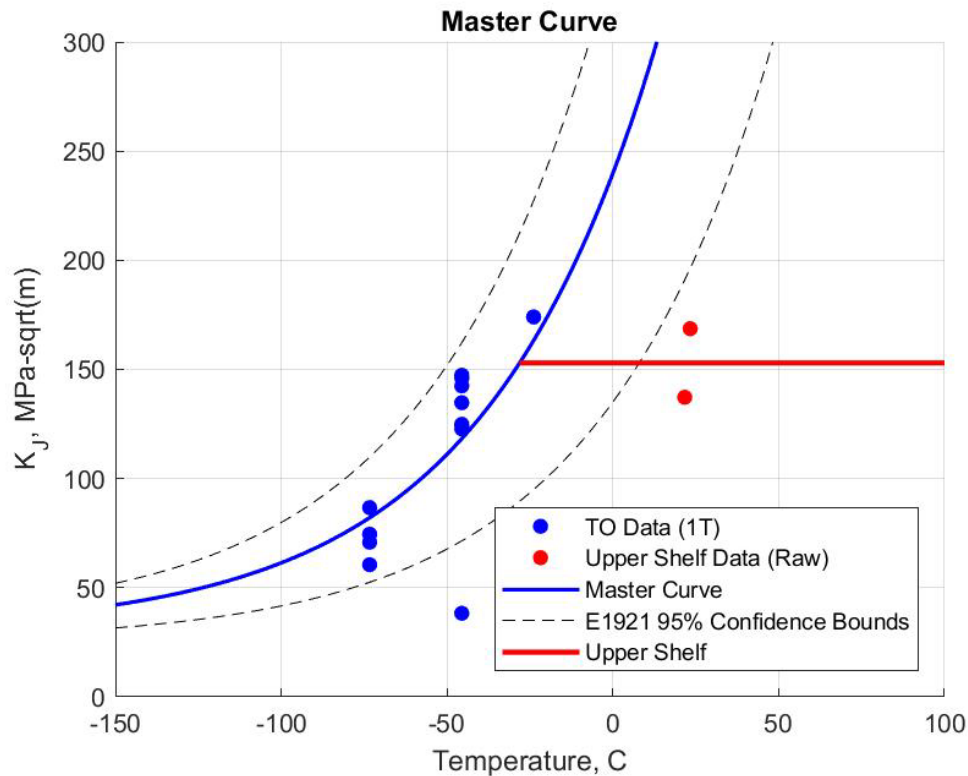


Figure 3.3-2: Master Curve Example

3.4 Fatigue Crack Growth Testing

Fatigue crack growth testing is used to measure the crack growth per cycle at a given fracture toughness value. The curves generated by testing according to ASTM E647 (11), can be used to determine the amount that a predicted flaw will grow under given cyclic conditions. When using programs such as NASGRO to evaluate the failure potential of a known flaw, these curves are particularly valuable. Fatigue crack growth testing should be performed in the weakest material orientation as should all other testing. For a proper evaluation of the full range of fatigue properties, it is recommended to conduct tests at R ratios (peak/valley stress ratios) of 0.1 and 0.7. This allows for a proper curve fit to be applied. Figure 3.4-1 is an example

of the results of a fatigue crack growth test, showing how the crack growth per cycle relates to the delta K applied during each cycle.

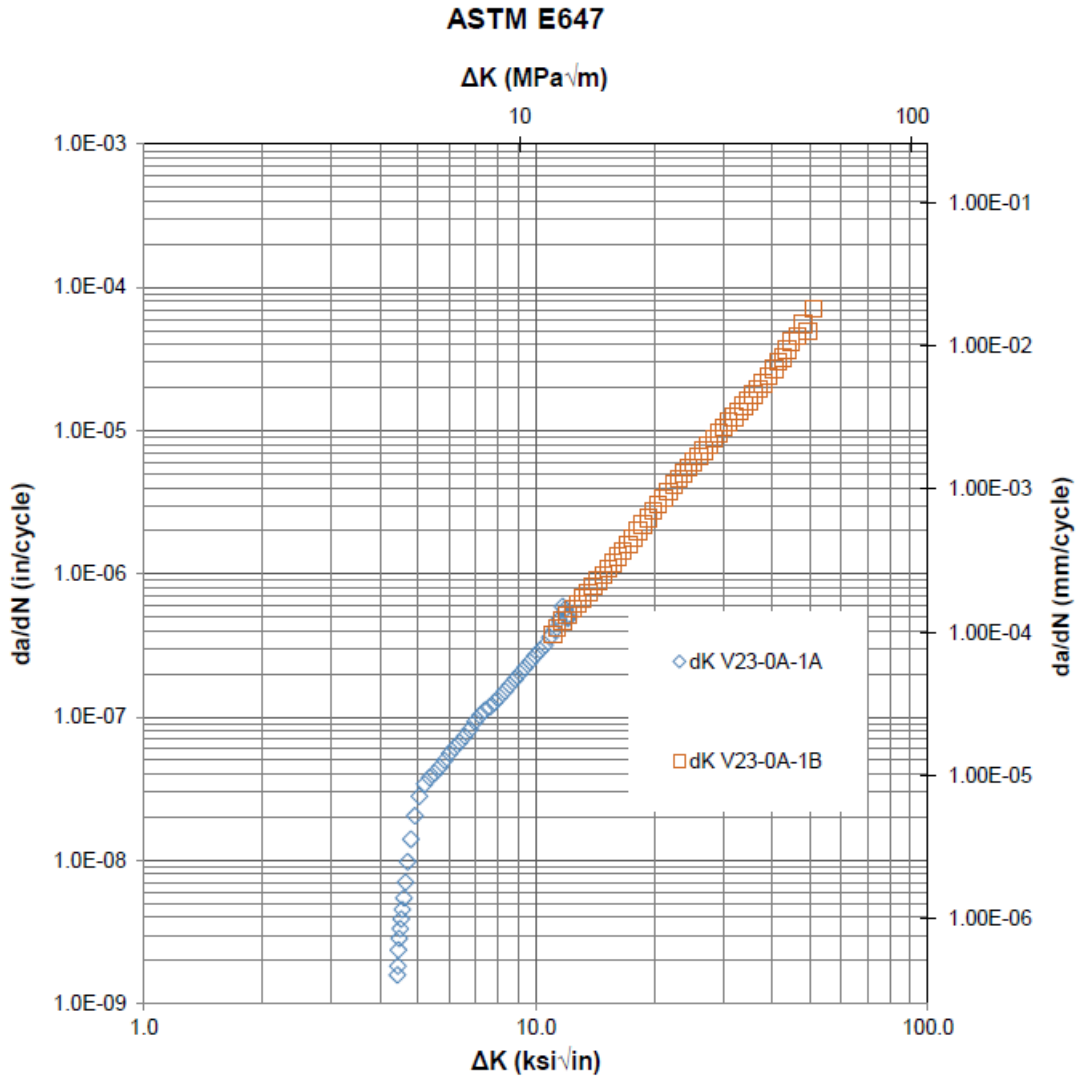


Figure 3.4-1: Example Fatigue Crack Growth Test Results

4 ASTM E1820 AND E1921 BACKGROUND

4.1 ASTM E1820 Background

ASTM E1820 (10) is a standard method of determining fracture toughness of metallic materials using the J integral to define the intensity of the stress and strain singularities near the crack tip. The J integral can be related to the Crack Tip Opening Displacement (CTOD) at the crack tip. E1820 measures the magnitude of the J integral as a function of crack extension from a pre-existing fatigue crack. E1820 uses unloading compliance, potential drop measurements, or a normalization procedure to estimate the change in crack length during the destructive specimen test. The set of data relating the J integral to crack extension is referred to as the J-R curve and is often fit with a power law relationship for transfer to applications. A measure of toughness near crack initiation, called J_{Ic} , is determined and is often the principal result of the E1820 test procedure. The J-R curve is a plot of the far-field J-integral versus stable crack extension, demonstrating the material's toughness at crack initiation and with continued crack growth.

Some metals demonstrate a high crack initiation toughness followed by a low resistance to further crack growth. This is typical of aluminum alloys, titanium alloys, and maraging or tool steels. Modern structural steels generally demonstrate a high initiation toughness but also a high resistance to further crack growth. Older structural steels, like those used in LPVs, are characterized by modest initiation toughness and mostly low resistance curve slopes beyond initiation.

In E1820, J_{Ic} is a property that describes the fracture toughness of a material at fracture instability without significant stable crack extension; essentially this is the measured fracture toughness when the laboratory specimen fails in an unstable manner abruptly ending the test. This occurs when the energy stored in the test machine exceeds the energy required to extend the crack in the test specimen as the crack grows and the specimen load capacity falls. The fracture can be ductile and consist of hole growth at the microscale or it can correspond to multigrain cleavage with cleavage occurring on specific planes in the metal's crystal structure. Ferritic steels are characterized by ductile behavior at an elevated temperature and cleavage behavior at a lower temperature with the intermediate "ductile-brittle" transition temperature being an important material characterization parameter. To evaluate the fracture toughness properties of a ferritic steel, one must evaluate the toughness when the steel is on the ductile upper shelf and determine the temperature at which the rather sudden transition to cleavage takes place.

Essentially, E1820 is used to evaluate the fracture toughness at the initiation of ductile crack growth denoted as J_{Ic} , and the resistance curve for crack extension beyond ductile initiation referred to as the J-R curve. E1820 is also used to measure the fracture toughness at the onset of cleavage, while E1921 (7) is used to evaluate the temperature at which the ductile-brittle transition takes place using data obtained from E1820 tests that exhibit cleavage. J_{Ic} and

the J-R curve depend on temperature, but only weakly across the limited operating temperature variations encountered by LPVs. The variability corresponds to normal statistics and accurate characterization of these properties requires only two or three repeat tests at a specified temperature.

J_{Ic} is the plane strain fracture toughness J-integral that provides the measurement of crack resistance near the start of stable crack extension during a Mode I test. This initiation toughness signals a transition from mostly elastic stretching typically found in the beginning of the test to stable crack extension found in the latter portion of the test. Depending on material characteristics, J_{Ic} may not be the sole significant indicator of material performance. Referring back to the J-R curve, if a material continues to show significant increase in J value past J_{Ic} , the material will continue to tear only with significant increase in load relative to crack length. This will correspond to an increase in plastic zone size and may eventually terminate in a failure via net section yield as opposed to crack extension. If a material demonstrates a "flat" J-R curve with J value remaining relatively stable after J_{Ic} , the crack will continue to extend under consistent load to crack length ratios. A material of this sort is more likely to fail via unstable crack extension. These are important factors to consider when evaluating material applications that approach the J_{Ic} boundary.

Fracture toughness measurements at the onset of cleavage demonstrate high variability, on the order of a factor of 50 from low to high, and the variability does not correspond to a normal statistical distribution. E1921 uses Weibull statistics to analyze the cleavage onset data in the temperature region, requires a data set of 6 to 10 specimens, and fits the data with a "master curve" which is taken to be applicable to analysis of all ferritic structural steels. The intersection of this curve and a toughness level of $K_J = 100 \text{ MPa}\sqrt{\text{m}}$ is defined as the T_0 reference temperature defining the transition temperature for the test steel.

K_J is a fracture toughness stress intensity value derived from the integral value J and is a measurement of crack extension resistance near the onset of stable crack extension under mostly elastic conditions. K_J is calculated from J using Equation 4.1 which incorporates Poisson's ratio (ν) and the elastic modulus (E) of the material.

$$K_J = \left[\left(\frac{E}{1 - \nu^2} \right) J \right]^{0.5}$$

Equation 4.1 (10)

Equation 5.1 can be used to relate J_c at the onset of instability to a linear elastic equivalent, K_{Jc} , which can be used in a predominantly elastic application. In a similar fashion, Equation 4.1 can relate the ductile initiation value J_{Ic} from E1820 to a linear elastic equivalent $K_{J_{Ic}}$, with the understanding that $K_{J_{Ic}}$ is only applicable to predominantly elastic conditions. In other words, small specimens can be tested in the laboratory to evaluate J_{Ic} or J_c and the results can be converted to linear elastic stress intensity values that can be used in very large and

nearly elastic applications like those found in LPVs. Cleavage onset only occurs in the intense stress field conditions that exist at the crack tip during linear elastic conditions, this explains both the E1921 Master Curve plot and why T_0 evaluation are done in terms of K_I rather than using the J integral directly.

4.2 ASTM E1921 Background

In the course of the LPV investigation, a crucial decision surrounded the characterization of an MDMT which is a common method of selecting appropriate material for vessel construction. Background on the relationship between this value described in UCS-66 (14) and the modern T_0 from E1921 is needed to fully understand the direction of material testing and its role in structural analysis.

To avoid confusion, RT_{NDT} is an index temperature determined from Charpy V-notch and nil-ductility temperature data that is intended to provide bounding fracture toughness values versus temperature. RT_{NDT} is related to the nil-ductility temperature from ASME Boiler and Pressure Vessel Code, 2019. Section III Rules for Constructions of Nuclear Facility Components-Division 1 (15) NB-2331 such that $RT_{NDT} = \text{MAX}\{T_{NDT}, T_{35/50} - 60\}$ (in °F) where T_{NDT} is the nil-ductility-temperature from ASTM E208 Standard Test Method for Conducting Drop-Weight Test to Determine Nil-Ductility Transition Temperature of Ferritic Steel (16) and $T_{35,50}$ is the transition temperature from Charpy V-notch specimens per ASTM E23 Standard Test Methods for Notched Bar Impact Testing of Metallic Materials (17). The use of RT_{NDT} versus T_{NDT} is intended to collapse the data more completely by accounting for the heat-to-heat differences in fracture toughness transition temperature, thereby collapsing fracture toughness into a single curve. The evidence suggests that RT_{NDT} does not do this as well as the T_0 reference temperature defined by ASTM E1921. The main reason for this is because of the more robust statistical and fracture-mechanics-based nature of the Master Curve methodology.

RTT_0 is a Master Curve-based index temperature determined from fracture toughness data that may be used as an alternative to RT_{NDT} as permitted by ASME Code Cases N-629 Use of Fracture Toughness Test Data to Establish Reference Temperature for Pressure Retaining Materials Section XI, Division 1 (18) and N-631 Use of Fracture Toughness Test Data to Establish Reference Temperature for Pressure Retaining Materials Other than Bolting for Class 1 Vessels Section III, Division 1 (19) that establishes an RT_{NDT} -like quantity from T_0 via the relationship $RTT_0 = T_0 + 35$ °F. It is similar to RT_{NDT} in the sense that it acts in the same way to bound fracture toughness versus temperature data, but the two are not equivalent since they are derived from different types of mechanical tests, i.e. impact tests and fracture toughness tests for RT_{NDT} and RTT_0 , respectively. In order to use RTT_0 as a substitute RT_{NDT} , it must be assumed that RTT_0 has the same implied margin as RT_{NDT} .

Kim Wallin demonstrated by statistical analysis that a K_{IC} curve indexed to RT_{NDT} corresponds very closely to a 97.5% tolerance bound for the original Welding Research Council (WRC) Bulletin 175 PVRC Recommendations on Toughness Requirements for Ferritic Materials,

1972 (20) K_{IC} reference dataset that was used in development of fracture toughness rules for the ASME BPVC, Section VIII (2). A later report issued in 2002 by the Office of Nuclear Regulatory Research with the US Nuclear Regulatory Commission (NRC) extended this statistical analysis to its then-existing data and confirmed that the relationship $RTT_0 = T_0 + 35^\circ\text{F}$ was defensible as their analysis showed that this 97.5% tolerance bound was maintained for an RTT_0 indexed K_{IC} curve.

According to the exemption curves in UCS-66, all LPV materials are identified as Curve A materials, i.e. carbon or low alloy steel. The thickness ranges for fleet LPVs are well over 2 inches routinely and possibly as thick as 4 or 5 inches for some of the largest vessels. Using these parameters to determine an MDMT from UCS-66 exemption curves would give an MDMT for the 4–5 inch thick components possibly as high as 120 °F. With this method, there is realistically no thickness that would be deemed acceptable for Class A LPV materials in any geographic location in winter. The Class A MDMT is approximately 85 °F for a 2 inch thick component. The Class A MDMT for a 0.394 inch component is approximately 20 °F, and LPV shell sections are much thinner. Additionally, the exemption curves only represent four T_0 values: (A = 114 °F, B = 76 °F, C = 48 °F, D = 12 °F), and it is difficult to justify a measure of T_0 that discretizes so drastically when a more direct and accurate measure of T_0 from E1921 is available.

While several attempts have been made to correlate Charpy impact and fracture tests, there is not yet enough consistency between materials to justify this connection with certainty. However, determining a structural evaluation temperature from the Master Curve is straightforward. The E1921 analysis procedure defines T_0 , the relationship between fracture toughness and temperature, and the statistical distribution of fracture toughness at a given temperature. Therefore, an MDMT can be directly determined by the intersection of the limiting Master Curve tolerance bound curve (at any desired confidence level) with fracture toughness where the fracture toughness is defined as the minimum fracture toughness required for safe operation based on a fracture mechanics analysis of a given vessel that accounts for the required pressure, vessel geometry, and assumed cracks. By defining a target minimum fracture toughness of the vessel and desired confidence level, engineers can determine MDMT directly from the E1921 Master Curve tolerance bounds.

The test method delineated in ASTM E1921 is used to determine a reference temperature T_0 that characterizes the fracture toughness of ferritic steels that experience onset of cleavage cracking at elastic, or elastic-plastic K_{Ic} instabilities, or both. The method uses the Master Curve concept to describe the transition in fracture toughness due to cleavage mechanisms as temperature decreases to the lower shelf. The Master Curve method defines the ductile-brittle transition temperature of structural steels using static tests of fatigue pre-cracked fracture mechanics samples. This is the recommended method when a limited number and size of specimens are available for testing. shows a schematic of the brittle to ductile material behavior of ferritic steels with a superimposed Master Curve.

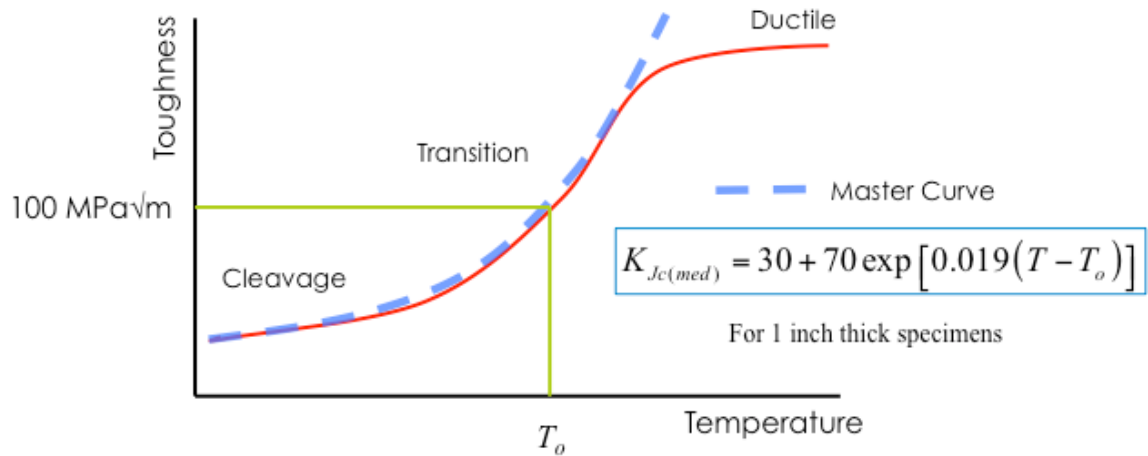
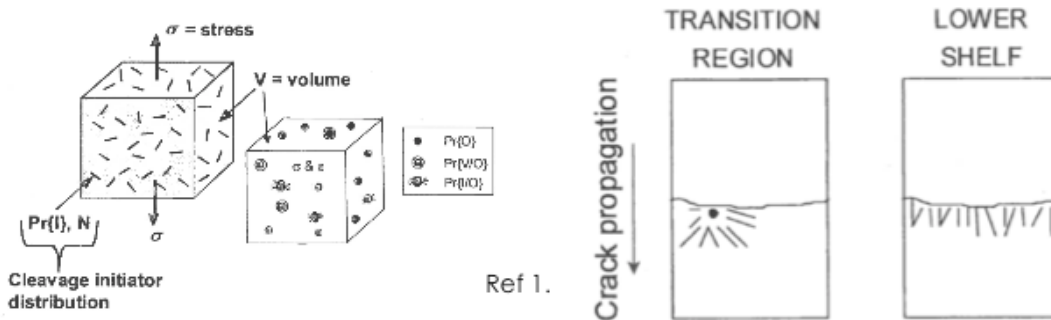
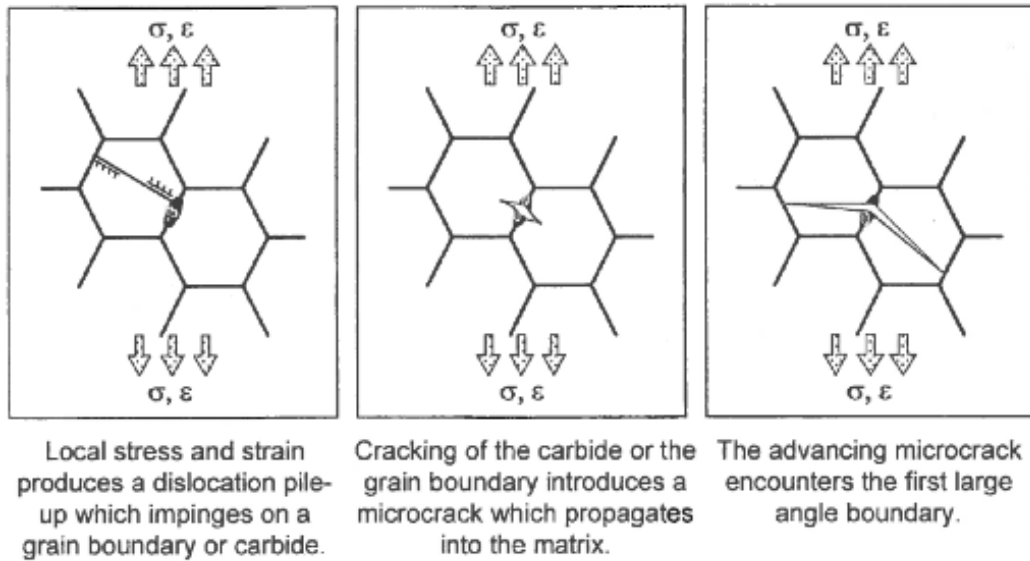


Figure 4.2-1: Example Cleavage with Master Curve Superimposed

The transition region exhibits a mixture of ductile and brittle fracture mechanisms. Fracture is governed by the statistics of local initiation mechanisms, giving rise to a “weakest link” pattern of failure. On the lower shelf, the fracture variability is dramatically reduced since many initiation sites exist and the toughness is fairly constant. Figure 4.2-2 shows schematics of the failure mechanisms.



References

1. Wallin, Kim, *Fracture Toughness of Engineering Materials, Estimation and Application*, EMAS Publishing, 2011
2. McCabe, D., Merkle, J., Wallin, K., *An introduction to the Development and Use of the Master Curve Method*, ASTM Manual 52, ASTM International, 2005

Figure 4.2-2: Schematics Depicting Cracking Mechanisms

This method is a physics-based model and can handle the data scatter problem. The statistical relationship between specimen size and K_{Jc} fracture toughness can be assessed using weakest-link theory, thus providing a relationship between specimen size and K_{Jc} .

The weakest link statistics in E1921 utilize a three-parameter Weibull model. Equation 4.2 defines J_c cumulative failure probability distribution for a finite sample drawn from an infinite population of data for the test material. The data is ranked in ascending order according to J_c fracture toughness instability and assigned a cumulative probability value as shown in Figure 4.2-3.

$$P[J_C \leq J_I] = 1 - \exp\left(-\left(\frac{J_C}{\theta}\right)^b\right)$$

Scaling parameter for 63.2% failure probability

Weibull slope (empirical)

Equation 4.2

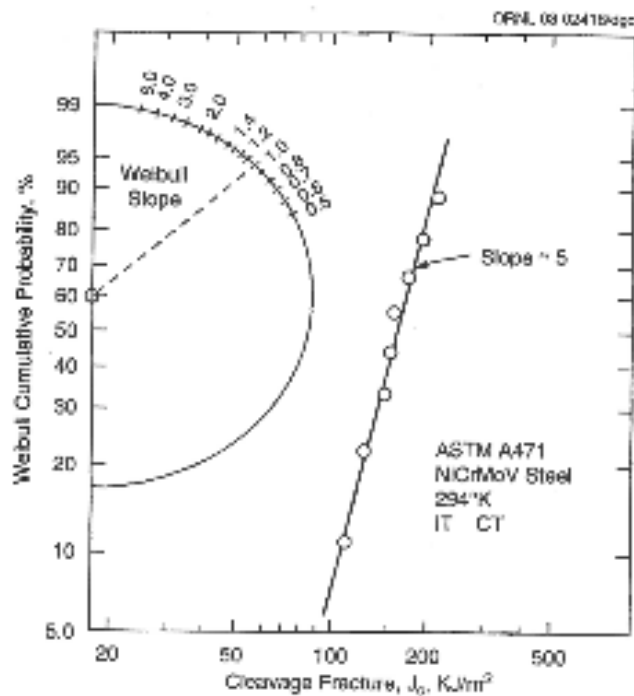


Figure 4.2-3: Probability of Failure (P_f) as a Function of J_C in Weibull Space

ASTM E1921 uses an engineering model where K_{min} defines the lower shelf toughness resulting in a three-parameter Weibull model where P is the probability of failure (P_f) at or before K_I as proposed by Wallin, Equation 4.2 (21). This model has been found to be a good fit for ferritic steels with $b = 4$ and $K_{min} = 20 \text{ MPa } \sqrt{m}$. Since only the scaling factor, K_0 , needs to be defined, only a small number of specimens need to be tested to fully define the Master Curve. Setting the Weibull slope at $b = 4$ pre-establishes scatter expectations so tolerance bounds are also fully defined with this method.

$$P[K_C \leq K_I] = 1 - \exp \left[- \left(\frac{K_I - K_{\min}}{K_o - K_{\min}} \right)^b \right]$$

Conditional probability after initiation models the K_{\min} lower shelf

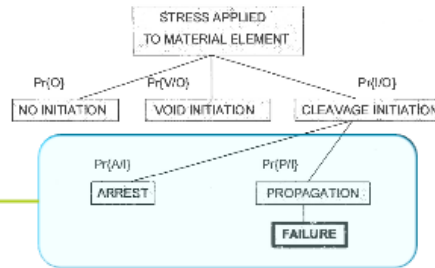


Figure 4.2-4: Determination of P and Pf by Weibull Distribution

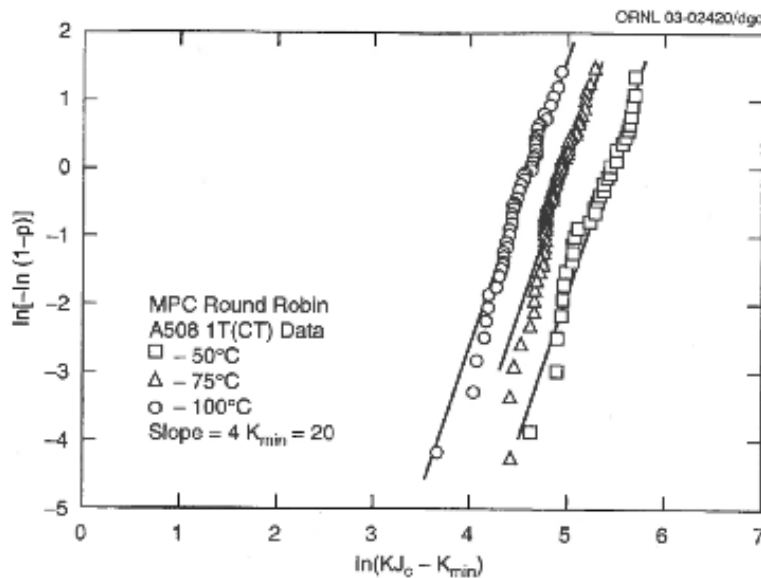


Figure 4.2-5: Round Robin Data Indicating Model Independence to Test Temperature.

The statistical size effect (length of crack front) needs to be considered. The weakest length statistics indicate that P_f will be a function of the volume of material tested. Therefore, the length of the crack front is important since a longer crack front increases the probability of fracture. Two parameters to be considered are the thickness of specimen in testing, and the assumed or identified length of crack in structure. E1921 test data is normalized using the statistical model to a 1T equivalent 25.4mm (1 inch) specimen thickness or crack length before evaluating the Master Curve parameter, K_o (and thus T_o). The E1921 statistical size correction is defined as:

$$K_{Jc(x)} = 20 + (K_{Jc(1)} - 20) \left(\frac{B_1}{B_x} \right)^{1/4}$$

Equation 4.3 (7)

where B_1 = thickness of the specimen, $B_x = 25.4$ mm, $K_{Jc(1)}$ = the K_{Jc} for the specimen size B_1 , and $K_{Jc(x)}$ = the K_{Jc} for the $B_x = 25.4$ mm thickness.

To apply the E1921 method, Equation 4.4 through Equation 4.7, replicate specimens are tested at a temperature near the estimated T_0 to obtain $J_{c(i)}$ and then $K_{Jc(i)}$ at the onset of cleavage. Some trial and error is generally required to estimate the test temperature so that specimens cleave. The $K_{Jc(i)}$ data is adjusted to the 1T (1 inch) thickness if necessary, then the scale parameter K_0 is evaluated from the following equation:

$$K_0 = \left[\sum_{i=1}^N \frac{(K_{Jc(i)} - 20)^4}{N} \right]^{1/4} + 20$$

Equation 4.4 (7)

where N is the number of specimens.

The E1921 Weibull scale parameter K_0 corresponds to a 63% cumulative probability of fracture and is converted to $K_{Jc(med)}$ corresponding to a 50% cumulative probability of fracture using Equation 4.5:

$$K_{Jc(med)} = 20 + (K_0 - 20)[\ln(2)]^{1/4}$$

Equation 4.5 (7)

The T_0 is calculated from (7) where T_{test} is the test temperature.

$$T_o = T_{test} - \left(\frac{1}{0.019} \right) \ln \left[\frac{K_{Jc(med)} - 30}{70} \right]$$

Equation 4.6 (7)

$$K_{Jc(med)} = 30 + 70 \exp[0.019(T - T_o)]$$

Equation 4.7 (7)

Figure 4.2-6 shows supporting data for the E1921 Master Curve method. Figure 4.2-7 shows the typical variability of a large set of weldment fracture data in comparison with the corresponding Master Curve. Figure 4.2-8 shows the E1921 tolerance bounds which are predicted to capture the 95% upper bound and the 5% lower bound of the fracture data for a homogeneous ferritic steel.

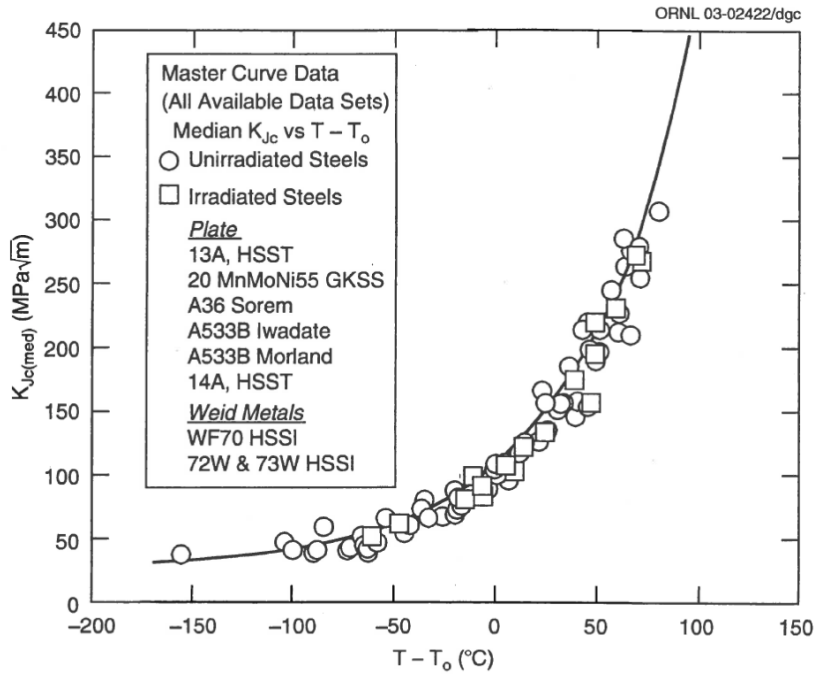


Figure 4.2-6: Supporting Data Used to Validate Master Curve

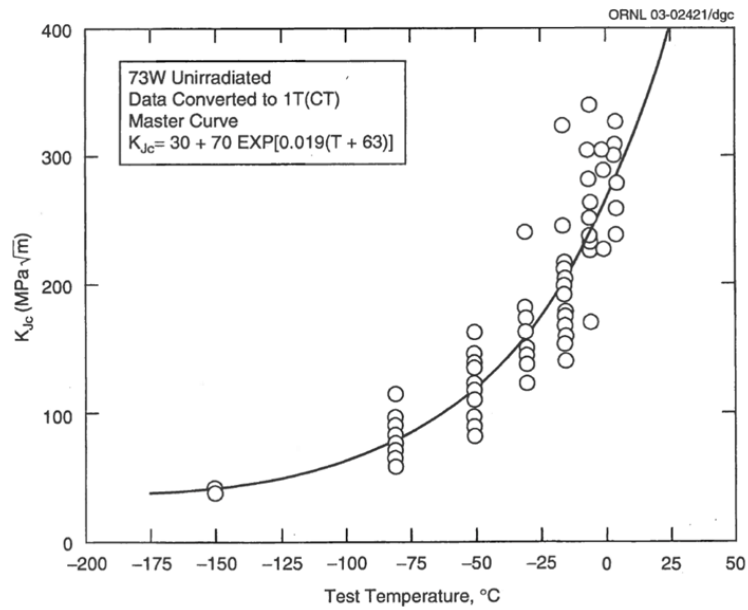


Figure 4.2-7: Example of Variability and Data Scatter Around Typical Master Curve

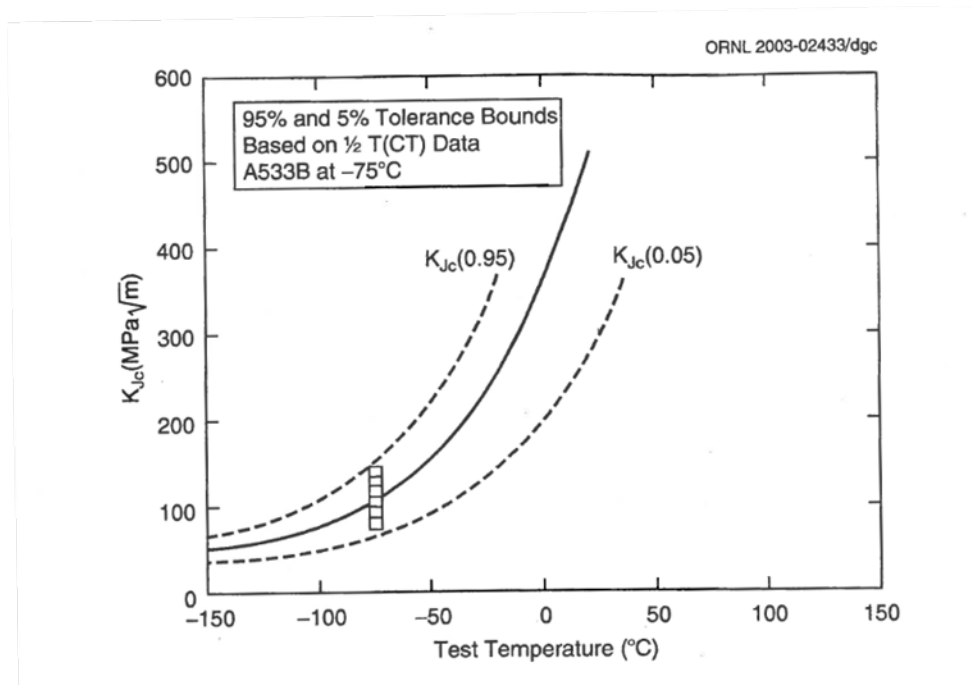


Figure 4.2-8: Master Curve Plotted Against the 95 % and 5 % Tolerance Bounding Curves

E1921 does provide a more complicated but equivalent method to evaluate T_0 when the test data is evaluated at more than one temperature. It also requires censoring of some data if the fracture toughness reached before cleavage is elevated above a set $K_{Jc(limit)}$ that implies a loss of adequate crack tip constraint.

E1921 has been predominantly developed by the commercial nuclear power industry to extend the life of commercial nuclear power plants. Defining the ductile to brittle transition of pressure vessel steels using Charpy based methods has been seen to be too conservative. This has resulted in almost all the data that has been developed to support the E1921 Master Curve and T_0 reference temperature method being measured on high quality, clean, and consistent steels that are used in modern nuclear pressure vessels and components. The steels found in LPVs are ferritic structural steels of an earlier generation and that has caused some concern that the E1921 method might not be applicable to these steels. It has been found, however, that the E1921 method works well for the LPV steels. The main issue has been the low upper shelf toughness demonstrated by several of the LPV steels with $K_{Jc} < 80$ MPa√m. Since this upper shelf toughness is less than 100 MPa√m, which is the toughness at which T_0 is evaluated, for these LPV steels cleavage only occurs at temperatures well below T_0 and the range of test temperatures that can be used to evaluate T_0 is very limited. While E1921 limits the test range to $T_0 \pm 50^\circ\text{C}$, the low upper shelf present in these steels limits the test temperature range only to temperatures below T_0 and, in some instances, to temperatures between $T_0 - 20^\circ\text{C}$ and $T_0 - 50^\circ\text{C}$. However, for all LPV steels of interest, a careful choice of test temperature has led to a successful evaluation of T_0 .

The original version of E1921 assumed that the data set was homogeneous and, hence, that the confidence bounds presented in E1921 would apply. More recently, revisions have been made to determine whether a data set is likely to be homogeneous or not. If the data set is determined to be inhomogeneous, the E1921 tolerance bounds would be non-conservative. This E1921 result suggests that the user should proceed to a newly provided Annex X5 to investigate the inhomogeneity and to develop more conservative tolerance bounds. The downside is that the inhomogeneity annex requires more test data to obtain a revised median curve equivalent to the Master Curve and the corresponding tolerance bounds. The analysis is also more complex.

In the following section, a code developed by NASA Marshall Space Flight Center (MSFC), named T_0 Test Evaluation Module (T_0 TEM), is presented which evaluates the E1921 master curve reference temperature T_0 but also is capable of doing the E1921 inhomogeneity analysis. Two types of inhomogeneity are investigated in the E1921 Annex X5. The first inhomogeneity possibility is that the data set is composed of two different but distinct distributions of specimens. An example of a data set of this type is presented in Figure 4.2-9 where specimens were taken from inner and outer plate layers of the vessel V0032 head. The standard analysis shown gives the T_0 reference temperature and the confidence bounds. The immediate concern is that 5 of the 18 data points lie outside of the $\pm 95\%$ tolerance bounds, more than the 2 that would be expected. Figure 4.2-10 shows the inner and outer layer data separately annotated and the bimodal inhomogeneity analysis of Annex X5 applied and plotted. The bimodal analysis determines that two data sets are in fact present with $T_b = -109\text{ }^\circ\text{C}$ and $T_a = -84\text{ }^\circ\text{C}$. The Annex X5 provides confidence bounds as shown in Figure 4.2-10 which are somewhat wider than those plotted in Figure 4.2-9 and now encompass the data set as expected.

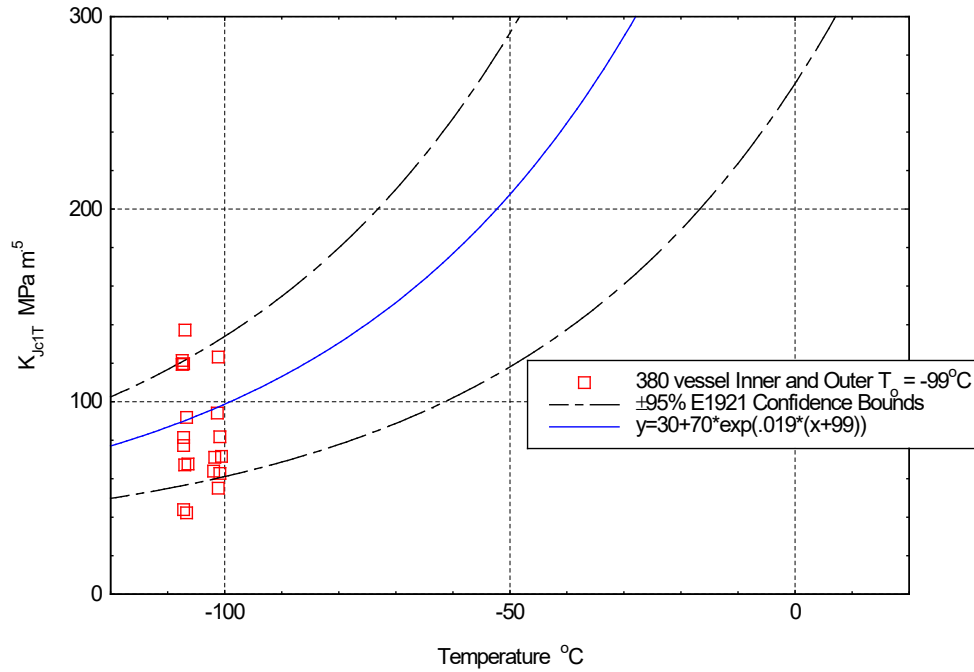


Figure 4.2-9: Vessel V0032 Data Set, Master Curve, and Confidence Bounds for A225 Steel

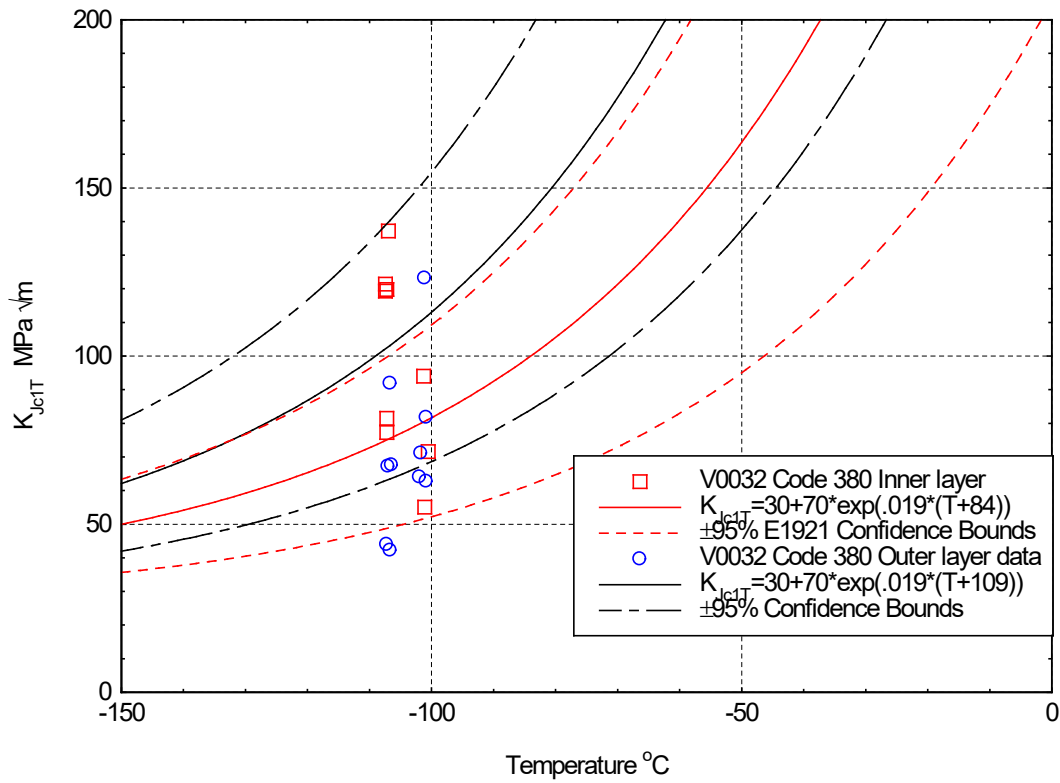


Figure 4.2-10: Bimodal Analysis of A225 Steel from the Hemispherical Head of Vessel V0032.

A nozzle weld heat affected zone data set is shown in Figure 4.2-11, demonstrating extensive variability beyond what would be expected by E1921. Figure 4.2-12 shows the application of both the bimodal and multimodal procedures of E1921 Annex X5 to this data set. The multimodal procedure assumes that the data set is a "smear" of Weibull distributions and obtains from the data a median equivalent to T_0 called T_m and a standard deviation referred to as σ_{Tm} . In this case, the multimodal analysis fits the data better than the bimodal analysis though it presents very wide tolerance bounds. However, the saving grace here is that all the estimates of the transition temperature, T_0 , T_A , T_B , T_m , and $T_m + 2\sigma_{Tm}$ are low with respect to the vessel operating temperature.

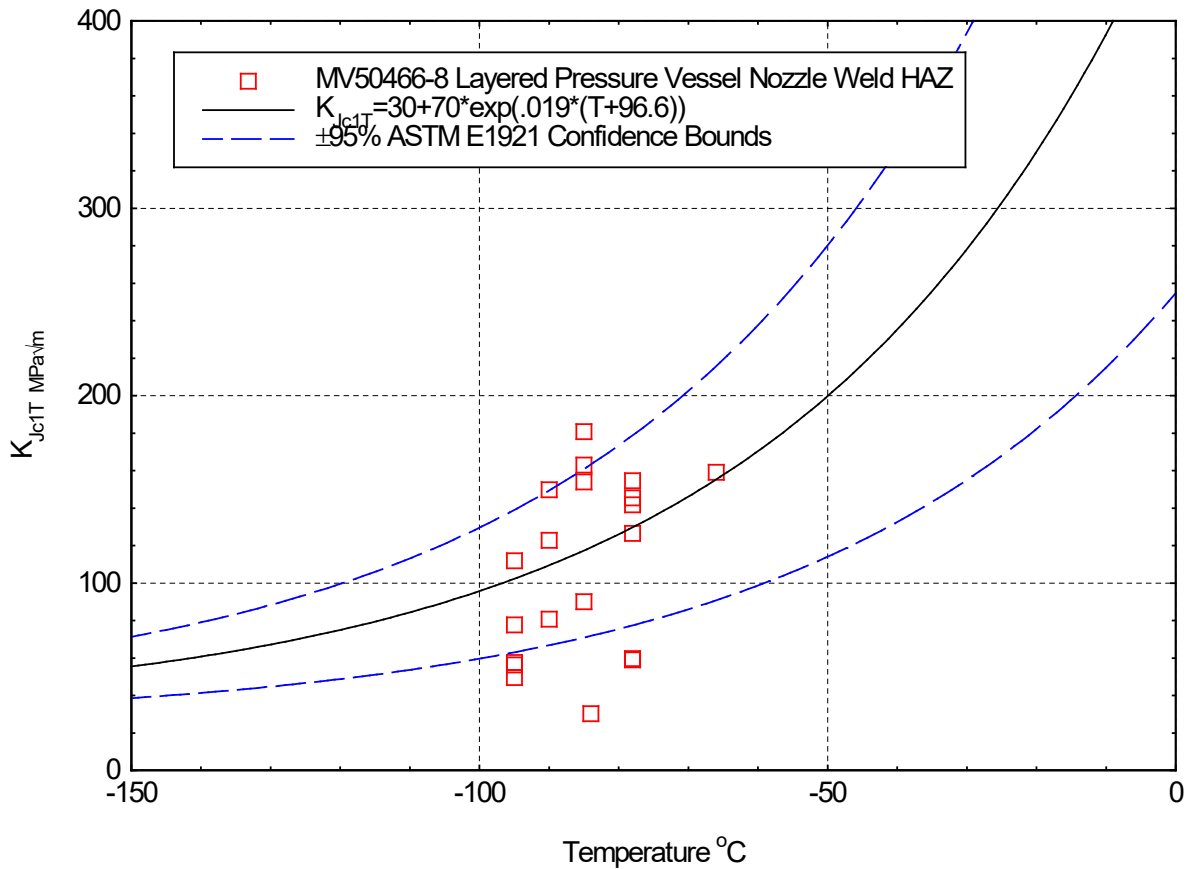


Figure 4.2-11: Nozzle Weld Data with Data Scatter Beyond E1921 Tolerance Bounds

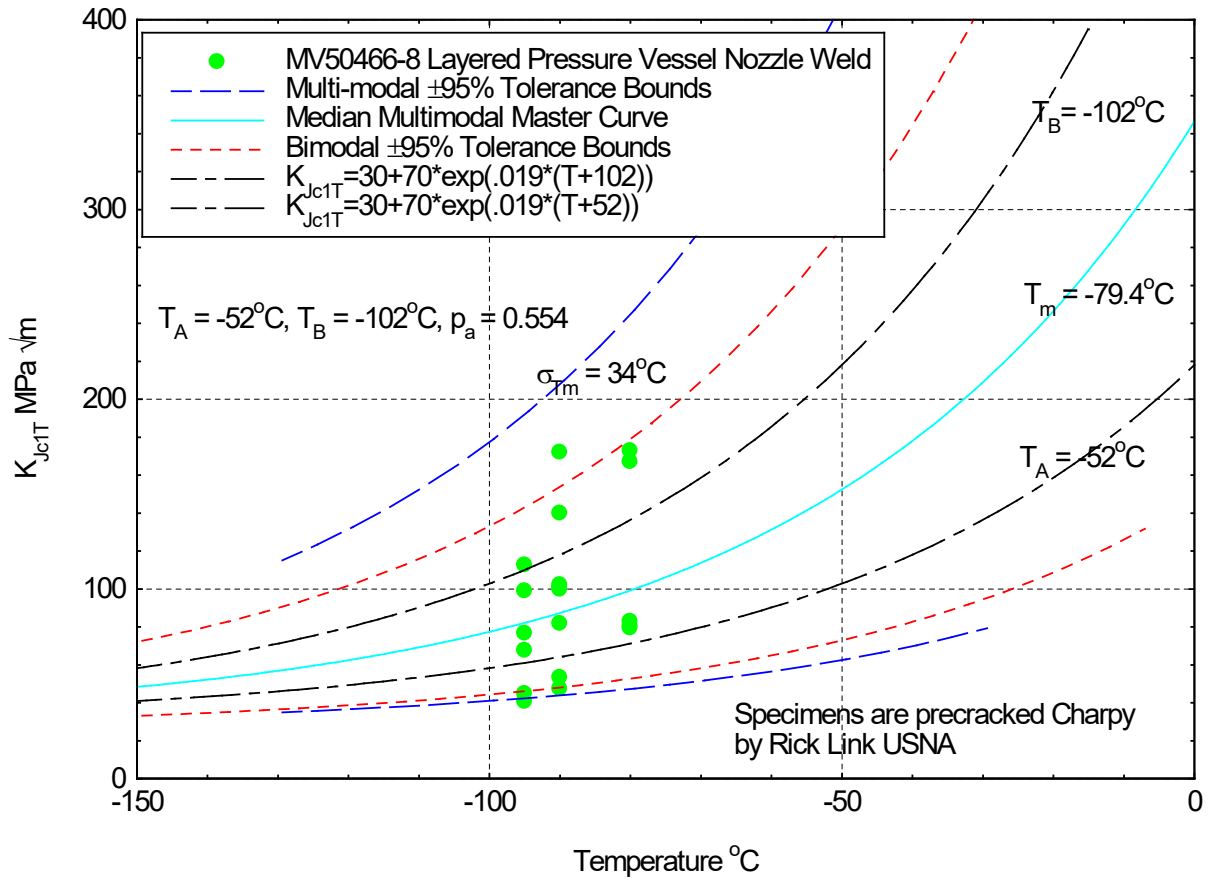


Figure 4.2-12: Application of Bimodal and Multimodal Analysis Methods of E1921 Annex X5

An alternate application for the E1921 Annex X5 multimodal analysis procedure is to evaluate a median transition toughness curve and corresponding tolerance bounds for a combined set of data that can be applied to the fleet of LPV applications. For example, the multimodal procedure has been applied in to a combined set of four A225 data sets. The A225 steel used in a majority of the NASA LPVs demonstrates dramatic variability. The specimen-to-specimen variability for a particular head is within the expectations of E1921, but the plate-to-plate variation is extreme. The four data sets in Figure 4.2-13, for instance, have T_0 values ranging from -99°C to -2°C . Applying the worst case result with $T_0 = -2^{\circ}\text{C}$ in a deterministic fashion to all vessels with A225 heads would be very conservative and likely require replacing every vessel. Treating the four data sets as a multimodal data set using the technique of Annex X5 gives the median curve and tolerance bounds shown in Figure 4.2-13. Using these results in a probabilistic analysis would give a much more reasonable and accurate analysis of the structural integrity of an LPV.

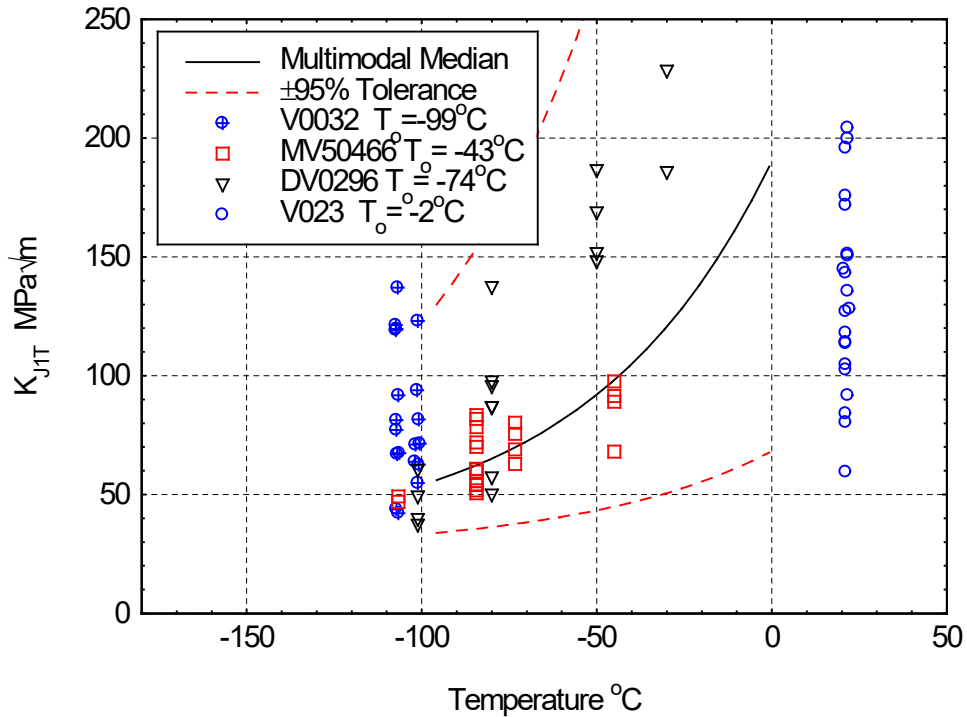


Figure 4.2-13: A225 Data Multimodal Median T_m Curve and Corresponding Bounds

TOTEM

TOTEM is a software code that was created to efficiently analyze the large number of E1921 data sets produced for the LPV Project. The goal was to produce a program that could rapidly calculate and plot the master curve for a material. In addition, the software performs all necessary size adjustments, censoring, and validity checks in accordance with ASTM E1921. Recently, the addition of Annex X5 *Treatment of Potentially Inhomogeneous Data Sets* to ASTM E1921 created the need for additional functionality of TOTEM to calculate master curve plots related to ferritic steels that exhibit inhomogeneity. These methods assess whether the data set is likely to be inhomogeneous and they provide methods to characterize the inhomogeneous data.

From ASTM E1921 X5.3.2.1:

The bimodal toughness distribution applies to data sets that contain two toughness populations; the first population is more brittle than the second. Typically, such toughness distributions are encountered in heat-affected zone (HAZ) materials where the crack tip can sample the low- or high toughness material. The combined bimodal toughness distribution is fully defined by three parameters: the reference temperature of population A, T_A , the reference temperature of population B, T_B , and the probability of sampling a specimen from population A, p_A . The probability of sampling a specimen

from population B is equal to $1-p_A$. Populations A and B are defined using the convention $T_B \leq T_A$.

From ASTM E1921 X5.3.3.1:

The multimodal toughness distribution applies to data sets that contain randomly distributed toughness populations. Typically, such cases are encountered in heterogeneous ferritic steels, for which the macroscopic heterogeneities are randomly distributed, or data sets of similar materials that are combined together. The overall data set is composed of several populations that individually follow the master curve distribution. The combined distribution is fully defined by two parameters: the mean reference temperature of all populations (T_m), and the standard deviation around the mean (σ_{Tm}).

TOTEM's integrated analysis and plotting tools allow the user to input raw data in the form of standard sample measurements and individual test values. The sample measurements and values do not require modification prior to input which saves significant time usually required to perform size adjustments. This data is then processed through the standard master curve evaluation, as well as the inhomogeneity evaluation. The results are plotted and exported in figures and tables as shown in Figure 4.2-14 through Figure 4.2-16. By doing this, this software allows for large data sets to be processed quickly with all required outputs and plots generated automatically within seconds.

	A	B	C	D	E	F	G	H	I
1	Specimen Name	W (mm)	ao (mm)	Crack Size (mm)	Test Temp (°C)	Yield Strength (MPa)	Raw Data K_{Ic} (MPa*m ^{0.5})	Modulus (GPa)	B (mm)
2	Specimen 1	25.4	12.7	0	-130	841	59.5	212.125	12.7
3	Specimen 2	25.4	12.7	0	-130	841	85.1	212.125	12.7
4	Specimen 3	25.4	12.7	0	-130	841	55.3	212.125	12.7
5	Specimen 4	25.4	12.7	0	-130	841	56.4	212.125	12.7
6	Specimen 5	25.4	12.7	0	-80	740	51.3	209	12.7
7	Specimen 6	25.4	12.7	0	-80	740	87.9	209	12.7
8	Specimen 7	25.4	12.7	0	-80	740	113.4	209	12.7
9	Specimen 8	50.8	25.4	0	-65	719	73.9	208.0625	25.4
10	Specimen 9	50.8	25.4	0	-65	719	126.8	208.0625	25.4
11	Specimen 10	25.4	12.7	0	-55	707	167.7	207.4375	12.7
12	Specimen 11	25.4	12.7	0	-55	707	88.5	207.4375	12.7
13	Specimen 12	25.4	12.7	0	-55	707	115.2	207.4375	12.7
14	Specimen 13	25.4	12.7	0	-55	707	81.4	207.4375	12.7
15	Specimen 14	25.4	12.7	0	-55	707	121.9	207.4375	12.7
16	Specimen 15	25.4	12.7	0	-55	707	145	207.4375	12.7
17	Specimen 16	25.4	12.7	0	-55	707	104.2	207.4375	12.7
18	Specimen 17	25.4	12.7	0	-55	707	64.4	207.4375	12.7
19	Specimen 18	25.4	12.7	0	-55	707	96.8	207.4375	12.7
20	Specimen 19	25.4	12.7	0	-55	707	114.5	207.4375	12.7
21	Specimen 20	25.4	12.7	0	-55	707	107.4	207.4375	12.7
22	Specimen 21	25.4	12.7	0	-55	707	81	207.4375	12.7
23	Specimen 22	25.4	12.7	0	-55	707	70	207.4375	12.7
24	Specimen 23	25.4	12.7	0	-55	707	131.8	207.4375	12.7
25	Specimen 24	25.4	12.7	0	-55	707	69.5	207.4375	12.7
26	Specimen 25	25.4	12.7	0	-55	707	67.5	207.4375	12.7
27	Specimen 26	25.4	12.7	0	-30	681	102.3	205.875	12.7
28	Specimen 27	25.4	12.7	0	-30	681	194	205.875	12.7
29	Specimen 28	25.4	12.7	0	-30	681	170.4	205.875	12.7

Figure 4.2-14: Example TOTEM Input Data

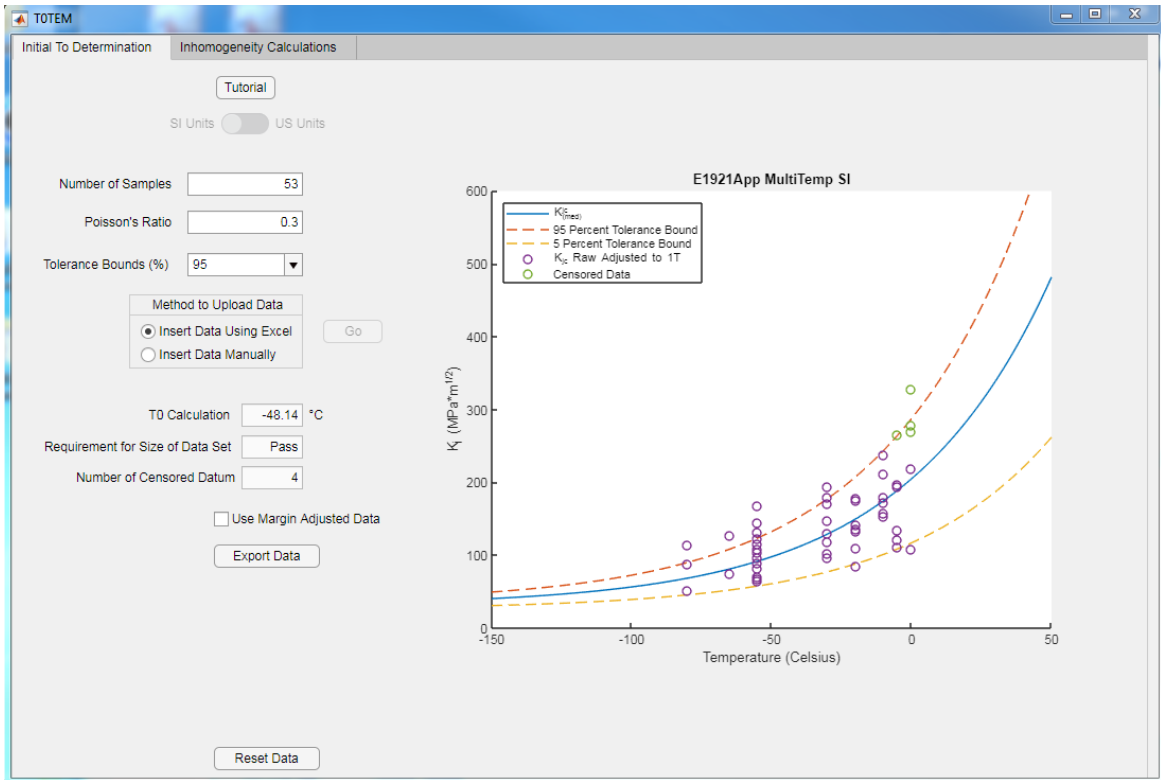


Figure 4.2-15: Example TOTEM Master Curve Plot

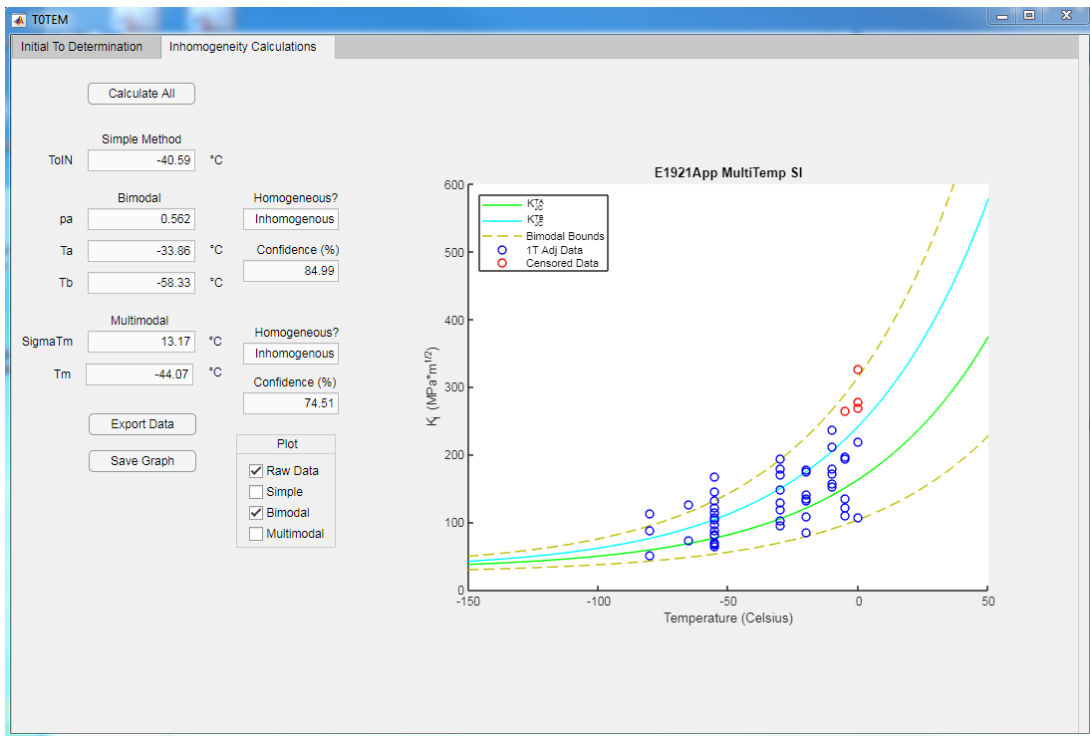


Figure 4.2-16: Example TOTEM Bimodal Master Curve Plot

The T0TEM Program has been evaluated by ASTM for accuracy and will continue to undergo verification and validation tests going forward. It is the goal of the committee to utilize T0TEM as a validated engineering software that will be accessible to users who may be new or unfamiliar with the detailed working of E1921.

Table 4.2-1: Comparison of T0TEM with ASTM Master Curve Results

	Standard	T0TEM	% Diff
T₀ (C)	-48.1	-48.1	0
N	53	53	0
R	49	49	0
Max ln(L)	-243.5	-243.5	0
P_A	0.56	0.56	0
T_A (C)	-33.8	-33.9	0.3
T_B (C)	-58.3	-58.3	0
MLNH	3.52	3.52	0
MLNH_{ec}	3.46	3.46	0
σ_{pA} (C)	0.066	0.066	0
σ_{TA} (C)	4.17	4.17	0
σ_{TB} (C)	3.85	3.86	0.26
% conf in MLNH	85	85	0

Table 4.2-2: Comparison of T0TEM with ASTM Bimodal Master Curve Results

T _i - T ₀ (°C)	T _i (°C)	Standard				T0TEM				Absolute Diff T0TEM/Standard		Percent Diff T0TEM/Standard	
		K _A (T) (MPa√m)	K _B (T) (MPa√m)	K _{Jc(0.05)} (MPa√m)	K _{Jc(0.95)} (MPa√m)	K _A (T) (MPa√m)	K _B (T) (MPa√m)	K _{Jc(0.05)} (MPa√m)	K _{Jc(0.95)} (MPa√m)	K _{Jc(0.05)} (MPa√m)	K _{Jc(0.95)} (MPa√m)	K _{Jc(0.05)} (MPa√m)	K _{Jc(0.95)} (MPa√m)
-50	-98	53.6	67.1	37.7	77.1	53.6	67.1	37.7	77.1	-0.01	0.04	-0.03	0.0
-45	-93	55.9	70.7	38.9	81.5	55.9	70.7	38.9	81.5	0.00	0.00	0.01	0.0
-40	-88	58.4	74.6	40.2	86.3	58.4	74.6	40.2	86.3	0.04	0.00	0.10	0.0
-35	-83	61.1	79	41.7	91.6	61.1	79.0	41.7	91.6	0.01	-0.02	0.03	-0.0
-30	-78	64.1	83.7	43.3	97.4	64.1	83.8	43.3	97.4	0.03	-0.01	0.06	-0.0
-25	-73	67.4	89	45.1	103.8	67.4	89.0	45.1	103.8	0.00	-0.03	0.00	-0.0
-20	-68	71.1	94.8	47.1	110.8	71.1	94.8	47.1	110.8	-0.05	-0.01	-0.10	-0.0
-15	-63	75.1	101.2	49.2	118.5	75.1	101.2	49.2	118.5	0.00	0.01	-0.01	0.0
-10	-58	79.4	108.2	51.6	127	79.5	108.2	51.6	127.0	-0.04	0.01	-0.09	0.0
-5	-53	84.3	115.8	54.1	136.3	84.3	115.9	54.1	136.3	0.05	0.04	0.09	0.0
0	-48	89.6	124.3	57	146.6	89.6	124.3	57.0	146.6	0.00	0.01	0.00	0.0
5	-43	95.4	133.6	60.1	157.9	95.4	133.6	60.1	157.9	0.03	0.00	0.05	0.0
10	-38	101.9	143.8	63.6	170.3	101.9	143.8	63.6	170.3	-0.02	0.02	-0.04	0.0
15	-33	108.9	155.1	67.4	184	108.9	155.1	67.4	184.0	-0.04	-0.03	-0.05	-0.0
20	-28	116.7	167.5	71.5	199	116.7	167.5	71.5	199.0	0.03	-0.01	0.04	0.0
25	-23	125.2	181.1	76.1	215.5	125.3	181.1	76.1	215.5	0.01	0.00	0.01	0.0
30	-18	134.6	196	81.1	233.7	134.7	196.0	81.1	233.7	0.05	-0.04	0.06	-0.0
35	-13	145	212.5	86.7	253.6	145.0	212.5	86.7	253.6	-0.02	0.03	-0.02	0.0
40	-8	156.3	230.6	92.8	275.6	156.4	230.6	92.8	275.6	-0.03	-0.02	-0.03	-0.0
45	-3	168.8	250.4	99.5	299.7	168.9	250.5	99.5	299.7	-0.03	0.03	-0.03	0.0
50	2	182.6	272.3	106.8	326.3	182.6	272.3	106.8	326.3	0.03	-0.02	0.03	-0.0

Table 4.2-3: Comparison of T0TEM with ASTM Multimodal Master Curve Results

$T_i - T_m$ (°C)	T_i (°C)	Standard			T0TEM			Percent Diff T0TEM/Standard		
		$K_{Jc(0.50)}$ (MPa√m)	$K_{Jc(0.05)}$ (MPa√m)	$K_{Jc(0.95)}$ (MPa√m)	$K_{Jc(0.50)}$ (MPa√m)	$K_{Jc(0.05)}$ (MPa√m)	$K_{Jc(0.95)}$ (MPa√m)	$K_{Jc(0.50)}$ (MPa√m)	$K_{Jc(0.05)}$ (MPa√m)	$K_{Jc(0.95)}$ (MPa√m)
-51	-95	56.24	38.11	79.50	56.24	38.11	79.50	0.00	0.01	0.01
-46	-90	58.83	39.35	84.09	58.83	39.35	84.10	-0.01	-0.01	0.01
-41	-85	61.69	40.72	89.16	61.69	40.72	89.16	0.01	0.00	0.01
-36	-80	64.82	42.23	94.72	64.83	42.23	94.72	0.01	0.01	0.00
-31	-75	68.27	43.88	100.85	68.28	43.88	100.85	0.01	0.01	0.00
-26	-70	72.07	45.69	107.58	72.07	45.69	107.58	0.00	0.00	0.00
-21	-65	76.24	47.68	114.99	76.24	47.68	115.00	0.00	-0.01	0.01
-16	-60	80.83	49.87	123.15	80.83	49.88	123.15	0.00	0.01	0.00
-11	-55	85.87	52.28	132.11	85.87	52.28	132.11	0.00	0.00	0.00
-6	-50	91.42	54.93	141.97	91.42	54.93	141.97	0.00	0.01	0.00
-1	-45	97.52	57.83	152.82	97.52	57.83	152.82	0.00	0.00	0.00
4	-40	104.23	61.03	164.74	104.23	61.03	164.74	0.00	0.00	0.00
9	-35	111.60	64.54	177.86	111.61	64.54	177.86	0.01	0.00	0.00
14	-30	119.71	68.40	192.28	119.72	68.40	192.29	0.00	0.00	0.00
19	-25	128.64	72.64	208.15	128.64	72.65	208.15	0.00	0.01	0.00
24	-20	138.44	77.31	225.59	138.45	77.31	225.60	0.00	0.00	0.00
29	-15	149.23	82.44	244.78	149.24	82.44	244.78	0.01	0.00	0.00
34	-10	161.09	88.08	265.88	161.10	88.08	265.88	0.00	0.00	0.00
39	-5	174.14	94.28	289.08	174.14	94.29	289.08	0.00	0.01	0.00
44	0	188.48	101.10	314.59	188.49	101.11	314.60	0.00	0.01	0.00

5 LPV FLEET CHARACTERIZATION

The NASA LPV fleet contains mostly non-code vessels manufactured in the late 1950s and early 1960s. Materials used in construction of these LPVs were considered the best available at the time, but in some cases, they have shown poor fracture properties when later studied. Another nuance of these construction materials is the variability in raw stock production techniques, and thus in mechanical properties. Each vessel purchased by NASA was typically delivered with material data sheets and drawings indicating the different steels used in fabrication. However, a number of LPVs in the current NASA fleet were acquired from other government organizations and paperwork did not always follow them. When available, this data was used at the start of the LPV effort not only to keep track of the different materials in use, but also to direct the testing most effectively.

When the decision was reached to acquire test specimens from decommissioned vessels to characterize the materials, it was decided that the focus should be on materials that would cover the greatest portion of the fleet. The LPV fleet database was created by collecting vessel data packages from each center’s pressure systems team and compiling them into a comprehensive list of LPVs and their materials. This allowed the LPV materials team to target materials for testing to cover the most in-service vessels.

There are four types of material characterizations for this effort. First, there are materials that have been tested as part of the effort, and therefore their properties have been properly characterized by modern test methods and analysis. Second are materials that have

been widely characterized in literature. Many of these are more modern materials whose contents and properties were more tightly controlled at time of production, or which saw significant service in other industries. They are considered to be bounded in literature and testing was minimal or not conducted at all. Next, are materials that are bounded by testing. These materials have been tested, however not necessarily in the target location. For example, the T-1 steel was tested in a thick wrapper layer, but not in the head. Head T-1 material is considered to be bounded by this testing as the investigation gave significant confidence in the similarity of these material locations. The last are a few materials which, due to proprietary blending or missing records, are unknown. These materials have little data available and are found in only a few vessels in the fleet. In general, it is impossible to test these materials since they are often in one-of-a-kind vessels created for a purpose unique to NASA. The risk associated with these vessels must be bought down through methods other than material property characterization, or the vessels must be removed from service.

5.1 Database Summary

It was common for LPVs to be manufactured using a variety of materials, depending on the component. Figure 5.1-1 through Figure 5.1-4 break down the quantity of vessels with certain materials by component. This demonstrates the logic used in selecting materials for testing, as well as the quantities of vessel components covered by testing, literature, or falling into the unknown/uncharacterized category. If a material was tested for one component, but not another, it may be considered bounded by the first component, or remain uncharacterized. Some materials behave differently depending on the produced thickness and the work required to form them into the proper shape.

The three main components of an LPV are the heads, nozzles, and layered shell course(s). Shell courses often include an inner layer which is thicker and of a different material. This layer provided a sufficiently stiff liner for wrapping of subsequent layers, provides the pressure boundary, shields the rest of the vessel layers from the contents of the vessel, and generally shares the loading due to pressure. As a result, the material fleet characterization of the inner layer is broken out separately from the standard wrapper layers.

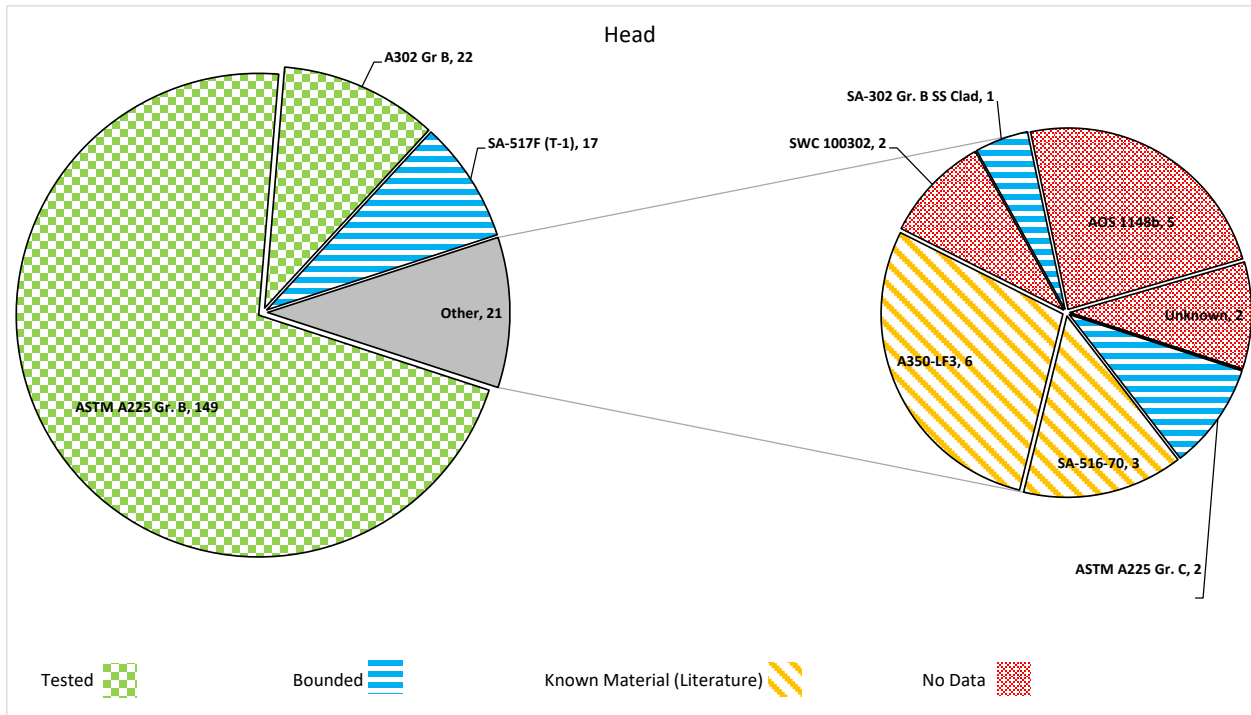


Figure 5.1-1: Fleet Characterization, Head Materials

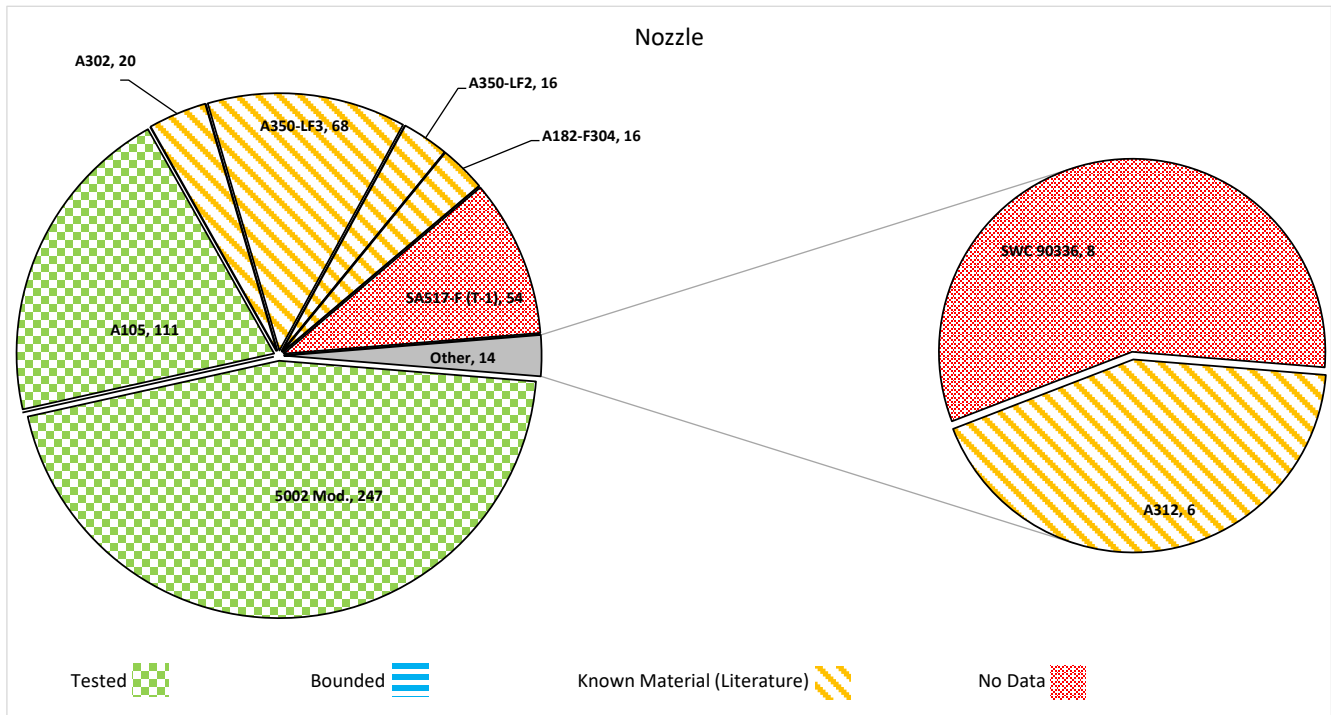


Figure 5.1-2: Fleet Characterization, Nozzle Materials (Head and Shell)

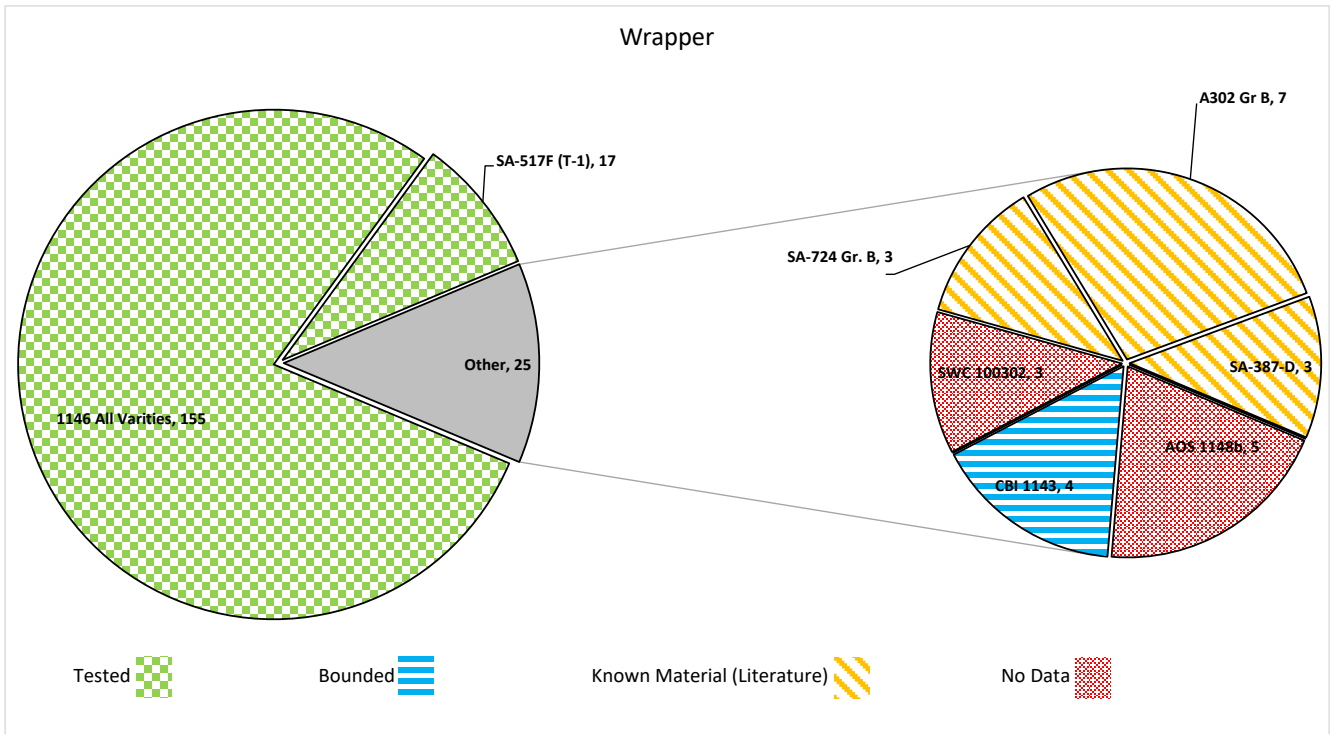


Figure 5.1-3: Fleet Characterization, Wrapper Materials

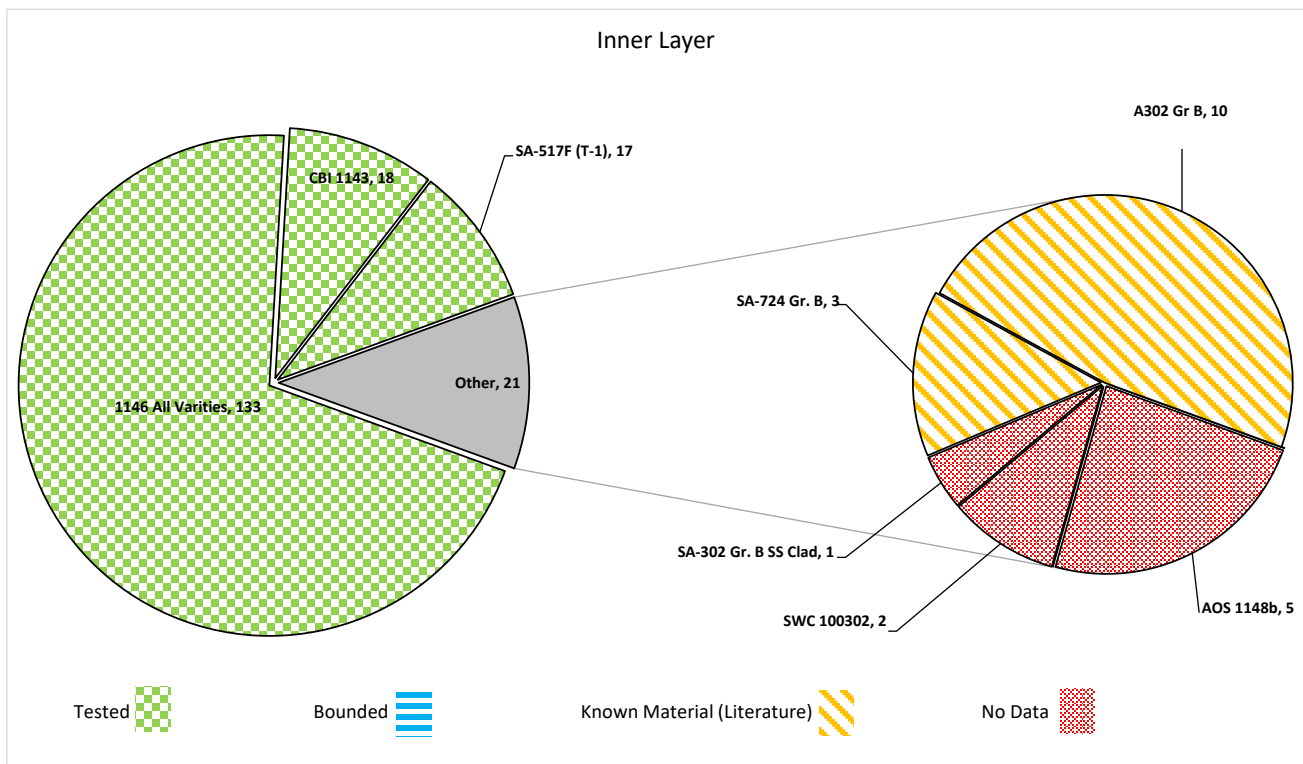


Figure 5.1-4: Fleet Characterization, Inner Layer Materials

6 REFERENCE LITERATURE MATERIALS

NASA oversees the operation and maintenance of a fleet of LPVs across the United States. Nearly 300 of the fleet's current vessels were constructed in the 1960s before LPVs were included in the ASME BPVC. Therefore, they were not built-in accordance with ASME BPVC requirements. Due to the inherent risk and potential catastrophic failure involved with pressure vessels that store compressed gas, the safety and risk of all aforementioned vessels must be examined to assess compliance with Occupational Safety and Health Administration (OSHA) standards as outlined by NASA Pressure System Recertification Programs.

As previously mentioned, many of the vessels in the fleet date from the 1960s and therefore have no viable original manufacturer contacts as many manufacturers are either no longer in business or do not have accessible records. Some vessels are also found in such small quantities in the fleet that testing is not an option. In an attempt to fill in missing information related to proprietary or discontinued materials, the LPV team has put together a data packet of relevant documentation, official documented correspondence with manufacturers, manufacturer specifications, etc. The following material sections give relevant properties of these materials as best can be discovered.

These materials can be broken down into three types, each with its own section to follow.

The first group contains materials that are code materials addressed by ASME BPVC VIII UCS-66. These materials have been evaluated by ASME and are considered to be code compliant construction materials. ASME designates ferrous alloys with "SA-" preceding the number, rather than simply "A" as is done by ASTM (the alloy number designations are the same). In some cases, the ASME specification is identical to the ASTM specification, but sometimes additional requirements are added. For simplicity materials will generally be referred to by their ASTM designations.

The second group contains materials that are not in the BPVC, but have significant reference literature. These may be ASTM-defined materials or materials that have been well studied and have well defined properties.

The third group contains proprietary legacy materials that have little or no information available. Often these materials are based on common materials but with chemistry and/or physical properties modified by the manufacturer, and with no traceability or history documented. What information can be found on these materials is usually in the form of mill certifications and does not match any known alloy.

6.1 Code Materials

Code materials are materials that are referenced by the ASME BPVC. These materials have been evaluated and accepted by ASME as compliant materials. Therefore, they were not

targeted during the testing phase of the LPV project. The information herein serves to reference and supplement the information contained within the BPVC.

6.1.1.1 A350

A350 is a carbon/low-alloy steel forging material governed by ASTM’s *Standard Specification for Carbon and Low-Alloy Steel Forgings, Requiring Notch Toughness Testing for Piping Components* (22).

6.1.1.1.1 Material Specification Properties

6.1.1.1.1.1 ASME BPVC Properties

Table 6.1.1.1.1-1: A350 ASME BPVC Material Properties (22)

Nominal Composition	Type/Grade	UNS No.	Min. Yield	Min. Tensile
Carbon Steel	LF2	K03011	36 ksi	70 ksi
3½Ni	LF3	K32025	37.7 ksi	70 ksi

6.1.1.1.2 ASTM Specification Properties

Table 6.1.1.1.2-1: ASTM A350 Mechanical Properties (22)

	Yield Stress min (ksi)	Tensile Stress (ksi)	Fracture Elongation (%)
LF1	30	60-85	25
LF2	36	70-95	22
LF3	37.5	70-95	22

Table 6.1.1.1.2-2: ASTM A350 Chemical Composition (22)

	C (max)	Mn	P (max)	S (max)	Si (max)	Ni	Cr (max)	Mo (max)	Cu (max)	V (max)
Grade LF1	0.3	0.60-1.35	0.035	0.04	0.15-0.30	0.4 (max)	0.3	0.12	0.4	0.08
Grade LF2	0.3	0.60-1.35	0.035	0.04	0.15-0.30	0.4 (max)	0.3	0.12	0.4	0.08
Grade LF3	0.2	0.60-1.35	0.035	0.4	0.20-0.35	3.3-3.7	0.3	0.12	0.4	0.03

6.1.1.2 Mill Test Report (MTR) Properties

No mill test reports were found containing test data for A350 materials used in LPV creation.

6.1.1.3 Fracture Results

A literature search identified an ASTM E1921 analysis that had been conducted on a section of A350 flange material for the purpose of offshore piping qualification. These flanges are similar to the flanges used in LPV nozzles. The results of these tests are published by F.M Haggag in *In-Situ Automated Ball Indentation Testing of A350 Steel Flanges at Ambient Temperature for Offshore Qualifications at -46°C (-50°F)* (23). Compact tension specimens from A350 flanges were tested according to E1921. The T_0 from the compact tension tests was found to be -115°C . A transition temperature at this level places A350 material lower than the majority of other LPV materials tested, and thus as a low concern from a material property standpoint. The Master Curve results as presented by F.M. Haggag are shown in Figure 6.1.1.3-1 (23)

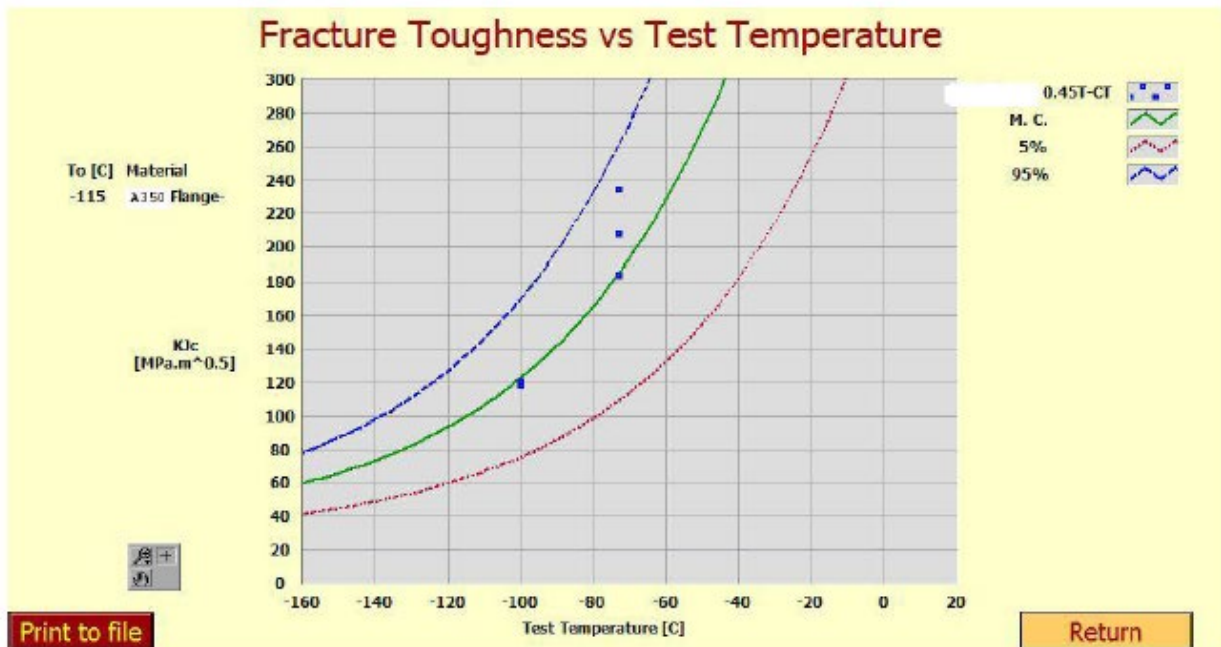


Figure 6.1.1.3-1: A350 Master Curve Results

6.1.2 A517 (T-1)

T-1 is the United States Steel Corporation (USS) trade name for a low-carbon, high-strength quenched and tempered alloy steel which has been accepted as both an ASTM and an ASME material, designated A517 (24) or SA-517, respectively. (The A517 specification includes a number of slightly different chemistries associated with different letter designations following the number, apparently for reasons related to the USS patent on the alloy. The material was used extensively in the pressure vessel industry around the time of its introduction. It exhibits good strength and toughness properties, but both weld and parent material have in some cases exhibited a tendency to crack. The governing material standards are the ASTM A517/A517M-84 Standard Specification for Pressure Vessel Plates, Alloy Steel, High-Strength, Quenched and Tempered and the comparable ASME SA-517/517M standard of the same name.

6.1.2.1 Material Specification Properties

6.1.2.1.1 ASME BPVC Properties

Table 6.1.2.1.1-1: SA-517 ASME BPVC Material Properties

Nominal Composition	Type/Grade	UNS No.	Min. Yield	Min. Tensile
$\frac{3}{4}\text{Ni}-\frac{1}{2}\text{Cr}-\frac{1}{2}\text{Mo}-\text{V}$	F	K11576	100 ksi	115 ksi

6.1.2.1.2 ASTM Material Properties

Table 6.1.2.1.2-1: ASTM A517 Mechanical Properties (24)

	Yield Stress min (ksi)	Tensile Stress (ksi)	Fracture Elongation in 2 in, min (%)	Reduction of Area, min (%)
Grade F	100	115-135	16	45

Table 6.1.2.1.2-2: ASTM A517 Chemical Composition (24)

	C	Mn	P (max)	S (max)	Si	Ni	Cr	Mo	Cu	V
Grade F	0.08-0.22	0.55-1.10	0.035	0.04	0.13-0.37	0.67-1.03	0.36-0.69	0.36-0.64	0.15-0.50	0.02-0.09

6.1.2.2 Mill Test Report (MTR) Properties

No mill test reports were found containing test data for A517F materials used in LPV creation.

6.1.2.3 Fracture Results

The transition temperature of A517F steel was investigated by John M. Barsom and Stanley T. Rolfe in *K_{IC} Transition Temperature Behavior of A517-F Steel* in 1971 (25). Their work details an investigation into the transition from ductile tearing to brittle fracture utilizing pre-cracked three-point bend specimens. This report is essentially a precursor to the ASTM E1921 test method, as it conducts tests in a similar manner and with a similar goal. However, at the time of its writing, the Master Curve method was not applied. Despite this, the test data shows exceptional similarity to the E1921 method.

In light of this, the original plot from Barsom and Rolfe was digitized, and the individual data points extracted as best possible in order to apply the modern Master Curve method found in E1921 and determine the T₀ of this data set. It is impossible to be certain of all validity criteria, however the data set is expansive enough to give confidence of its validity. The Barsom and Rolfe analysis also noted that the fractography of the fracture specimens indicated that the

transition was a result of microscopic fracture mode, exactly as would be later defined in ASTM E1921.

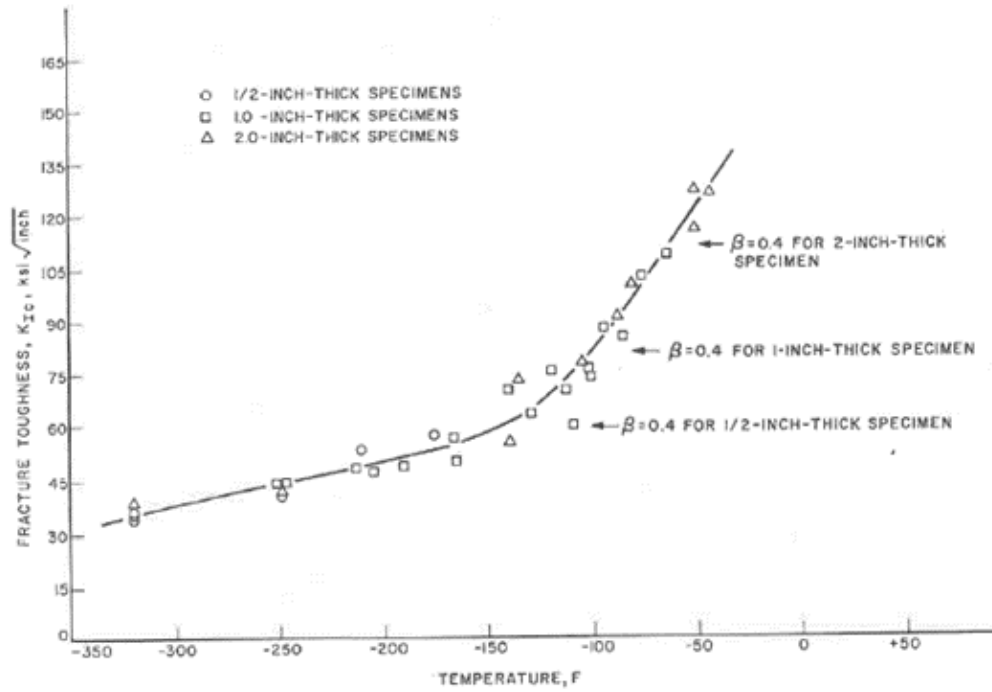


Figure 6.1.2.3-1: A517F Original Plot and Curve Fit from Barsom and Rolfe (25)

Table 6.1.2.3-1: A517F Raw Test Data

Specimen Name	Temperature (°C)	KjcRaw (MPa*m ^{0.5})	1T Data (MPa*m ^{0.5})	δi	Test Temp -T0 (°C)
1	-196	36.5	33.8	1	-130
2	-196	38.3	35.4	1	-130
3	-196	39.4	36.3	1	-130
4	-156	44.2	40.3	1	-91
5	-135	58.8	52.6	1	-70
6	-116	62.8	56.0	1	-50
7	-158	48.5	48.5	1	-92
8	-155	48.4	48.4	1	-89
9	-136	53.0	53.0	1	-71
10	-132	51.8	51.8	1	-66
11	-124	53.3	53.3	1	-58
12	-110	62.2	62.2	1	-45
13	-110	55.0	55.0	1	-44
14	-90	69.6	69.6	1	-24
15	-79	66.3	66.3	1	-13
16	-96	76.9	76.9	1	-30
17	-84	83.1	83.1	1	-19
18	-80	77.0	77.0	1	-15
19	-74	81.1	81.1	1	-8
20	-75	83.5	83.5	1	-9
21	-65	93.8	93.8	1	0
22	-70	96.5	96.5	1	-5
23	-60	112.8	112.8	1	5
24	-53	119.7	119.7	1	12
27	-93	80.3	91.7	1	-28
28	-76	85.9	98.4	1	-11
29	-67	100.2	115.3	1	-1
30	-63	110.2	127.3	1	3
31	-46	127.6	147.9	1	19
32	-46	139.5	162.1	1	19
33	-42	138.7	161.1	1	23

Table 6.1.2.3-2: A517F Master Curve Results

Initial T ₀ (°C)	-66
Total Samples	33
Number of Samples Between +50/-50°C (N)	20
Number of Uncensored Data (r)	20
Poisson's Ratio	0.3
$\Sigma(r_i n_i)$	3.1
Samples Between T _i - T ₀ 50 to -14 °C	13
Samples Between T _i - T ₀ -15 to -35 °C	5
Samples Between T _i - T ₀ -36 to -50 °C	2
T ₀ scrn (°C)	-66
Homogenous or Inhomogeneous	Homogeneous

Table 6.1.2.3-1

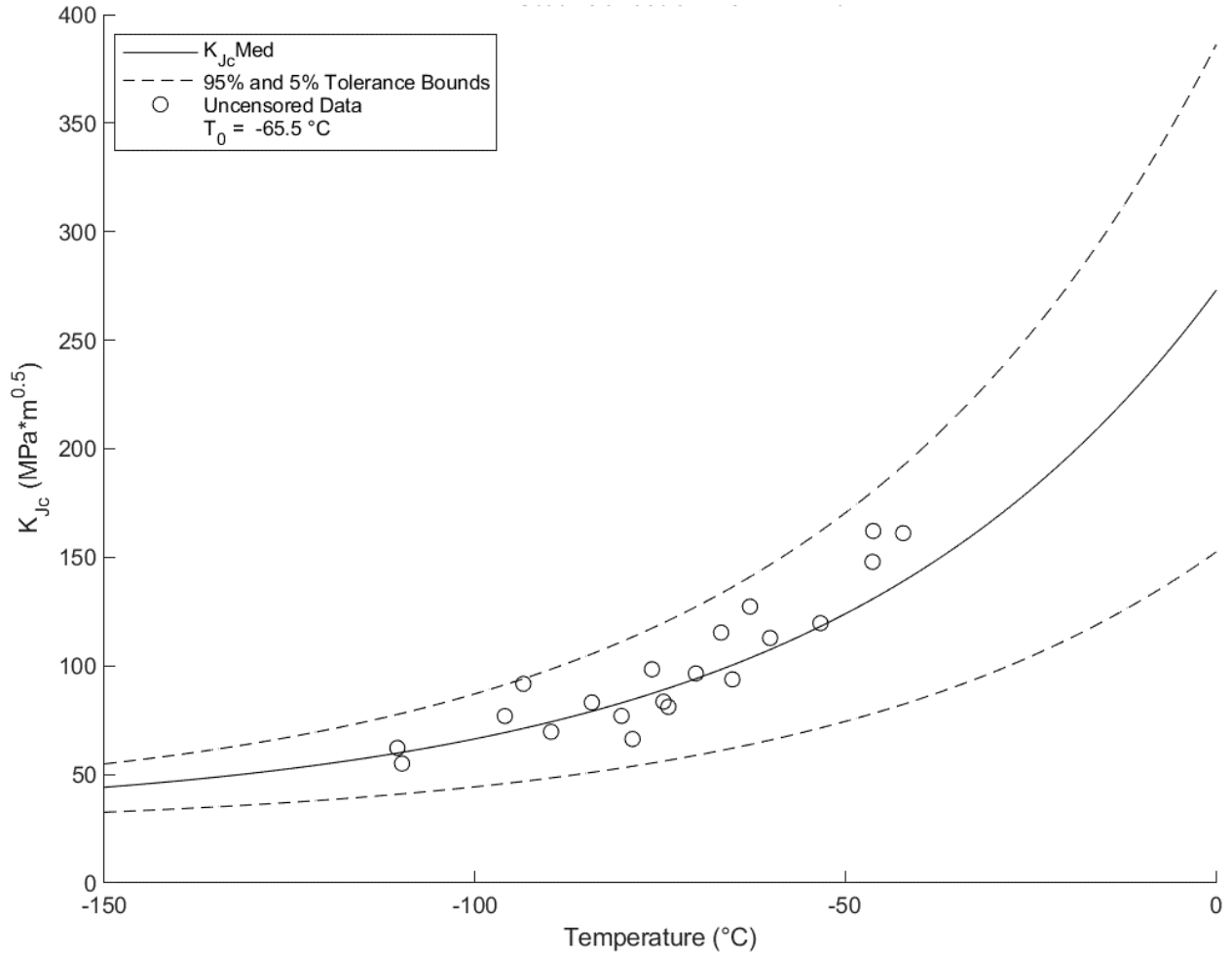


Figure 6.1.2.3-2: A517F Master Curve ($T_0 = -66^{\circ}\text{C}$)

Table 6.1.2.3-1, Table 6.1.2.3-2, Figure 6.1.2.3-1 and Figure 6.1.2.3-2 show the results of the digitized Barsom and Rolfe data (25). As expected, the data fits well in the context of the E1921 master curve. While the digitized data likely contains some degree of error, the final result of $T_0 = -66^{\circ}\text{C}$ is directly in family with modern data. This gives significant confidence to the continued use of verified A517F (T-1) steel in LPVs.

6.1.3 SA-724

A724 Grade B is a low-alloy steel plate material. The governing material standard specification is *ASTM Standard Specification for Pressure Vessel Plates, Carbon-Manganese-Silicon Steel, Quenched and Tempered, for Welded Layered Pressure Vessels*, also known as ASTM Designation: A 724/A 724M – 97 (26).

6.1.3.1 Material Specification Properties

Numerous standards and specifications exist for the SA-724 material. However, only the most widely accepted records have been listed below.

6.1.3.1.1 ASME BPVC Properties

Table 6.1.3.1.1-1: ASME SA-724 BPVC Material Properties

Type/Grade	UNS No.	Min. Yield	Min. Tensile
B	K12031	75 ksi	95 ksi

6.1.3.1.2 ASTM Specification Properties

Table 6.1.3.1.2-1: ASTM A724 Mechanical Properties (26).

Type/Grade	Elongation	Min. Yield	Tensile
B	17%	75 ksi	95-115 ksi

Table 6.1.3.1.2-2: ASTM A724 Chemical Composition (26).

Analysis	C	Mn [max]	P [max]	S [max]	Si [max]	Cu [max]	Ni [max]	Cr [max]	Mo	V
Heat	0.20	1.00-1.60	0.035	0.035	0.50	0.35	0.25	0.25	0.08	0.08
Product	0.24	0.92-1.72	0.035	0.035	0.55	0.38	0.28	0.29	0.09	0.09

6.1.3.2 Mill Test Report (MTR) Properties

No mill test reports were found containing test results for A724 materials used in LPV creation.

6.1.3.3 Fracture Results

There are no test results for A724.

6.1.4 A387

387 Grade D is an alloy steel and is intended for use in the petrochemical/pressure vessel industry. The governing material standard specification is *ASTM A387 Standard Specification for Pressure Vessel Plates, Alloy Steel, Chromium-Molybdenum (27)*

6.1.4.1 Material Specification Properties

Numerous standards and specifications exist for the SA-387 material. However, only the most widely accepted records have been listed below.

6.1.4.1.1 ASME BPVC Materials

Table 6.1.4.1.1-1: SA-387 ASME BPVC Material Properties

Type/Grade	UNS No.	Class	Min. Yield	Min. Tensile
22	K21590	2	45 ksi	75 ksi

6.1.4.1.2 ASTM Specification Properties

Table 6.1.4.1.2-1: ASTM A387 Mechanical Properties (27)

Class	Reduction of Area	Elongation	Yield	Tensile
1	40%	18%	30 ksi	60-85 ksi
2	40%	18%	45 ksi	75-100 ksi

Table 6.1.4.1.2-2: ASTM A387 Chemical Properties (27)

	C	Mn	P	S	Si	Cr	Mo
Heat	0.05-0.015	0,30-0.60	0.035	0.035	0.50	2.00-2.50	0.90-1.10
Product	0.04-0.15	0.25-0.66	0.035	0.035	0.50	1.88-2.62	0.85-1.15

6.1.4.1.3 Welding Research Council Technical Review

In 1980, Alan Pense presented the Adams Lecture: Twenty Years of Pressure Vessel Steel Research (28), which included the following properties for ASTM A387:

Table 6.1.4.1.3-1: Technical Paper/Review Material Mechanical Properties (28)

15 ft-lb transition temperature	Elongation %	Min. Yield	Min. Tensile
-25 °F	28 %	40 ksi	70 ksi

Table 6.1.4.1.3-2: Technical Paper/Review Chemical Composition (28)

C [max]	Mn [max]	P [max]	S [max]	Si [max]	Cr [Max]	Mo [Max]
0.11	0.37	0.010	0.010	0.26	2.20	0.96

6.1.4.2 Mill Test Report (MTR) Properties

Available data package reports for current fleet vessels provide some vessel-specific properties. According to the records, data was obtained from the U1-A data package provided by the manufacturer (Taylor Forge) and included in reference (29). Note that the values provided appear to be specification values, not values from MTRs.

Table 6.1.4.2-1: MARS Vessel U Package (29)

Vessels	Description	Yield [ksi]	Tensile [ksi]
289661 V-1 (MARS 1)	Outer Bands	82.5	115
289661 V-3 (MARS 2)	Outer Bands	82.5	115
289661 V-4 (MARS 3)	Outer Bands	82.5	115

6.1.4.3 Fracture Results

There are no test results for A387/SA-387.

6.1.5 SA-182

SA-182 Grade F 316L is a forged austenitic stainless steel. The governing material standard specification is *ASTM A182/A182M-20 Standard Specification for Forged or Rolled Alloy and Stainless-Steel Pipe Flanges, Forged Fittings, and Valves and Parts for High-Temperature Service (30)*.

6.1.5.1 Material Specification Properties

Numerous standards and specifications exist for the A182 material. However, only the most widely accepted records have been listed below.

6.1.5.1.1 ASME BPVC Properties

Table 6.1.5.1.1-1: ASME SA-182 ASME BPVC Material Properties

Nominal Composition	Type/Grad	UNS No.	Min. Yield	Min. Tensile
16Cr-12Ni-2Mo	F316L	S31603	25 ksi	65 ksi

6.1.5.1.2 ASTM Specification Properties

Table 6.1.5.1.2-1: ASTM A182 Mechanical Properties (30)

Type/Grade	Min. Yield	Min. Tensile	Elongation	Reduction of Area
F 316L	25 ksi	70ksi	30%	50%

Table 6.1.5.1.2-2: ASTM A182 Chemical Composition (30)

C [max]	Mn [max]	P [max]	S [max]	Si [max]	Ni	Cr	Mo	N [max]
0.030	2.00	0.045	0.030	1.00	10.0-15.0	16.0-18.0	2.00-3.00	0.10

6.1.5.2 Mill Test Report (MTR) Properties

No mill test reports were found containing tests of A182 Grade F316L materials used in LPV creation.

6.1.5.3 Fracture Results

There are no internal test results for A182.

6.1.6 A312

6.1.6.1 General Material Properties

A312 Grade T304 is an austenitic stainless steel pipe material. The governing material standard specification is *ASTM A 312/A 312M – 95a Standard Specification for Seamless and Welded Austenitic Stainless-Steel Pipes*, (31). Later versions of the standard, with a slightly different name, cover a wider range of materials and forms, including heavily worked materials.

6.1.6.2 Material Specification Properties

Numerous standards and specifications exist for the A312 material. However, only the most widely accepted records have been listed below.

6.1.6.2.1 ASME BPVC Materials

Table 6.1.6.2.1-1: ASME SA-312 BPVC Material Properties

Nominal Composition	Type/Grad	UNS No.	Min. Yield	Min. Tensile
18Cr-8Ni	TP304	S30400	30 ksi	75 ksi

6.1.6.2.2 ASTM Specification Properties

Table 6.1.6.2.2-1: ASTM A312 Mechanical Properties (31)

Type/Grade	Min. Yield	Min. Tensile	Elongation Longitudinal	Elongation Transverse
TP304	30 ksi	75 ksi	35%	25%

Table 6.1.6.2.2-2: ASTM A312 Chemical Composition (31)

C [max]	Mn [max]	P [max]	S [max]	Si [max]	Ni	Cr
0.08	2.00	0.040	0.030	0.75	8.00-11.0	18.0-20.0

6.1.6.3 Mill Test Reports (MTR)

No mill test reports were found containing tests of A312 materials used in LPV creation.

6.1.6.4 Fracture Results

There are no internal test results for A312.

6.1.7 SA-516

SA-516 Grade 70 is a low-alloy steel plate material frequently used for pressure vessel shells and heads. The governing material standard specification is *ASTM A516/A516M-70 Standard Specification for Pressure Vessel Plates, Carbon Steel, for Moderate and Lower-Temperature Service* (32).

6.1.7.1 Material Specification Properties

Numerous standards and specifications exist for the SA-516 material. However, only the most widely accepted records have been listed below.

6.1.7.1.1 ASME BPVC Materials

Table 6.1.7.1.1-1: SA-516 ASME BPVC Material Properties

Type/Grade	UNS No.	Min. Yield	Min. Tensile
70	K02700	38 ksi	70 ksi

6.1.7.1.2 ASTM Specification Properties

Table 6.1.7.1.2-1: ASTM A516 Mechanical Properties (32)

Type/Grade	Elongation	Min. Yield	Tensile
70	22% (Flange), 23 % (Firebox)	38 ksi	70-85 ksi

Table 6.1.7.1.2-2: ASTM A516 Chemical Composition (32)

Analysis	C* [max]	Mn*	P [max]	S [max]	Si [max]
Heat	0.27	0.85-1.20	0.04 (Flange),	0.04 (Flange),	0.15-0.30
Product	0.27	0.80-1.25	0.035 (Firebox)	0.035 (Firebox)	0.13-0.33

*Thickness dependent. Consult Specification.

6.1.7.1.3 Welding Research Institute Supplement 311-S

Pense (28), provided material properties and chemistry values for 516-70:

Table 6.1.7.1.3-1: 516-70 Normalized Condition Mechanical Properties) (28)

Type/Grade	Elongation	Min. Yield	Tensile	15 ft-lb transition temperature
70	32%	50 ksi	82 ksi	-50 °F

Table 6.1.7.1.3-2: 516-70 Chemical Composition (28)

C	Mn [max]	P [max]	S [max]	Si [max]	Cr [max]	Mo [max]
0.27	1.09	0.010	0.010	0.26	2.20	0.96

6.1.7.2 Mill Test Report (MTR) Properties

No mill test reports were found containing tests of A516 materials used in LPV creation.

6.1.7.3 Fracture Results

There are no internal test results for SA-516.

6.1.8 A302B Plates

6.1.8.1 General Material Information

This section consists of a compilation of relevant material properties for ASTM A302 Grade B, herein after referred to as A302B. A302B is a manganese-molybdenum alloy that was created for welded boilers and other pressure vessels in accordance with ASTM A302 Specification for Pressure Vessel Plates, Alloy Steel, Manganese-Molybdenum and Manganese-Molybdenum-Nickel (33). At the time, there were four standard grades of A302, however A302B is the only one found in the LPV fleet. It should be noted that the A302B specification was discontinued in 1989. A302B was most commonly found in nuclear pressure vessels, where the majority of research data has been obtained. In addition, the LPV program tested A302B material taken from an out-of-service vessel. The results of the NASA investigation can be found in Section 7.2.3.

Most of the data presented in this report comes from U.S. Nuclear Regulatory Commission NUREG reports or other research work sponsored by the U.S. Nuclear Regulatory Commission since several early commercial nuclear plants had pressure vessels constructed of A302B modified steels. A302B steel was used in several of the early commercial nuclear reactors and its fracture toughness was extensively studied after these vessels were built and put in operation. A302B steel was one of the first post-World War II steels that could be heat treated and welded when used in the construction of large-scale pressure vessels. The original A302 Standard did not control nickel and, as time went on, up to 1% nickel (Ni) was added to A302B to improve the fracture properties and to improve hardenability. This version of A302 was termed "A302B modified" and generally contains from 0.2% to 0.7% Ni, leading to a variety of properties.

A302B is generally air-cooled or cooled in a water spray to 500°F or cooler, then tempered in the range of 1225-1275°F for several hours. In most applications, the steel was then stress-relieved for 30 hours or more at a lower temperature of about 1150°F and then furnace cooled to 600°F or lower from which it was air cooled to ambient temperature.

6.1.8.2 Material Specification Properties

A302B is not a proprietary material, therefore the mechanical properties and chemical compositions should be by ASME or ASTM standard. However, in-house adjustments, resulting in "A302B modified" were common and often not fully documented. Therefore, only the base material specification is provided.

6.1.8.2.1 ASME BPVC Materials

6.1.8.2.2 ASTM Specification Properties

Table 6.1.8.2.2-1: ASTM A302 Mechanical Properties (33)

	Yield Stress min (ksi)	Tensile Stress (ksi)	Fracture Elongation in 8 in,min (%)	Fracture Elongation in 2 in,min (%)
Grade B	45	80-100	15	18

Table 6.1.8.2.2-2: ASTM Specification Chemical Composition (33)

	C (max)	Mn	P (max)	S (max)	Si	Mo
Grade B	0.25	1.07-1.62	0.035	0.04	0.13-0.45	0.41-0.64

6.1.8.3 Mill Test Report (MTR) Properties

The available data package reports for current fleet vessels provide the melt slab-specific mechanical properties and chemical compositions listed in Table 6.1.8.3-1 and Table 6.1.8.3-2.

Table 6.1.8.3-1 MTR Mechanical Properties

Melt/Heat	Yield Stress (ksi)	Tensile Stress (ksi)	Elongation (%)
A9149	72	100	28
412992	40	77	30
B4634	74	95	27
84065	78	99	28
151425	51	75	26
011966	68	88	27
011863	66	85	30
011927	69	83	29

Table 6.1.8.3-2: MTR Chemical Compositions

Melt/Heat	Cert Origin	Chemistry (%)							
		C	Mn	P	S	Si	Ni	V	Mo
A9149	Lukens Steel Co	0.22	1.36	0.013	0.016	0.26	0.54	---	0.46
412992	US Steel	0.34	0.78	0.011	0.023	0.22	---	---	---
B4634	Lukens Steel Co	0.19	1.39	0.009	0.016	0.24	0.52	---	0.46
84065	Lukens Steel Co	0.21	1.29	0.01	0.01	0.23	0.53	0.45	---
151425	US Steel	0.19	0.93	0.016	0.029	0.18	---	---	---
011966	US Steel	0.21	1.34	0.019	0.024	0.21	0.62	0.54	---
011863	US Steel	0.19	1.33	0.012	0.021	0.2	0.58	---	0.51
011927	US Steel	0.18	1.26	0.01	0.019	0.2	0.6	---	0.54

6.1.8.4 Fracture Data

The large test program of A302B steel plate properties was conducted by Don McCabe at Oak Ridge National Laboratory (ORNL) and reported extensively in NUREG/CR6426 Ductile Fracture Toughness of Modified A302 Grade B Plate Materials, Data Analysis (34). The results showed that the J-R curves developed using what became the ASTM E1820 test procedure were specimen size independent, at least if the specimens were all scaled compact tension (C(T))

specimens. The test matrix of this program is shown in Table 6.1.8.4-1, the steel chemistries are presented in Table 6.1.8.4-2, and the tensile mechanical properties are presented in Table 6.1.8.4-3. This program resulted in a wealth of upper shelf toughness data for applications using A302B steel as is the case for the present layered pressure vessel study.

Table 6.1.8.4-4 presents NDT and RTNDT results for the seven A302B plates and Charpy V notch test results are presented in Table 6.1.8.4-5. The results showed that there is considerable variability in the seven test plates, but generally the lowest toughness occurred for specimens with the cracks oriented in the L-T orientation.

Since it is difficult to compare J-R curves directly, Figure 6.1.8.4-1 and Figure 6.1.8.4-2 show the measurements taken from each J-R curve and tabulated for comparison. These measurements were then summarized in tables like that of Table 6.1.8.4-4 and Table 6.1.8.4-6 for the subset of test specimens with the T-L oriented crack planes. The McCabe NUREG report included J-R curves for all specimens plus curve fits and additional comparisons. Study of the test results led to the conclusion that there was no size dependence present in the 1/2T to 4T J-R curves measured in this study. The results at the bottom of the table in Table 6.1.8.4-6 show, for comparison, the results of the A.L. Hiser (35) study which did show a distinct trend in toughness with specimen size.

Figure 6.1.8.4-2 shows a typical J-R curve taken from the NUREG/CR6426. In this case the specimen is a 1/2T size specimen from plate Z6A tested at 180°F. Figure 6.1.8.4-3 shows average J-R curves for each of the seven test plates of the McCabe study, as well as an average (in some way that was not explained) specimen from the Hiser study. The material variability over the seven A302B plates was much more pronounced than the specimen geometry dependence with the V50 Hiser plate being by far the lowest toughness plate.

Table 6.1.8.4-7 presents fracture toughness parameters averaged over repeat specimens to demonstrate how the crack plane orientation affects the measured fracture toughness. It is clear that the T-L orientation is the lowest toughness orientation. The L-T and L-S orientations do not show a pattern of consistent relative toughness, with the L-T results sometimes higher in toughness, and sometimes the L-S toughness higher. The McCabe et al. (34) report included hundreds of plots of J-R curves and CTOD-R curves. One example is shown in Figure 6.1.8.4-4 to demonstrate the high quality of the data obtained in this study.

Table 6.1.8.4-1: Fracture Property Study Test Matrix from McCabe et al. (34)

Table 1. Fracture toughness of modified A 302 grade B – test matrix

Specimen size	Plate code	Test temperatures (°F)	Orientation*	Duplicates	Number of specimens per plate
1/2T C(T)	Z1, Z2	180, 400, 550	T-L, L-S	2	12
	Z3	180, 400, 550	T-L, L-S	2	12
	Z4	180, 400, 550	T-L, L-S	2	12
	Z5	180, 400, 550	T-L, L-S	2	12
	Z6A	180, 400, 550	T-L, L-S	2	12
	Z6B	180, 400, 550	T-L, L-S	2	12
	Z7	180, 400, 550	T-L, L-S	2	12
	Z8	180, 400, 550	T-L, L-S	2	12
	Total				
1T C(T)	Z2	180, 400, 550	T-L, L-S	2	12
	Z3	180, 550	T-L, L-S	2	8
	Z5	180, 550	L-T	2	4
	Z6A	180, 550	T-L, L-S	2	8
	Z6B	180, 550	T-L, L-S	2	8
	Z7	180, 400, 550	T-L, L-S	2	12
Total					52
2T C(T)	Z1	550	T-L, L-T	2	4
	Z2	180, 400	T-L, L-S	2	8
	Z3	180, 550	T-L, L-S, L-T	2	8
	Z4	180, 550	T-L, L-S	2	8
	Z5	180, 550	T-L, L-S	2	8
	Z6A	180, 550	T-L, L-S	2	8
	Z6B	550	T-L, L-S, L-T	2	6
	Z7	180, 400, 550	T-L, L-S, L-T	2	16
	Z8	180, 550	T-L, L-S	2	8
Total					74
4T C(T)	Z2	180, 550	T-L	2	2
	Z3	180	T-L	1	1
	Z4	180	T-L	1	1
	Z7	180, 550	T-L, L-T	3	6
	Z8	180	T-L	1	1
Total					11
Charpy	Z1	b	T-L, L-S, L-T	14	42
	Z3	b	T-L, L-S, L-T	15	45
	Z4	b	T-L, L-S	14	28
	Z5	b	T-L, L-S, L-T	14	42
	Z6	b	T-L, L-S, L-T	15	45
	Z7	b	T-L, L-S, L-T	15	45
	Z8	b	T-L, L-S, L-T	14	42
Total					289

*T-L = transverse, L-T = longitudinal, and L-S = short transverse.
 *A full ductile-brittle transition curve to be developed.

Table 6.1.8.4-2: A302B-Modified Chemical Compositions from McCabe et al. (34)

Plate code	Heat	Composition (wt %)												
		C	Mn	P	S	Si	Ni	Cr	Mo	V	Nb	Co	Cu	Al
Z1, Z2	B3990-2	0.18	1.35	0.007	0.011	0.23	0.47	0.11	0.44	0.003	0.004	0.011	0.17	0.03
Z3	A0237-1 ^a	0.24	1.47	0.008	0.014	0.25	0.52	0.11	0.50	0.002	0.003	0.011	0.11	0.026
Z4	C1290-2 ^a	0.22	1.42	0.006	0.013	0.24	0.50	0.11	0.48	0.002	0.003	0.011	0.10	0.027
Z5	P2130-2	0.17	1.16	0.013	0.016	0.17	0.60	0.10	0.50	0.002	0.004	0.012	0.16	0.012
Z6A	C1079-1	0.17	1.35	0.006	0.013	0.23	0.49	0.10	0.45	0.002	0.003	0.012	0.18	0.028
Z6B	B5013-2	0.22	1.39	0.009	0.023	0.20	0.51	0.15	0.48	0.002	0.003	0.017	0.21	0.035
Z7	C2463-1	0.26	1.47	0.008	0.014	0.15	0.53	0.09	0.52	0.002	0.003	0.011	0.16	0.017
Z8	C2220-2	0.27	1.49	0.006	0.015	0.23	0.68	0.12	0.45	0.002	0.003	0.012	0.16	0.016

^aThere was some uncertainty in heat identifications. Values were determined by ABB-Combustion Engineering.

Table 6.1.8.4-3: Modified Tensile Properties from McCabe et al. (34)

Table 3. Tensile properties for seven heats of modified A 302 grade B (Z1-Z7) and one vintage heat of A 533 grade B material (Z8)

Plate code	Test temperature (°F)	Yield strength* (ksi)			Ultimate strength* (ksi)			Elongation (%)		
		T	L	S _T	T	L	S _T	T	L	S _T
Z1	75	65.2	64.0	64.2	84.5	84.7	80.1	25.5	25.0	13.5
	180	62.4	64.2	58.1	80.7	80.8	79.0	22.5	23.0	17, 7 ^b
	400	57.0	58.8	57.7	79.3	79.7	72.2	21.0	21.5	15, 8 ^b
	550	60.3	60.1	58.9	84.8	84.0	57.0	24.5	24.0	8
Z3	75	67.9	67.8	67.0	89.7	90.0	89.3	23.0	27.5	16.5
	180	64.8	64.4	64.0	85.2	85.2	84.7	21.5	23.5	15.0
	400	59.8	59.5	52.9	84.9	84.2	80.5	20.5	23.0	11.0
	550	61.7	61.0	62.2	88.2	89.0	88.3	25.0	25.5	15.0
Z4	75	67.8	68.1	66.5	89.2	89.8	88.2	25.0	24.5	21.5
	180	63.8	64.4	63.5	83.9	84.7	83.6	22.5	23.5	20.5
	400	60.3	c	c	83.3	c	c	22.0	c	c
	550	61.2	61.0	60.4	88.0	87.9	87.1	24.0	26.0	20.0
Z5	75	58.1		55.2	78.1		72.0	24.5		17.5
	180	55.6		52.8	74.4		68.6	22.4		13.5
	400	53.8		49.0	75.8		68.5	21.5		13.0
	550	54.2		49.6	79.8		74.1	23.4		11.5
Z6A	75	61.8	63.7	57.6	81.0	82.4	62.5	28.5	28.0	7.5
	180	57.9	59.1	58.4	70.8	77.0	61.5	16.0	25.0	4.5
	400	55.0	55.6	55.7	76.2	75.8	74.9	21.0	23.5	12.5
	550	55.8	57.7	57.5	81.2	84.0	76.8	21.5	22.0	12.0
Z6B	75	64.9	68.8	62.6	86.3	89.1	77.9	24.5	28.0	9.5
	180	64.5	63.2	61.0	83.6	82.3	78.0	20.5	24.0	11.0
	400	59.3	59.8	57.5	83.7	83.4	69.0	20.5	22.5	4.5
	550	60.7	61.5	60.7	86.2	87.2	64.7	21.5	24.0	5.0
Z7	75	68.5	69.1	68.2	91.7	92.5	92.2	24.5	23.5	17.5
	180	65.5	66.7	66.7	86.7	87.7	87.7	22.5	23.5	17.0
	400	60.1	60.3	61.4	85.6	86.0	86.2	21.5	22.5	13.0
	550	62.3	63.6	62.3	90.0	91.3	90.6	23.4	26.0	11.5
Z8	75	61.9	63.1	61.6	88.2	88.9	87.2	23.5	26.0	17.5
	180	59.8	59.2	58.4	83.4	82.5	81.5	22.5	24.0	17.0
	400	56.7	54.7	55.8	82.7	80.2	80.0	21.0	23.0	14.5
	550	58.0	57.4	54.6	88.2	87.2	84.6	22.5	26.5	11.5

*MPa = (ksi) × 6.894.
^bUnaveraged values.
^cOmitted because of questionable results.

Table 6.1.8.4-4 shows T-L Orientation Reference temperature results for the seven A302B steel plates in the weaker T-L crack plane orientation

Table 6.1.8.4-4: Tabulated A302B Reference Temperature Results from McCabe et al. (34)

Plate code	NDT ^a temperature		Charpy properties at NDT ^a + 60°F, T-L (transverse) orientation				RT _{NDT} ^b	
			Energy		Lateral expansion			
	(°F)	(°C)	(ft-lb)	(J)	(in.)	(mm)	(°F)	(°C)
Z1, Z2	-5	-20	93	127	0.063	1.6	-5	-20
Z3	-15	-26	60	82	0.046	1.2	-15	-26
Z4	-15	-26	64	88	0.058	1.5	-15	-26
Z5	-30	-34	56	77	0.048	1.2	-30	-34
Z6A	-30	-34	65	89	0.052	1.3	-30	-34
Z6B	-30	-34	38	52	0.034	0.9	13 ^c	-10
Z7	-15	-26	64	88	0.056	1.4	-15	-26
Z8	-20	-29	33	45	0.038	1.0	24 ^c	-4

^aNDT = nil-ductility-transition temperature.
^bRT_{NDT} = reference nil-ductility-transition temperature.
^cDetermined from Charpy V-notch 50-ft-lb (lower-bound) temperature - 60°F.

Table 6.1.8.4-5: A302B Charpy Toughness Results from McCabe et al. (34)

Plate code	Orientation ^a	Temperature, °F (°C)			RT _{NDT} ^b		Upper-shelf energy	
		30 ft-lb	50 ft-lb	50% shear	(°F)	(°C)	(ft-lb)	(J)
Z1, Z2	T-L	-33 (-36)	-4 (-20)	25 (-4)	-5	-20	126	173
	L-T	-45 (-43)	-20 (-29)	10 (-12)			160	219
	L-S	-19 (-28)	8 (-13)	30 (-1)			171	234
Z3	T-L	0 (-18)	33 (0)	35 (2)	-15	-26	85	116
	L-T	-37 (-38)	-9 (-23)	25 (-4)			129	177
	L-S	-16 (-27)	21 (-6)	55 (13)			127	174
Z4	T-L	-38 (-39)	11 (-12)	30 (-1)	-15	-26	111	152
	L-S	-56 (-49)	-17 (-27)	35 (2)			130	178
Z5	T-L	-19 (-28)	18 (-8)	20 (-7)	-30	-34	95	130
	L-T	-30 (-34)	-2 (-19)	25 (-4)			153	209
	L-S	-59 (-50)	-41 (-40)	-1 (-23)			171	234
Z6A	T-L	-17 (-27)	11 (-12)	40 (4.4)	-30	-34	113	155
	L-T	-28 (-33)	-2 (-19)	25 (-4)			129	177
	L-S	-41 (-40)	-10 (-23)	35 (2)			130	178
Z6B	T-L	11 (-12)	60 (16)	40 (4.4)	13	-10	64	88
	L-T	-33 (-36)	-1 (-18)	5 (-15)			117	160
	L-S	-32 (-36)	-5 (-20)	10 (-12)			114	156
Z7	T-L	-21 (-29)	19 (-7)	5 (-15)	-15	-26	96	131
	L-T	-45 (-43)	-12 (-24)	10 (-12)			126	173
	L-S	-50 (-46)	-20 (-29)	0 (-18)			120	164
Z8	T-L	27 (-3)	72 (22)	30 (-1)	24	-4.4	96	131
	L-T	25 (-4)	48 (9)	65 (18)			134	184
	L-S	-5 (-20)	29 (-2)	55 (13)			154	211

^aT-L = transverse, L-T = longitudinal, and L-S = short transverse.
^bRT_{NDT} = reference nil-ductility-transition temperature.

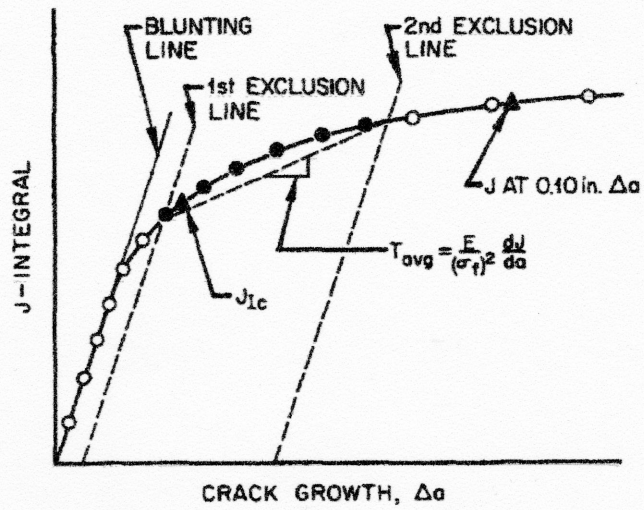


Figure 4. Schematic of J-R curve plot and measurements taken. Filled data points represent the points used in the power law curve fit.

Figure 6.1.8.4-1: J-Integral Versus Crack Growth from McCabe et al (34)

Test results in Table 6.1.8.4-6 show that the fracture tests in the T-L orientation did not demonstrate any specimen size effects.

Table 6.1.8.4-6: T-L Orientation Fracture Test Results from McCabe et al. (34)

Table 6. Evaluation of specimen size on J-R curves of modified A 302 grade B steel [averaged values; T-L (transverse) orientation and 180°F (82°C); all specimens 20% side grooved]

Plate code	Size (T)	T ^a	J _{0.1} ^b (in.-lb/in. ²)	J _c ^c (in.-lb/in. ²)
Z1, Z2	1/2	115	3200	1330
	1	130	3410	1360
	2	120	4030	2050
	4	75	2990	1590
Z3	1/2	85	2615	1230
	1	80	2515	1175
	2	115	3055	1095
	4	95	2755	1310
Z4	1/2	105	3050	1360
	2	95	3200	1600
	4	95	2840	1200
Z5	1/2	55	1655	815
	2	50	1825	1080
Z6A	1/2	80	2370	905
	1	85	2535	1065
	2	55	2070	1075
Z6B	1/2	50	1470	715
	1	45	1505	785
	2	35	1430	930
Z7	1/2	80	2600	1290
	1	95	2995	1210
	2	100	3325	1685
	4	125	3120	1270
Z8	1/2	95	2770	1290
	2	85	2525	1160
	4	70	2800	1740
MEA^d report on plate V50				
p. 58	1/2	36	1293	600
p. 61	1	36	1129	659
p. 66	2	20.4	863	653
p. 70	4	14.3	704	543
p. 74	6	19.4	686	500
^a T = E/σ _r ² (dJ/da) _r . ^b J at 0.1 in. of slow-stable crack growth. ^c J after 0.008 in. of slow-stable crack growth. ^d MEA = Materials Engineering Associates, Lanham, Maryland.				

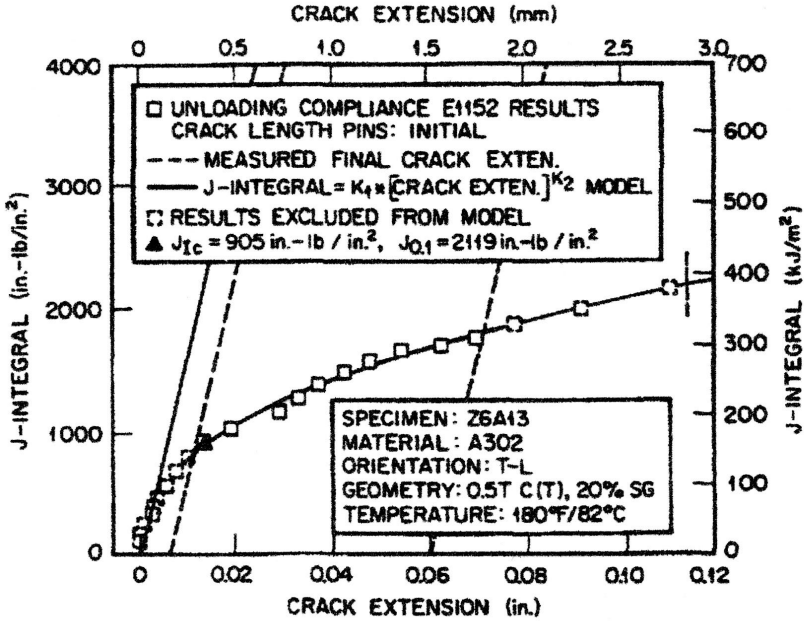


Figure 6.1.8.4-2: Typical J-R Curve for A302B from McCabe et al. (34)

Figure 6.1.8.4-3 shows the average J-R curves for each plate and the material variability present in the seven A302B plates tested by McCabe et al. (14), the Hiser V50 plate, and a "vintage" ASTM A533 Specification for Pressure Vessel Plates, Alloy Steel, Quenched and Tempered, Manganese-Molybdenum and Manganese-Molybdenum-Nickel (36) plate.

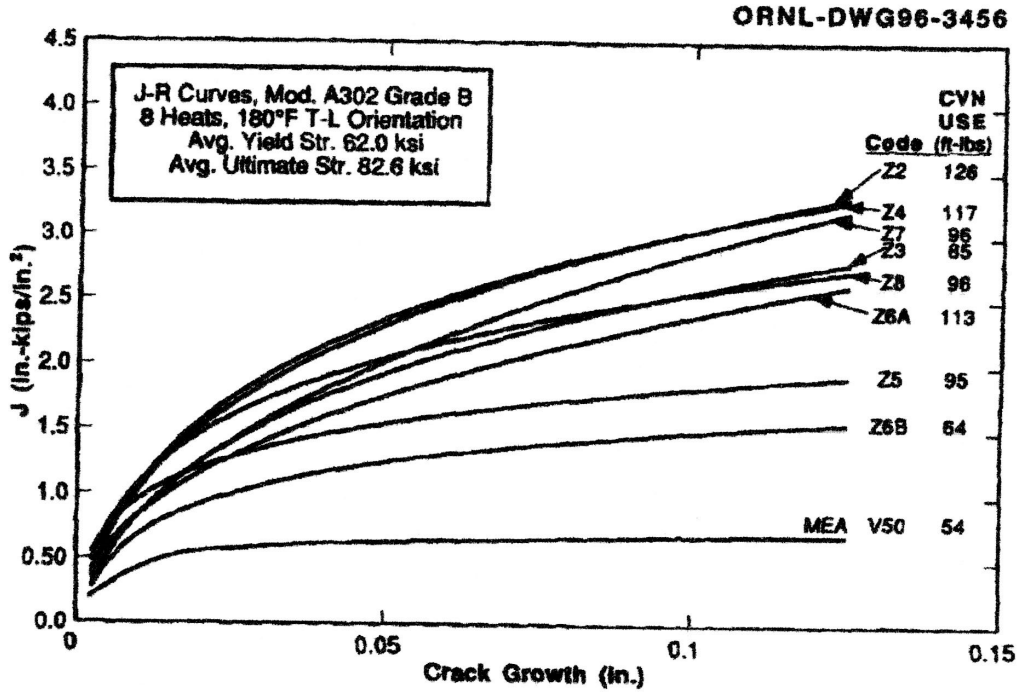


Figure 6.1.8.4-3: J-R Results from McCabe et al. (34)

Table 6.1.8.4-7 shows the effect of crack plane orientation on the measured fracture parameters. The T-L crack plane orientation generally has lower fracture toughness when measured using a J-R curve.

Table 6.1.8.4-7: Tabulated Averaged Results from McCabe et al. (34)

Plate code	Orientation*	Charpy V-notch upper-shelf energy (ft-lb)	T slope	J _{0.2} ^b (in./lb/in. ²)	J _{0.6} ^b (in./lb/in. ²)	Fitting curves	J = A · Δa ^B · exp (C/Δa ^{1/2})		
							A	B	C
Z1, Z2	T-L	126	120	3300	1350	Z2B2-1T	7.110	0.287	-0.0596
	L-T	160	130	3810	1360	Z2B16-1T	9.513	0.300	-0.0761
	L-S	171	130	3480	1570	Z2B2-1/2T	8.715	0.259	-0.0846
Z3	T-L	85	90	2730	1200	Z310-1/2T	6.030	0.275	-0.0699
	L-T	129							
	L-S	127	70	2000	870	Z34-1/2T	5.633	0.435	-0.0014
Z4	T-L	111	100	3060	1420	Z49-1/2T	6.517	0.226	-0.0368
	L-S	130	130	4080	1880	Z47-2T	13.333	0.446	-0.0246
Z5	T-L	95	45	1630	1075	Z55-2T	3.043	0.177	-0.0329
	L-T	153	90	2640	1225	Z51-1T	6.178	0.318	-0.0348
	L-S	171	160	3895	1195	Z57-1/2T	15.718	0.567	-0.0199
Z6A	T-L	113	75	2325	1040	Z6A8-1T	6.377	0.410	-0.0131
	L-T	129	115	3570	1570	Z6A1-1T	12.299	0.518	-0.0114
	L-S	130	120	3550	1620	Z6A3-1/2T	8.542	0.267	-0.0752
Z6B	T-L	64	45	1470	810	Z6B9-1/2T	2.407	0.100	-0.0790
	L-T	117	70	2360	1130	Z6B1-1T	5.193	0.341	-0.0140
	L-S	114	85	2730	1183	Z6B8-1/2T	1.340	0.079	-0.0235
Z7	T-L	96	95	3000	1250	Z711-1T	8.742	0.446	-0.0279
	L-T	126	140	4500	2120	Z78-1T	12.057	0.383	-0.0501
	L-S	120	145	4405	2045	Z71-1/2T	10.637	0.326	-0.0780
Z8	T-L	96	85	2715	1245	Z83-1/2T	4.963	0.218	-0.0514
	L-T	134							
	L-S	154	145	4190	1860	Z816-1/2T	12.594	0.378	-0.0566

*T-L = transverse, L-T = longitudinal, and L-S = short transverse.
^bTo obtain J in units of kPa-m, multiply by 0.175.

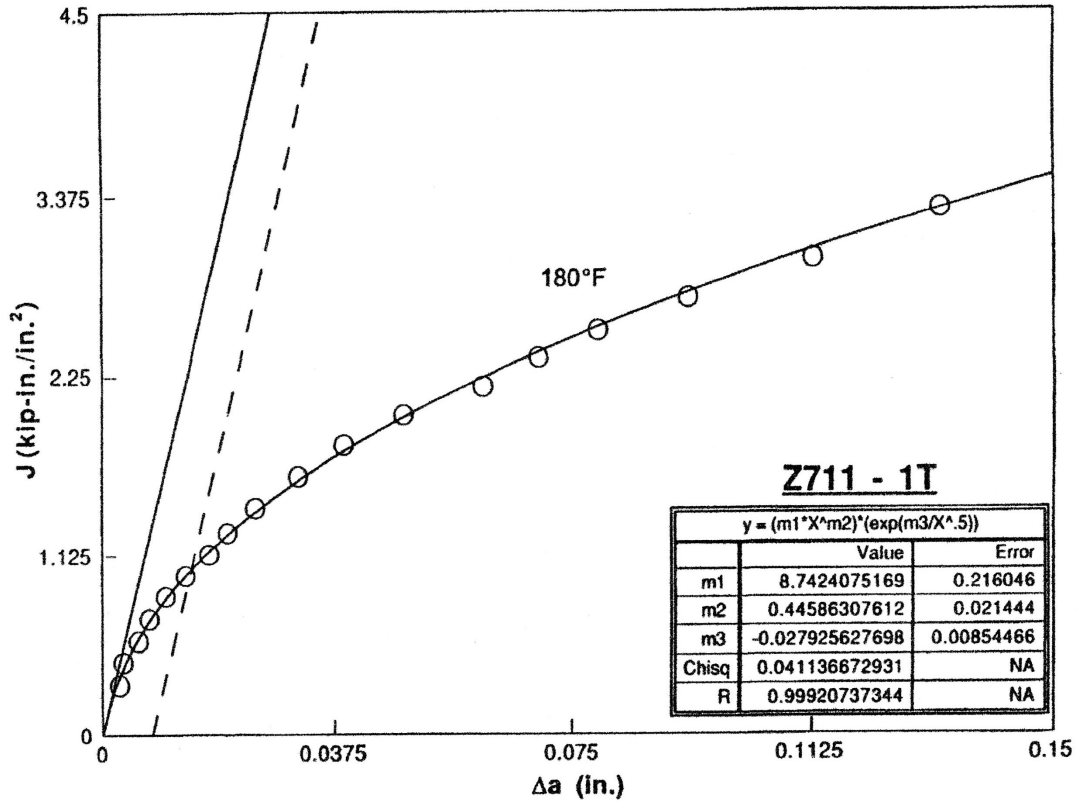


Figure 6.1.8.4-4: Typical Analysis Plot from McCabe et al. (34)

Besides defining the upper shelf toughness, it is important to identify the temperature of the ductile-brittle transition of the A302B steel since it is a ferritic pressure vessel steel developed generally for elevated temperature applications. In LPV application at NASA research facilities, the LPVs operate at ambient temperature which can sometimes be well below 0°C. Most data characterizing the ductile-brittle transition temperature for A302B steels are available as Charpy impact test results, as shown in Figure 6.1.8.4-5. To quantify this data set, the intersection of the "French Curve" fit and a convenient toughness level, like 20 ft-lb (28 Joules) or 30 ft-lb (41 Joules) was taken as the transition temperature. In this example taken from Hiser (35), the 30 ft-lb transition temperature would be approximately 0°C while the 20 foot-pound transition temperature would be -10°C.

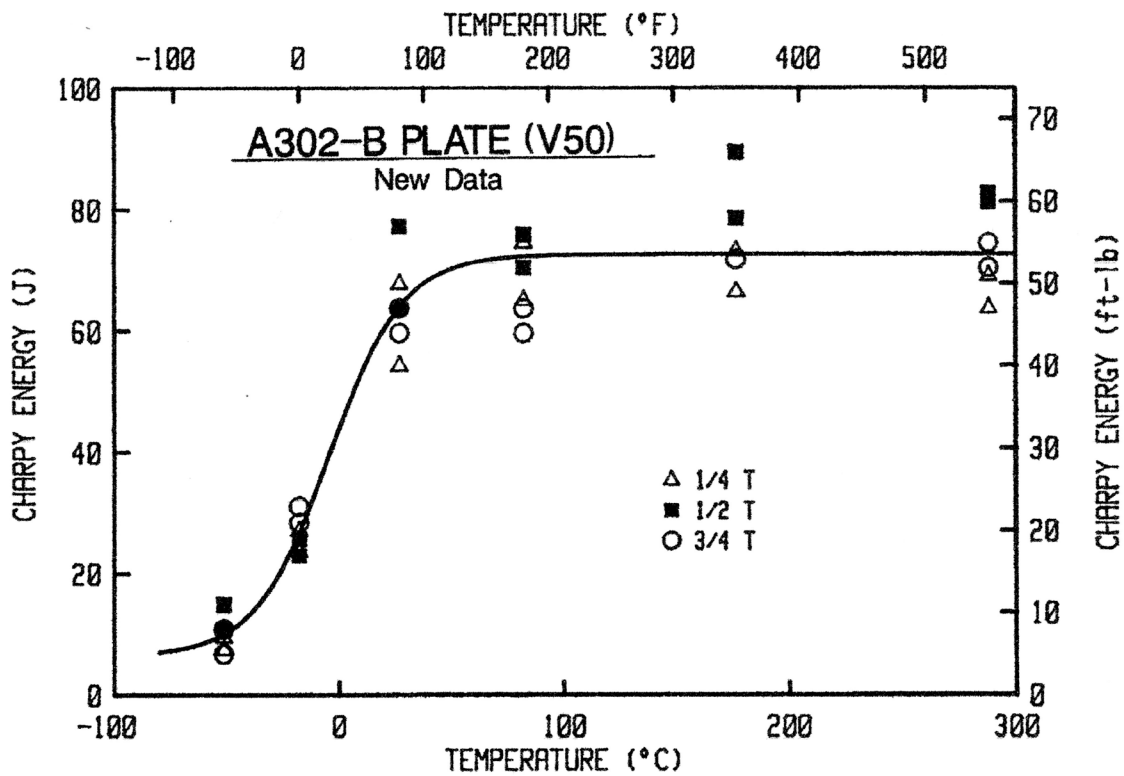


Figure 6.1.8.4-5: Charpy Ductile-Brittle Characterization Plot for A302B Steel (34)

Searching for more recent data utilizing the ASTM E1921 T_0 reference temperature does not result in many hits. At present, only three such data sets seem to be reported in the literature. One example is the data set reported by R. Chaouadi et al. (37) and two other examples are reported in ASTM Manual 52 (38). The Chaouadi result is $T_0 = -61^\circ\text{C}$ and corresponds to tests samples removed from an A302B modified steel vessel of the decommissioned ORNL research reactor BR3 that had been irradiated and then "wet annealed" at 343°C (650°F) for a week. Hence, the history and heat treatment were not typical of standard A302B as shipped by the original vendor, and the low T_0 result here has to be considered a data point corresponding to an annealed A302B modified steel. The reported tensile properties of 58 ksi for the yield stress and 90 ksi for the ultimate strength are typical of A302B steel. The nickel content of 0.47% in the sample is consistent with the modified version of A302B steel, which is now considered to be A302 Grade C.

The two T_0 results that were reported in the ASTM Manual 52 were widely divergent with one being $T_0 = -87^\circ\text{C}$ and the other being $T_0 = 69^\circ\text{C}$. The first result corresponds to the plate Z7 which was part of the McCabe A302B study reported in reference (34). The Z7 plate was the second toughest plate in terms of the J-R curve, though the J_{IC} was average. The material with the high T_0 reported in the second case was referred to as normalized A302B in the Manual 52, but no clear information was provided on the heat treatment process and the

data set was referred to as unpublished ORNL data. The following information summary is provided regarding common heat treatments applied to A302B steel.

Plates between 2 inches and 4 inches in thickness are normalized. This means that they are air cooled from the austenitizing temperature and subsequently tempered in the range of 1100-1300°F (595-705°C). The example above with the high value of $T_0 = 69^\circ\text{C}$ was apparently normalized but not subsequently tempered. The Z7 plate was one of seven heats of modified A302B plate that were donated to the McCabe investigation by General Electric Company of San Jose, California. All were archival materials that were being saved for possible future tests, as needed, for fracture toughness verification purposes. It is highly likely that these plates were all normalized and then tempered and stress relieved, though the details of the process used are unknown.

The wide range in T_0 shown by A302B steel is reminiscent of results reported earlier by Pellini and Puzak (39) which are reproduced here in Figure 6.1.8.4-6. Wide differences in NDT toughness are related to additional alloy content of the A302B steel and to the cooling rate of the plates and the resulting grain size present. It is not clear at present how to compare the NDT toughness to the E1921 reference temperature. The wide range of NDT shown is clearly due to various heat treatments that were applied to the A302B steel. The normal process is to use more rapidly quenched procedures with subsequent tempering and stress relief processes. The key observation to make from this plot is that A302 has a higher transition temperature than A212 steel. This is consistent with results presented later in this report.

Figure 6.1.8.4-6 is a schematic showing the wide measured range of NDT toughness.

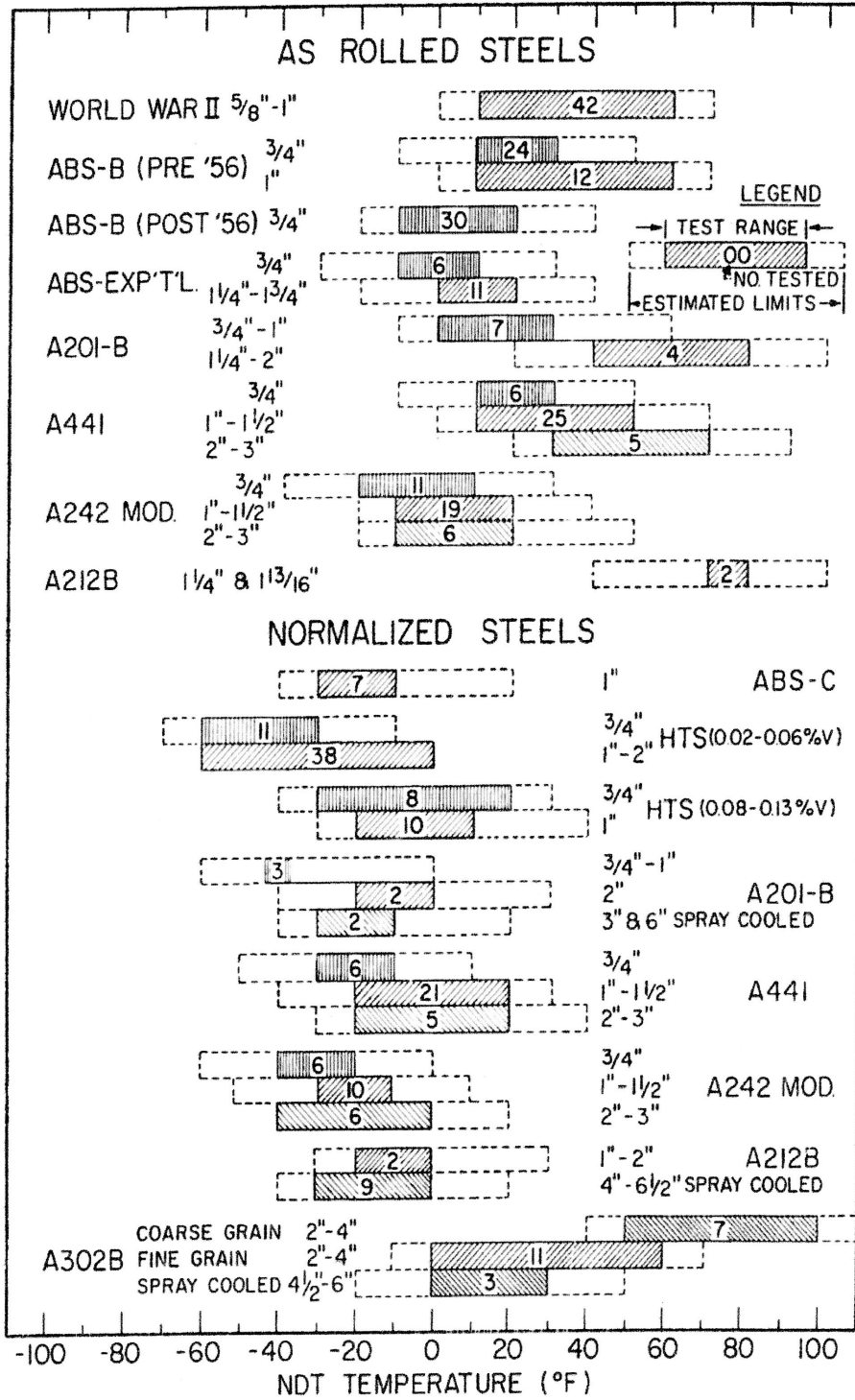


Figure 6.1.8.4-6: NDT Toughness Reported by Pellini and Puzak (39)

Charpy transition data for A302B modified steel has been developed by the commercial nuclear power industry and is available in the literature. Much of this data comes from the surveillance program that has measured the shift in the ductile-brittle transition temperature as a function of neutron fluence which is an important concern for the continued operation of nuclear power plants. Of value for this program is the baseline data that reports the Charpy 30 ft-lb transition temperature as shown in Figure 6.1.8.4-5. The largest assembly of this data is in the NUREG/CR6413 report of J.A. Wang (40) which gives Charpy transition results from all nuclear plants that have A302B steel in their pressure vessels. Also included are data from the McCabe report (34) on the seven A302B modified steels tested there and three data sets from Stofanak et al. (41). Considerable scatter is present in these results. Frequency plots are constructed and presented in Figure 6.1.8.4-6 and Figure 6.1.8.4-7 showing the frequency of the Charpy transition measurements as a function of temperature.

More data are available for the tougher L-T orientation since the major concern was for the center beltline region of the cylindrical section of the pressure vessels where the neutron fluence was most intense and the hoop stress was dominant. In most instances, these vessels were manufactured with the longitudinal plate rolling direction perpendicular to the hoop stress such that the L-T crack orientation was perpendicular to the hoop stress and was hence of primary concern. A comparison of Figure 6.1.8.4-6 and Figure 6.1.8.4-7 shows that the transition temperature defined by the Charpy test was about 20°F higher in the T-L orientation than in the L-T orientation. The L-T orientation average transition temperature was -11°F while the T-L orientation average was 10°F. The broad distribution of the Charpy transition temperatures in Figure 6.1.8.4-6 and Figure 6.1.8.4-7 is possibly due to the rather loose nature of the ASTM A302 standard and to variations in the heat treatments applied to the A302B steel plates.

Figure 6.1.8.4-7 shows absorbed energy for A302B steels with the crack plane oriented in the L-T orientation.

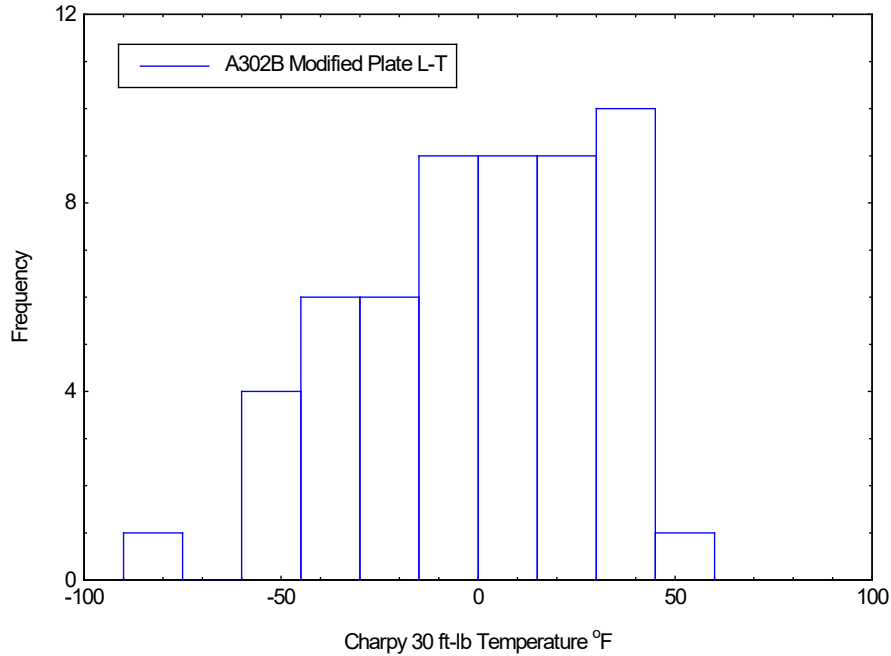


Figure 6.1.8.4-7: L-T Charpy V Transition Temperatures at 30 ft-lb

Charpy transition data are based on small, fixed-size three point notched bend specimens tested at an elevated impact speed to estimate the transition temperature applicable to a much larger surface cracked pressure vessel loaded statically, predominantly in tension. The transferability of the laboratory data to the pressure vessel application is somewhat of a reach. More recently, ASTM proposed a fracture mechanics based approach in standard E1921 which uses a statically loaded, pre-cracked specimen that is generally much larger than the Charpy specimen to predict a transition curve called a Master Curve and an associated reference temperature, T_0 . Size transferability is also possible using statistical methods with the E1921 approach providing the transition temperature for a one inch thick C(T) geometry which can, in theory, be related to pressure vessel flaws using constraint based methods.

Testing in the LPV Program has been conducted according to E1921, and it is desirable to relate the Charpy transition data to the E1921 T_0 reference temperature. The commercial nuclear research programs have again suggested correlations between the Charpy transition temperatures and T_0 . The original correlation by Wallin (42) is shown in Figure 6.1.8.4-8. This data set includes a large number of pressure vessel steels and also weld data, HAZ data, and results from irradiated surveillance specimens. The relationship found was a simple linear equation with an offset between T_0 and T_{28J} of -18°C in Figure 6.1.8.4-9.

Figure 6.1.8.4-8 contains measurements showing a linear relationship for pressure vessel steels.

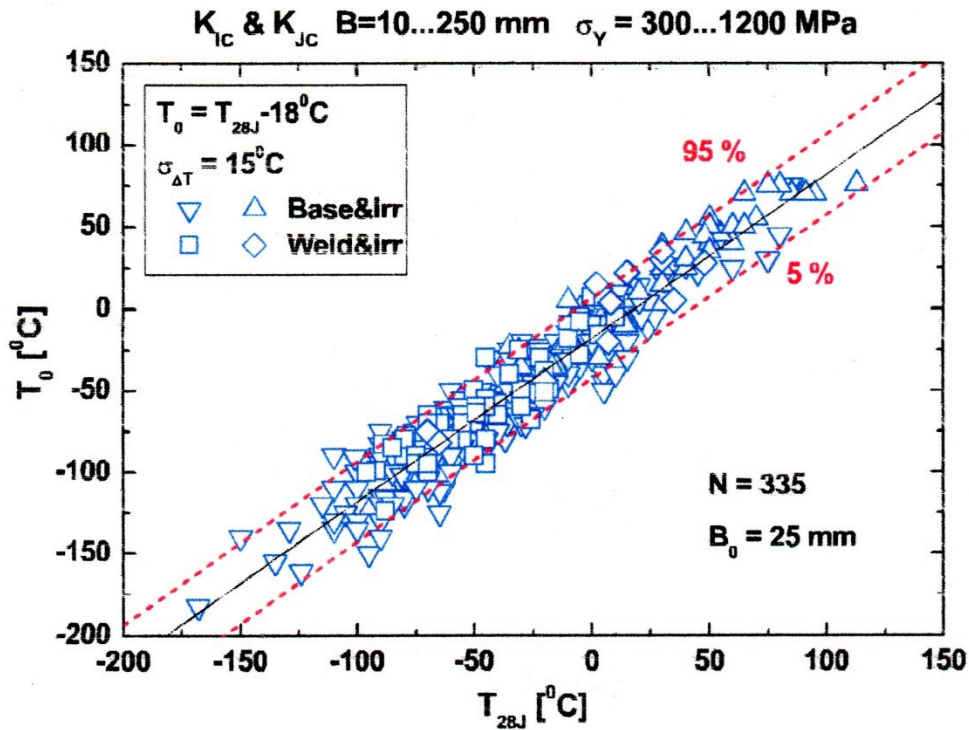


Figure 6.1.8.4-8: T_0 Versus 20 ft-lb (28J) Charpy Transition from Wallin (42)

The Charpy transition number that was used here was for a 20 ft-lb or 28 Joule energy level rather than the more universal 30 ft-lb energy level. A revised correlation using 30 ft-lb Charpy transition data was proposed by M. Sokolov and R.K. Nanstad of ORNL (43) as shown in Figure 6.1.8.4-9. A linear correlation still works though the offset increases from -18°C to -24°C and the standard deviation increases somewhat.

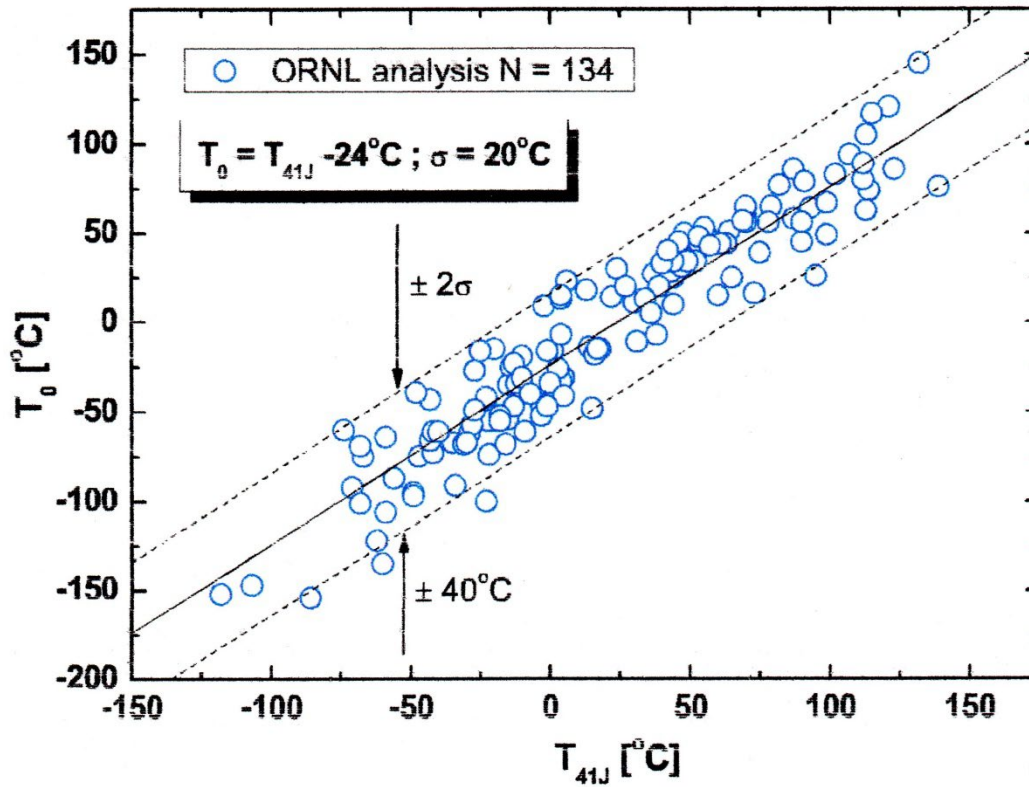


Figure 6.1.8.4-9: Revised T_0 Versus 30 ft-lb Charpy Correlation from Sokolov and Nanstad (43)

Returning to the ASTM Manual 52 and setting $T_0 = 69^\circ\text{C}$ for the normalized A302B steel, the correlation would result in a $T_{41J} = 93^\circ\text{C}$ or 199°F , which is outside the range of Figure 6.1.8.4-10 and shows clearly that it is proper to ignore this result. As discussed below, the data in Figure 6.1.8.4-11 above $T_0 = 0^\circ\text{C}$ corresponds to irradiated steel data which can be ignored as well for the LPV study.

The main issue with this result for the purpose of the LPV study is that it includes a large amount of irradiated steel data without indicating which are unirradiated and which are irradiated. A more recent study by Iradj Sattari-Far and Kim Wallin (44) separates the irradiated and unirradiated data sets as shown in Figure 6.1.8.4-11. This data is also restricted to A302B, A508B, and A533B steels, welds, and HAZ though it does not make clear which individual data points are A302B steel. The correlation's proposed equation is essentially the same as the ORNL relationship with an offset of -26°C . It is definitely of interest here to observe that the unirradiated data appears capped at a T_0 of approximately -10°C (14°F) when only unirradiated data is considered while Charpy transition data for the irradiated case extends as high as 80°C or 176°F , which is the largest value of T_{41J} for an unirradiated data set that is shown in Figure 6.1.8.4-11. In other words, while the Charpy transition number of 80°C would predict a T_0 of

54°C if the correlation that $T_0 = T_{41J} - 26^\circ\text{C}$ was used, no value of T_0 was in fact observed for any of the three steels making up Figure 6.1.8.4-10 that exceeded -10°C . The measured value for $T_{0\text{EST}} = -15^\circ\text{C}$ in Figure 6.1.8.4-9. It is likely that some of the highest T_0 values in Figure 6.1.8.4-9 correspond to A302B steel.

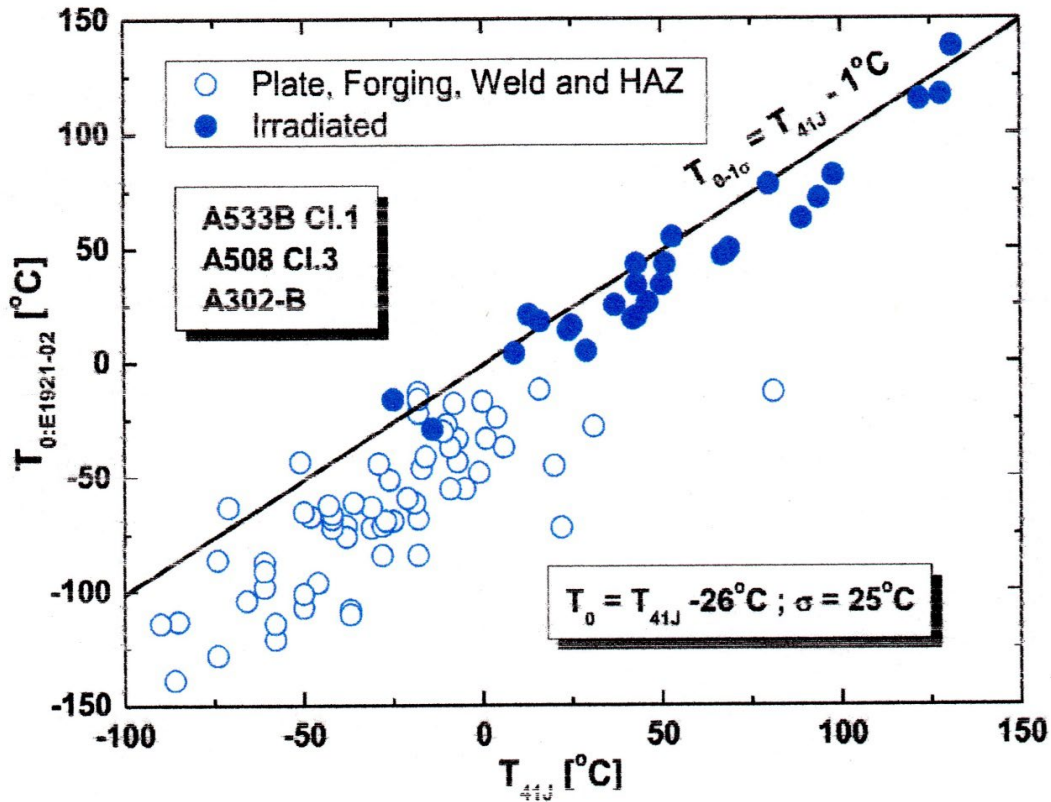


Figure 6.1.8.4-10: T_0 Versus 30 ft-lb Charpy Correlation from Sattari-Far and Wallin (44)

The correlation equation of Figure 6.1.8.4-10 can easily be applied to the frequency plots in Figure 6.1.8.4-6 and Figure 6.1.8.4-7 to give the T_0 frequency plots shown in Figure 6.1.8.4-11 and Figure 6.1.8.4-12. These results show that the T_0 for A302B obtained using the linear correlation equation is at maximum about 0°C with the highest results corresponding to the T-L crack plane orientation.

Figure 6.1.8.4-11 shows an L-T frequency plot for T_0 estimated from the 30 ft-lb/ T_{41J} plot shown in Figure 6.1.8.4-9.

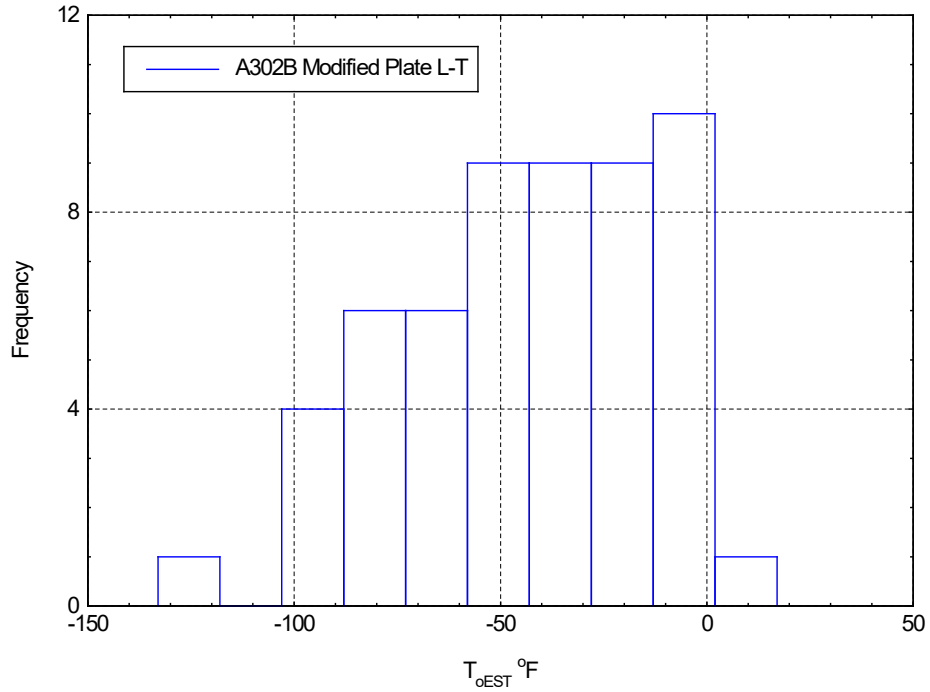


Figure 6.1.8.4-11: Proposed Linear Correlation Frequency Results for A302 L-T

Figure 6.1.8.4-12 contains an A302 T-L frequency plot for T_0 estimated from the 30 ft-lb/ $T_{4.1}$ Charpy transition data plot shown in Figure 6.1.8.4-9 using a proposed linear correlation function.

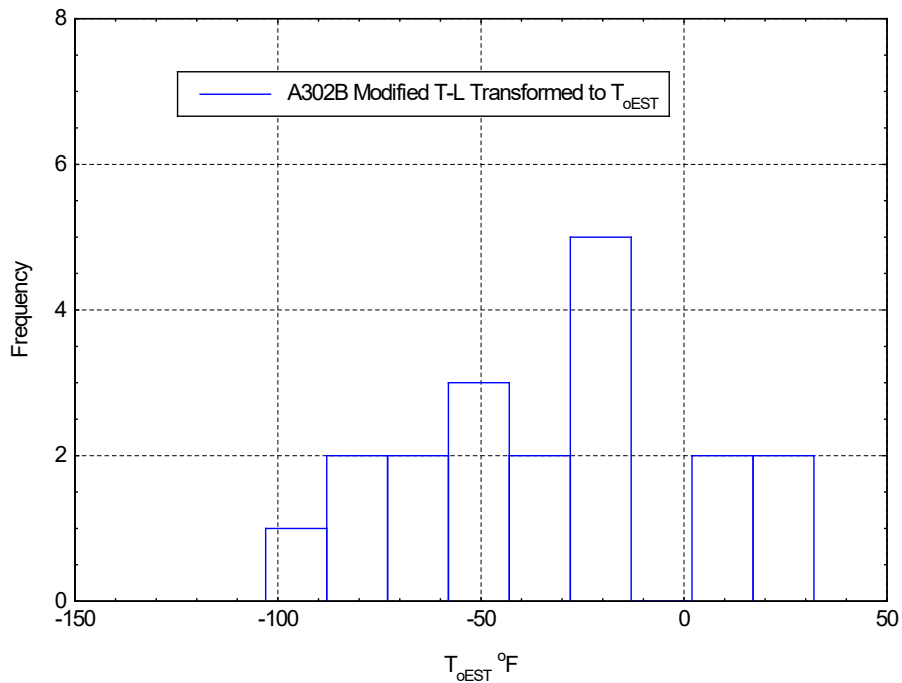


Figure 6.1.8.4-12: Proposed Linear Correlation Frequency Results for A302 T-L

In summary, the upper shelf toughness as characterized by the ASTM E1820 J_{IC} and J at 0.1 inch of crack extension was investigated by McCabe et al. (34) on seven prototypical A302B modified plates provided by the General Electric Company. The results show a relatively high toughness compared to other steels studied in the present LPV program, but also high variability for steels that were heat-treated similarly. Only three T_0 values were located in this study and only one of these, obtained from the Z7 General Electric plate, can be assured to have a standard quench and temper heat treatment. One very high result from McCabe in the ASTM Manual 52 was normalized only, meaning quenched and not tempered, and is thus not comparable to the T_0 values one would expect for a structural plate. The third value from Chaouadi et al. (37) was obtained from an annealed research reactor vessel with a high neutron fluence history.

A large number of Charpy test ductile-brittle transition temperature measurements are available from surveillance programs used by the U.S. Nuclear Regulatory Commission to assure the safety of commercial power plant pressure vessels. These results have been assembled in this report in frequency plots. These plots show Charpy transitions defined by the 30 ft-lb (41 Joules) toughness level extend as high as 75°F in the T-L crack plane orientation. Linear correlations have been proposed to relate the Charpy transitions to the more modern T_0 quantity. These correlations essentially shift the Charpy transition numbers leftward by 24-26°C or 43-47°F. Applying this shift results then in the estimated T_0 values from the Charpy data of around 0°C or 30°F.

Looking more closely at the Charpy test to T_0 correlation data for unirradiated A302B, A508B, and A533B steels, the T_0 values appear to be capped at -10°C with higher Charpy 30 ft-lb transition measurements observed, but apparently not corresponding to higher T_0 . The correlation data beyond a T_0 of about -10°C is all from irradiated specimens and should not be the basis of T_0 estimations. However, because irradiation degrades toughness, unless actual test data is obtained for a target vessel containing A302B material, this estimate can be considered a worst-case value.

6.2 Non-Code Materials with Reference Literature

6.2.1 AO Smith 1148B

6.2.1.1 General Material Information

1148B is a proprietary material manufactured by A.O. Smith that was subsequently and exclusively manufactured by Chicago Bridge and Iron (CB&I) in the 1960s (45). A.O. Smith (AOS) was acquired by CB&I around the same time that many of the NASA LPVs were manufactured (45). This is relevant because when CB&I acquired AO Smith in 1963, they continued making the

1148 material, but modified the original specification by increasing the required mechanical properties and changing the number designation.

6.2.1.2 Material Specification Properties

Table 6.2.1.2-1: Material Specification Equivalents (46)

A.O. Smith Spec.	CBI Standard No.	ASTM
1148B	626-48-2 (High Strength Low-Alloy Steel Plates 1148)	ASTM-A225 Gr. B (Modified)

Physical properties for plate thicknesses ranging from 0.180 inches through 0.580 inches outlined per CB&I's Standard 626-48-2 are shown in Table 6.2.1.2-2 and Table 6.2.1.2-3.

Table 6.2.1.2-2: Manufacturer Specification Mechanical Properties (46)

Thickness Range [in.]	Yield [ksi]	Tensile [ksi]	Elongation % [2 in.]
0.180 thru 0.375	62	82-107	20.0% min.
0.375 thru 0.580	60	80-105	20.0% min.

Table 6.2.1.2-3: Manufacturer Specification Chemical Composition (46)

C [max]	Mn [max]	P [max]	S [max]	Si	V
0.21	1.5	0.04	0.05	0.15-0.30	0.10-0.15

According to documented correspondence between the NASA LPV Team and AO Smith, 1148B is a modified ASTM 225 Grade B steel (47). According to the ASTM standard for A225, the material properties and chemical composition of the original material that the 1148 is derived from are listed in Table 6.2.1.2-4 and Table 6.2.1.2-5 (47):

Table 6.2.1.2-4: ASTM A225 (Parent) Mechanical Properties (47)

Material	Yield [ksi]	Tensile [ksi]	Elongation % [2 in.]
ASTM A225 (Grade B)	43	75-90	20.0% min.

Table 6.2.1.2-5: ASTM A225 (Parent) Chemical Composition (47)

C [max]	Mn [max]	P [max]	S [max]	Si*	V*
0.2	1.45	0.035	0.04	0.13-0.32	0.09-0.14
*Check analysis composition					

6.2.1.3 Mill Test Report (MTR) Properties

Available data package reports for some current fleet vessels provide the melt slab-specific mechanical properties and chemical compositions listed in Table 6.2.1.3-1 and Table 6.2.1.3-2.

Table 6.2.1.3-1: MTR Mechanical Properties (48)

Melt Slab / Serial No.	Type	Yield [ksi]	Tensile [ksi]	Elongation
198847	Inner Shell	70.65	92.56	35%
198847	Shell Layers	75	93.55	20%

Table 6.2.1.3-2: MTR Chemical Compositions (48)

Melt Slab	C	Mn	P	S	Si	V
198847	0.17	1.34	0.018	0.026	0.27	0.12

6.2.1.4 Fracture Data

No fracture data was found for 1148B.

6.2.2 AO Smith 1135

6.2.2.1 General Material Properties

VMS-W135G (also known as 1135G) is a proprietary steel used by A.O. Smith. Official correspondence with A.O. Smith Corporation personnel equates 1135 with ASTM A212B modified steel. The ASTM specification A-212B Modified was replaced with what is now A-516-70. The governing material standard specification is ASTM A516/A516M-90 *Standard Specification for Pressure Vessel Plates, Carbon Steel, High Strength, for Moderate and Lower Temperature Service*.

6.2.2.2 Material Specification Properties

The manufacturer’s material specification and mechanical and chemical requirements are included in Table 6.2.2.2-1 and Table 6.2.2.2-2. These are obtained from AOS VMS-W135G *Special Grade A Specification Properties*.

6.2.2.2.1 Manufacturer Specification Properties

Table 6.2.2.2-1: AOS 1135 Specification Mechanical Properties (46)

Elongation	Min. Yield	Tensile
26.0%	41.25 ksi	75-92 ksi

Table 6.2.2.2-2: AOS Specification Chemical Composition (46)

C* [max]	Si [max]	P [max]	S[max]	Mn [max]
0.20-0.30	0.20	0.045	0.050	1.25

6.2.2.3 Mill Test Report (MTR) Properties

Product analysis from instances of AOS1135 within LPV fleet vessels provide records from mill test reports. The data from these records is not a comprehensive list of all heat or slab numbers.

Table 6.2.2.3-1: V- AOS 1135 Mechanical Properties

Data Package	Melt No.	Yield	Min. Tensile	Elongation
075	16011-11	55.6 ksi	87.2 ksi	25%
075	16011-22	54.4 ksi	86.8 ksi	26%
076	16011-15	53.8 ksi	86.7 ksi	24%

Table 6.2.2.3-2: V- AOS 1135 Chemical Composition

Data Package	Melt No.	C	Mn	P	S	Si
075	16011-11	0.22	0.98	0.019	0.038	0.20
075	16011-22	0.22	0.98	0.019	0.038	0.20
076	16011-15	0.22	0.98	0.019	0.038	0.20

6.2.2.4 Fracture Results

There are no internal test results for 1135.

6.3 Non-Code Materials with No Reference

6.3.1 SWC 100302

6.3.1.1 General Material Properties

Struthers Wells Corporation (SWC)'s 100302 is a proprietary steel. It is primarily used for shells in SWC's multilayered vessel designs. Because it is a proprietary steel that has been created from the modification of an existing ASTM steel, it has no governing ASTM specification. Therefore, the governing material specification is the manufacturer's internal

specification for the material: *Struthers Wells 100302 Rev. 11/8/1963 Mod. For Chemistry Physicals and Charpy Firebox (Fbx)*. (49) Though the LPV Team currently does not have access to this specific document, references to the specifications and data are provided in data packages where the steel is used.

As mentioned above, SWC100302 is a proprietary steel that has been modified from a standard steel. Though no official record of verification can be found to confirm what the parent material is, it can be observed that ASME SA-533, otherwise known as the *Specification for Pressure Vessel Plates, Alloy Steel, Quenched and Tempered, Manganese-Molybdenum and Manganese-Molybdenum-Nickel*, maintains similar chemical composition and mechanical property requirements to SWC100302. Additionally, SA-533 is attached to the manufacturer's data package index and is not used on any parts in the drawings. A summary of SA-533 chemical composition limits and mechanical properties can be seen in Section 6.3.1.2.2.

Additionally, most instances of SWC100302 occur in LPV that were manufactured in the mid-1960s, which was around the time that the pressure vessel industry had begun to use SA-533 as the replacement for the previous industry standard that was A302B (33). The new SA-533B was created by modifying A302B.

Though other potential parent materials such as a modified T-1 (otherwise known as SA-517 Gr. F) may satisfy mechanical and/or chemical requirements similar to those for SWC100302, they have not been included in this summary. This is because they are not mentioned in the manufacturer's data packages where SWC100302 is used. Additionally, SWC won a contract appeal decision (50) with the United States Armed Services Board in 1963 that revolved around the difficulties they experienced when they tried to use T-1 steel instead of A302B steel, making it more likely that they modified A302 or its replacement SA-533. Further anecdotal evidence supporting the characterization of SWC100302 as a modified A302B steel can be found in the form of documented correspondence between SWC and NASA.

6.3.1.2 Material Specification Properties

6.3.1.2.1 SWC 100302 Mechanical Properties

According to the notes on the drawing for V-106, the mechanical properties shown in Table 6.3.1.2.1-1 are referenced for SWC100302 minimum requirements.

Table 6.3.1.2.1-1: SWC100302 Mechanical Properties (49)

Min. Yield	Min. Tensile	Charpy V-Notch
83.5 ksi	100 ksi	15 ft.lbs. (Average) at -40F and +50F

6.3.1.2.2 ASTM SPECIFICATION PROPERTIES

Chemical and mechanical requirements of possible parent material are outlined in ASTM A533 (1993), shown in Table 6.3.1.2.2-1 and Table 6.3.1.2.2-2.

Table 6.3.1.2.2-1: ASTM A533 Chemical Composition (36)

Type	C [max]	Mn	P [max]	S [max]	Si	Mo	Ni
A	0.25	1.07-1.62	0.035	0.035	0.13-0.45	0.41-0.64	---
B	0.25	1.07-1.62	0.035	0.035	0.13-0.45	0.41-0.64	0.37-0.73
C	0.25	1.07-1.62	0.035	0.035	0.13-0.45	0.41-0.64	0.67-1.03
D	0.25	1.07-1.62	0.035	0.035	0.13-0.45	0.41-0.64	0.17-0.43

Table 6.3.1.2.2-2: ASTM A533 Mechanical Properties (36)

Class	Min. Yield	Tensile	Elongation (2 in)
1	50 ksi	80-100 ksi	18 %
2	70 ksi	90-115 ksi	16 %
3	83 ksi	100-125 ksi	16 %

6.3.1.3 Mill Test Report (MTR) Properties

Product analysis from instances of SWC100302 within LPV fleet vessels provide records from mill test reports, shown in Table 6.3.1.3-1 and Table 6.3.1.3-2. The data from these records is not a comprehensive list of all heat or slab numbers.

Table 6.3.1.3-1: MTR SWC100302 Mechanical Properties

Melt No.	Yield	Min. Tensile	Elongation	Reduction Area	Average Charpy (-40°F)	Average Charpy (+50°F)
A90009	85.7 ksi	105.6 ksi	26%	67.9%	77 ft.lbs.	95.7 ft.lbs.
A9149	106.5 ksi	119.5 ksi	24%	64.3%	85.7 ft.lbs.	89 ft.lbs.

Table 6.3.1.3-2: MTR SWC100302 Mechanical Properties

Melt No.	C	Mn	P	S	Si	Ni	Mo
A9009	0.22	1.22	0.010	0.018	0.27	0.60	0.46
A9149	0.22	1.36	0.013	0.016	0.26	0.54	0.46

6.3.1.4 Fracture Results

There are no fracture results available at this time.

6.3.2 SWC 90336

6.3.2.1 General Material Properties

SWC90336 is primarily used for nozzles in SWC’s multilayered vessel designs. Like the SWC100302 specification for plate material, this is a proprietary steel that was created by modifying an existing ASTM steel, and it has no equivalent ASTM reference. Therefore, the governing material specification is the manufacturer’s internal specification for the steel. Though the LPV team currently does not have access to this specific document, reference to the specifications data is provided in some of the data packages for LPVs using the steel and mechanical and chemical characteristics are shown in Table 6.3.2.2-1 and Table 6.3.2.2-2.

6.3.2.2 Material Specification Properties

The governing specification for SWC90336 outlines the chemical and mechanical requirements below:

Table 6.3.2.2-1: 90336 Mechanical Properties Requirements (49)

Min. Yield	Min. Tensile	Elongation	Reduction Area	Charpy V-Notch
50 ksi	90 ksi	18%	45.0%	15 ft.lbs. (Average) at -40F and +50F

Table 6.3.2.2-2: 90336 Chemical Composition Requirements (49)

C	Mn	P [max]	S [max]	Si	Ni	Cr	V	Mo
0.30	0.40-0.90	0.020	0.030	1.00-1.50	0.45-0.75	0.45-0.75	0.03-0.08	0.50-0.70

6.3.2.3 Mill Test Report (MTR) Properties

Product analysis from instances of SWC90336 within LPV fleet vessels provide records from mill test reports. The data from these records is not a comprehensive list of all heat or slab numbers, but available information is provided in Table 6.3.2.3-1 and Table 6.3.2.3-2.

Table 6.3.2.3-1: 90336 MTR Mechanical Properties (49)

Melt No.	Yield	Tensile	Elongation	Reduction Area	Average Charpy (-40°F)	Average Charpy (+50°F)
120N244VA3F1-4 LC	79.5 ksi	99 ksi	24.5%	69.5%	73.8 ft.lbs.	144 ft.lbs.
120N244VA3F1-4 LCA	82.5 ksi	102 ksi	24.0%	69.5%		

Table 6.3.2.3-2: 90336 MTR Chemical Composition (49)

Heat No.	C	Mn	P	S	Si	Ni	Cr	V	Mo
120N244	0.24	0.62	0.009	0.011	0.26	1.34	0.50	0.05	0.47*
*Out of spec, approved by customer									

6.3.2.4 Fracture Results

There are no fracture results available for SWC90336 at this time.

7 MATERIAL TEST DATA

Introduction

This section of the materials report contains data collected from various tests conducted on the materials found in LPVs. Many different types of tests were conducted with a focus on accurately describing the material properties of steels found in common LPVs at NASA facilities. Not all types of tests were conducted for each material, particularly when it was determined that the material was of consistent mechanical properties, or that the properties discovered were of low risk. Many tests were conducted on multiple steels obtained from several vessels to obtain data on the variability of the properties. Material types and the tests conducted are described in sections 7.1 and 7.2.

7.1 Description of Test Types and Analysis Methods

Smooth Tensile: Smooth tensile tests are documented under ASTM E8 (51) “Standard Test Methods for Tension Testing of Metallic Materials” and were performed on most materials typically found in LPVs. This test is the basic method for determining yield strength, ultimate strength, and elongation of materials.

Notch Tensile: Notch tensile tests are documented under ASTM G142 (52) and were performed only on materials where hydrogen embrittlement was a concern. This test gives strength information as related to the effect of a vessel operating in a hydrogen environment.

Fracture Toughness: Fracture toughness tests are documented under ASTM E1820 (10) and were performed on most materials. This test gives information on the resistance of the material to the ductile extension of cracks. This information is used as a basis for identifying critically sized flaws in vessels, which may vary depending on location.

Transition Temperature (T_0): T_0 tests are documented under ASTM E1921 (7) and were performed on most materials. This test locates the ductile-brittle transition temperature of ferritic steels, which is the primary component of layered pressure vessels. The T_0 is the temperature below which the material’s fracture toughness drops to a level where uncontrolled crack growth can occur.

Fatigue Crack Growth (da/dN): Fatigue crack growth tests are documented under ASTM E647 (11) and were performed on some of the most common materials and welds. This test creates a curve of crack growth per load cycle at various K values and load ratios. These curves are then uploaded into NASGRO and used to help calculate critical initial crack size and remaining life.

Chemistry: Chemical analysis was performed on all tested materials. These tests were conducted using an optical emissive spectrometer which characterizes the percentage of elements present in the material. The use of a portable testing apparatus allows the chemistry of vessels in the fleet to be compared with the steels tested in the lab.

Metallography: Metallographic tests were performed on several common layered pressure vessel materials. These tests are used to evaluate the microstructure, grain size, grain structure, weld passes, heat affected zone, and other material characteristics using a microscopic examination of samples cut from the steel components, polished, and chemically etched using standard procedures. These tests are particularly useful in determining a materials principal rolling orientation, welding process details, and differences in heat treatment, processing, or manufacturing.

Hardness: Hardness measurements were taken for all materials. Hardness values were obtained using a standard hardness tester for small pieces and a portable unit for large in-situ pieces. Hardness in steels correlates well with ultimate strength and can be used as a non-destructive evaluation (comparison) method.

Fractography: Fractography is the process of examining the fracture surface of existing cracks or cracks obtained in the laboratory, and inspecting them for indications of different types of growth and clues as to how the crack formed. This process was used specifically on weld material taken from LPVs to determine how and when the cracks were formed. It is also used extensively during laboratory fracture toughness testing to determine the crack size present when failure occurred under known test conditions.

Test Matrices: The test matrices shown in Table 7.1-1 through Table 7.1-8 were used to track LPV materials of interest and the tests performed on them. With a limited number of disposable LPVs available to test, materials that cover a larger portion of the fleet were prioritized with multiple lots.

Table 7.1-1: V0023 Test Matrix

Material Location	V0023										
	Material	RT Fracture	To Fracture	da/dN	Tensiles	Notch Tensiles	HCF	Metallography	Chemistry	Hardness	Charpy
Parent Material											
Head (stress relieved)	A225										
Nozzle	A105										
Inner layer (stress relieved)	1146										
Wrapper shell	1146										
Weld Material, Center											
Head-to-shell circumferential weld (green)											
Shell-to-shell circumferential weld (green)											
Longitudinal welds (green)											
Inner layer welds (stress relieved)											
Nozzle-to-head weld (stress relieved)											
Nozzle-to-shell weld (green)											
Weld Material, HAZ											
Head-to-shell circumferential weld, shell side (green)											
Head-to-shell circumferential weld, head side (green)											
Shell-to-shell circumferential weld (green)											
Longitudinal welds (green)											
Inner layer welds (stress relieved)											
Nozzle-to-head weld, nozzle side (stress relieved)											
Nozzle-to-head weld, head side (stress relieved)											
Nozzle-to-shell weld, shell side (green)											
Nozzle-to-shell weld, nozzle side (green)											
Tested											

Table 7.1-2: V0032 Test Matrix

Material Location	V32										
	Material	RT Fracture	To Fracture	da/dN	Tensiles	Notch Tensiles	HCF	Metallography	Chemistry	Hardness	Charpy
Parent Material											
Head (stress relieved)	A225										
Nozzle	A105										
Inner layer (stress relieved)	1146										
Wrapper shell	1146										
Weld Material, Center											
Head-to-shell circumferential weld (green)											
Shell-to-shell circumferential weld (green)											
Longitudinal welds (green)											
Inner layer welds (stress relieved)											
Nozzle-to-head weld (stress relieved)											
Nozzle-to-shell weld (green)											
Weld Material, HAZ											
Head-to-shell circumferential weld, shell side (green)											
Head-to-shell circumferential weld, head side (green)											
Shell-to-shell circumferential weld (green)											
Longitudinal welds (green)											
Inner layer welds (stress relieved)											
Nozzle-to-head weld, nozzle side (stress relieved)											
Nozzle-to-head weld, head side (stress relieved)											
Nozzle-to-shell weld, shell side (green)											
Nozzle-to-shell weld, nozzle side (green)											
Tested											

Table 7.1-3: MV50466-8 Test Matrix

Material Location	MV 50466-8										
	Material	RT Fracture	To Fracture	da/dN	Tensiles	Notch Tensiles	HCF	Metallography	Chemistry	Hardness	Charpy
Parent Material											
Head (stress relieved)	A225										
Nozzle	5002										
Inner layer (stress relieved)	1146										
Wrapper shell	1146										
Weld Material, Center											
Head-to-shell circumferential weld (green)											
Shell-to-shell circumferential weld (green)											
Longitudinal welds (green)											
Inner layer welds (stress relieved)											
Nozzle-to-head weld (stress relieved)											
Nozzle-to-shell weld (green)											
Weld Material, HAZ											
Head-to-shell circumferential weld, shell side (green)											
Head-to-shell circumferential weld, head side (green)											
Shell-to-shell circumferential weld (green)											
Longitudinal welds (green)											
Inner layer welds (stress relieved)											
Nozzle-to-head weld, nozzle side (stress relieved)											
Nozzle-to-head weld, head side (stress relieved)											
Nozzle-to-shell weld, shell side (green)											
Nozzle-to-shell weld, nozzle side (green)											
Tested											

Table 7.1-4: V0125 Test Matrix

Material Location	V125										
	Material	RT Fracture	To Fracture	da/dN	Tensiles	Notch Tensiles	HCF	Metallography	Chemistry	Hardness	Charpy
Parent Material											
Head (stress relieved)	A225										
Nozzle	5002										
Inner layer (stress relieved)	1143										
Wrapper shell	1146										
Weld Material, Center											
Head-to-shell circumferential weld (green)											
Shell-to-shell circumferential weld (green)											
Longitudinal welds (green)											
Inner layer welds (stress relieved)											
Nozzle-to-head weld (stress relieved)											
Nozzle-to-shell weld (green)											
Weld Material, HAZ											
Head-to-shell circumferential weld, shell side (green)											
Head-to-shell circumferential weld, head side (green)											
Shell-to-shell circumferential weld (green)											
Longitudinal welds (green)											
Inner layer welds (stress relieved)											
Nozzle-to-head weld, nozzle side (stress relieved)											
Nozzle-to-head weld, head side (stress relieved)											
Nozzle-to-shell weld, shell side (green)											
Nozzle-to-shell weld, nozzle side (green)											
Tested											

Table 7.1-5: PV0296 Test Matrix

Material Location	PV296										
	Material	RT Fracture	To Fracture	da/dN	Tensiles	Notch Tensiles	HCF	Metalography	Chemistry	Hardness	Charpy
Parent Material											
Head (stress relieved)	A225										
Nozzle	5002										
Inner layer (stress relieved)											
Wrapper shell											
Weld Material, Center											
Head-to-shell circumferential weld (green)											
Shell-to-shell circumferential weld (green)											
Longitudinal welds (green)											
Inner layer welds (stress relieved)											
Nozzle-to-head weld (stress relieved)											
Nozzle-to-shell weld (green)											
Weld Material, HAZ											
Head-to-shell circumferential weld, shell side (green)											
Head-to-shell circumferential weld, head side (green)											
Shell-to-shell circumferential weld (green)											
Longitudinal welds (green)											
Inner layer welds (stress relieved)											
Nozzle-to-head weld, nozzle side (stress relieved)											
Nozzle-to-head weld, head side (stress relieved)											
Nozzle-to-shell weld, shell side (green)											
Nozzle-to-shell weld, nozzle side (green)											
Tested											

Table 7.1-6: V0348 Test Matrix

Material Location	V348										
	Material	RT Fracture	To Fracture	da/dN	Tensiles	Notch Tensiles	HCF	Metallography	Chemistry	Hardness	Charpy
Parent Material											
Head (stress relieved)	A212										
Nozzle	A105										
Inner layer (stress relieved)	A225										
Wrapper shell	A225										
Weld Material, Center											
Head-to-shell circumferential weld (green)											
Shell-to-shell circumferential weld (green)											
Longitudinal welds (green)											
Inner layer welds (stress relieved)											
Nozzle-to-head weld (stress relieved)											
Nozzle-to-shell weld (green)											
Weld Material, HAZ											
Head-to-shell circumferential weld, shell side (green)											
Head-to-shell circumferential weld, head side (green)											
Shell-to-shell circumferential weld (green)											
Longitudinal welds (green)											
Inner layer welds (stress relieved)											
Nozzle-to-head weld, nozzle side (stress relieved)											
Nozzle-to-head weld, head side (stress relieved)											
Nozzle-to-shell weld, shell side (green)											
Nozzle-to-shell weld, nozzle side (green)											
Tested											

Table 7.1-7: V0071 Test Matrix

Material Location	V071										
	Material	RT Fracture	To Fracture	da/dN	Tensiles	Notch Tensiles	HCF	Metalography	Chemistry	Hardness	Charpy
Parent Material											
Head (stress relieved)	A302										
Nozzle											
Inner layer (stress relieved)											
Wrapper shell											
Weld Material, Center											
Head-to-shell circumferential weld (green)											
Shell-to-shell circumferential weld (green)											
Longitudinal welds (green)											
Inner layer welds (stress relieved)											
Nozzle-to-head weld (stress relieved)											
Nozzle-to-shell weld (green)											
Weld Material, HAZ											
Head-to-shell circumferential weld, shell side (green)											
Head-to-shell circumferential weld, head side (green)											
Shell-to-shell circumferential weld (green)											
Longitudinal welds (green)											
Inner layer welds (stress relieved)											
Nozzle-to-head weld, nozzle side (stress relieved)											
Nozzle-to-head weld, head side (stress relieved)											
Nozzle-to-shell weld, shell side (green)											
Nozzle-to-shell weld, nozzle side (green)											
Tested											

Table 7.1-8: V066 Test Matrix

Material Location	V066										
	Material	RT Fracture	To Fracture	da/dN	Tensiles	Notch Tensiles	HCF	Metallography	Chemistry	Hardness	Charpy
Parent Material											
Head (stress relieved)	T-1										
Nozzle											
Inner layer (stress relieved)	T-1										
Wrapper shell	T-1										
Weld Material, Center											
Head-to-shell circumferential weld (green)											
Shell-to-shell circumferential weld (green)											
Longitudinal welds (green)											
Inner layer welds (stress relieved)											
Nozzle-to-head weld (stress relieved)											
Nozzle-to-shell weld (green)											
Weld Material, HAZ											
Head-to-shell circumferential weld, shell side (green)											
Head-to-shell circumferential weld, head side (green)											
Shell-to-shell circumferential weld (green)											
Longitudinal welds (green)											
Inner layer welds (stress relieved)											
Nozzle-to-head weld, nozzle side (stress relieved)											
Nozzle-to-head weld, head side (stress relieved)											
Nozzle-to-shell weld, shell side (green)											
Nozzle-to-shell weld, nozzle side (green)											
Tested											

7.2 Parent Head Materials

Parent head materials are materials commonly used on LPVs to form the monolithic heads attached to the layered shell courses. These heads range from 1.5 inches to over 8 inches in thickness. The most common thicknesses are 3 to 4 inches. Typically, the heads are formed by roll forming a flat plate into a semi-elliptical dome of the same diameter as the vessel. In some cases, the heads are thinner than the shell course with weld material bridging the difference. The head materials investigated are A225, A212, and A302.

Investigations of head materials from seven vessels are reported on in this document. Five of those vessels are A225 steel which represents the largest single material

characterization, as well as the majority of the fleet. These lots of A225 vary in their material properties, but have little disparity in their chemical compositions. This indicates that post-processing and forming methods likely have a significant impact on the final mechanical properties of the material. An attempt has been made to characterize the transition temperature of all of the lots combined utilizing the E1921 (7) inhomogeneity annex. Using a multimodal analysis applied to all of the test data, a Master Curve using T_m has been created. However, this curve is extremely conservative based on the large amount of data scatter. In general cases it would be most efficient to conduct tests on materials known to be similar, creating a Master Curve from that data that would be specific to the application.

7.2.1 A225

ASTM A225 (47) is primarily used as the head material of LPVs. The results reported include vessels manufactured by AOS and one by CB&I. All heads are nominally A225B FBX, also referred to herein as A225.

7.2.1.1 Chemical Composition

Table 7.2.1.1-1 shows the standard ASTM chemical specification for A225 material. Some values may vary depending on the time during the process that they are checked. Ladle analysis refers to a chemical test on the molten steel, while check analysis is a final product check.

Table 7.2.1.1-1: Standard Chemical Composition for A225

	C	Mn	P	S	Si		V	
					Ladle Analysis	Check Analysis	Ladle Analysis	Check Analysis
Grade B	0.2	0.145	0.035	0.04	0.15-0.30	0.13-0.32	0.09-0.14	0.07-0.16

Table 7.2.1.1-2 shows data collected from mill certifications of vessels at MSFC. Table 7.2.1.1-3 arc-spark data collected from tested vessel materials.

Table 7.2.1.1-2: Manufacturer Mill Certification Chemistry

Melt/Heat	Cert Origin	Chemistry (%)					
		C	Mn	P	S	Si	V
590437	US Steel	0.16	1.25	0.012	0.028	0.22	0.1
699746	US Steel	0.17	1.35	0.008	0.024	0.22	0.11
919705	US Steel	0.15	1.32	0.008	0.021	0.21	0.01
589611	US Steel	0.17	1.32	0.01	0.021	0.24	0.11
699804	US Steel	0.18	1.4	0.009	0.025	0.24	0.11
630099	US Steel	0.16	1.4	0.009	0.026	0.24	0.11
589503	US Steel	0.16	1.36	0.008	0.021	0.26	0.11
630102	US Steel	0.17	1.44	0.03	0.026	0.25	0.11
700200	US Steel	0.15	1.26	0.008	0.023	0.23	0.11
639905	US Steel	0.15	1.35	0.01	0.028	0.25	0.12
710211	US Steel	0.17	1.4	0.012	0.024	0.21	0.11
589577	US Steel	0.16	1.33	0.009	0.027	0.22	0.12
910261	US Steel	0.17	1.32	0.01	0.029	0.26	0.12
599662	US Steel	0.16	1.35	0.01	0.028	0.25	0.11
10639	US Steel	0.17	1.38	0.013	0.03	0.24	0.11
11546	US Steel	0.19	1.32	0.018	0.025	0.26	0.13
20503	US Steel	0.17	1.43	0.014	0.02	0.19	0.12
679370	US Steel	0.18	1.3	0.01	0.024	0.24	0.11
679519	US Steel	0.19	1.32	0.014	0.023	0.21	0.11
709390	US Steel	0.19	1.35	0.009	0.019	0.26	0.12
719581	US Steel	0.16	1.2	0.02	0.028	0.22	0.11
622618	US Steel	0.17	1.27	0.01	0.016	0.21	0.1
672031	US Steel	0.18	1.32	0.027	0.022	0.21	0.1
622618	US Steel	0.17	1.27	0.01	0.016	0.21	0.1

Table 7.2.1.1-3: A225 Collected Chemistry Data

Vessel	Location	C	Si	Mn	P	S	Cr	Mo	Ni	V
MV50466-8	Head 1	0.19	0.21	1.46	0.032	0.063	0.19	0.028	0.21	0.11
MV50466-8	Head 2	0.16	0.2	1.46	0.03	0.023	0.19	0.02	0.21	0.1
PV0296	Head	0.1505	0.2345	1.311	0.0123	0.0133	0.0191	0.00685	0.0076	0.103
V0023	Head	0.21	0.2	1.43	0.025	0.023	0.25	0.056	0.35	0.09
V32	Intact Head	0.17	0.25	1.36	0.027	0.046	0.21	0.059	0.024	0.09
V125	Head	0.17	0.19	1.25	0.013	0.023	0.17	0.05	0.011	0.11
GRC Head 10	Head	0.162	0.257	1.3	0.021	0.018	0.046	0.003	0.016	0.10
GRC Head 9	Head	0.184	0.252	1.3	0.02	0.015	0.046	0.003	0.015	0.10
V32	Dissected Head	0.26	0.23	1.38	0.032	0.048	0.21	0.062	0.027	0.09

7.2.1.2 Metallography

Studies:

Grain Orientation study - yes

Grain size study – no

Grain size through thickness study - no

Carburization layer thickness - no

Macro cubes if showing multiple surfaces- Metallographic studies on this material included a grain orientation study and macro cubes. No grain size, grain size through thickness, or carburization layer thickness studies were performed.

Preliminary testing previously performed by SwRI on Ames Vessel MV-50466-8 confirmed that the fracture toughness for the LPV materials was orientation dependent. Although tensile strength was not strongly dependent on orientation, fracture testing showed considerable anisotropy. Of particular interest in the LPV materials characterization effort performed at MSFC was the head material, ASTM designation A225B, which was thought to likely have the highest ductile-brittle transition temperature out of all of the LPV materials. In order to machine and test fracture toughness test samples in an appropriate orientation to produce bounding material properties, the vessel orientation for each LPV component tested needed to be reconciled with the corresponding material orientation from the original plate from which the vessel was manufactured. The identification of the original longitudinal (L) versus transverse (T) material orientations for the starter plate for the shell material was straightforward since there are only two logical scenarios for how the vessel shell was manufactured from a flat starting plate: Either the vessel circumferential direction corresponds to the initial longitudinal direction of the plate, or the vessel longitudinal direction corresponds to the initial longitudinal direction of the plate. For shells, this means that fracture toughness samples can be tested in only two orientations to determine the bounding orientation. In the case of the head, the fully symmetric circular geometry makes determining the L and T directions of the original plate difficult because the L and T directions, while orthogonal to each other, are randomly oriented with respect to the pressure vessel head.

Consistent with the approach used by SwRI, the potential of identifying the plate orientation in the heads by conducting a macroscopic query of the surfaces was attempted. Metallographic specimens were extracted from the heads of sacrificial vessels V0032 and GRC 0296 at three angular locations, 0°, 45°, and 90° around the heads. The coordinate axes were arbitrarily chosen since there was no way to anchor the heads to the original orientation of their plates.

The specimen dimensions were selected such that each face would be identifiable to prevent any confusion with the face being queried. The directions were meridional (M), circumferential (C), and radial (R). The surfaces of the specimen were mounted, polished, and imaged at 50X and 100X magnification with a light Nital etch to reveal the grain structure. The evaluation was conducted by Element Material Technology.

For the specimens evaluated, there were no conclusive results to identify the plate orientation with respect to the head. The images of the faces were difficult to interpret to definitively establish the weakest orientation.

- Microstructural analysis was performed to determine the material orientation in the head relative to the original plate for:
 - A225 head from SwRI MV50466-8
 - A225 head from MSFC Vessel V0032
 - A225 head from GRC PV0296
 - Samples were extracted from circumferential locations around each head
 - Radial, Circumferential, and Meridional faces were evaluated at each location.
 - Microstructural analysis was performed at 50X and 100X with a light Nital etch.
 - A225 head from MSFC V0023

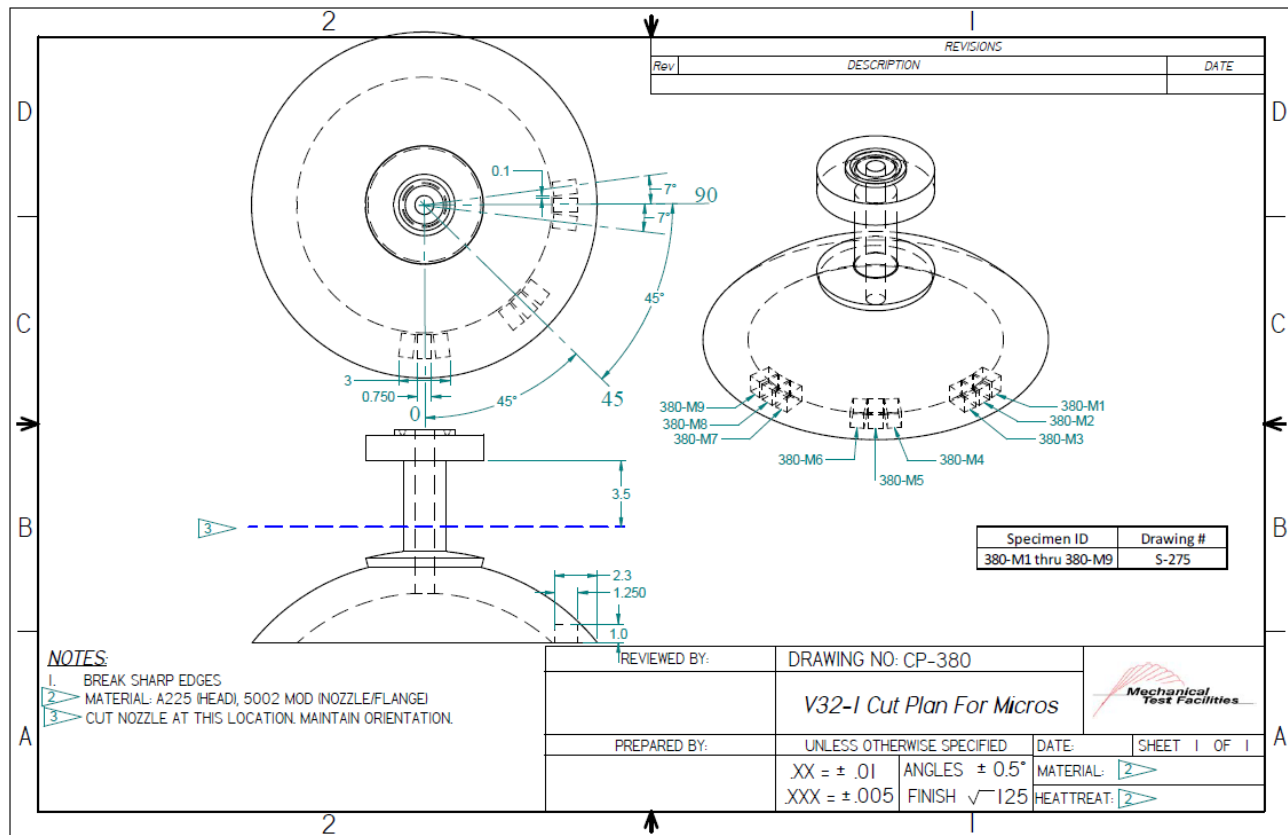


Figure 7.2.1.2-1: V0032 Head Cut Plan Metallography Specimens

Table 7.2.1.2-1: A225 Microstructure Specimen List, Vessels V0032 and PV0296

Sample ID	Description	Angle	Face
380-M1;	.75 x 1.0 Specimen	90	Radial
380-M2	1.0 x 1.25 Specimen	90	Circumferential
380-M3	1.25 x .75 Specimen	90	Meridional
380-M4	.75 x 1.0 Specimen	45	Radial
380-M5	1.0 x 1.25 Specimen	45	Circumferential
380-M6	1.25 x .75 Specimen	45	Meridional
380-M7	.75 x 1.0 Specimen	0	Radial
380-M8	1.0 x 1.25 Specimen	0	Circumferential
380-M9	1.25 x .75 Specimen	0	Meridional
393-M0-1	1.25 x 1.0 Specimen	0	Circumferential
393-M0-2	1.0 x .75 Specimen	0	Radial
393-M0-3	.75 x 1.25 Specimen	0	Meridional
393-M45-1	1.25 x 1.0 Specimen	45	Circumferential
393-M45-2	1.0 x .625 Specimen	45	Radial
393-M45-3	.625 x 1.25 Specimen	45	Meridional
393-M90-1	1.25 x 1.0 Specimen	90	Circumferential
393-M90-2	1.0 x .5 Specimen	90	Radial
393-M90-3	.5 x 1.25 Specimen	90	Meridional

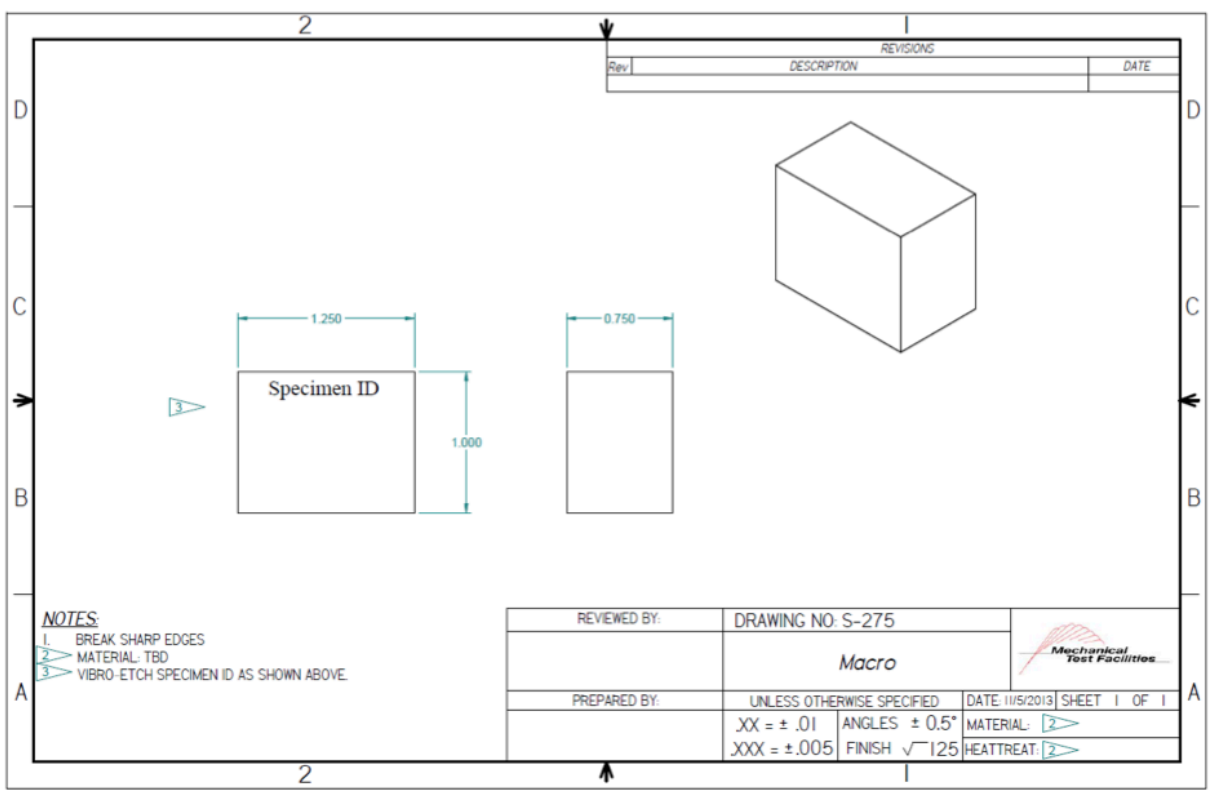


Figure 7.2.1.2-2: Macro Specimen Drawing

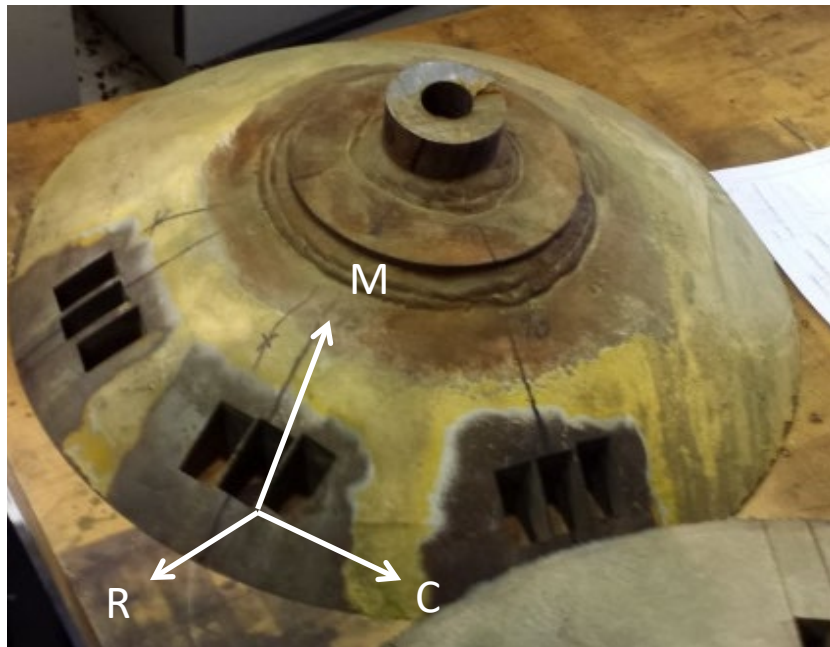


Figure 7.2.1.2-3: V0032 Macro Specimen

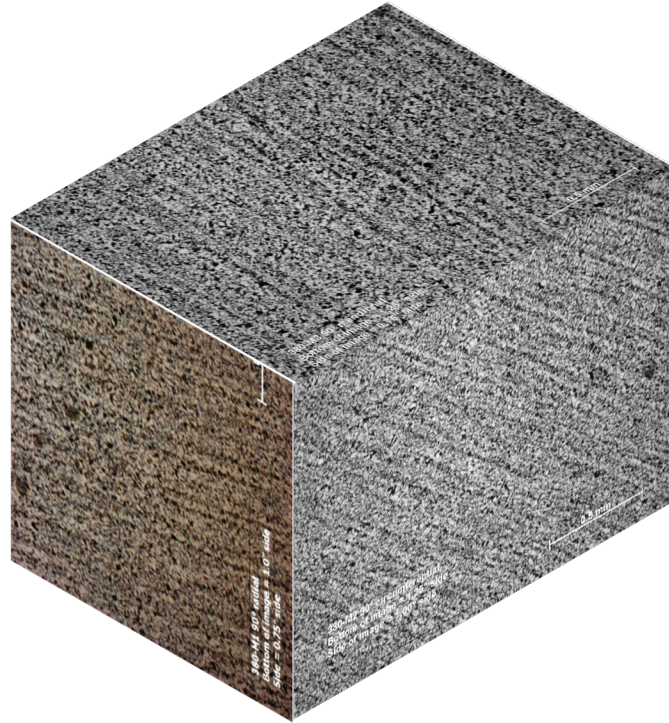
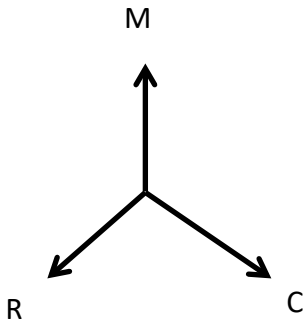


Figure 7.2.1.2-4: Micrographs of V0032 CP-380 90 Degree Location, 50X

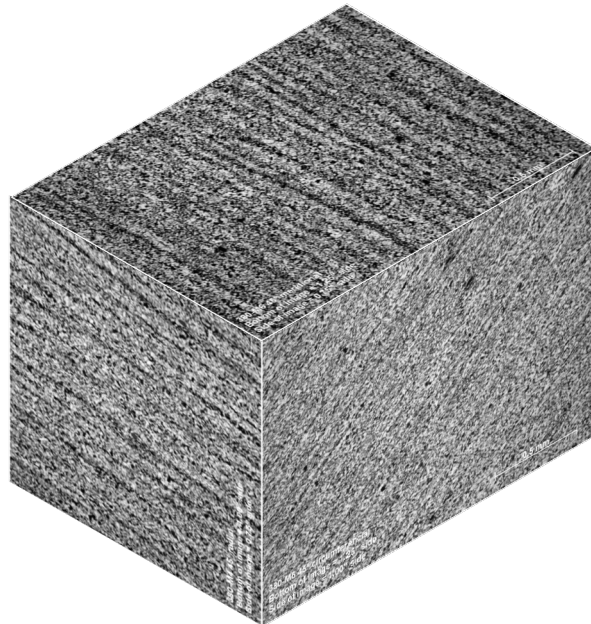
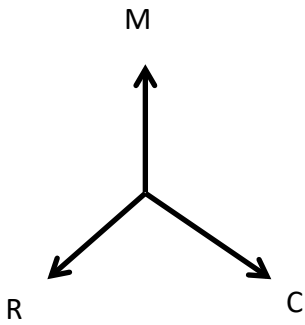


Figure 7.2.1.2-5: Micrographs of V0032 CP-380 at 45 Degree Location, 50X

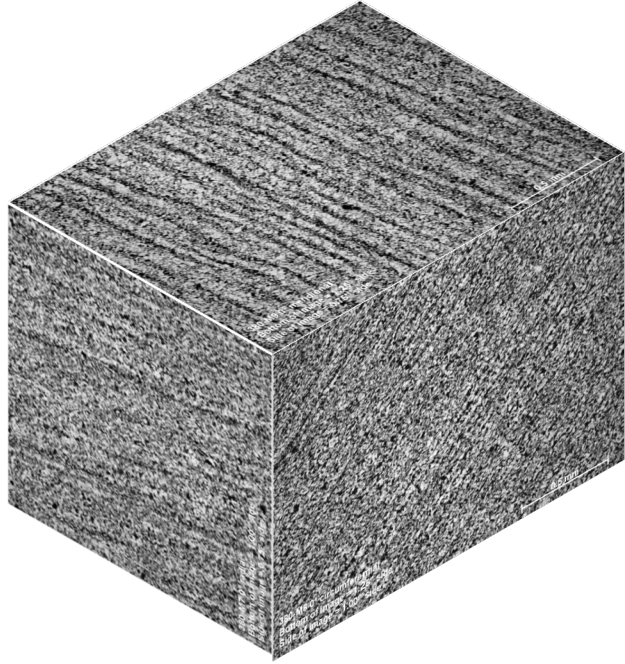
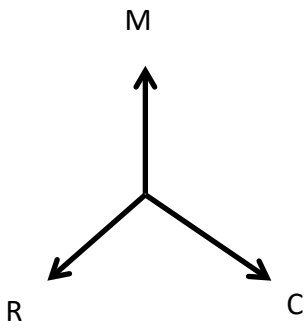


Figure 7.2.1.2-6: Micrographs of V0032 CP-380 at 0 Degree Location, 50X

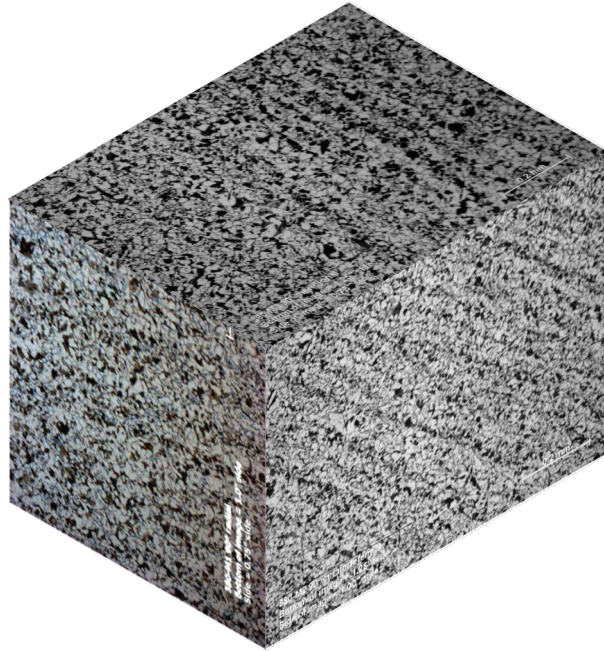
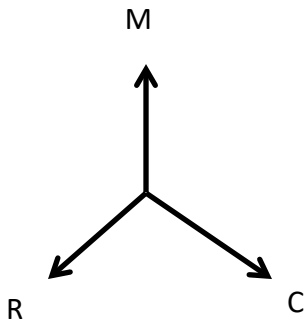


Figure 7.2.1.2-7: Micrographs of V0032 CP-380 at 90 Degree Location, 100X

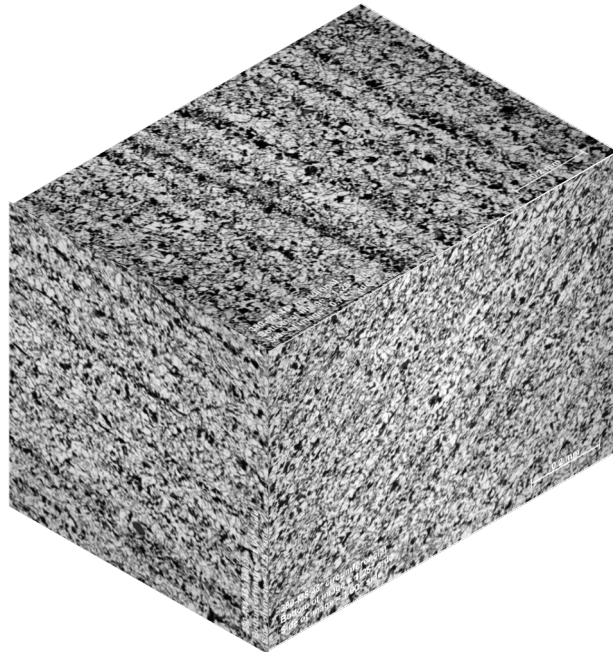
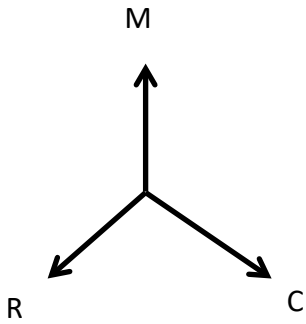


Figure 7.2.1.2-8: Micrographs of V0032 CP-380 at 45 Degree Location, 100X

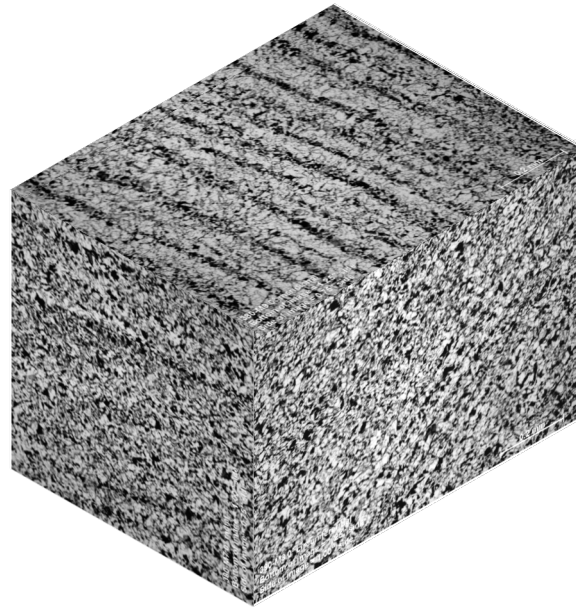
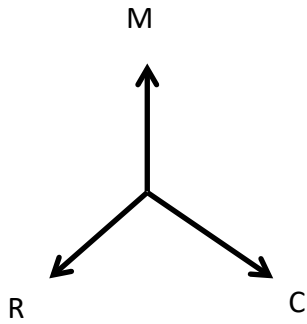


Figure 7.2.1.2-9: Micrographs of V0032 CP-380 at 0 Degree Location, 100X

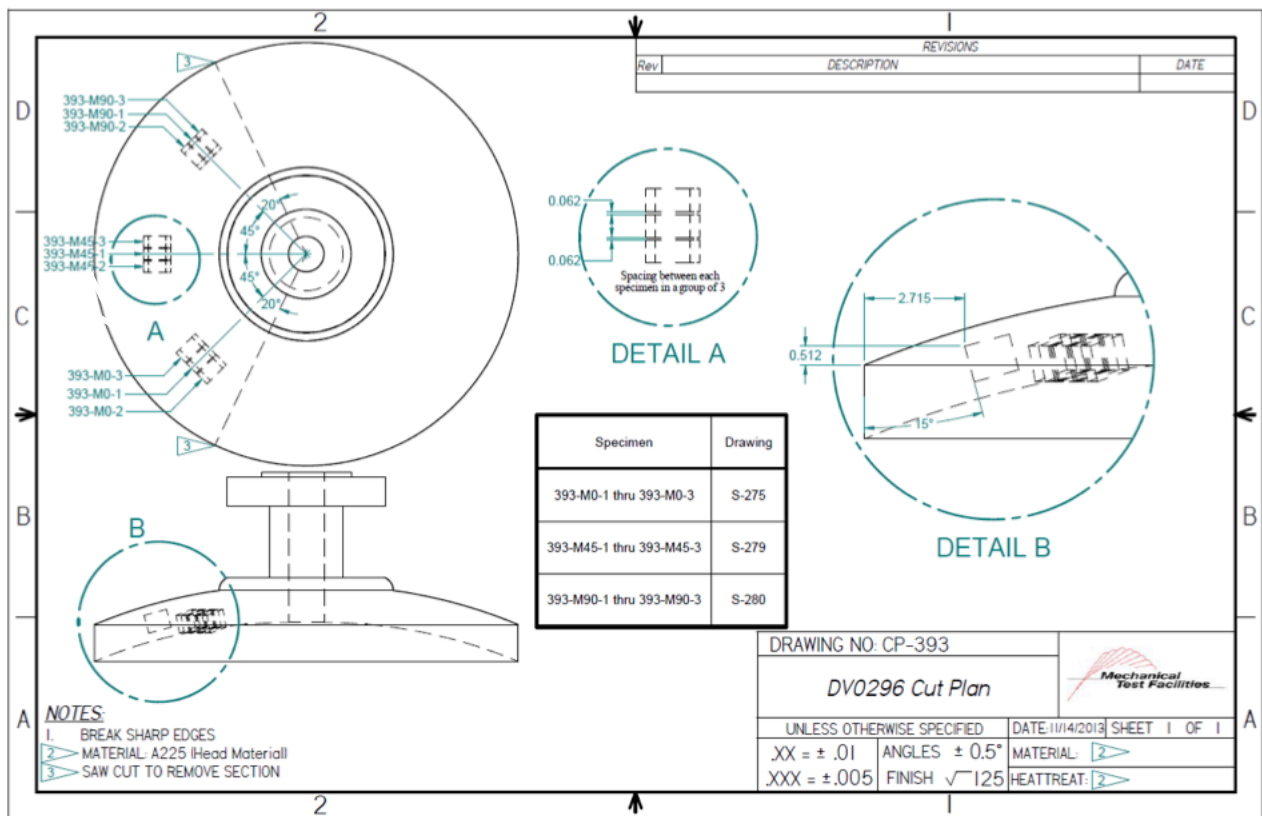


Figure 7.2.1.2-10: PV0296 Cut Plan for Macro Specimens

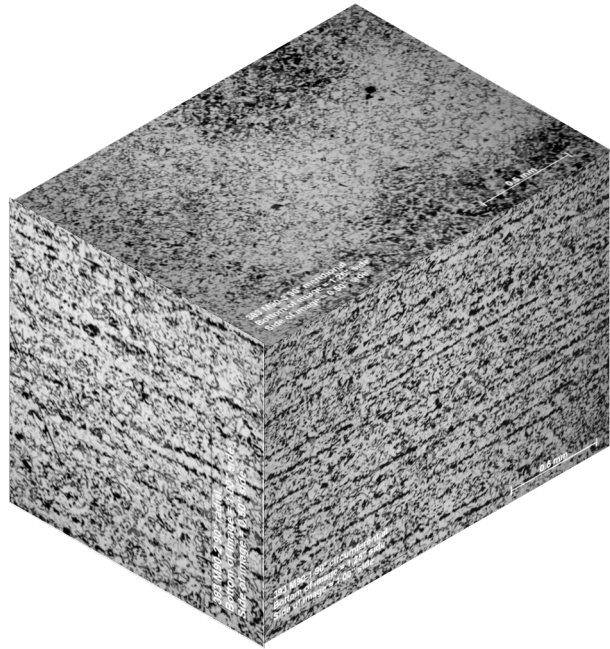
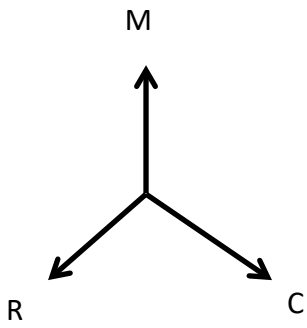


Figure 7.2.1.2-11: Micrographs of PV0296 CP-280 at 90 Degree Location, 50X

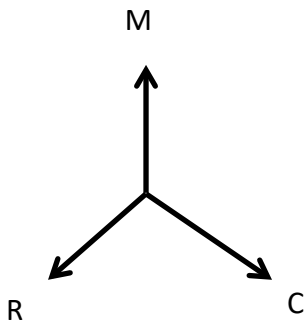


Figure 7.2.1.2-12: Micrographs of PV0296 CP-279 at 45 Degree Location, 50X

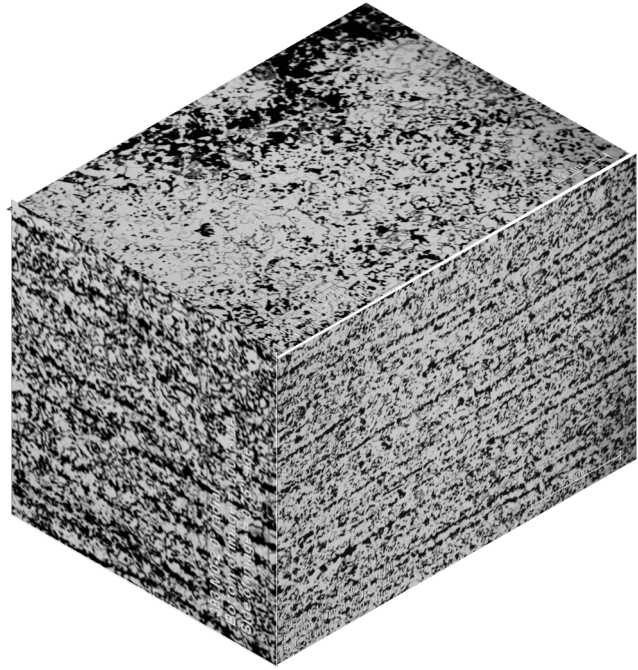
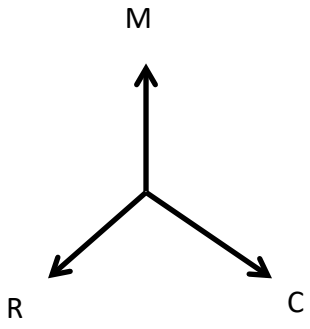


Figure 7.2.1.2-13: Micrographs of PV0296 CP-275 at 0 Degree Location, 50X

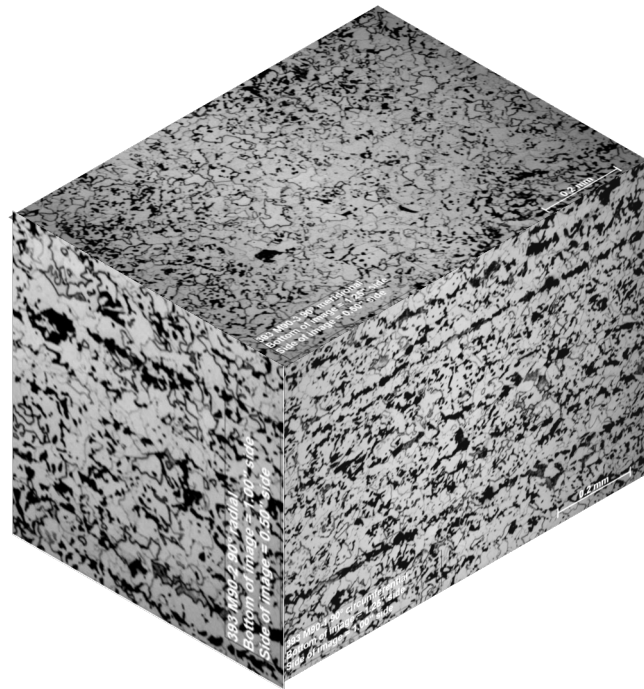
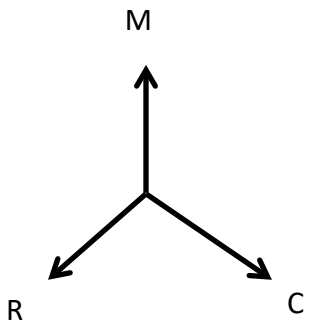


Figure 7.2.1.2-14: Micrographs of PV0296 CP-280 at 90 Degree Location, 100X

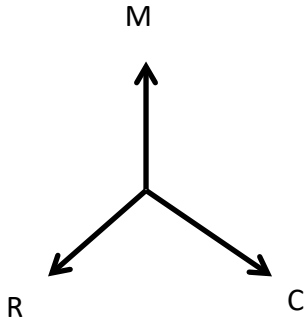


Figure 7.2.1.2-15: Micrographs of PV0296 CP-279 at 45 Degree Location, 100X

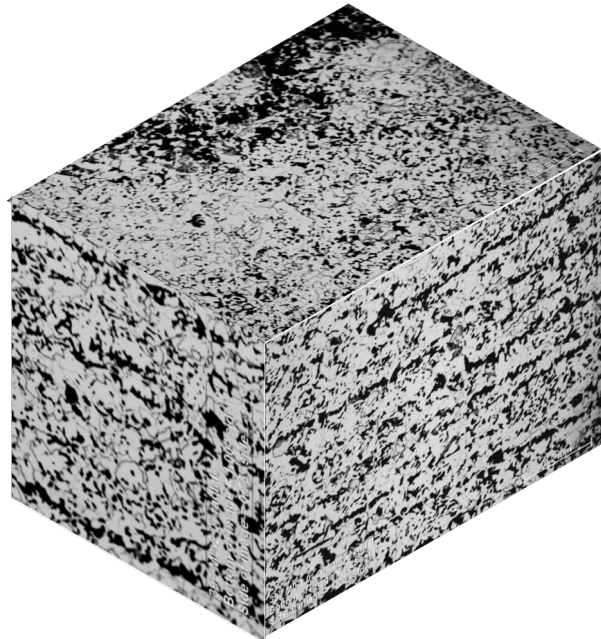
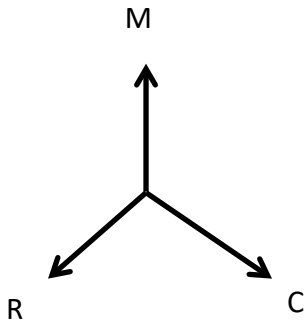


Figure 7.2.1.2-16: Micrographs of PV0296 CP-275 at 0 Degree Location, 100X

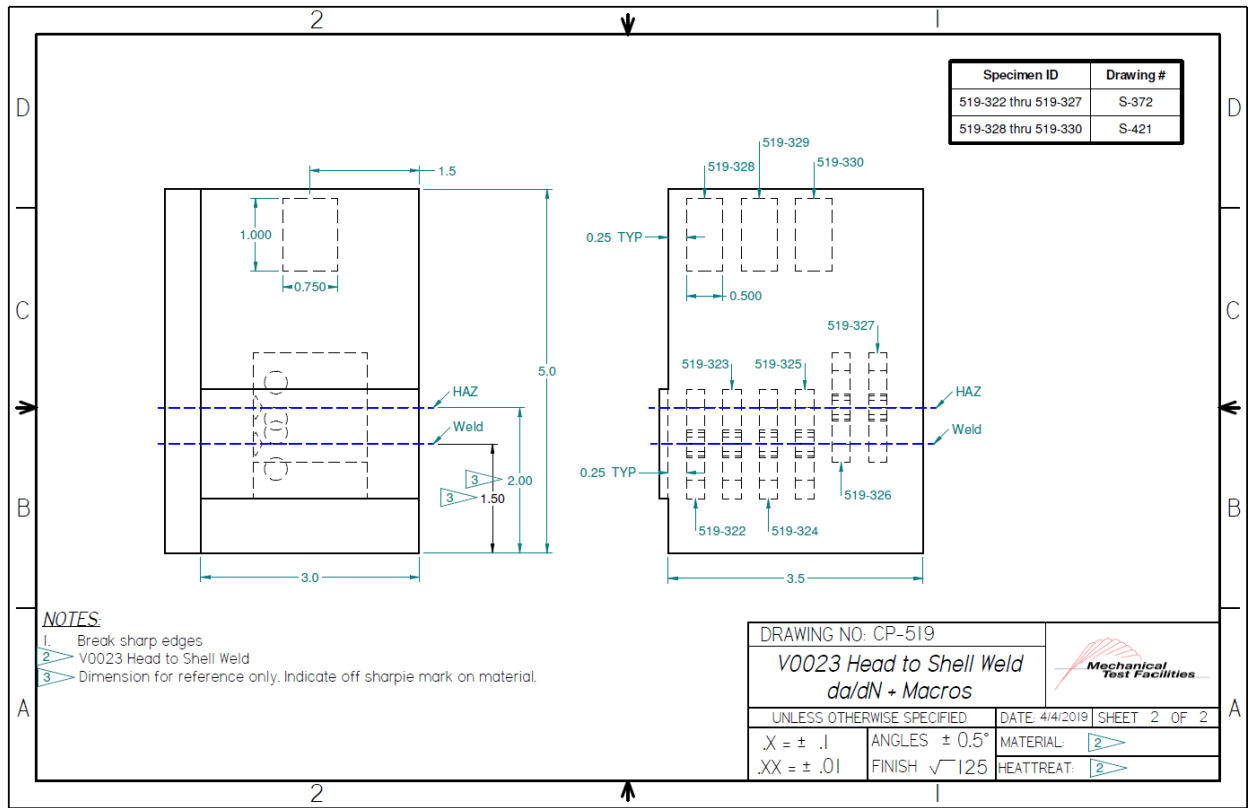


Figure 7.2.1.2-17: Macro Cut Plan V0023 A225 Head Material

Table 7.2.1.2-2: Macro Analysis V0023 A225

Face	Face Dimensions	As-polished observations	Etched observations
519-328	1.00" x 0.75"	Sample exhibits equiaxed manganese sulfide inclusions, indicating face is transverse to metal working direction.	Microstructure consists of equiaxed ferrite and pearlite.
519-329	1.00" x 0.50"	Sample exhibits elongated manganese sulfide inclusions, indicating face is parallel with metal working direction.	Microstructure consists of predominately equiaxed ferrite and pearlite. However, a minor amount of segregation is noticeable.
519-330	0.75" x 0.50"	Sample exhibits elongated manganese sulfide inclusions, indicating face is parallel with metal working direction.	Microstructure consists of equiaxed ferrite and pearlite.

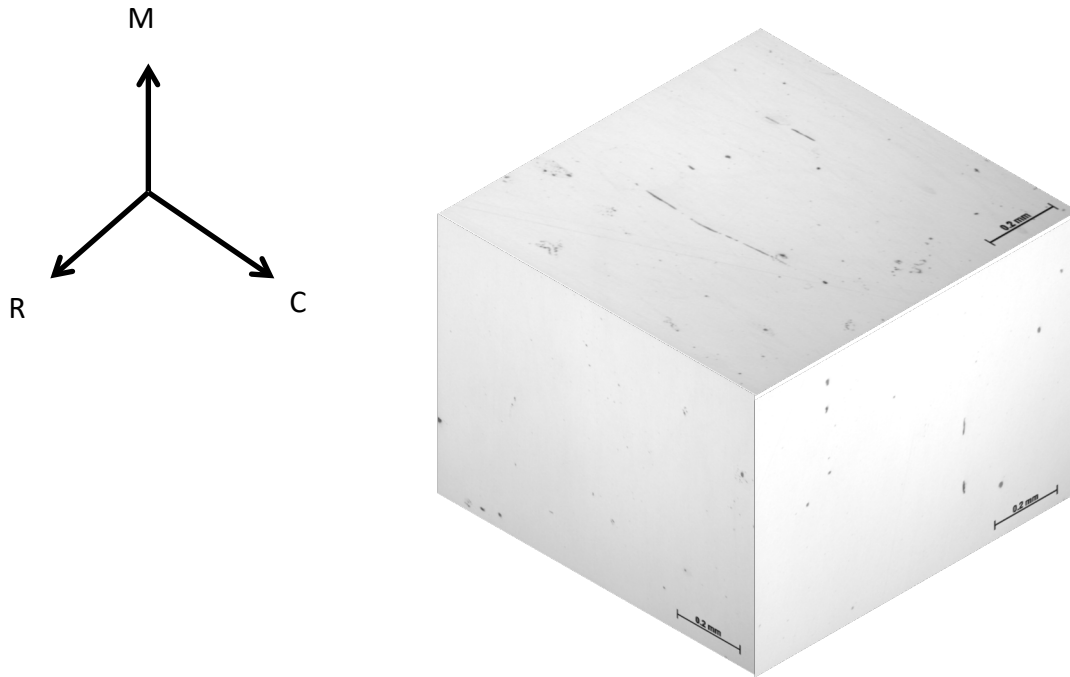


Figure 7.2.1.2-18: Metallography Cube As-Polished V0023 A225 100X

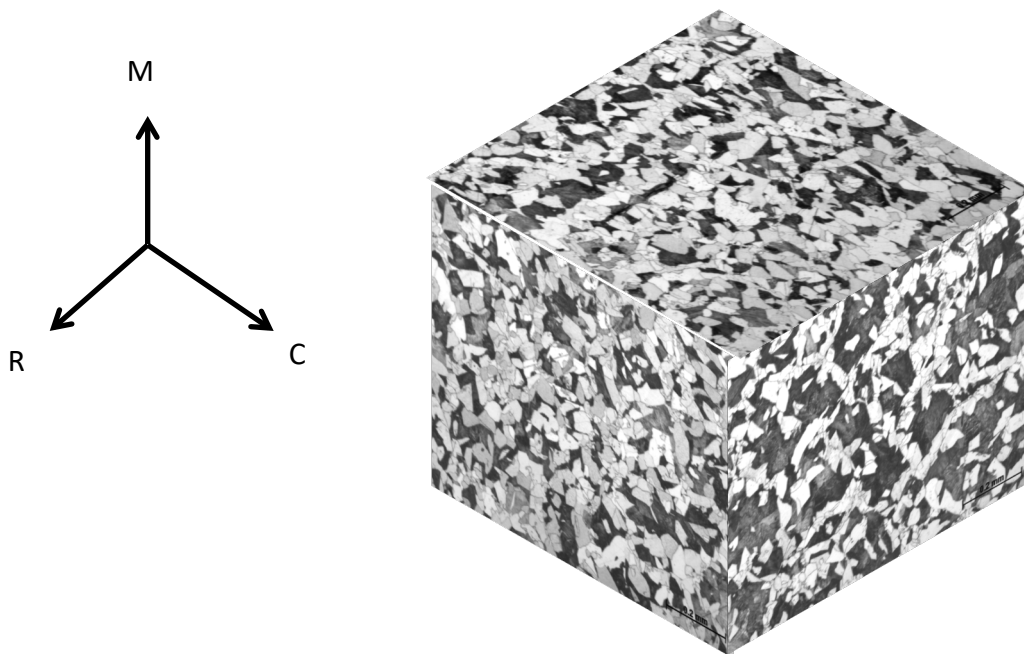


Figure 7.2.1.2-19: Metallography Cube Nital Etched V0023 A225 100X

7.2.1.3 Mechanical Properties

Table 7.2.1.3-1 shows minimum values for tensile properties required in the ASTM material specification for A225 Grade B steel.

Table 7.2.1.3-1: A225 Minimum Material Specifications

	Yield Stress (ksi)	Tensile Stress (ksi)	Fracture Elongation in 8 in. (%)	Fracture Elongation in 2 in. (%)
Grade B	43	75-90	16	20

Table 7.2.1.3-2 provides the results obtained from mill certifications from all the vessels available at MSFC.

Table 7.2.1.3-2: LPV Mill Certification Material Properties A225

Melt/Heat	Yield Stress (ksi)	Tensile Stress (ksi)	Elongation in 2in. (%)
590437	45	75	34
699746	65	89	26
919705	49	74	34
589611	57	79	34
699804	65	87	28
630099	65	88	29
589503	60	83	31
630102	62	84	30
700200	52	75	35
639905	51	75	32
710211	58	82	32
589577	64	81	27
910261	52	79	34
599662	54	86	29
10639	62	90	20
11546	56	81	34
20503	57	77	31
7-8311A	54	82	30
679370	52	75	35
679519	44	75	31
709390	53	78	33
719581	54	77	35
622618	54	77	34
672031	60	88	29
622618	53	77	33

7.2.1.3.1 Smooth Tensile Tests

MSFC conducted smooth tensile tests on round specimens in accordance with ASTM E8, (51) using specimen design S-58. The mechanical test frame consisted of a servo-hydraulic actuator and reaction frame. The frame used a linear variable differential transformer (LVDT) for displacement feedback. Stress measurements were derived from load measurements and the initial specimen measurements. Strain measurements were derived using an extensometer and the initial specimen measurements.

Test were conducted for five different vessels: MV50466, PV0296, V0032, V0023, and V0125. The results of these tests are presented in Table 7.2.1.3.1-1 through Table 7.2.1.3.1-5.

Table 7.2.1.3.1-1: A225 Smooth Tensile Data, MV50466-8

Specimen ID	Test Temp. (°C)	ASTM Orientation	Tensile Stress	Yield Stress (ksi)	Fracture Elongation (%)
440-28	21	C	75.3	51.8	30.2
440-29	21	C	74.4	49.6	33.6
440-30	-107	C	93.4	63.4	N/A
440-31	-107	C	94.7	64.2	N/A

Table 7.2.1.3.1-2: A225 Smooth Tensile Data, PV0296

Specimen ID	Test Temp. (°C)	ASTM Orientation	Tensile Stress	Yield Stress (ksi)	Fracture Elongation (%)
393-2	26	C	81.6	51.4	22.2
393-8	26	C	84.6	51.1	21.2
393-12	-50	C	92.1	58.7	22.1
393-4	-50	C	86.2	50.1	23.9
393-3	-100	C	103.0	72.6	20.9
393-9	-100	C	99.2	71.6	21.8

Table 7.2.1.3.1-3: A225 Smooth Tensile Data, V0032

Specimen ID	Test Temp. (°C)	ASTM Orientation	Tensile Stress	Yield Stress (ksi)	Fracture Elongation (%)
380-106	21	C	77.8	55.4	34.7
380-107	21	C	78.9	57.1	35.8
380-108	21	C	80.7	58.2	35.5
380-100	21	M	79.2	57.2	36.1
380-101	21	M	76.9	55.4	34.8
380-102	21	M	78.5	55.5	36.4
380-103	21	M	79.8	58.1	34.9
380-104	21	M	78.2	56.1	36.8
380-97	21	M	79.8	57.0	36.3
380-98	21	M	78.2	56.1	35.5
380-99	21	M	77.9	55.6	34.5

Table 7.2.1.3.1-4: A225 Smooth Tensile Data, V0023

Specimen ID	Test Temp. (°C)	ASTM Orientation	Tensile Stress	Yield Stress (ksi)	Fracture Elongation (%)
519-245	21	C	92.4	61.9	25.3
519-246	21	C	90.8	61.5	23.3
519-247	-46	C	97.4	65.7	23.7
519-248	-46	C	99.0	66.2	25.8
519-249	-101	C	109.3	78.4	27.7
519-250	-101	C	105.4	73.6	27.9

Table 7.2.1.3.1-5: A225 Smooth Tensile Data, V0125

Specimen ID	Test Temp. (°C)	ASTM Orientation	Tensile Stress	Yield Stress (ksi)	Fracture Elongation (%)
CP-344-10	21	C	76.8	51.4	N/A
CP-344-11	21	C	81.2	54.4	N/A
CP-344-12	21	M	82.1	55.4	N/A
CP-344-13	21	M	83.1	55.1	N/A

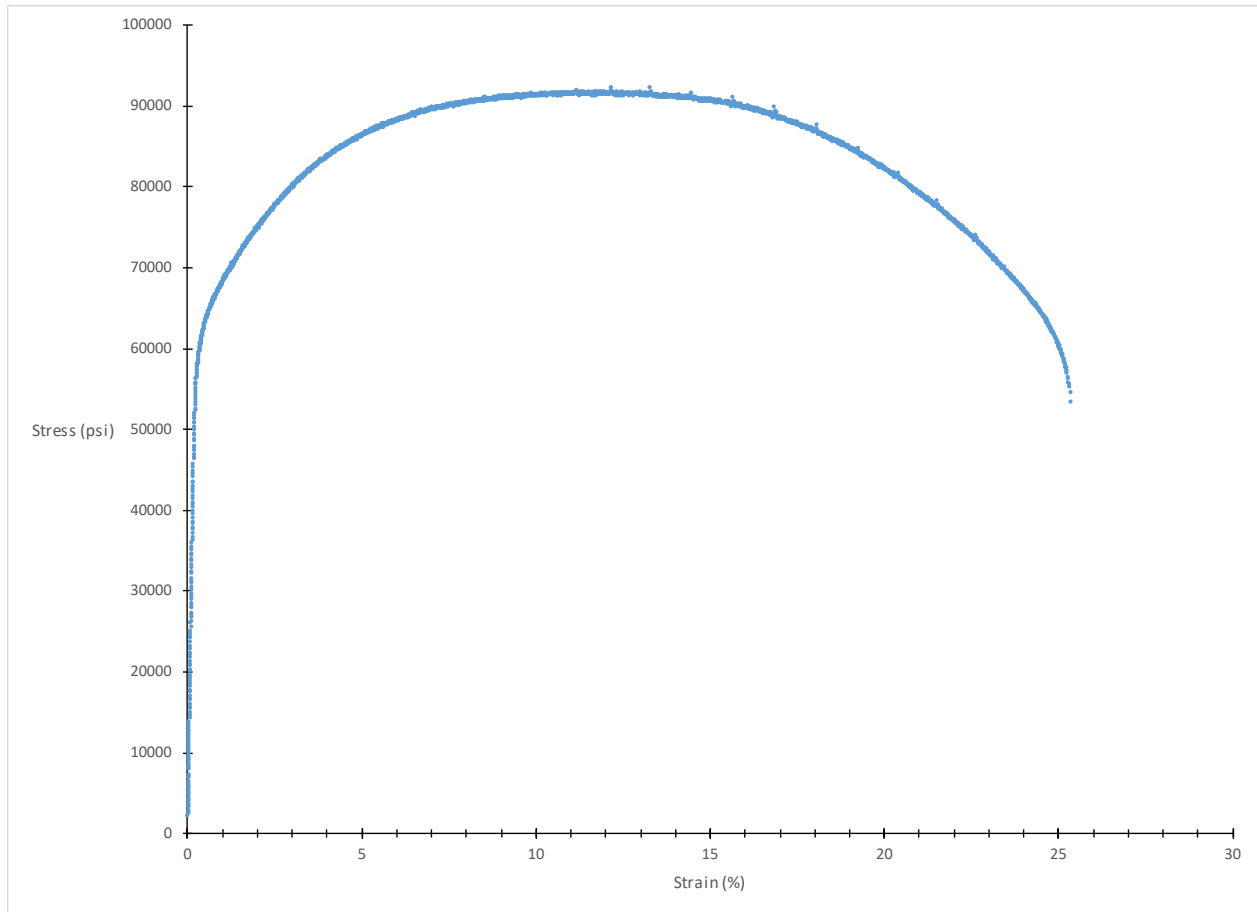


Figure 7.2.1.3.1-1: A225 Smooth Specimen Tensile Plot for Sample 519-245

7.2.1.3.2 Notch Tensile Test

Notch tensile tests of A225 specimens were conducted according to ASTM G142, “Standard Test Method for Determination of Susceptibility of Metals to Embrittlement in Hydrogen Containing Environments at High Pressure, High Temperature, or Both” (52). The test specimens were standard notch tensile design S-40-B with notch diameter = 0.25 inches and had a Kt value of 6.0 (5.55 – 6.48).

A total of five specimens removed from the MV50466-8 LPV vessel head underwent two baseline tests and four gaseous hydrogen tests. The environment for the two baseline tests was 5000 psi gaseous helium at an ambient temperature of approximately 31°C. The environment for the three hydrogen embrittlement tests was 5000 psi gaseous hydrogen at an ambient temperature of approximately 30°F. The test frame was equipped with a servo-hydraulic mechanical actuator and reaction member. Stress measurements were derived from a load cell and specimen pre-test dimension measurements. Displacement measurements were derived from an LVDT. The tests were performed in displacement control at an actuator speed of 0.0005 in/min.

The average tensile stress for baseline Gaseous Helium (GHe) tests was 132.84 ksi, with a minimum value of 132.47 ksi. The average tensile stress for Gaseous Hydrogen (GH2) tests was 108.71 ksi with a minimum value of 103.13 ksi. The results are reported in Table 7.2.1.3.2-1 and Figure 7.2.1.3.2-1.

Table 7.2.1.3.2-1: A225 Notch Tensile Data, MV50466-8

Specimen ID	Test Temp. (°C)	ASTM Orientation	Tensile Stress (ksi)	Notes
440-184	31	C	132.47	5000 psi, Ambient, GHe
440-185	32	C	133.2	5000 psi, Ambient, GHe
440-186	31	C	112.46	5000 psi, Ambient, GH2
440-188	28	C	104.37	5000 psi, Ambient, GH2
440-189	28	C	103.13	5000 psi, Ambient, GH2

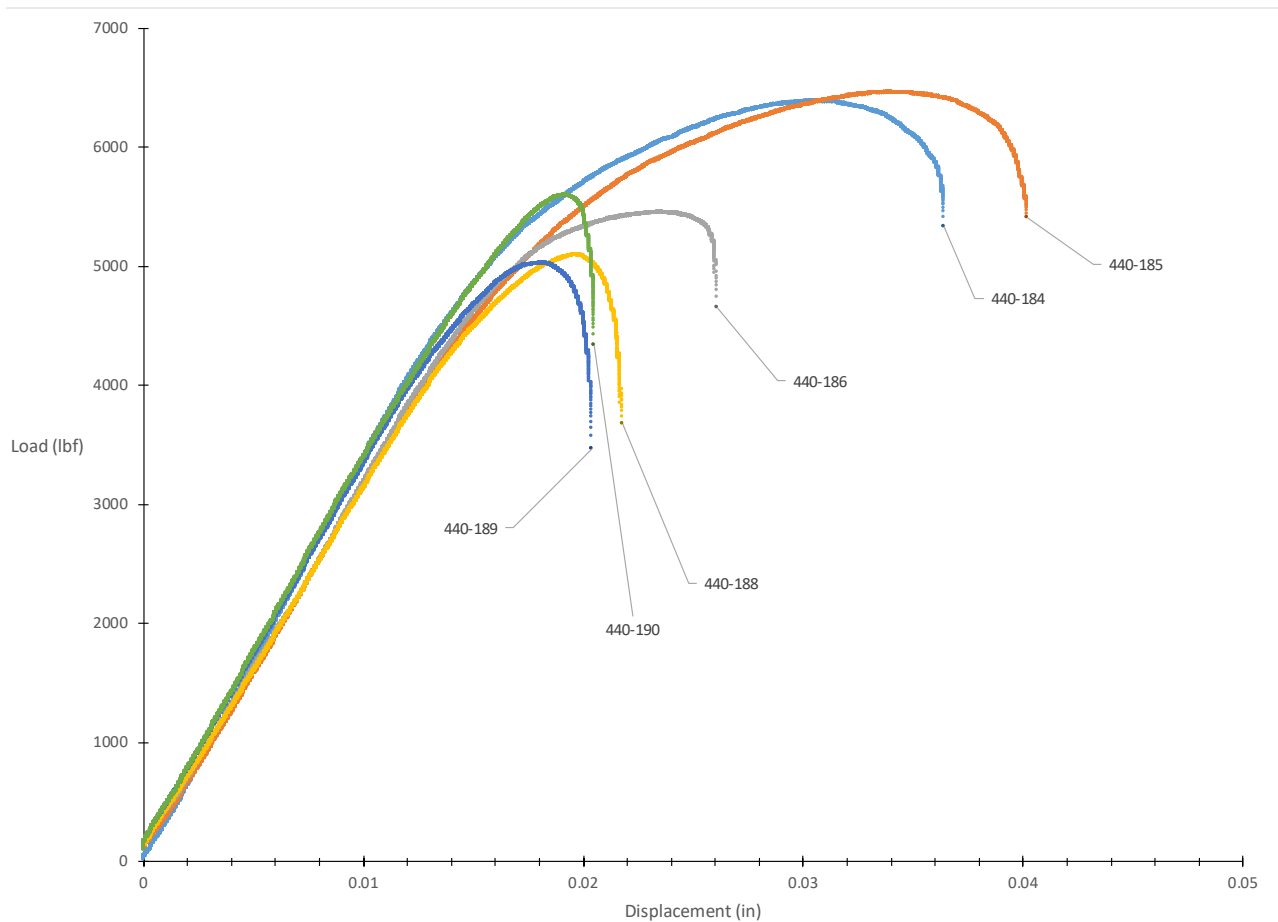


Figure 7.2.1.3.2-1: A225 Notch Tensile Plot, MV50466-8

7.2.1.3.3 Fracture Properties

All room temperature testing was performed in accordance with ASTM E1820 (10). All other temperatures were tested per ASTM E1921 (7). Testing for both standards use specimen design S-318 Rev A. All A225 fracture tests came from LPVs V0023, MV50466-8, V0032, PV0296, and V0125 and were tested with the crack plane in the C-M orientation as defined by ASTM (both grain and vessel orientations). The specimens used were ASTM E1820 (C(T)) specimens with $W = 2.0$ in., $B = 1.0$ in., and $a/W = 0.5$. All specimens were side grooved to a total thickness reduction of 20%. The cutting diagram used to remove the C(T) specimens from the 32 head is shown in Figure 7.2.1.3.3-3. Examples of load versus Crack Opening Displacement (COD) and J_q versus Δa plots are shown in Figure 7.2.1.3.3-1 and Figure 7.2.1.3.3-2. One vessel, PV0296, was tested by US Naval Academy personnel whereas the rest were tested at MSFC.

The parent A225 head material was tested by selecting representative material within the head away from flame cuts or welds that may have been detrimentally affected by further processing in HAZ. Unlike layer materials, no orientation down-selection was performed for heads based on past metallographic and Charpy impact testing results of other vessels. Specimens were extracted around the full head circumference where possible, from remnant material, as well as at multiple radial locations.

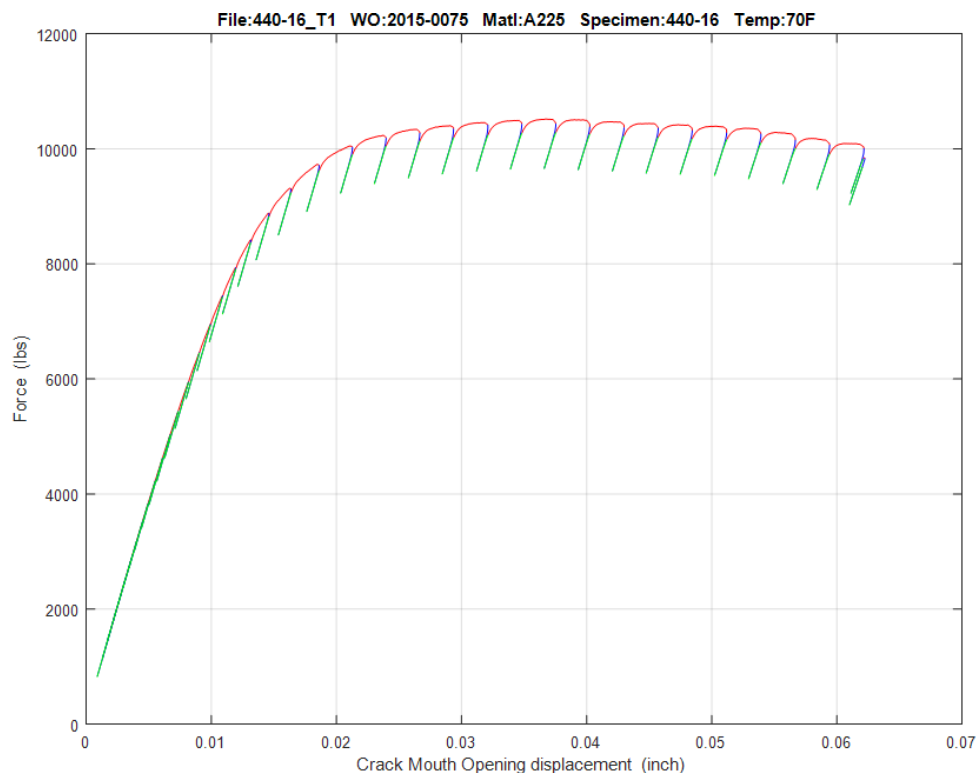


Figure 7.2.1.3.3-1: A225 Load Versus COD Plot, Sample 440-16

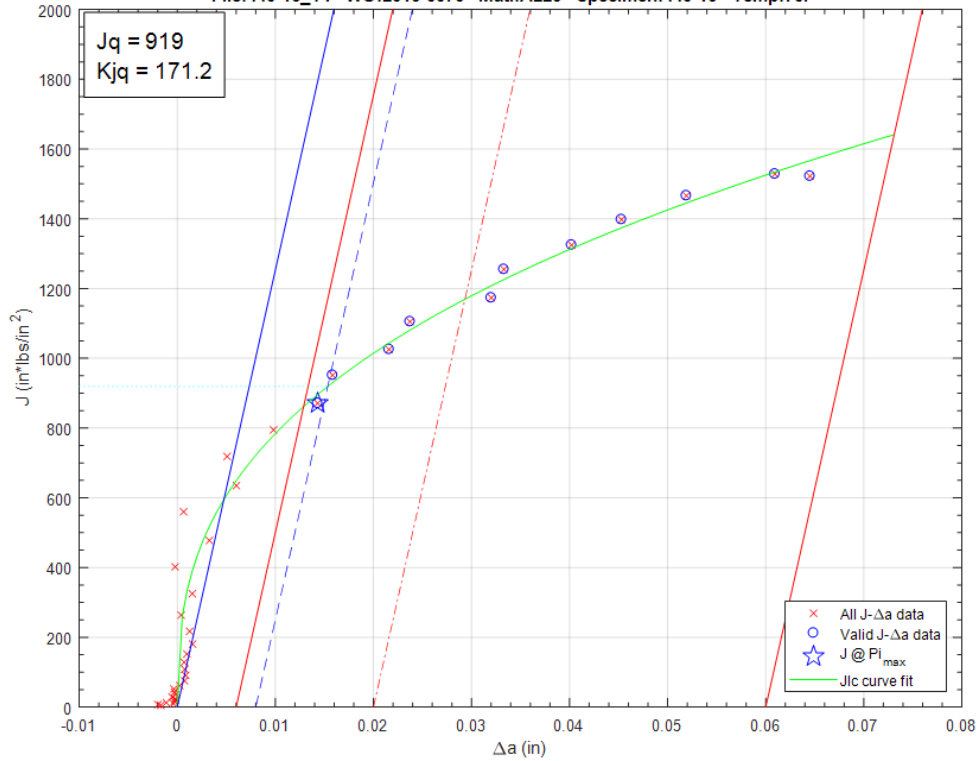


Figure 7.2.1.3.3-2: A225 J_q Versus Δa Plot, Sample 440-16

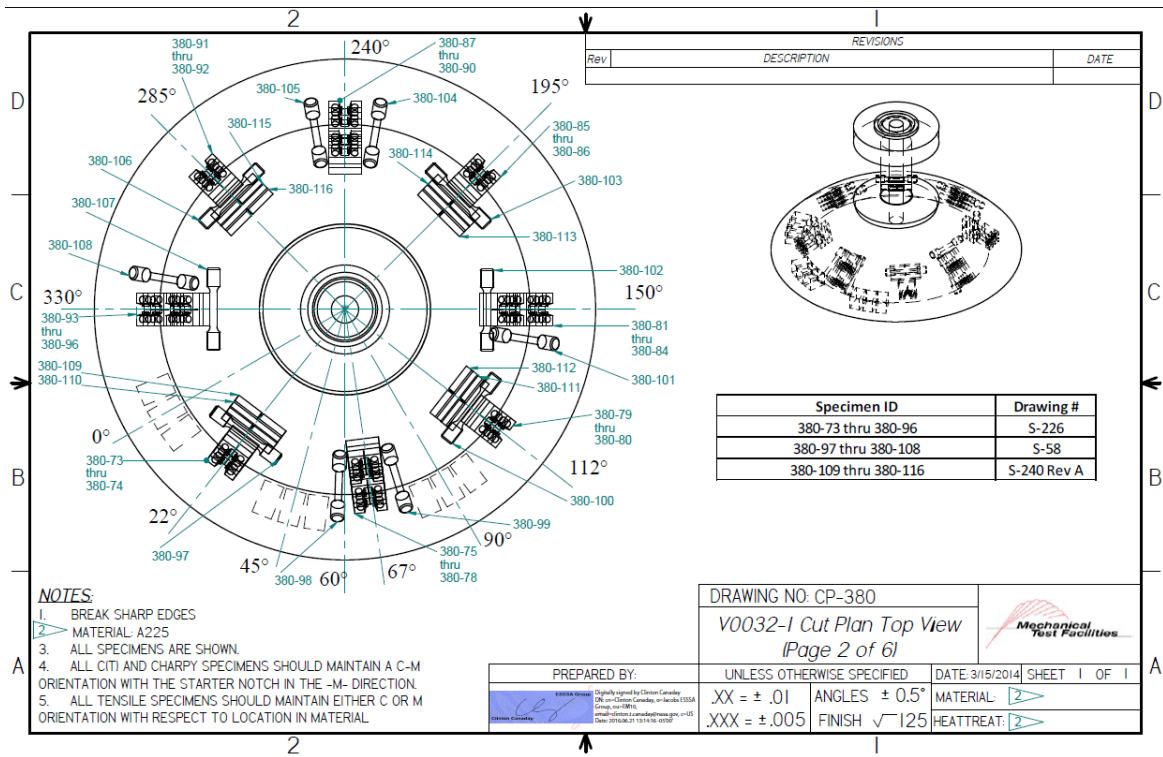


Figure 7.2.1.3.3-3: V0032 Specimen Layout

The test data in Table 7.2.1.3.3-1 are raw values obtained from fracture tests conducted on V0125 A225 head material. Tests that are considered upper shelf are listed under ASTM E1820, while transition temperature tests are listed under E1921. Tests that meet the complete validity requirements for $J_q = J_{1C}$ and $K_{Jq} = K_{J1C}$ are denoted with an asterisk. Despite invalidities, J_q and K_{Jq} convey valuable fracture toughness information, especially when the test results are applied directly to the sample material source.

Table 7.2.1.3.3-1: V0125 A225 Head Fracture Data

Specimen ID	Test Temp. (°C)	ASTM Crack Plane Orientation	W (in)	a ₀ (in)	a _f (in)	B ₀ (in)	B _N (in)	J _q (kJ/m ²)	K _{Jq} (MPa√m)	K _{JC1T} (MPa√m)	ASTM Standard
CP-344-6	21	M-C	1.0017	0.4944	0.5734	0.3775	0.3004	184	203	---	E1820
CP-344-8	20	C-M	1.0015	0.5083	0.6060	0.3772	0.2983	213	218	---	E1820
CP-344-3	-29	R-M	1.0022	0.5272	0.6440	0.3749	0.3600	51	107	---	E1820
CP-344-1	-29	R-M	1.0055	0.5206	0.5726	0.3738	0.2983	97	147	---	E1820
CP-344-7	-29	C-M	1.0010	0.4991	0.5805	0.3750	0.2990	222	223	---	E1820
CP-344-9	-29	C-M	1.0025	0.5083	0.5938	0.3767	0.3007	224	224	---	E1820

E1921 transition temperature tests were not conducted on the A225 material from V0125. The low temperature tests conducted were not at temperatures low enough to induce cleavage failure. Therefore, it is relatively safe to assume that the T_0 is somewhere below the -29°C lowest test temperature.

The test data in Table 7.2.1.3.3-2 are raw values obtained from fracture tests conducted on MV50466-8 A225 head material. Tests that are considered upper shelf are listed under ASTM E1820, while transition temperature tests are listed under E1921. Tests that meet the complete validity requirements for $J_q = J_{1C}$ and $K_{Jq} = K_{J1C}$ are denoted with an asterisk. Despite invalidities, J_q and K_{Jq} convey valuable fracture toughness information, especially when the test results are applied directly to the sample material source.

Table 7.2.1.3.3-2: MV50466-8 A225 Head Fracture Data

Specimen ID	Test Temp. (°C)	ASTM Crack Plane Orientation	W (in)	a ₀ (in)	a _r (in)	B ₀ (in)	B _N (in)	J _q (kJ/m ²)	K _{Iq} (MPa √m)	K _{JCI,T} (MPa √m)	ASTM Standard
440-13	23	C-M	1.9926	1.0257	1.0841	1.0025	0.8041	303	260	---	E1820
440-49	22	C-M	1.9959	1.0125	1.0307	1.0028	0.8008	186	204	---	E1820
440-16	21	C-M	2.0010	1.0240	1.0905	1.0061	0.8021	158	188	---	E1820
440-50	-45	C-M	1.9933	1.0179	1.0249	1.0020	0.8037	38	92	92	E1921
440-51	-45	C-M	1.9922	1.0140	1.0154	1.0067	0.8030	36	89	89	E1921
440-52	-45	C-M	1.9933	1.0190	1.0344	1.0021	0.8090	43	98	98	E1921
440-53	-45	C-M	1.9935	1.0164	1.0177	0.9969	0.8010	21	68	68	E1921
440-18	-73	C-M	1.9920	1.0168	1.0183	1.0035	0.8027	18	63	63	E1921
440-19	-73	C-M	1.9912	1.0152	1.0232	1.0034	0.8001	26	76	76	E1921
440-20	-73	C-M	1.9921	1.0126	1.0216	1.0032	0.8043	29	80	81	E1921
440-21	-73	C-M	1.9989	1.0168	1.0302	1.0038	0.8021	21	69	69	E1921
440-26	-84	C-M	1.9973	1.0159	1.0183	1.0023	0.8020	28	78	79	E1921
440-17	-84	C-M	1.9928	1.0126	1.0175	1.0007	0.7995	23	72	72	E1921
440-22	-84	C-M	1.9933	1.0188	1.0220	1.0013	0.8020	17	61	61	E1921
440-23	-84	C-M	1.9915	1.0180	1.0205	1.0023	0.7986	17	61	61	E1921
440-24	-84	C-M	1.9927	1.0118	1.0159	1.0019	0.7999	22	70	70	E1921
440-25	-84	C-M	1.9910	1.0027	1.0054	1.0023	0.8050	30	82	82	E1921
440-27	-84	C-M	1.9937	1.0096	1.0134	1.0028	0.7987	31	84	84	E1921
440-43	-84	C-M	1.9918	1.0191	1.0191	1.0003	0.7930	13	55	55	E1921
440-44	-84	C-M	1.9934	1.0123	1.0161	1.0021	0.8006	12	52	52	E1921
440-45	-84	C-M	2.0026	1.0167	1.0167	1.0023	0.7990	11	50	50	E1921
440-46	-84	C-M	1.9943	1.0153	1.0195	1.0024	0.8007	13	54	54	E1921
440-47	-84	C-M	1.9912	1.0124	1.0160	1.0025	0.8039	16	60	60	E1921
440-48	-84	C-M	1.9919	1.0145	1.0185	1.0013	0.7994	14	56	56	E1921
440-15	-101	C-M	1.9917	1.0117	1.0145	1.0037	0.8040	11	49	49	E1921
440-14	-107	C-M	1.9935	1.0166	1.0182	1.0019	0.8025	10	46	46	E1921

Results from the 23 E1921 tests are presented in Figure 7.2.1.3.3-4, Table 7.2.1.3.3-3 and Table 7.2.1.3.3-4. These results were obtained using the T₀TEM Code described in Section 4.2. The T₀ reference temperature for this data set was evaluated as -43°C using the E1921 Master Curve shown in Figure 7.2.1.3.3-4. The data set is considered to be macroscopically homogenous.

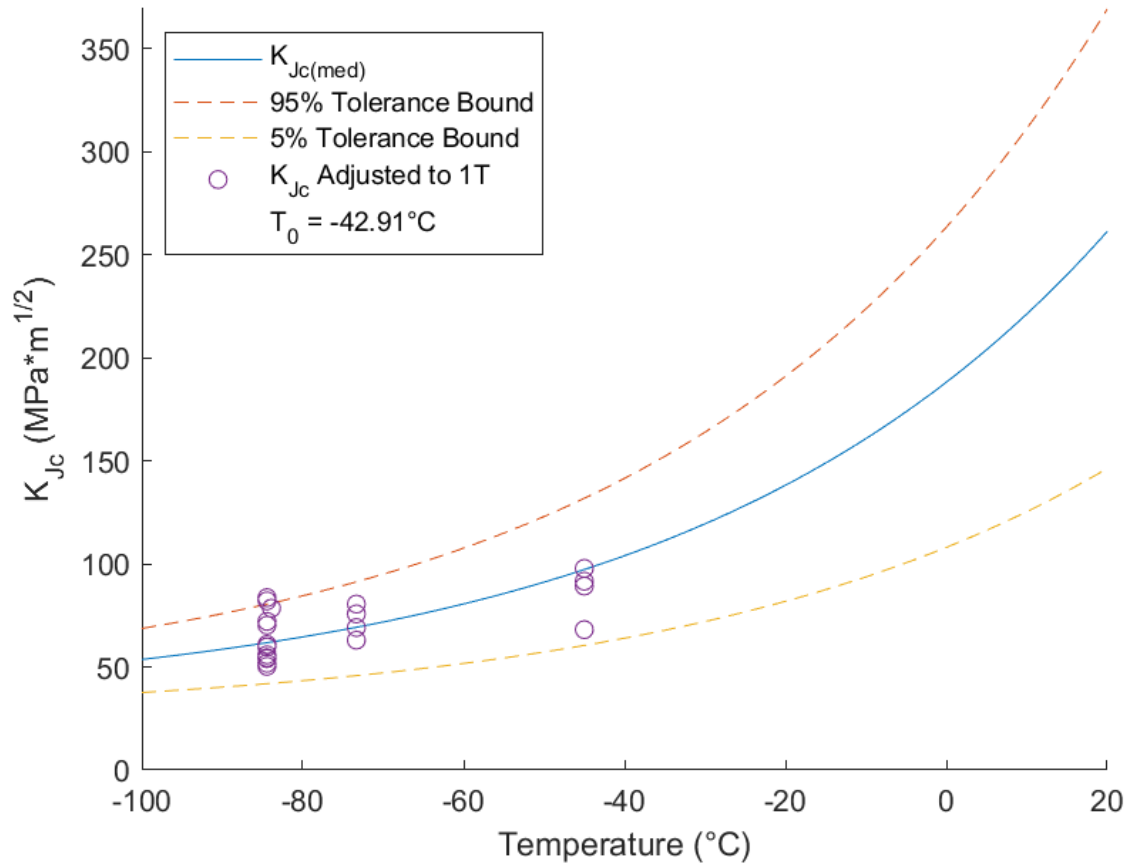


Figure 7.2.1.3.3-4: MV50466-8 A225 Head T_0 Plot ($T_0T_0 = -43^\circ\text{C}$)

Table 7.2.1.3.3-3: MV50466-8 A225 Head T₀ Individual Specimen Results

Specimen Name	Temperature (°C)	K _{Jc} Raw (MPa*m ^{0.5})	1T Data (MPa*m ^{0.5})	Uncensored Data	Test Temp -T ₀ (°C)
440-17	-84	72.1	72.1	1	-42
440-18	-73	63.0	63.0	1	-30
440-19	-73	75.7	75.7	1	-30
440-20	-73	80.5	80.5	1	-30
440-21	-73	69.1	69.1	1	-30
440-22	-84	60.9	60.9	1	-42
440-23	-84	60.9	60.9	1	-42
440-24	-84	70.3	70.3	1	-42
440-25	-84	82.0	82.1	1	-42
440-26	-84	78.5	78.5	1	-41
440-27	-84	83.6	83.6	1	-42
440-43	-84	54.5	54.5	1	-42
440-44	-84	51.8	51.8	1	-42
440-45	-84	50.3	50.3	1	-42
440-46	-84	54.1	54.1	1	-42
440-47	-84	59.7	59.8	1	-42
440-48	-84	55.9	55.9	1	-42
440-50	-45	91.6	91.6	1	-2
440-51	-45	89.2	89.3	1	-2
440-52	-45	97.8	97.8	1	-2
440-53	-45	68.2	68.1	1	-2

Table 7.2.1.3.3-4: MV50466-8 A225 Head T₀ Calculation Results

Initial T ₀ (°C)	-43
Total Samples	21
Samples within T ₀ ± 50°C (N)	21
Number of Uncensored Data (r)	21
Poisson's Ratio	0.3
Σ(r _i n _i)	2.86
Samples Between T _i - T ₀ 50 to -14 °C	4
Samples Between T _i - T ₀ -15 to -35 °C	4
Samples Between T _i - T ₀ -36 to -50 °C	13
T ₀ scrn (°C)	-40
Homogenous or Inhomogeneous	Homogenous

The test data in Table 7.2.1.3.3-5 are raw values obtained from fracture tests conducted on V0023 A225 head material. Test results that are considered upper shelf are listed under ASTM E1820, while transition temperature test results are listed under E1921. Tests that meet the complete validity requirements for $J_q = J_{1C}$ and $K_{Jq} = K_{J1C}$ are denoted with an asterisk.

Despite invalidities, J_q and K_{Jq} convey valuable fracture toughness information, especially when the test results are applied directly to the sample material source. No upper shelf tests were performed as the material exhibited cleavage failure at room temperature and at temperatures as high as 100°C which was the highest temperature possible for the test apparatus.

Table 7.2.1.3.3-5: V0023 A225 Head Fracture Data

Specimen ID	Test Temp. (°C)	ASTM Crack Plane Orientation	W (in)	a_0 (in)	a_f (in)	B_0 (in)	B_N (in)	J_q (kJ/m ²)	K_{Jq} (MPa√m)	$K_{JCI T}$ (MPa√m)	ASTM Standard
519-226	100	C-M	1.9998	1.0327	1.0694	0.9983	0.7905	191	207	207	E1921
519-229	50	C-M	1.9985	1.0403	1.0622	0.9985	0.7989	158	188	188	E1921
519-231	22	C-M	1.9994	1.0430	1.0490	0.9992	0.7925	74	128	128	E1921
519-222	22	C-M	2.0047	1.0340	1.0436	1.0011	0.7964	82	136	136	E1921
519-224	22	C-M	2.0012	1.0381	1.0481	1.0011	0.7965	101	151	151	E1921
519-234	22	C-M	2.0044	1.0336	1.0390	1.0018	0.7931	38	92	92	E1921
519-236	22	C-M	2.0010	1.0346	1.0617	1.0009	0.7972	187	204	205	E1921
519-237	22	C-M	2.0008	1.0371	1.0651	0.9992	0.7874	179	200	200	E1921
519-238	22	C-M	1.9983	1.0278	1.0371	0.9990	0.7901	103	151	151	E1921
519-221	21	C-M	2.0041	1.0371	1.0371	1.0003	0.8310	72	127	127	E1921
519-225	21	C-M	2.0002	1.0307	1.0356	0.9975	0.7956	63	118	118	E1921
519-228	21	C-M	1.9983	1.0319	1.0420	0.9996	0.7940	92	144	143	E1921
519-230	21	C-M	1.9976	1.0248	1.0376	0.9997	0.7974	133	172	172	E1921
519-233	21	C-M	2.0017	1.0299	1.0380	0.9995	0.8153	58	114	114	E1921
519-235	21	C-M	2.0024	1.0346	1.0465	0.9994	0.8164	139	176	176	E1921
519-242	21	C-M	1.9981	1.0390	1.0423	0.9993	0.8044	47	103	103	E1921
519-243	21	C-M	1.9973	1.0405	1.0619	0.9990	0.7953	172	196	196	E1921
519-244	21	C-M	1.9980	1.0341	1.0373	0.9989	0.7899	58	114	114	E1921
519-241	21	C-M	2.0016	1.0395	1.0469	0.9989	0.7963	94	145	145	E1921
519-223	-46	C-M	2.0019	1.0410	1.0410	1.0000	0.8146	7	40	40	E1921

Results from the twenty E1921 tests are presented in. These results were obtained using the T_0 TEM Code described in Section 4.2. The T_0 reference temperature for this data set was evaluated as -2°C using the E1921 Master Curve shown in Figure 7.2.1.3.3-5.

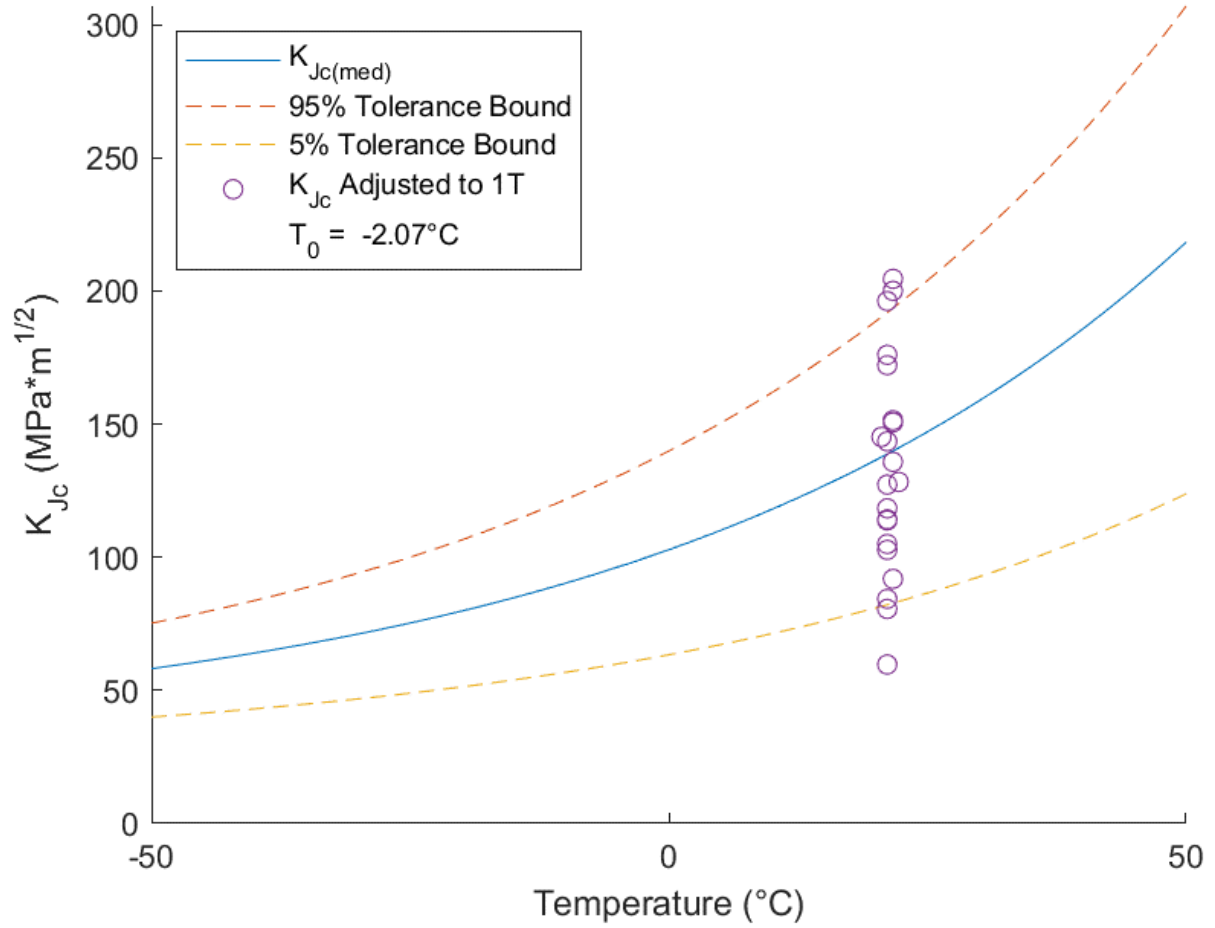


Figure 7.2.1.3.3-5: V0023 A225 Head T_0 Plot ($T_0 = -2^{\circ}\text{C}$)

Table 7.2.1.3.3-6: V0023 A225 Head T₀ Individual Specimen Results

Specimen Name	Temperature (°C)	KjcRaw (MPa*m ^{0.5})	1T Data (MPa*m ^{0.5})	Uncensored Data	Test Temp -T ₀ (°C)
519-221	21	127.2	127.3	1	23
519-222	22	135.8	135.8	1	24
519-224	22	150.6	150.6	1	24
519-225	21	118.4	118.3	1	23
519-228	21	143.5	143.5	1	23
519-230	21	172.1	172.1	1	23
519-231	22	128.3	128.3	1	24
519-233	21	114.2	114.2	1	23
519-234	22	91.8	91.9	1	24
519-235	21	176.0	176.0	1	23
519-236	22	204.5	204.5	1	24
519-237	22	200.0	200.0	1	24
519-238	22	151.4	151.4	1	24
519-241	21	145.2	145.1	1	23
519-242	21	102.7	102.7	1	23
519-243	21	196.2	196.2	1	23
519-244	21	113.8	113.8	1	23
519-232	21	105.0	105.0	1	23
519-240	21	59.7	59.7	1	23
519-239	21	80.6	80.6	1	23
519-227	21	84.4	84.3	1	23

Table 7.2.1.3.3-7 V0023 A225 Head T₀ Calculation Results

Initial T ₀ (°C)	-2
Total Samples	21
Samples within T ₀ ± 50°C (N)	21
Number of Uncensored Data (r)	21
Poisson's Ratio	0.3
Σ(ri ni)	3.5
Samples Between T _i - T ₀ 50 to -14 °C	21
Samples Between T _i - T ₀ -15 to -35 °C	0
Samples Between T _i - T ₀ -36 to -50 °C	0
T ₀ scrn (°C)	5
Homogenous or Inhomogeneous	Homogeneous

The test data in Table 7.2.1.3.3-8 are raw values obtained from fracture tests conducted on V0032 A225 head material. Test results that are considered upper shelf are listed under ASTM E1820, while transition temperature test results are listed under E1921. Tests that meet the complete validity requirements for $J_q = J_{1C}$ and $K_{Jq} = K_{J1C}$ are denoted with an asterisk. Despite invalidities, J_q and K_{Jq} convey valuable fracture toughness information, especially when the test results are applied directly to the sample material source.

Table 7.2.1.3.3-8 V0032 A225 Head Fracture Data

Specimen ID	Test Temp. (°C)	ASTM Crack Plane Orientation	W (in)	a ₀ (in)	a _f (in)	B ₀ (in)	B _N (in)	J _q (kJ/m ²)	K _{Jq} (MPa√m)	K _{JC1T} (MPa√m)	ASTM Standard
380-76	-57	C-M	0.9983	0.5309	0.5566	0.3752	0.3003	190	206	---	E1820
380-80	-59	C-M	0.9987	0.5239	0.5620	0.3761	0.3026	213	218	---	E1820
380-95	-101	C-M	0.9994	0.5243	0.5243	0.3745	0.3060	33	86	72	E1921
380-84	-101	C-M	1.0015	0.5085	0.5089	0.3737	0.3000	24	73	62	E1921
380-73	-101	C-M	0.9964	0.5183	0.5183	0.3746	0.3009	111	158	128	E1921
380-93	-101	C-M	0.9989	0.5315	0.5318	0.3749	0.3021	22	71	60	E1921
380-74	-101	C-M	1.0033	0.5240	0.5240	0.3645	0.2993	57	113	93	E1921
380-96	-102	C-M	1.0005	0.5242	0.5242	0.3741	0.3001	44	99	82	E1921
380-94	-102	C-M	1.0005	0.5197	0.5197	0.3743	0.3034	33	85	71	E1921
380-77	-102	C-M	0.9979	0.5183	0.5186	0.3743	0.3027	25	75	63	E1921
380-75	-106	C-M	0.9985	0.5181	0.5181	0.3736	0.3024	29	81	68	E1921
380-82	-107	C-M	1.0011	0.5157	0.5163	0.3753	0.3013	10	48	42	E1921
380-85	-107	C-M	0.9988	0.5438	0.5438	0.3750	0.3017	54	110	90	E1921
380-88	-107	C-M	1.0001	0.5164	0.5172	0.3748	0.2998	169	194	156	E1921
380-89	-107	C-M	1.0003	0.5267	0.5284	0.3740	0.3004	28	79	66	E1921
380-79	-107	C-M	1.0010	0.5293	0.5302	0.3754	0.2979	37	91	76	E1921
380-86	-107	C-M	1.0008	0.5186	0.5186	0.3741	0.3002	42	97	80	E1921
380-87	-107	C-M	1.0004	0.5138	0.5138	0.3733	0.3068	11	50	43	E1921
380-91	-107	C-M	1.0020	0.5180	0.5180	0.3762	0.2988	97	148	120	E1921
380-78	-107	C-M	0.9986	0.5200	0.5201	0.3741	0.3004	115	161	130	E1921
380-81	-107	C-M	1.0008	0.5365	0.5365	0.3740	0.3002	93	144	117	E1921

Results from the 19 E1921 tests are presented in Figure 7.2.1.3.3-6 and Table 7.2.1.3.3-9, Table 7.2.1.3.3-10 . These results were obtained using the TOTEM Code described in Section 4.2. The T₀ reference temperature for this data set was evaluated as -104°C using the E1921 Master Curve shown in Figure 7.2.1.3.3-6.

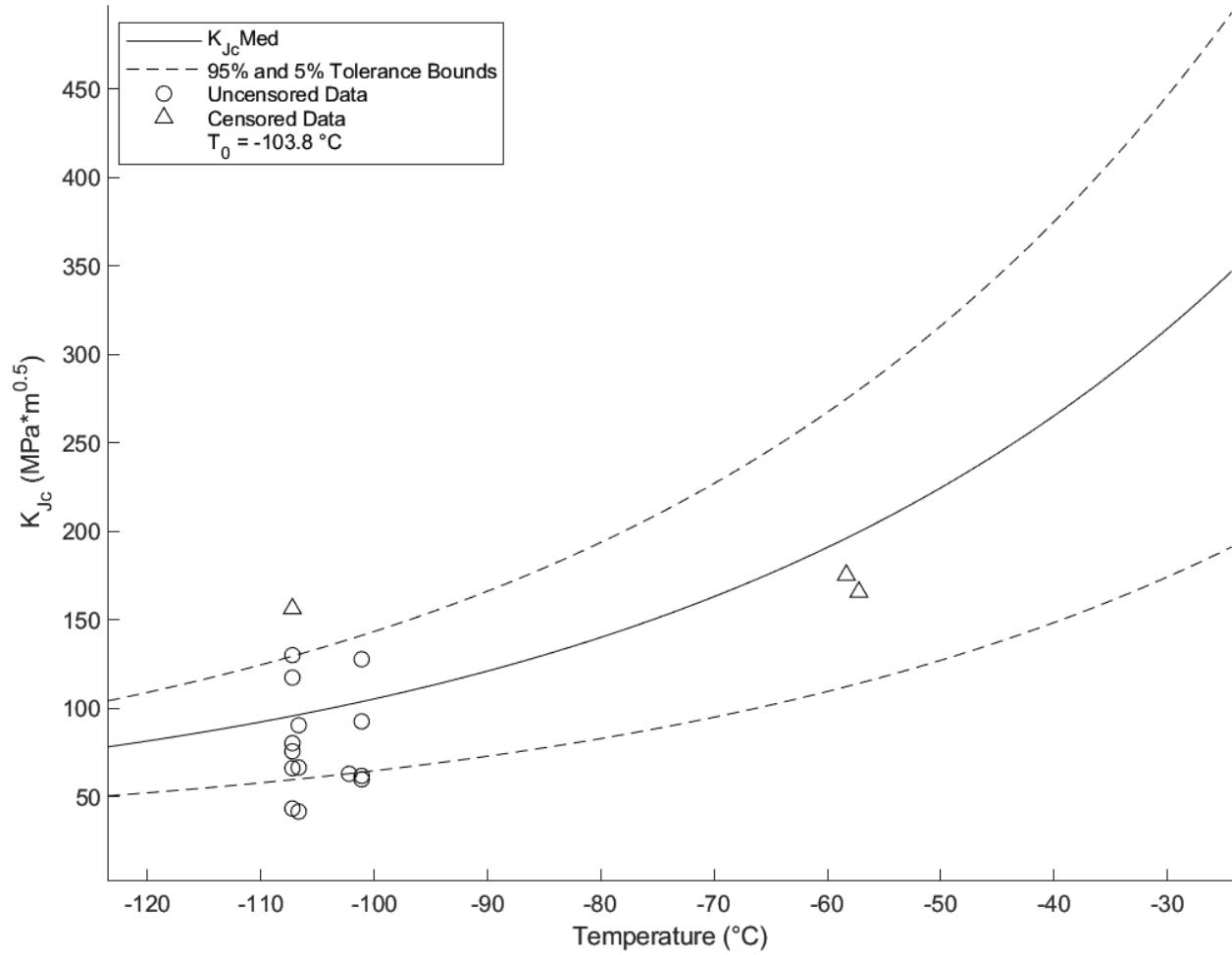


Figure 7.2.1.3.3-6: V0032 A225 Head T_0 Plot ($T_0 = -104^{\circ}\text{C}$)

Table 7.2.1.3.3-9: V0032 A225 Head T₀ Individual Specimen Results

Specimen Name	Temperature (°C)	KjcRaw (MPa*m ^{0.5})	1T Data (MPa*m ^{0.5})	Uncensored Data	Test Temp -T0 (°C)
380-73	-101	157.6	127.7	1	3
380-74	-101	113.3	92.5	1	3
380-75	-107	79.4	66.5	1	-3
380-76	-57	206.1	130.0	0	47
380-77	-102	74.8	62.9	1	2
380-78	-107	160.6	130.0	1	-3
380-79	-107	91.0	75.6	1	-3
380-80	-58	218.2	130.0	0	45
380-81	-107	144.4	117.3	1	-3
380-82	-107	47.6	41.6	1	-3
380-84	-101	73.4	61.7	1	3
380-85	-107	109.9	90.4	1	-3
380-86	-107	97.0	80.2	1	-3
380-87	-107	49.8	43.3	1	-3
380-88	-107	194.2	146.4	0	-3
380-89	-107	78.9	66.1	1	-3
380-93	-101	70.8	59.7	1	3

Table 7.2.1.3.3-10: V0032 A225 Head T₀ Calculation Results

Initial T0 (°C)	-104
Total Samples	17
Samples within T0 ± 50°C (N)	17
Number of Uncensored Data (r)	14
Poisson's Ratio	0.3
Σ(ri ni)	2.33
Samples Between Ti - T0 50 to -14 °C	14
Samples Between Ti - T0 -15 to -35 °C	0
Samples Between Ti - T0 -36 to -50 °C	0
T0scrn (°C)	-76
Homogenous or Inhomogeneous	Inhomogeneous

According to the E1921 inhomogeneity annex, this material is macroscopically inhomogeneous with a 95% confidence in multimodal inhomogeneity. Therefore, it is recommended that the multimodal median transition temperature value T_m = -89°C be recognized as the final value. This gives a more accurate reflection of the material properties

and the associated confidence bounds include a more acceptable number of specimens as shown in Figure 7.2.1.3.3-7

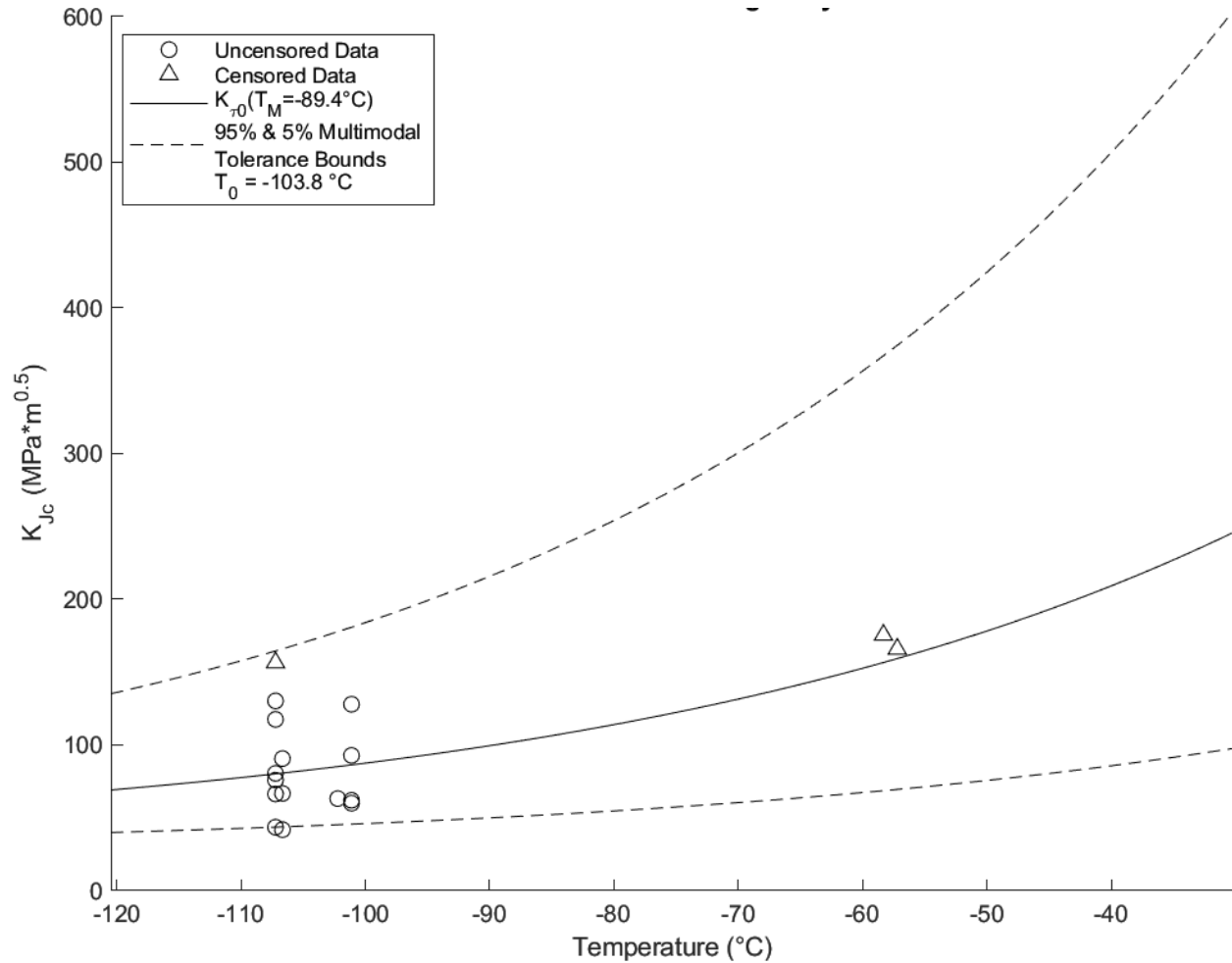


Table 7.2.1.3.3-11: V0032 A225 Head Multimodal T_m Calculation Results

T_m ($^\circ\text{C}$)	-89
σT_m ($^\circ\text{C}$)	29
Multimodal Homogeneity	Inhomogeneous
Multimodal Confidence	94.81
Number of samples within $T_m \pm 50^\circ\text{C}$	17

The test data in Table 7.2.1.3.3-12 are raw values obtained from fracture tests conducted on PV0296 A225 head material. Upper shelf tests are listed under ASTM E1820, while transition temperature tests are listed under E1921. Tests that meet the complete validity

requirements for $J_q = J_{1C}$ and $K_{Jq} = K_{J1C}$ are denoted with an asterisk. Despite invalidities, J_q and K_{Jq} convey valuable fracture toughness information, especially when the test results are applied directly to the sample material source.

Table 7.2.1.3.3-12: PV0296 A225 Head Fracture Data

Specimen ID	Test Temp. (°C)	ASTM Crack Plane Orientation	W (in)	a_0 (in)	a_f (in)	B_0 (in)	B_N (in)	J_q (kJ/m ²)	K_{Jq} (MPa \sqrt{m})	K_{J1C} (MPa \sqrt{m})	ASTM Standard
393-22	0	C-M	1.0010	0.5200	0.0000	0.3720	0.2990	498	334	---	E1820
393-27	-30	C-M	0.9980	0.5200	0.0000	0.3730	0.2800	242	232	183	E1921
393-34	-30	C-M	0.9990	0.5210	0.0000	0.3730	0.3060	369	287	183	E1921
393-24	-50	C-M	0.9980	0.5110	0.0000	0.3740	0.2970	244	233	187	E1921
393-25	-50	C-M	0.9990	0.5220	0.0000	0.3730	0.3000	152	184	149	E1921
393-28	-50	C-M	0.9970	0.5200	0.0000	0.3710	0.3010	160	189	152	E1921
393-32	-50	C-M	0.9980	0.5200	0.0000	0.3730	0.3040	199	211	169	E1921
393-19	-80	C-M	1.0000	0.5190	0.0000	0.3730	0.3000	61	117	96	E1921
393-21	-80	C-M	0.9990	0.5210	0.0000	0.3730	0.2940	64	120	98	E1921
393-30	-80	C-M	0.9970	0.5140	0.0000	0.3730	0.2920	15	59	50	E1921
393-31	-80	C-M	0.9990	0.5160	0.0000	0.3730	0.3010	50	106	87	E1921
393-33	-80	C-M	0.9980	0.5180	0.0000	0.3730	0.3080	130	171	138	E1921
393-35	-80	C-M	0.9990	0.5180	0.0000	0.3730	0.3080	50	106	87	E1921
393-36	-80	C-M	0.9990	0.5180	0.0000	0.3750	0.3030	21	68	58	E1921
393-20	-101	C-M	1.0000	0.5140	0.0000	0.3730	0.3000	23	72	61	E1921
393-23	-101	C-M	0.9980	0.5170	0.0000	0.3720	0.2990	9	46	40	E1921
393-26	-101	C-M	0.9990	0.5150	0.0000	0.3720	0.2980	15	58	50	E1921
393-29	-101	C-M	0.9980	0.5160	0.0000	0.3720	0.2910	8	43	38	E1921

Results from the 17 E1921 tests are presented in Figure 7.2.1.3.3-8, Table 7.2.1.3.3-13, and Table 7.2.1.3.3-14. These results were obtained using the T_0 TEM Code described in Section 4.2. The T_0 reference temperature for this data set was evaluated as -75°C using the E1921 Master Curve shown in Figure 7.2.1.3.3-8.

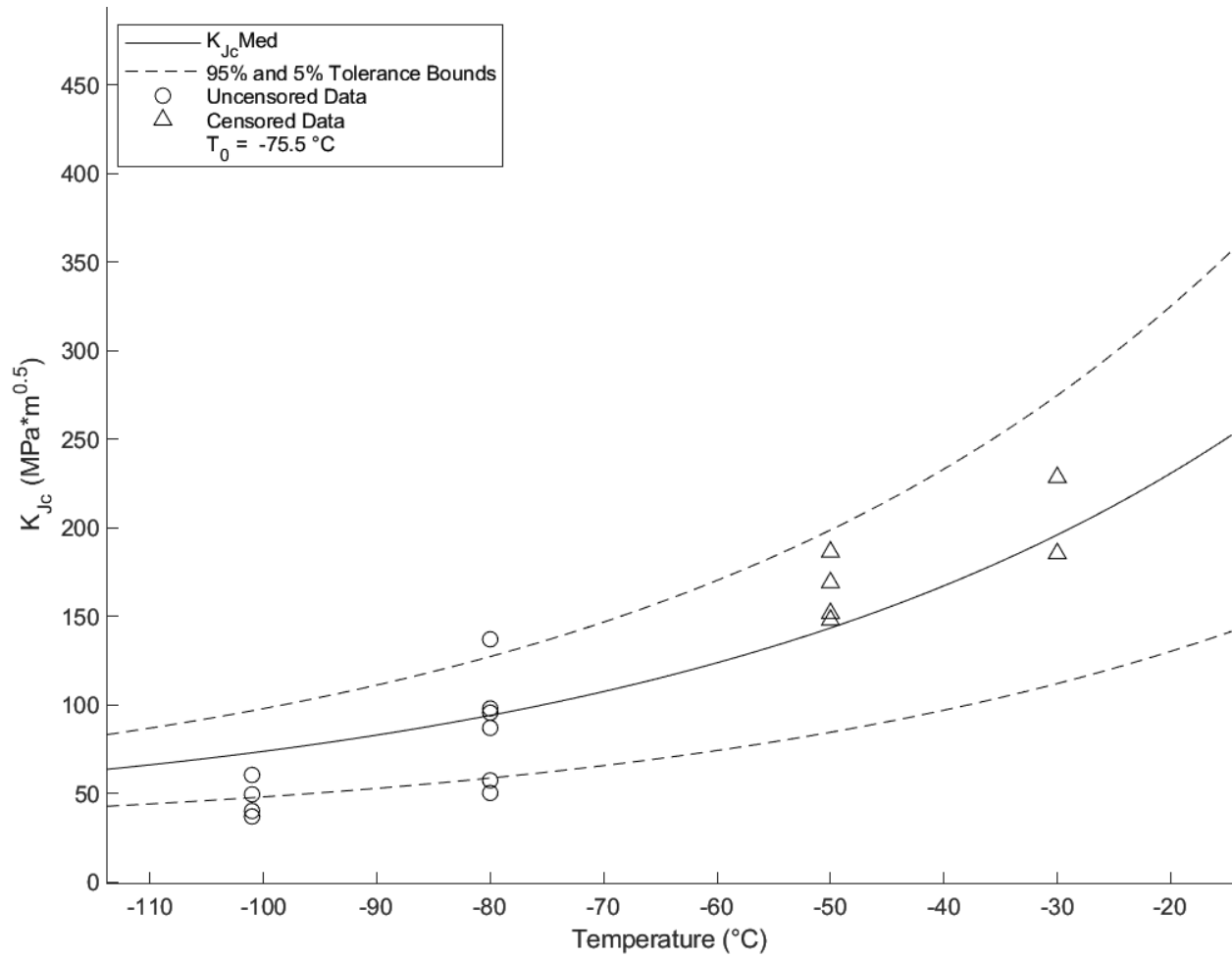


Figure 7.2.1.3.3-8: PV0296 A225 Head T_0 Plot ($T_0 = -75^\circ\text{C}$)

Table 7.2.1.3.3-13: PV0296 A225 Head T₀ Individual Specimen Results

Specimen Name	Temperature (°C)	KjcRaw (MPa*m ^{0.5})	1T Data (MPa*m ^{0.5})	Uncensored Data	Test Temp -T ₀ (°C)
393-19	-80	117.0	95.8	1	-5
393-20	-101	72.0	60.6	1	-26
393-21	-80	120.0	98.1	1	-5
393-23	-101	46.0	40.3	1	-26
393-26	-101	58.0	49.7	1	-26
393-29	-101	42.0	37.2	1	-26
393-30	-80	59.0	50.5	1	-5
393-31	-80	106.0	87.2	1	-5
393-33	-80	170.0	137.2	1	-5
393-35	-80	106.0	87.2	1	-5
393-36	-80	68.0	57.6	1	-5
393-24	-50	233.0	148.5	0	25
393-25	-50	184.0	146.9	0	25
393-27	-30	232.0	146.0	0	45
393-28	-50	189.0	146.7	0	25
393-34	-30	287.0	146.0	0	45
393-32	-50	211.0	147.0	0	25

Table 7.2.1.3.3-14: PV0296 A225 Head T₀ Calculation Results

Initial T₀ (°C)	-75
Total Samples	17
Samples within T₀ ± 50°C (N)	17
Number of Uncensored Data (r)	11
Poisson's Ratio	0.3
Σ(ri ni)	1.74
Samples Between T_i - T₀ 50 to -14 °C	7
Samples Between T_i - T₀ -15 to -35 °C	4
Samples Between T_i - T₀ -36 to -50 °C	0
T₀scrn (°C)	-65
Homogenous or Inhomogeneous	Inhomogeneous

According to the E1921 inhomogeneity annex, this material is macroscopically inhomogeneous with a 96% confidence in multimodal inhomogeneity. Therefore, it is recommended that the multimodal median transition temperature value T_m = -70°C be recognized as the final value. This gives a more accurate reflection of the material properties and the associated confidence bounds include a more acceptable number of specimens as shown in Figure 7.2.1.3.3-9.

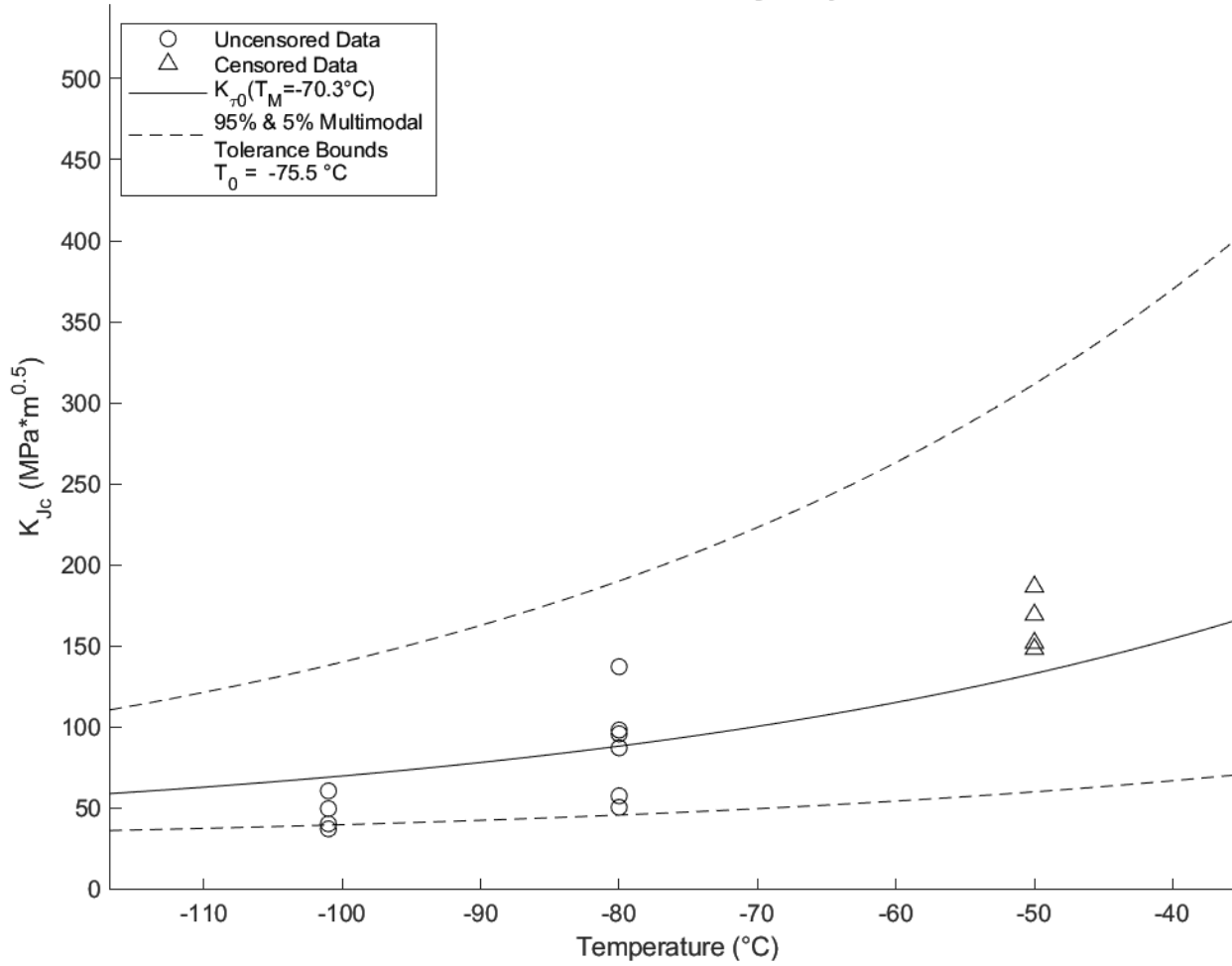


Figure 7.2.1.3.3-9: PV0296 A225 Head Multimodal T_m Plot ($T_m = -70^\circ\text{C}$)

Table 7.2.1.3.3-15: PV0296 A225 Head Multimodal T_m Calculation Results

T_m (°C)	-70
σT_m (°C)	31
Multimodal Homogeneity	Inhomogeneous
Multimodal Confidence	96.25
Number of samples within $T_m \pm 50^\circ\text{C}$	17

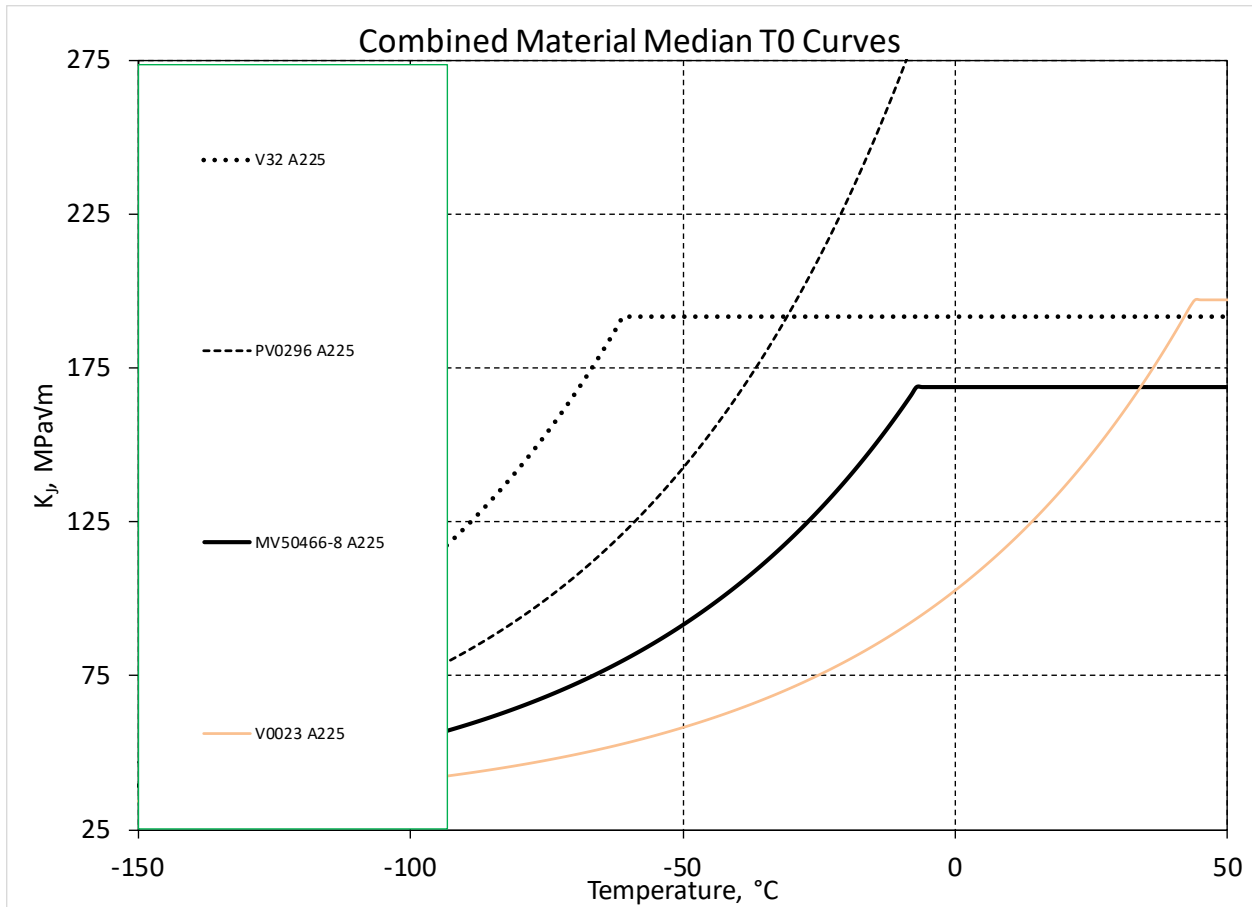


Figure 7.2.1.3.3-10: A225 Fracture Toughness Plot

The plot in Figure 7.2.1.3.3-10 shows the T_0 Master Curves for each A225 data set plotted against each other. Given the wide range of transition temperatures obtained from each individual lot, it is difficult to characterize the A225 material as a whole based on these values. A multimodal analysis has been performed on the combined data sets, treating them as one large inhomogenous data lot. The results of this evaluation are shown in Table 7.2.1.3.3-16, Table 7.2.1.3.3-17, Figure 7.2.1.3.3-11, and Figure 7.2.1.3.3-12.

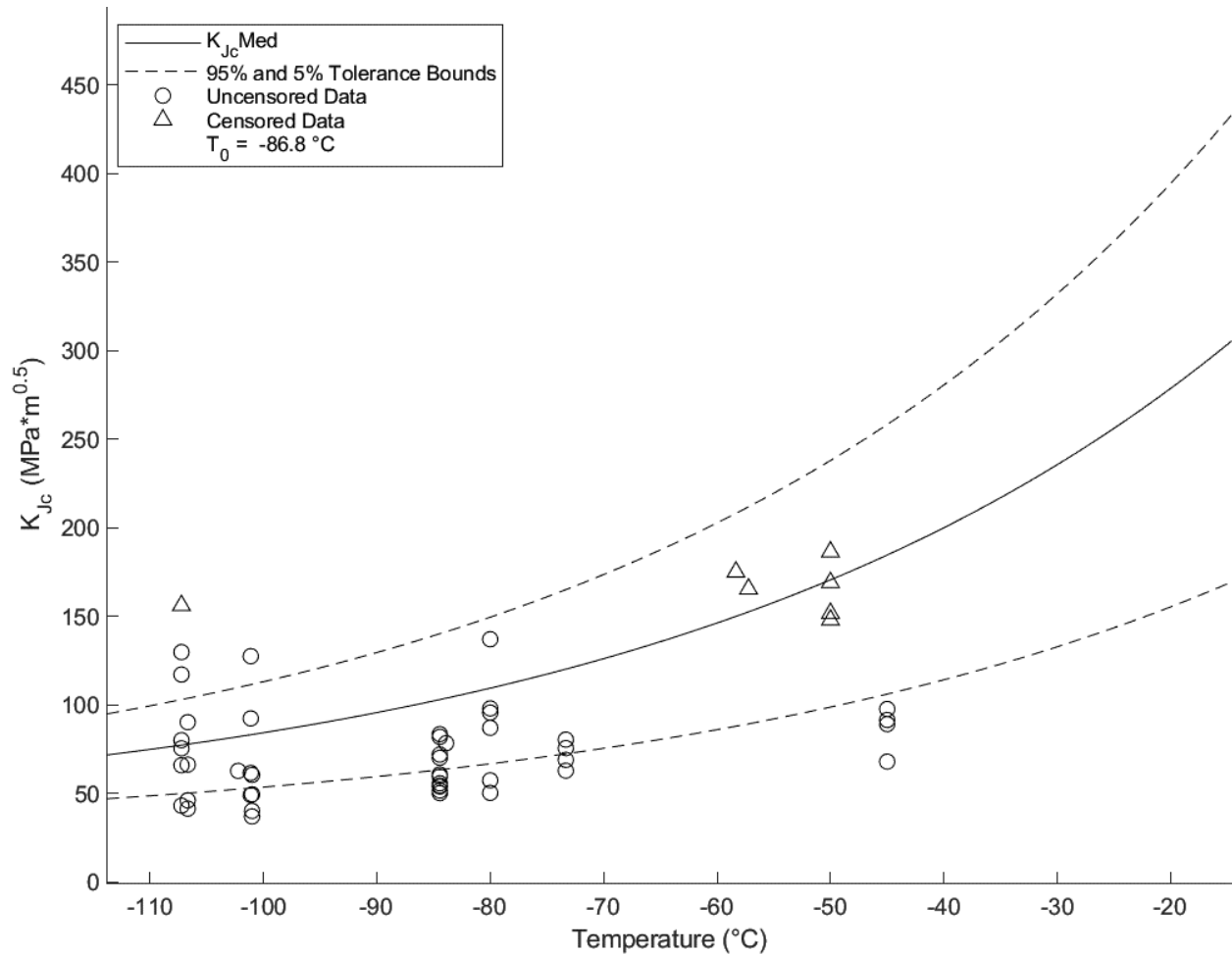


Figure 7.2.1.3.3-11: A225 Combined Set T_0 Plot ($T_0 = -87$ °C)

Table 7.2.1.3.3-16 A225 Combined Set T_0 Calculation Results

Initial T_0 (°C)	-87
Total Samples	60
Number of Samples Between +50/-50°C (N)	54
Number of Uncensored Data (r)	47
Poisson's Ratio	0.3
$\sum(r_i n_i)$	7.38095
Samples Between $T_i - T_0$ 50 to -14 °C	28
Samples Between $T_i - T_0$ -15 to -35 °C	19
Samples Between $T_i - T_0$ -36 to -50 °C	0
T_{0scrn} (°C)	-56
Homogenous or Inhomogeneous	Inhomogeneous

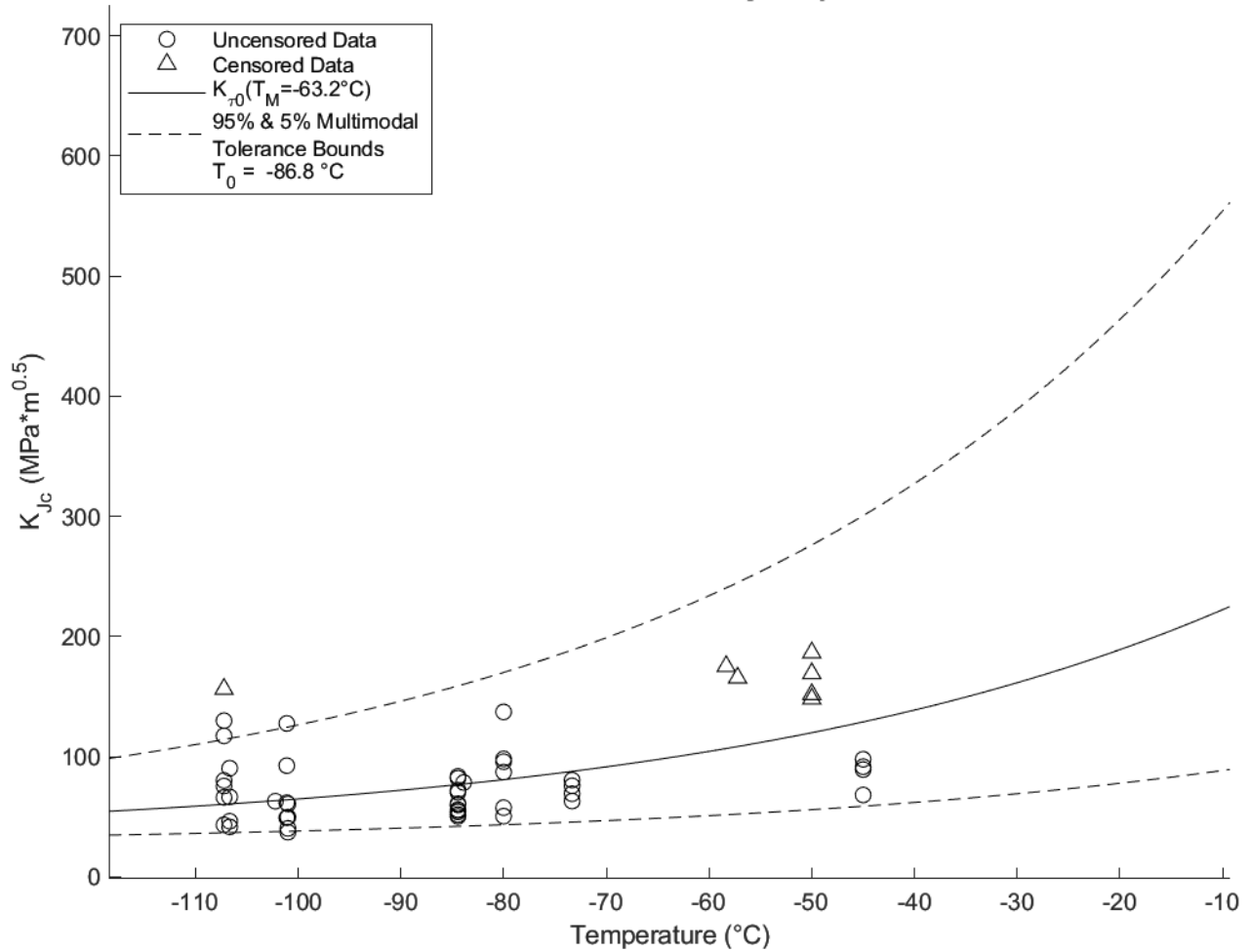


Figure 7.2.1.3.3-12: A225 Combined Set Multimodal T_m Plot ($T_m = -63^\circ\text{C}$)

Table 7.2.1.3.3-17: A225 Combined Set Multimodal T_m Calculation Results

T_m (°C)	-63
Sigma T_m (°C)	31
Multimodal Max $\ln(L)$	226.196
MLNH Criterion	2
MLNH from Multimodal	6.26995
Multimodal Homogeneity?	Inhomogeneous
Multimodal Confidence (%)	100

The results of the inhomogeneity analysis on combined data sets from LPVs V0023, V0032, MV50466-8, and PV0296 give a result of $T_m = -63^\circ\text{C}$ with 100% confidence in the characterization as multimodal. The overall confidence bounds include significantly more data and should be considered sufficient as a worst-case assumption of material properties. As discussed in the introduction, it is always best to conduct tests on the lot of material under investigation to achieve the most reliable data.

7.2.1.3.4 Fatigue Crack Growth Testing

Sections of V0023 were tested to determine the fatigue crack growth rates in accordance with ASTM E647 (11). Since V0023 head material was the worst performing material in the A225 family, using the da/dN (crack growth rate) values from V0023 provided a worst-case analysis when evaluating other vessels containing A225. Load ratios of $R = 0.1$ and $R = 0.7$ were chosen corresponding to load cycles associated with slight pressure variations and nearly full pressure releases of the LPVs. These tests were conducted on material taken from the center of the head thickness as shown in Figure 7.2.1.3.4-1. Figure 7.2.1.3.4-2 shows the combined fatigue crack growth curves for the A225 head material from LPV V0023. These curves are input into NASGRO to create material data packages used for structural analysis and crack growth prediction.

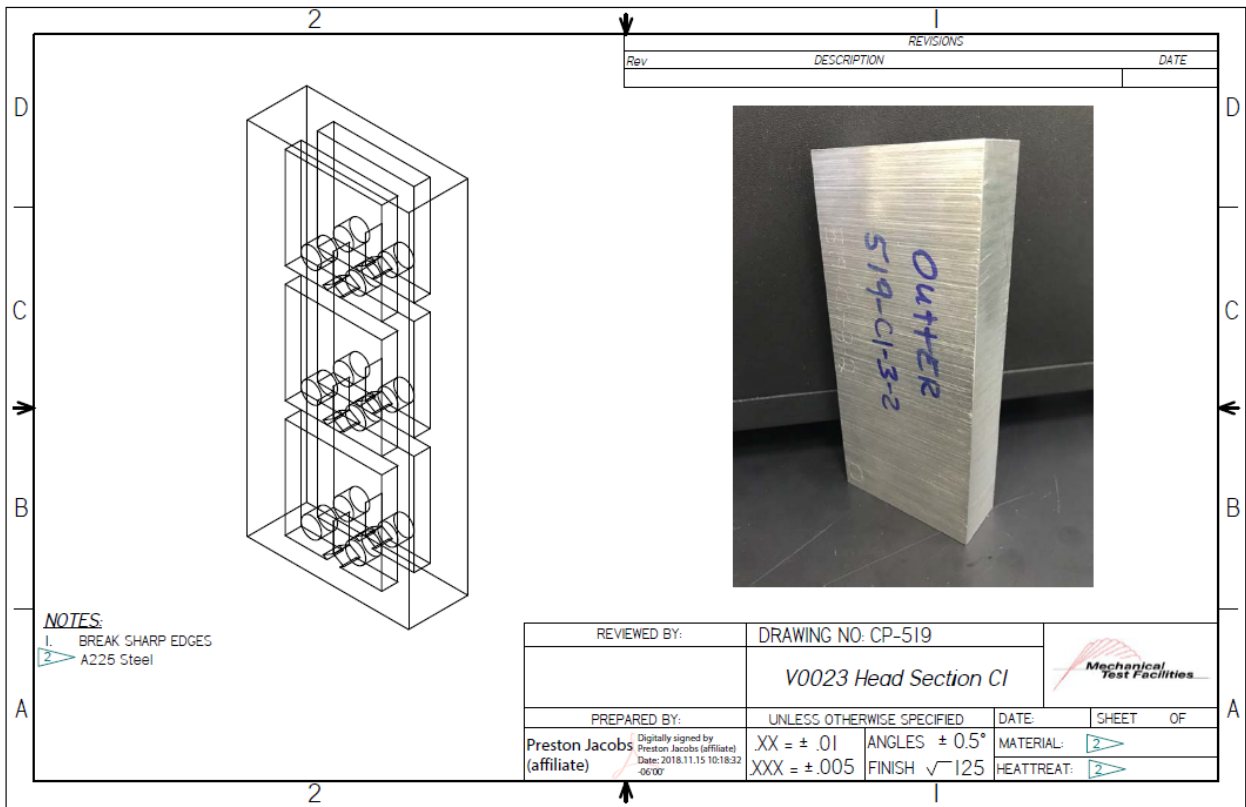


Figure 7.2.1.3.4-1: V0023 A225 Cut Plan for da/dN Specimen

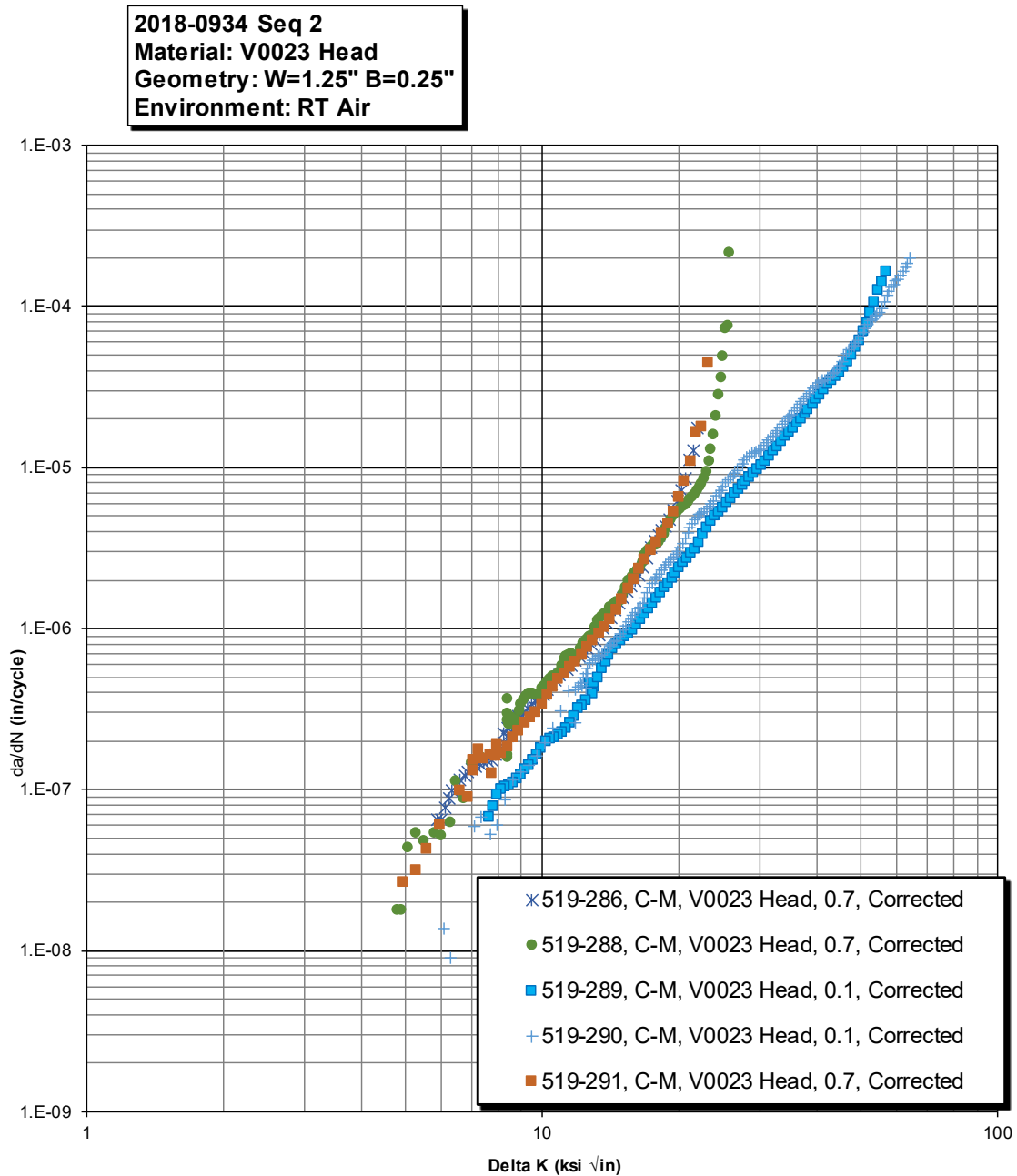


Figure 7.2.1.3.4-2: A225 Fatigue Crack Growth Plot, V0023

7.2.1.3.5 Charpy Impact

Charpy impact tests were conducted by Westmoreland Mechanical Testing and Research, Inc (WMT&R Report No. 4-50582). The specimens were extracted from V0032, A225 head material and tested according to the methods established in ASTM E2298 (8) and ASTM E23 (17).

C-M is the worst orientation, showing impact energy levels as low as 34 ft-lbs. However, the Charpy test method is too fast, describing only dynamic cracking. This prompted the use of the ASTM E1921 approach to obtain T_0 . Charpy impact is not recommended as a method of determining the proper evaluation temperatures for this vintage steel.

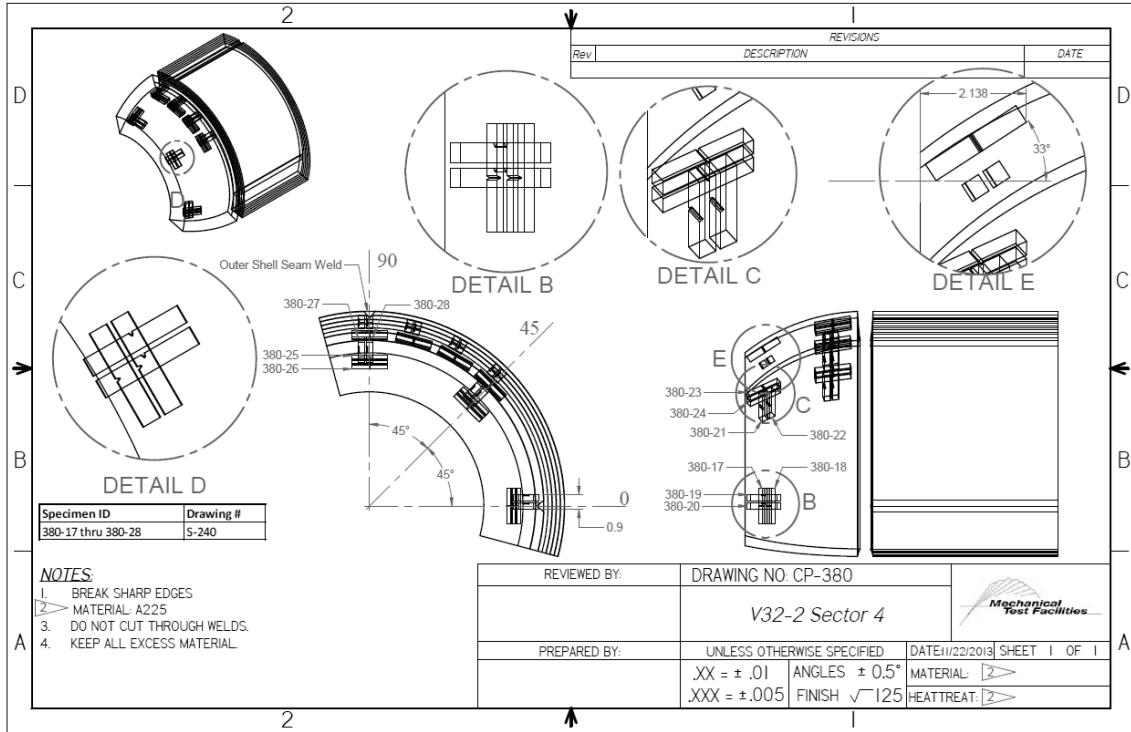


Figure 7.2.1.3.5-1: Section of V0032 Showing Charpy Specimen Location

Table 7.2.1.3.5-1: V0032 A225 Charpy Test Results

Sample ID	Vendor Test ID	Temp (F)	Theta (deg)	Meridional Location	Orientation	Impact Energy (ft-lbs)	Lat Exp (mils)	% Shear
CP-380-17	U09577	0	0	1	C-M	73.88	39	80
CP-380-18	U09578	0	0	1	C-M	66.83	34	40
CP-380-19	U09579	0	0	1	M-C	84.60	42	40
CP-380-20	U09580	0	0	1	M-C	90.85	44	40
CP-380-21	U09581	0	45	1	C-M	39.36	20	30
CP-380-22	U09582	0	45	1	C-M	34.28	20	30
CP-380-23	U09583	0	45	1	M-C	142.86	71	90
CP-380-24	U09584	0	45	1	M-C	135.21	71	80
CP-380-25	U09585	0	90	1	C-M	43.74	23	50
CP-380-26	U09586	0	90	1	C-M	42.60	22	30
CP-380-27	U09587	0	90	1	M-C	123.06	57	80
CP-380-28	U09588	0	90	1	M-C	111.80	55	70
CP-380-45	U33589	0	60	2	C-M	36.03	19	20
CP-380-46	U33590	0	60	2	C-M	36.91	18	20
CP-380-47	U33591	0	60	2	M-C	136.89	66	80
CP-380-48	U33592	0	60	2	M-C	186.76	81	100
CP-380-49	U33593	0	75	2	C-M	47.24	24	30
CP-380-50	U33594	0	75	2	C-M	44.66	26	35
CP-380-51	U33595	0	75	2	M-C	168.58	72	100
CP-380-52	U33596	0	75	2	M-C	163.52	75	100
CP-380-65	U47089	0	45	2	C-M	43.89	27	20
CP-380-66	U47090	0	45	2	C-M	39.18	19	20
CP-380-67	U47091	0	45	2	M-C	167.64	74	80
CP-380-68	U47092	0	45	2	M-C	200.16	72	100
CP-380-69	U47093	0	90	2	C-M	44.31	23	30
CP-380-70	U47094	0	90	2	C-M	44.50	27	40
CP-380-71	U47095	0	90	2	M-C	177.24	78	100
CP-380-72	U47096	0	90	2	M-C	162.75	67	90

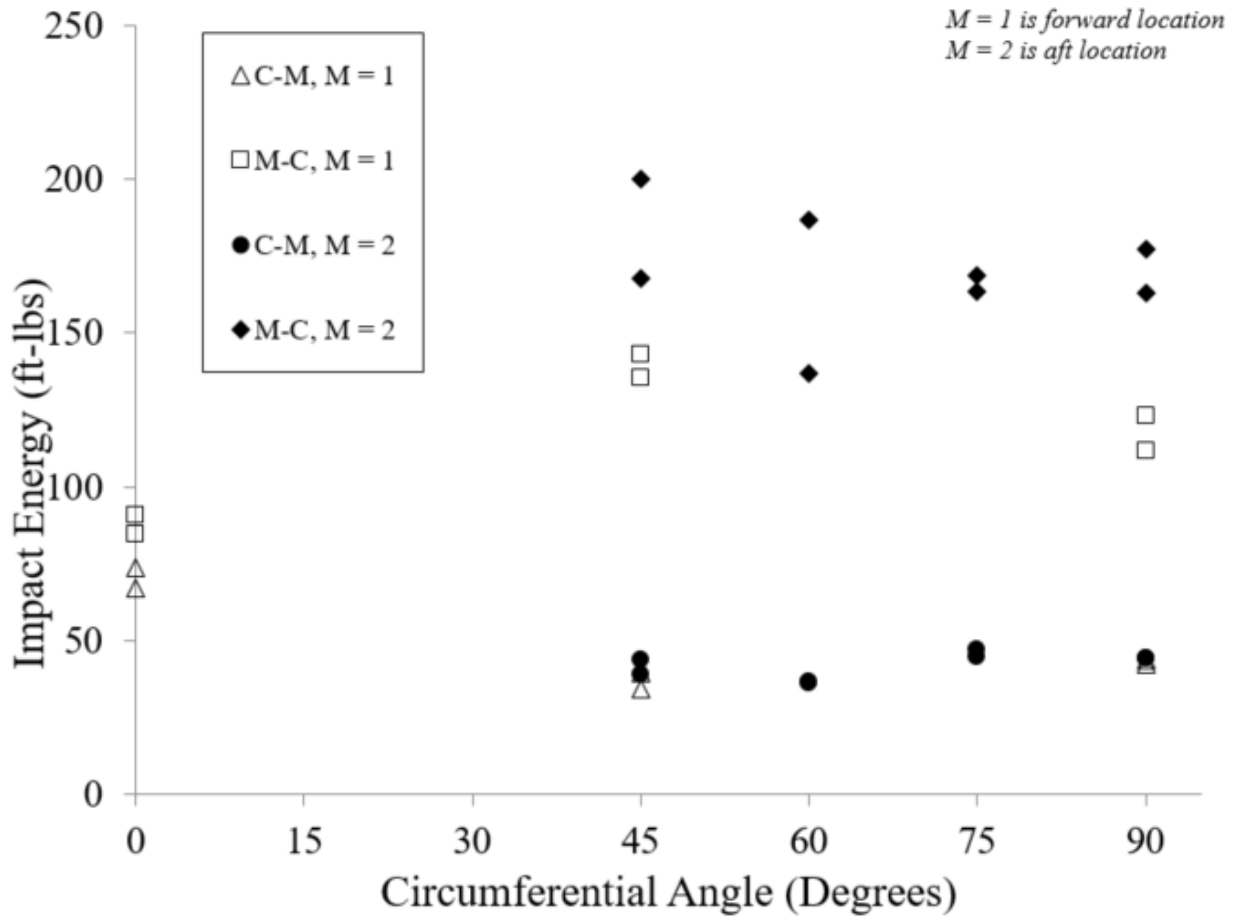


Figure 7.2.1.3.5-2: Charpy Impact Energy as a Function of Circumferential Angle

7.2.2 A212

ASTM A212 (53) is used as the head material for a number of LPVs. The results reported include those for LPVs manufactured by A.O. Smith. All LPV heads are nominally A212 Grade B FBX, and will be referred to as A212 herein for brevity. The V0348 head has an outside radius of approximately 12 inches and a thickness of 1-5/8 inches.

7.2.2.1 Chemical Composition

Table 7.2.2.1-1 provides the maximum percent content values for alloying elements listed in the A212 material specification.

Table 7.2.2.1-1: ASTM A212-64 Standard Chemistry Values (53)

	C			Mn	P		S		Si	
	Thickness				Flange	Firebox	Flange	Firebox	Ladle analysis	Check analysis
	< 1"	1" to 2"	2" to 8"							
Grade B	0.31	0.33	0.35	0.9	0.035	0.035	0.04	0.04	0.15 to 0.30	0.13 to 0.33

Table 7.2.2.1-2 provides data collected from mill certifications of vessels at MSFC.

Table 7.2.2.1-2: Manufacturer Mill Certification Chemistry

Melt/Heat	Cert Origin	C	Mn	P	S	Si
4D-3379-4	Spencer	0.28	0.72	0.012	0.031	0.018
70-5741-3	Spencer	0.27	0.6	0.01	0.025	0.17
7G5710-6B	Spencer	0.26	0.7	0.014	0.023	0.16
7G5710-6T	Spencer	0.26	0.7	0.014	0.023	0.16
4D3379	Spencer	0.27	0.72	0.012	0.031	0.18
6F7160-10B	Spencer	0.26	0.72	0.012	0.027	0.16
4D379-4B	Spencer	0.28	0.72	0.012	0.031	0.18
7G5741-4B	Spencer	0.27	0.6	0.01	0.025	0.14
7G5741-4T	Spencer	0.27	0.6	0.01	0.025	0.14
7G5741-3B	Spencer	0.27	0.6	0.01	0.025	0.17
7G5741-3T	Spencer	0.27	0.6	0.01	0.025	0.017
6F7160-13	Spencer	0.26	0.72	0.012	0.027	0.16
D-3379-3	Spencer	0.28	0.72	0.012	0.031	0.18
4D-3379-5	Spencer	0.28	0.72	0.012	0.031	0.18
7G-5741-4	Spencer	0.27	0.6	0.01	0.025	0.17
7-G5710-6B	Spencer	0.26	0.7	0.014	0.023	0.16
7G5710-6T	Spencer	0.26	0.7	0.014	0.023	0.16
6F7160-10B	Spencer	0.26	0.72	0.012	0.027	0.16
4D3379-3B	Spencer	0.28	0.72	0.012	0.031	0.18
7G5741	Spencer	0.27	0.6	0.01	0.025	0.17
7G5741-3B	Spencer	0.27	0.6	0.01	0.025	0.17
7G5471-3T	Spencer	0.27	0.6	0.01	0.025	0.17
27343	T.C. & J	0.32	0.84	0.018	0.031	0.257
32492	T.C. & J	0.28	0.83	0.017	0.035	0.252
34327	T.C. & J	0.3	0.8	0.028	0.033	0.243
23683	T.C. & J	0.27	0.79	0.01	0.037	0.248
674053	T.C. & J	0.28	0.71	0.011	0.026	0.22

Table 7.2.2.1-3 provides the chemistry of the A212 head of LPV V0348 at MSFC as determined by Arc Spark analyses. The V0348 plate falls comfortably within the A212 specification.

Table 7.2.2.1-3: V0348 Collected Chemistry Data

Vessel	Material	Location	C	Si	Mn	P	S	Cr	Mo	Ni	Cu	Nb	V	B
V0348	A212	Dissected Head	0.26	0.26	0.82	0.019	0.03	0.021	0.005	0.007	0.024	0.003	0.002	0.001
V0348	A212	Intact Head	0.26	0.27	0.85	0.028	0.047	0.022	0.012	0.005	0.031	0.005	0.002	0.0008

7.2.2.2 Metallography

Various metallographic studies were performed on the A212 material. These included: grain orientation, grain size, grain size through thickness, carburization layer thickness, and macro cubes if showing multiple surfaces.

Studies:

Grain Orientation study - yes

Grain size study – yes

Grain size through thickness study - yes

Carburization layer thickness - yes

Macro cubes if showing multiple surfaces- yes

Grain Orientation Study

Two sets of three metallographic blocks were initially taken from the centerline of the head material to correlate the grain orientation with the tensile and fracture toughness testing. The cut plan in Figure 7.2.2.2-1 shows how the blocks were removed from the head. The blocks were polished, etched, and photographed, and the photographs were reconstructed as shown in Figure 7.2.2.2-2 and Figure 7.2.2.2-3.

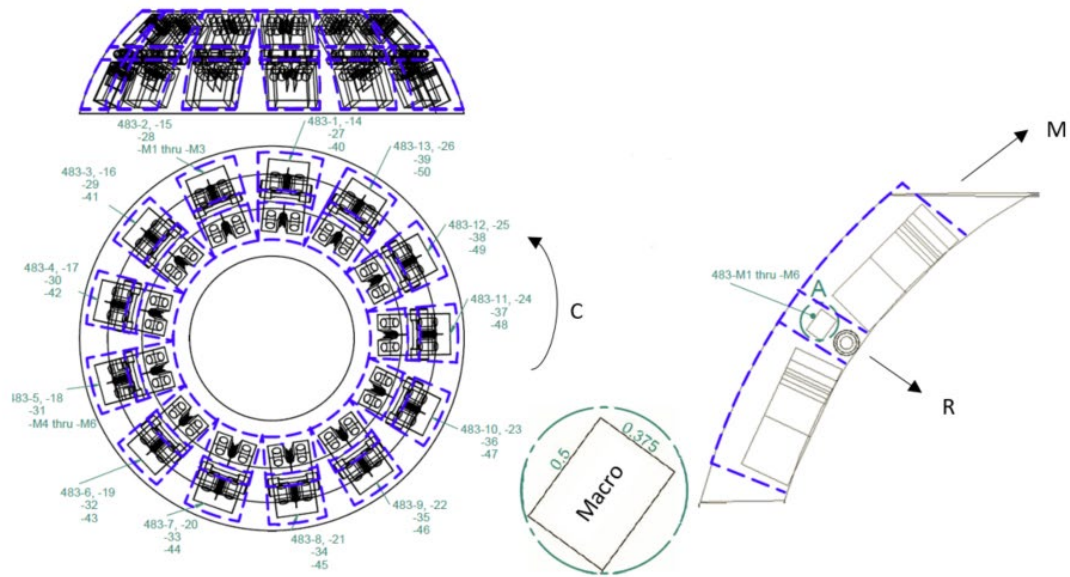


Figure 7.2.2.2-1: Sample Cut Plan for Macros from V0348 Head

These macros show that the grains are elongated in the M-C plane with the greatest elongation in the circumferential direction. This implies that the grains were approximately equiaxial until the head was formed and the grains were only then elongated due to forming into the hemispherical shape.

Head 1 Specimen Orientation Location 0°

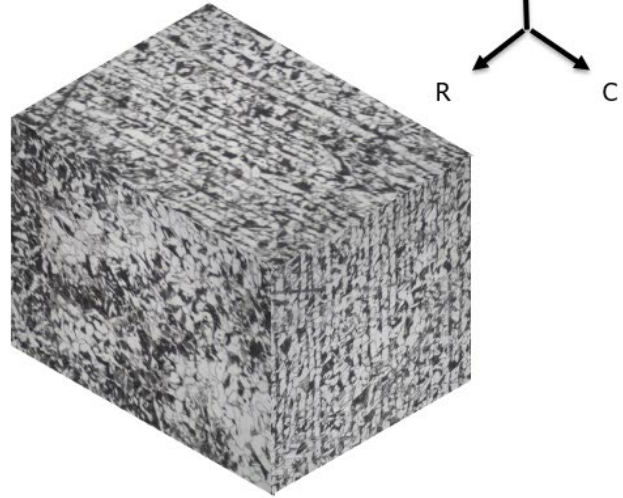
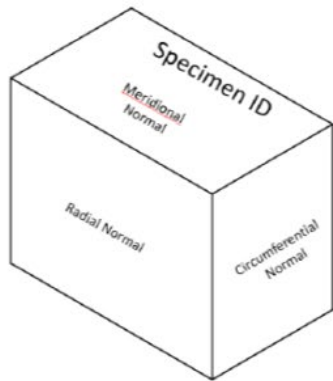


Figure 7.2.2.2-2: Macro from V0348 Head Material at 0 Degrees 10X Magnification

Head 1 Specimen Orientation Location 90°

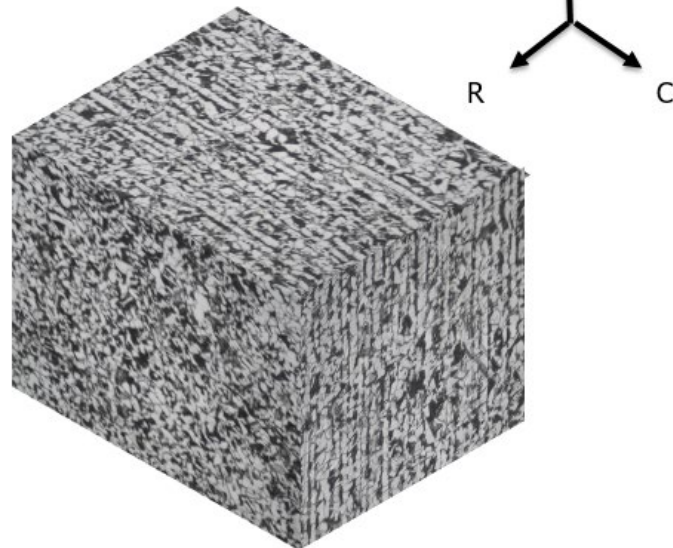
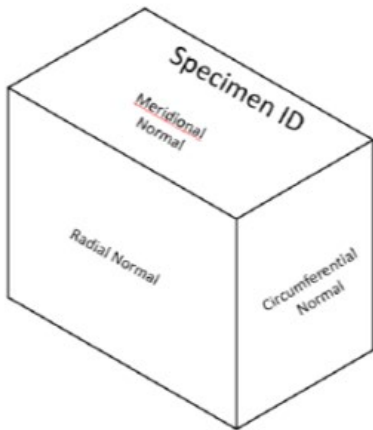
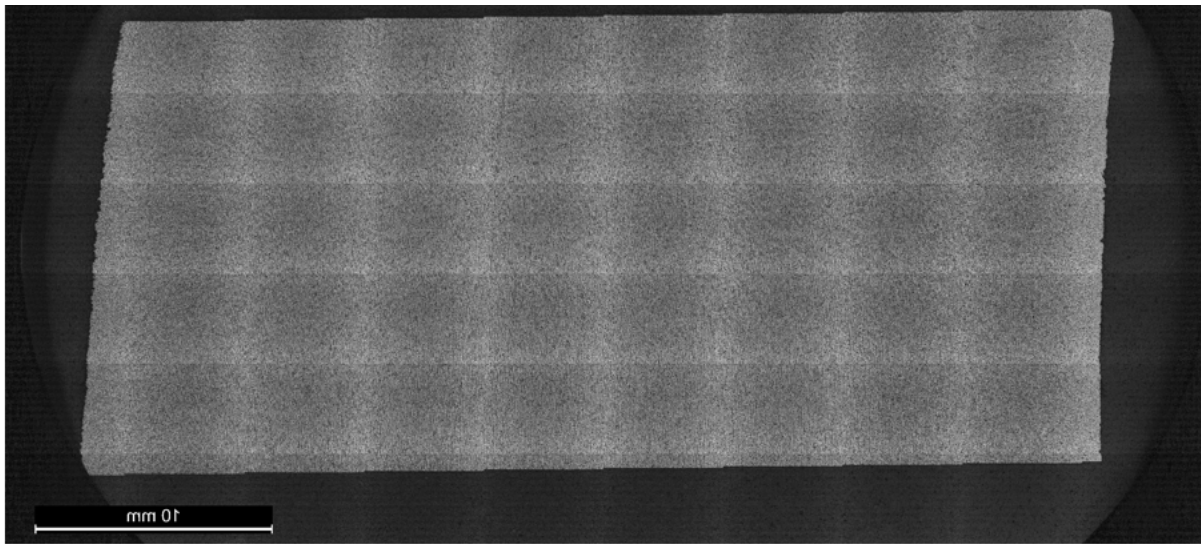


Figure 7.2.2.2-3: Macro from V0348 Head Material at 90 Degrees 10X Magnification

Grain Size Study

ASTM A212 head material was subjected to a grain size study in an effort to classify the V0348 head material as “coarse” or “fine” grain in accordance with ASTM E112, *Standard Test Methods for Determining Average Grain Size* (54). ASTM E112 covers procedures for estimating average grain size in

single phase metals. A through thickness sample, spanning from the inner to the outer surfaces was taken to investigate whether any dramatic variation in metallurgy was present through the thickness of the head. Multiple high resolution photos were taken of a through thickness macro and stitched together to produce Figure 7.2.2.2-4. Figure 7.2.2.2-5, Figure 7.2.2.2-6, and Figure 7.2.2.2-7 provide individual high resolution photos which were examined to determine the grain characteristics at each location through the thickness. Since grain size was consistent throughout the head thickness, an average location was selected and measured, with results as shown in Figure 7.2.2.2-8. The study revealed an average grain size of 7.2 as defined in ASTM E112. For A212, grain size above 5 indicates fine grained, and grain size from 1-5 indicates coarse grained. Standard A212 Grade B FBX steel is coarse grained, therefore this sample cannot be considered representative of standard structure or properties.



Outside Surface

25X Multi-Step

Inside Surface

Figure 7.2.2.2-4: Through-Thickness Macro

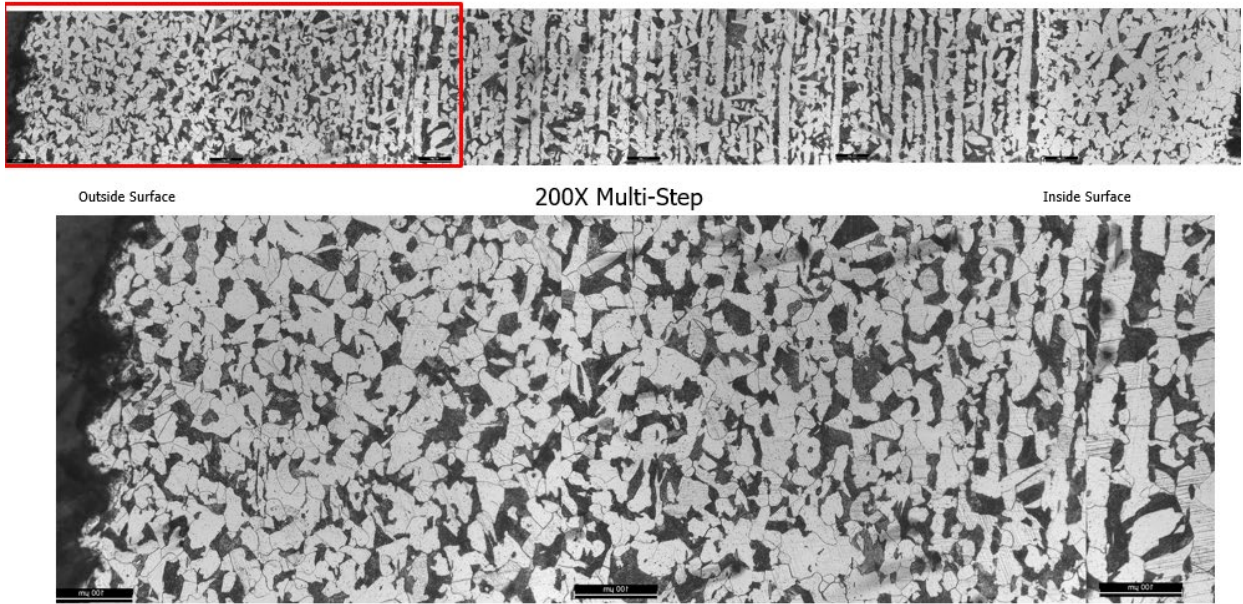


Figure 7.2.2.2-5: Outside Surface Grain Size

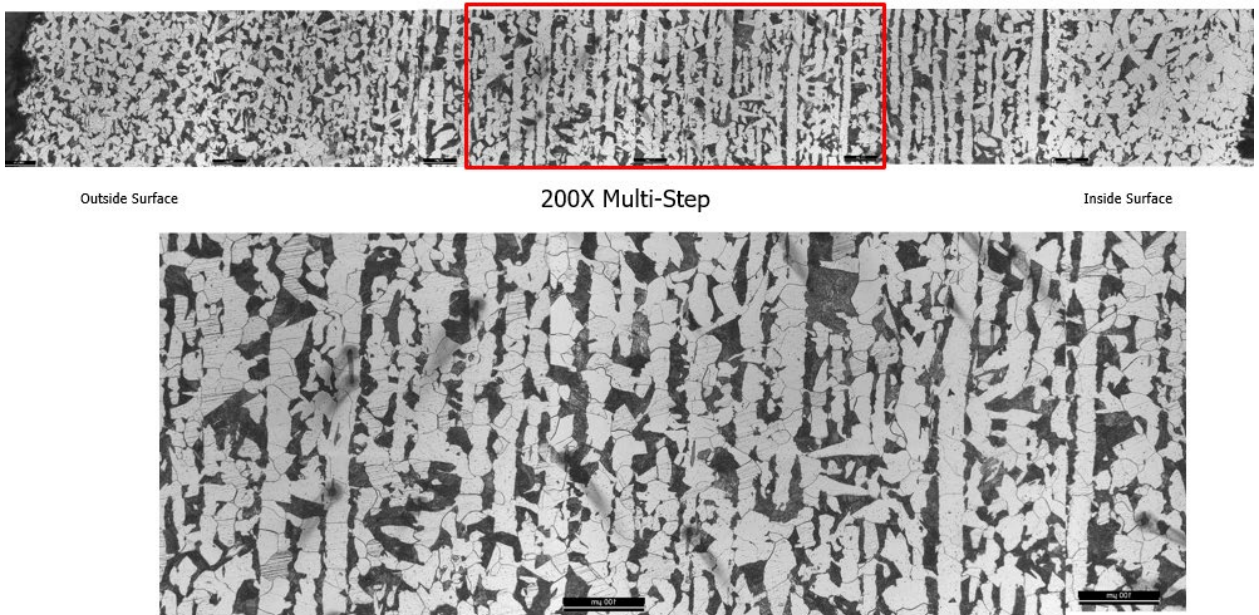


Figure 7.2.2.2-6: Mid-Thickness Grain Size



Outside Surface

200X Multi-Step

Inside Surface

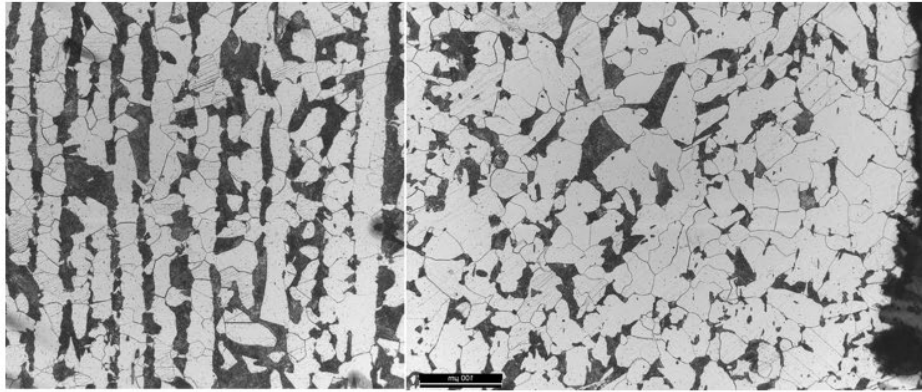


Figure 7.2.2.2-7: Inside Surface Grain Size

LAS Grain Analysis Report ASTM E112 3 Circles

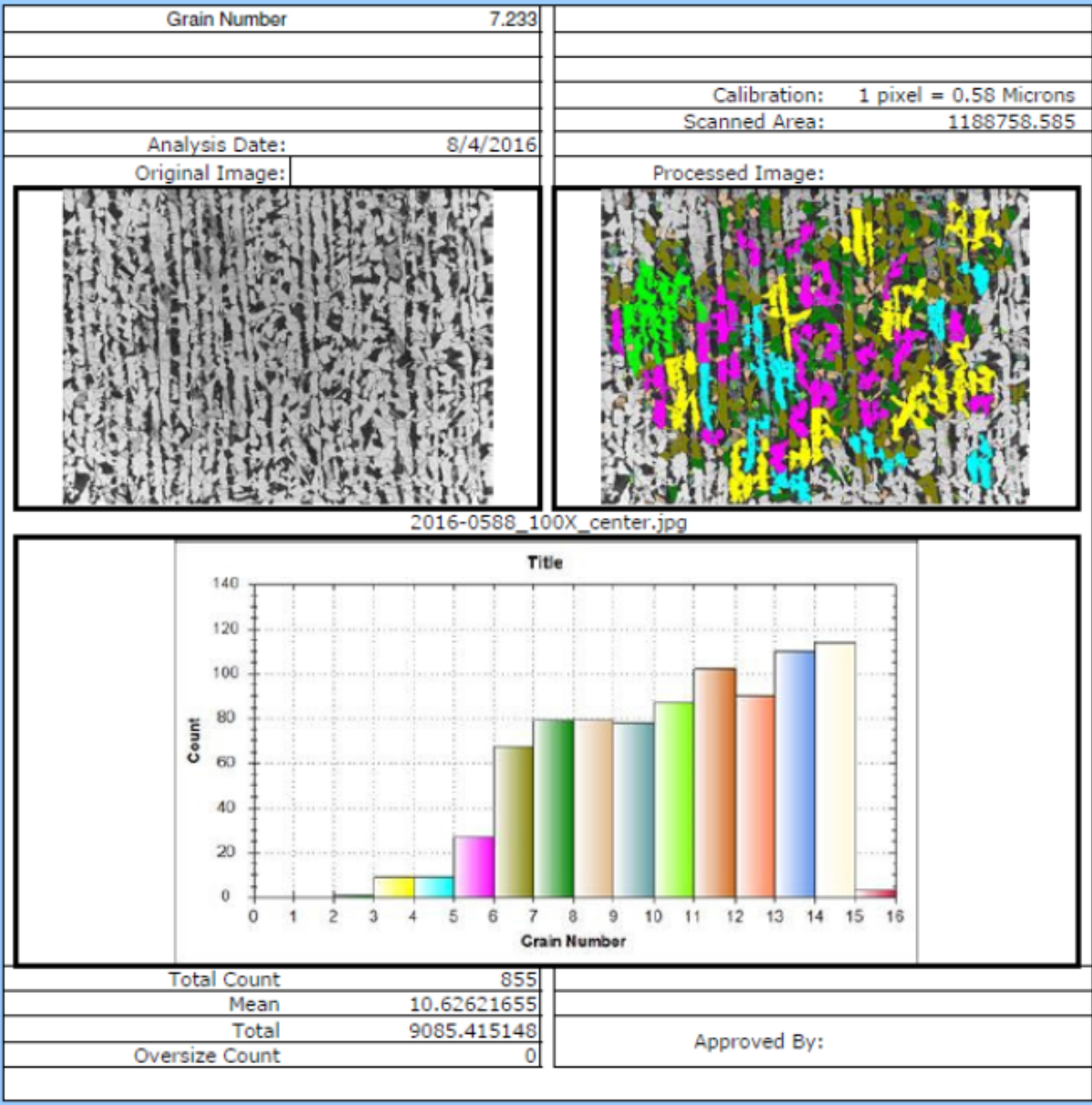


Figure 7.2.2.2-8: V0348 Grain Count Head Material Center of Thickness 100X Magnification

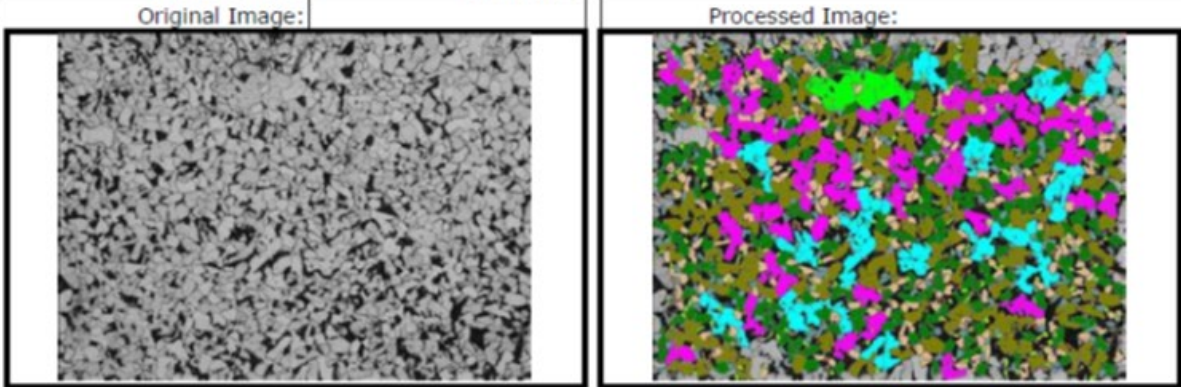
7.2.2.2.1 Carburization Layer Thickness Study

A study was conducted to determine the necessary requirements for analyzing grain size from the outer surface of a vessel. The objective was to determine whether checking grain size in the field for an in-situ active vessel was feasible. Once the outer coatings were removed, a 0.75 inch diameter flat surface was ground. For the 24 inch diameter head this corresponded to a 0.010 inch grind depth.

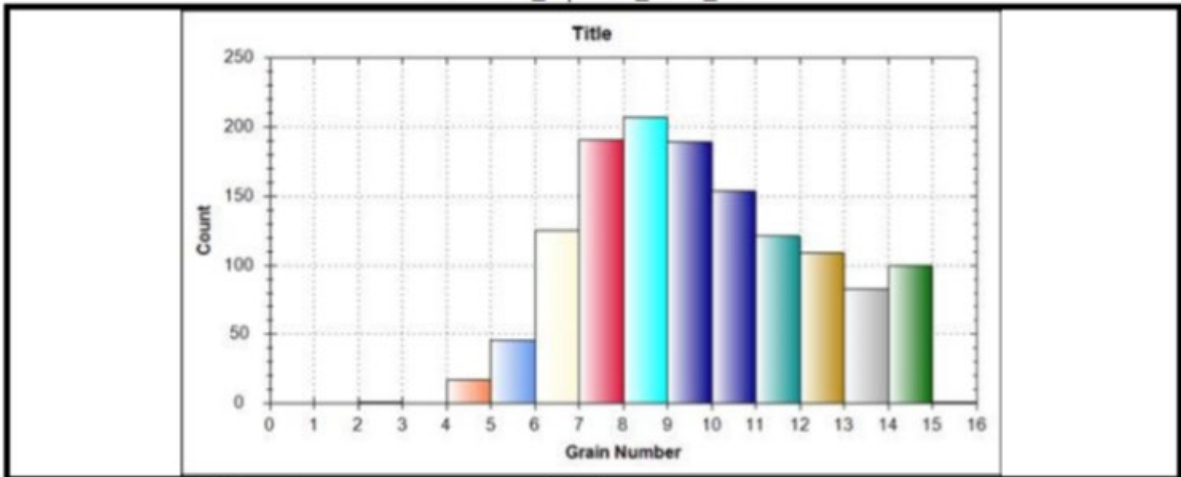
LAS Grain Analysis Report ASTM E112 3 Circles



Grain Number	7.725	Technologist	B. Tucker
Project	2016-0622		
Preparation	3% Nital etch		
Specimen	Top View	Calibration:	1 pixel = 0.58 Microns
Observation	100X	Scanned Area:	1188758.585
Analysis Date:	8/18/2016		

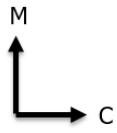


2016-0622_top view_100X_01.tif

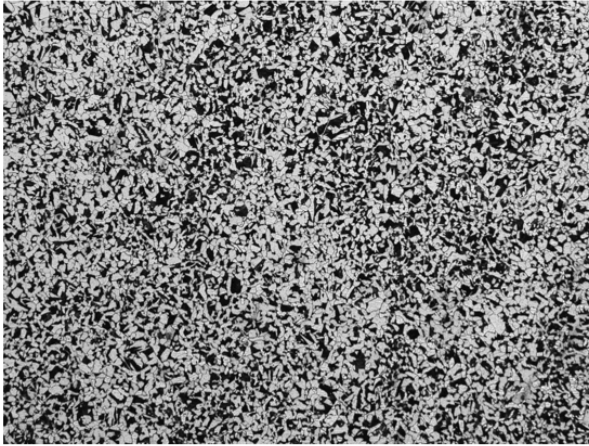


Total Count	1344	Approved By:
Mean	9.755877748	
Total	13111.89969	
Oversize Count	0	

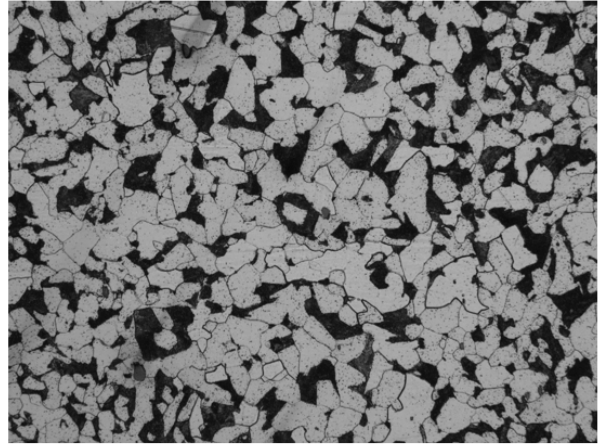
Figure 7.2.2.2.1-2: V0348 Grain Analysis Head Material Outer Surface (0.01 Inch Grind Depth)



483-M8
0.035" Grind Depth



50X



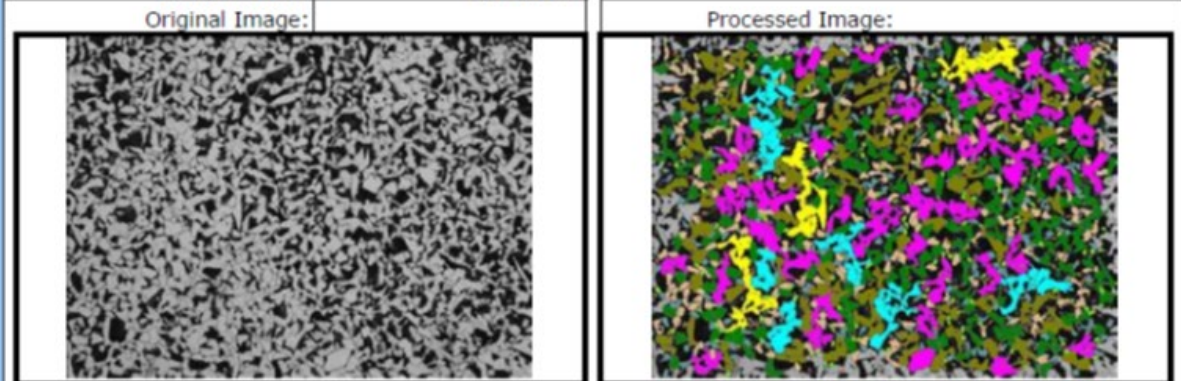
200X

Figure 7.2.2.2.1-3: V0348 Surface study Head Material Outer Surface (0.035 Inch Grind Depth)

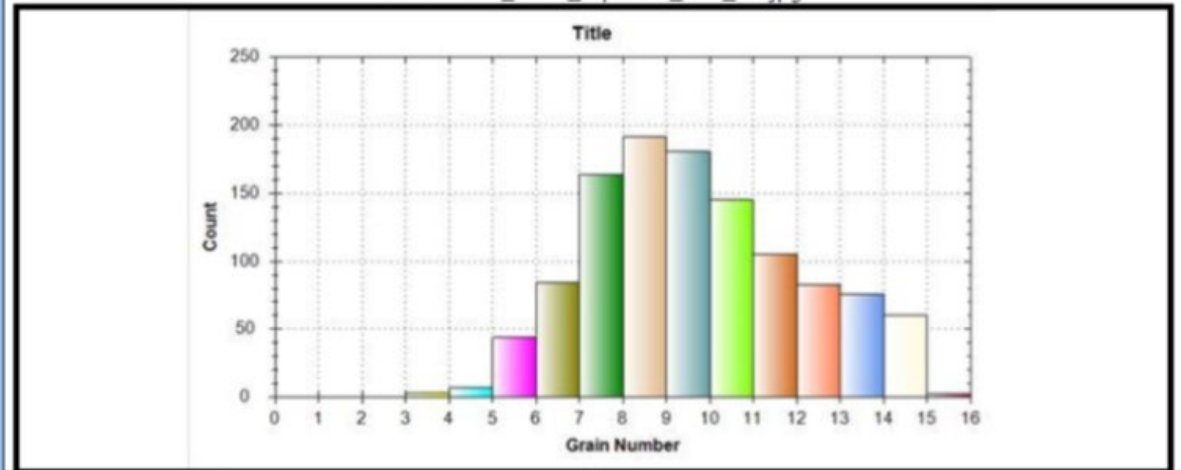
LAS Grain Analysis Report ASTM E112 3 Circles



Grain Number	8.358	Technologist	B. Tucker
Project	2016-0622		
Preparation	3% Nital etch		
Specimen	Top View (ref.887)	Calibration:	1 pixel = 0.58 Microns
Observation	100X	Scanned Area:	1188758.585
Analysis Date:	8/19/2016		



2016-0622_100X_top view_887_02.jpg



Total Count	1146	Approved By:
Mean	9.695950874	
Total	11111.5597	
Oversize Count	0	

Figure 7.2.2.2.1-4: V0348 Grain Analysis Head Material Outer Surface (0.035 Inch Grind Depth)

From these tests, two key observations were made. First, the forming of the head left elongated grains in the circumferential direction. This agrees with previous head investigations. Second, the grain has minimal variation from the outer surface to the inner surface of the head, with grain size number ranging from 7.5-8.5. This falls under the definition of fine grain, low carbon steel. A surface study was also conducted to determine the necessary requirements to correctly characterize grain size with minimal impact to the structure. It was determined that a flat surface of 0.75 inches in diameter

minimum and 0.035 inches total below the bare metal surface was sufficient to pass through the decarburization layer and display the typical grain size characteristics existing through the head thickness.

Summary

The grain size of the head of LPV V0348 has been characterized as fine grained with negligible difference in size through the thickness. The principal longitudinal grain direction is circumferential in the fabricated head. Morphology changes through the thickness show a layer of decarburization on the inner and outer surfaces, indicating that the material has been quenched and tempered. The typical grain through the thickness can be observed by grinding the head to a depth of 0.035 inch to penetrate through the decarburization layer.

7.2.2.3 Mechanical Properties

Table 7.2.2.3-1 provides minimum values for tensile properties required in the ASTM material specification for A212 Grade B steel.

Table 7.2.2.3-1: A212 Minimum Material Specifications

	Yield Stress (ksi)	Tensile Stress (ksi)	Fracture Elongation in 8 in. (%)		Fracture Elongation in 2 in. (%)	
			Flange	Firebox	Flange	Firebox
Grade B	38	70 to 85	18	19	21	22

Table 7.2.2.3-2 provides material properties results obtained from mill certifications from all the vessels available at MSFC.

Table 7.2.2.3-2: LPV Mill Certification Material Properties A212B

Melt/Heat	Yield Stress (ksi)	Tensile Stress (ksi)	Elong in 2 in. (%)
4D-3379-4	42.0	73.8	28.0
70-5741-3	42.0	74.5	35.0
7G5710-6B	42.0	73.5	31.0
7G5710-6T	42.0	73.5	31.0
4D3379	42.0	73.8	28.0
6F7160-10B	43.0	77.3	30.0
4D379-4B	42.0	73.8	28.0
7G5741-4B	41.5	72.5	37.0
7G5741-4T	41.5	72.5	37.0
7G5741-3B	42.0	74.5	35.0
7G5741-3T	42.0	74.5	35.0
6F7160-13	43.0	73.3	35.0
D-3379-3	42.5	77.9	31.0
4D-3379-5	42.5	77.8	31.0
7G-5741-4	41.5	72.5	37.0
7-G5710-6B	42.0	73.5	31.0
7G5710-6T	42.0	73.5	31.0
6F7160-10B	43.0	77.3	30.0
4D3379-3B	42.5	76.8	32.0
7G5741	42.0	74.5	35.0
7G5741-3B	42.0	74.5	35.0
7G5471-3T	42.0	74.5	35.0
27343	44.2	79.9	25.0
32492	54.1	76.3	23.7
34327	45.2	81.0	25.0
23683	39.3	71.6	27.5
674053	46.7	77.7	30.0
Average	42.83	75.05	31.5

7.2.2.3.1 Smooth Tensile Tests

Smooth tensile tests were conducted on round specimens according to ASTM E8, “Standard Test Methods for Tension Testing of Metallic Materials” (51) using specimen design S-58. These specimens were tested at MSFC. The mechanical test frame consisted of a servo-hydraulic actuator and reaction frame. The frame used an LVDT for displacement feedback. Stress measurements were derived from load measurements and the initial specimen measurements. Strain measurements were derived from an extensometer and the initial specimen measurements.

The results obtained from testing A212 from vessel V0348 are presented in Table 7.2.2.3.1-1. A typical engineering stress-strain curve for this material is shown in Figure 7.2.2.3.1-1.

Table 7.2.2.3.1-1: A212 Tensile Data V0348

Specimen ID	Test Temp. (°C)	ASTM Orientation	Tensile Stress (ksi)	Yield Stress (ksi)	Fracture Elongation (%)
483-27	21	C	75.9	39.8	34.5
483-28	21	C	74.8	40.1	35.2
483-29	21	C	80.1	44.0	33.6
483-30	21	C	79.3	43.0	36.0
483-31	-46	C	81.2	45.7	36.7
483-32	-46	C	81.3	46.2	36.1
483-33	-73	C	85.5	52.1	38.9
483-34	-73	C	86.6	53.3	39.4

*Note: C denotes circumferential orientation

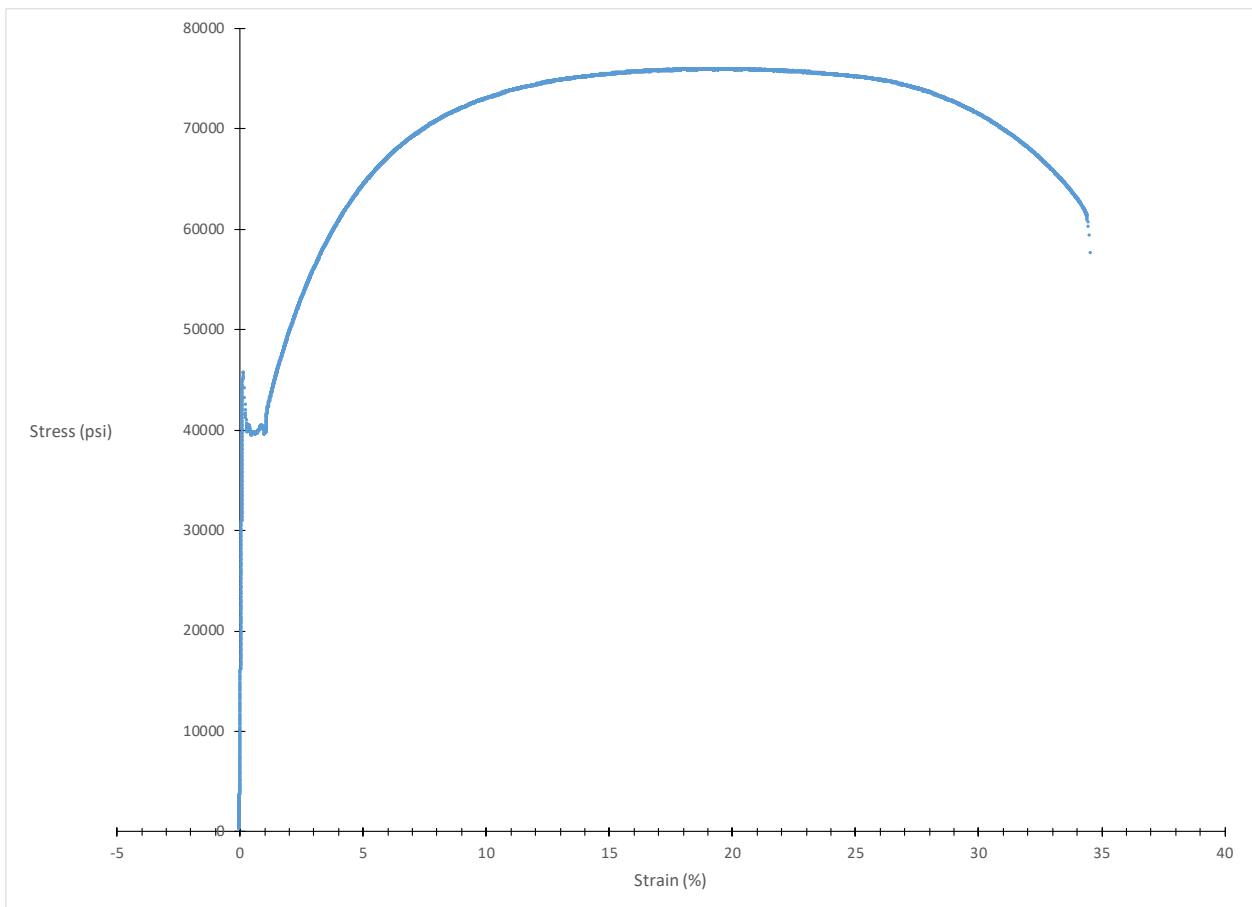


Figure 7.2.2.3.1-1: A212 Smooth Specimen Tensile Plot for Sample 483-27

7.2.2.3.2 Notch Tensile Tests

Notch tensile tests of A212 specimens were conducted according to ASTM G142, “Standard Test Method for Determination of Susceptibility of Metals to Embrittlement in Hydrogen Containing

Environments at High Pressure, High Temperature, or Both” (52). The test specimens were standard notch tensile design S-40-B with notch diameter = 0.25 inches. Kt value 6.0 (5.55 – 6.48).

A total of six specimens were removed from the V0348 LPV head and underwent two baseline tests and four gaseous hydrogen tests. The environment for the two baseline tests was 5000 psi gaseous helium at an ambient temperature of approximately 85°F. The environment for the four hydrogen embrittlement tests was 5000 psi gaseous hydrogen at an ambient temperature of approximately 85°F. The test frame was equipped with a servo-hydraulic mechanical actuator and reaction member. Stress measurements were derived from a load cell and specimen pre-test dimension measurements. Displacement measurements were derived from an LVDT. The tests were performed in displacement control at an actuator speed of 0.0005 inches/minute.

The average tensile stress for the baseline GHe tests was 104 ksi, with a minimum value of 103 ksi. The average tensile stress for GH2 tests was 78 ksi, with a minimum value of 77 ksi. Due to lack of ductility in GH2 after yielding, A212 is not recommended for GH2 service. The results of these tests are presented in Table 7.2.2.3.2-1 and Figure 7.2.2.3.2-1.

Table 7.2.2.3.2-1: A212 Notch Tensile Data, V0348

Specimen ID	Test Temp. (°C)	ASTM Orientation	Tensile Stress (ksi)	Notes
483-40	21	C	78	5000 psi, Ambient, GH2
483-41	21	C	77	5000 psi, Ambient, GH2
483-42	21	C	78	5000 psi, Ambient, GH2
483-43	21	C	79	5000 psi, Ambient, GH2
483-44	21	C	104	5000 psi, Ambient, GHe
483-45	21	C	104	5000 psi, Ambient, GHe

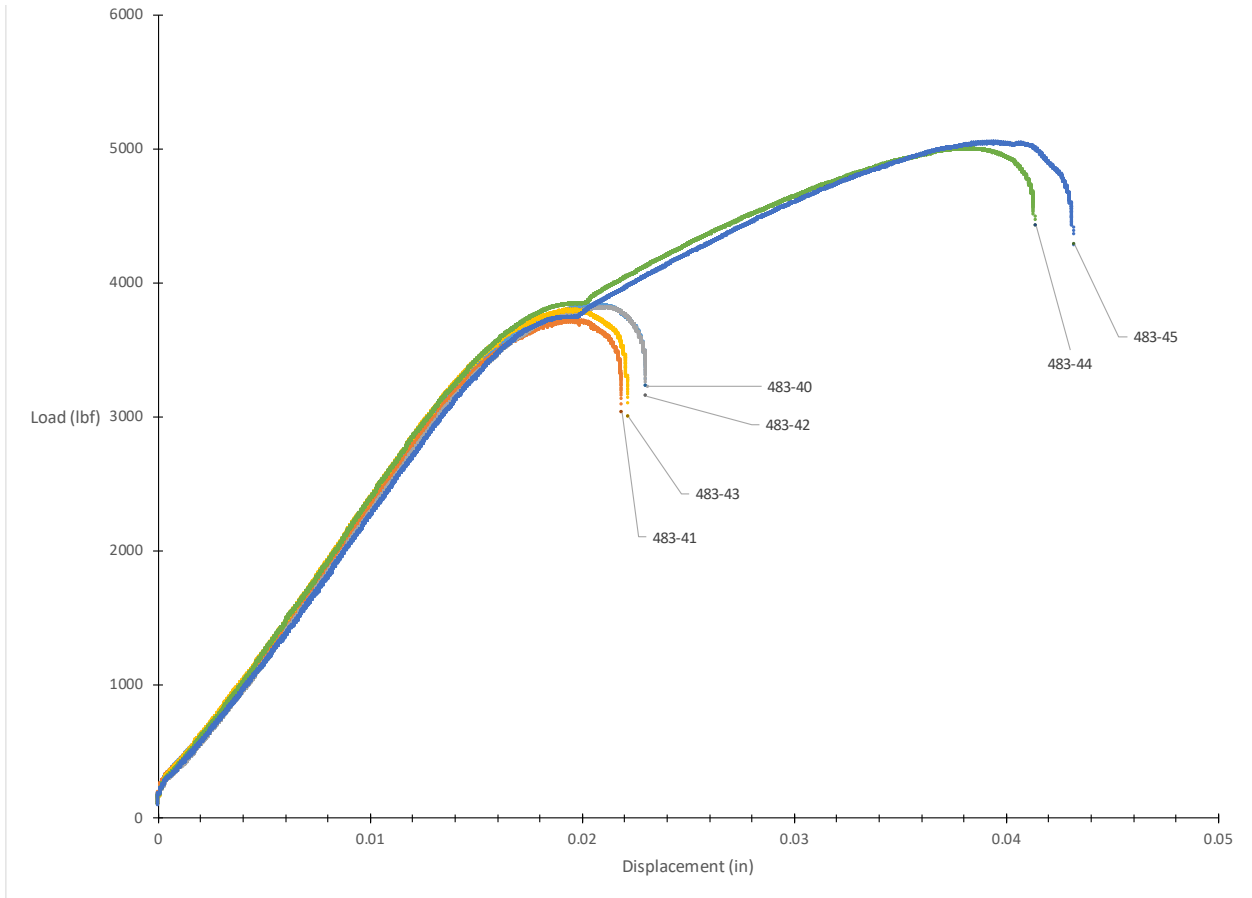


Figure 7.2.2.3.2-1: A212 Notch Tensile Plot, V0348

7.2.2.3.3 Fracture Properties

All room temperature testing was performed in accordance with ASTM E1820 (10) All other temperatures were tested in accordance with ASTM E1921. Testing for both standards use specimen design S-318 Rev A. All A212 fracture tests came from vessel V0348 and were tested with the crack plane in the C-M orientation as defined by ASTM (both grain and vessel orientations). The specimens used were ASTM E1820 compact specimens (C(T)) with $W = 2.0$ inches and $B = 1.0$, $a/W = 0.5$ and all specimens were side grooved to a total thickness reduction of 20%. The cutting diagram used to remove the C(T) specimens from the V0348 head is shown in Figure 7.2.2.3.3-1.

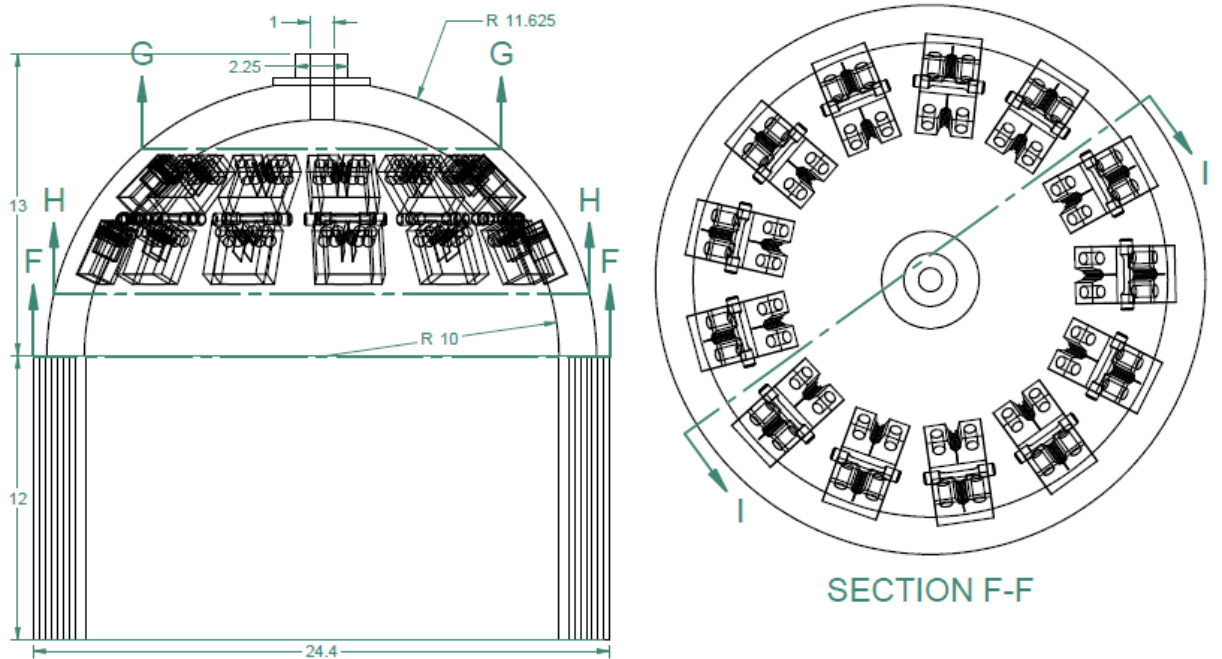


Figure 7.2.2.3.3-1: Cut Plan for V0348 Fracture Specimens (C-M Orientation)

Table 7.2.2.3.3-1 provides raw values of test data obtained from fracture tests conducted on V0348 A212 head material. Tests with results identified as upper shelf are listed under ASTM E1820, while transition temperature tests are listed under E1921 (7). Tests that meet the complete validity requirements for $J_q = J_{1C}$ and $K_{Jq} = K_{J1C}$ are denoted with an asterisk. Despite invalidities, J_q and K_{Jq} convey valuable fracture toughness information, especially when the test results are applied directly to the sample material source. Although it was tested in the transition temperature window, Specimen 483-4 did not display the characteristics of an E1921 test and as such was analyzed as an upper shelf test.

Table 7.2.2.3.3-1: A212 Fracture Data V0348

Specimen ID	Test Temp. (°C)	ASTM Crack Plane Orientation	W (in)	a ₀ (in)	a _f (in)	B ₀ (in)	B _N (in)	J _q (kJ/m ²)	K _{Jq} (MPa √m)	K _{JCT} (MPa √m)	ASTM Standard
483-2	23	C-M	2.0019	1.0164	1.0721	0.9993	0.8025	145	180	---	E1820
483-1	22	C-M	2.0022	1.0075	1.0610	1.0000	0.7985	93	144	---	E1820
483-4	-24	C-M	2.0025	1.0029	1.0701	1.0003	0.8021	95	146	---	E1820
483-3	-24	C-M	2.0021	0.9950	1.0330	0.9990	0.8015	163	191	191	E1921
483-12	-46	C-M	1.9997	1.0097	1.0191	0.9993	0.7977	52	108	108	E1921
483-13	-46	C-M	1.9998	1.0032	1.0207	0.9983	0.7972	81	135	135	E1921
483-14	-46	C-M	2.0076	1.0116	1.0150	0.9930	0.7970	98	148	148	E1921
483-17	-46	C-M	2.0043	1.0077	1.0285	0.9993	0.7952	110	156	156	E1921
483-5	-46	C-M	2.0024	1.0163	1.0294	1.0000	0.7995	84	137	137	E1921
483-6	-46	C-M	2.0014	1.0103	1.0248	1.0000	0.7967	117	162	162	E1921
483-7	-46	C-M	2.0026	1.0166	1.0363	0.9993	0.8000	83	136	136	E1921
483-8	-46	C-M	2.0020	1.0141	1.0320	0.9997	0.7988	115	160	160	E1921
483-10	-73	C-M	2.0023	1.0478	1.0506	0.9987	0.7960	30	82	82	E1921
483-11	-73	C-M	2.0024	1.0166	1.0236	0.9987	0.7960	20	66	66	E1921
483-15	-73	C-M	2.0019	1.0026	1.0219	0.9997	0.7970	27	78	78	E1921
483-16	-73	C-M	2.0007	1.0080	1.0207	0.9990	0.7971	41	95	95	E1921

Figure 7.2.2.3.3-2 shows a typical load versus crack opening displacement record for an upper shelf E1820 test and the resulting J integral resistance curve (J-R curve) is presented in Figure 7.2.2.3.3-3, which shows the evaluation of J_q according to E1820.

Results from the 13 E1921 tests are presented in Table 7.2.2.3.3-2 and Table 7.2.2.3.3-3. These results were obtained using the T₀TEM Code described in Section 4.2. The T₀ reference temperature for this data set was evaluated as -57°C using the E1921 Master Curve shown in Figure 7.2.2.3.3-4.

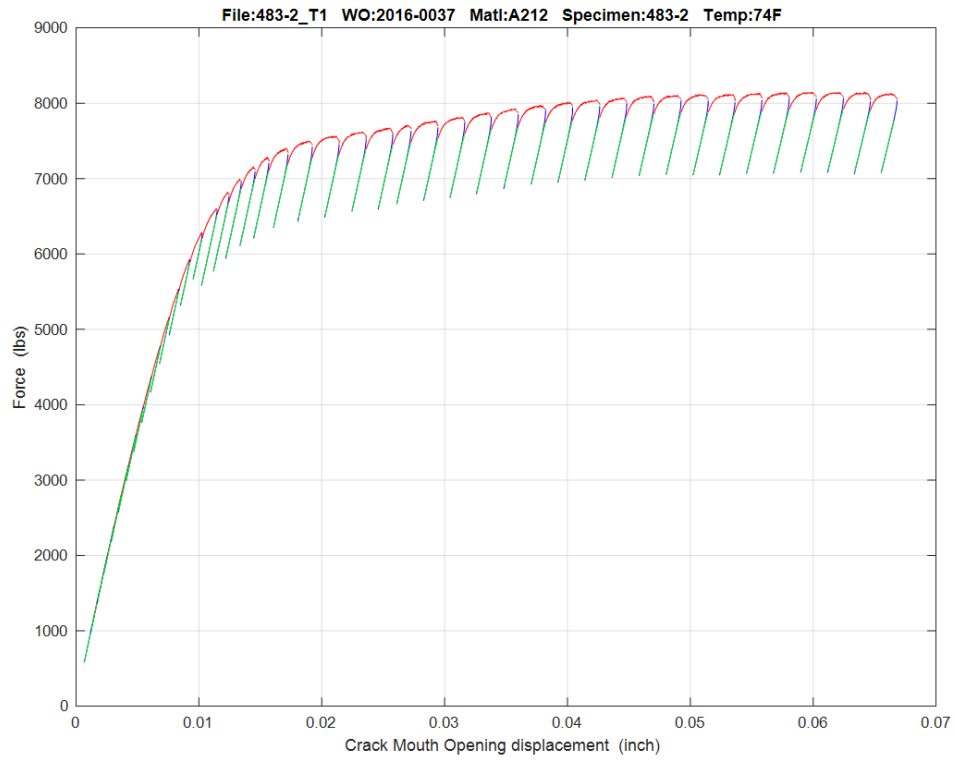


Figure 7.2.2.3.3-2: A212 Load Versus COD Plot, Sample 483-2

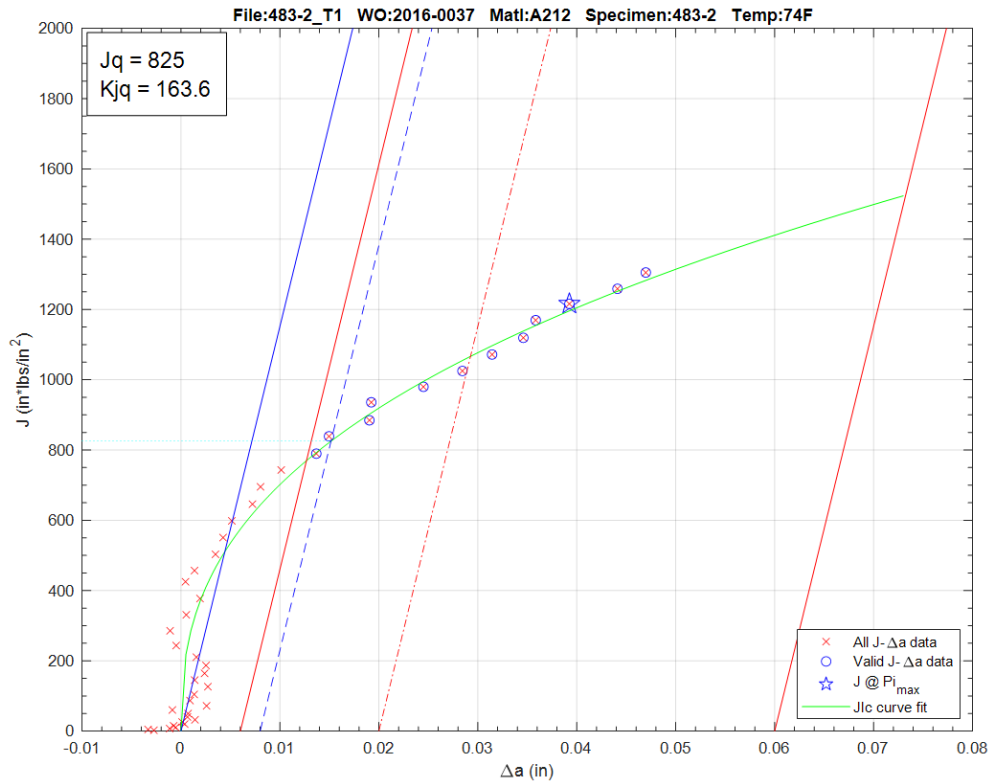


Figure 7.2.2.3.3-3: A212 J_q Versus Δa Plot, Sample 483-2

Table 7.2.2.3.3-2: T₀ Individual Specimen Results

Specimen Name	Temperature (°C)	KjcRaw (MPa*m ^{0.5})	1T Data (MPa*m ^{0.5})	Uncensored Data	Test Temp -T ₀ (°C)
483-3	-24	173.9	173.9	1	33
483-5	-46	124.8	124.8	1	11
483-6	-46	147.2	147.2	1	11
483-7	-46	124.2	124.2	1	11
483-8	-46	146	146.0	1	11
483-10	-73	74.5	74.5	1	-16
483-11	-73	60.5	60.5	1	-16
483-12	-46	98.2	98.2	1	11
483-13	-46	122.7	122.7	1	11
483-14	-46	134.7	134.7	1	11
483-15	-73	70.8	70.8	1	-16
483-16	-73	86.7	86.7	1	-16
483-17	-46	142.4	142.4	1	11

Table 7.2.2.3.3-3: T₀ Calculation Results

T₀ (°C)	-57
Total Samples	13
Samples within T₀ ± 50°C (N)	13
Number of Uncensored Data (r)	13
Poisson's Ratio	0.3
Σ(r_i n_i)	2.07
Samples Between T_i - T₀ 50 to -14 °C	9
Samples Between T_i - T₀ -15 to -35 °C	4
Samples Between T_i - T₀ -36 to -50 °C	0
T₀scrn (°C)	-57
Homogenous or Inhomogeneous	Homogenous

The results of the E1921 analysis show that the A212 material removed from the V0348 head is macroscopically homogenous, indicating consistent properties throughout the sampled material. For this data set, the ductile-brittle transition temperature was found to be -57°C. This result also meets the E1921 validity criteria for a sufficient number of samples tested in an appropriate temperature range with $\Sigma(r_i n_i) \geq 1.0$.

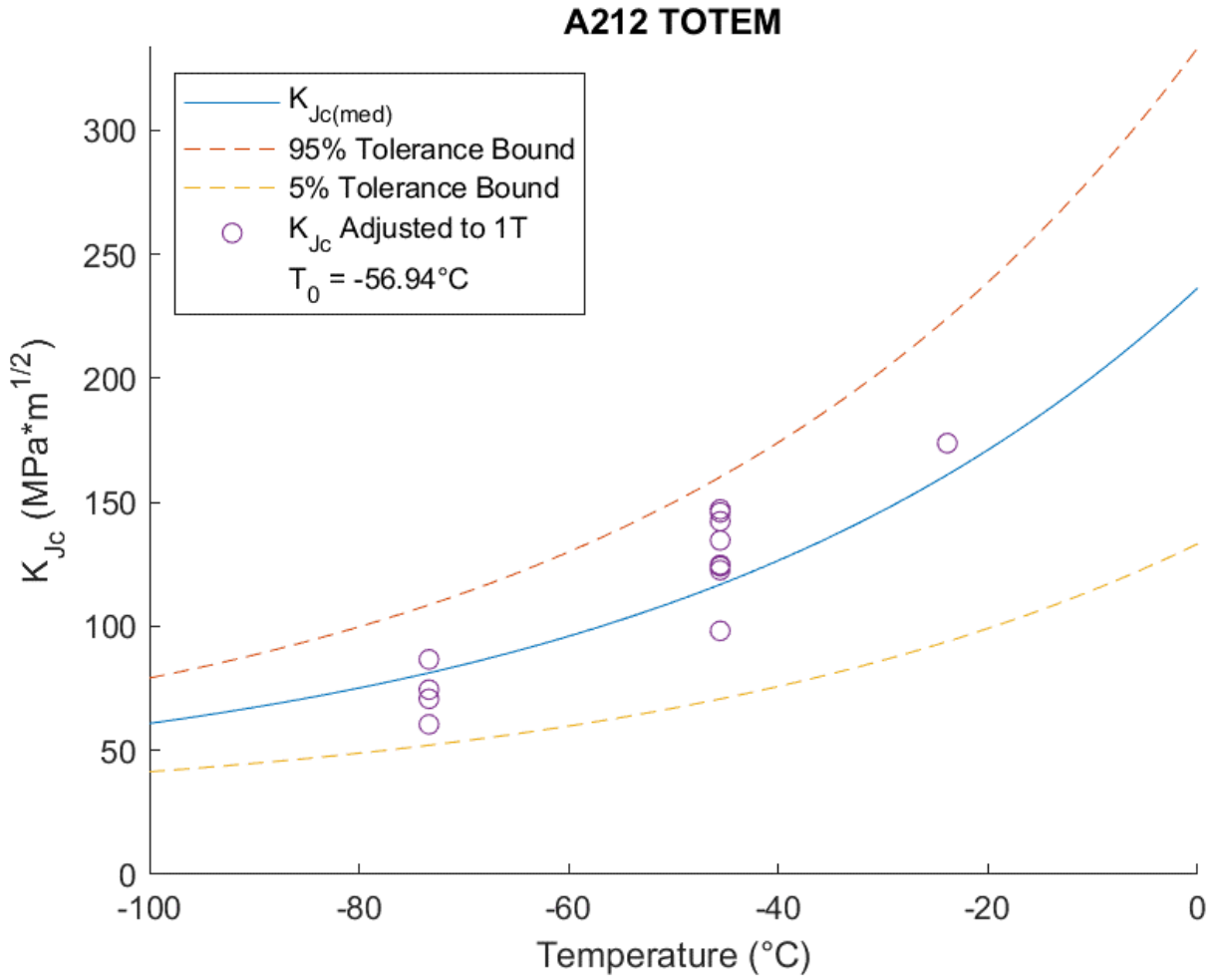


Figure 7.2.2.3.3-4: A212 T₀ Plot

7.2.2.3.4 Fatigue Crack Growth

Fatigue crack growth tests were not performed on this material.

7.2.2.3.5 Charpy Impact

Charpy impact tests were not performed on this material.

7.2.3 A302B Modified

A302B is also used as the head material of LPVs. The chemistry data reported in Figure 7.2.3.1-1 are from vessel V0071, dissected at Stennis Space Center and tested at MSFC. This particular material sample is listed as A302B-Modified which likely signifies the addition of more nickel to help add toughness, prior to the addition of A302C to the ASTM standard. Many literature searches for this material produced mostly irradiated Charpy data for nuclear reactor vessels which differed significantly from the tested LPV head material. However, the Charpy to fracture correlation appears to remain intact as detailed in Section 7.2.3.3.5.

7.2.3.1 Chemical Composition

Figure 7.2.3.1-1 provides the maximum percent content or ranges listed in the ASTM A302 material specification.

Elements	Composition, %			
	Grade A	Grade B	Grade C	Grade D
Carbon, max ^A :				
Up to 1 in. [25 mm], incl, in thickness	0.20	0.20	0.20	0.20
Over 1 to 2 in. [50 mm], incl	0.23	0.23	0.23	0.23
Over 2 in. [50 mm] in thickness	0.25	0.25	0.25	0.25
Manganese:				
Heat analysis	0.95–1.30	1.15–1.50	1.15–1.50	1.15–1.50
Product analysis	0.87–1.41	1.07–1.62	1.07–1.62	1.07–1.62
Phosphorus, max ^A	0.035	0.035	0.035	0.035
Sulfur, max ^A	0.040	0.040	0.040	0.040
Silicon:				
Heat analysis	0.15–0.40	0.15–0.40	0.15–0.40	0.15–0.40
Product analysis	0.13–0.45	0.13–0.45	0.13–0.45	0.13–0.45
Molybdenum:				
Heat analysis	0.45–0.60	0.45–0.60	0.45–0.60	0.45–0.60
Product analysis	0.41–0.64	0.41–0.64	0.41–0.64	0.41–0.64
Nickel:				
Heat analysis	0.40–0.70	0.70–1.00
Product analysis	0.37–0.73	0.67–1.03

^A Applies to both heat and product analyses.

Figure 7.2.3.1-1: ASTM A302/A302M-82 Standard Chemistry Values (33)

Table 7.2.3.1-1 provides data collected from Arc Spark analyses of vessel V0071.

Table 7.2.3.1-1: A302 Collected Chemistry Data, V0071

Chemistry (%)											
C	Si	Mn	P	S	Cr	Mo	Ni	Cu	Nb	V	B
0.190	0.220	1.340	0.008	0.020	0.140	0.450	0.510	0.220	0.003	0.003	0.0006

7.2.3.2 Metallography

This section reports the results of the grain orientation and macro cubes studies performed on the material samples from V0071. No grain size, through thickness grain size, or carburization studies were performed.

Grain Orientation Study

One set of three metallographic blocks was taken from the centerline of the head material to correlate the grain orientation with the tensile and fracture toughness testing. The cut plan in Figure 7.2.3.2-1 shows how the blocks were removed from the head. The blocks were polished, etched, and photographed, and the photographs were reconstructed as shown in Figure 7.2.3.2-2 through Figure 7.2.3.2-5, and Table 7.2.3.2-1 gives the descriptions of the metallographic structures observed.

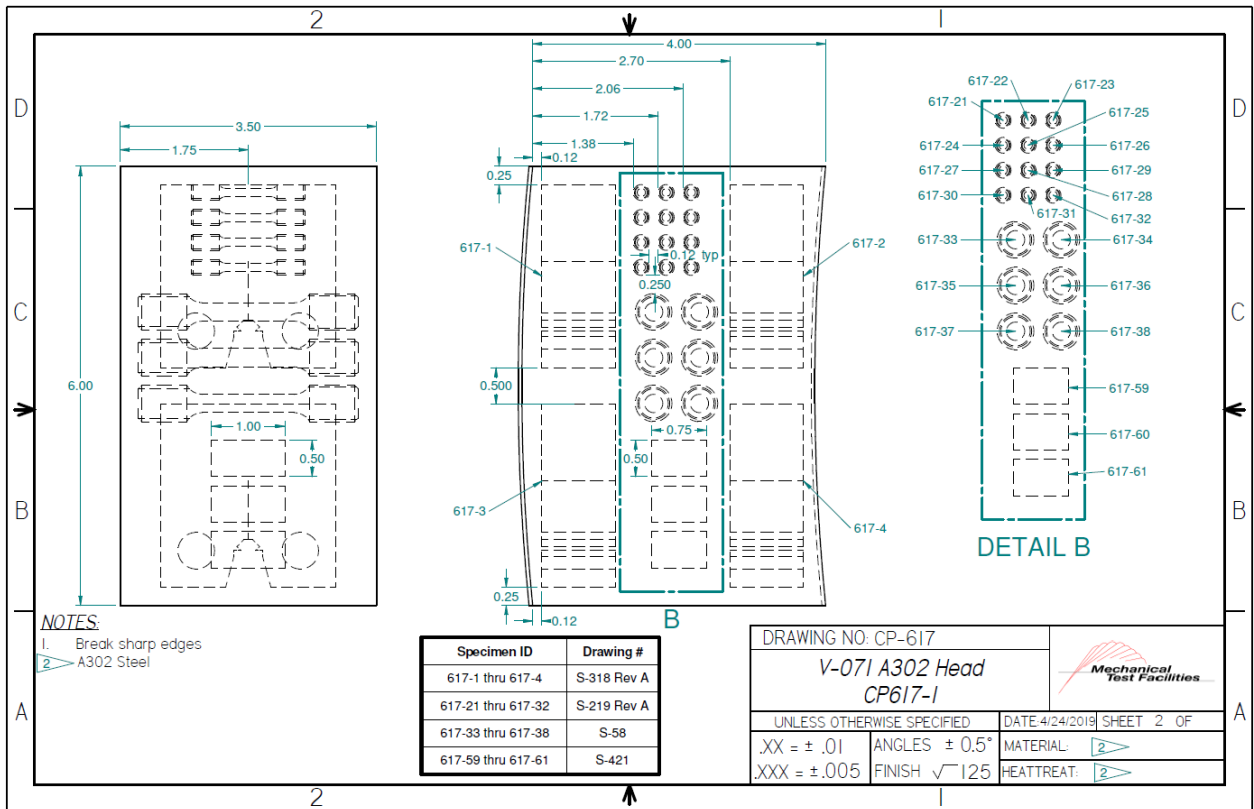


Figure 7.2.3.2-1: Cut Plan for Macros from V0071 Head

Table 7.2.3.2-1: A302 Macro Observations, V0071

Face	Face Dimensions	As-polished observations	Etched observations
617-59	1.00" x 0.75"	Elongated manganese sulfide inclusions. Indicates that the face is parallel to the metal working direction.	Martensitic microstructure consisting of equiaxed grains
617-60	1.00" x 0.50"	Equiaxed manganese sulfide inclusions. Indicates that the face is transverse to the metal working direction.	Martensitic microstructure consisting of equiaxed grains
617-61	0.75" x 0.50"	Elongated manganese sulfide inclusions. Indicates that the face is parallel to the metal working direction.	Martensitic microstructure consisting of equiaxed grains

The macros shown in Figure 7.2.3.2-2 through Figure 7.2.3.2-5 were extracted from the center of thickness of the V0071 head as shown in Figure 7.2.3.2-1.

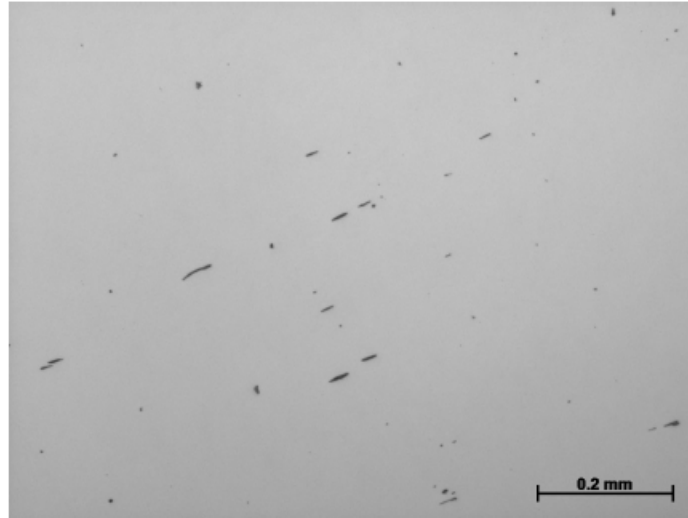


Figure 7.2.3.2-2: A302 Macro 617-59

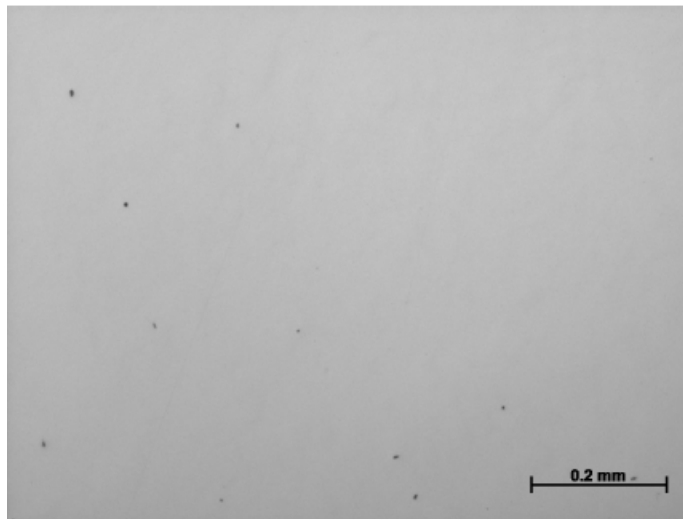


Figure 7.2.3.2-3: A302 Macro 617-60

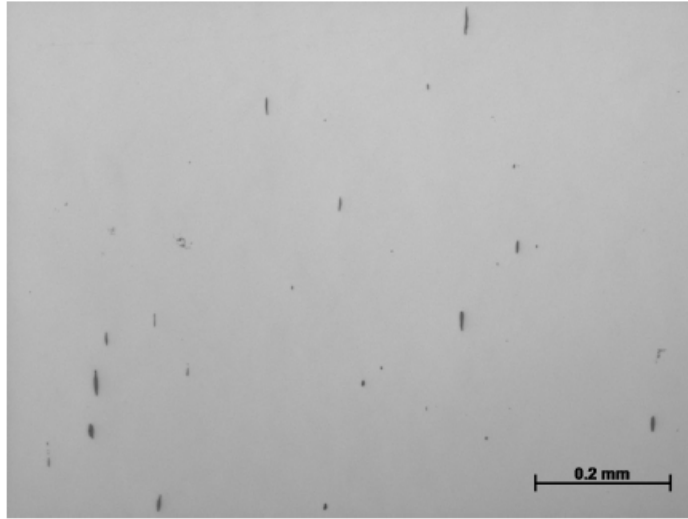


Figure 7.2.3.2-4: A302 Macro 617-61

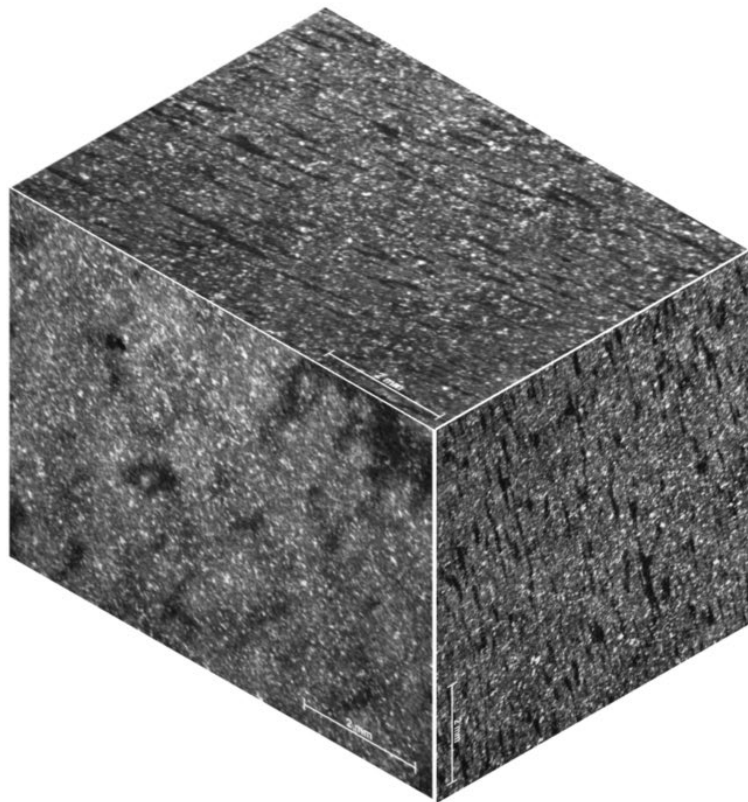
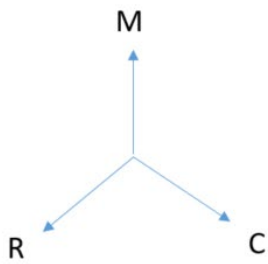


Figure 7.2.3.2-5: A302 Macro Cube, V0071

These macros show that the grains are elongated in the M-C plane with the greatest elongation in the circumferential direction. This implies that the grains were approximately equiaxial until the head was formed and the grains were only then elongated due to forming to the hemispherical shape.

The results of the macro cubes are as expected with the material working direction being in the circumferential direction. Fracture testing will be conducted in the C-M orientation, which while not the absolute weakest orientation, is the weakest orientation in which cracks could appear.

7.2.3.3 Mechanical Properties

Figure 7.2.3.3-1 provides the mechanical properties listed in the ASTM A302 material specification (33).

	Grade A	Grade B	Grade C	Grade D
Tensile strength, ksi [MPa]	75-95 [515-655]	80-100 [550-690]	80-100 [550-690]	80-100 [550-690]
Yield strength, min, ksi [MPa]	45 [310]	50 [345]	50 [345]	50 [345]
Elongation in 8 in. [200 mm], min, %	15 ^A	15 ^A	17 ^A	17 ^A
Elongation in 2 in. [50 mm], min, %	19 ^A	18 ^A	20 ^A	20 ^A

^A See Specification A 20/A 20M.

Figure 7.2.3.3-1: A302 Minimum Material Specifications (33)

7.2.3.3.1 Smooth Tensile Tests

Smooth tensile tests were conducted at MSFC on round specimens according to ASTM E8, “Standard Test Methods for Tension Testing of Metallic Materials” (51) using specimen design S-219 Revision A. The mechanical test frame consisted of a servo-hydraulic actuator and reaction frame. The frame used an LVDT for displacement feedback. Stress measurements were derived from load measurements and the initial specimen measurements. Strain measurements were derived from an extensometer and the initial specimen measurements.

The results obtained from testing of A302 from vessel V0071 are presented in Table 7.2.3.3.1-1. A typical engineering stress-strain curve is shown in Figure 7.2.3.3-1.

Table 7.2.3.3.1-1: A302 Tensile Data V0071

Specimen ID	Test Temp. (°C)	ASTM Orientation	Tensile Stress (ksi)	Yield Stress (ksi)	Fracture Elongation (%)
617-24	21	C	91.7	70.3	25.5
617-32	21	C	90.4	68.9	27.4
617-26	-46	C	96.3	71.3	26.5
617-29	-46	C	96.4	72.3	27.2
617-23	-101	C	106.8	82.2	28.6
617-31	-101	C	104.1	78.6	30.6

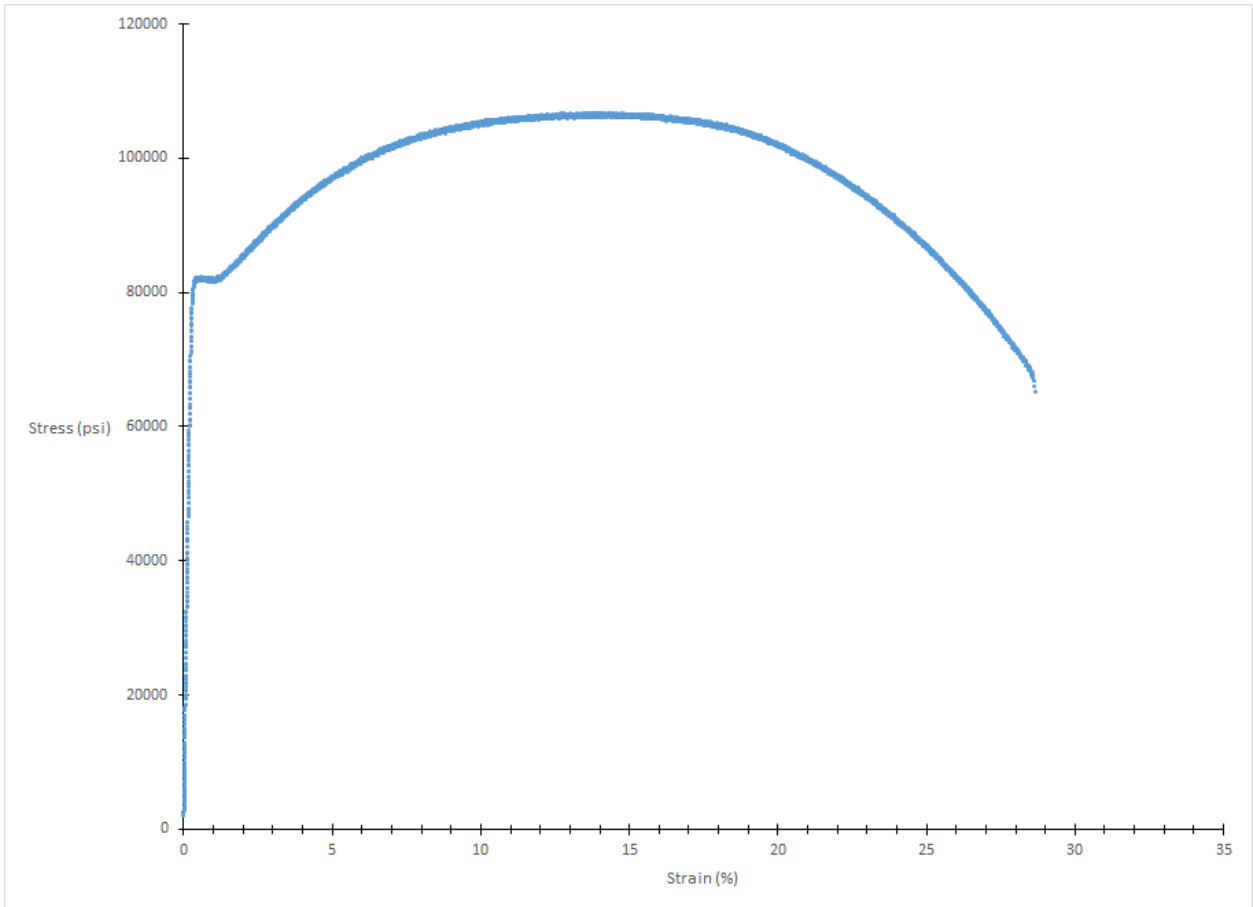


Figure 7.2.3.3.1-1: A302 Smooth Tensile Plot for Sample 617-23

7.2.3.3.2 Notch Tensile Tests

Notch tensile tests were not performed on this material.

7.2.3.3.3 Fracture Properties

All room temperature testing was performed in accordance with ASTM E1820 (10). All other temperatures were tested in accordance with ASTM E1921 (7). Testing for both standards use specimen design S-318 Rev A. All A302 fracture tests came from vessel V0071 and were tested with the crack plane in the C-M orientation as defined by ASTM (both grain and vessel orientations). The specimens used were ASTM E1820 compact specimens (C(T)) with $W = 2.0$ inches and $B = 1.0$ inch, $a/W = 0.5$ and all specimens were side grooved to a total thickness reduction of 20%. The cutting diagram used to remove the C(T) specimens from the V0071 head is shown in Figure 7.2.3.3.3-1.

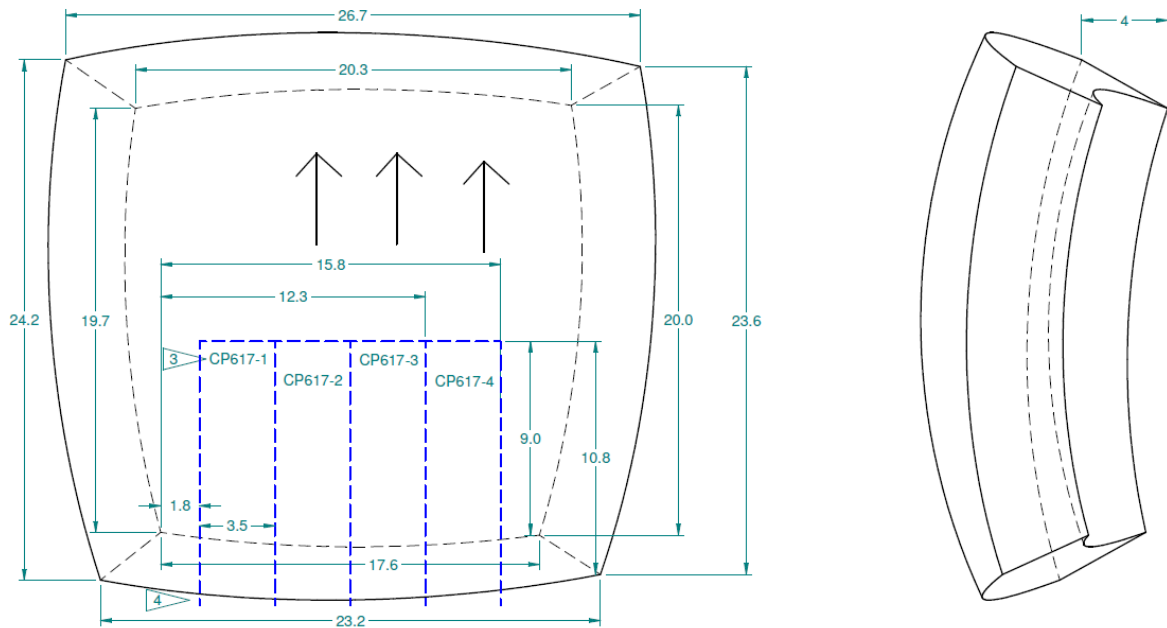
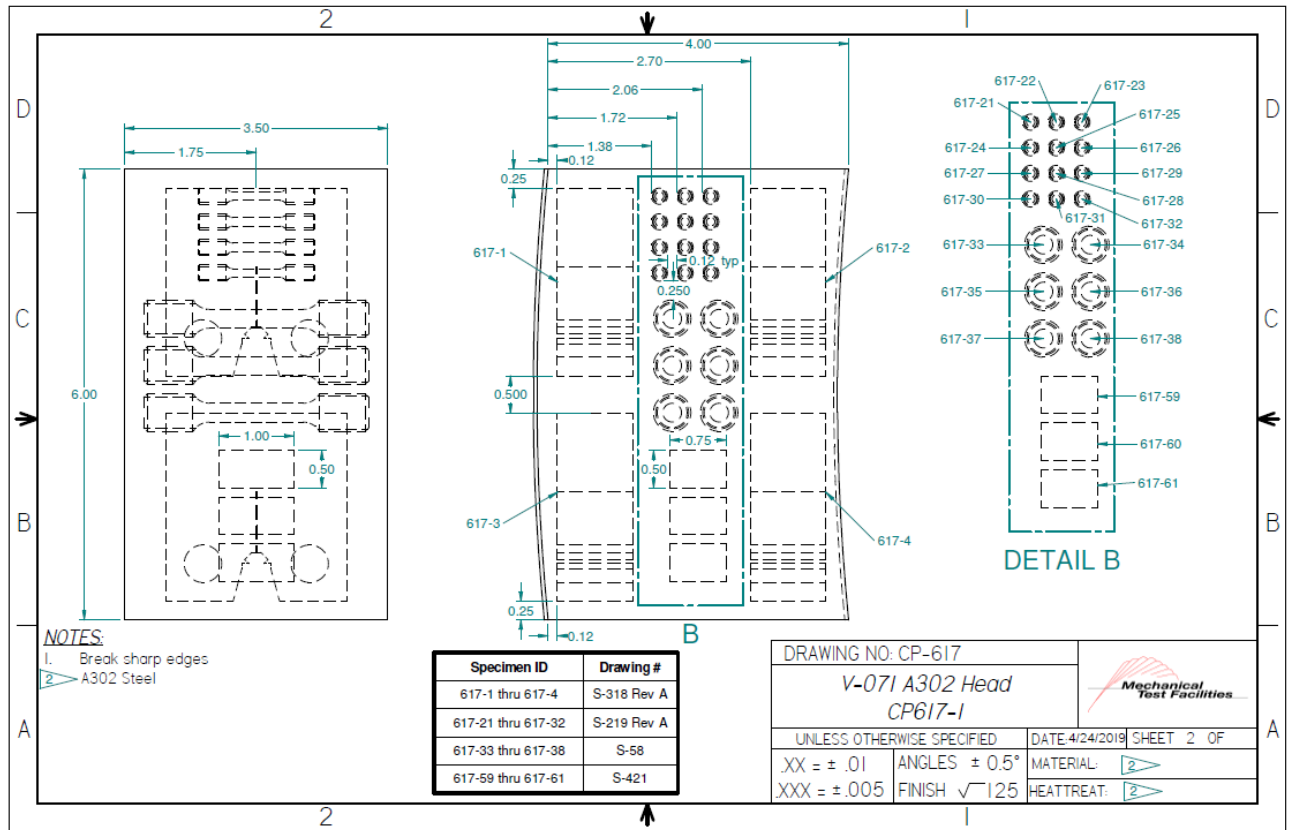


Figure 7.2.3.3.3-1: Example Cut Plan for V0071 Fracture Specimens (C-M Orientation)

Table 7.2.3.3.3-1 raw values obtained from fracture tests conducted on V0071 A302 head material. Test results identified as upper shelf are listed under ASTM E1820, while transition

temperature tests are listed under E1921. Tests that meet the complete validity requirements for $J_q = J_{1C}$ and $K_{Jq} = K_{J1C}$ are denoted with an asterisk. Despite invalidities, J_q and K_{Jq} convey valuable fracture toughness information, especially when the test results are applied directly to the sample material source.

Table 7.2.3.3.3-1: A302 Fracture Data V0071

Specimen ID	Test Temp. (°C)	ASTM Crack Plane Orientation	W (in)	a ₀ (in)	a _r (in)	B ₀ (in)	B _N (in)	J _q (kJ/m ²)	K _{Jq} (MPa√m)	K _{JC1T} (MPa√m)	ASTM Standard
617-7	21	C-M	1.9997	1.0438	1.3361	0.9998	0.8078	237	230	---	E1820
617-8	21	C-M	1.9998	1.0389	1.2255	1.0023	0.8050	223	223	---	E1820
617-11	-30	C-M	2.0003	1.0414	1.0414	0.9996	0.8050	46	101	101	E1921
617-12	-30	C-M	2.0026	1.0381	1.0407	0.9991	0.8014	96	147	147	E1921
617-14	-30	C-M	2.0000	1.0421	1.0421	0.9999	0.8032	128	169	169	E1921
617-16	-30	C-M	2.0015	1.0343	1.0375	0.9987	0.8011	77	131	131	E1921
617-9	-50	C-M	2.0004	1.0422	1.0529	0.9999	0.8000	160	189	189	E1921
617-10	-50	C-M	2.0014	1.0408	1.0454	1.0000	0.8013	57	112	112	E1921
617-13	-50	C-M	1.9998	1.0448	1.0503	0.9986	0.8007	70	125	125	E1921
617-15	-50	C-M	2.0004	1.0409	1.0484	0.9980	0.8010	163	191	191	E1921
617-1	-73	C-M	2.0013	1.0362	1.0362	1.0005	0.8058	178	199	199	E1921
617-2	-107	C-M	2.0002	1.0319	1.0356	1.0007	0.8054	20	68	68	E1921
617-3	-107	C-M	1.9993	1.0452	1.0452	0.9997	0.8031	45	101	101	E1921
617-4	-107	C-M	2.0008	1.0363	1.0363	1.0005	0.8075	35	89	89	E1921
617-5	-107	C-M	1.9996	1.0469	1.0475	0.9998	0.8044	38	92	92	E1921
617-6	-107	C-M	1.9998	1.0352	1.0375	1.0006	0.8039	21	68	68	E1921

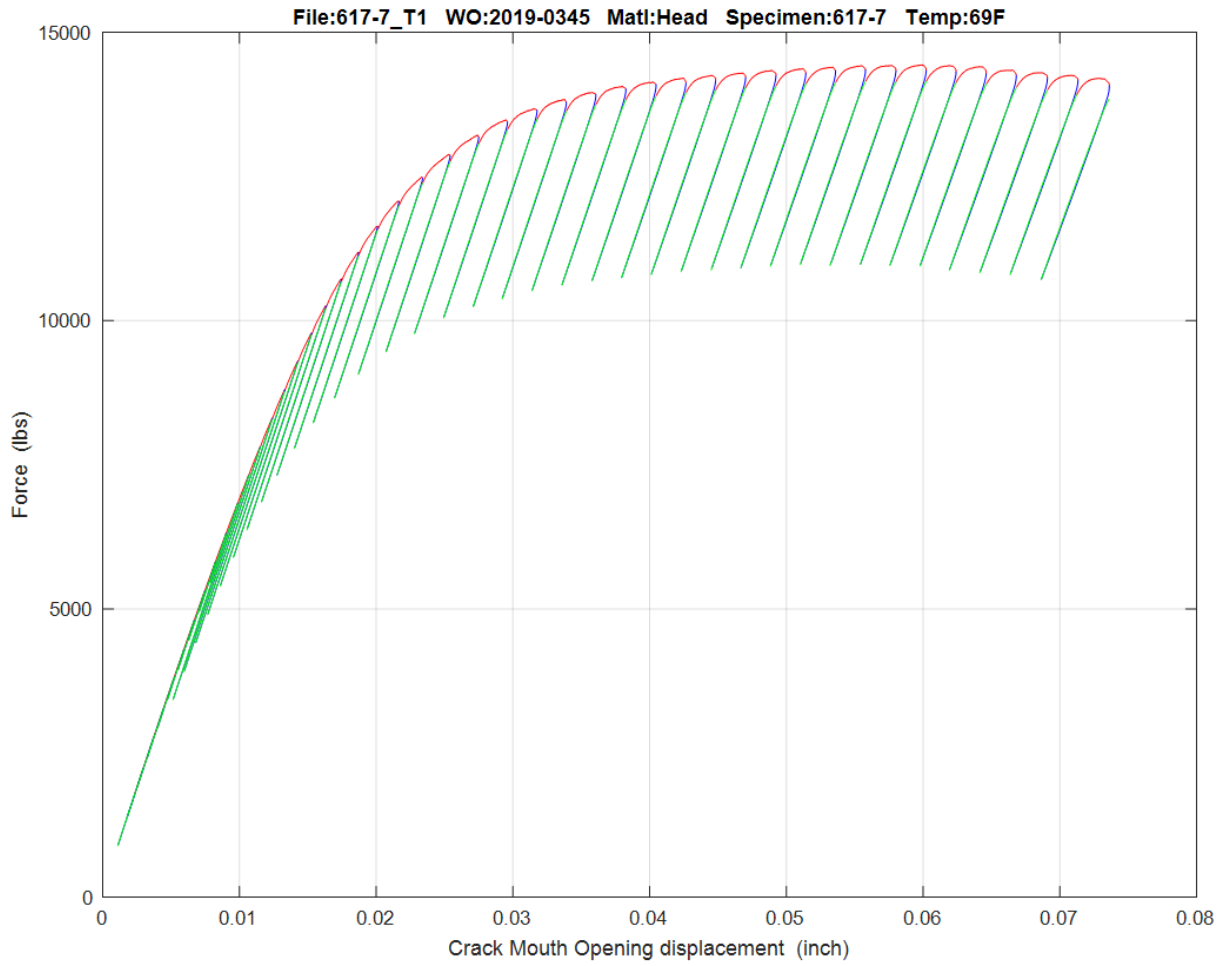


Figure 7.2.3.3.3-2: A302 Load Versus COD Plot, Sample 617-7

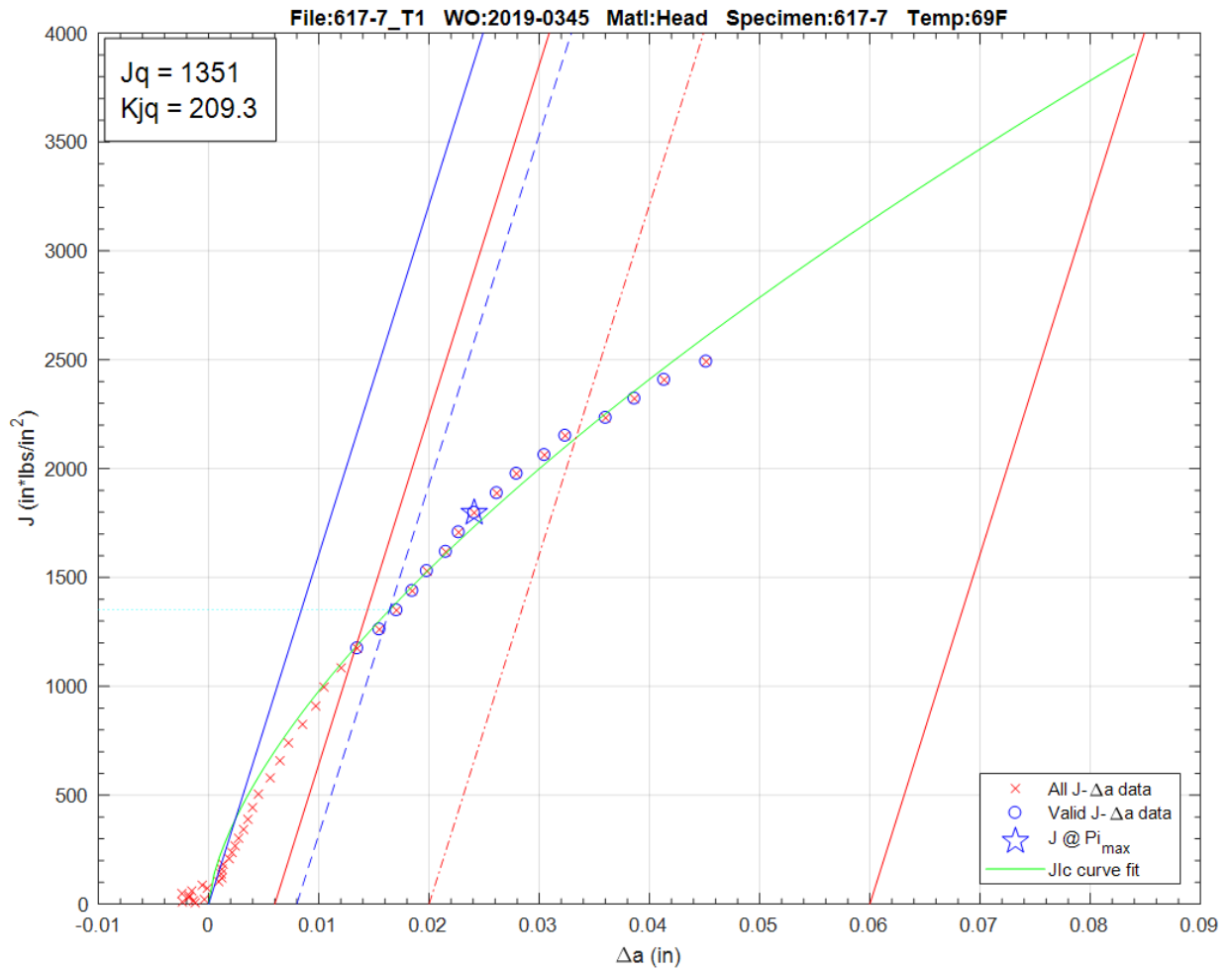


Figure 7.2.3.3.3-3: A302 J_q Versus Δa Plot, Sample 617-7

Table 7.2.3.3.3-2: T_0 Individual Specimen Results

Specimen Name	Temperature (°C)	KjcRaw (MPa*m ^{0.5})	1T Data (MPa*m ^{0.5})	Uncensored Data	Test Temp -T0 (°C)
617-1	-73	199.3	199.3	1	20
617-2	-107	67.6	67.6	1	-13
617-3	-107	100.8	100.8	1	-13
617-4	-107	89.1	89.1	1	-13
617-5	-107	92.0	92.0	1	-13
617-6	-107	68.3	68.3	1	-13
617-9	-50	189.2	189.2	1	43
617-10	-50	112.5	112.5	1	43
617-13	-50	125.3	125.2	1	43
617-15	-50	190.7	190.6	1	43

Table 7.2.3.3.3-3: T₀ Calculation Results

Initial T₀ (°C)	-93
Total Samples	10
Samples within T₀ ± 50°C (N)	10
Number of Uncensored Data (r)	10
Poisson's Ratio	0.3
Σ(r_i n_i)	1.67
Samples Between T_i - T₀ 50 to -14 °C	10
Samples Between T_i - T₀ -15 to -35 °C	0
Samples Between T_i - T₀ -36 to -50 °C	0
T₀scrn (°C)	-92
Homogenous or Inhomogeneous	Homogenous

The results of the E1921 analysis show that the A302 material removed from the V0071 head is macroscopically homogenous, indicating consistent properties throughout the sampled material. For this data set, the ductile-brittle transition temperature was found to be -93°C. This result also meets the E1921 validity criteria for a sufficient number of samples tested in an appropriate temperature range with $\Sigma(r_i n_i) \geq 1.0$.

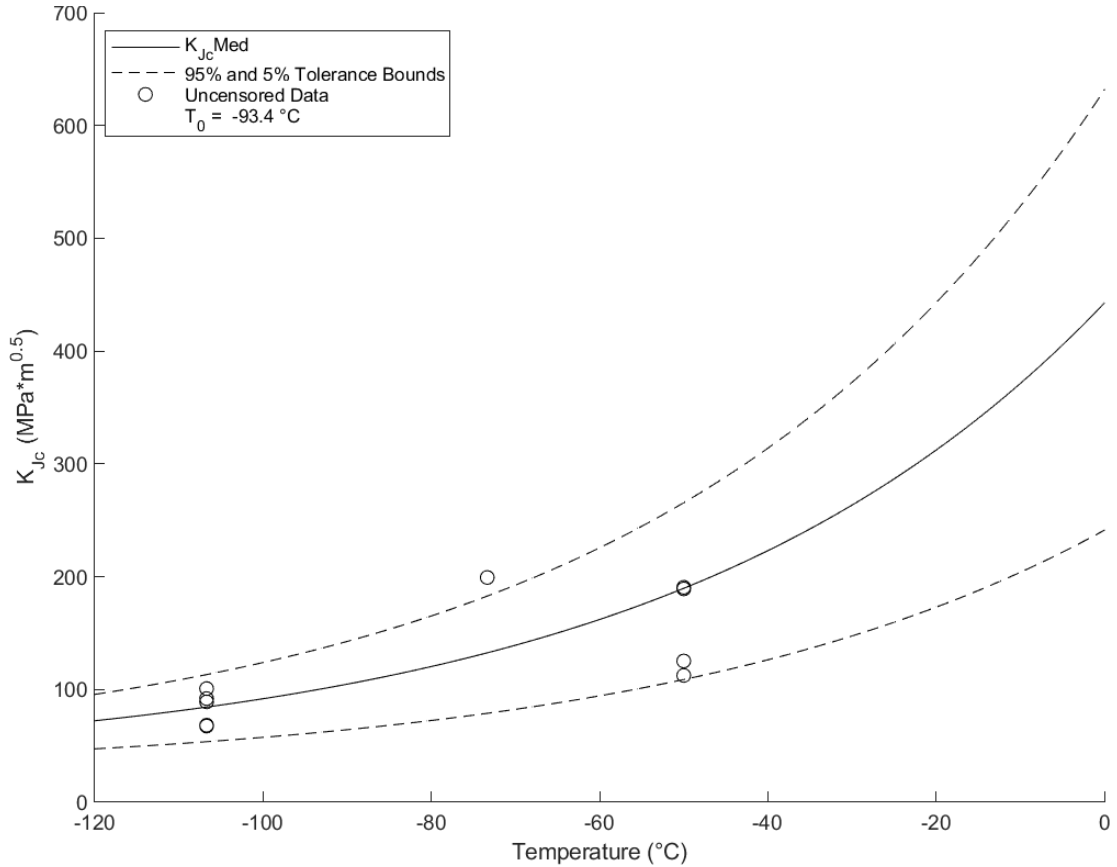


Figure 7.2.3.3.3-4: A302 T₀ Plot

7.2.3.3.4 Fatigue Crack Growth

Fatigue crack growth tests were not performed on this material.

7.2.3.3.5 Charpy Impact

Charpy impact tests were performed on this material per ASTM E23 (17) with the intention of comparing the results to historical Charpy test data. Significant numbers of Charpy tests have been A302B materials in the past. If the current data shows similarity, then an argument can be made for accepting the previous results as relevant to LPVs.

Twenty Charpy impact specimens were machined from the V0071 A302 head material in the C-M orientation, the same orientation used for the E1820/E1921 fracture specimens.

Table 7.2.3.3.5-1: A302 Charpy Impact Results V0071
Impact Testing - Charpy Trans Curve Ref/Heat

Test Method	ASTM A 370
Sample Direction	As Received
Sample Size	10 x 10 x 55mm
Notch Type	V-Notch

Specimen	Sample ID	Temperature (°C)	Impact 1 (Ft-Lbs)	Impact 2 (Ft-Lbs)	Impact 3 (Ft-Lbs)	Impact Avg (Ft-lbs)	Lat Exp 1 (mils)	Lat Exp 2 (mils)	Lat Exp 3 (mils)	% Shear 1	% Shear 2	% Shear 3
617	39, 40, 41	19.7	105	89	119	104	77	64	84	95	60	100
617	42, 43, 44	-75	4	11	4	6	4	10	2	<5	<5	<5
617	45, 46, 47	-50	9	21	19	16	9	16	14	10	10	10
617	48, 49, 50	-30	29	46	65	47	24	36	47	10	20	35
617	51, 58, 57	-40	36	31	35	34	29	23	27	20	20	25
617	52, 53, 54	Ø -45	19	61	19	33	33	45	18	10	30	10
617	55, 56	-35	13	37	-	25	10	30	-	10	25	-

Figure 7.2.3.3.5-1 through Figure 7.2.3.3.5-4 provide plots and charts comparing toughness data for the A302B steel removed from the hemispherical head of the LPV designated V0071 to fracture toughness data on A302B obtained from the literature in references (35), (37), (40), (33), (34).

The V0071 A302B is shown to be superior to legacy A302B steels reported in the references. It is not clear at this time whether this is caused by the relatively more recent date of manufacture of the V0071 vessel, hence cleaner steel, or simple variability between material samples. Nonetheless, it is proposed that the larger data set obtained from the technical literature will be useful to establish the material variability present in A302B steel, and hence this data and this comparison will be useful in the structural integrity analysis of other LPVs.

Table 7.2.3.3.5-2 provides the chemical analysis reported for the ORNL A302 plates and for the MSFC vessel V0071 head A302 steel. Note that the Z8 plate was an A533B steel that ORNL included in their report. Data for it is not included in this analysis because the alloy is not found in any NASA LPVs.

Table 7.2.3.3.5-2: A302 Chemistry ORNL (58)

Table 2. Modified A 302 grade B test materials, heat code, and chemistries

Plate code	Heat	Composition (wt %)												
		C	Mn	P	S	Si	Ni	Cr	Mo	V	Nb	Co	Cu	Al
Z1, Z2	B3990-2	0.18	1.35	0.007	0.011	0.23	0.47	0.11	0.44	0.003	0.004	0.011	0.17	0.03
Z3	A0237-1*	0.24	1.47	0.008	0.014	0.25	0.52	0.11	0.50	0.002	0.003	0.011	0.11	0.026
Z4	C1290-2*	0.22	1.42	0.006	0.013	0.24	0.50	0.11	0.48	0.002	0.003	0.011	0.10	0.027
Z5	P2130-2	0.17	1.16	0.013	0.016	0.17	0.60	0.10	0.50	0.002	0.004	0.012	0.16	0.012
Z6A	C1079-1	0.17	1.35	0.006	0.013	0.23	0.49	0.10	0.45	0.002	0.003	0.012	0.18	0.028
Z6B	B5013-2	0.22	1.39	0.009	0.023	0.20	0.51	0.15	0.48	0.002	0.003	0.017	0.21	0.035
Z7	C2463-1	0.26	1.47	0.008	0.014	0.15	0.53	0.09	0.52	0.002	0.003	0.011	0.16	0.017
Z8	C2220-2	0.27	1.49	0.006	0.015	0.23	0.68	0.12	0.45	0.002	0.003	0.012	0.16	0.016

*There was some uncertainty in heat identifications. Values were determined by ABB-Combustion Engineering.

10

Table 7.2.3.3.5-3: A302 Chemistry V0071

Chemistry (%)											
C	Si	Mn	P	S	Cr	Mo	Ni	Cu	Nb	V	B
0.190	0.220	1.340	0.008	0.020	0.140	0.450	0.510	0.220	0.003	0.003	0.0006

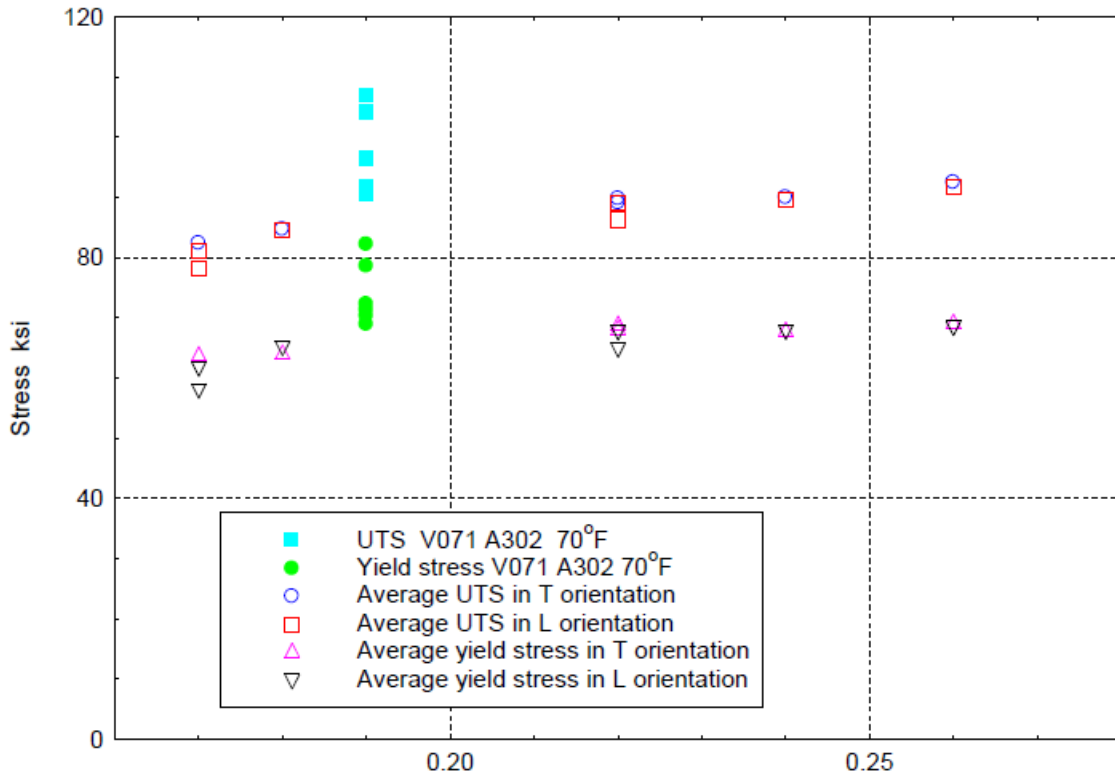


Figure 7.2.3.3.5-1: Tensile Properties of V0071 A302B Modified and ORNL A302B

The yield stress and ultimate tensile strength for each of the ORNL plates and the V0071 head steel are plotted versus carbon content in Figure 7.2.3.3.5-1. The V0071 steel has a very high yield stress and the ultimate tensile strength exceeds the maximum ultimate strength allowed for A302 steel plates.

Figure 7.2.3.3.5-2 shows a typical Charpy data set result from the Hiser (57) work. This figure shows the Charpy-defined toughness transition and can be utilized to obtain a ductile-brittle transition temperature at a toughness level of 20 ft-lbs (28 J), 30 ft-lbs (41 J), or 40 ft-lbs (56 J), etc., as desired for the application at hand. In this work, a 30 ft-lb toughness level is used to quantify the Charpy transition temperature.

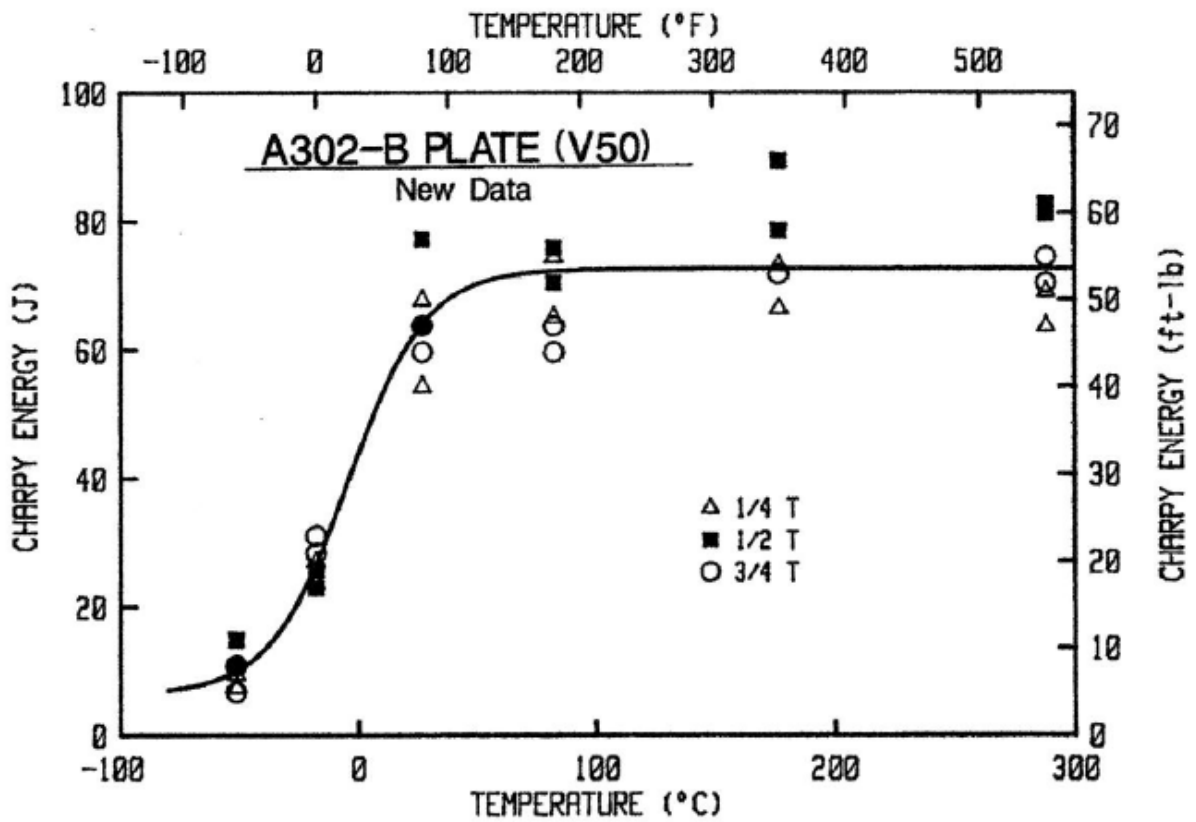


Figure 7.2.3.3.5-2: Typical Charpy Data Set (57)

Figure 7.2.3.3.5-3 and Figure 7.2.3.3.5-4 show data obtained from Wang (40) who did a large study of the effects of irradiation on A302B and A533B steels. These figures show the baseline un-irradiated toughness data measured for a large number of A302 steels that were used in commercial and research nuclear power plants during the 1950s and 1960s.

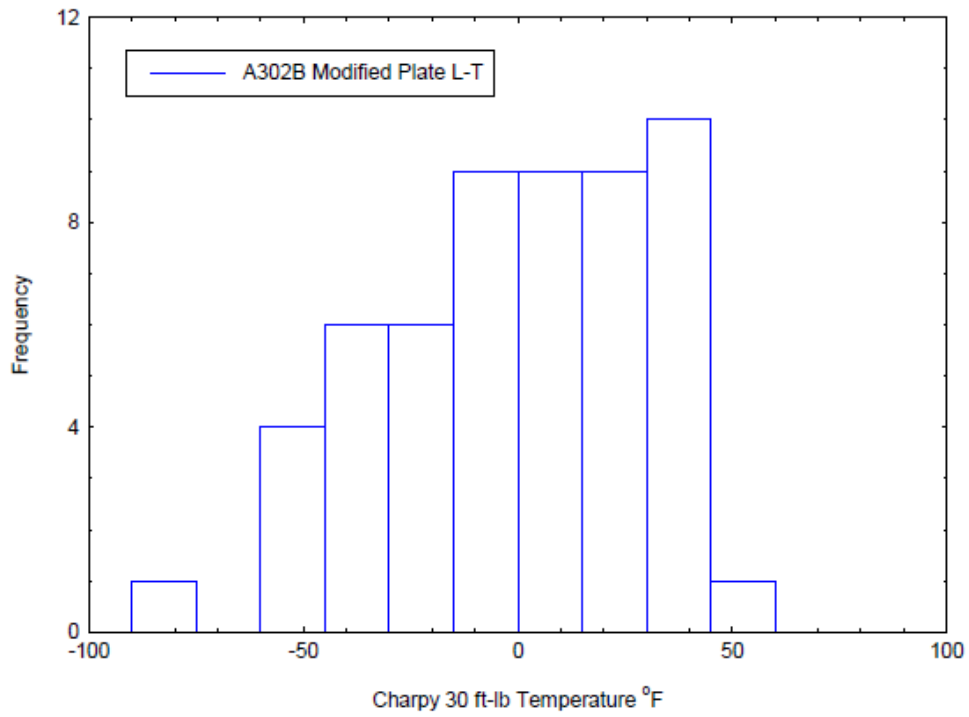


Figure 7.2.3.3.5-3: A302 30 ft-lb Transition Temperatures L-T Orientation (43)

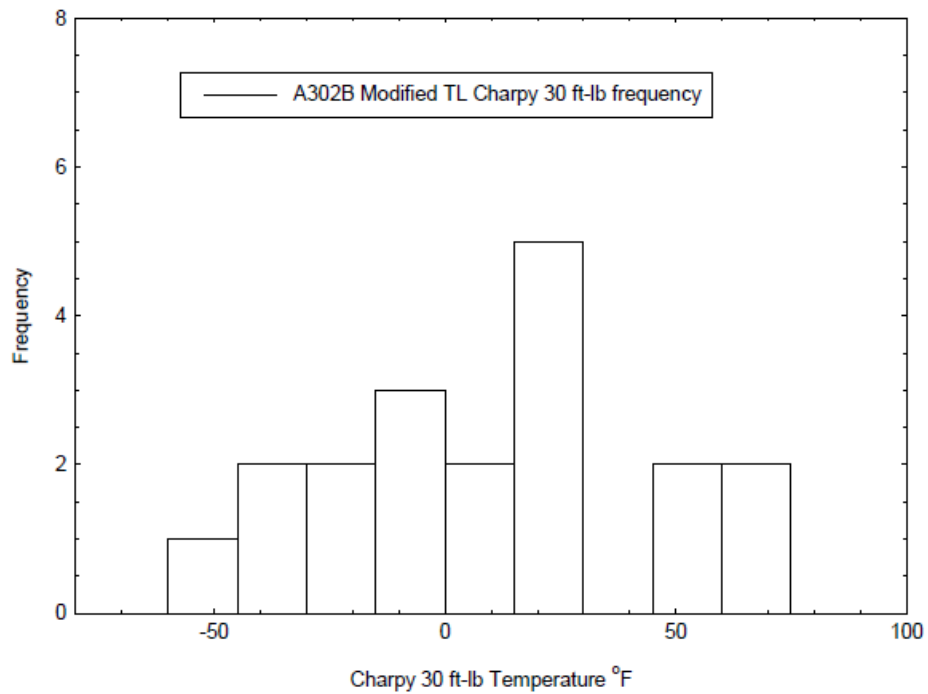


Figure 7.2.3.3.5-4: A302 30 ft-lb Transition Temperatures T-L Orientation (43)

The Wang Charpy data can be used to estimate the E1921 T_0 reference temperature as shown in Figure 7.2.3.3.5-5 and Figure 7.2.3.3.5-6 using correlations developed by Wallin (21) and Sokolov and Nanstad (43). The original correlation between the legacy Charpy transition temperature and T_0 was presented by Wallin as shown in Figure 7.2.3.3.5-5 used a 20 ft-lb toughness level to define the transition temperature. The second correlation shown in Figure 7.2.3.3.5-6 based on the 30 ft-lb transition temperature was presented by Sokolov and Nanstad.

Figure 7.2.3.3.5-7 and Figure 7.2.3.3.5-8 show the estimated T_0 obtained from the Charpy transition data by applying the Sokolov and Nanstad proposed 24°C (43°F) shift defined in Figure 7.2.3.3.5-6 to the Wang Charpy transition results of Figure 7.2.3.3.5-3 and Figure 7.2.3.3.5-4.

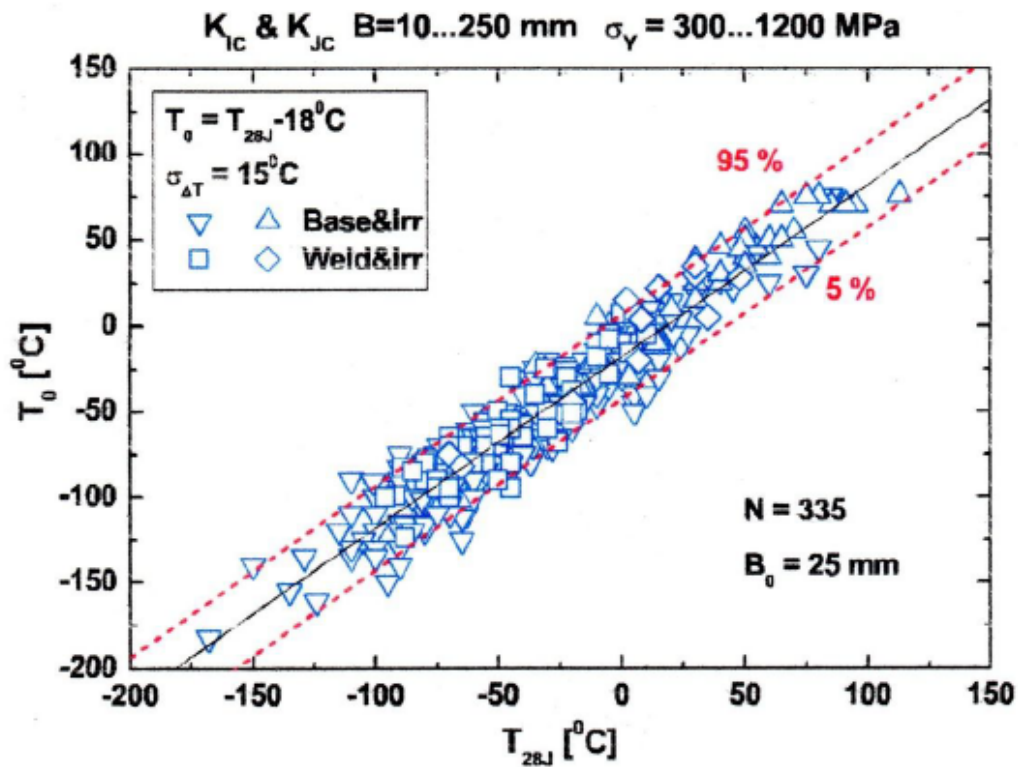


Figure 7.2.3.3.5-5: Wallin Correlation Between T_0 and 20 ft-lb Charpy Transition (43), (21)

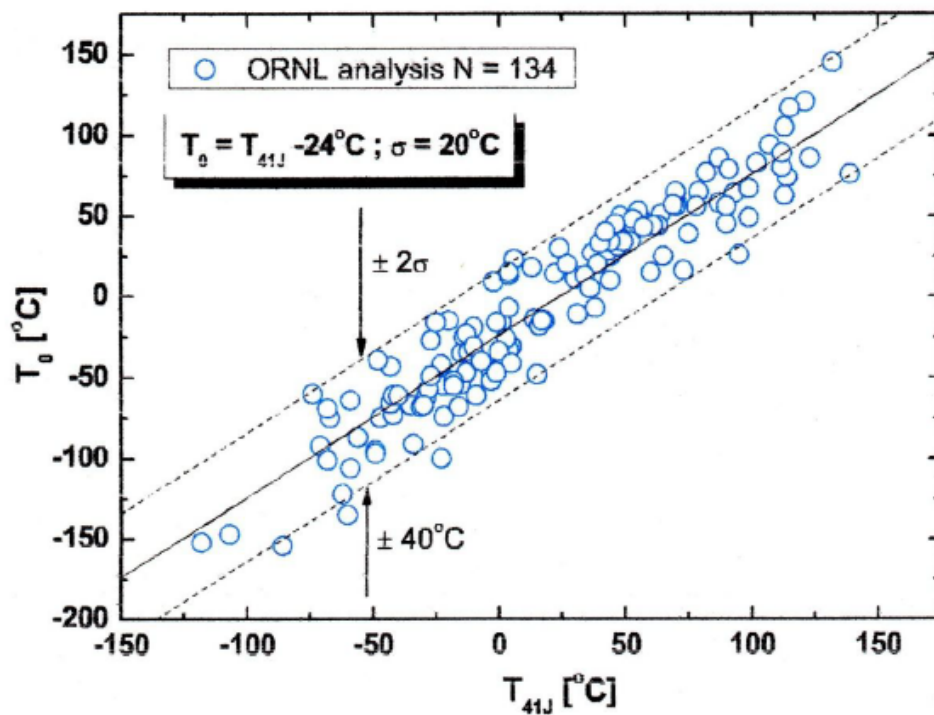


Figure 7.2.3.3.5-6: Revised T_0 to 30 ft-lb Charpy Correlation (43), (21)

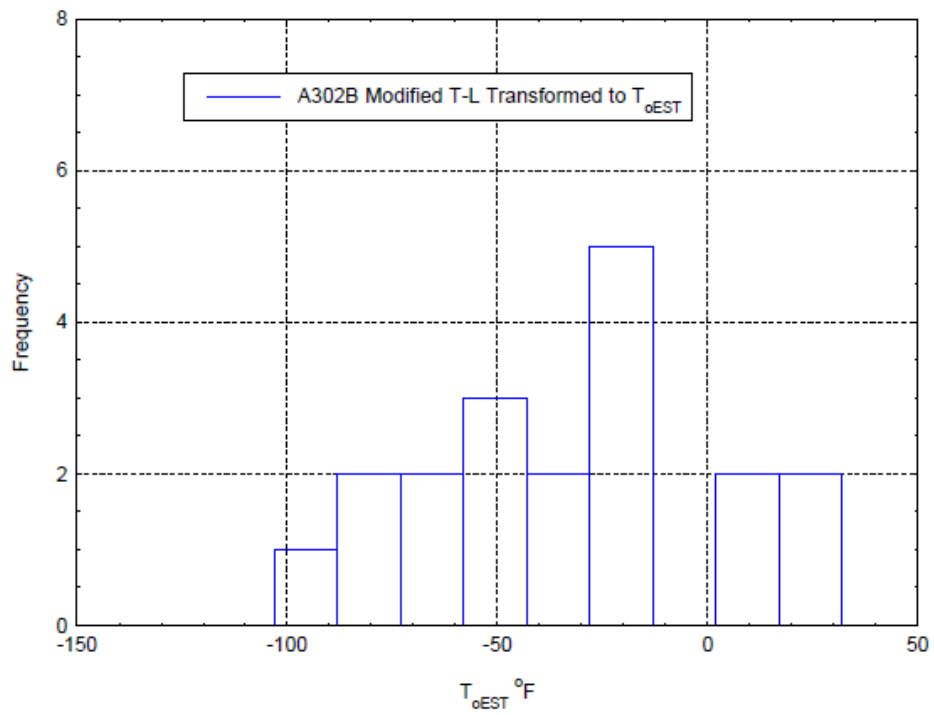


Figure 7.2.3.3.5-7: A302B T_0 ORNL Correlation Wang (43), (21)

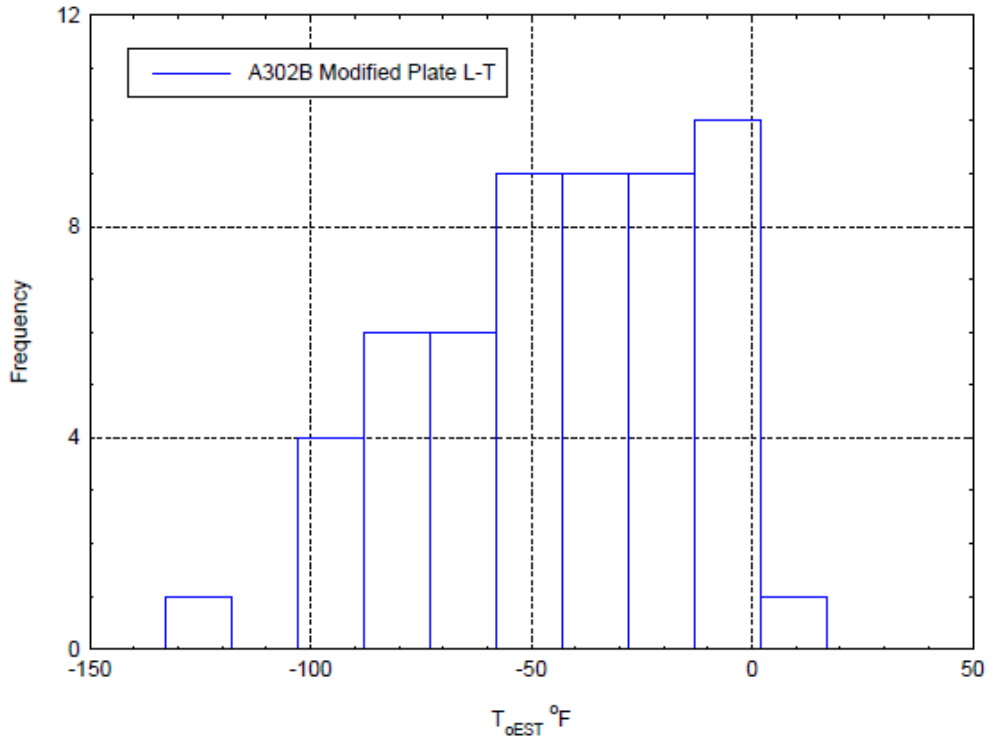


Figure 7.2.3.3.5-8: A302B T_0 ORNL Correlation Wang (43), (21)

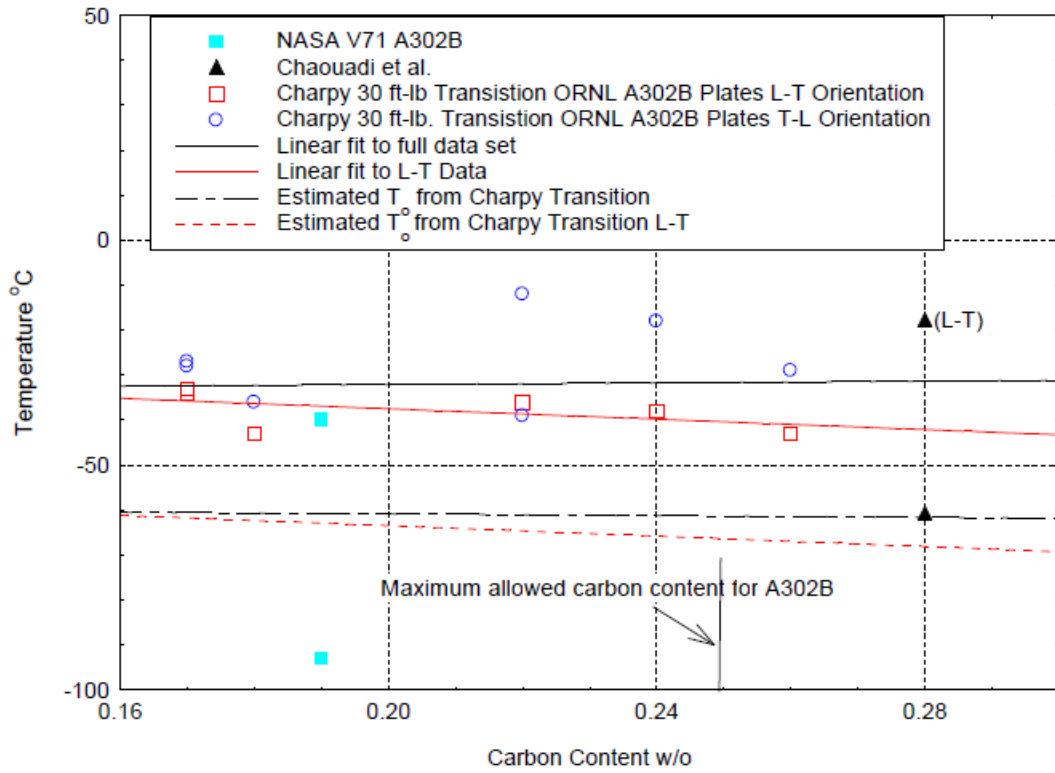


Figure 7.2.3.3.5-9: 30 ft-lb Transition ORNL Charpy, V0071 for A302B (43), (21)

Figure 7.2.3.3.5-9 shows the 30 ft-lb transition Charpy results obtained by ORNL on the seven A302 plates (34). Also shown are two fit equations which were then shifted by -24°C to show the predicted T_0 values corresponding to the ORNL Charpy results. In addition, the graph includes the results obtained by Chaouadi et al. (37) for an A302B steel removed from an ORNL test reactor. The Chaouadi results are quite consistent with the ORNL Charpy predictions and the T_0 from the ORNL T_0 to Charpy transition predictions. The Chaouadi Master Curve plot is presented in Figure 7.2.3.3.5-10 with $T_0 = -64^{\circ}\text{C}$ and is the only data set that was found in the literature for A302 steel. In this case, the steel was removed from a decommissioned ORNL reactor as part of an irradiation study. The data presented here was from material removed from a portion of the reactor pressure vessel that received very limited radiation. Other A302 data is presented by McCabe (34), but in that case the A302 had been specially heat treated to simulate irradiation and the T_0 resulting from that study is not comparable with the steel used in the head of MSFC vessel V0071. The Charpy result of -40°C falls close to the ORNL data while the V0071 $T_0 = -93^{\circ}\text{C}$ falls relatively low, but within the $2\sigma = 40^{\circ}\text{C}$ (72°F) confidence bound predicted by Sokolov and Nanstad in Figure 7.2.3.3.5-6.

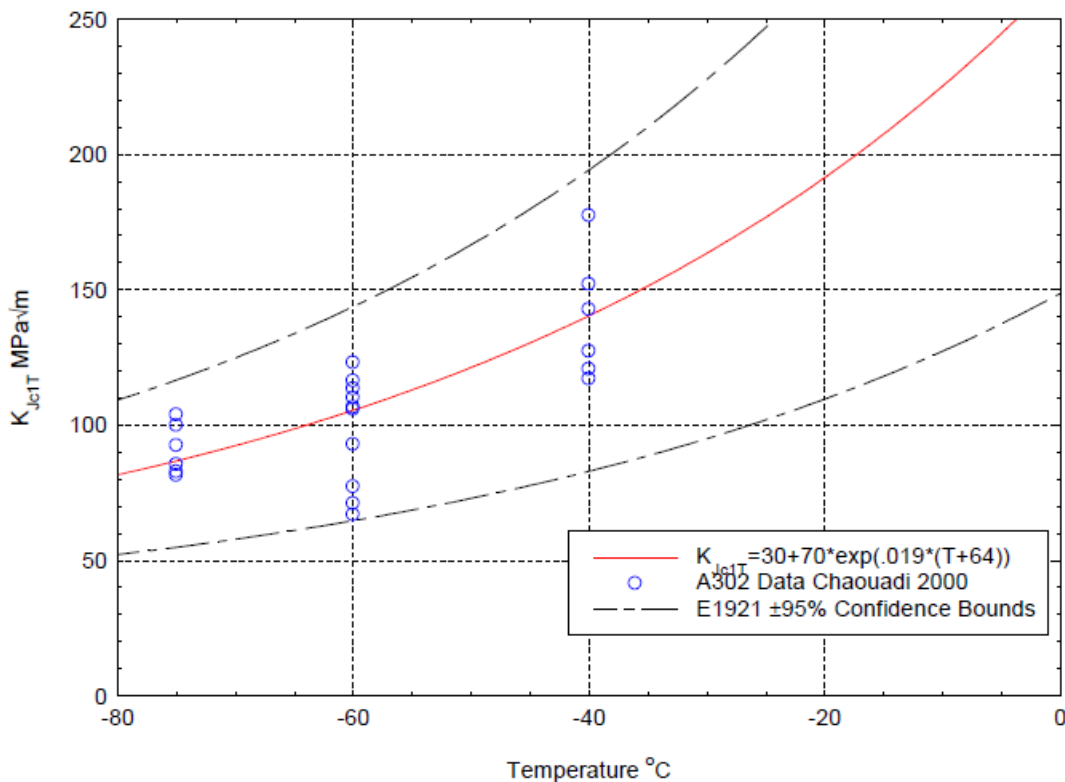


Figure 7.2.3.3.5-10: Chaouadi (37) Master Curve for ORNL A302B

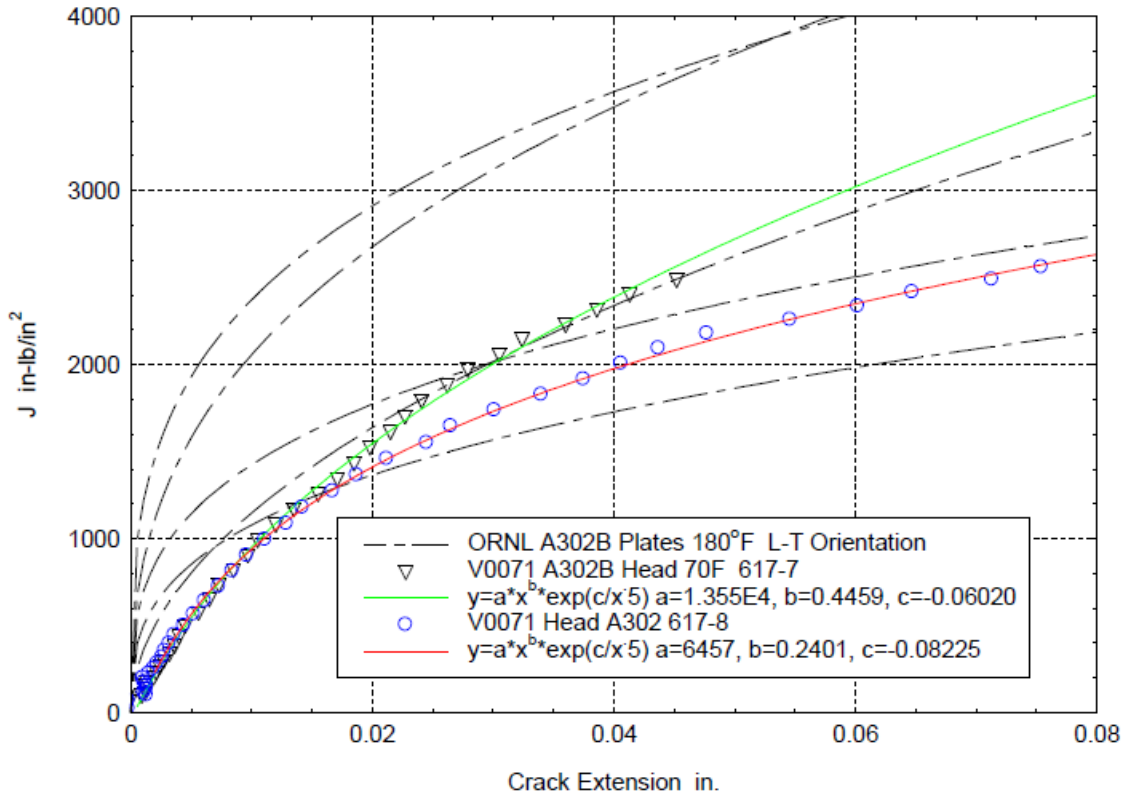


Figure 7.2.3.3.5-11: Upper Shelf J-R Curve; V0071 Versus ORNL (37) Average in L-T Orientation

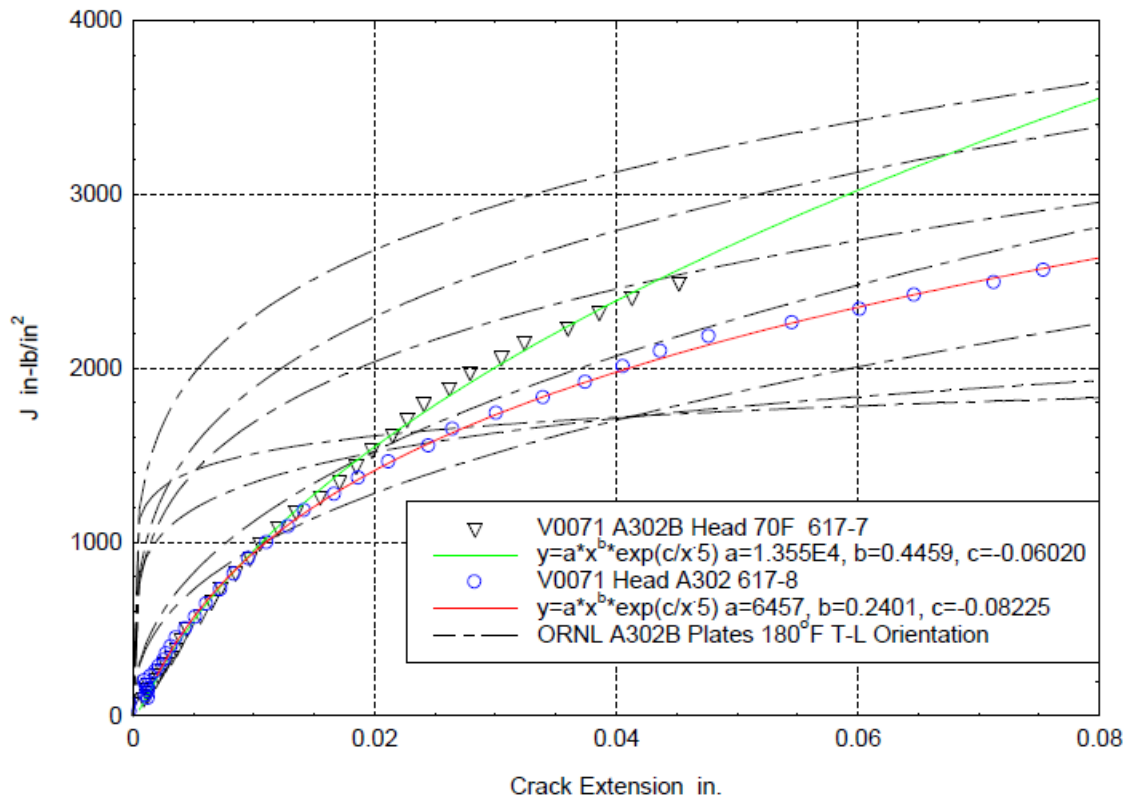


Figure 7.2.3.3.5-12: Upper Shelf J-R Curve, V0071 Versus Average ORNL (37) in T-L Orientation

Figure 7.2.3.3.5-11 and Figure 7.2.3.3.5-12 compare the E1820 J-R curves obtained at MSFC for V0071 with average J-R curves obtained by ORNL (37) on their seven A302 plates. Clearly, the correlation is good in both cases. The difference between toughness measured in the two crack orientations is not great in this case since the thick plates have not been rolled as much as would be the case in 0.25 inch thick plates, as found in the layers of the cylindrical section of the LPVs.

The upper shelf Charpy toughness measured for the ORNL plates is shown versus carbon content in Figure 7.2.3.3.5-13. The average upper shelf Charpy toughness measured for the V0071 A302B was 104 ft-lb as shown in Figure 7.2.3.3.5-14. This result is comparable to the results obtained by ORNL. There is no established correlation between upper shelf toughness measured by the Charpy test and toughness measurements taken from J-R curves. The trend in toughness behavior is similar to more elevated J-R curves corresponding to higher upper shelf Charpy toughness, but the Charpy test result is soon saturated since the specimen is small compared to the specimen allowed and required by E1820 for the J_{Ic} and J-R results to be valid.

The E1921 T_0 reference temperature for the V0071 has been measured as $T_0 = -93^\circ\text{C}$. This is at the lower limit of what would be expected based on the Wang results converted to an estimated T_0 as shown above in Figure 7.2.3.3.5-7 and Figure 7.2.3.3.5-8. Results in Figure 7.2.3.3.5-9 show the Charpy transition temperature to be between -10°C and -50°C for the seven plates tested which is consistent

with the Wang data. Applying the Charpy to T_0 correlation estimates T_0 to be -64°C , which is considerably higher than the MSFC V0071 result of -93°C , but the V0071 value is within the $2\sigma = 40^{\circ}\text{C}$ correlation window for the seven plates, which extends to -104°C as shown in Figure 7.2.3.3.5-6.

The $T_0 = -93^{\circ}\text{C}$ and the upper shelf toughness measured in terms of $K_{J} \sim 230 \text{ MPa}\sqrt{\text{m}}$ in Figure 7.2.3.3.5-11 demonstrate much higher toughness than that found previously by MSFC for the A212 and A225 steel heads present in the majority of NASA LPVs.

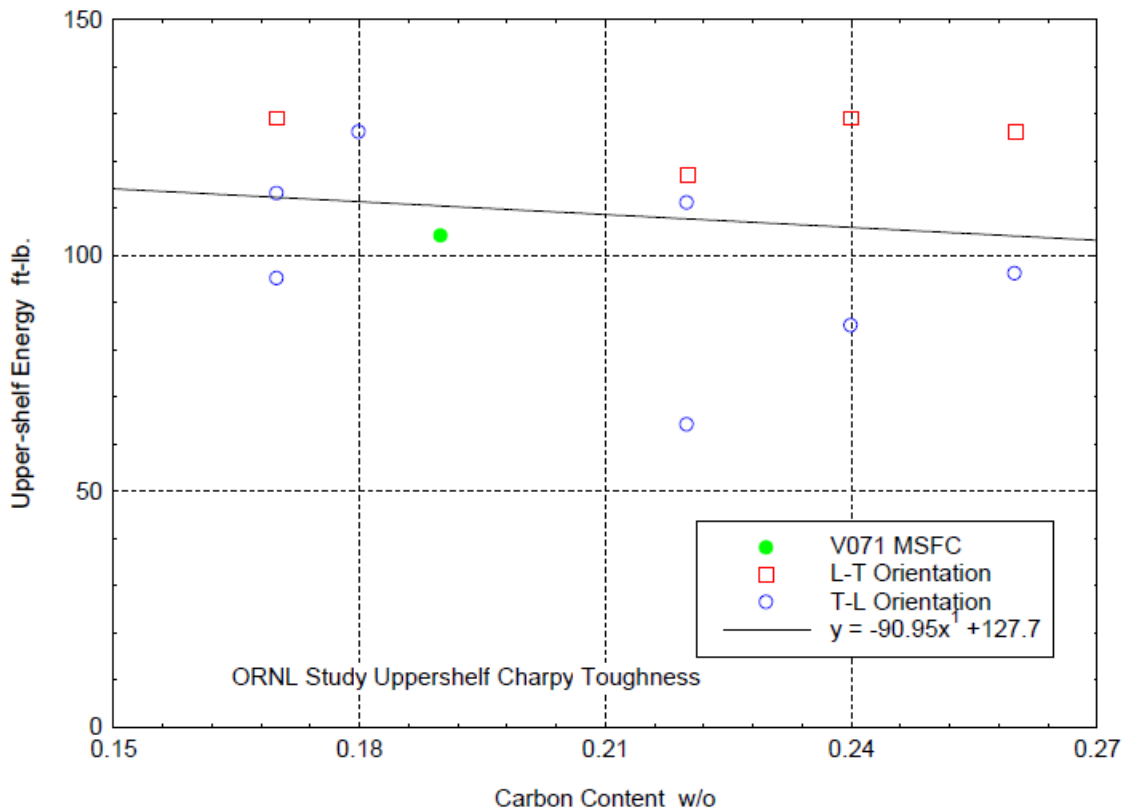


Figure 7.2.3.3.5-13: Upper Shelf Charpy Toughness, V0071 Versus ORNL (37)

The Charpy transition temperature for the V0071 A302B steel was obtained using the data set plotted in Figure 7.2.3.3.5-14. The 30 ft-lb transition gives $T_{30} = -39.7^{\circ}\text{C}$ or essentially -40°C . Figure 7.2.3.3.5-15 shows the ORNL correlation plot of Figure 7.2.3.3.5-6 with the new V0071 data added. The data falls within the ORNL proposed confidence bounds.

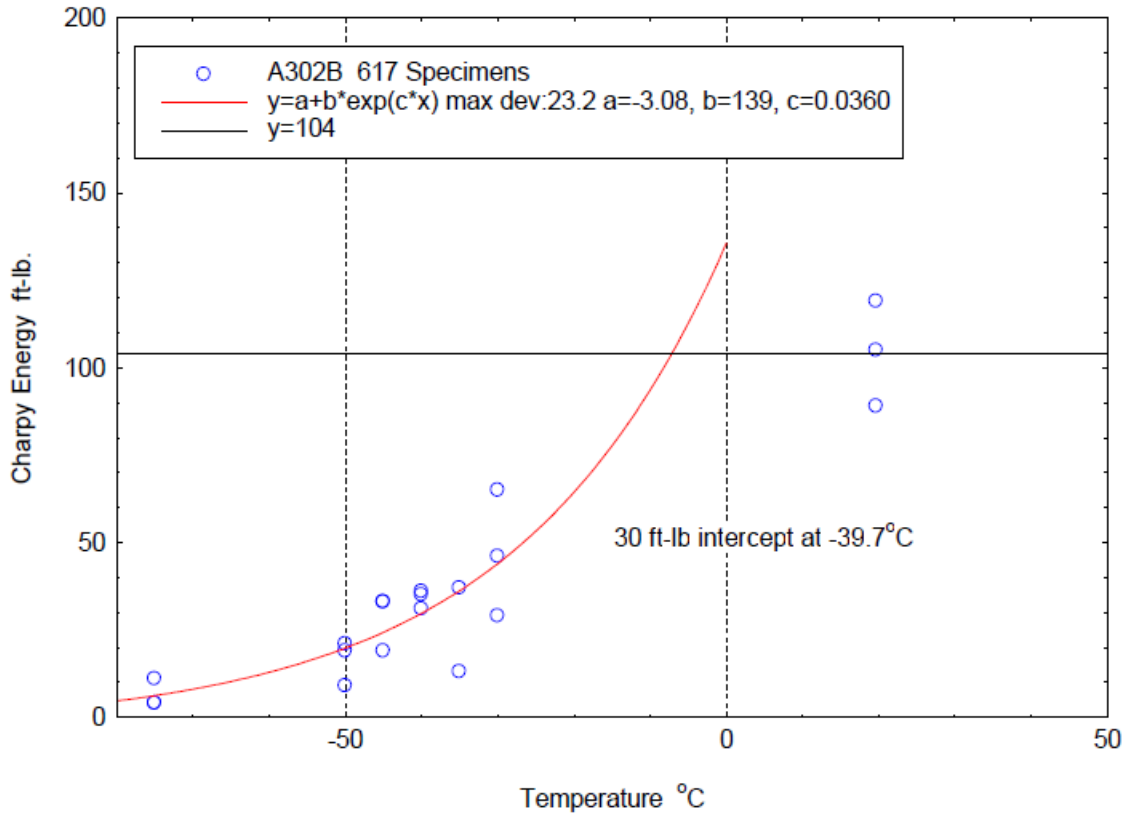


Figure 7.2.3.3.5-14: Charpy Transition Evaluation for V0071 A302B Modified

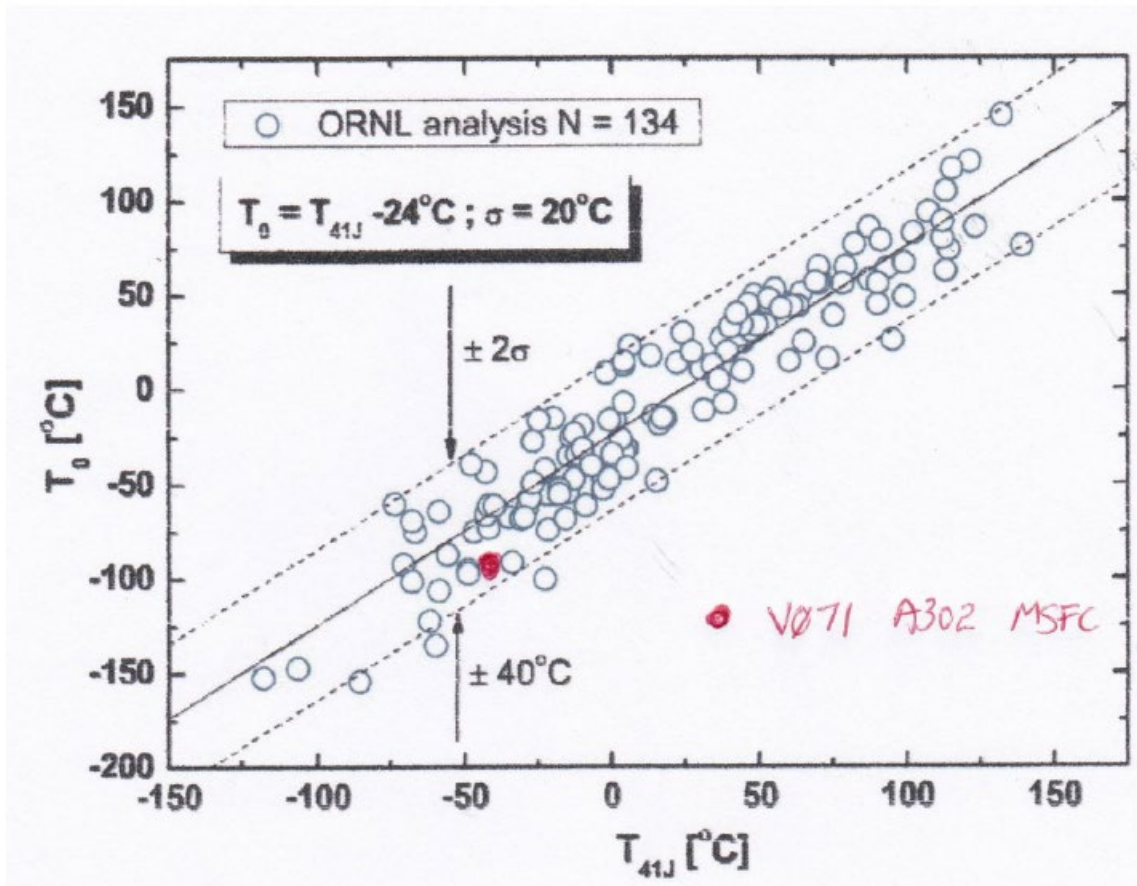


Figure 7.2.3.3.5-15: ORNL T_0 to Charpy T_{30} Correlation with V0071 Point Added

Summary

The MSFC V0071 vessel head A302 steel is clearly superior in toughness to most A302B steels reported in the literature. The tensile properties are high and even exceed what is allowed by the ASTM A302 standard while the transition temperature approaches the lowest number previously measured for this steel. The upper shelf toughness for the V0071 A302B steel defined by ASTM E1820 is in line with what has been reported by ORNL for this steel. The Charpy test results are also consistent with historical results with an average upper shelf toughness of 104 ft-lbs. and a ductile-brittle transition temperature at 30 ft-lbs, $T_{30} = -40^\circ\text{C}$. The comparison of T_0 and T_{30} results shows that they are consistent with standard correlations developed to predict T_0 from T_{30} , and vice versa.

7.3 Parent Shell Course Materials

Parent shell steels are used in LPVs to construct the wrapped layers of the cylindrical section of the LPV. These steels are fabricated as rolled plates between 0.25 inches and 0.5 inches thick. They are rolled dramatically and cold finished to tensile properties in excess of 72 ksi yield strength and 100 ksi ultimate strength. This combination yields poor fracture toughness properties, properties which were not well understood when these vessels were fabricated. Some vessels may have layers up to 1.75 inch thick, but this is not common. The materials investigated in this section are 1146, 1143, and T-1 (A517). The 1146 variety was specified somewhat differently by A.O Smith (56) and CB&I (58) and is designated here as 1146a for the A.O. Smith Version and 1146 for the CB&I version.

Wrapper steels from four LPVs have been investigated in this report. One vessel, V0023 demonstrated a strong variation in tensile and fracture properties around the circumference of the inner layer, but had consistent tensile and fracture properties along the length of the vessel. This observation caused a considerable effort to be undertaken involving the follow four items: 1) Additional tensile and fracture toughness tests were conducted at locations around the circumference of the inner layer, 2) Hardness was measured at every 30 degrees around the circumference of the V0023 vessel, 3) An extensive microstructural and metallurgical study was conducted on the V0023 inner layer to understand the causes of the observed property variations, and 4) hardness measurements were taken around the circumferences of the other available LPV inner layers to determine whether the property variation existed in the other vessels for which this information could be obtained. This study is described in the Section 7.3.1.3.1.

The principal observations of this work were to determine whether the property variation displayed by vessel V0023 was found in the inner layers of other LPVs (It was not.) It was also observed that the steel microstructure corresponded to the observed variation in fracture and tensile properties with the microstructure varying from a spheroidized carbide microstructure to an equiaxial ferrite structure. It was not determined how such variation could have been introduced into the inner layer of this vessel. Since the spheroidized structure requires a very slow cooling process, it was most likely introduced into the plate during the manufacturing process when the ferrite structure can result from a more rapid cooling. Because the inner layer is basically a membrane used to maintain the vessel pressure and, hence, contributes only slightly to the vessel integrity, it is not extremely concerning that the properties of this layer of vessel V0023 were found to be so variable.

7.3.1 1146

1146 is a carbon manganese steel defined by a proprietary standard which was commonly used by both A.O. Smith and CB&I in the construction of LPV wrapper layers and inner layers. A proprietary melt common to the time period, 1146 is a high strength steel that has marginal to poor fracture properties under the standard heat treatment. The steel used in the LPVs is typically 0.25 inch rolled plate for wrapper layers and 0.375 inch to 0.5 inch plate for inner layers. LPV drawings indicate that the inner layers were stress relieved post-welding, while the wrapper layers were not.

7.3.1.1 Chemical Composition

The variations of 1146 produced during this time period were typically governed by internal manufacturer specifications. The values from the manufacturer documentation are found in Table 7.3.1.1-1.

Table 7.3.1.1-1: 1146 Manufacturer Specifications (% Composition) (56), (58)

Material	Thickness	Chemical Content (%)						
		C	Mn	P	S	Si	Ni	V
AOS 1146a	0.18" ≤ t ≤ 0.375"	0.18-0.25	1.1-1.5	0-0.04	0-0.05	0.2-0.35	0.4-0.7	0.13-0.18
AOS 1146a	0.375" < t ≤ 0.580"	0.18-0.25	1.1-1.5	0-0.04	0-0.05	0.2-0.35	0.4-0.7	0.13-0.18
CB&I 1146	0.18" ≤ t ≤ 0.375"	0.18-0.25	1.1-1.5	0-0.04	0-0.05	0.2-0.35	0.4-0.7	0.13-0.18
CB&I 1146	0.375" < t ≤ 0.580"	0.18-0.25	1.1-1.5	0-0.04	0-0.05	0.2-0.35	0.4-0.7	0.13-0.18

The data in Figure 7.3.1.1-1 were collected from mill certifications of vessels at MSFC. The differences between the AOS and CB&I designations relate to different tensile requirements as shown in Table 7.3.1.1-1.

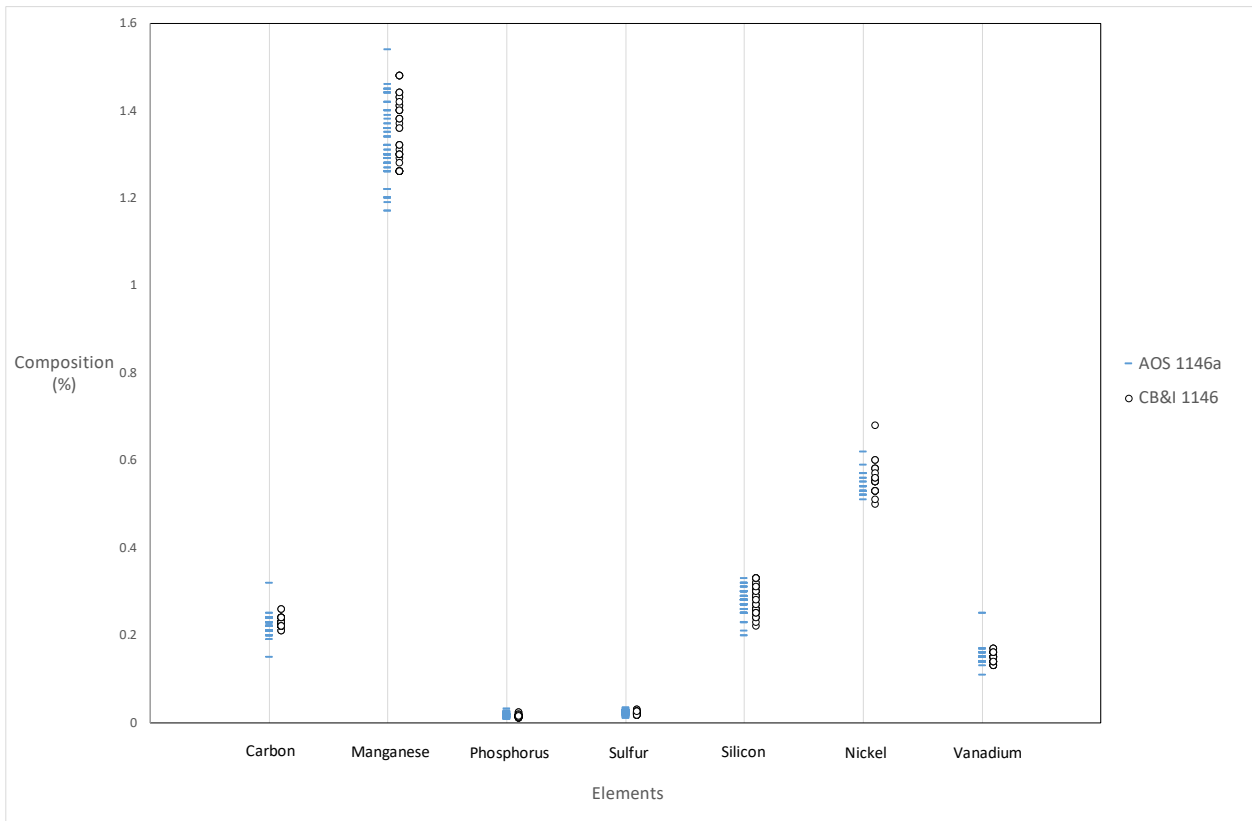


Figure 7.3.1.1-1: 1146 Material Chemistry Mill Certifications (Percent Composition) (56), (58)

Table 7.3.1.1-2 presents data collected from Arc Spark analyses of LPV chemistries at MSFC. For V0023, Inner Layer A and Inner Layer B are the locations at which significantly different material

properties were located. Chemistry measurements were performed at each location to ensure consistent content.

Table 7.3.1.1-2: 1146 Material Chemistry Collected Data (Percent Composition)

Vessel	Material	Location	C	Si	Mn	P	S	Cr	Mo	Ni	Cu	V
MV50466-8	1146	Inner Layer	0.17	0.25	1.41	0.027	0.029	0.18	0.01	0.56	0.05	0.15
V32	1146	Inner Layer	0.18	0.22	1.19	0.016	0.017	0.064	0.017	0.51	0.028	0.14
V0023	1146	Inner Layer A	0.25	0.32	1.58	0.021	0.035	0.11	0.034	0.57	0.04	0.15
V0023	1146	Inner Layer B	0.24	0.32	1.59	0.021	0.035	0.11	0.034	0.58	0.041	0.15
V0023	1146	Layer 1 Plate A	0.23	0.25	1.3	0.023	0.012	0.081	0.016	0.52	0.042	0.12
V0023	1146	Layer 2 Plate B	0.23	0.24	1.37	0.03	0.018	0.088	0.022	0.52	0.045	0.14
V0023	1146	Layer 6 Plate A	0.24	0.27	1.38	0.023	0.018	0.084	0.017	0.51	0.041	0.14
MV50466-8	1146	Mid Layer	0.22	0.24	1.33	0.02	0.017	0.066	0.014	0.5	0.036	0.13
V125	1146	Mid Layer	0.25	0.27	1.39	0.015	0.03	0.044	0.01	0.52	0.03	0.15
V32	1146	Mid Layer	0.25	0.27	1.28	0.014	0.02	0.039	0.009	0.5	0.026	0.14

7.3.1.2 Metallography

Metallography studies performed on the inner layer of LPV V0023 included grain structure and hardness, grain orientation, and macro cubes if showing multiple surfaces. Grain size, through thickness grain size, and carburization layer thickness studies were not conducted.

Hardness Study

Hardness measurements were taken at multiple locations on all available 1146 vessels. In general, hardness did not vary between locations with the exception of within the V0023 inner layer. Around the circumference of the V0023 inner layer, there were significant differences in hardness. These correlated with the L plate direction which is the C vessel orientation. The difference was initially noticed at the inner layer weld seam that joins Plate A to Plate B. Inner layer plates are rolled into cylinders, welded longitudinally to themselves, and then joined together via circumferential welds to produce the full vessel length. At the first point of investigation, Plate A was found to be on average 5 Rockwell Hardness B scale (HRB) softer than Plate B. (See Figure 7.3.1.2-1 and Table 7.3.1.2-1).

It was initially assumed that the difference was between the two separate plates, however further investigation showed the plates to be nearly identical. The actual hardness difference occurred within the individual plates, varying around the circumference of the vessel and thus along the length of each plate as manufactured. This variation prompted a check of the hardness of all other tested vessel inner layers. V0023 was the only vessel to demonstrate this anomaly, and therefore was the only vessel to receive an in-depth study.

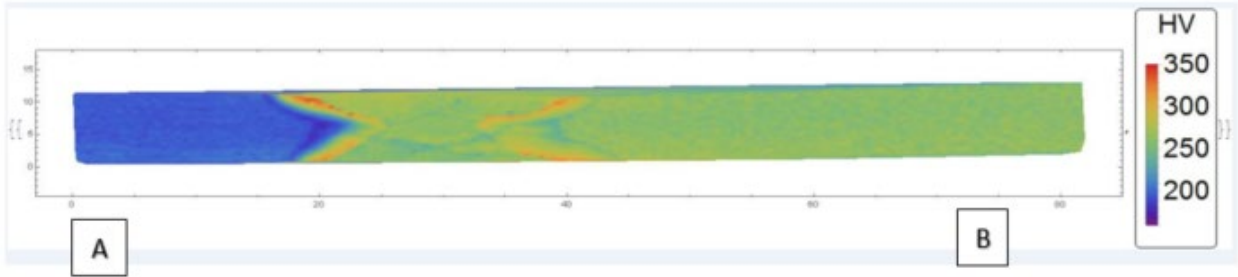


Figure 7.3.1.2-1: V0023 Inner Layer Circumferential Weld Hardness Map

Table 7.3.1.2-1: Average Hardness Values

	HRB	
	Side A	Side B
	91.6	97.4
	91.0	95.5
	91.7	98.2
Average	91.43	• 97.03

For both Plates A and B, as described above in this section, hardness measurements were taken at regular intervals around the circumference of the vessel, which is the length of the plate as it was originally produced. Inner layer longitudinal welds are offset from each other to prevent the formation of a continuous weld path along the length of the vessel (see Figure 7.3.1.2-2). Thus, when the hardness measurements were taken according to a zero location on the vessel, initially the pattern did not present itself (see Figure 7.3.1.2-3). In Figure 7.3.1.2-4, the measurements were rotated such that the longitudinal welds were aligned, giving a hardness map from beginning to end of the original plate length for Plates A and B. This revealed a pattern with the highest hardness values located towards the center of the original plate and the lowest hardness values located towards the ends of the plate. Later tests conducted on Plate C (an inner 1146 layer from a different LPV remnant) are also shown on Figure 7.3.1.2-4. These test results showed no inconsistency throughout the plate, except in the seam weld, and values were similar to the low hardness sections of Plates A and B. This indicates that Plate C is likely the intended material treatment and therefore would have properties similar to the low hardness sections of Plates A and B.

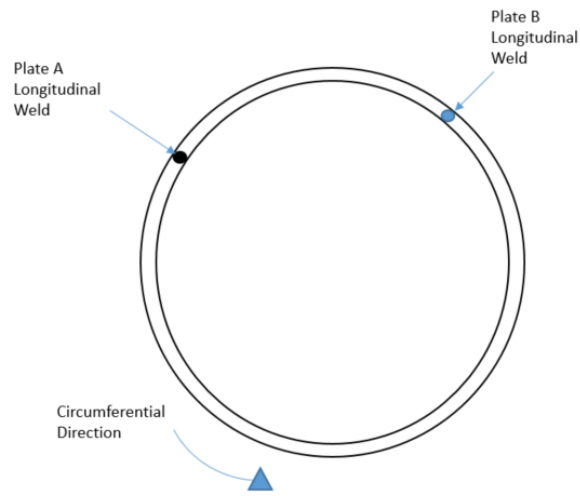


Figure 7.3.1.2-2: V0023 Inner Layer Weld

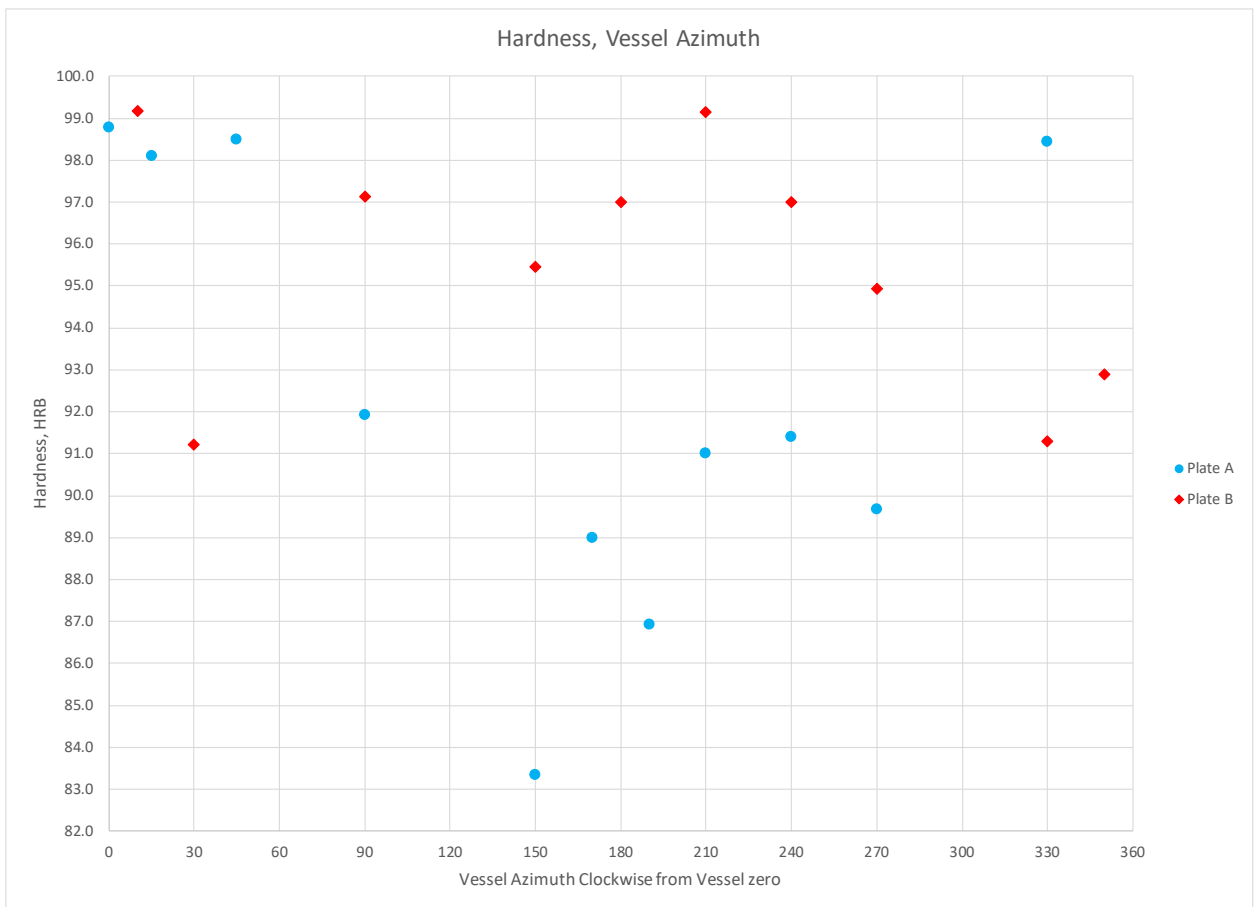


Figure 7.3.1.2-3: Hardness Data from Plates A and B, Oriented by Vessel Location

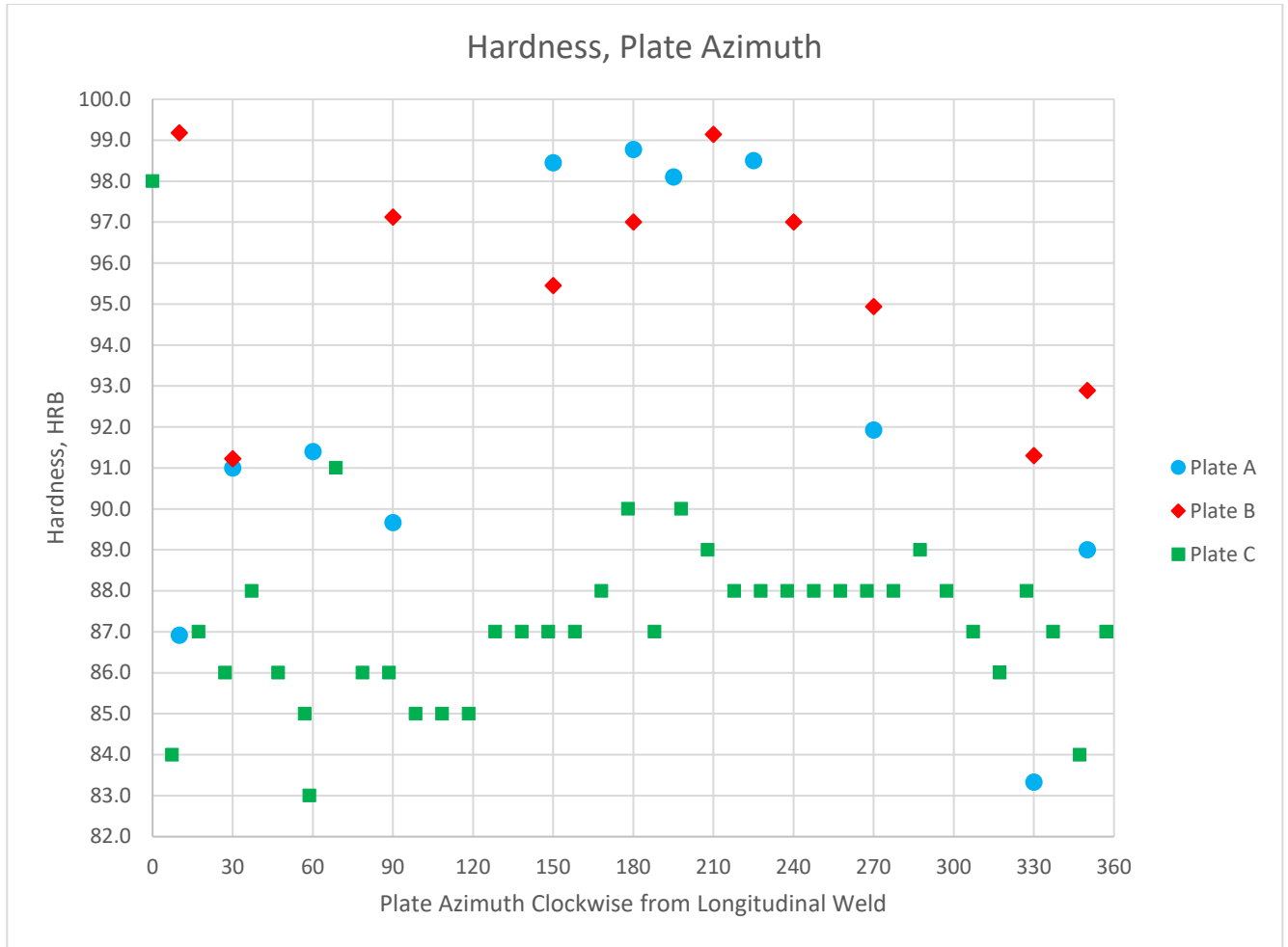


Figure 7.3.1.2-4: Hardness Data from Plates A, B, and C, Aligned by Original Plate Length

Grain Orientation Study

The results of the previously discussed hardness study prompted the creation and analysis of macro cubes from two different locations of the B plate, C4-2 0B and C3-1 0B. Cut plans and macro design are shown in Figure 7.3.1.2-5. The assembled macro cube photos in Figure 7.3.1.2-7 and Figure 7.3.1.2-8 exhibit clear differences in microstructure which are detailed in Table 7.3.1.2-2.

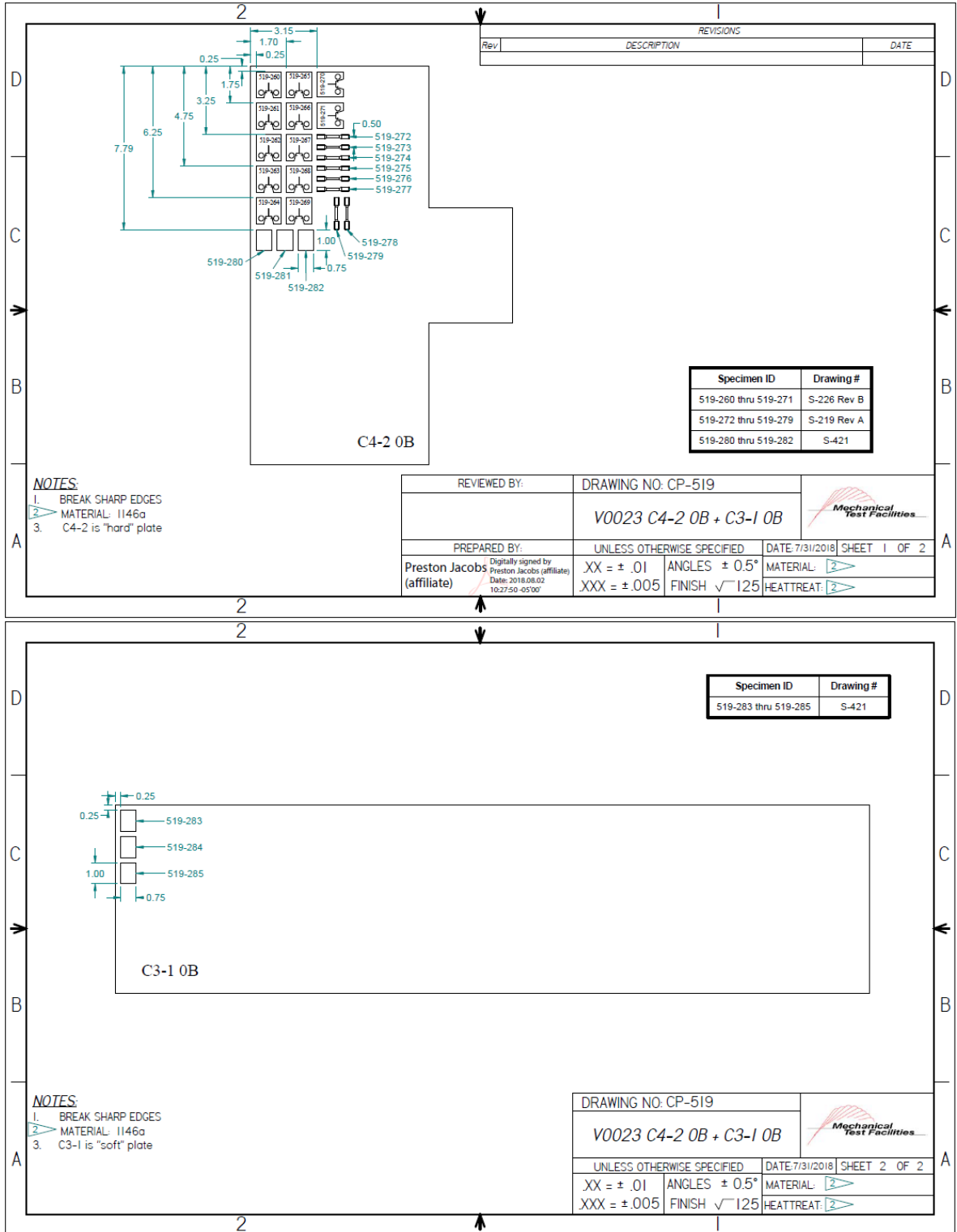


Figure 7.3.1.2-5: Cut Plan for Macros from V0023 Inner Layer

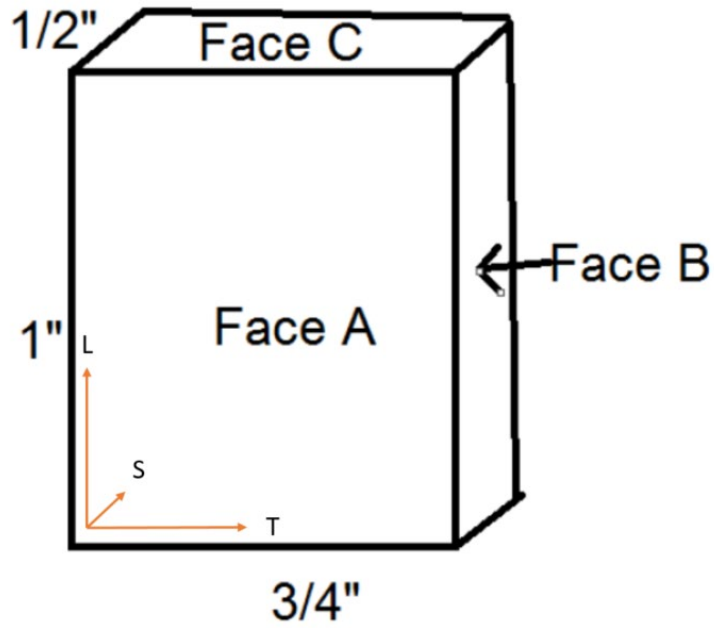


Figure 7.3.1.2-6: Macro Size and Face Orientation

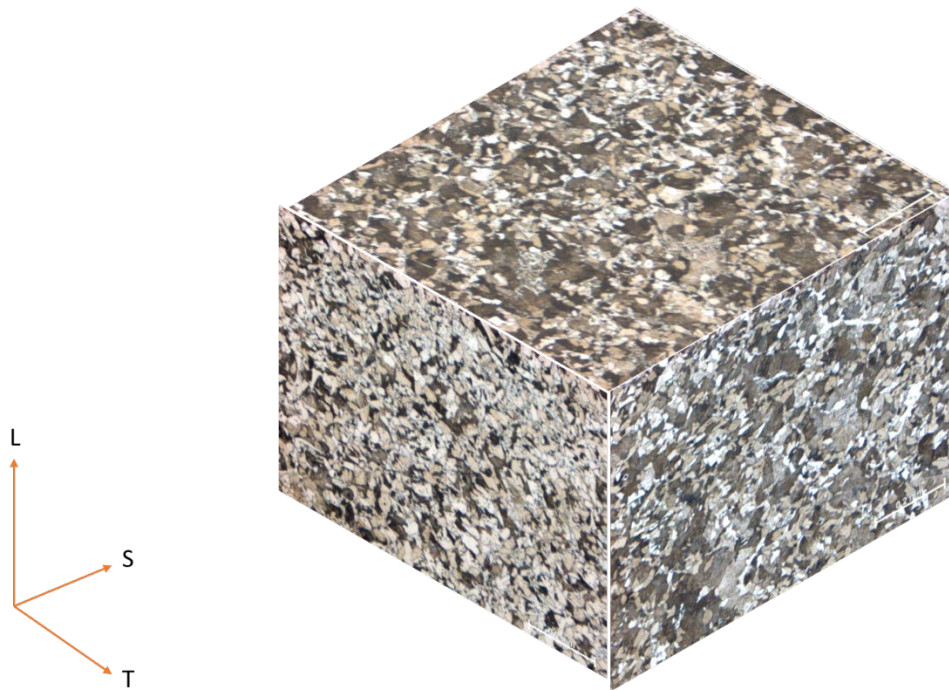


Figure 7.3.1.2-7: C4-2 0B at 100x Magnification

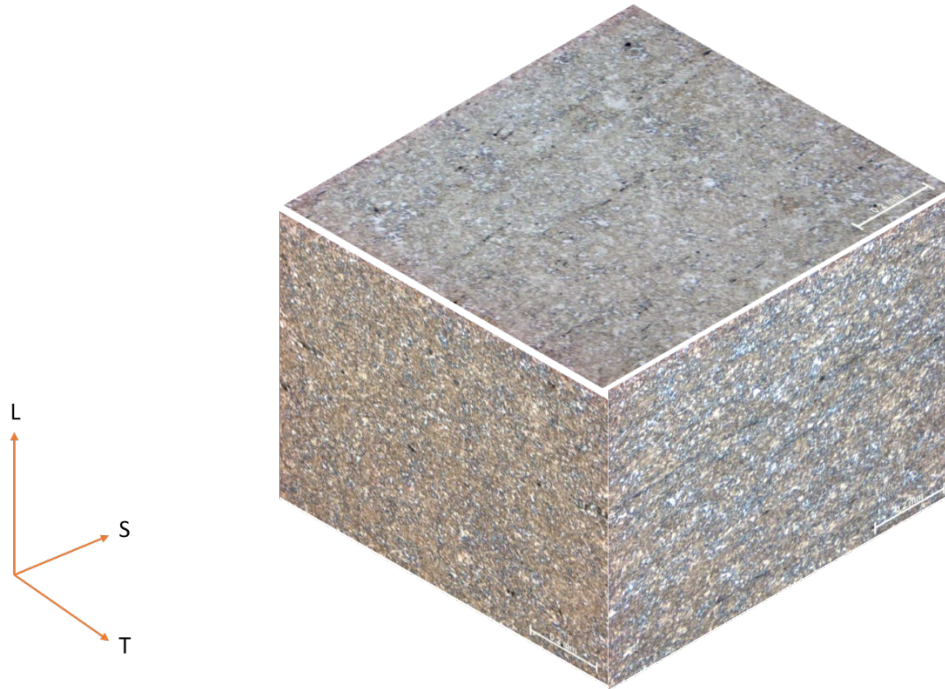


Figure 7.3.1.2-8: C3-10B at 100x Magnification

Table 7.3.1.2-2: Analysis of Macros

Sample	Lot	Face ID	Face Dimensions	Microstructure
519-280	C4-2 0B 1	A	1.0" x ¾"	Equiaxed ferrite and lamellar pearlite; note lower amount of pearlite relative to the other two orientations, due to decarburization of this face. No evidence of banding. Equiaxed manganese sulfide non-metallic inclusions suggest this face is transverse to working direction.
519-281		B	1.0" x ½"	Equiaxed ferrite and pearlite. Elongated manganese sulfide non-metallic inclusions suggest this face is longitudinal to working direction. No evidence of banding.
519-282		C	¾" x ½"	Equiaxed ferrite and lamellar pearlite. No evidence of banding.
519-283	C3-1 0B 2	A	1.0" x ¾"	Spheroidized carbide in a matrix of equiaxed ferrite. Carbides are nearly randomly distributed, and show little correlation with the original pearlite colonies. Equiaxed manganese sulfide non-metallic inclusions suggest this face is transverse to working direction.
519-284		B	1.0" x ½"	Spheroidized carbide in a matrix of equiaxed ferrite. Carbides are nearly randomly distributed, and show little correlation with the original pearlite colonies. Elongated manganese sulfide non-metallic inclusions suggest this face is longitudinal to working direction.
519-285		C	¾" x ½"	Spheroidized carbide in a matrix of equiaxed ferrite. Carbides are nearly randomly distributed, and show little correlation with the original pearlite colonies.

The results reported in Table 7.3.1.2-2 show that distinctly different microstructures were found in areas C4 and C3 of the B Plate. Achieving these microstructures could not have happened without application of markedly different heat treatments to different areas of the plate. The spheroidized microstructure requires a slow furnace cool and was likely the desired process. The ferritic structure was

then achieved by a local heating and cooling of the plate at some point during the LPV fabrication. Spheroidized carbide is achieved using a specific anneal that is designed to make the material very soft and must be intentionally produced by heating material to a high temperature and then slow cooling ~50°F/hour in the furnace. This had to be done first as part of the material creation. The equiaxed ferrite and lamellar pearlite come from experiencing extremely high temperatures after anneal and then being air cooled. The locations of each of the different metallographic characteristics are consistent throughout the original plate length, but not through the length of the vessel. No indications were found that the length of the vessel had any impact on this anomaly. This indicates that these properties were introduced in the production of the plate and not during the production of the vessel, and most likely the spheroidized carbide anneal was the intended structure of the plate.

7.3.1.3 Mechanical Properties

The following are minimum values and ranges listed in the material specification.

Table 7.3.1.3-1: 1146 Standard Material Properties, Minimums and Ranges (58), (60)

Material	Thickness	Yield Stress (ksi)	Tensile Stress (ksi)	Fracture Elongation (%)
AOS 1146a	0.18" ≤ t ≤ 0.375"	77	105-135	22
AOS 1146a	0.375" < t ≤ 0.580"	74	100-130	22
CB&I 1146	0.18" ≤ t ≤ 0.375"	83	105	22
CB&I 1146	0.375" < t ≤ 0.580"	75	100	22

Table 7.3.1.3-2 shows a compilation of mill certification values collected from vessels at MSFC. Compiling hundreds of certifications shows that the average mechanical values of the materials used meet the most stringent specifications and are well within the standard deviation.

Table 7.3.1.3-2: 1146 Collected Mill Certification Values

Manufacturer	Material	Average Yield Stress (ksi)	Yield Stress Std Dev (ksi)	Average Tensile Stress (ksi)	Tensile Stress Std Dev (ksi)	Average Fracture Elongation (%)	Fracture Elongation Std Dev (%)
A.O.Smith	1146a	88	5	115	7	29	3
CB&I	1146	90	3	117	5	30	3

7.3.1.3.1 Smooth Tensile Tests

Smooth tensile tests were conducted at MSFC on round specimens according to ASTM E8, “Standard Test Methods for Tension Testing of Metallic Materials” (51) using specimen design S-219 Rev A. The mechanical test frame consisted of a servo-hydraulic actuator and reaction frame. The frame used an LVDT for displacement feedback. Stress measurements were derived from load measurements and the initial specimen measurements. Strain measurements were derived from an extensometer and the initial specimen measurements.

The results obtained from testing of 1146 samples taken from LPVs MV50466-8, V0023, V0032 and V0125 are presented Table 7.3.1.3.1-1, Table 7.3.1.3.1-2, Table 7.3.1.3.1-3, and Table 7.3.1.3.1-4. A typical engineering stress-strain curve is shown in Figure 7.3.1.3.1-1.

Table 7.3.1.3.1-1: 1146 Smooth Tensile Data, Vessel MV50466-8

Specimen ID	Test Temp. (°C)	ASTM Orientation	Tensile Stress (ksi)	Yield Stress (ksi)	Fracture Elongation (%)	Location
440-79	23	T	95.1	70.7	16.9	Inner Layer
440-237	22	T	99.8	74.2	23.7	Inner Layer
440-239	22	T	99.6	74.1	21.6	Inner Layer
440-241	22	T	99.8	74.0	21.5	Inner Layer
440-80	22	T	93.6	70.2	19.0	Inner Layer
440-236	20	T	94.6	70.8	22.4	Inner Layer
440-238	20	T	95.1	72.1	22.7	Inner Layer
440-240	20	T	94.1	69.8	22.1	Inner Layer
440-145	2	T	88.1	61.0	29.8	Inner Layer
440-146	2	T	88.2	59.4	28.0	Inner Layer
440-143	-14	T	90.1	62.4	30.4	Inner Layer
440-144	-14	T	91.6	63.4	28.7	Inner Layer
440-141	-30	T	92.1	61.7	28.2	Inner Layer
440-142	-30	T	93.0	65.5	28.3	Inner Layer
440-81	-51	T	101.4	74.9	20.0	Inner Layer
440-82	-51	T	99.2	72.0	20.3	Inner Layer
440-139	-82	T	100.6	69.2	31.3	Inner Layer
440-140	-82	T	101.8	71.0	32.0	Inner Layer
440-137	-196	T	148.0	132.7	28.9	Inner Layer
440-138	-196	T	148.2	134.3	27.9	Inner Layer
440-105	21	L	121.3	96.6	22.4	Wrap Layer 5
440-106	21	L	116.9	96.5	20.0	Wrap Layer 5
440-107	21	L	119.6	97.1	N/A	Wrap Layer 5
440-111	21	L	118.8	86.4	16.9	Wrap Layer 5
440-112	21	L	120.4	87.6	16.6	Wrap Layer 5
440-115	-51	L	128.8	92.4	N/A	Wrap Layer 5
440-116	-51	L	125.9	89.9	16.9	Wrap Layer 5

Table 7.3.1.3.1-2: 1146 Smooth Tensile Data, Vessel V0023

Specimen ID	Test Temp. (°C)	ASTM Orientation	Tensile Stress (ksi)	Yield Stress (ksi)	Fracture Elongation (%)	Location
519-7	21	L	124.0	92.0	20.5	C4-1 Layer 0B
519-8	21	L	123.4	90.9	20.0	C4-1 Layer 0B
519-9	21	L	122.6	89.9	20.6	C4-1 Layer 0B
519-1	27	T	125.9	93.8	17.6	C4-1 Layer 0B
519-2	27	T	126.3	94.5	17.5	C4-1 Layer 0B
519-3	27	T	126.3	94.1	17.9	C4-1 Layer 0B
519-10	21	T	121.4	91.6	19.0	C4-1 Layer 3B
519-11	21	T	121.1	90.9	18.3	C4-1 Layer 3B
519-12	21	T	121.4	91.5	19.9	C4-1 Layer 3B
519-4	27	L	121.7	90.1	23.1	C4-1 Layer 3B
519-5	27	L	120.7	89.4	23.2	C4-1 Layer 3B
519-6	27	L	120.1	89.6	23.3	C4-1 Layer 3B
519-150	21	T	95.5	68.4	25.3	C4-1 Layer 0A
519-151	21	T	97.5	71.4	24.9	C4-1 Layer 0A
519-152	21	T	100.0	72.3	24.6	C4-1 Layer 0A
519-153	21	L	98.2	69.8	28.4	C4-1 Layer 0A
519-154	21	L	96.9	68.2	28.9	C4-1 Layer 0A
519-155	21	L	97.4	70.2	27.9	C4-1 Layer 0A
519-276	-29	T	130.8	98.1	19.7	C4-2 0B
519-277	-29	T	139.4	104.2	17.5	C4-2 0B
519-274	0	T	134.0	100.3	17.8	C4-2 0B
519-275	0	T	139.5	104.1	19.7	C4-2 0B
519-272	21	T	131.7	99.0	17.5	C4-2 0B
519-273	21	T	132.3	98.6	18.3	C4-2 0B
519-278	21	L	133.0	100.1	19.4	C4-2 0B
519-279	21	L	131.8	98.7	19.9	C4-2 0B

Table 7.3.1.3.1-3: 1146 Smooth Tensile Data, Vessel V0032

Specimen ID	Test Temp. (°C)	ASTM Orientation	Tensile Stress (ksi)	Yield Stress (ksi)	Fracture Elongation (%)	Location
380-1	21	T	80.2	52.4	37.4	Inner Layer
380-2	21	T	80.8	45.3	33.8	Inner Layer
380-21 (33)	21	L	74.0	48.1	34.4	Inner Layer
380-22 (34)	21	L	74.5	49.1	35.5	Inner Layer
380-3	21	L	82.0	51.1	32.4	Inner Layer
380-4	21	L	82.1	53.3	29.9	Inner Layer
CP380-11-1A-13 (380-13)	21	L	76.6	50.8	32.3	Inner Layer
CP380-11-1A-14 (380-14)	21	L	77.1	50.8	32.5	Inner Layer
380-19 (31)	21	L	124.1	93.0	24.1	Wrap Layer 2
380-20 (32)	21	L	124.6	92.5	24.5	Wrap Layer 2
380-40	21	L	119.5	88.5	24.8	Wrap Layer 6
380-41	21	L	120.0	87.1	24.7	Wrap Layer 6

Table 7.3.1.3.1-4: 1146 Smooth Tensile Data, Vessel V0125

Specimen ID	Test Temp. (°C)	ASTM Orientation	Tensile Stress (ksi)	Yield Stress (ksi)	Fracture Elongation (%)	Location
CP344-3-49	25	L	122.6	93.3	16.8	Wrap Layer
CP344-3-25	24	L	122.6	89.4	16.8	Wrap Layer
CP344-3-37	24	L	128.8	94.5	17.3	Wrap Layer
CP344-3-38	24	L	124.9	90.8	17.4	Wrap Layer
CP344-3-50	24	L	122.2	94.5	17.1	Wrap Layer
CP344-3-24	24	L	122.6	90.4	17.4	Wrap Layer
CP344-3-26	-46	L	137.8	104.3	20.5	Wrap Layer
CP344-3-39	-46	L	136.8	97.6	20.4	Wrap Layer
CP344-4-61	21	L	130.3	97.1	19.6	Wrap Layer 1
CP344-4-62	21	L	128.8	96.9	19.1	Wrap Layer 1
CP344-4-63	21	L	130.3	97.0	18.4	Wrap Layer 1
CP344-4-64	21	L	129.9	97.3	19.1	Wrap Layer 1
CP344-4-65	21	L	133.0	98.7	18.0	Wrap Layer 1
CP344-4-66	21	L	129.0	96.7	19.6	Wrap Layer 1
CP344-4-67	21	L	133.1	99.0	18.6	Wrap Layer 1
CP344-4-68	21	T	133.1	97.6	14.1	Wrap Layer 1
CP344-4-69	21	T	132.7	97.8	13.9	Wrap Layer 1
CP344-4-71	21	T	133.7	98.9	14.7	Wrap Layer 1
CP344-4-72	21	T	132.7	99.9	15.0	Wrap Layer 1
CP344-4-73	21	T	132.4	97.6	14.8	Wrap Layer 1
CP344-4-74	21	T	132.4	99.0	14.7	Wrap Layer 1
CP344-4-75	21	T	134.3	100.8	15.0	Wrap Layer 1

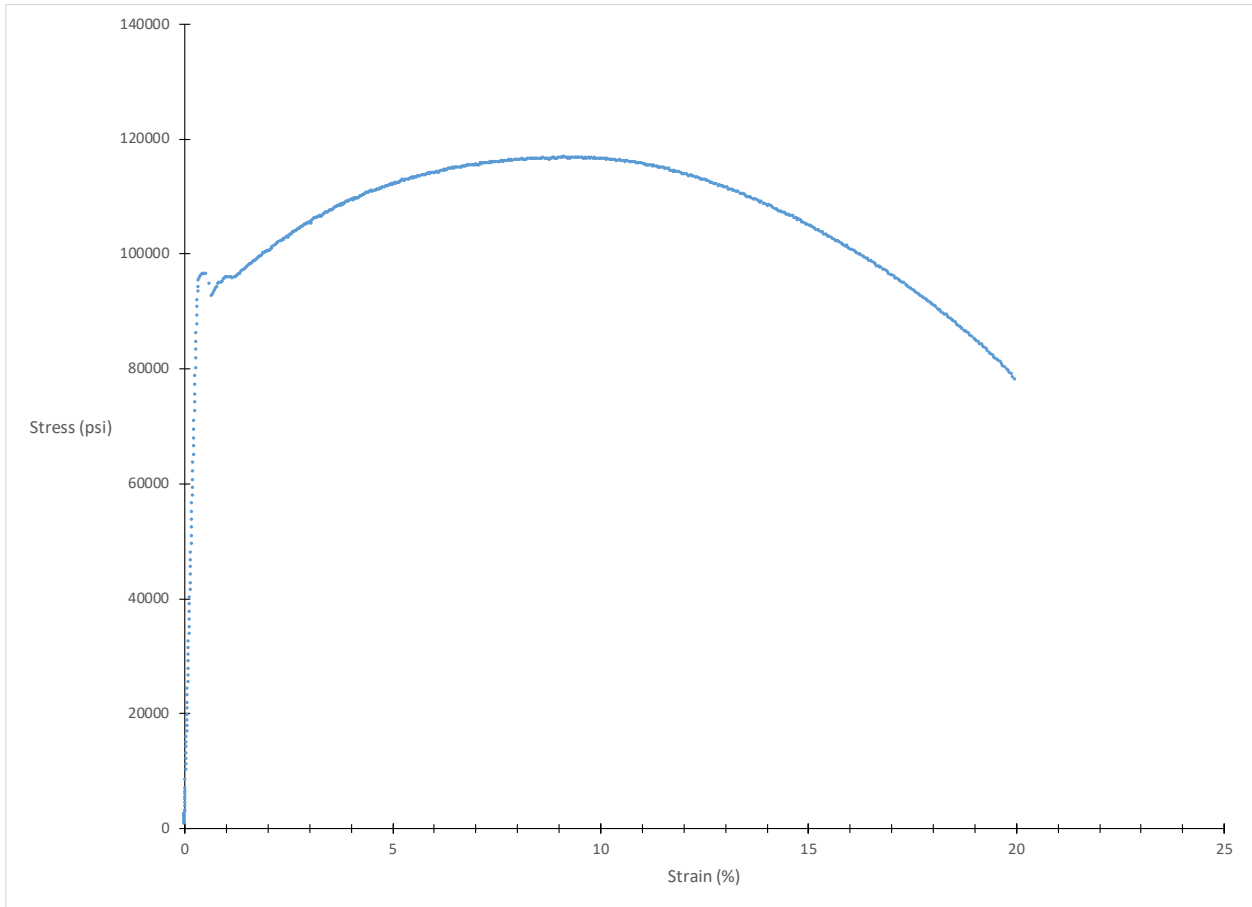


Figure 7.3.1.3.1-1: 1146 Smooth Specimen Tensile Plot for Sample 440-106

7.3.1.3.2 Notch Tensile

Notch tensile tests were not performed on this material.

7.3.1.3.3 Fracture Properties

All room temperature testing was performed per ASTM E1820 (10). All other temperatures were tested per ASTM E1921 (7). Testing for both standards use specimen design S-226 Rev B, with the thickness machined to maximum allowable thickness. All 1146 fracture tests came from vessels V0125, V0032, MV50466-8, and V0023 and were tested with the crack plane in the T-L and L-T orientations as defined by ASTM. The specimens used were ASTM E1820 compact specimens (C(T)) with $W = 1.0$ inches and $0.2 \text{ inches} \leq B \leq 0.375 \text{ inches}$, $a/W = 2.0$, and all specimens were side grooved to a total thickness reduction of 20%. The cutting diagram used to remove the C(T) specimens from the MV50466-8 wrapper is shown in Figure 7.3.1.3.3-3. Examples of Load Versus COD and J_q Versus Δa plots are shown in Figure 7.3.1.3.3-1 and Figure 7.3.1.3.3-2.

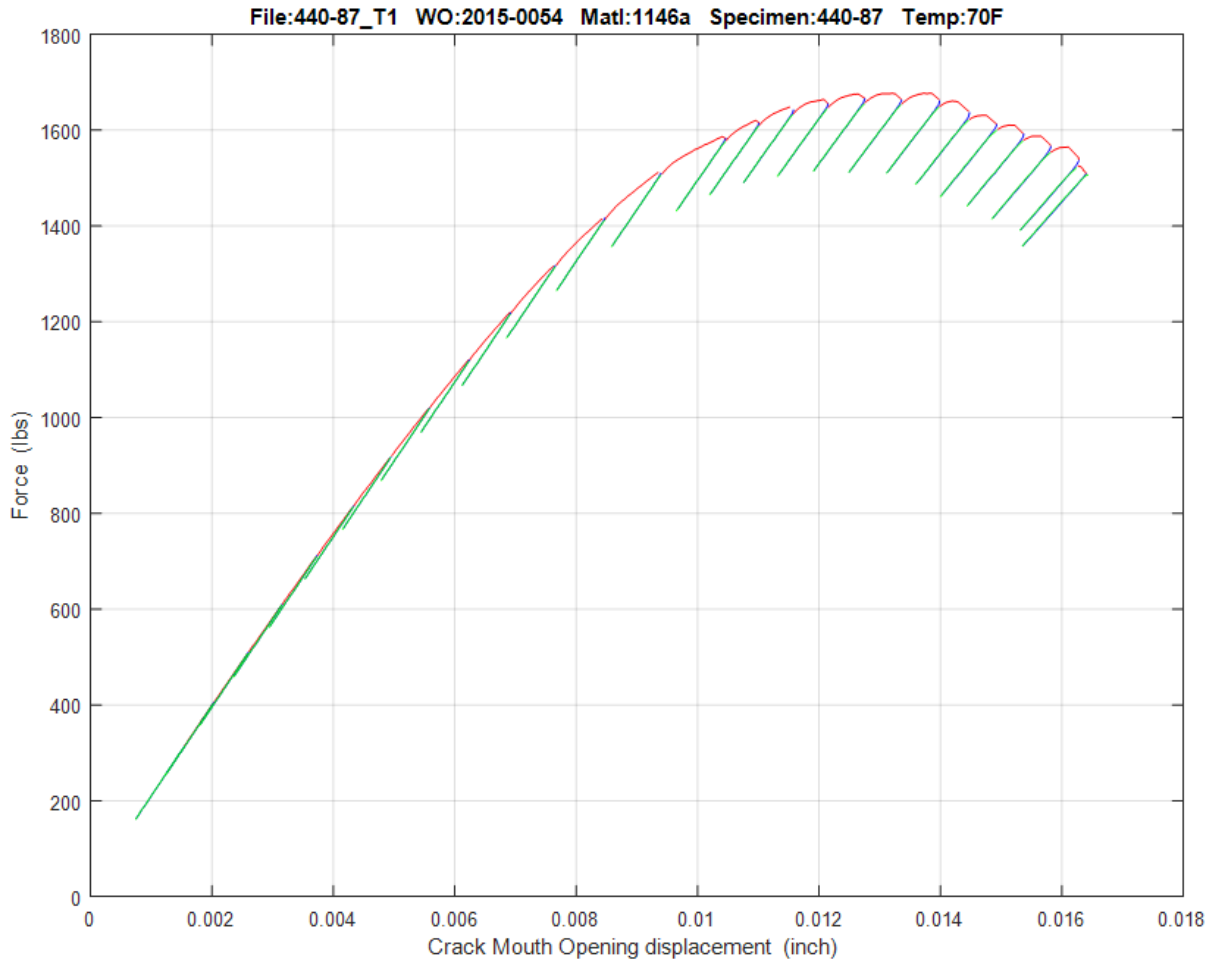


Figure 7.3.1.3.3-1: 1146 Load Versus COD Plot, Sample 440-87

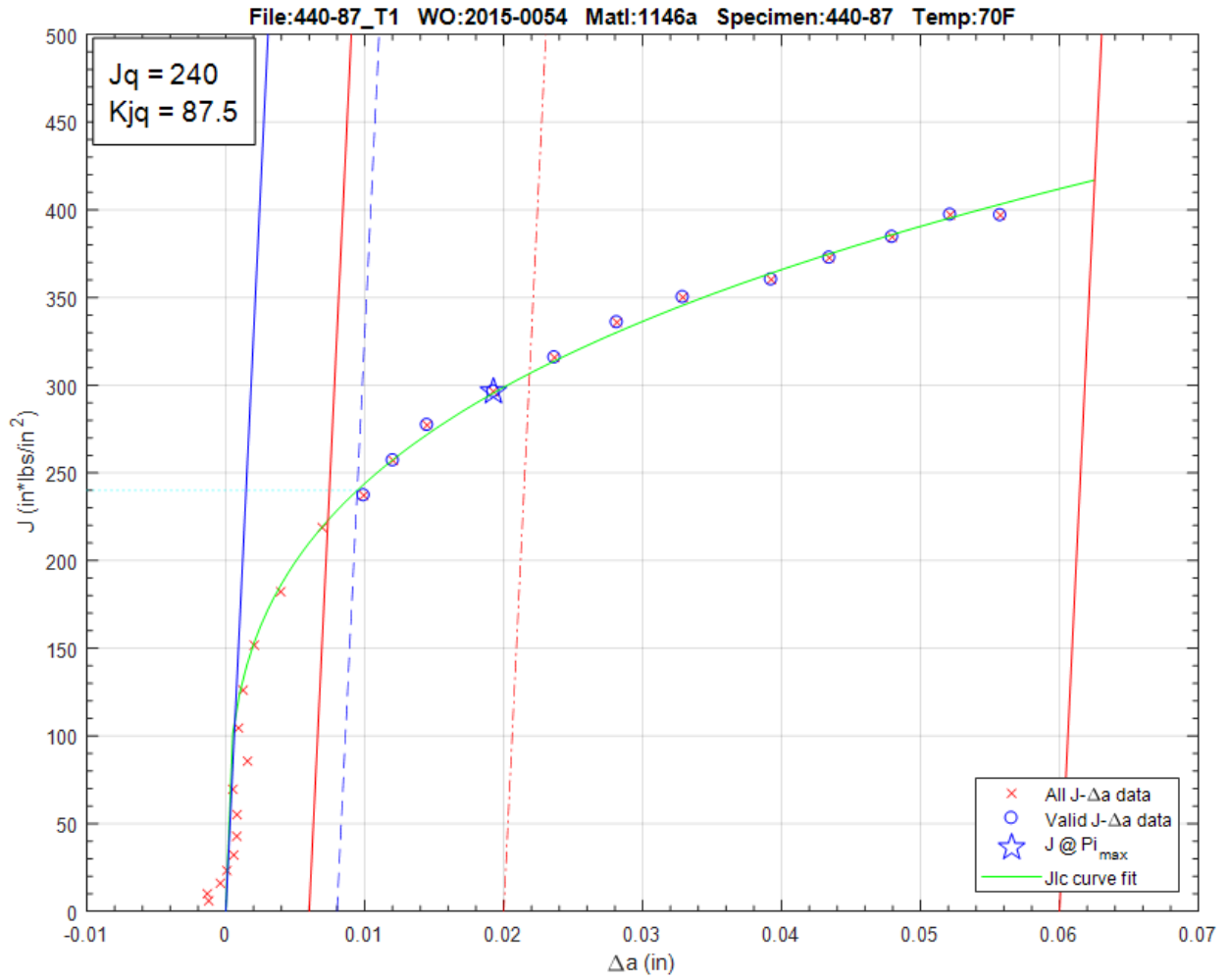


Figure 7.3.1.3.3-2: 1146 J_q Versus Δa Plot, Sample 440-87

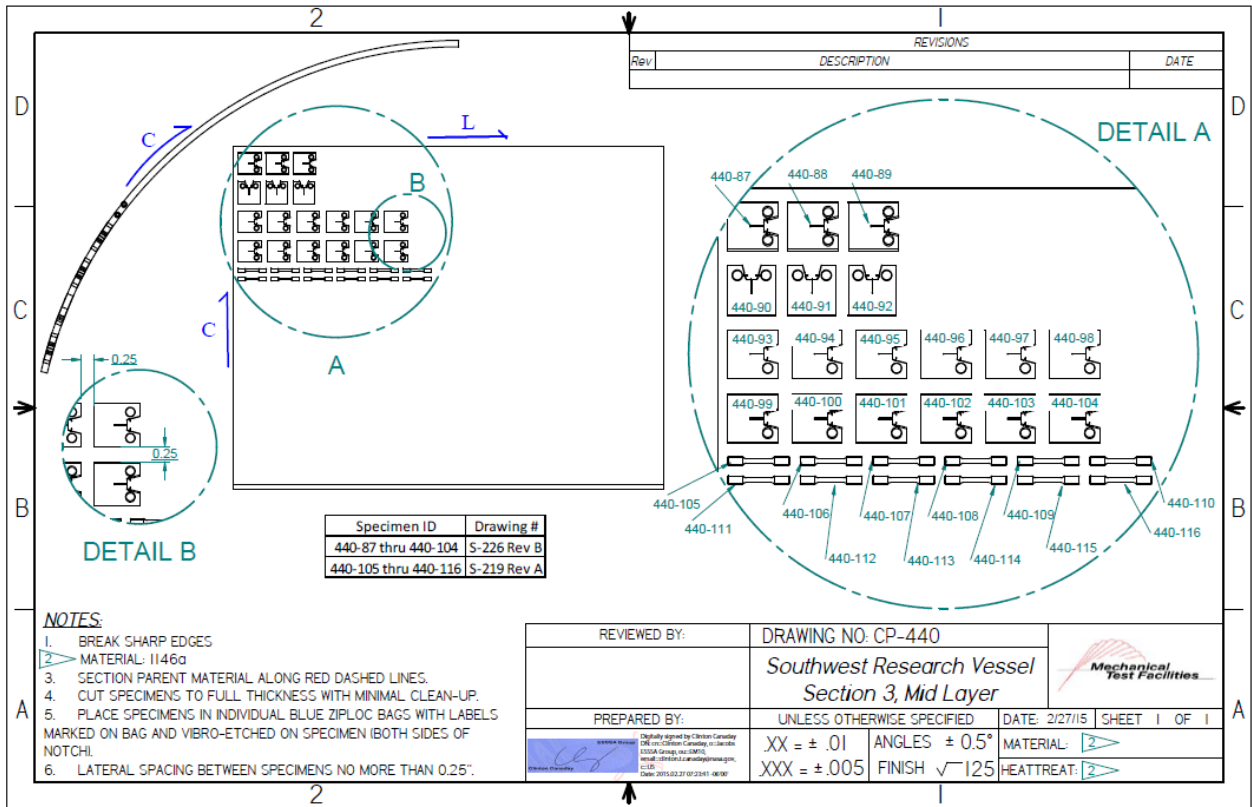


Figure 7.3.1.3.3-3: Cut Plan for MV50466-8 Fracture Specimens

The test data in Table 7.3.1.3.3-1 are raw values obtained from fracture tests conducted on V0125 1146 wrap layer material. Test results that are considered upper shelf are listed under ASTM E1820, while transition temperature test results are listed under E1921. Tests that meet the complete validity requirements for $J_q = J_{1C}$ and $K_{Iq} = K_{I1C}$ are denoted with an asterisk. Despite invalidities, J_q and K_{Iq} convey valuable fracture toughness information, especially when the test results are applied directly to the sample material source.

Table 7.3.1.3.3-1: V0125 1146 Wrapper Fracture Data

Specimen ID	Test Temp. (°C)	ASTM Crack Plane Orientation	W (in)	a ₀ (in)	a _f (in)	B ₀ (in)	B _N (in)	J _q (kJ/m ²)	K _{Jq} (MPa √m)	K _{JCI,T} (MPa √m)	ASTM Standard
CP344-4-7	24	T-L	0.9998	0.5624	0.6316	0.2332	0.1843	41	96	---	E1820
CP-344-3-18	23	T-L	0.9975	0.5963	0.6779	0.1877	0.1470	36	90	---	E1820
CP-344-3-19	23	T-L	0.9975	0.6010	0.6573	0.1876	0.1425	31	83	---	E1820
CP-344-3-31	22	T-L	0.9979	0.6053	0.7002	0.1881	0.1425	39	94	---	E1820
CP-344-3-44	22	T-L	0.9990	0.6010	0.6835	0.1888	0.1440	40	95	---	E1820
CP344-4-10	21	L-T	0.9997	0.5457	0.6515	0.2363	0.1829	131	171	---	E1820
CP344-4-8	21	T-L	0.9992	0.5600	0.6332	0.2335	0.1841	34	87	---	E1820
CP344-4-9	21	L-T	1.0005	0.5539	0.6364	0.2360	0.1854	127	168	---	E1820
CP344-4-16	0	T-L	1.0007	0.5585	0.8512	0.1985	0.1566	38	92	68	E1921
CP344-4-11	-29	T-L	1.0008	0.5493	0.9515	0.1968	0.1524	46	102	74	E1921
CP344-4-12	-46	T-L	0.9998	0.5563	0.6000	0.1962	0.1539	41	96	70	E1921
CP344-4-13	-46	T-L	1.0003	0.5440	0.7422	0.1993	0.1502	44	99	73	E1921
CP344-4-15	-51	T-L	1.0011	0.5570	0.5672	0.1978	0.1582	31	83	62	E1921
CP344-4-29	-51	T-L	1.0005	0.6108	0.6194	0.2453	0.1885	24	74	58	E1921
CP344-4-32	-51	T-L	1.0008	0.5563	0.6074	0.2435	0.1956	43	98	75	E1921
CP344-4-33	-51	T-L	1.0016	0.5534	0.5713	0.2435	0.1958	33	86	66	E1921
CP344-4-34	-51	T-L	1.0009	0.5570	0.5656	0.2440	0.1946	31	83	64	E1921
CP344-4-35	-51	T-L	1.0021	0.5854	0.5908	0.2442	0.1880	24	74	58	E1921
CP344-4-49	-51	T-L	0.9992	0.5432	0.5432	0.1910	0.1501	16	60	47	E1921
CP344-4-50	-51	T-L	0.9983	0.5440	0.5529	0.1906	0.1486	28	80	59	E1921
CP344-4-52	-51	T-L	0.9990	0.5421	0.5487	0.1901	0.1520	28	80	59	E1921
CP344-4-14	-52	T-L	1.0016	0.5691	0.5764	0.1995	0.1596	25	74	56	E1921
CP344-4-30	-52	T-L	1.0005	0.5650	0.5819	0.2450	0.1886	43	98	75	E1921
CP344-4-48	-52	T-L	1.0000	0.5824	0.6095	0.1901	0.1496	36	90	66	E1921
CP344-4-51	-52	T-L	0.9975	0.5437	0.5437	0.1905	0.1502	20	67	51	E1921

Results from the 17 E1921 tests are presented in Table 7.3.1.3.3-2 and summarized in Table 7.3.1.3.3-3. These results were obtained using the T₀TEM code described in Section 4.2. The T₀ reference temperature for this data set was evaluated as -13°C using the E1921 Master Curve shown in Figure 7.3.1.3.3-4.

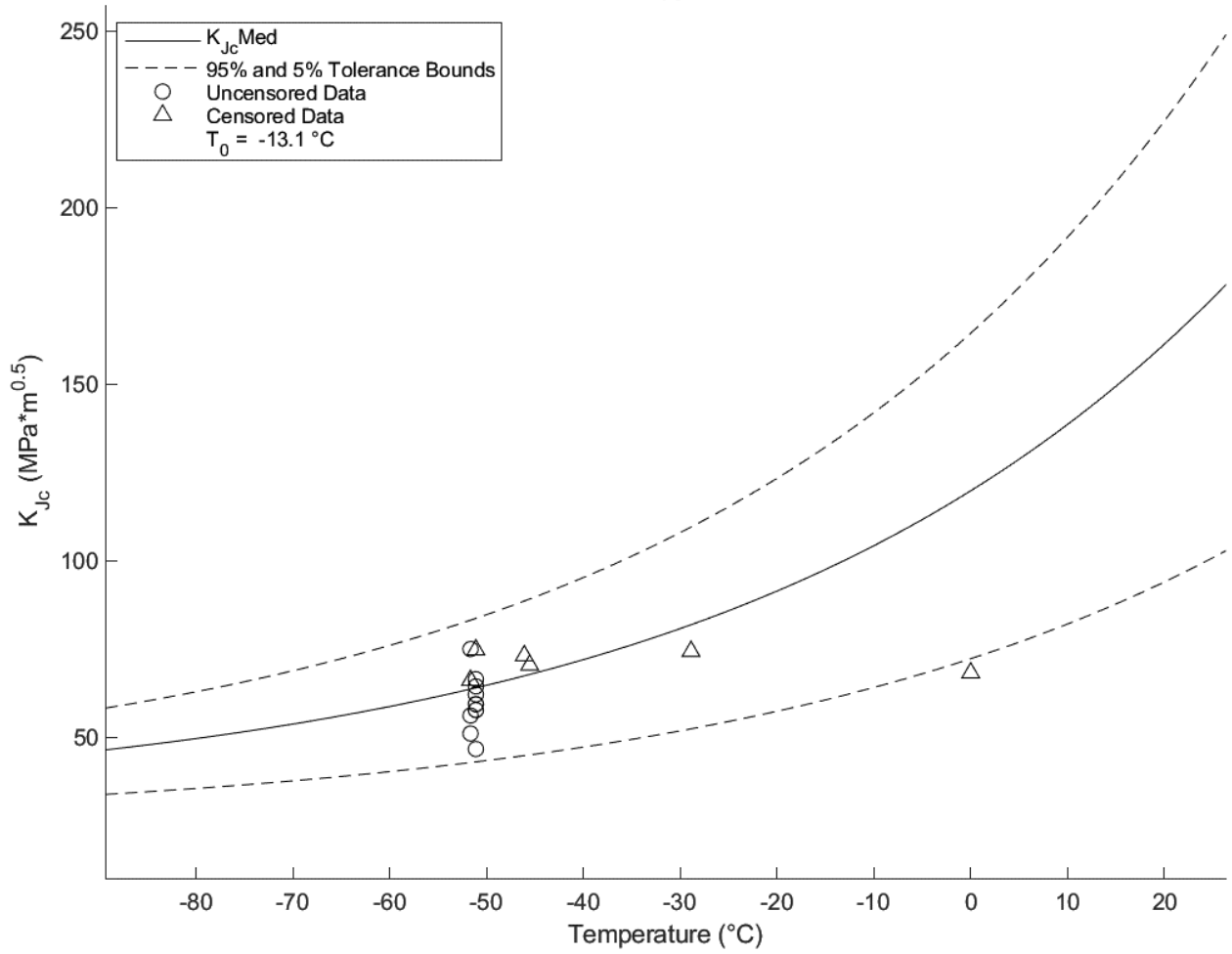


Figure 7.3.1.3.3-4: V0125 1146 Wrapper Layer T_0 Plot ($T_0 = -13^{\circ}\text{C}$)

Table 7.3.1.3.3-2: V0125 1146 Wrapper Layer T₀ Individual Specimen Results

Specimen Name	Temperature (°C)	K _{Jc} Raw (MPa*m ^{0.5})	1T Data (MPa*m ^{0.5})	Uncensored Data	Test Temp -T ₀ (°C)
CP344-4-11	-29	101.6	74.4	0	-16
CP344-4-12	-46	95.8	70.5	0	-32
CP344-4-13	-46	99.5	73.1	0	-33
CP344-4-14	-52	74.1	56.2	1	-39
CP344-4-15	-51	83.2	62.1	1	-38
CP344-4-16	0	92.3	68.3	0	13
CP344-4-29	-51	73.5	57.7	1	-38
CP344-4-30	-52	98.2	75.0	1	-39
CP344-4-32	-51	98.0	74.8	0	-38
CP344-4-33	-51	86.1	66.4	1	-38
CP344-4-34	-51	83.2	64.4	1	-38
CP344-4-35	-51	73.7	57.8	1	-38
CP344-4-48	-52	89.9	66.1	0	-39
CP344-4-49	-51	60.3	46.7	1	-38
CP344-4-50	-51	79.7	59.4	1	-38
CP344-4-51	-52	67.0	51.1	1	-39
CP344-4-52	-51	79.5	59.3	1	-38

Table 7.3.1.3.3-3: V0125 1146 Wrapper Layer T₀ Calculation Results

Initial T ₀ (°C)	-13
Total Samples	17
Samples within T ₀ ± 50°C (N)	17
Number of Uncensored Data (r)	11
Poisson's Ratio	0.3
Σ(r _i n _i)	1.38
Samples Between T _i - T ₀ 50 to -14 °C	0
Samples Between T _i - T ₀ -15 to -35 °C	0
Samples Between T _i - T ₀ -36 to -50 °C	11
T ₀ scrn (°C)	-8
Homogenous or Inhomogeneous	Homogenous

The following test data are raw values obtained from fracture tests conducted on V0032 1146 wrap and inner layer material. Test results that are considered upper shelf are listed under ASTM E1820, while transition temperature test results are listed under E1921. Tests that meet the complete validity requirements for $J_q = J_{1C}$ and $K_{Jq} = K_{J1C}$ are denoted with an asterisk. Despite invalidities, J_q and K_{Jq} convey valuable fracture toughness information, especially when the test results are applied directly to the sample material source. Tests on V0032 1146 wrapper material were only conducted for upper shelf temperatures, therefore no transition temperature was determined.

Table 7.3.1.3.3-4: V0125 1146 Wrapper Layer T₀ Calculation Results

Specimen ID	Test Temp. (°C)	ASTM Crack Plane Orientation	W (in)	a ₀ (in)	a _f (in)	B ₀ (in)	B _N (in)	J _q (kJ/m ²)	K _{Jq} (MPa √m)	K _{JCT} (MPa √m)	ASTM Standard
380-192	21	T-L	0.9985	0.5283	0.6339	0.2283	0.1826	29	80	---	E1820
380-193	21	T-L	1.0012	0.5953	0.7085	0.2266	0.1845	30	81	---	E1820
380-194	21	L-T	1.0002	0.5136	0.5890	0.2266	0.1801	123	166	---	E1820
380-195	21	L-T	0.9998	0.5255	0.5910	0.2267	0.1795	120	164	---	E1820

Table 7.3.1.3.3-5: V0032 Inner Layer 1146 Fracture Data

Specimen ID	Test Temp. (°C)	ASTM Crack Plane Orientation	W (in)	a ₀ (in)	a _f (in)	B ₀ (in)	B _N (in)	J _q (kJ/m ²)	K _{Jq} (MPa √m)	K _{JCT} (MPa √m)	ASTM Standard
380-11-1A-11	24	L-T	1.0013	0.5480	0.5884	0.4670	0.3700	232	228	---	E1820
380-11-1A-10	24	L-T	1.0006	0.6556	0.7468	0.4573	0.3600	230	227	---	E1820
380-11-1A-9	23	L-T	1.0003	0.6515	0.7413	0.3030	0.2349	248	236	---	E1820
380-8	26	T-L	1.0018	0.5697	0.6758	0.4258	0.3588	88	140	---	E1820
380-7	21	T-L	1.0014	0.5571	0.6602	0.4250	0.3596	88	141	---	E1820
380-6	19	T-L	1.0034	0.5667	0.7328	0.4250	0.3519	87	140	---	E1820
380-9	-28	T-L	1.0014	0.5697	0.6170	0.4585	0.3628	17	61	54	E1921
380-12	-29	T-L	1.0014	0.5604	0.6271	0.4588	0.3670	46	101	87	E1921
380-10	-29	T-L	1.0007	0.5449	0.5891	0.4590	0.3617	36	90	77	E1921
380-15	-31	T-L	1.0016	0.5300	0.5790	0.4583	0.3664	177	199	167	E1921
380-16	-31	T-L	1.0009	0.5481	0.5481	0.4578	0.3611	119	163	138	E1921
380-35	-31	T-L	1.0001	0.5593	0.6280	0.4578	0.3605	222	223	177	E1921
380-36	-31	T-L	0.9989	0.5502	0.5955	0.4590	0.3576	162	190	160	E1921
380-37	-31	T-L	0.9988	0.5467	0.5588	0.4558	0.3574	89	141	120	E1921
380-38	-31	T-L	1.0005	0.5486	0.5540	0.4562	0.3569	85	137	117	E1921
380-39	-31	T-L	0.9999	0.5450	0.5665	0.4557	0.3563	139	176	149	E1921
380-13	-57	T-L	1.0000	0.5537	0.5537	0.4587	0.3669	21	68	60	E1921
380-14	-57	T-L	1.0021	0.5482	0.5482	0.4588	0.3645	21	68	60	E1921

Results from the 12 E1921 tests are presented in Table 7.3.1.3.3-6 and Table 7.3.1.3.3-7. These results were obtained using the T₀TEM code described in Section 4.2. The T₀ reference temperature for this data set was evaluated as -52°C using the E1921 Master Curve shown in Figure 7.3.1.3.3-5.

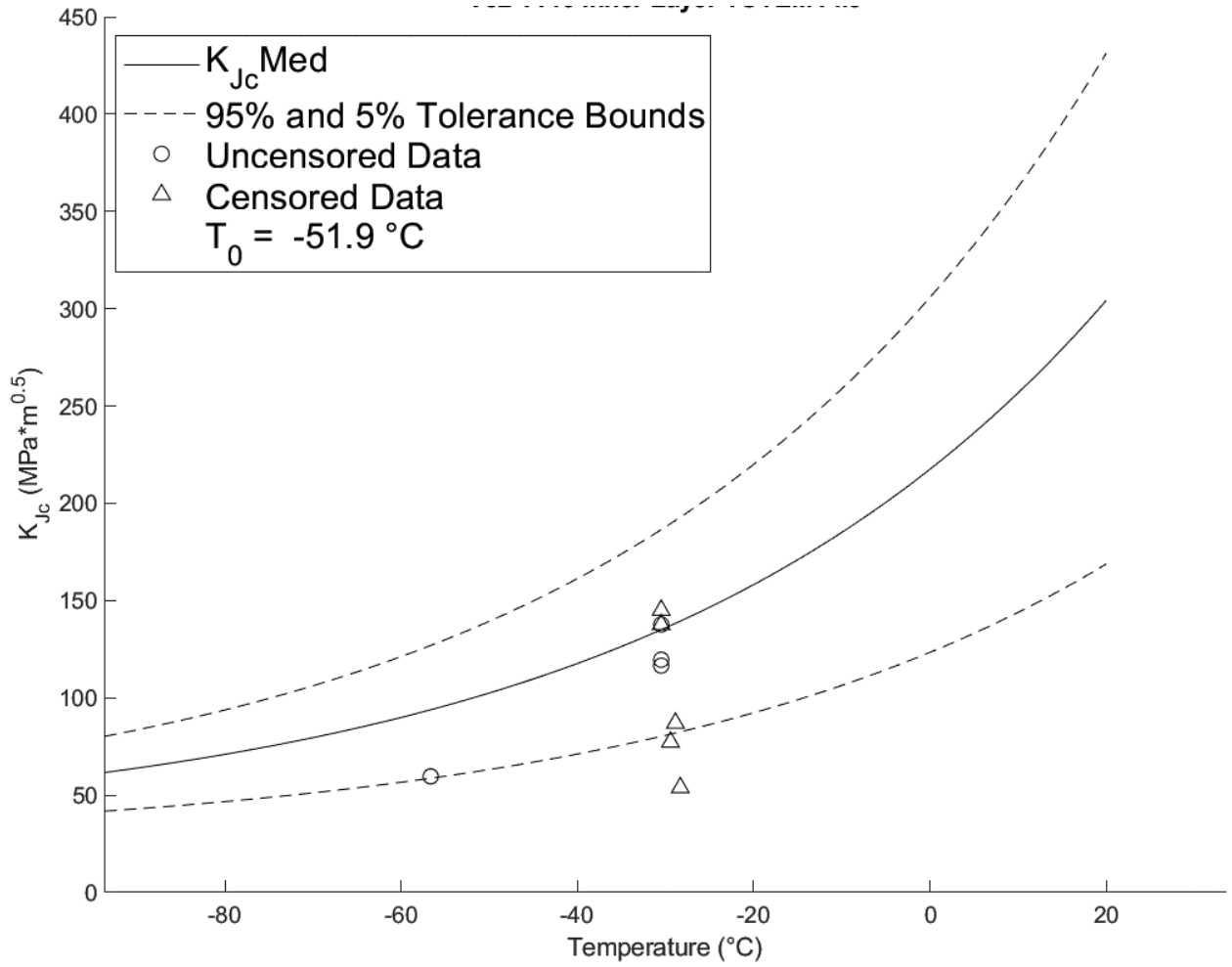


Figure 7.3.1.3.3-5: V0032 Inner Layer T_0 Plot ($T_0 = -52^{\circ}\text{C}$)

Table 7.3.1.3.3-6: V0032 Inner Layer T₀ Plot (T₀ = -52°C)

Specimen Name	Temperature (°C)	KjcRaw (MPa*m ^{0.5})	1T Data (MPa*m ^{0.5})	Uncensored Data	Test Temp -T0 (°C)
380-10	-29	89.6	77.3	0	22
380-12	-29	101.5	87.0	0	23
380-13	-57	68.1	59.6	1	-5
380-14	-57	68.2	59.7	1	-5
380-15	-31	198.7	137.7	0	21
380-16	-31	163.1	137.7	1	21
380-9	-28	61.2	53.9	0	24
380-35	-31	222.8	137.7	0	21
380-36	-31	190.0	137.7	0	21
380-37	-31	141.2	119.6	1	21
380-38	-31	137.5	116.5	1	21
380-39	-31	176.5	145.0	0	21

Table 7.3.1.3.3-7: V0032 Inner Layer 1146 T₀ Calculation Results

Initial T ₀ (°C)	-52
Total Samples	12
Samples within T ₀ ± 50°C (N)	12
Number of Uncensored Data (r)	5
Poisson's Ratio	0.3
Σ(ri ni)	0.83
Samples Between Ti - T ₀ 50 to -14 °C	5
Samples Between Ti - T ₀ -15 to -35 °C	0
Samples Between Ti - T ₀ -36 to -50 °C	0
T ₀ scrn (°C)	-40
Homogenous or Inhomogeneous	Inhomogeneous

For the V0032 inner layer, the listing of inhomogeneous is a result of having too few valid specimens to allow assessment of the data set as truly homogenous.

The test data in Table 7.3.1.3.3-8 are raw values obtained from fracture tests conducted on MV50466-8 1146 inner layer material. Test results that are considered upper shelf are listed under ASTM E1820, while transition temperature test results are listed under E1921. Tests that meet the complete validity requirements for $J_q = J_{1C}$ and $K_{Iq} = K_{J1C}$ are denoted with an asterisk. Despite invalidities, J_q and K_{Iq} convey valuable fracture toughness information, especially when the test results are applied directly to the sample material source.

Table 7.3.1.3.3-8: V50466-8 1146 Inner Layer Fracture Data

Specimen ID	Test Temp. (°C)	ASTM Crack Plane Orientation	W (in)	a ₀ (in)	a _r (in)	B ₀ (in)	B _N (in)	J _q (kJ/m ²)	K _{Iq} (MPa √m)	K _{ICIT} (MPa √m)	ASTM Standard
440-4	23	L-T	0.9999	0.4992	0.5822	0.3754	0.2985	164	192	---	E1820
440-7	23	L-T	1.0008	0.4999	0.5588	0.3756	0.2987	159	189	---	E1820
440-9	23	L-T	1.0009	0.5043	0.5539	0.3751	0.2962	145	180	---	E1820
440-1	22	L-T	1.0000	0.5048	0.5634	0.3756	0.3010	162	191	---	E1820
440-3	22	L-T	0.9990	0.5284	0.5735	0.3739	0.2955	133	173	---	E1820
440-8	22	L-T	0.9999	0.5014	0.5587	0.3751	0.2979	173*	197	---	E1820
440-90	22	L-T	0.9998	0.4991	0.5354	0.2354	0.1898	138	175	---	E1820
440-91	22	L-T	0.9999	0.4931	0.5277	0.2338	0.1936	195	209	---	E1820
440-5	23	T-L	0.9998	0.4994	0.5589	0.3748	0.2975	60	116	---	E1820
440-11	23	T-L	1.0020	0.5027	0.5908	0.3751	0.2955	64	120	---	E1820
440-2	22	T-L	0.9998	0.5031	0.5979	0.3742	0.2943	60	115	---	E1820
440-10	22	T-L	1.0011	0.5094	0.6042	0.3754	0.2982	58	114	---	E1820
440-12	22	T-L	1.0002	0.4947	0.5915	0.3757	0.2982	65	120	---	E1820
440-6	22	T-L	1.0002	0.4952	0.5936	0.3755	0.2956	74	129	---	E1820
440-88	22	T-L	0.9996	0.4937	0.5618	0.2380	0.1909	43	98	---	E1820
440-87	21	T-L	0.9997	0.4909	0.5556	0.3758	0.1913	40	95	---	E1820
440-132	2	T-L	0.9997	0.4997	0.5764	0.3559	0.2863	67	122	---	E1820
440-133	2	T-L	0.9997	0.4935	0.5420	0.3565	0.2848	69	124	---	E1820
440-134	2	T-L	0.9999	0.4956	0.5616	0.3756	0.3016	73	127	---	E1820
440-135	2	T-L	1.0002	0.4891	0.5520	0.3566	0.2863	82	135	---	E1820
440-127	-14	T-L	0.9994	0.4940	0.5760	0.3568	0.2856	62	118	96	E1921
440-128	-14	T-L	1.0001	0.4891	0.5552	0.3561	0.2854	67	123	99	E1921
440-148	-29	T-L	0.9951	0.4883	0.4969	0.3766	0.3005	61	117	96	E1921
440-149	-30	T-L	0.9974	0.4939	0.5556	0.3758	0.3010	51	107	88	E1921
440-71	-45	T-L	0.9992	0.4955	0.5001	0.3787	0.3074	38	93	77	E1921
440-72	-45	T-L	0.9993	0.4985	0.5043	0.3797	0.3054	52	108	89	E1921
440-69	-46	T-L	0.9994	0.4956	0.4959	0.3787	0.3063	27	78	65	E1921
440-70	-46	T-L	0.9993	0.4985	0.5019	0.3786	0.3017	46	101	84	E1921
440-73	-46	T-L	0.9989	0.5030	0.5095	0.3790	0.3066	62	118	97	E1921
440-74	-46	T-L	0.9982	0.5030	0.5205	0.3785	0.3032	88	140	114	E1921
440-150	-47	T-L	0.9994	0.4879	0.5531	0.3768	0.3000	67	122	100	E1921
440-151	-47	T-L	0.9958	0.4863	0.5503	0.3751	0.3000	61	117	96	E1921
440-158	-49	T-L	0.9988	0.5044	0.5624	0.3769	0.3000	49	105	86	E1921
440-157	-50	T-L	0.9966	0.4862	0.5377	0.3765	0.2970	73	128	105	E1921
440-66	-50	T-L	0.9997	0.4992	0.5002	0.3788	0.3048	21	68	58	E1921
440-67	-51	T-L	0.9984	0.4996	0.5009	0.3794	0.3050	27	78	65	E1921
440-65	-51	T-L	0.9981	0.5711	0.5723	0.3795	0.3037	20	67	57	E1921
440-75	-51	T-L	0.9999	0.5107	0.5118	0.3785	0.3014	33	85	71	E1921
440-76	-51	T-L	0.9988	0.4976	0.4976	0.3785	0.3021	16	59	51	E1921
440-136	-65	T-L	0.9992	0.4890	0.5460	0.3558	0.2865	79	133	107	E1921
440-153	-81	T-L	0.9935	0.5222	0.5262	0.3763	0.2993	18	64	54	E1921
440-147	-82	T-L	0.9941	0.5136	0.5160	0.3770	0.2981	18	63	54	E1921
440-152	-82	T-L	0.9883	0.5141	0.5141	0.3765	0.2999	15	58	50	E1921
440-156	-82	T-L	0.9880	0.4923	0.4947	0.3766	0.2840	23	71	60	E1921
440-118	-82	T-L	1.0006	0.5203	0.5322	0.3563	0.2866	67	122	99	E1921
440-119	-82	T-L	0.9991	0.5201	0.5407	0.3561	0.2860	99	149	119	E1921
440-120	-82	T-L	0.9998	0.5060	0.5072	0.3563	0.2841	36	89	73	E1921
440-154	-82	T-L	0.9977	0.5170	0.5211	0.3745	0.2997	14	56	48	E1921
440-159	-82	T-L	0.9947	0.5486	0.5754	0.3671	0.2910	55	111	91	E1921
440-130	-196	T-L	0.9995	0.5099	0.5099	0.3755	0.3000	2	19	19	E1921
440-131	-196	T-L	1.0004	0.5199	0.5199	0.3546	0.2850	2	22	22	E1921

Results from the 31 E1921 tests are presented in Table 7.3.1.3.3-9 and Table 7.3.1.3.3-10. These results were obtained using the T₀TEM code described in Section 4.2. The T₀ reference temperature for this data set was evaluated as -44°C using the E1921 master curve shown in Figure 7.3.1.3.3-6. Given the number of specimens tested, the material was able to be properly characterized as macroscopically inhomogeneous with a 91% confidence in multimodal inhomogeneity. This gives a multimodal transition temperature of T_m = -38°C. The multimodal master curve and confidence bounds are shown in Figure 7.3.1.3.3-7.

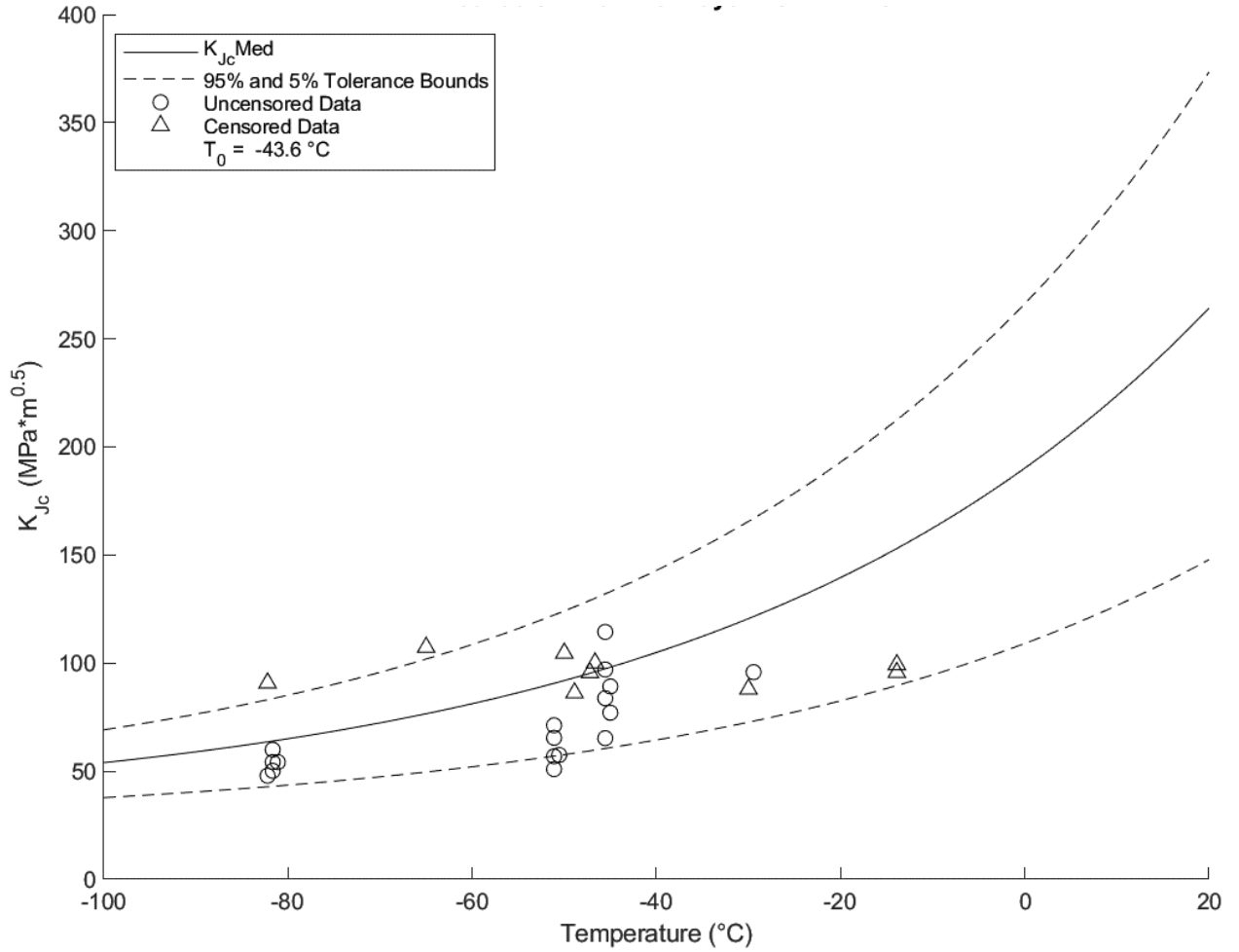


Figure 7.3.1.3.3-6: MV50466-8 1146 Inner Layer Fracture Data

Table 7.3.1.3.3-9: MV50466-8 1146 Inner Layer T₀ Individual Specimen Results

Specimen Name	Temperature (°C)	KjcRaw (MPa*m ^{0.5})	1T Data (MPa*m ^{0.5})	Uncensored Data	Test Temp -T0 (°C)
440-65	-51	67.0	56.9	1	-8
440-66	-51	67.8	57.5	1	-7
440-67	-51	77.9	65.4	1	-8
440-69	-46	77.8	65.3	1	-2
440-70	-46	101.3	83.7	1	-2
440-71	-45	92.7	77.0	1	-1
440-72	-45	108.2	89.2	1	-1
440-73	-46	118.2	97.0	1	-2
440-74	-46	140.4	114.4	1	-2
440-75	-51	85.3	71.2	1	-8
440-76	-51	59.5	51.0	1	-8
440-127	-14	117.9	95.7	0	30
440-128	-14	122.7	99.3	0	30
440-136	-65	133.1	107.3	0	-21
440-147	-82	63.7	54.2	1	-38
440-148	-29	116.8	95.8	1	14
440-149	-30	106.8	88.0	0	14
440-150	-47	122.2	100.1	0	-3
440-151	-47	116.6	95.6	0	-4
440-152	-82	58.5	50.2	1	-38
440-153	-81	63.7	54.2	1	-38
440-154	-82	55.7	47.9	1	-39
440-156	-82	71.0	60.0	1	-38
440-157	-50	128.0	104.6	0	-6
440-158	-49	104.5	86.2	0	-5
440-159	-82	111.0	90.8	0	-39
440-130	-196	19.2	19.4	1	-152
440-131	-196	21.9	21.5	1	-152

Table 7.3.1.3.3-10: MV50466-8 1146 Inner Layer T_0 Calculation Results

Initial T_0 (°C)	-44
Total Samples	28
Samples within $T_0 \pm 50^\circ\text{C}$ (N)	26
Number of Uncensored Data (r)	17
Poisson's Ratio	0.3
$\Sigma(r_i n_i)$	2.63
Samples Between $T_i - T_0$ 50 to -14°C	12
Samples Between $T_i - T_0$ -15 to -35°C	0
Samples Between $T_i - T_0$ -36 to -50°C	5
$T_{0\text{scrn}}$ (°C)	-25
Homogenous or Inhomogeneous	Inhomogeneous

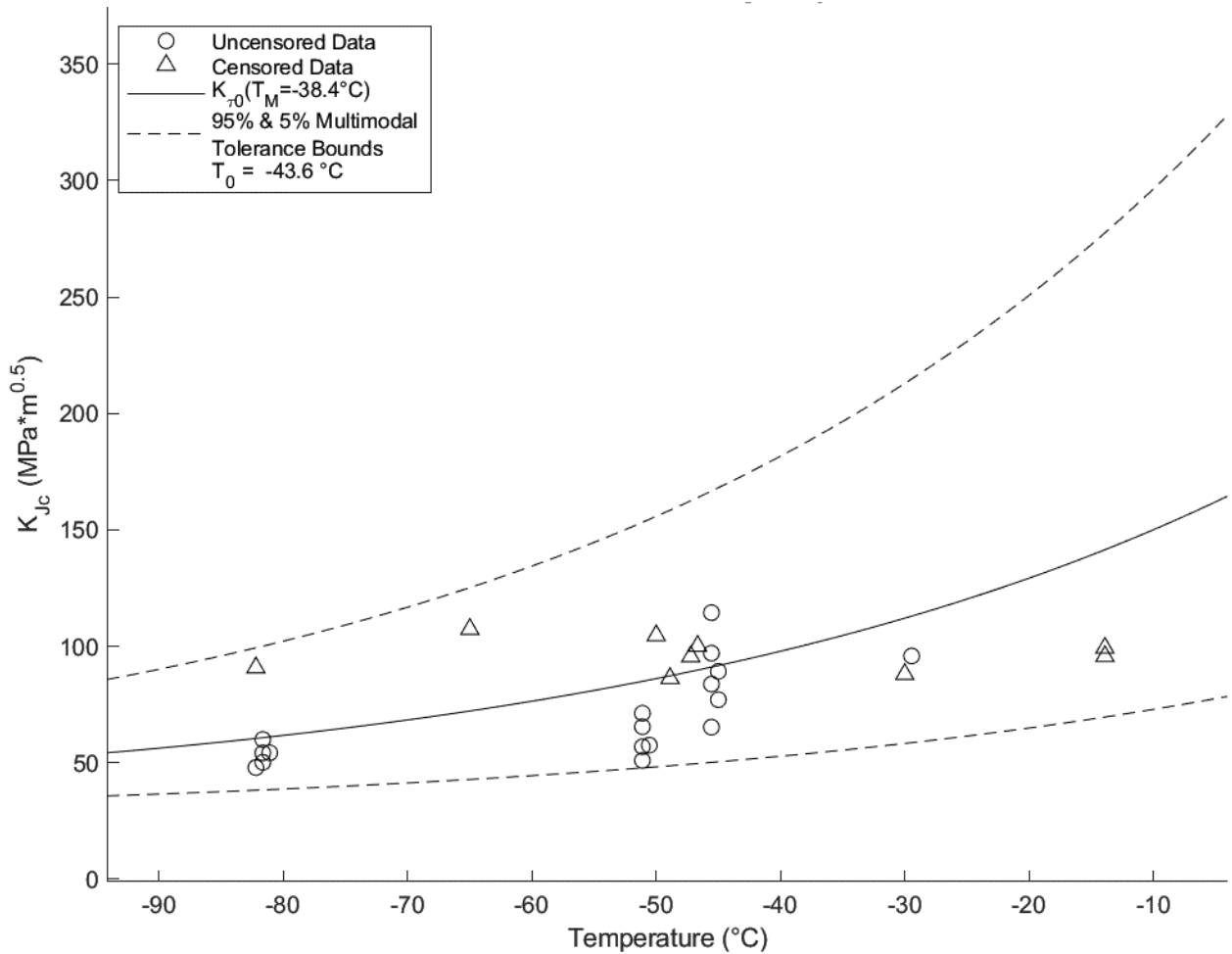


Figure 7.3.1.3.3-7: MV50466-8 1146 Inner Layer Multimodal T_m Plot ($T_m = -38^\circ\text{C}$)

Table 7.3.1.3.3-11: MV50466-8 1146 Inner Layer Multimodal T_m Calculation Results

T_m (°C)	-38
σT_m (°C)	22
Multimodal Homogeneity	Inhomogeneous
Multimodal Confidence	91
Number of samples within $T_m \pm 50$ °C	26

The multimodal T_m value moves the transition temperature 6°C higher and expands the confidence bounds to more accurately reflect the composition of the data set.

The test data in Table 7.3.1.3.3-12 are raw values obtained from fracture tests conducted on MV50466-8 1146 wrap layer material. Test results that are considered upper shelf are listed under ASTM E1820, while transition temperature test results are listed under E1921. Tests that meet the complete validity requirements for $J_q = J_{1C}$ and $K_{Jq} = K_{J1C}$ are denoted with an asterisk. Despite invalidities, J_q and K_{Jq} convey valuable fracture toughness information, especially when the test results are applied directly to the sample material source.

Table 7.3.1.3.3-12: MV50466-8 1146 Wrapper Layer Fracture Data

Specimen ID	Test Temp. (°C)	ASTM Crack Plane Orientation	W (in)	a_0 (in)	a_f (in)	B_0 (in)	B_N (in)	J_q (kJ/m ²)	K_{Jq} (MPa \sqrt{m})	K_{JCT} (MPa \sqrt{m})	ASTM Standard
440-100	-51	T-L	1.0011	0.4919	0.4949	0.2314	0.1839	23	72	56	E1921
440-101	-51	T-L	1.0014	0.4923	0.4978	0.2319	0.1877	16	59	47	E1921
440-102	-51	T-L	1.0008	0.4887	0.4975	0.2320	0.1874	46	101	76	E1921
440-103	-51	T-L	1.0016	0.4915	0.4984	0.2317	0.1870	35	89	68	E1921
440-104	-51	T-L	1.0012	0.4913	0.4960	0.2315	0.1839	13	55	44	E1921
440-93	-50	T-L	1.0012	0.4958	0.4974	0.2317	0.1869	27	78	60	E1921
440-94	-50	T-L	1.0007	0.4921	0.5013	0.2320	0.1864	45	100	76	E1921
440-95	-50	T-L	1.0012	0.4911	0.4945	0.2314	0.1861	34	87	66	E1921
440-96	-50	T-L	1.0009	0.4926	0.5012	0.2306	0.1850	41	96	73	E1921
440-97	-50	T-L	1.0014	0.4971	0.5003	0.2307	0.1880	37	90	69	E1921
440-98	-50	T-L	1.0014	0.4939	0.4951	0.2318	0.1854	34	87	66	E1921
440-99	-50	T-L	1.0011	0.4929	0.4963	0.2317	0.1802	28	79	61	E1921

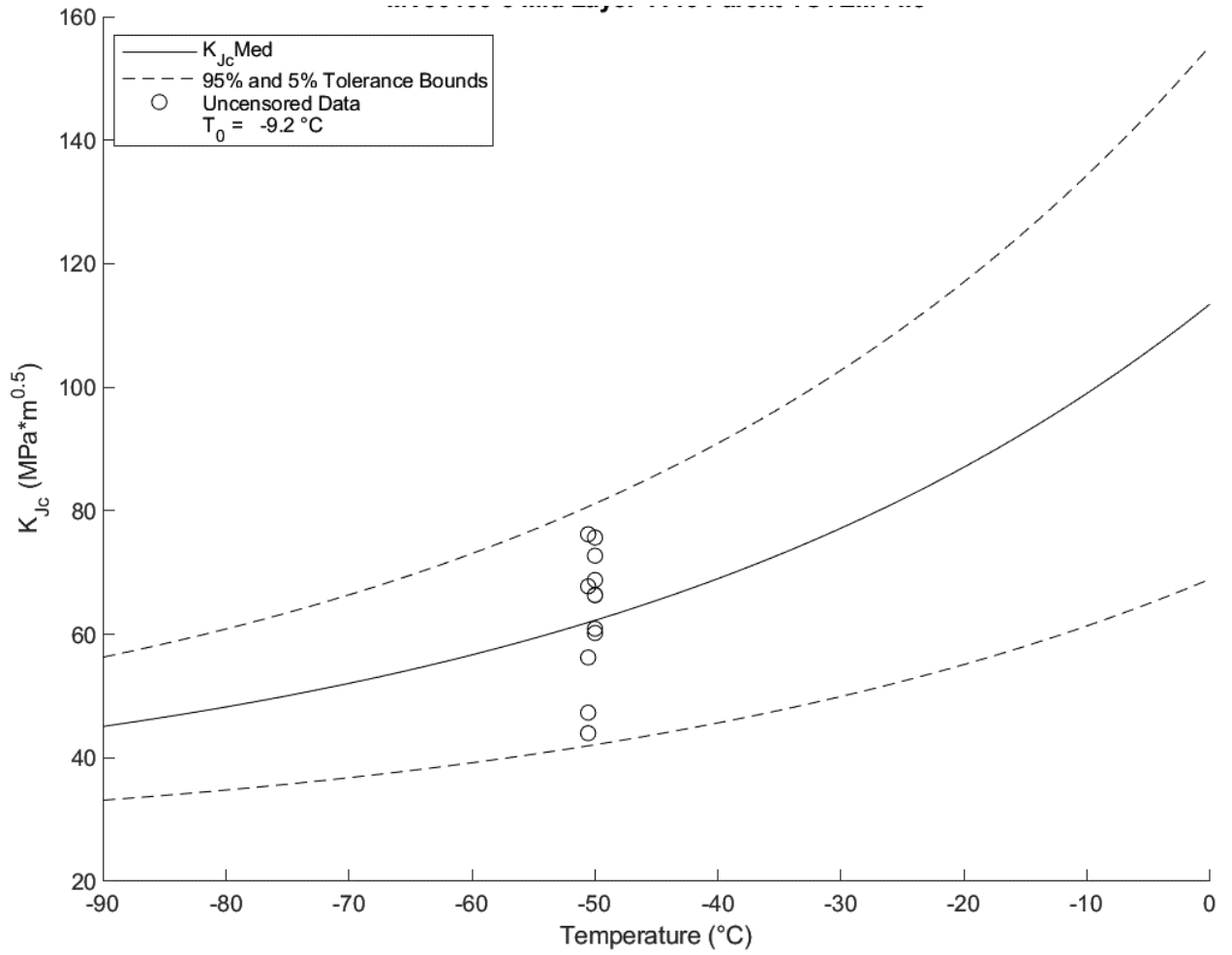


Figure 7.3.1.3.3-8: MV50466-8 1146 Wrapper Layer T_0 Plot ($T_0 = -9^{\circ}\text{C}$)

Table 7.3.1.3.3-13: MV50466-8 1146 Wrapper Layer T₀ Individual Specimen Results

Specimen Name	Temperature (°C)	KjcRaw (MPa*m ^{0.5})	1T Data (MPa*m ^{0.5})	Uncensored Data	Test Temp -T0 (°C)
440-93	-50	78.0	60.2	1	-41
440-94	-50	100.2	75.7	1	-41
440-95	-50	86.8	66.3	1	-41
440-96	-50	96.1	72.7	1	-41
440-97	-50	90.4	68.8	1	-41
440-98	-50	86.8	66.4	1	-41
440-99	-50	79.0	60.9	1	-41
440-100	-51	72.3	56.2	1	-41
440-101	-51	59.4	47.3	1	-41
440-102	-51	101.0	76.2	1	-41
440-103	-51	88.8	67.8	1	-41
440-104	-51	54.6	44.0	1	-41

Table 7.3.1.3.3-14: MV50466-8 1146 Wrapper Layer T₀ Calculation Results

Initial T0 (°C)	-9
Total Samples	12
Samples within T0 ± 50°C (N)	12
Number of Uncensored Data (r)	12
Poisson's Ratio	0.3
Σ(ri ni)	1.5
Samples Between Ti - T0 50 to -14 °C	0
Samples Between Ti - T0 -15 to -35 °C	0
Samples Between Ti - T0 -36 to -50 °C	12
T0scrn (°C)	-9
Homogenous or Inhomogeneous	Homogenous

As noted in Table 7.3.1.2-1, the initial discovery of variation in a single inner layer plate was revealed during a hardness trace of the longitudinal weld found in Section C4-1. Down select tests were conducted on the respective sides of the weld. From Table 7.3.1.2-1, the A side demonstrated low hardness values, while the B side demonstrated high hardness values. Table 7.3.1.3.3-15 shows the difference in toughness at these two locations, as well as the difference in orientation. The results confirm that the plate orientation is consistently weakest in the T-L direction, however the K_{JQ} is an average of 36 Mpavm higher for the A side with lower hardness. These tests confirm that the plate itself has varying property values in accordance with the hardness.

Table 7.3.1.3.3-15: V0023 1146 Inner Layer C4-1 0A and 0B Fracture Data

Specimen ID	Test Temp. (°C)	ASTM Crack Plane Orientation	W (in)	a ₀ (in)	a _f (in)	B ₀ (in)	B _N (in)	J _q (kJ/m ²)	K _{Jq} (MPa √m)	K _{JCT} (MPa √m)	ASTM Standard	Location
519-13	22	L-T	1.0045	0.5242	0.5274	0.3747	0.2987	63	119	---	E1820	C4-1 Layer 0B
519-14	24	L-T	1.0043	0.5331	0.5400	0.3752	0.3002	74	129	---	E1820	C4-1 Layer 0B
519-15	22	T-L	0.9819	0.5462	0.5496	0.3747	0.2978	40	95	---	E1820	C4-1 Layer 0B
519-16	27	T-L	1.0036	0.5322	0.5366	0.3170	0.2551	27	78	---	E1820	C4-1 Layer 0B
519-144	21	L-T	1.0011	0.5207	0.6049	0.3723	0.3160	166	193	---	E1820	C4-1 Layer 0A
519-145	21	L-T	1.0016	0.5147	0.5949	0.3744	0.3160	141	177	---	E1820	C4-1 Layer 0A
519-146	21	L-T	1.0012	0.5229	0.5817	0.3745	0.3197	149	182	---	E1820	C4-1 Layer 0A
519-147	19	T-L	1.0011	0.5133	0.5879	0.3345	0.2780	68	123	---	E1820	C4-1 Layer 0A
519-148	21	T-L	1.0016	0.5148	0.5907	0.3403	0.2843	81	135	---	E1820	C4-1 Layer 0A
519-149	21	T-L	1.0012	0.5228	0.6095	0.3383	0.2855	61	117	---	E1820	C4-1 Layer 0A

As noted in Table 7.3.1.2-1, some sections of the inner layer of vessel V0023 displayed inconsistent hardness levels around the circumference of the vessel. Section C3-1 0B was tested in order to confirm a mechanical (fracture) property difference in the area where lower hardness values were seen. The results are shown in Table 7.3.1.3.3-16. As a result of this, a separate T₀ curve was created in Figure 7.3.1.3.3-9 to describe the areas of lower hardness, with a transition temperature of T₀ = -100°C.

Table 7.3.1.3.3-16: V0023 1146 Inner Layer C3-1 0B Fracture Data

Specimen ID	Test Temp. (°C)	ASTM Crack Plane Orientation	W (in)	a ₀ (in)	a _f (in)	B ₀ (in)	B _N (in)	J _q (kJ/m ²)	K _{Jq} (MPa √m)	K _{JCT} (MPa √m)	ASTM Standard
519-168	-40	T-L	1.0000	0.5270	0.6450	0.3750	0.2990	123	166	---	E1820
519-170	-60	T-L	1.0000	0.5310	0.6000	0.3750	0.2990	135	174	---	E1820
519-171	-90	T-L	1.0010	0.5270	0.5700	0.3740	0.3010	104	153	124	E1921
519-169	-100	T-L	1.0000	0.5320	0.5530	0.3760	0.2990	83	136	111	E1921
519-172	-100	T-L	0.9990	0.5330	0.5530	0.3740	0.3000	83	136	111	E1921
519-173	-110	T-L	1.0000	0.5300	0.5300	0.3760	0.3000	44	99	82	E1921
519-174	-110	T-L	1.0000	0.5270	0.5370	0.3750	0.3000	62	118	96	E1921
519-175	-110	T-L	1.0010	0.5290	0.5530	0.3740	0.2990	87	140	113	E1921
519-176	-110	T-L	0.9990	0.5410	0.5410	0.3760	0.2990	41	96	79	E1921
519-177	-110	T-L	1.0010	0.5270	0.5270	0.3750	0.2990	26	76	64	E1921
519-178	-110	T-L	0.9900	0.5250	0.5250	0.3760	0.2990	29	80	67	E1921
519-179	-110	T-L	1.0000	0.5320	0.5420	0.3770	0.2990	52	108	89	E1921

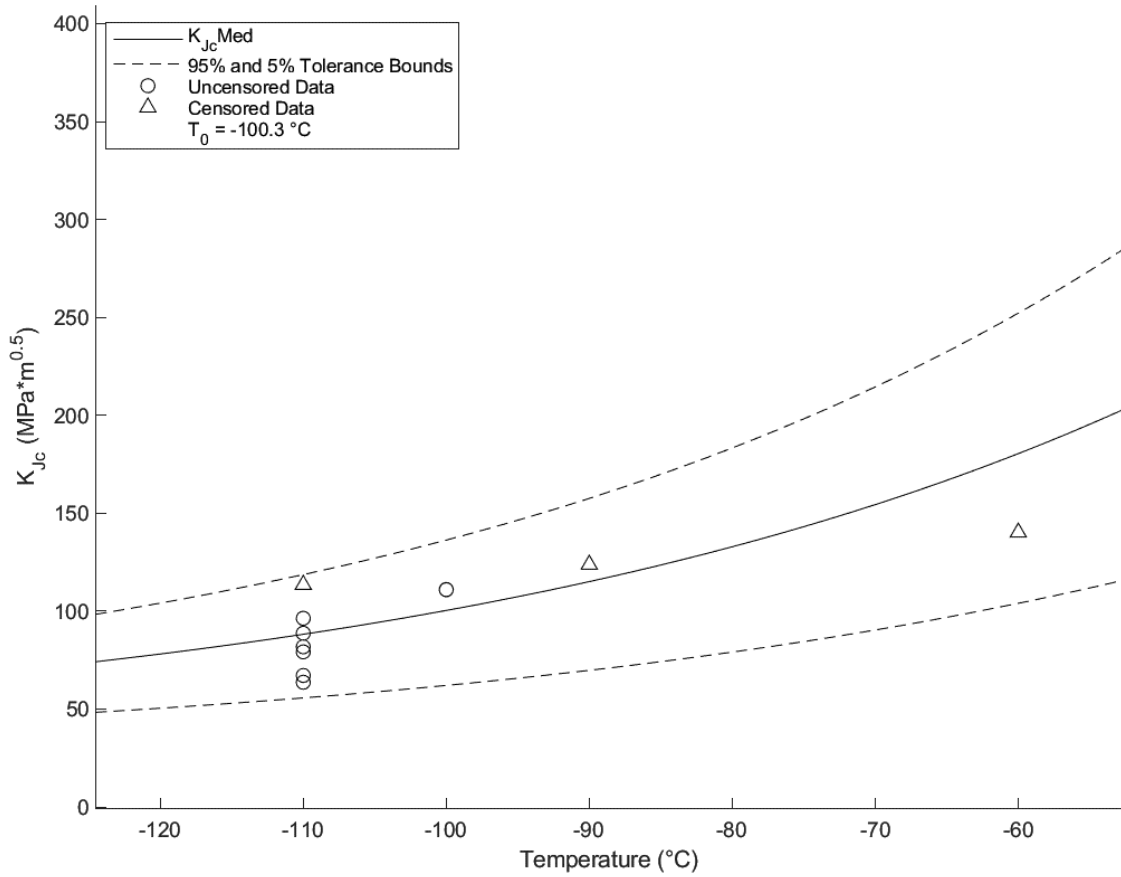


Figure 7.3.1.3.3-9: V0023 1146 Inner Layer C3-1 OB T_0 Plot ($T_0 = -100^\circ\text{C}$)

Table 7.3.1.3.3-17: V0023 1146 Inner Layer C3-1 0B T₀ Individual Specimen Results

Specimen Name	Temperature (°C)	KjcRaw (MPa*m ^{0.5})	1T Data (MPa*m ^{0.5})	Uncensored Data	Test Temp -T0 (°C)
519-168	-40	165.9	111.0	0	60
519-169	-100	136.3	111.0	1	0
519-170	-60	173.6	111.0	0	40
519-171	-90	152.7	111.0	0	10
519-172	-100	136.3	110.9	1	0
519-173	-110	98.9	81.8	1	-10
519-174	-110	117.6	96.4	1	-10
519-175	-110	139.6	111.0	0	-10
519-176	-110	95.6	79.2	1	-10
519-177	-110	75.8	63.7	1	-10
519-178	-110	80.2	67.2	1	-10
519-179	-110	107.7	88.7	1	-10

Table 7.3.1.3.3-18: V0023 1146 Inner Layer C3-1 0B T₀ Calculation Results

Initial T ₀ (°C)	-100
Total Samples	12
Samples within T ₀ ± 50°C (N)	11
Number of Uncensored Data (r)	8
Poisson's Ratio	0.3
Σ(r _i n _i)	1.33
Samples Between T _i - T ₀ 50 to -14 °C	8
Samples Between T _i - T ₀ -15 to -35 °C	0
Samples Between T _i - T ₀ -36 to -50 °C	0
T ₀ scrn (°C)	-96
Homogenous or Inhomogeneous	Homogenous

Section C4-2 0B was tested in order to confirm a mechanical property difference in the area where higher hardness values were seen. As a result of this, a separate T₀ curve was created in Figure 7.3.1.3.3-10 to describe the areas with higher hardness, with a transition temperature of T₀ = 61°C. The results are shown in Table 7.3.1.3.3-19.

Table 7.3.1.3.3-19: V0023 1146 Inner Layer C4-2 OB Fracture Data

Specimen ID	Test Temp. (°C)	ASTM Crack Plane Orientation	W (in)	a ₀ (in)	a _f (in)	B ₀ (in)	B _N (in)	J _q (kJ/m ²)	K _{Jq} (MPa √m)	K _{JcIT} (MPa √m)	ASTM Standard
519-260	23	T-L	1.0002	0.5212	0.5253	0.3747	0.2967	40	95	79	E1921
519-261	23	T-L	1.0010	0.5259	0.5285	0.3737	0.2988	30	82	68	E1921
519-262	23	T-L	1.0011	0.5158	0.5179	0.3730	0.2958	27	78	65	E1921
519-263	23	T-L	1.0013	0.5354	0.5368	0.3737	0.2979	23	72	61	E1921
519-264	23	T-L	1.0014	0.5200	0.5219	0.3728	0.2964	27	77	65	E1921
519-265	23	T-L	1.0005	0.5281	0.5339	0.3710	0.2985	34	87	72	E1921
519-266	23	T-L	1.0013	0.5251	0.5273	0.3740	0.3006	31	84	70	E1921
519-267	23	T-L	1.0011	0.5237	0.5268	0.3733	0.2961	26	76	64	E1921
519-270	21	L-T	1.0003	0.5306	0.5370	0.3740	0.3055	76	131	107	E1921
519-271	21	L-T	1.0006	0.5359	0.5362	0.3743	0.3080	20	67	57	E1921

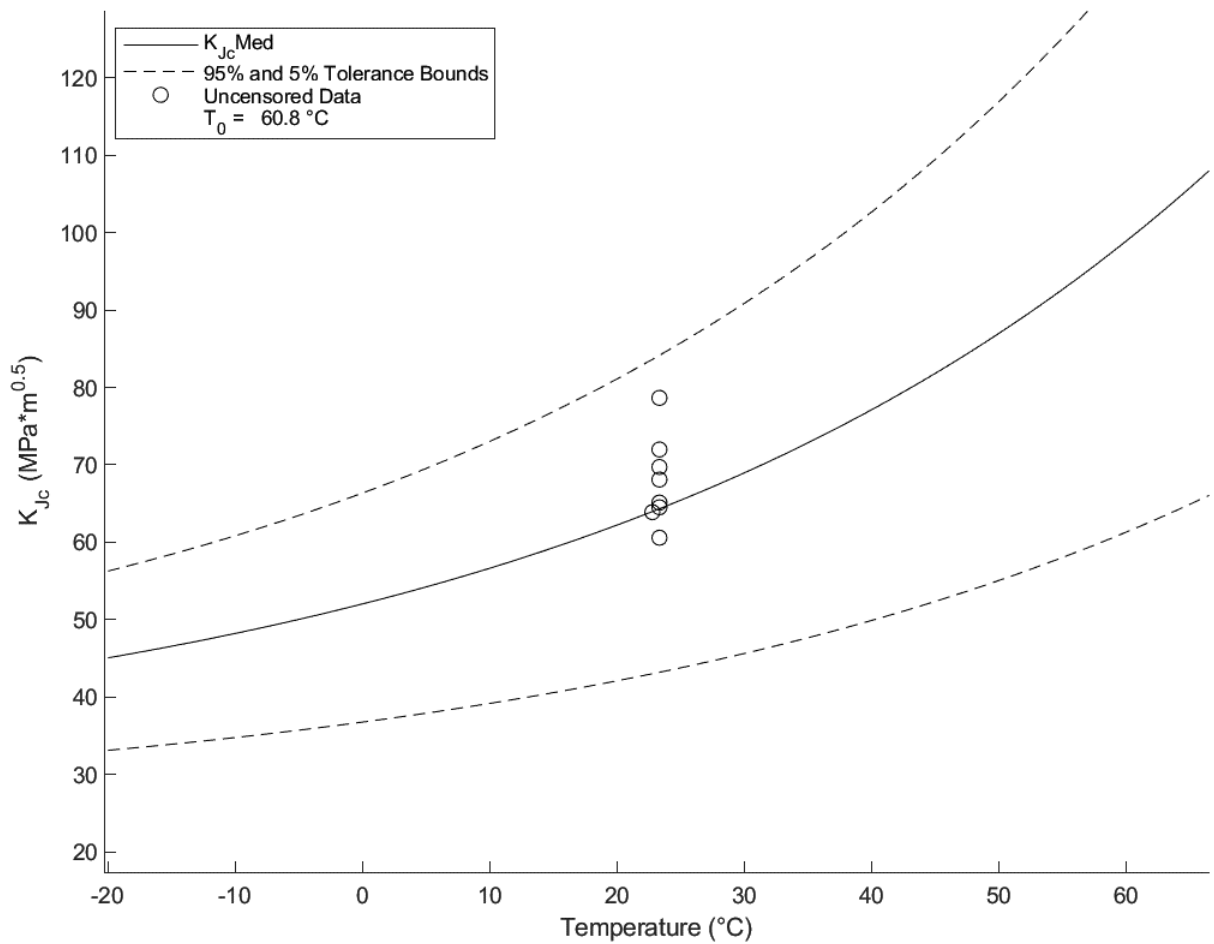


Figure 7.3.1.3.3-10: V0023 1146 Inner Layer C4-2 OB T_0 Plot ($T_0 = 61^\circ\text{C}$)

Table 7.3.1.3.3-20: V0023 1146 Inner Layer C4-2 0B T₀ Individual Specimen Results

Specimen Name	Temperature (°C)	KjcRaw (MPa*m ^{0.5})	1T Data (MPa*m ^{0.5})	Uncensored Data	Test Temp -T ₀ (°C)
519-260	23	95.0	78.6	1	-38
519-261	23	81.5	68.1	1	-38
519-262	23	77.7	65.1	1	-38
519-263	23	71.9	60.6	1	-38
519-264	23	77.0	64.5	1	-38
519-265	23	86.6	72.0	1	-38
519-266	23	83.6	69.7	1	-38
519-267	23	76.1	63.9	1	-38

Table 7.3.1.3.3-21: V0023 1146 Inner Layer C4-2 0B T₀ Calculation Results

Initial T ₀ (°C)	61
Total Samples	8
Samples within T ₀ ± 50°C (N)	8
Number of Uncensored Data (r)	8
Poisson's Ratio	0.3
Σ(ri ni)	1
Samples Between Ti - T ₀ 50 to -14 °C	0
Samples Between Ti - T ₀ -15 to -35 °C	0
Samples Between Ti - T ₀ -36 to -50 °C	8
T ₀ scrn (°C)	61
Homogenous or Inhomogeneous	Homogenous

The test data in Table 7.3.1.3.3-22 are raw values obtained from fracture tests conducted on V0023 1146 wrap layer material. Test results that are considered upper shelf are listed under ASTM E1820, while transition temperature test results are listed under E1921. Tests that meet the complete validity requirements for $J_q = J_{1C}$ and $K_{Jq} = K_{J1C}$ are denoted with an asterisk. Despite invalidities, J_q and K_{Jq} convey valuable fracture toughness information, especially when the test results are applied directly to the sample material source. No E1921 tests were conducted on the V0023 wrapper material and as such there is not associated T₀ or Master Curve.

Table 7.3.1.3.3-22: V0023 1146 Wrapper Layer Fracture

Specimen ID	Test Temp. (°C)	ASTM Crack Plane Orientation	W (in)	a ₀ (in)	a _f (in)	B ₀ (in)	B _N (in)	J _q (kJ/m ²)	K _{Jq} (MPa√m)	K _{JCLT} (MPa√m)	ASTM Standard
519-20	27	L-T	1.0044	0.5337	0.5916	0.2624	0.2096	105	153	---	E1820
519-19	22	L-T	1.0046	0.5291	0.5867	0.2623	0.2115	137	175	---	E1820
519-125	21	L-T	0.9998	0.4603	0.5915	0.2688	0.2261	172	196	---	E1820
519-124	21	L-T	1.0010	0.4609	0.6079	0.2692	0.2240	197	210	---	E1820
519-18	27	T-L	1.0041	0.5242	0.5857	0.2627	0.2101	47	102	---	E1820
519-17	22	T-L	1.0047	0.5420	0.6390	0.2626	0.2100	39	93	---	E1820
519-121	21	T-L	1.0021	0.4621	0.5386	0.2688	0.2223	31	83	---	E1820
519-122	21	T-L	1.0012	0.4612	0.6156	0.2698	0.2242	43	98	---	E1820
519-123	21	T-L	1.0020	0.4623	0.6325	0.2694	0.2312	30	82	---	E1820

Figure 7.3.1.3.3-11 shows the combined Master Curves of the 1146 material test lots plotted against each other. Each curve is terminated at the apparent upper shelf value of the material. With many of these lots, the upper shelf value itself is below the 100 Mpa√m evaluation level set for T₀. This presents a unique issue as the lots have a low transition temperature, but do not exhibit the commonly expected high upper shelf K_J value.

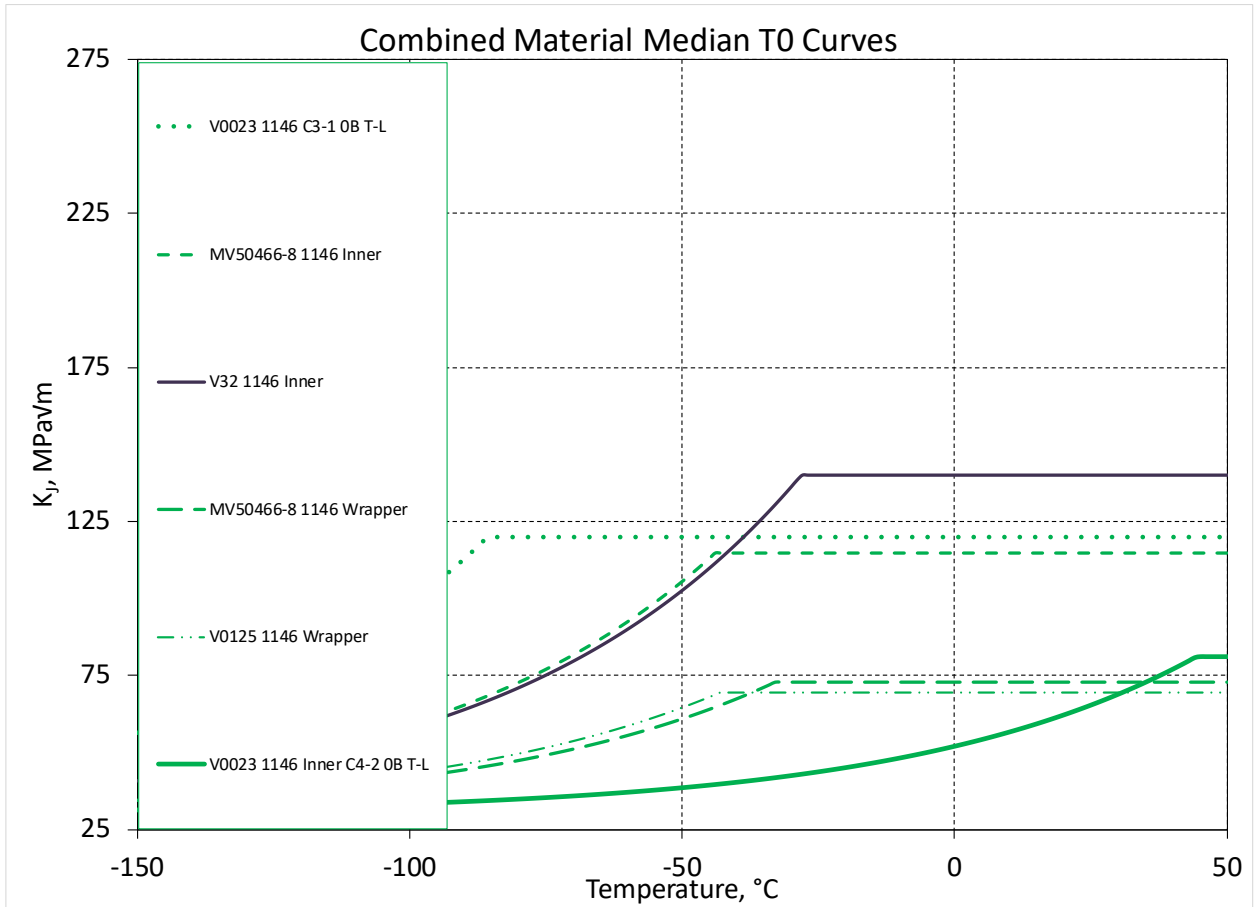


Figure 7.3.1.3.3-11: 1146 Combined T_0 Plots

7.3.1.3.4 Fatigue Crack Growth

Sections of V0023 were tested to determine the fatigue crack growth rates according to ASTM E647 (11). Load ratios of $R = 0.1$ and $R = 0.7$ were chosen corresponding to load cycles associated with slight pressure variations and nearly full pressure releases of the LPVs. These tests were conducted on the wrapper material, the soft inner (0A) and the hard inner (0B) material as shown in Figure 7.3.1.2-1. Table 7.3.1.3.4-1 and Table 7.3.1.3.4-2 show the test matrix and threshold result of each E647 test conducted. The individual fatigue growth curves are shown in Figure 7.3.1.3.4-1 through Figure 7.3.1.3.4-12. These curves are input into NASGRO to create material data packages used for structural analysis and crack growth prediction.

Table 7.3.1.3.4-1: V0023 da/dN Test Matrix

Lot	Material	Orientation	Stock Thickness	Specimen Thickness	Machine	R=0.1	R=0.7	Spares
V23 Inner 0A	1146a	T-L	0.5	0.375	6	2	2	2
V23 Inner 0B	1146a	T-L	0.5	0.375	6	2	2	2
V23 Wrapper, 2A	1146a	T-L	0.28	0.2-0.25	6	2	2	2
Total:					18	6	6	6

Table 7.3.1.3.4-2: V0023 da/dN Results

Specimen ID	Temperature °F	R-Ratio	Segment	C (1/in)	Frequency	Threshold (ΔK) (KSI \sqrt{in})	Location
V23-0A-1	75	0.1	A	-20	25 Hz	4.469	Inner
			B	6	25 Hz		
V23-0A-2	75	0.1	A	-20	20 Hz	4.56	Inner
			B	6	20 Hz		
V23-0A-3	75	0.7	A	-20	25 Hz	2.676	Inner
			B	6	25 Hz		
V23-0A-4	75	0.7	A	-20	25 Hz	2.857	Inner
			B	6	25 Hz		
V23-0B-1	75	0.1	A	-20	25 Hz	5.282	Inner
			B	6	25 Hz		
V23-0B-2	75	0.1	A	-20	25 Hz	4.515	Inner
			B	6	25 Hz		
V23-0B-3	75	0.7	A	-20	20 Hz	2.511	Inner
			B	6	20 Hz		
V23-0B-4	75	0.7	A	-20	25 Hz	2.547	Inner
			B	6	25 Hz		
V23-2A-1	75	0.1	A	-20	30 Hz	5.116	Wrapper
			B	6	30 Hz		
V23-2A-2	75	0.1	A	-20	30 Hz	4.735	Wrapper
			B	6	30 Hz		
V23-2A-3	75	0.7	A	-20	30 Hz	2.894	Wrapper
			B	6	30 Hz		
V23-2A-4	75	0.7	A	-20	30 Hz	2.878	Wrapper
			B	6	30 Hz		

ASTM E647

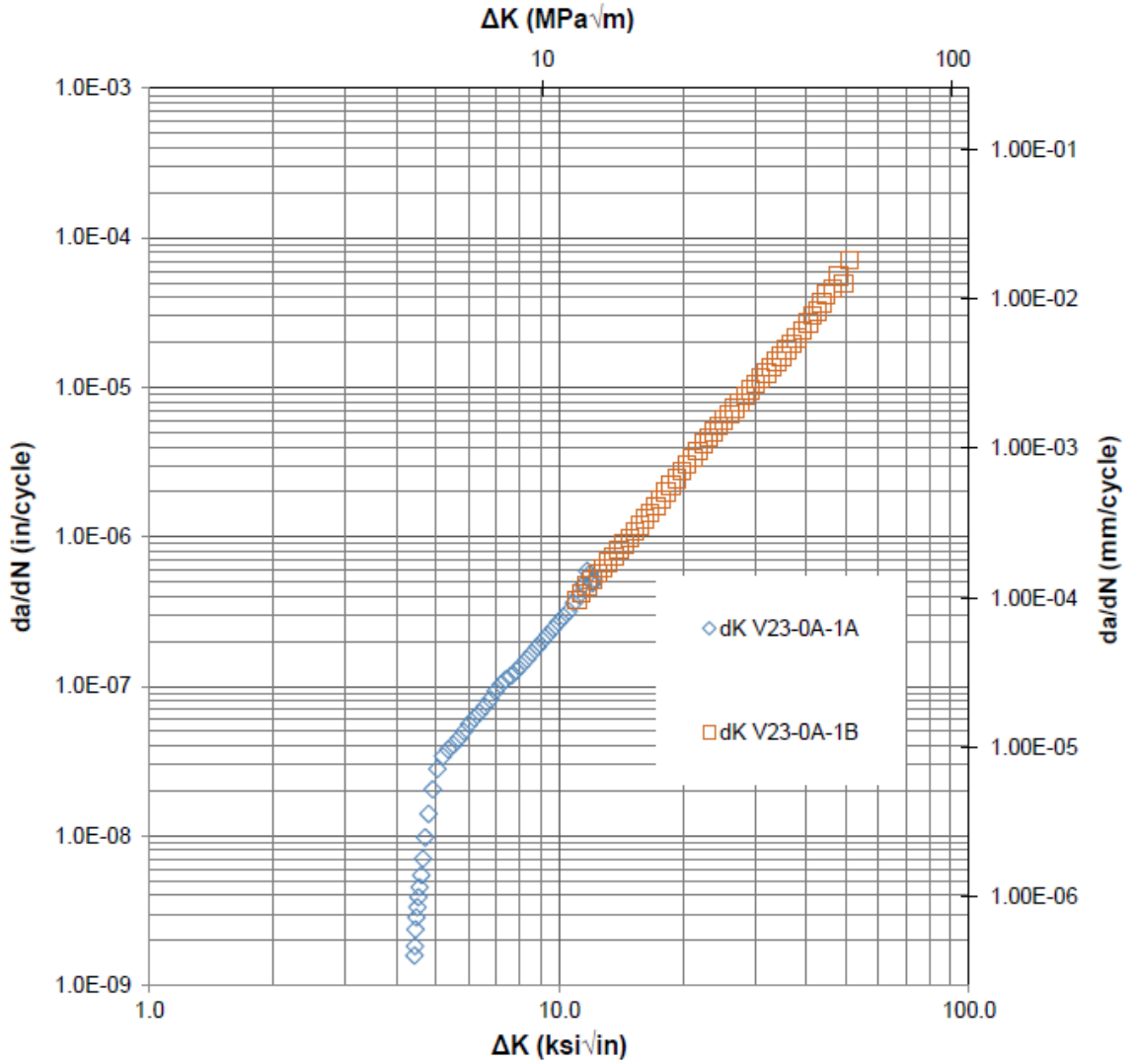


Figure 7.3.1.3.4-1: V0023-0A-1A/1B Plot R = 0.1

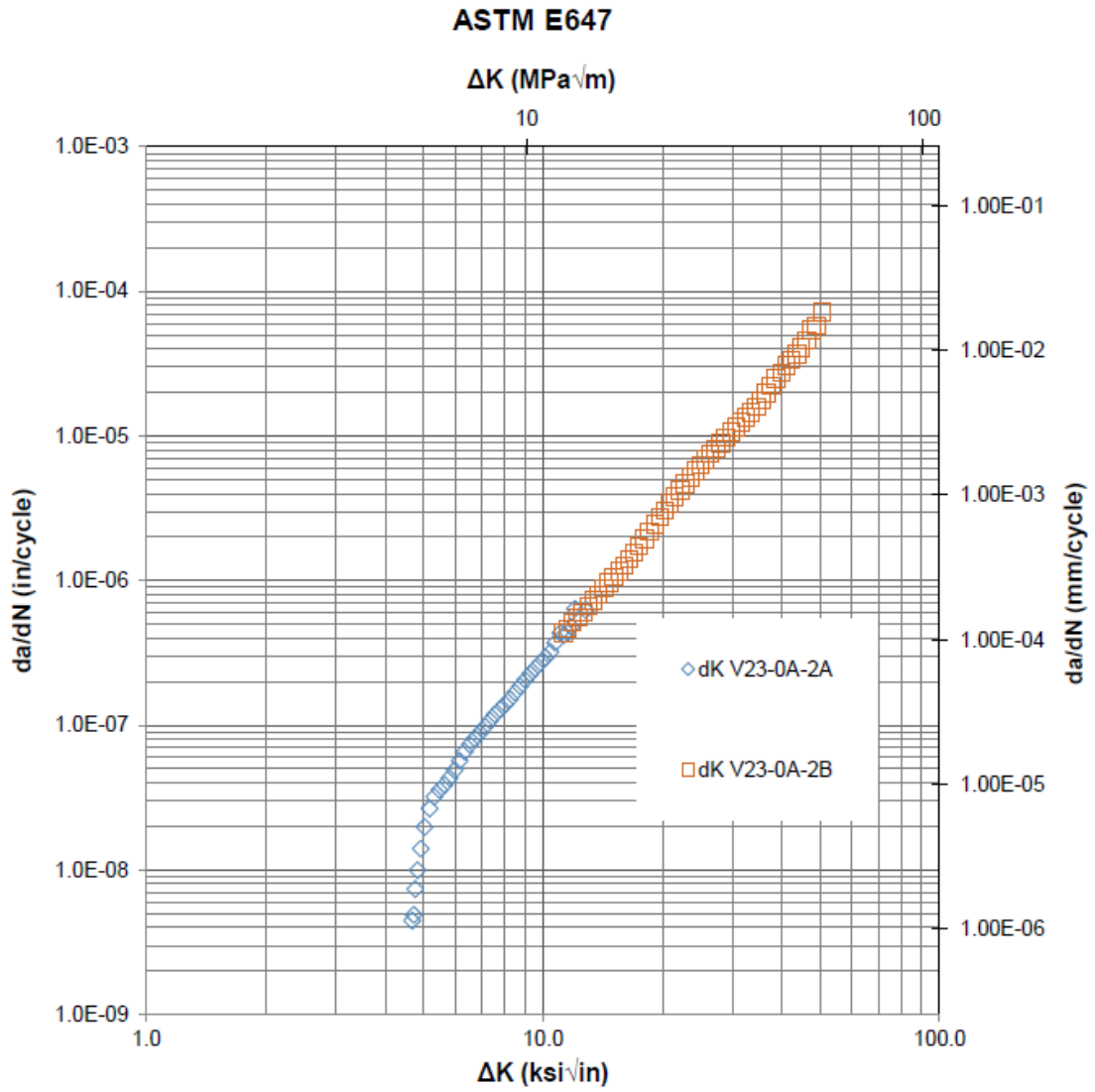


Figure 7.3.1.3.4-2: V0023-0A-2A/2B Plot R = 0.1

ASTM E647

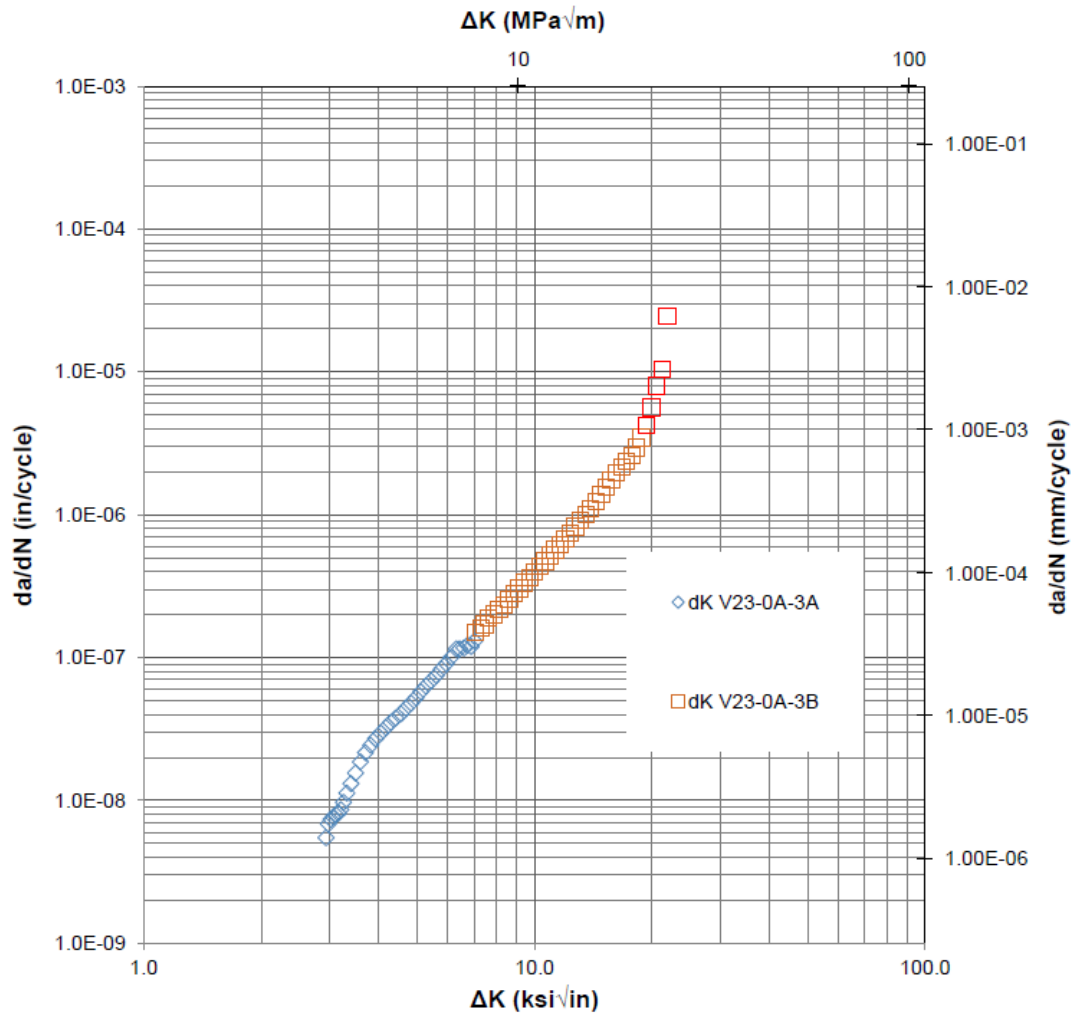


Figure 7.3.1.3.4-3: V0023-0A-3A/3B Plot R = 0.7

ASTM E647

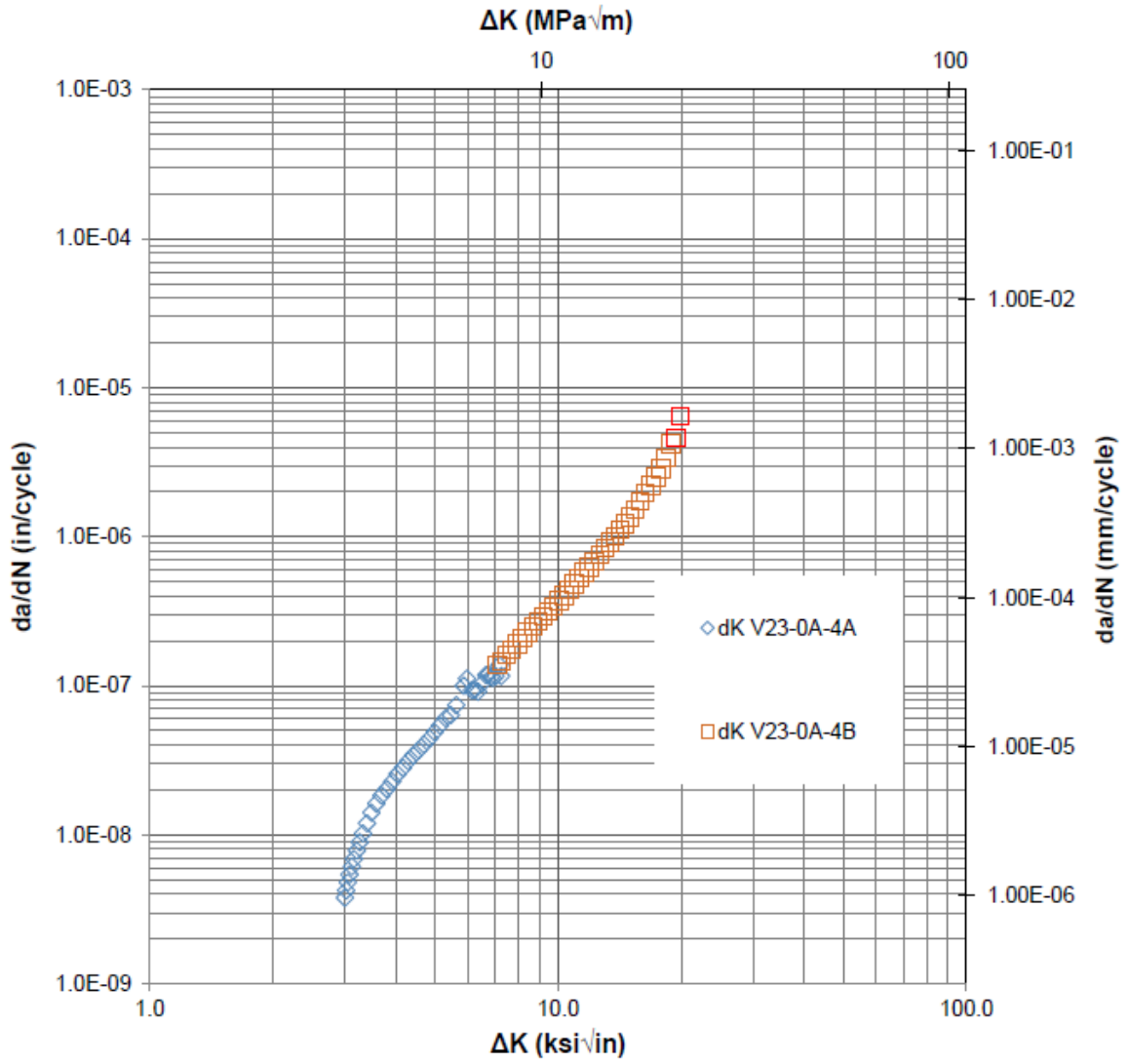


Figure 7.3.1.3.4-4: V0023-0A-4A/4B Plot R = 0.7

ASTM E647

ΔK (MPa \sqrt{m})

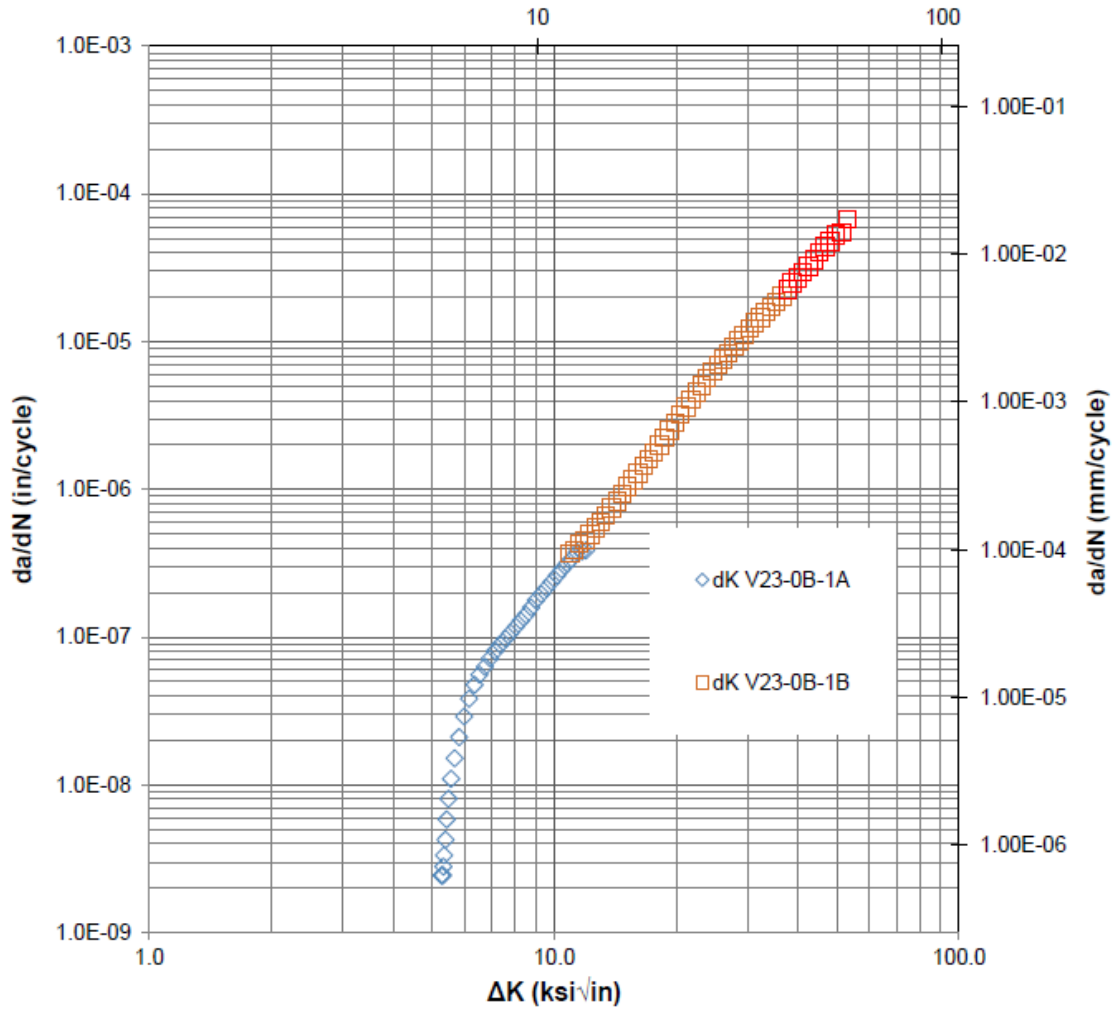


Figure 7.3.1.3.4-5: V0023-0B-1A/1B Plot R=0.1

ASTM E647

ΔK (MPa \sqrt{m})

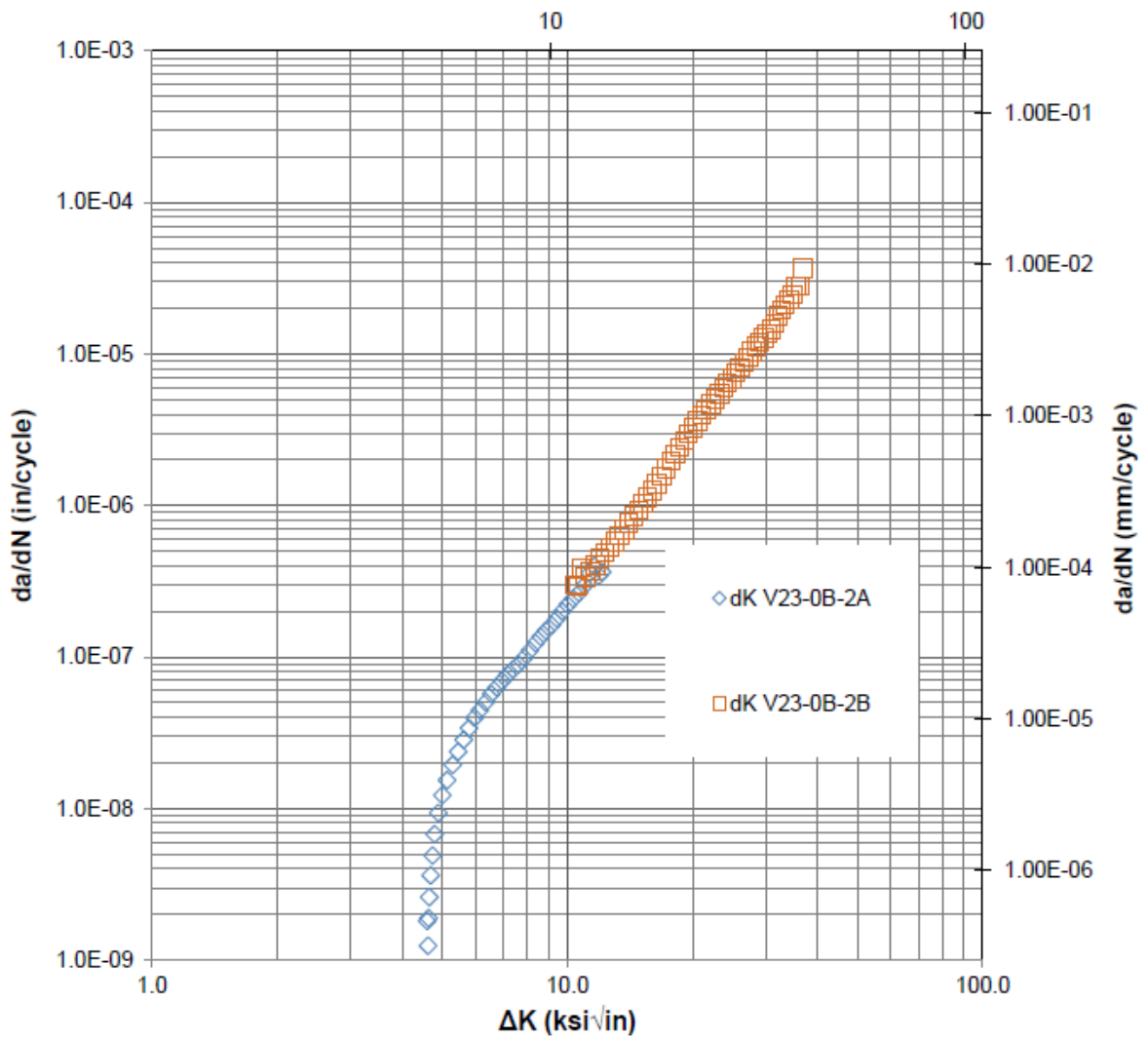


Figure 7.3.1.3.4-6: V0023-0B-2A/2B Plot R = 0.1

ASTM E647

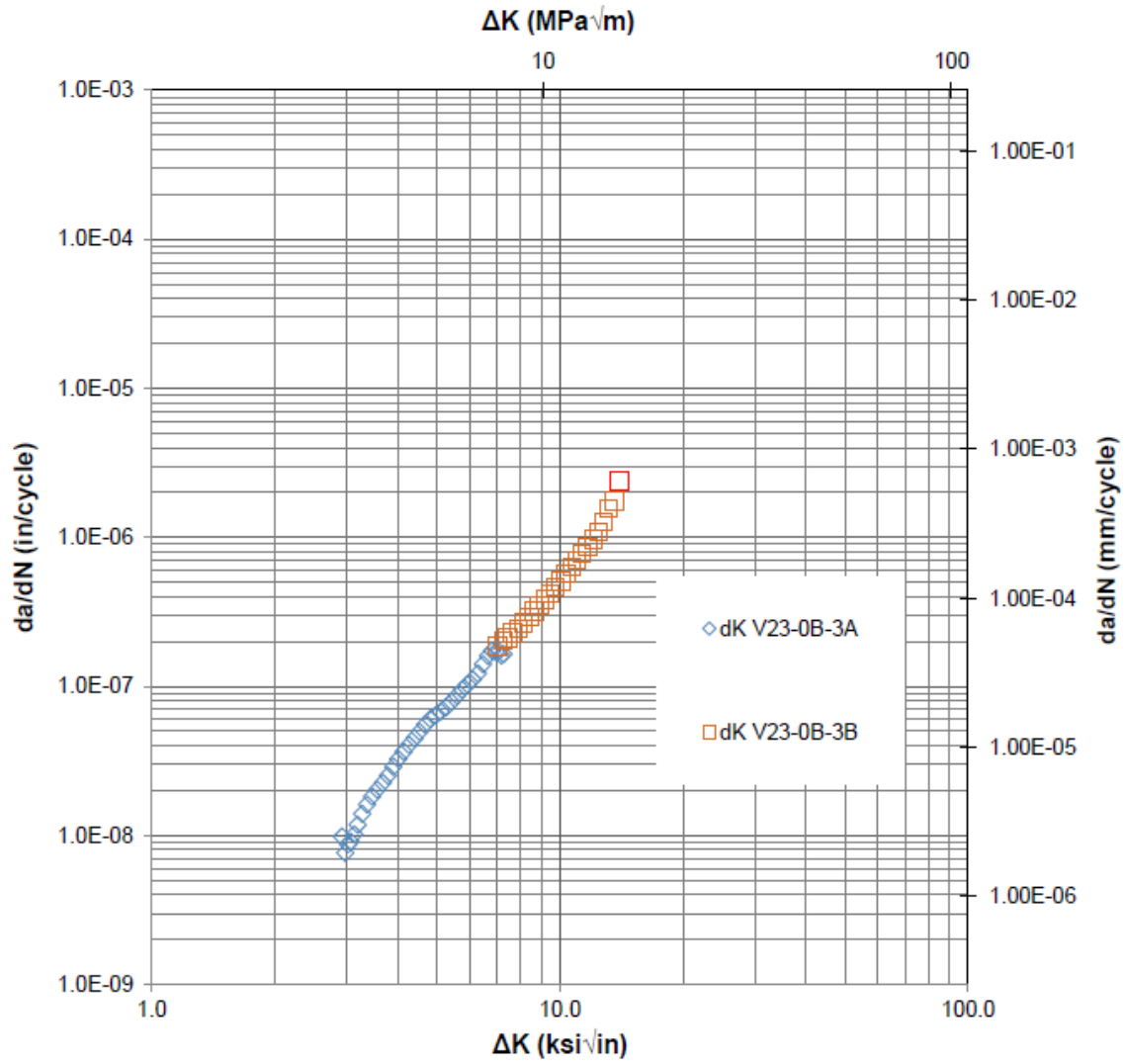


Figure 7.3.1.3.4-7: V0023-0B-3A/3B Plot R = 0.7

ASTM E647

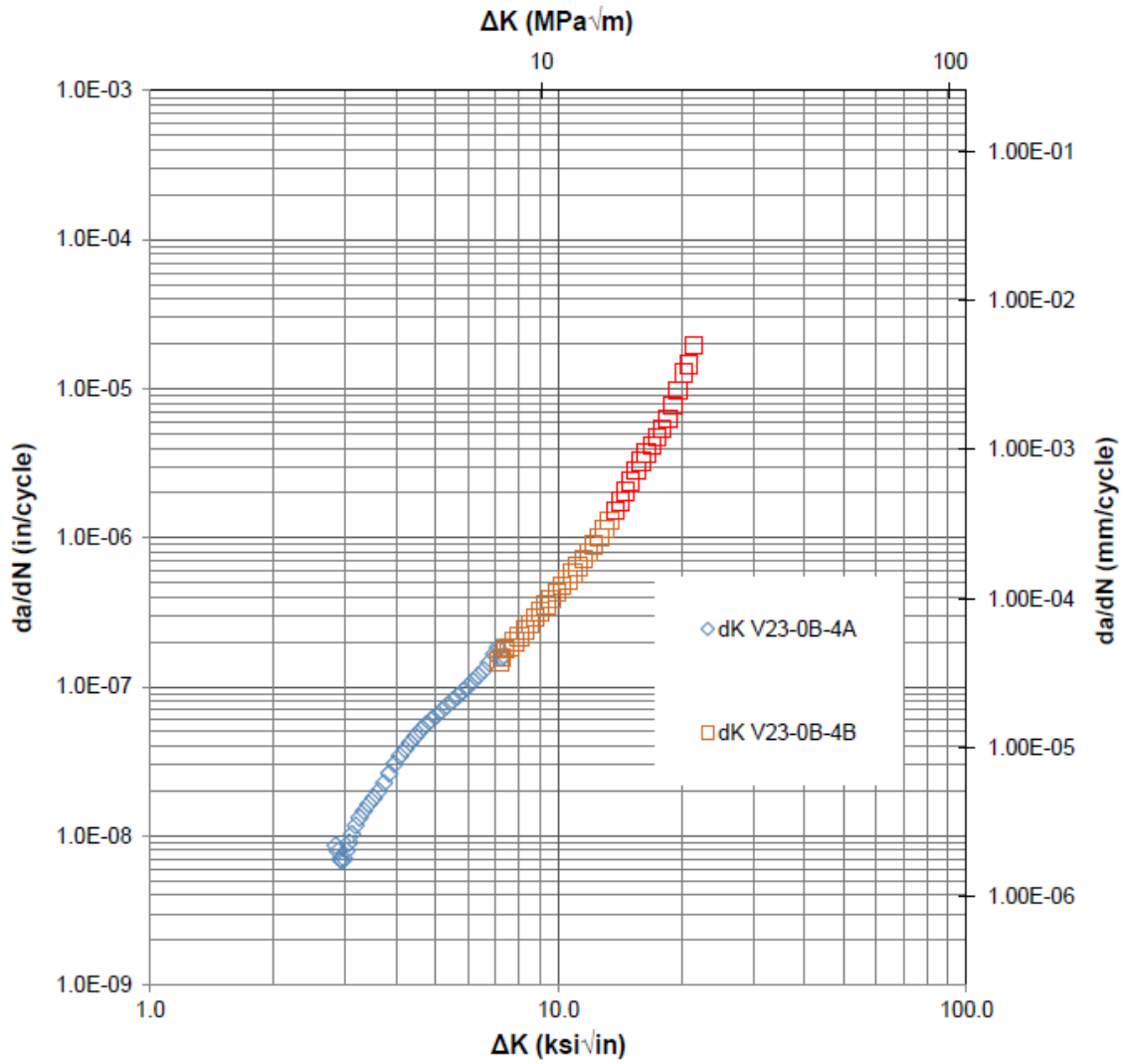


Figure 7.3.1.3.4-8: V0023-0B-4A/4B Plot R = 0.7

ASTM E647

ΔK (MPa \sqrt{m})

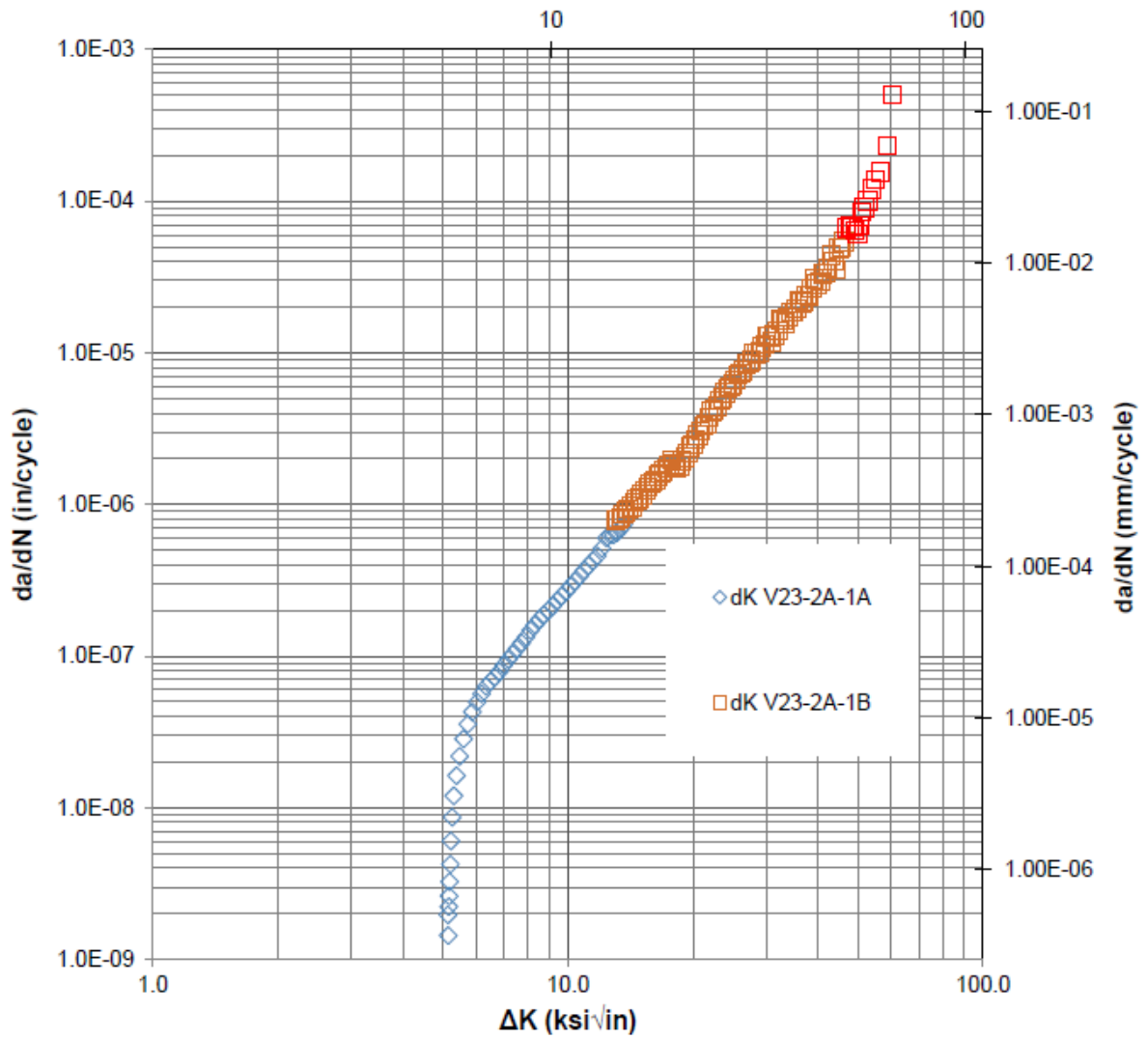


Figure 7.3.1.3.4-9: V0023-2A-1A/1B Plot R = 0.1

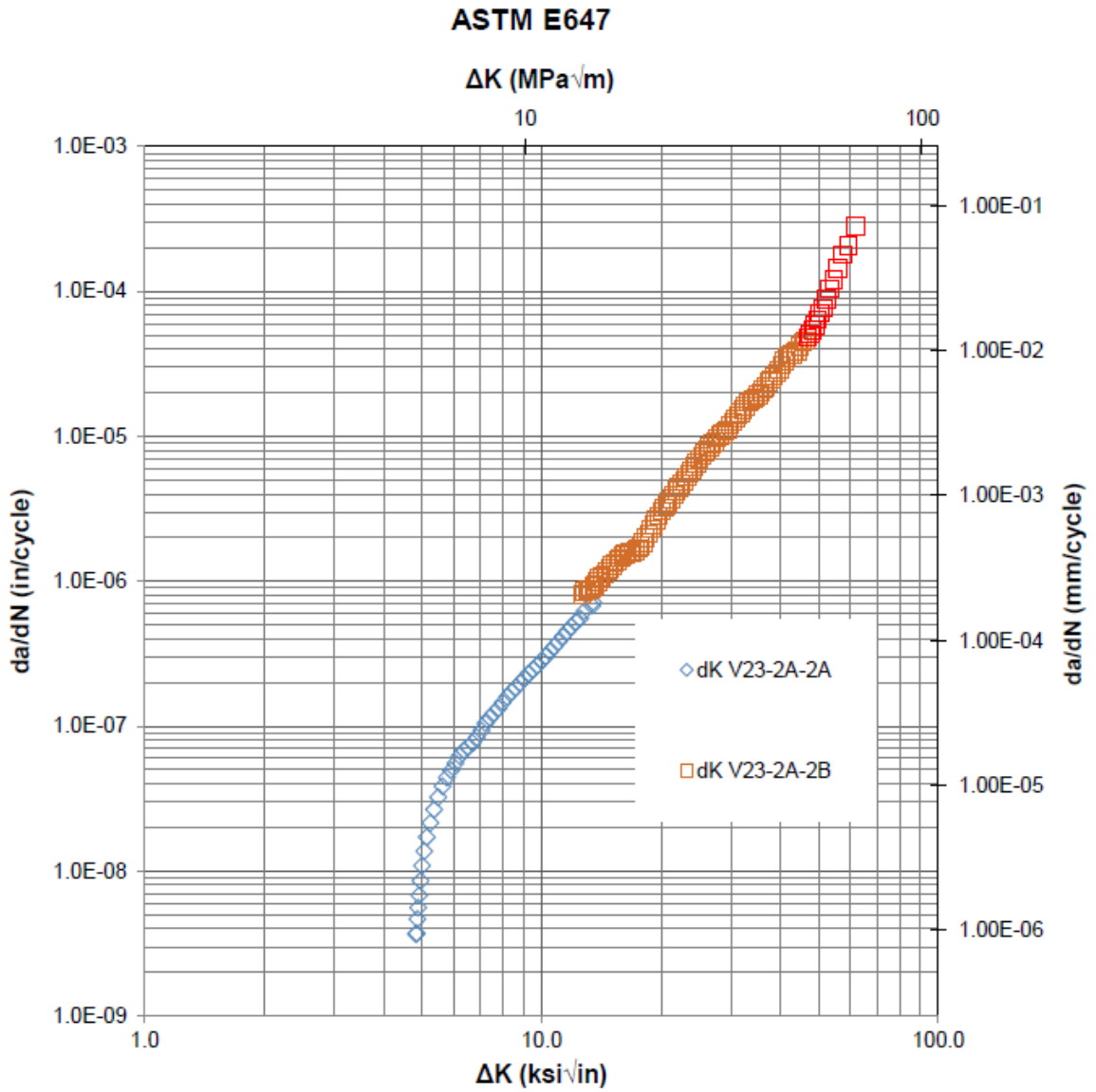


Figure 7.3.1.3.4-10: V0023-2A-2A/2B Plot R = 0.1

ASTM E647

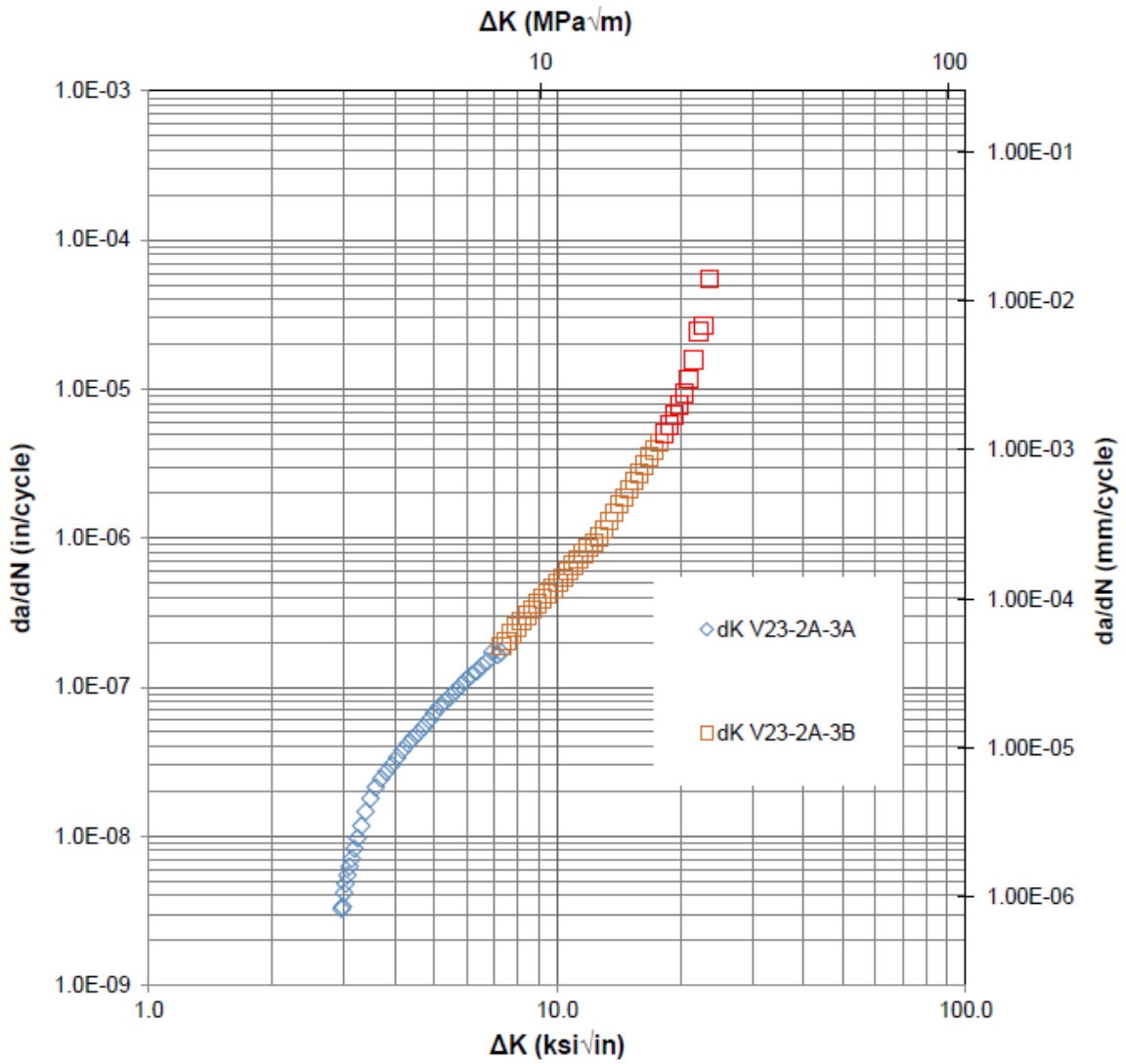


Figure 7.3.1.3.4-11: V0023-2A-3A/3B Plot R = 0.7

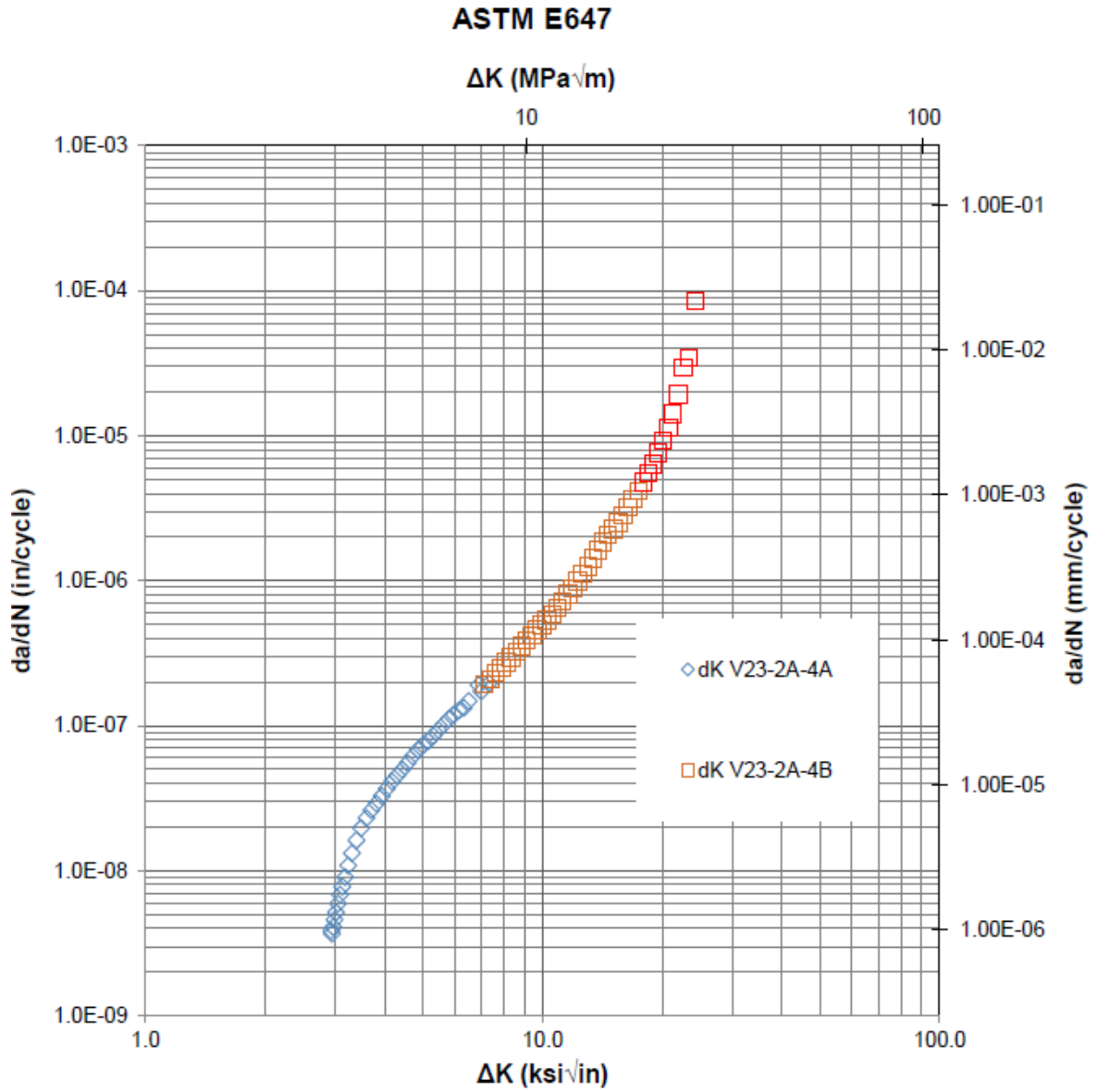


Figure 7.3.1.3.4-12: V0023-2A-4A/4B Plot R = 0.7

7.3.1.3.5 Charpy Impact

Charpy impact tests were not performed on this material.

7.3.2 1143

1143 is a commonly used steel in LPVs constructed in the early 1960s. It is typically used as an inner shell material. All NASA LPVs containing 1143 (59) were constructed by CB&I.

7.3.2.1 Chemical Composition

Table 7.3.2.1-1 provides the chemistry listed in the material specification.

Table 7.3.2.1-1: CB&I 1143 Material Chemistry Specification (59)

Chemistry (%)							
Material	C	Si	Mn	P	S	Ni	V
CB&I 1143	0.18-0.25	0.2-0.35	1.1-1.5	0-0.04	0-0.05	0.4-0.7	0.1-XX

Table 7.3.2.1-2 provides chemistry data collected from mill certifications of LPVs at MSFC. CB&I was the manufacturer of all LPVs investigated.

Table 7.3.2.1-2: Manufacturer Mill Certification Chemistry

Melt/Heat	Cert Origin	C	Mn	P	S	Si	Ni	V
35L429	US Steel	0.22	1.43	0.013	0.029	0.31	0.58	0.15
58L144	US Steel	0.23	1.42	0.018	0.023	0.25	0.55	0.17
69L332	US Steel	0.23	1.48	0.011	0.018	0.32	0.68	0.13
N14159	US Steel	0.23	1.38	0.01	0.015	0.22	0.57	0.15
82L709	US Steel	0.22	1.32	0.015	0.023	0.22	0.55	0.14
58L393	US Steel	0.23	1.29	0.012	0.022	0.24	0.6	0.15
581416	US Steel	0.22	1.4	0.013	0.021	0.23	0.53	0.14
58L144	US Steel	0.23	1.42	0.018	0.023	0.25	0.55	0.17
58L393	US Steel	0.23	1.29	0.012	0.022	0.24	0.6	0.15
N52335	US Steel	0.23	1.37	0.01	0.011	0.29	0.6	0.15
633906	US Steel	0.23	1.37	0.017	0.025	0.27	0.65	0.16
583274	US Steel	0.22	1.34	0.011	0.022	0.26	0.56	0.17
613215	US Steel	0.22	1.33	0.014	0.02	0.26	0.61	0.16
105208	US Steel	0.2	1.38	0.032	0.019	0.2	0.65	0.25
11786	US Steel	0.23	1.44	0.02	0.019	0.26	0.6	0.14
831955	US Steel	0.25	1.4	0.009	0.018	0.28	0.57	0.16
11786	US Steel	0.23	1.44	0.02	0.019	0.26	0.6	0.14
613215	US Steel	0.22	1.33	0.014	0.02	0.26	0.61	0.16
633906	US Steel	0.23	1.37	0.017	0.025	0.27	0.55	0.16
831955	US Steel	0.25	1.4	0.009	0.018	0.28	0.57	0.16
69L332	US Steel	0.23	1.48	0.011	0.018	0.32	0.68	0.13
N14159	US Steel	0.23	1.38	0.01	0.015	0.22	0.57	0.15
581416	US Steel	0.22	1.4	0.013	0.021	0.23	0.53	0.14
69L332	US Steel	0.23	1.48	0.011	0.018	0.32	0.68	0.13
N14954	US Steel	0.24	1.45	0.014	0.016	0.28	0.65	0.15

Table 7.3.2.1-3 provides chemistry data collected from Arc Spark analyses of vessels at MSFC.

Table 7.3.2.1-3: V0125 1143 Inner Layer Chemistry Data

Material	Vessel	Chemistry (%)											
		C	Si	Mn	P	S	Cr	Mo	Ni	Cu	Nb	V	B
1143 Inner	V125	0.26	0.28	1.35	0.025	0.028	0.071	0.013	0.5	0.026	0.003	0.13	0.0005

7.3.2.2 Metallography

Metallography studies were not performed on this material.

7.3.2.3 Mechanical Properties

Table 7.3.2.3-1 provides minimum values listed in the material specification (59)

Table 7.3.2.3-1: 1143 Standard Mechanical Properties (59)

Material	Thickness (heads)	σ_{YS} (ksi)	U_{TS} (ksi)	Elong. (%)
CB&I 1143	0.18" \geq t \leq 0.375"	75	90	22
CB&I 1143	0.375" $>$ t \leq 0.580"	70.5	85	22

Table 7.3.2.3-2 provides results obtained from mill certifications from all the vessels available at MSFC using 1143 material.

Table 7.3.2.3-2: Mill Certification Mechanical Properties

Melt/Heat	Yield Stress (ksi)	Tensile Stress (ksi)	Fracture Elongation (%)
35L429	90	118	31
58L144	78	94	46
69L332	73	93	41
N14159	79	94	42
82L709	78	99	24
58L393	75	93	40
581416	79	101	41
58L144	77	93	46
58L393	78	96	44
N52335	76	96	21
633906	81	99	40
583274	83	100	41
613215	76	101	40
105208	83	99	46
11786	74	101	35
831955	78	99	38
11786	76	106	34
613215	77	101	37
633906	79	102	29
831955	73	98	39
69L332	73	93	41
N14159	79	94	42
581416	86	102	42
69L332	80	97	34
N14954	81	98	42

7.3.2.3.1 Smooth Tensile Tests

Smooth tensile tests were conducted at MSFC on round specimens according to ASTM E8, “Standard Test Methods for Tension Testing of Metallic Materials” (51) using specimen design S-219 Rev A. The mechanical test frame consisted of a servo-hydraulic actuator and reaction frame. The frame used an LVDT for displacement feedback. Stress measurements were derived from load measurements and the initial specimen measurements. Strain measurements were derived from an extensometer and the initial specimen measurements.

The results obtained from testing of 1143 from vessel V0125 are presented in Table 7.3.2.3.1-1. A typical engineering stress-strain curve is shown in Figure 7.3.2.3.1-1. Note that final fracture elongation is unknown due to saturation of the extensometer.

Table 7.3.2.3.1-1: V0125 1143 Inner Layer Tensile Data

Specimen ID	Test Temp. (°C)	ASTM Orientation	Tensile Stress	Yield Stress (ksi)	Fracture Elongation
CP-344-3-7	21	T	94.1	71.3	N/A
CP-344-3-8	21	T	94.7	72.7	N/A
CP344-4-76	21	L	93.0	68.9	N/A
CP344-4-77	21	L	93.8	69.2	N/A
CP344-4-78	21	L	92.6	68.8	N/A
CP344-4-79	21	L	95.5	71.0	N/A
CP344-4-84	21	T	94.5	70.4	N/A
CP344-4-85	21	T	93.7	69.0	N/A
CP344-4-86	21	T	94.9	70.0	N/A
CP344-4-87	21	T	93.2	69.3	N/A

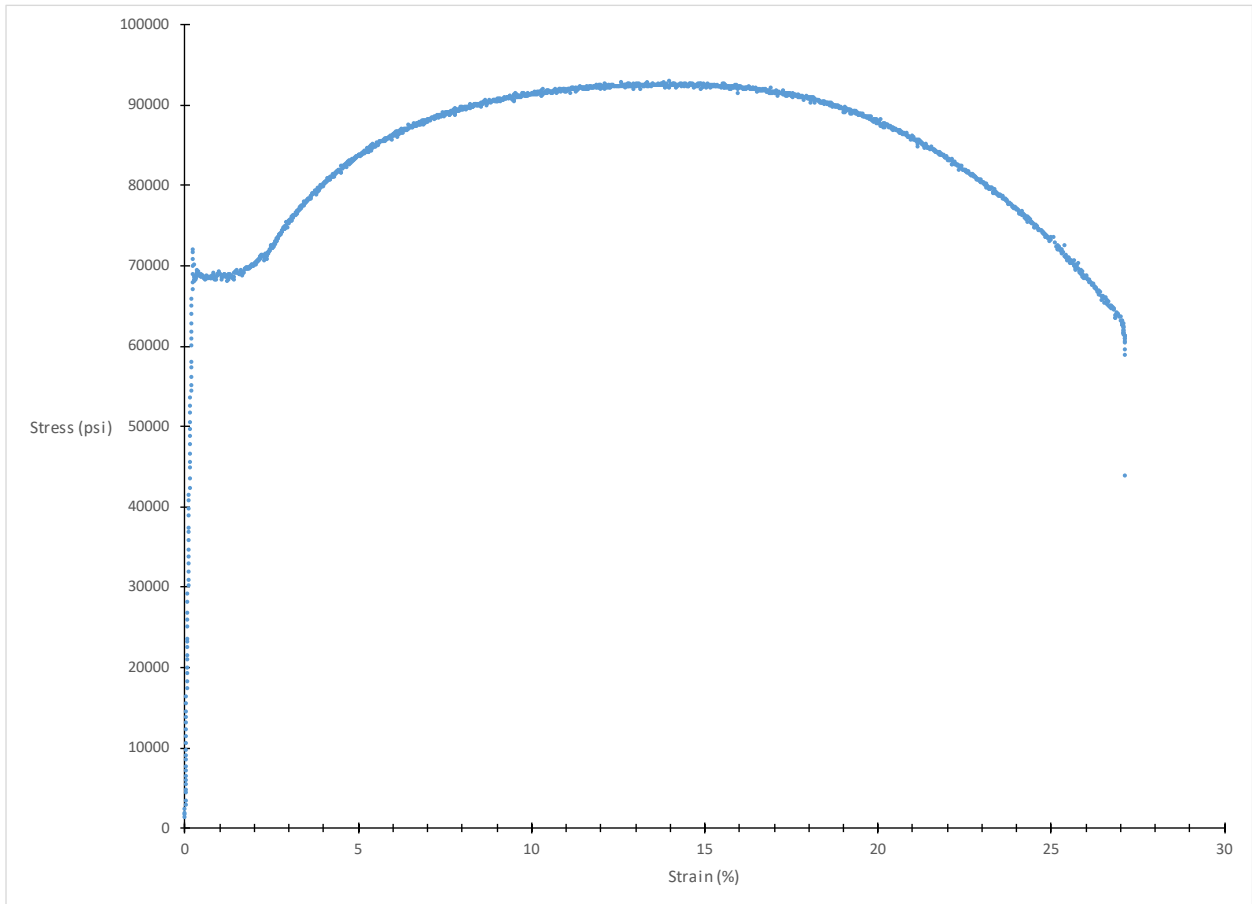


Figure 7.3.2.3.1-1: V0125 1143 Smooth Specimen Tensile Plot for Sample CP344-4-76

7.3.2.3.2 Notch Tensile Test

Notch tensile tests were not conducted on this material.

7.3.2.3.3 Fracture Properties

All room temperature testing was performed in accordance with ASTM E1820 (10). Testing at all other temperatures was performed in accordance with ASTM E1921 (7). Testing for both standards used specimen design S-226 Rev A. All 1143 fracture tests came from vessel V0125 and were tested with the crack plane in the T-L orientation as defined by ASTM (C-L vessel orientation). The specimens used were ASTM E1820 compact specimens (C(T)) with $W = 1.0$ inches and $B = 0.5$ inch, $a/W = 0.5$ and all specimens were side grooved to a total thickness reduction of 20%. The cutting diagram used to remove the C(T) specimens from the V0125 inner layer is shown in Figure 7.3.2.3.3-1.

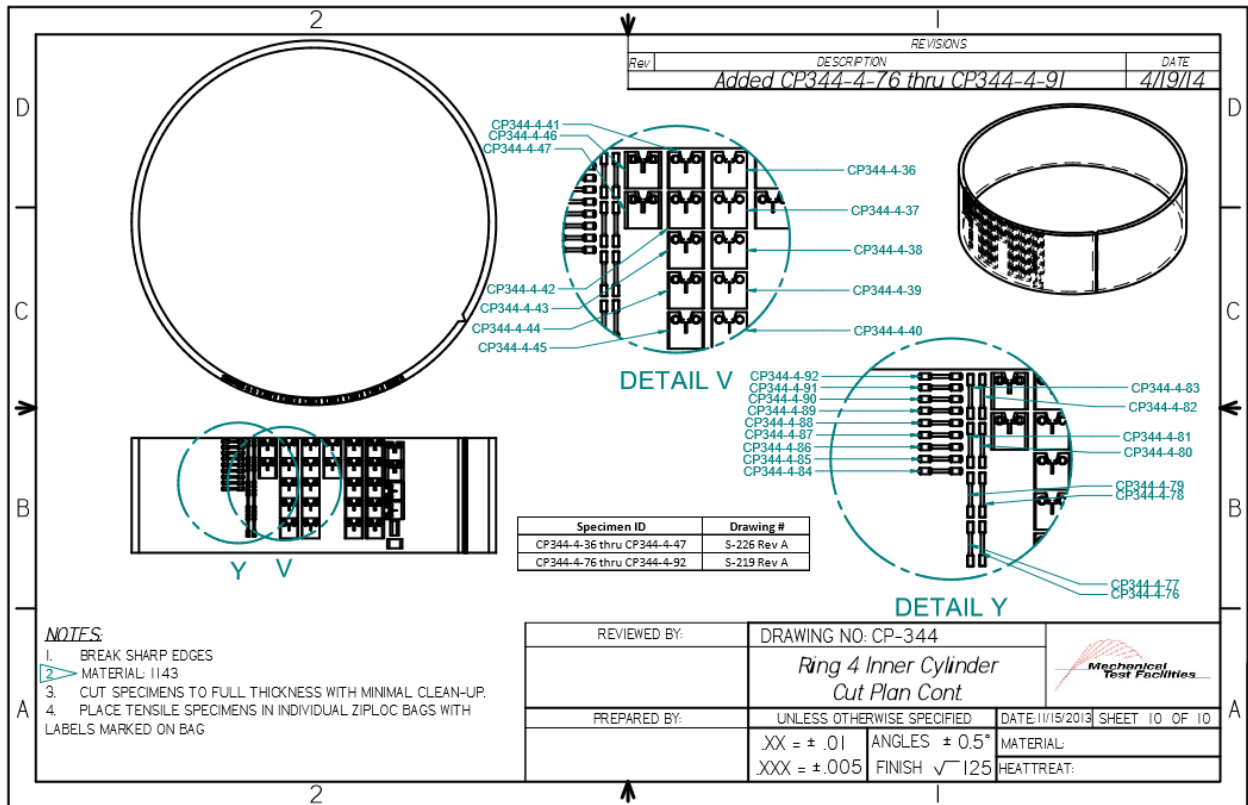


Figure 7.3.2.3.3-1: Cut Plan for V0125 Inner Specimens

The following test data are raw values obtained from fracture tests conducted on V0348 A212 head material. Test results that are considered upper shelf are listed under ASTM E1820, while transition temperature test results are listed under E1921. Tests that meet the complete validity requirements for $J_q = J_{1C}$ and $K_{Jq} = K_{J1C}$ are denoted with an asterisk. Despite invalidities, J_q and K_{Jq} convey valuable fracture toughness information, especially when the test results are applied directly to the sample material source.

Table 7.3.2.3.3-1: 1143 Fracture Data V03487

Specimen ID	Test Temp. (°C)	ASTM Crack Plane Orientation	W (in)	a ₀ (in)	a _f (in)	B ₀ (in)	B _N (in)	J _q (kJ/m ²)	K _{Jq} (MPa√m)	K _{JcIT} (MPa√m)	ASTM Standard
CP344-4-43	28	T-L	1.0002	0.4939	0.6169	0.3742	0.2896	74	129	---	E1820
CP-344-3-2	22	T-L	1.0002	0.5958	0.6765	0.3765	0.3010	66	121	---	E1820
CP-344-3-1	21	T-L	1.0012	0.6115	0.6761	0.3773	0.2990	57	113	---	E1820
CP344-4-3	21	L-T	0.9994	0.4810	0.5704	0.3755	0.2963	248	235	---	E1820
CP344-4-4	21	L-T	1.0002	0.4939	0.5954	0.3748	0.2956	230	227	---	E1820
CP344-4-6	21	T-L	1.0006	0.4901	0.6264	0.3752	0.2999	89	141	---	E1820
CP-344-3-3	-46	T-L	1.0006	0.6618	0.7419	0.3770	0.3032	80	134	---	E1820
CP344-4-27	-83	T-L	1.0014	0.5027	0.6233	0.3740	0.2875	73	128	---	E1820
CP344-4-26	-86	T-L	1.0003	0.5009	0.6198	0.3752	0.2706	70	125	---	E1820
CP344-4-17	-29	T-L	1.0003	0.4889	0.7888	0.3770	0.2893	58	114	93	E1921
CP344-4-18	-57	T-L	1.0010	0.4914	0.7649	0.3767	0.2886	69	125	102	E1921
CP344-4-23	-85	T-L	1.0011	0.4909	0.5359	0.3748	0.2885	38	92	76	E1921
CP344-4-19	-85	T-L	1.0013	0.4960	0.5940	0.3743	0.2842	70	125	102	E1921
CP344-4-22	-85	T-L	1.0009	0.4934	0.5228	0.3752	0.2931	42	96	80	E1921
CP344-4-20	-85	T-L	1.0010	0.4943	0.6498	0.3757	0.2921	61	117	96	E1921
CP344-4-24	-112	T-L	1.0009	0.5012	0.5012	0.3748	0.2884	20	67	57	E1921
CP344-4-25	-112	T-L	1.0006	0.4902	0.4902	0.3762	0.2913	39	94	78	E1921
CP344-4-42	-113	T-L	0.9992	0.4892	0.4892	0.3743	0.2913	16	60	51	E1921
CP344-4-44	-113	T-L	1.0007	0.4922	0.4922	0.3735	0.2988	17	62	53	E1921
CP344-4-28	-113	T-L	1.0010	0.4936	0.4936	0.3742	0.2910	40	95	79	E1921
CP344-4-38	-118	T-L	0.9987	0.4936	0.4936	0.3738	0.2929	10	48	42	E1921
CP344-4-39	-118	T-L	0.9997	0.4893	0.4893	0.3742	0.2902	34	88	73	E1921
CP344-4-41	-118	T-L	1.0005	0.5000	0.5000	0.3753	0.2911	12	52	45	E1921
CP344-4-46	-118	T-L	1.0002	0.4927	0.4927	0.3735	0.2917	18	64	54	E1921
CP344-4-40	-118	T-L	0.9995	0.4911	0.4911	0.3755	0.2931	39	94	78	E1921

Figure 7.3.2.3.3-2 shows a typical load versus crack opening displacement record for an upper shelf E1820 test. The resulting J integral resistance curve (J-R curve) is presented in Figure 7.3.2.3.3-3 which shows the evaluation of J_Q according to E1820.

Results from the 18 E1921 tests are presented in Table 7.3.2.3.3-2 and Table 7.3.2.3.3-3. These results were obtained using the T₀TEM code described in Section 4.2. The T₀ reference temperature for this data set was evaluated as -79°C using the E1921 Master Curve shown in Figure 7.3.2.3.3-4.

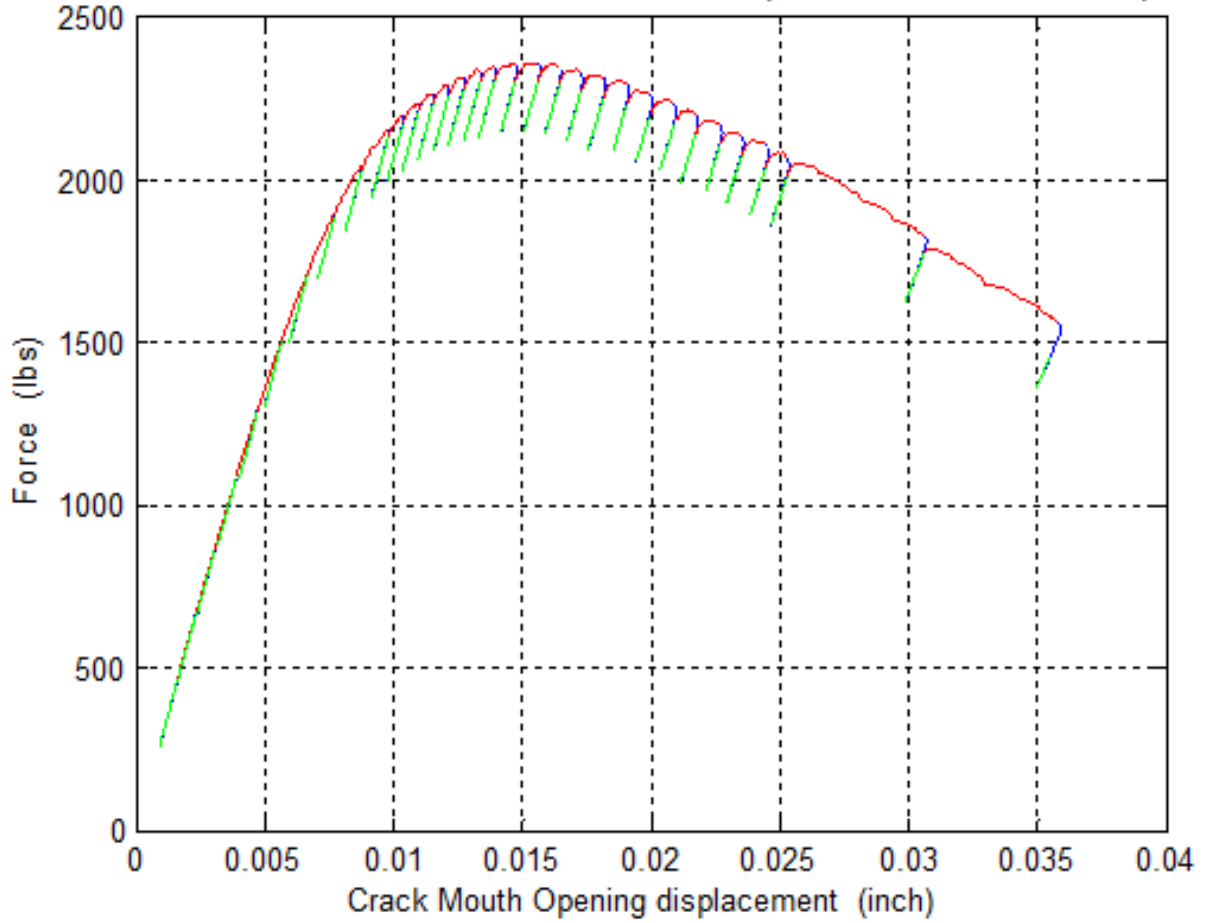


Figure 7.3.2.3.3-2: 1143 Load Versus COD Plot, Sample CP344-4-43

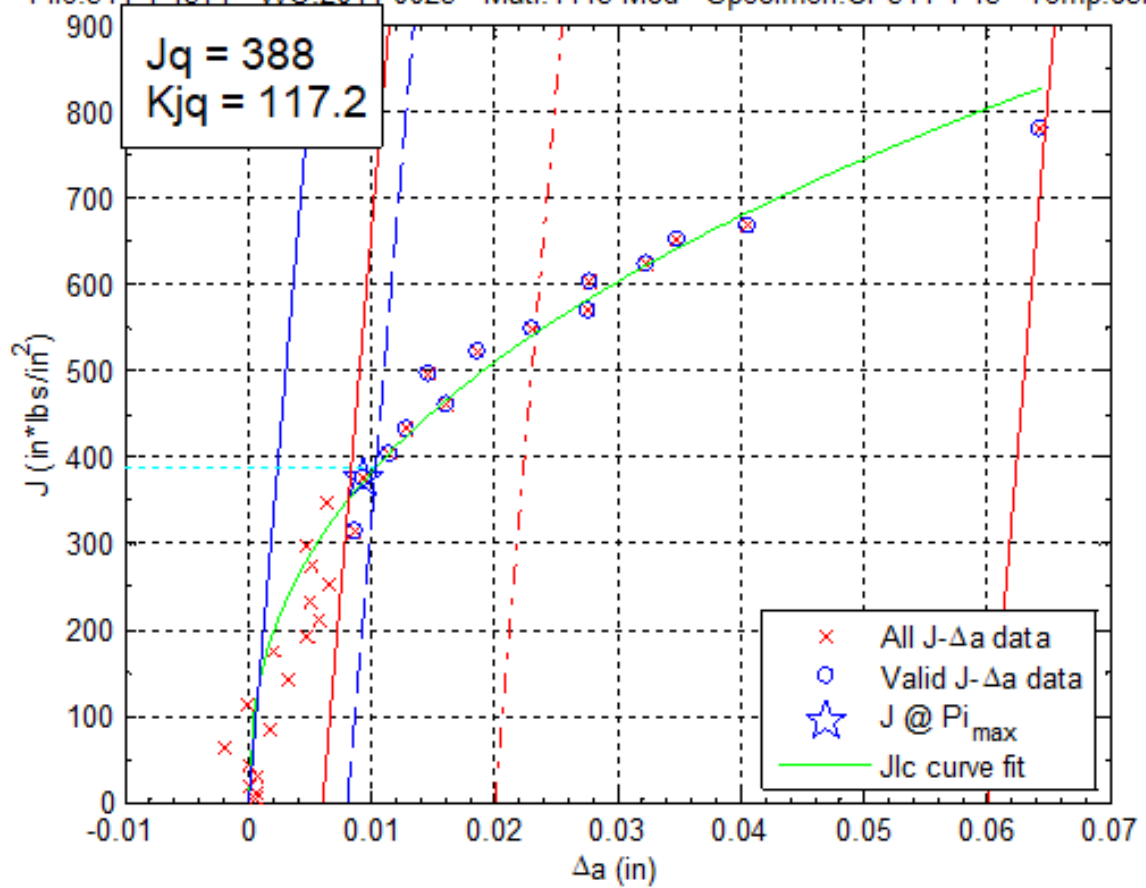


Figure 7.3.2.3.3-3: 1143 J_q Versus Δa Plot, Sample CP344-4-43

Table 7.3.2.3.3-2: V0125 1143 T₀ Individual Specimen Results

Specimen Name	Temperature (°C)	KjcRaw (MPa*m ^{0.5})	1T Data (MPa*m ^{0.5})	Uncensored Data	Test Temp -T0 (°C)
CP-344-3-3	-46	133.9	78.6	0	33
CP344-4-18	-57	124.5	78.6	0	22
CP344-4-19	-85	124.9	78.6	0	-6
CP344-4-20	-85	116.6	78.6	0	-7
CP344-4-22	-85	96.4	78.6	0	-7
CP344-4-23	-85	92.0	76.3	0	-6
CP344-4-24	-112	67.3	57.0	1	-34
CP344-4-25	-112	93.5	77.6	1	-34
CP344-4-26	-86	124.7	78.6	0	-8
CP344-4-27	-83	128.1	78.6	0	-4
CP344-4-28	-113	94.9	78.6	1	-34
CP344-4-38	-118	48.1	42.0	1	-39
CP344-4-39	-118	87.6	72.9	1	-39
CP344-4-40	-118	93.6	77.6	1	-40
CP344-4-41	-118	51.6	44.7	1	-39
CP344-4-42	-113	60.1	51.4	1	-34
CP344-4-44	-113	62.1	52.9	1	-34
CP344-4-46	-118	64.1	54.4	1	-39

Table 7.3.2.3.3-3: V0125 1143 T₀ Calculation Results

Initial T ₀ (°C)	-79
Total Samples	18
Samples within T ₀ ± 50°C (N)	18
Number of Uncensored Data (r)	10
Poisson's Ratio	0.3
Σ(r _i n _i)	1.34
Samples Between T _i - T ₀ 50 to -14 °C	0
Samples Between T _i - T ₀ -15 to -35 °C	5
Samples Between T _i - T ₀ -36 to -50 °C	5
T ₀ scrn (°C)	-62
Homogenous or Inhomogeneous	Homogenous

The results of the E1921 analysis show that the 1143 material removed from the V0125 inner layer is macroscopically homogenous, indicating consistent properties throughout the sampled material. For this data set, the ductile-brittle transition temperature was found to be -79°C. This result also meets the E1921 validity criteria for a sufficient number of samples tested in an appropriate temperature range with $\Sigma(r_i n_i) \geq 1.0$.

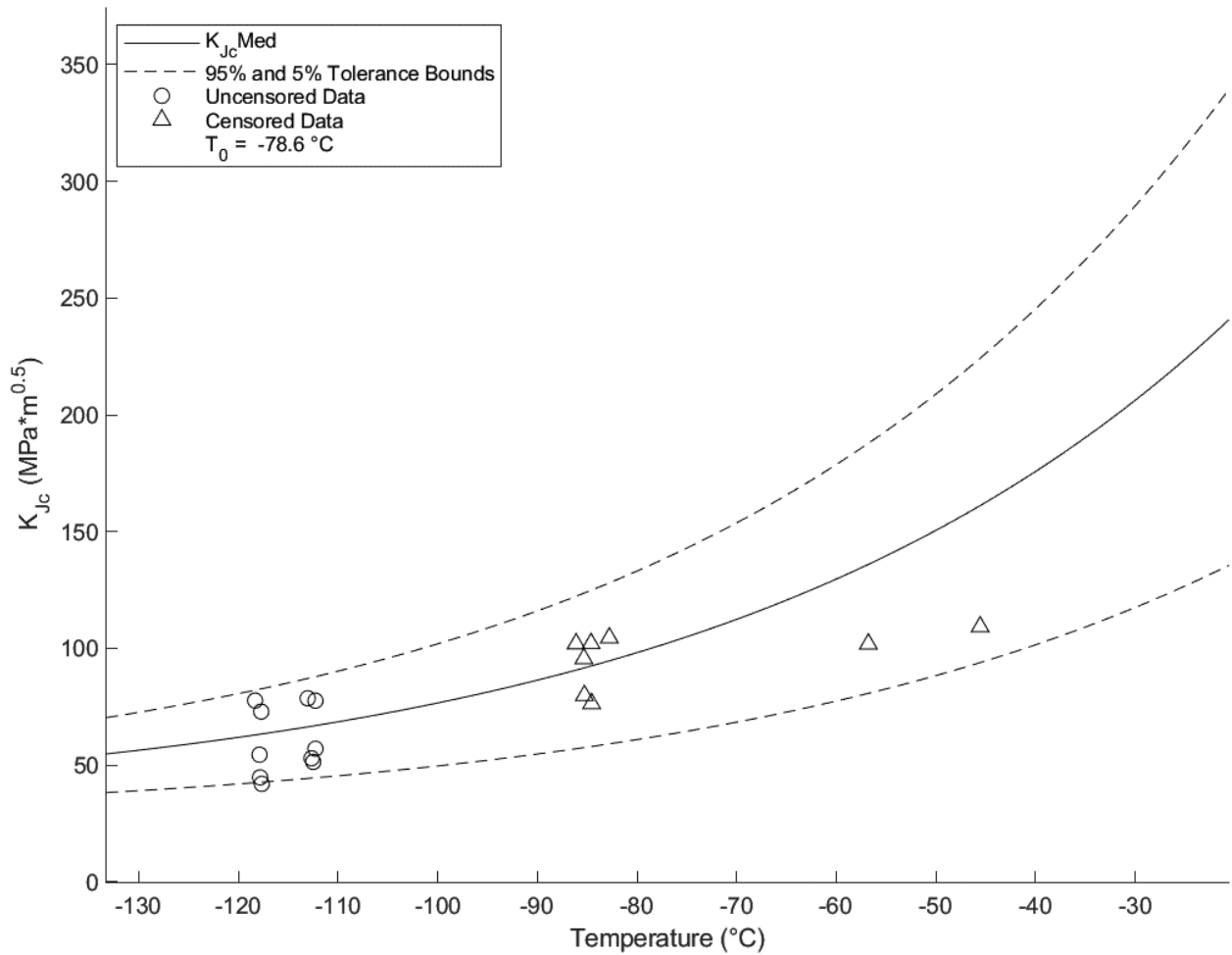


Figure 7.3.2.3.3-4: V0125 1143 T₀ Plot

7.3.2.3.4 Fatigue Crack Growth

Fatigue crack growth tests were not performed on this material.

7.3.2.3.5 Charpy Impact

Charpy impact tests were conducted on V0125 inner layer material by Westmoreland Mechanical Testing and Research Incorporated (60) in accordance with ASTM E23 (17).

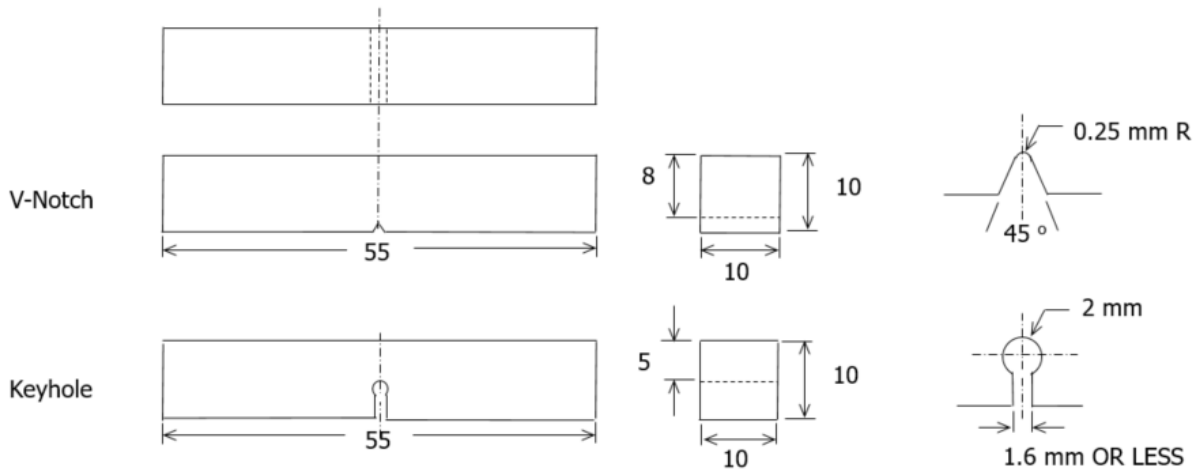


Figure 7.3.2.3.5-1: V0125 Charpy Cut Plan

Table 7.3.2.3.5-1: V0125 1143 Charpy Data

Westmoreland Mechanical Testing & Research, Inc.
WMT&R Report No. 3-55107
2-Apr-13

Impact Results: ASTM E23-12c
 Material: MLP 1143 MOD
 Sample Type: Charpy V-Notch

Sample	Test Log No.	Sample Size	Temp. F	Energy ft-lbs	Mils Lat Exp	% Shear Fracture	A\U\R
CVN-3	S36920	Standard	-40	23	22	5	Report
CVN-4	S36921	Standard	-40	18	16	5	Report
CVN-1	S36918	Standard	74	23	25	5	Report
CVN-2	S36919	Standard	74	24	25	5	Report

Impact Results: ASTM E23-12c
 Material: MLP 1143 MOD
 Sample Type: Charpy Keyhole

Sample	Test Log No.	Sample Size	Temp. F	Energy ft-lbs	A\U\R
Keyhole-3	S36924	Standard	-40	16	Report
Keyhole-4	S36925	Standard	-40	16	Report
Keyhole-1	S36922	Standard	74	17	Report
Keyhole-2	S36923	Standard	74	17	Report

Impact Results: ASTM E23-12c
 Material: MLP 1143 MOD
 Sample Type: Charpy V-Notch

Sample	Test Log No.	Sample Size	Temp. F	Energy ft-lbs	Mils Lat Exp	% Shear Fracture
CVN-1	S36918	Standard	74	23	25	5



Figure 7.3.2.3.5-2: V0125 1143 V-Notch Charpy Fracture Surface 74°F

Impact Results: ASTM E23-12c
 Material: MLP 1143 MOD
 Sample Type: Charpy V-Notch

Sample	Test Log No.	Sample Size	Temp. F	Energy ft-lbs	Mils Lat Exp	% Shear Fracture
CVN-4	S36921	Standard	-40	18	16	5



Figure 7.3.2.3.5-3: V0125 1143 V-Notch Charpy Fracture Surface -40°F

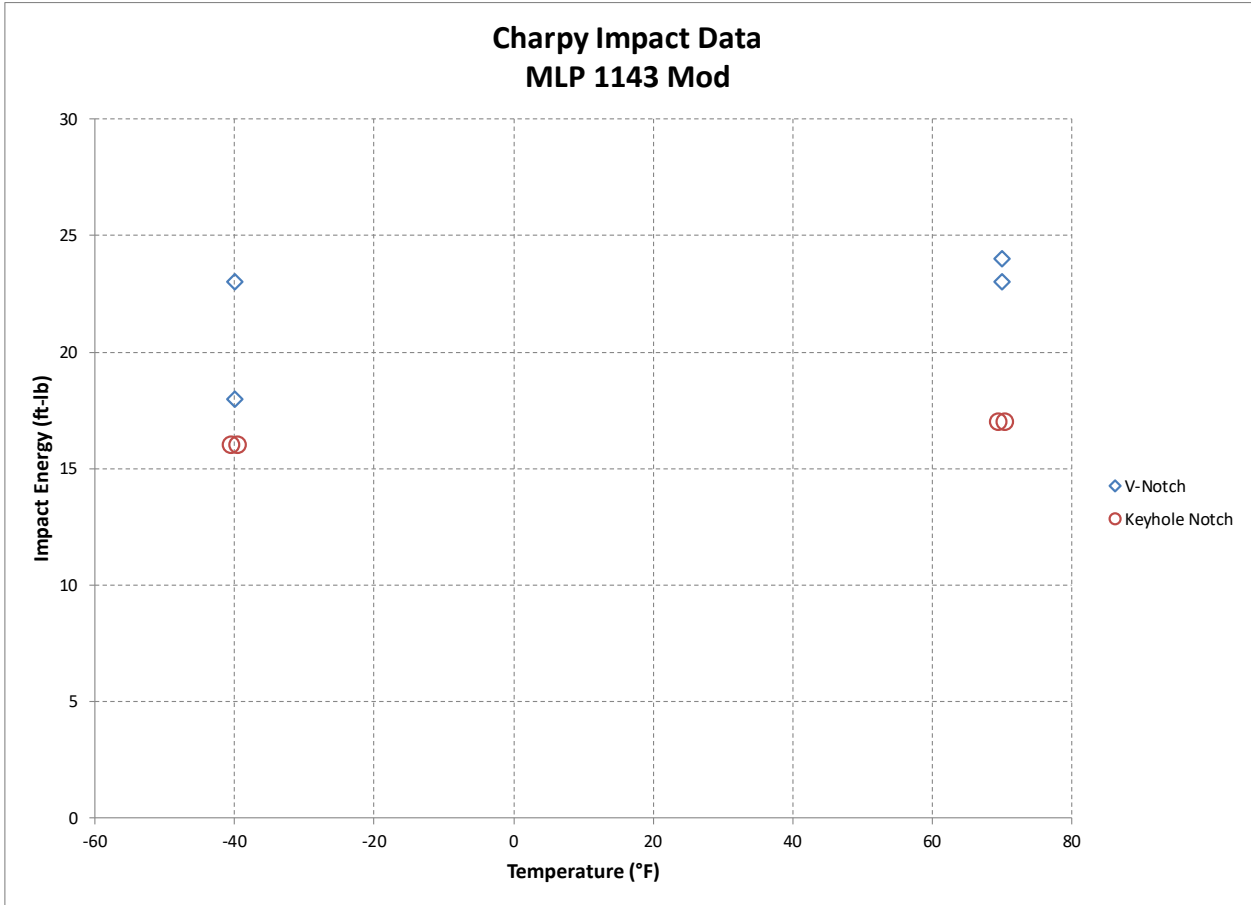


Figure 7.3.2.3.5-4: V0125 1143 Charpy Plot

The results of the Charpy impact tests show a drop in impact energy and lateral expansion from the room temperature tests to the -40°F tests. This is expected as the material is tested at colder temperatures. Too few specimens were tested to accurately compile a transition curve from this data, and therefore the newer E1921 Master Curve transition temperature is recommended for use when establishing fracture toughness values and critical operating temperatures.

7.3.3 T-1/A517

T-1 steel, designated as ASTM-517, is used as both a head and shell material in LPVs. The vessel investigated in this instance is V0066 and was constructed of T-1 steel for both the head and shell. By examining the chemistry on both the head and shell, the material is determined to be ASTM A517 Grade F for both. The wrapper material is plate and approximately 1-3/8 inches thick. Down select specimens and macros were examined to confirm testing in the weakest orientation.

7.3.3.1 Chemical Composition

Table 7.3.3.1-1 provides percent content values listed in the ASTM A517-84 material specification.

Table 7.3.3.1-1: ASTM A517-84 Standard Chemistry Values (24)

	C	Mn	P *max	S *max	Si	Ni	Cr	Mo	V	Cu
Grade F	0.08-0.22	0.55-1.10	0.035	0.04	0.13-0.37	0.67-1.03	0.36-0.69	0.36-0.64	0.02-0.09	0.12-0.53

Table 7.3.3.1-2 provides data collected from Arc Spark analyses of the T-1 wrapper and head of vessel V0066. The V0066 plate falls comfortably within the A517 Grade F specification.

Table 7.3.3.1-2: T-1 Collected Chemistry Data Vessel V0066

Location	C	Si	Mn	P	S	Cr	Mo	Ni	Cu
Head	0.15	0.25	0.84	0.014	0.027	0.41	0.48	0.9	0.26
Wrap Layer	0.15	0.25	0.88	0.014	0.025	0.68	0.46	0.82	0.27

7.3.3.2 Metallography

Metallography studies on T-1 material included grain orientation and macro cubes. Grain size, grain size through thickness, and carburization layer thickness studies were not conducted.

Grain Orientation Study

One set of three metallographic blocks was taken from the centerline of the wrapper layer material to correlate the grain orientation with the tensile and fracture toughness testing. The cut plan in Figure 7.3.3.2-1 shows how the blocks were removed from the layer. The blocks were polished, etched and photographed and the photographs were reconstructed as shown in Figure 7.3.3.2-2 and Figure 7.3.3.2-3.

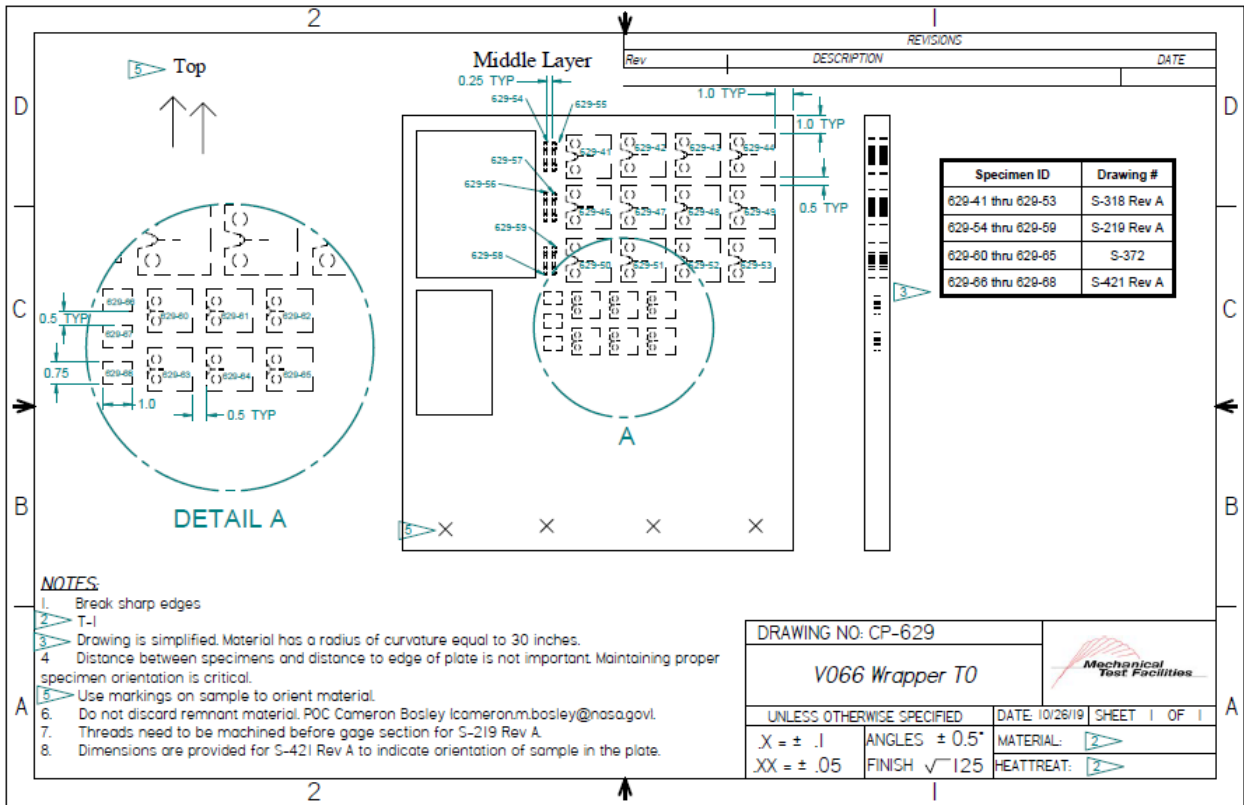


Figure 7.3.3.2-1: Cut Plan for Macros from V066 Layer

These macros show that the grains are elongated in the L-C and C-L vessel planes with the greatest elongation in the circumferential direction. This implies that the plates were arranged such that the plate L direction (weakest crack orientation) corresponds to the vessel C direction.

Table 7.3.3.2-1: Macro Observations

Face	Face Dimensions	As-polished observations	Etched observations
L-T Face 629-66	1.00"x0.75"	Equiaxed manganese sulfide inclusions. Indicates that the face is transverse to the metal working direction.	Transformed martensite matrix consisting of equiaxed prior austenite grains.
L-R Face 629-67	1.00"x0.50"	Highly elongated manganese sulfide inclusions. Indicates that the face is parallel to the metal working direction.	Transformed martensite matrix consisting of equiaxed prior austenite grains.
T-R Face 629-68	0.75"x0.50"	Elongated manganese sulfide inclusions. Indicates that the face is parallel to the metal working direction.	Transformed martensite matrix consisting of equiaxed prior austenite grains.

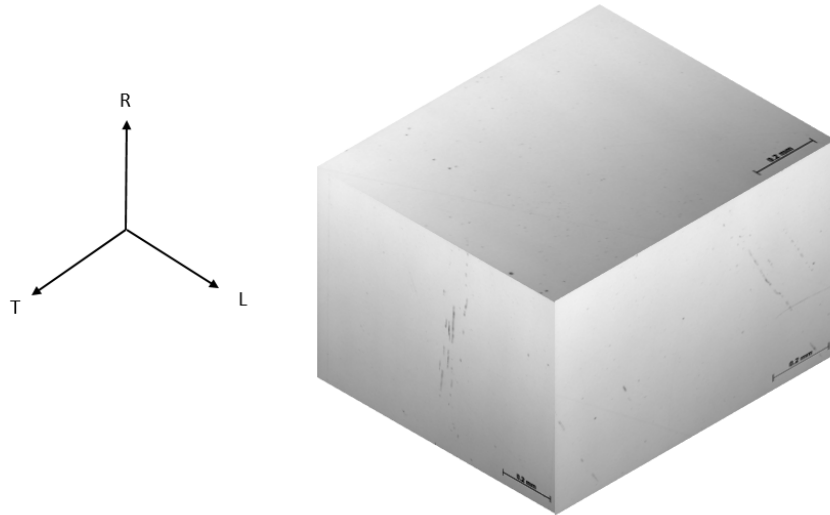


Figure 7.3.3.2-2: Macro from V0066 as Polished

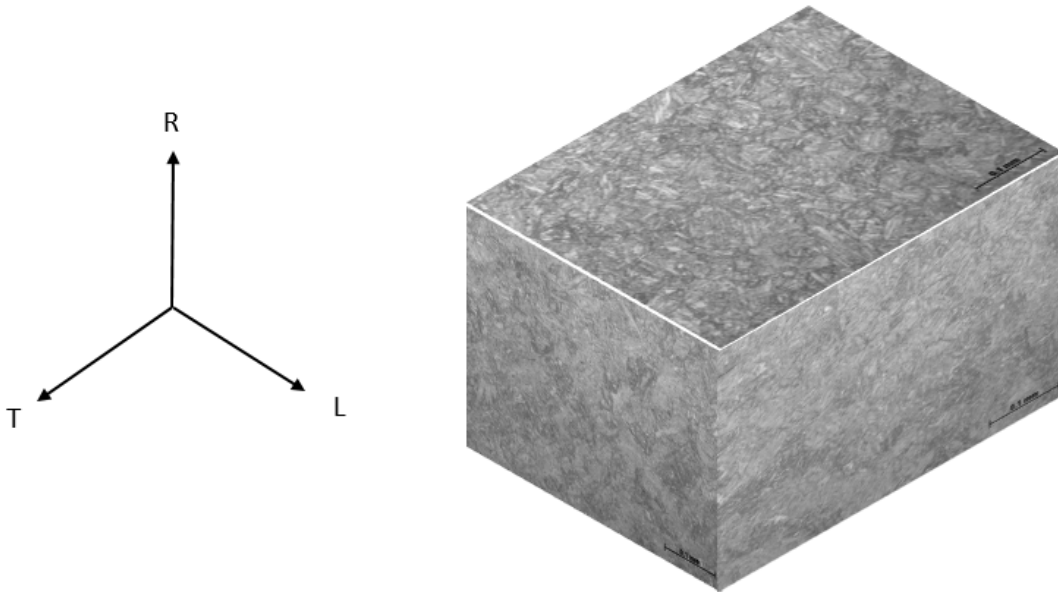


Figure 7.3.3.2-3: Macro from V0066 Etched

7.3.3.3 Mechanical Properties

Table 7.3.3.3-1 provides ASTM A517F specification tensile properties minimums.

Table 7.3.3.3-1: A517 Minimum Material Specifications (24)

Thickness	Yield Stess (ksi)	Tensile Stress (ksi)	Fracture Elongation in 2 in. (%)
2.5" or less	100	115-135	16
2.5" to 6"	90	105-135	14

7.3.3.3.1 Smooth Tensile Tests

Smooth tensile tests were conducted at MSFC on round specimens in accordance with ASTM E8, "Standard Test Methods for Tension Testing of Metallic Materials" (51) using specimen designs S-58 and S219 Rev A. The mechanical test frame consisted of a servo-hydraulic actuator and reaction frame. The frame used an LVDT for displacement feedback. Stress measurements were derived from load measurements and the initial specimen measurements. Strain measurements were derived from an extensometer and the initial specimen measurements.

The results obtained from testing T-1 steel from vessel V0066 are presented in Table 7.3.3.3.1-1. A typical engineering stress-strain curve is shown in Figure 7.3.3.3.1-1.

Table 7.3.3.3.1-1: T-1 Tensile Data V00667

Specimen ID	Test Temp. (°C)	ASTM Orientation	Tensile Stress (ksi)	Yield Stress (ksi)	Fracture Elongation
629-7	21	T	117.2	105.9	20.4
629-8	21	T	118.3	107.1	20.7
629-9	21	T	118.9	108.0	20.8
629-10	21	L	117.3	106.7	21.6
629-11	21	L	116.8	106.7	23.2
629-12	21	L	116.5	106.0	22.7
629-54	20	T	119.5	108.4	19.0
629-55	20	T	122.3	110.3	19.0
629-56	-46	T	129.8	115.8	22.2
629-57	-46	T	131.8	118.6	22.1
629-58	-101	T	137.7	123.7	24.2
629-59	-101	T	137.2	123.3	24.1

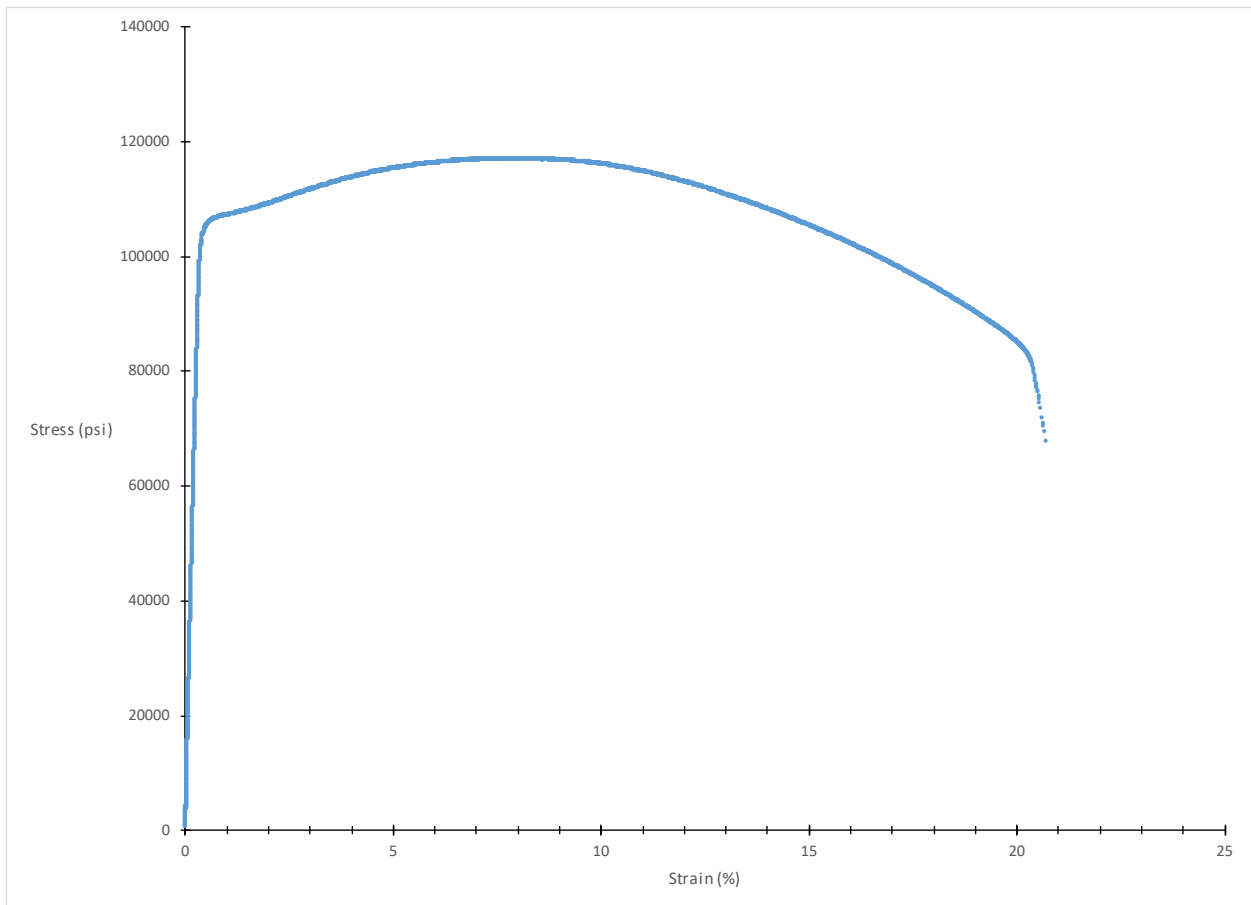


Figure 7.3.3.3.1-1: T-1 Smooth Specimen Tensile Plot for Sample 629-7

7.3.3.3.2 Notch Tensile Tests

Notch tensile tests were not performed on this material.

7.3.3.3.3 Fracture Properties

All room temperature testing was performed in accordance with ASTM E1820. Testing at all other temperatures was in accordance with ASTM E1921. Testing for both standards used specimen design S-318 Rev A. All T-1 fracture test samples came from vessel V0066. Down selects were tested in both T-L and L-T orientations, and cleavage tests were tested with the crack plane in the T-L orientation as defined by ASTM. The specimens used were ASTM E1820 compact specimens (C(T)) with $W = 2.0$ inches and $B = 1.0$ inch, $a/W = 0.5$ and all specimens were side grooved to a total thickness reduction of 20%. The cutting diagram used to remove the C(T) specimens from the V0066 layer is shown in Figure 7.3.3.3.3-1.

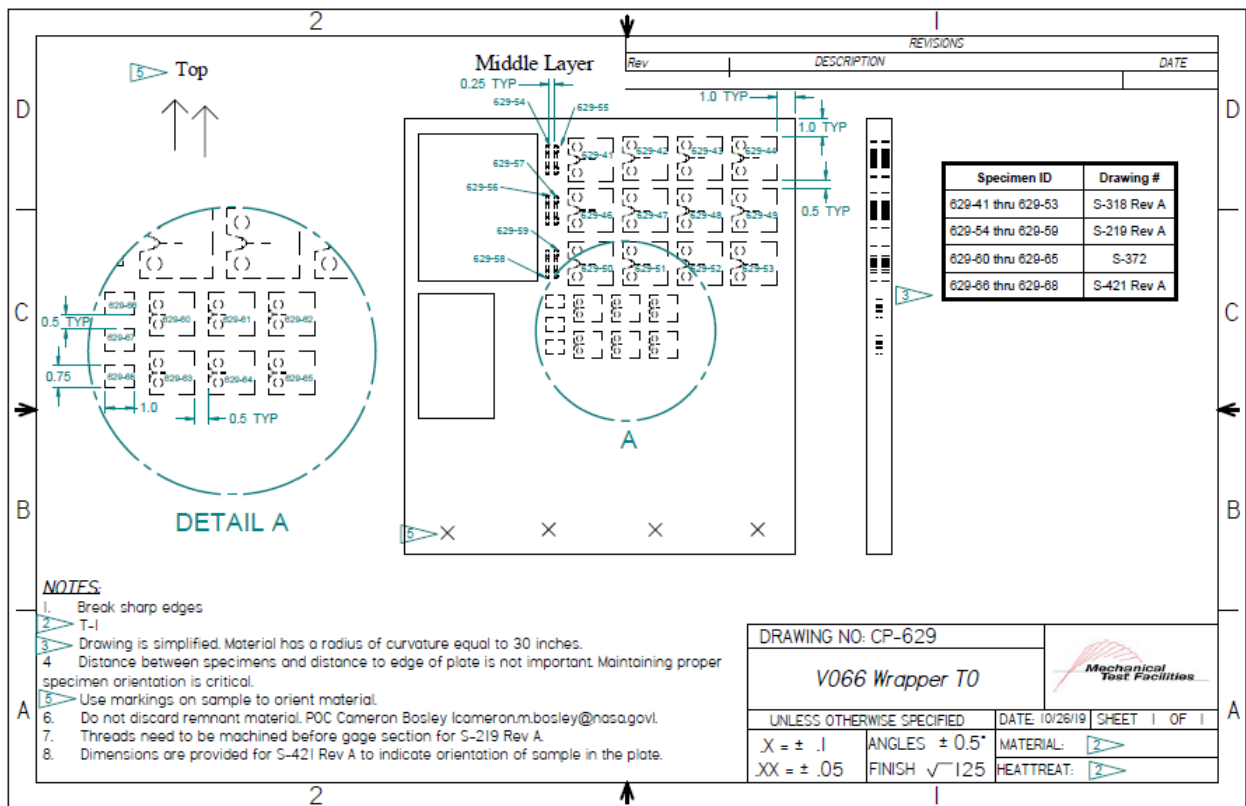


Figure 7.3.3.3.3-1: Cut Plan for V0066 Fracture Specimens

The following test data are raw values obtained from fracture tests conducted on V0066 T-1 wrapper material. Test results that are considered upper shelf are listed under ASTM E1820, while transition temperature test results are listed under E1921. Tests that meet the complete validity requirements for $J_q = J_{1C}$ and $K_{Jq} = K_{J1C}$ are denoted with an asterisk. Despite invalidities, J_q and K_{Jq} convey valuable fracture toughness information, especially when the test results are applied directly to the sample material source.

For the T-1 material tested, it is important to note that significant ductile instability was observed in non-cleavage tests after the test reached J_Q . Ductile instability is defined as unpredictable crack extension without a true cleavage mechanism. Practically the result is the same, once the crack has reached an initiation toughness, it will grow unstably. In a test environment, this is controlled somewhat by the load/unload cycles of the unloading compliance method. However, in a real world situation without load shedding, the result would most likely be catastrophic failure.

Table 7.3.3.3-1: T-1 Fracture Data V0066

Specimen ID	Test Temp. (°C)	ASTM Crack Plane Orientation	W (in)	a_0 (in)	a_f (in)	B_0 (in)	B_N (in)	J_q (kJ/m ²)	K_{Jq} (MPa√m)	K_{JcIT} (MPa√m)	ASTM Standard
629-1	21	T-L	2.0026	1.0272	1.0275	1.0006	0.8055	66	121	---	E1820
629-2	21	T-L	2.0016	1.0232	1.0232	1.0004	0.8101	67	122	---	E1820
629-3	21	T-L	2.0029	1.0315	1.0319	1.0011	0.8042	68	124	---	E1820
629-4	21	L-T	2.0041	1.0348	1.2305	1.0011	0.8021	82	135	---	E1820
629-5	20	L-T	2.0027	1.0319	1.1551	1.0020	0.8023	94	145	---	E1820
629-6	21	L-T	2.0036	1.0258	1.0712	1.0009	0.8029	74	129	---	E1820
629-41	21	T-L	1.9989	1.0485	1.0669	1.0002	0.8013	83	136	---	E1820
629-42	21	T-L	1.9985	1.0414	1.1889	1.0003	0.7997	64	119	---	E1820
629-43	21	T-L	1.9989	1.0462	1.0998	0.9988	0.8007	130	170	---	E1820
629-44	-18	T-L	1.9991	1.0532	1.2264	0.9992	0.8003	94	145	---	E1820
629-46	-73	T-L	1.9988	1.0609	1.0875	1.0000	0.8002	121	164	164	E1921
629-47	-101	T-L	1.9989	1.0653	1.1645	0.9992	0.8019	111	157	157	E1921
629-48	-101	T-L	1.9990	1.0694	1.0806	0.9998	0.8026	77	131	131	E1921
629-49	-101	T-L	1.9993	1.0534	1.1282	0.9987	0.8040	73	128	128	E1921
629-50	-129	T-L	1.9992	1.0551	1.0607	0.9989	0.8027	46	101	101	E1921
629-51	-129	T-L	1.9987	1.0539	1.0548	0.9999	0.8025	43	98	98	E1921
629-52	-129	T-L	1.9990	1.0562	1.0606	0.9997	0.8047	44	100	100	E1921
629-53	-129	T-L	1.9988	1.0546	1.0551	1.0000	0.8016	29	80	80	E1921

Figure 7.3.3.3-2 shows a typical load versus crack opening displacement record for an upper shelf E1820 test. The resulting J integral resistance curve (J-R curve) is presented in Figure 7.3.3.3-3 which shows the evaluation of J_Q according to E1820. Here the effect of ductile instability can be observed as the crack length begins to jump significantly without the load reaching the previous maximum.

Results from the seven E1921 tests are presented in Table 7.3.3.3-2 and Table 7.3.3.3-3. These results were obtained using the T_0 TEM code described in Section 4.2. The T_0 reference temperature for this data set was evaluated as -123°C using the E1921 Master Curve shown in Figure 7.3.3.3-4.

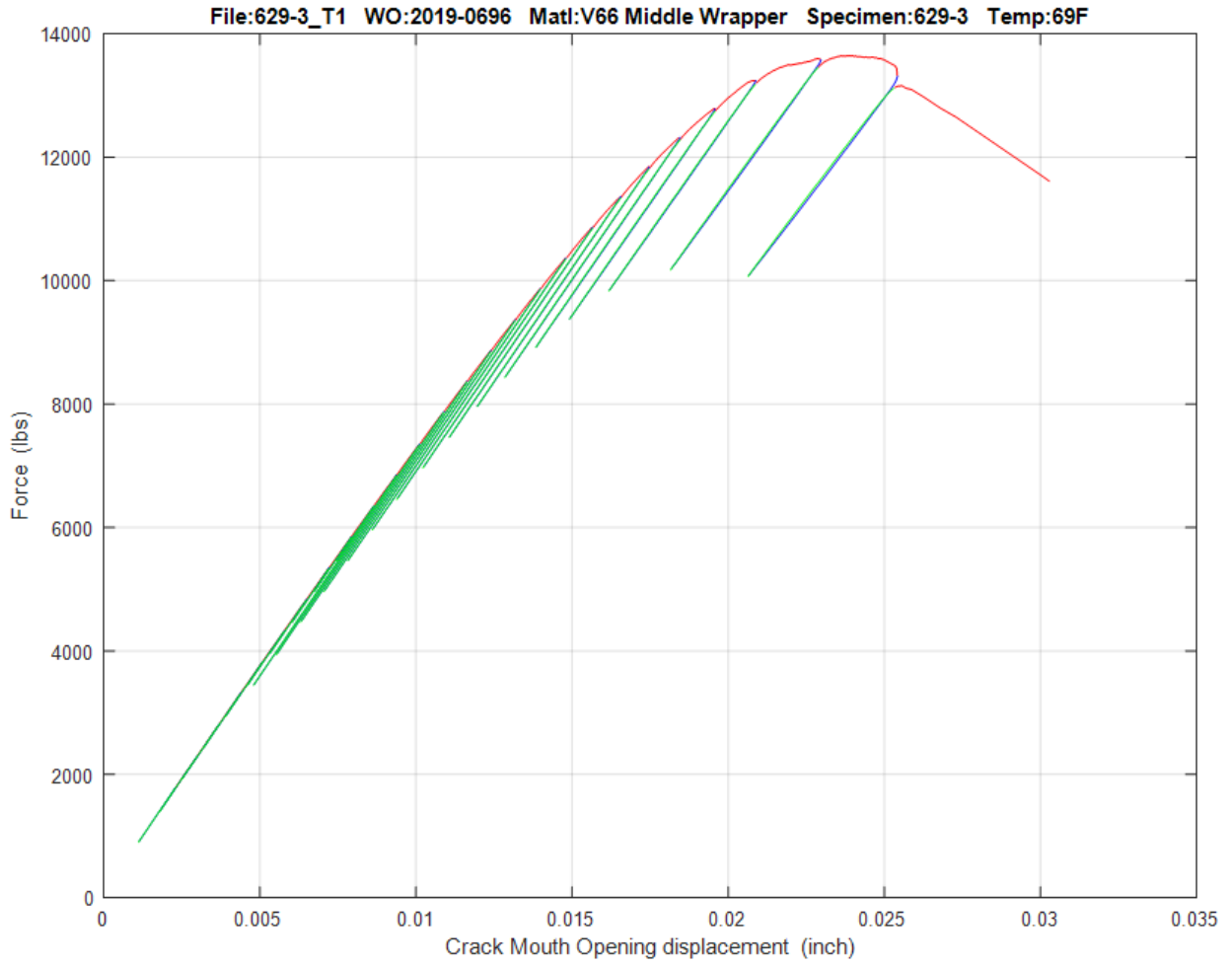


Figure 7.3.3.3.3-2: T-1 Load Versus COD Plot, Sample 629-3

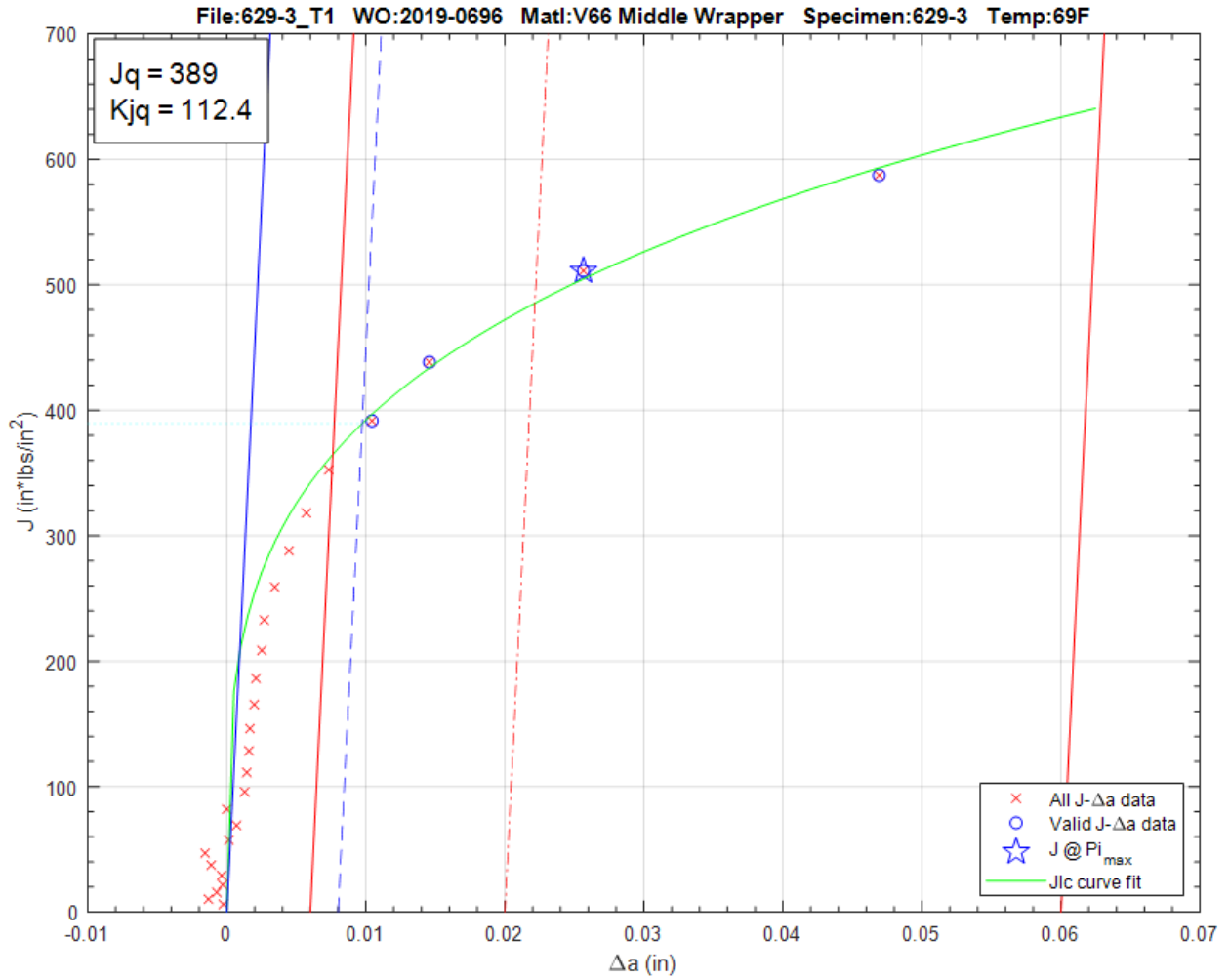


Figure 7.3.3.3.3-3: T-1 J_q Versus Δa Plot, Sample 629-3

Table 7.3.3.3.3-2: T_0 Individual Specimen Results

Specimen Name	Temperature (°C)	KjcRaw (MPa*m ^{0.5})	1T Data (MPa*m ^{0.5})	Uncensored Data	Test Temp -T0 (°C)
629-47	-101	157.3	131.5	0	22
629-48	-101	131.5	131.5	1	22
629-49	-101	128.0	128.0	0	22
629-50	-129	100.9	100.9	1	-6
629-51	-129	98.3	98.3	1	-6
629-52	-129	99.5	99.5	1	-6
629-53	-129	79.8	79.8	1	-6

Table 7.3.3.3.3-3: T₀ Calculation Results

Initial T₀ (°C)	-123
Total Samples	7
Samples within T₀ ± 50°C (N)	7
Number of Uncensored Data (r)	5
Poisson's Ratio	0.3
Σ(r_i n_i)	0.83
Samples Between T_i - T₀ 50 to -14 °C	5
Samples Between T_i - T₀ -15 to -35 °C	0
Samples Between T_i - T₀ -36 to -50 °C	0
T₀scrn (°C)	-123
Homogenous or Inhomogeneous	Homogenous

The results of the E1921 analysis show that the T-1 material removed from the V0066 wrapper is macroscopically homogenous, indicating consistent properties throughout the sampled material. For this data set, the ductile-brittle transition temperature was found to be -123°C. This result does not meet the E1921 validity criteria for a sufficient number of samples tested in an appropriate temperature range since $\Sigma(r_i n_i) < 1.0$. The resulting temperature and confidence bounds still provide valuable fracture information. The material itself demonstrates high initiation toughness at low temperatures. However, as mentioned previously, this material shows significant ductile instability even at high temperatures. The high initiation toughness makes this an unlikely scenario, but it should be considered in any vessel application.

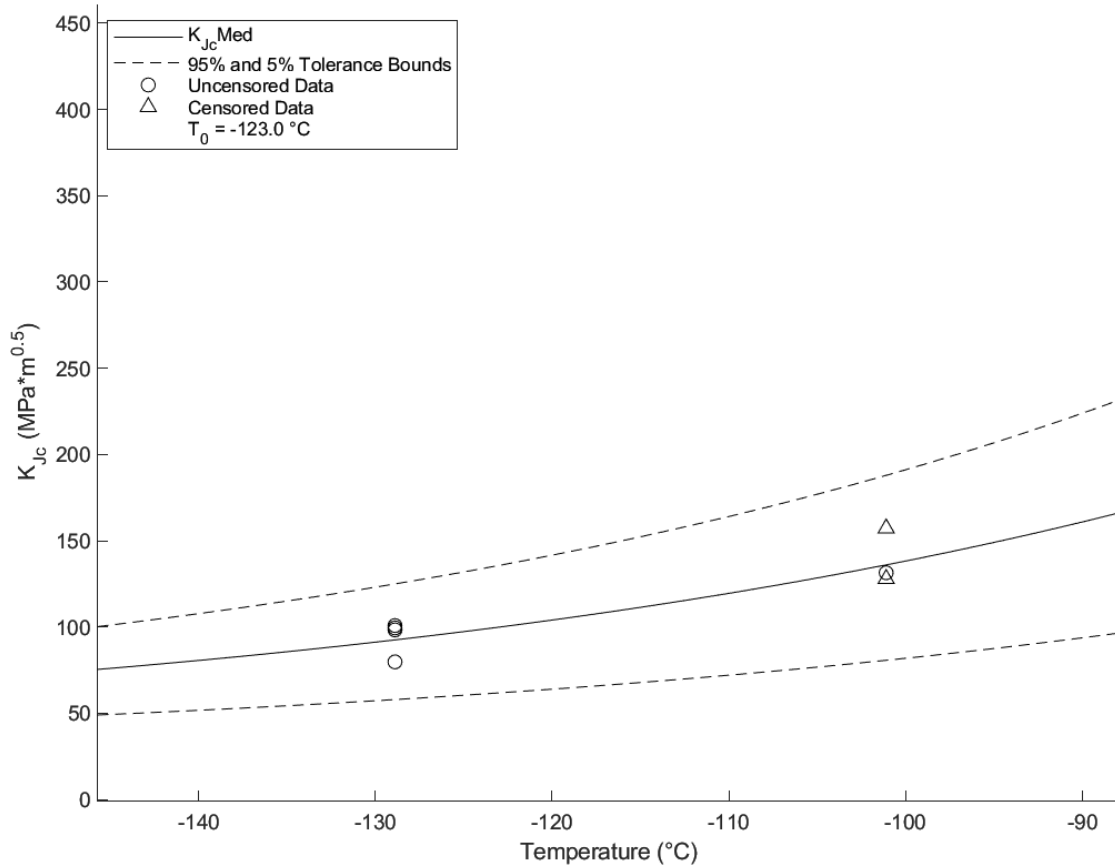


Figure 7.3.3.3-4: T-1 T₀ Plot

7.3.3.3.4 Fatigue Crack Growth

Sections of V0066 were tested in accordance with ASTM E647 to determine the fatigue crack growth rates. Load ratios of $R = 0.1$ and $R = 0.7$ were chosen corresponding to load cycles corresponding to slight pressure variations and nearly full pressure releases of the LPVs. These tests were conducted on material taken from the center of the layer in the thickness direction. Figure 7.3.3.3.4-1 and Figure 7.3.3.3.4-2 show the individual fatigue crack growth curves for the T-1 layer material from vessel V0066 at different R ratios. The combined plot with both curves is shown in Figure 7.3.3.3.4-3. These curves are input into NASGRO to create material data packages used for structural analysis and crack growth prediction.

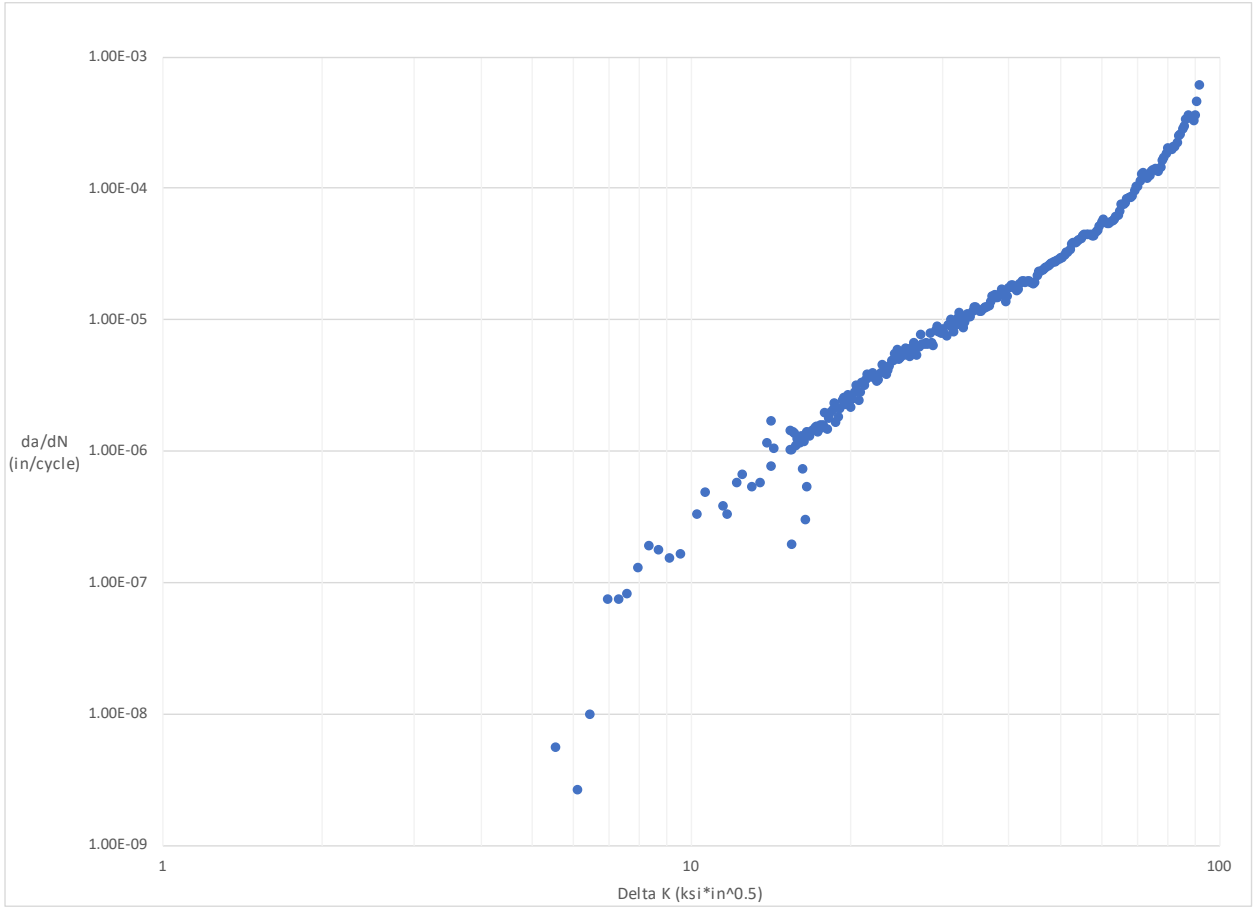


Figure 7.3.3.3.4-1: T-1 Fatigue Crack Growth Plot, R = 0.11

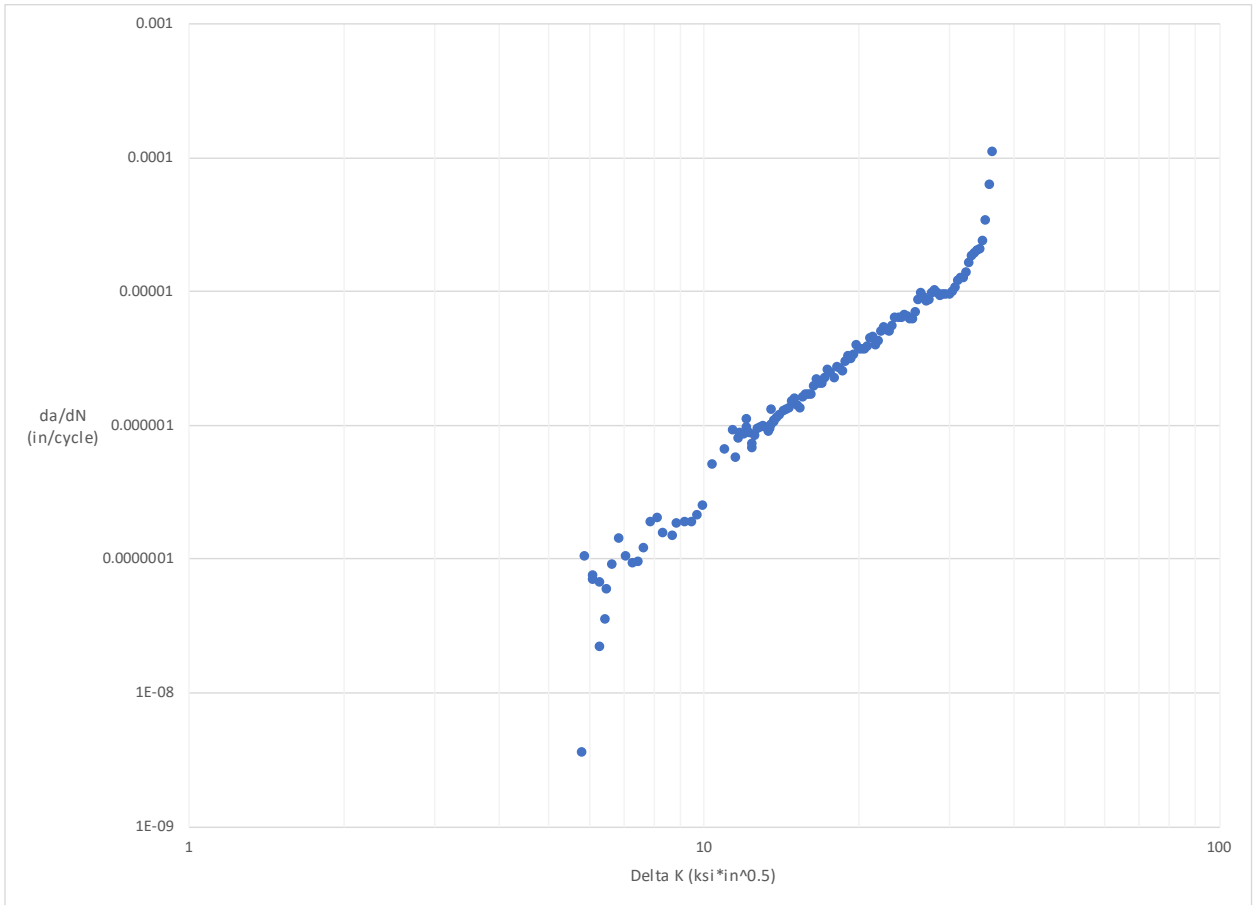


Figure 7.3.3.3.4-2: T-1 Fatigue Crack Growth Plot, R = 0.7

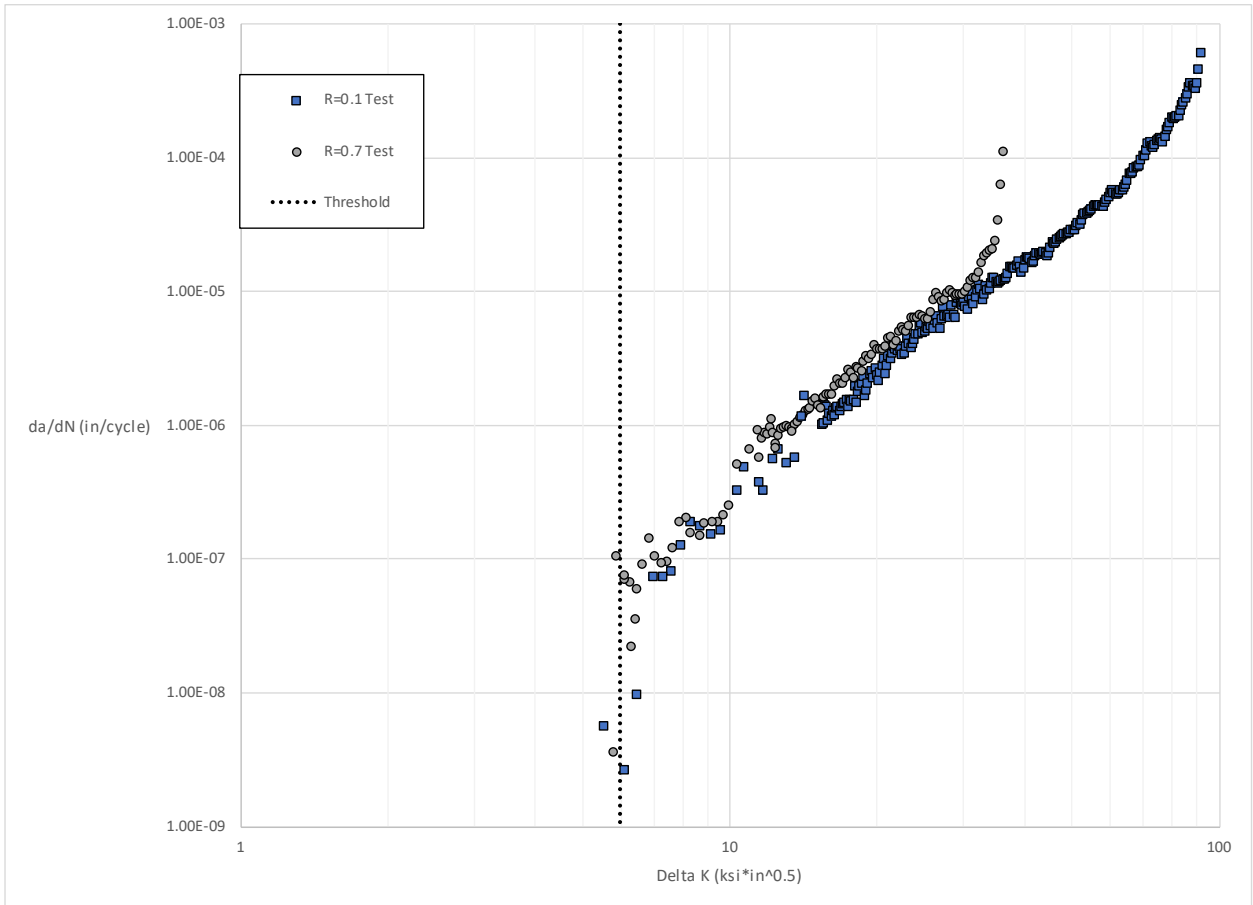


Figure 7.3.3.4-3: T-1 Fatigue Crack Growth Plot, Combined

7.3.3.3.5 Charpy Impact

Charpy impact tests were not performed on this material.

7.4 Parent Nozzle Materials

The nozzles found in layered pressure vessels are typically single piece forgings welded into the head, although some vessels contain nozzles located in shell courses. The most common nozzle materials are AOS A-5002-mod (5002) and ASTM A105 Grade II (hereafter referred to as A105), and these were the only nozzle materials investigated. No dissected vessels contained nozzles in the shell course, so only head nozzles were examined. In the nozzle materials tested, ductile-brittle transition temperatures were found to be exceptionally low, well beyond normal operational temperatures. This indicates that the nozzle material itself is stable and will likely not be susceptible to cold weather.

7.4.1 AOS A-5002-Mod

A.O. Smith A-5002-mod is used as a nozzle material in LPVs. The results reported in this section include vessels manufactured by A.O. Smith.

7.4.1.1 Chemical Composition

Table 7.4.1.1-1 provides the percent content values listed in the material specification, provided by A.O. Smith as construction reference. Exact melt chemistry is unavailable.

Table 7.4.1.1-1: AOS 5002 Chemistry Specification (60)

AO Smith Specification % Chemical Content											
C	Mn	P	S	Si	Ni	V	Cu	Cr	Mo	B	Nb
0.19-0.25	1.1-1.5	0-0.04	0-0.04	0.2-0.35	0.4-0.7	0.13-0.18	0-0.3	0-0.3	0-0.06	0-0.001	-

Table 7.4.1.1-2 provides data collected from Arc Spark analyses of vessels V125 and MV50466-8 at MSFC.

Table 7.4.1.1-2: 5002 Collected Chemistry Data

Vessel	C	Mn	P	S	Si	Ni	V	Cu	Cr	Mo	B	Nb
MV50466-8	0.25	1.34	0.011	0.019	0.27	0.66	0.12	0.095	0.071	0.035	0.0005	0.003
V125	0.28	1.61	0.02	0.14	0.25	0.56	0.13	0.075	0.095	0.044	0.002	0.003

7.4.1.2 Metallography

Metallography tests were not performed on this material.

7.4.1.3 Mechanical Properties

Table 7.4.1.3-1 provides minimum values listed in the material specification.

Table 7.4.1.3-1: AO Smith 5002 Mechanical Specification (60)

F _{ty} (ksi)	F _{tu} (ksi)	Elong in 2 in., min %	Reduction of Area, min %
65	95	18	35

7.4.1.3.1 Smooth Tensile Tests

Smooth tensile tests were not conducted on the material due to size constraints in the base material. AO Smith specification values were used to direct fracture testing.

7.4.1.3.2 Notch Tensile

Notch tensile tests were not performed on this material.

7.4.1.3.3 Fracture Properties

All room temperature testing was performed in accordance with ASTM E1820 (10). All other temperatures were tested in accordance with ASTM E1921 (7). Testing for both standards use specimen design S-226 Rev B. All 5002 fracture tests came from vessel MV50466-8 and were tested with the crack plane in the C-R orientation as defined by ASTM (both grain and vessel orientations). The specimens used were ASTM E1820 compact specimens (C(T)) with W = 1.0 inches and B = 0.375 inch, a/W = 0.5 and all specimens were side grooved to a total thickness reduction of 20%. The cutting diagram used to remove the C(T) specimens from the MV50466-8 Head 1 nozzle (2 inch diameter nozzle) is shown in Figure 7.4.1.3.3-1.

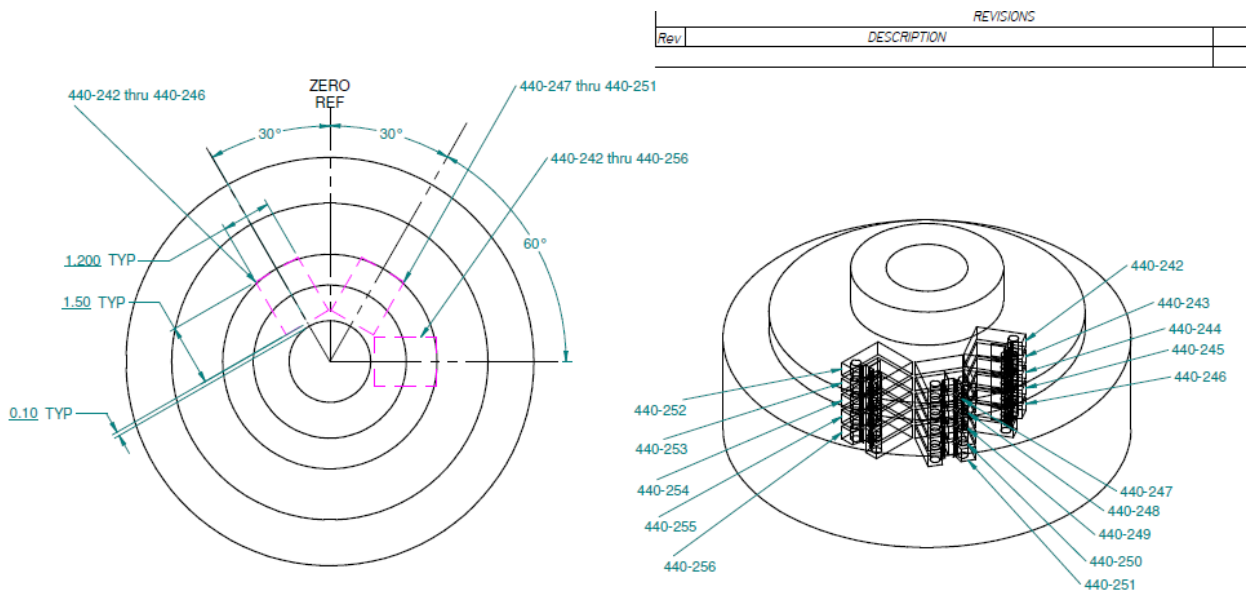


Figure 7.4.1.3.3-1: MV50466-8 Nozzle Fracture Cut Plan

The following test data are raw values obtained from fracture tests conducted on MV50466-8 nozzle material. Test results that are considered upper shelf are listed under ASTM E1820, while transition temperature test results are listed under E1921. Tests that meet the complete validity requirements for $J_q = J_{1C}$ and $K_{Jq} = K_{J1C}$ are denoted with an asterisk. Despite invalidities, J_q and K_{Jq} convey valuable fracture toughness information, especially when the test results are applied directly to the sample material source.

Table 7.4.1.3.3-1: AOS 5002 Fracture Data MV50466-8

Specimen ID	Test Temp. (°C)	ASTM Crack Plane Orientation	W (in)	a ₀ (in)	a _f (in)	B ₀ (in)	B _N (in)	J _q (kJ/m ²)	K _{Jq} (MPa√m)	K _{JC1T} (MPa√m)	ASTM Standard
440-253	21	C-R	1.0023	0.5340	0.6046	0.3748	0.3000	152	184	---	E1820
440-254	21	C-R	1.0029	0.5312	0.5959	0.3762	0.3010	140	177	---	E1820
440-255	-72	C-R	1.0008	0.5144	0.5238	0.3758	0.3018	69	124	102	E1921
440-249	-72	C-R	1.0028	0.5366	0.5405	0.3753	0.3012	42	96	80	E1921
440-243	-73	C-R	1.0015	0.5364	0.5366	0.3763	0.3032	51	107	88	E1921
440-244	-73	C-R	1.0022	0.5465	0.5492	0.3767	0.3014	40	94	78	E1921
440-245	-73	C-R	1.0023	0.5352	0.5361	0.3766	0.3000	10	48	42	E1921
440-246	-73	C-R	1.0012	0.5272	0.5318	0.3761	0.3017	50	106	87	E1921
440-247	-73	C-R	1.0036	0.5336	0.5356	0.3759	0.3012	36	89	74	E1921
440-248	-73	C-R	1.0025	0.5369	0.5387	0.3766	0.3012	32	84	70	E1921
440-250	-73	C-R	1.0018	0.5280	0.5286	0.3766	0.3012	33	86	72	E1921
440-252	-73	C-R	1.0024	0.5335	0.5358	0.3763	0.3023	34	88	73	E1921
440-256	-73	C-R	1.0031	0.5550	0.5552	0.3755	0.3000	35	89	74	E1921
440-251	-74	C-R	1.0024	0.5470	0.5490	0.3758	0.3030	55	111	91	E1921

Figure 7.4.1.3.3-2 shows a typical load versus crack opening displacement record for an upper shelf E1820 test. The resulting J integral resistance curve (J-R curve) is presented in Figure 7.4.1.3.3-3 which shows the evaluation of J_q according to E1820.

Results from the 12 E1921 tests are presented in Table 7.4.1.3.3-2 and Table 7.4.1.3.3-3. These results were obtained using the T₀TEM Code described in Section 4.2. The T₀ reference temperature for this data set was evaluated as -56°C using the E1921 master curve shown in Figure 7.4.1.3.3-4.

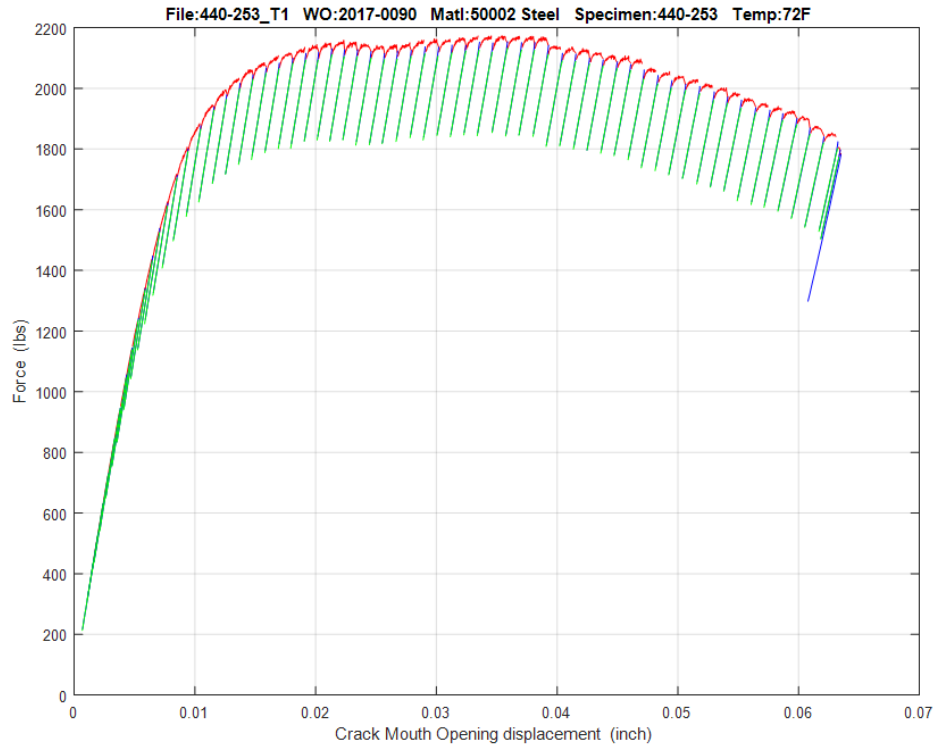


Figure 7.4.1.3.3-2: AOS 5002 Load Versus COD Plot, Sample 440-253

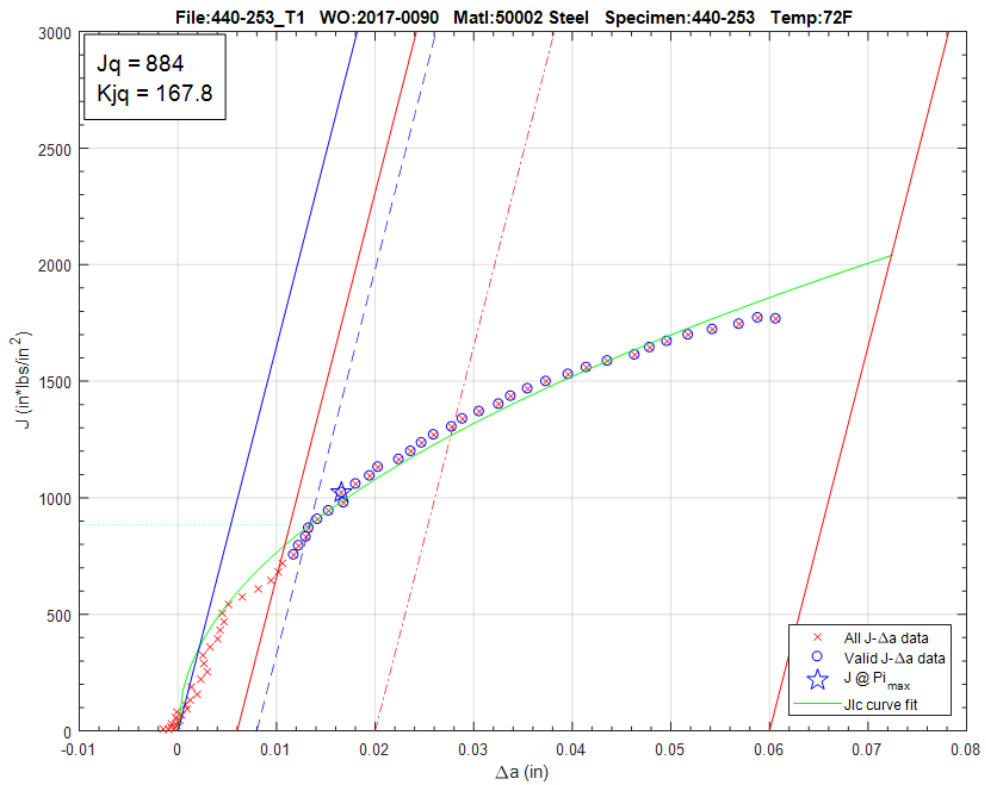


Figure 7.4.1.3.3-3: AOS 5002 J_q Versus Δa Plot, Sample 440-253

Table 7.4.1.3.3-2: T₀ Individual Specimen Results

Specimen Name	Temperature (°C)	K _{Jc} Raw (MPa*m ^{0.5})	1T Data (MPa*m ^{0.5})	Uncensored Data	Test Temp -T ₀ (°C)
440-243	-73	113.8	93.5	1	-17
440-244	-73	100.3	83.0	1	-17
440-245	-73	51.1	44.4	1	-17
440-246	-73	112.2	92.2	1	-17
440-247	-73	95.4	79.0	1	-17
440-248	-73	90.0	74.9	1	-17
440-249	-72	102.7	84.7	1	-16
440-250	-73	91.8	76.2	1	-17
440-251	-74	117.3	96.2	1	-19
440-252	-73	93.1	77.3	1	-17
440-255	-72	132.3	107.9	1	-16
440-256	-73	94.1	78.0	1	-17

Table 7.4.1.3.3-3: T₀ Calculation Results

Initial T ₀ (°C)	-56
Total Samples	12
Samples within T ₀ ± 50°C (N)	12
Number of Uncensored Data (r)	12
Poisson's Ratio	0.3
Σ(r _i n _i)	1.71
Samples Between T _i - T ₀ 50 to -14 °C	0
Samples Between T _i - T ₀ -15 to -35 °C	12
Samples Between T _i - T ₀ -36 to -50 °C	0
T ₀ scrn (°C)	-56
Homogenous or Inhomogeneous	Homogenous

The results of the E1921 analysis show that the 5002 material removed from the MV50466-8 nozzle is macroscopically homogenous, indicating consistent properties throughout the sampled material. For this data set, the ductile-brittle transition temperature was found to be -56°C. This result also meets the E1921 validity criteria for a sufficient number of samples tested in an appropriate temperature range with $\Sigma(r_i n_i) \geq 1.0$.

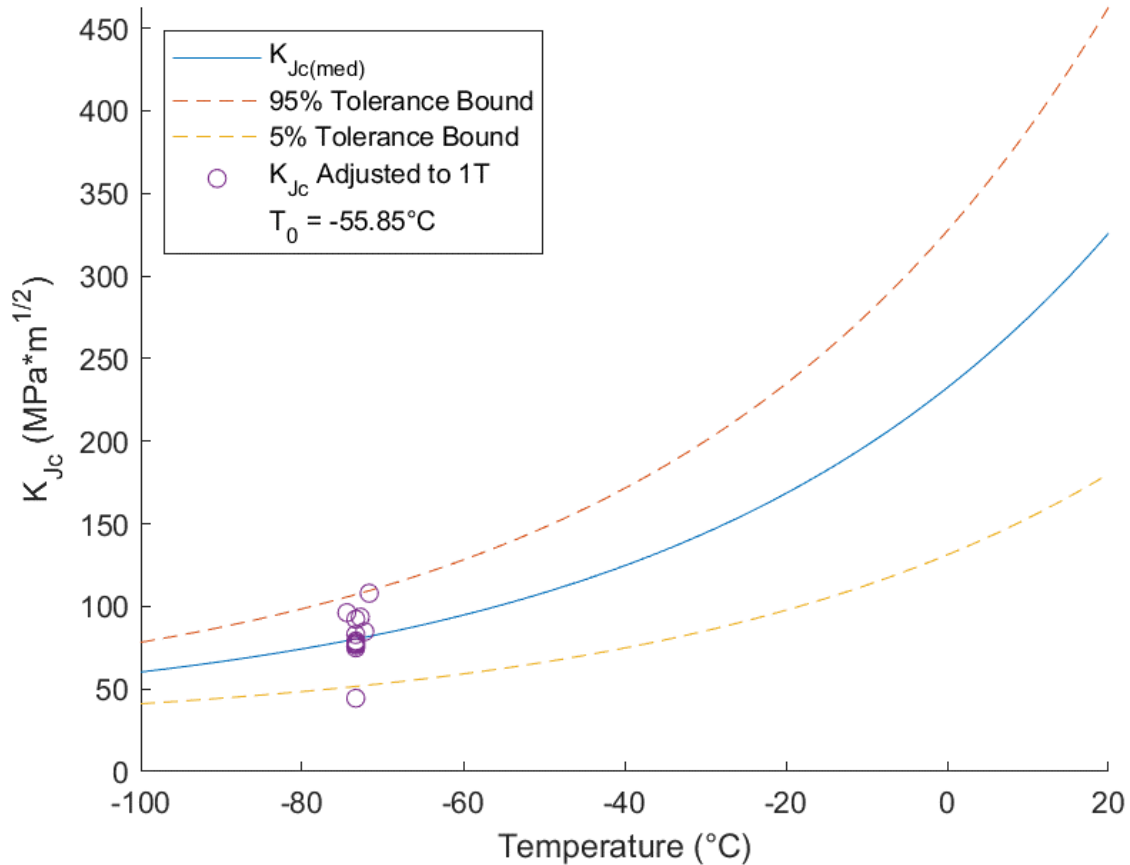


Figure 7.4.1.3.3-4: AOS 5002 T_0 Plot

7.4.1.3.4 Fatigue Crack Growth

Fatigue crack growth tests were not performed on this material.

7.4.1.3.5 Charpy Impact

Charpy impact tests were not performed on this material.

7.4.2 A105

A105 is used as the nozzle material for many LPVs. The results reported in this section are based on vessels manufactured by A.O. Smith. All nozzles reported on in this section are nominally A105 Grade II and are referred to as A105.

7.4.2.1 Chemical Composition

Table 7.4.2.1-1 provides maximum percent content values listed in the A105 material specification.

Table 7.4.2.1-1: A105 Chemistry Requirements (61)

	C	Mn	P	S
Grade II	0.35	0.9	0.05	0.05

Table 7.4.2.1-2 shows chemistry values reported on the mill certification of the V0032 nozzle.

Table 7.4.2.1-2: A105 V0032 Mill Certification Values

	C	Mn	P	S	Si
V32	0.26	0.67	0.015	0.021	0.2

Table 7.4.2.1-3 provides data collected from Arc Spark analyses of A105 nozzles from LPVs at MSFC.

Table 7.4.2.1-3: A105 Nozzle Collected Chemistry Data

Vessel	C	Mn	P	S	Si	Ni	V	Cu	Cr	Mo	B	Nb
V0023	0.390	0.900	0.027	0.067	0.240	0.005	0.002	0.010	0.020	0.003	0.001	0.003
V0032	0.260	0.660	0.006	0.015	0.220	0.038	0.002	0.048	0.025	0.010	0.001	0.003
V0348	0.270	0.760	0.012	0.031	0.200	0.100	0.002	0.240	0.081	0.036	0.001	0.003

7.4.2.2 Metallography

Metallographic studies performed on A105 material included grain orientation and macro cubes. No grain size, grain size through thickness, or carburization layer thickness studies were performed.

Grain Orientation Study

One set of three metallographic blocks was taken from the between the bolt holes of the nozzle material to correlate the grain orientation with the tensile and fracture toughness testing. The cut plan Figure 7.4.2.2-1 shows how the blocks were removed from the head. The blocks were polished, etched, and photographed, and the photographs were reconstructed as shown in Figure 7.4.2.2-2 and Figure 7.4.2.2-3. Table 7.4.2.2-1 details the observations of each macro.

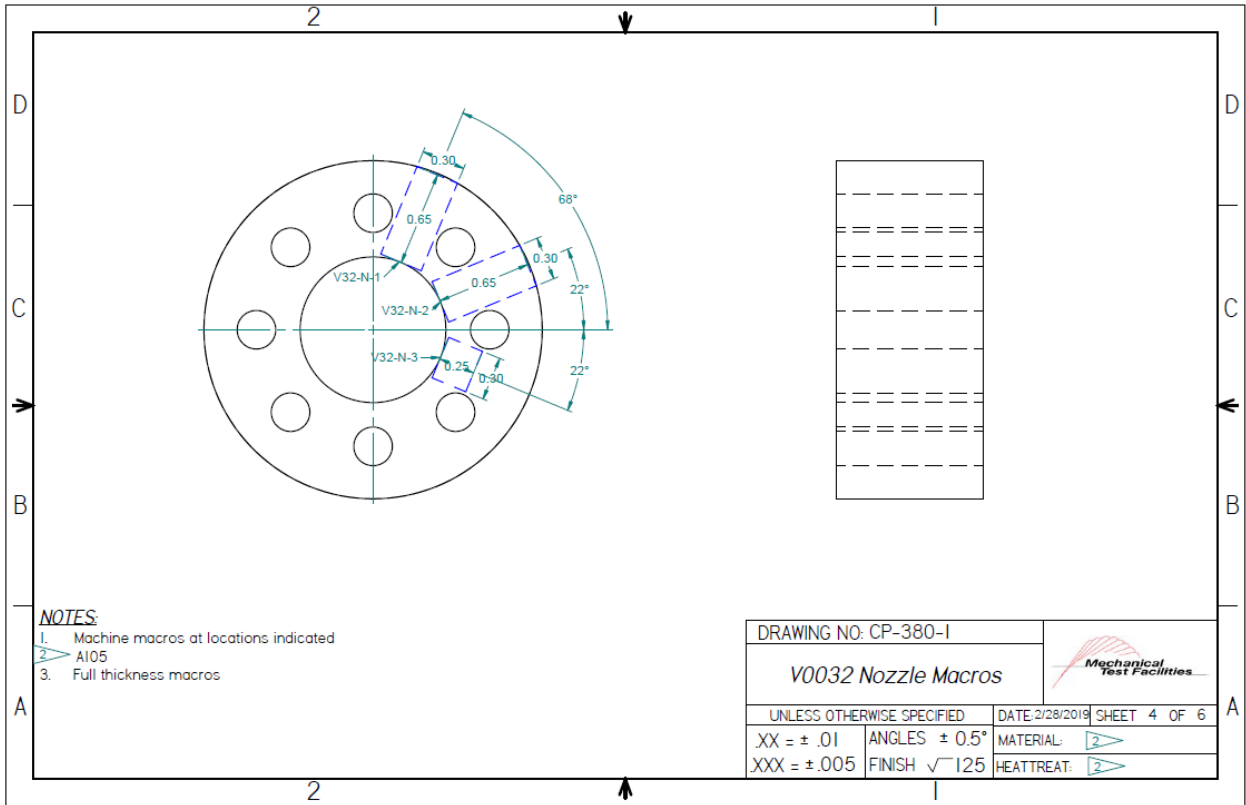


Figure 7.4.2.2-1: Cut Plan for Macros from V0032 A105 Nozzle

Table 7.4.2.2-1: A105 Nozzle Macro Evaluations

Face	Face Dimensions	As-polished observations	Etched observations
V32-N-1	0.3"x0.65"	Sample exhibits equiaxed manganese sulfide inclusions, indicating face is transverse to metal working direction.	Microstructure consists of ferrite and lamellar pearlite. The phases appear equiaxed.
V32-N-2	0.65"x1"	Sample exhibits elongated manganese sulfide inclusions, indicating face is parallel with metal working direction.	Microstructure consists of ferrite and lamellar pearlite. The phases appear equiaxed.
V32-N-3	0.3"x1"	Sample exhibits elongated manganese sulfide inclusions, indicating face is parallel with metal working direction.	Microstructure consists of ferrite and lamellar pearlite. The phases appear equiaxed. A minor amount of segregation is apparent in this section.

NOTES:

V0032-N-1: Evaluated face corresponds to the C-R plane.

V0032-N-2: Evaluated face corresponds to the L-R plane.

V0032-N-3: Evaluated face corresponds to the C-L plane.

The macros shown in Figure 7.4.2.2-2 and Figure 7.4.2.2-3 were extracted from the nozzle of V0032 as shown in Figure 7.4.2.2-1.

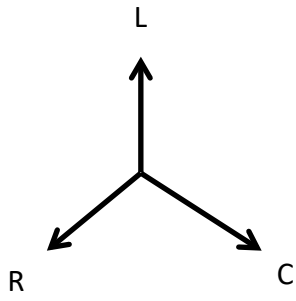


Figure 7.4.2.2-2: A105 Nozzle Macro Cube As-Polished 100X

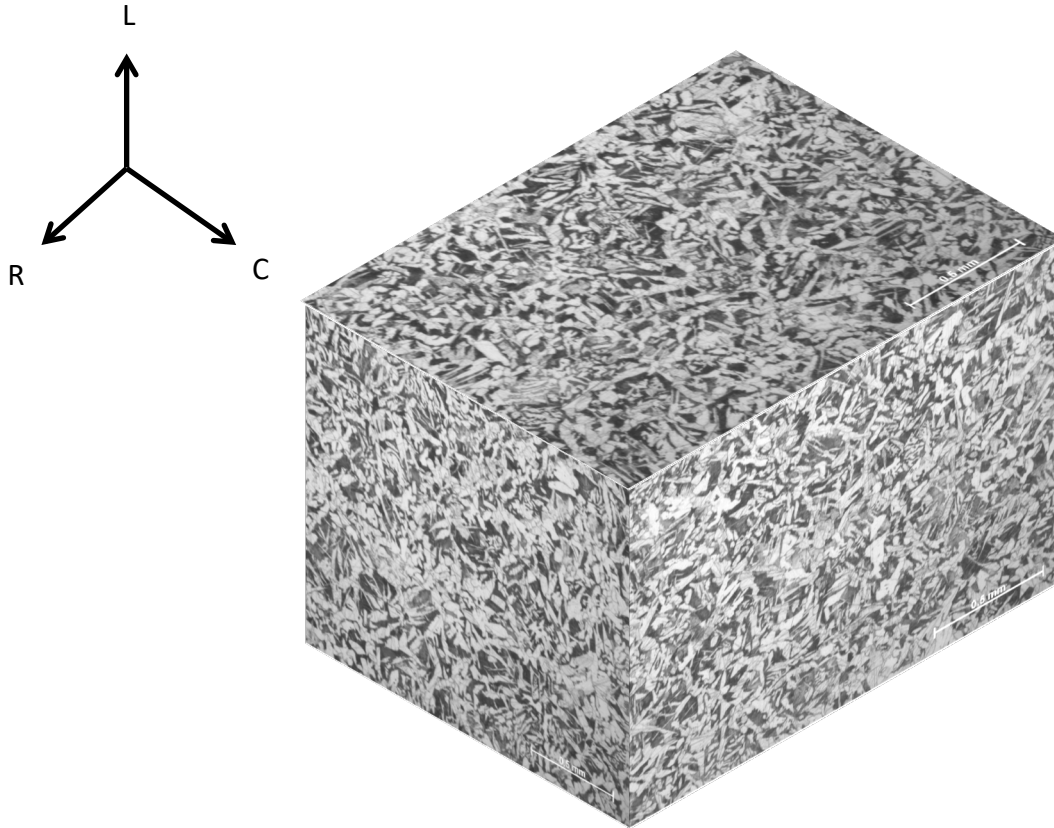


Figure 7.4.2.2-3: A105 Nozzle Macro Cube Nital Etch 50X

7.4.2.3 Mechanical Properties

Table 7.4.2.3-1 provides minimum values listed in the A105 material specification (61)

Table 7.4.2.3-1: A105 Standard Specification Value (61)

	Yield Stess (ksi)	Tensile Stress (ksi)	Fracture Elongation in 2 in. (%)	Reduction of Area (%)
Grade II	36	70	22	30

Table 7.4.2.3-2 provides tensile properties obtained from the mill certification of V0032.

Table 7.4.2.3-2: A105 Standard Specification Value

	Yield Stress (ksi)	Tensile Stress (ksi)	Elongation in 2in. (%)
V32	48	70	31

7.4.2.3.1 Smooth Tensile Tests

Smooth tensile tests were conducted at MSFC on round specimens according to ASTM E8, “Standard Test Methods for Tension Testing of Metallic Materials” (51) using specimen design S-219 Rev A. The mechanical test frame consisted of a servo-hydraulic actuator and reaction frame. The frame

used an LVDT for displacement feedback. Stress measurements were derived from load measurements and the initial specimen measurements. Strain measurements were derived from an extensometer and the initial specimen measurements.

The results obtained from testing of A105 from vessel V0032 are presented in Table 7.4.2.3.1-1, results from V0348 are in Table 7.4.2.3.1-2. A typical engineering stress-strain curve is shown in Figure 7.4.2.3.1-1.

Table 7.4.2.3.1-1: A105 Nozzle Tensile Data V0032

Specimen ID	Test Temp. (°C)	ASTM Orientation	Tensile Stress (ksi)	Yield Stress (ksi)	Fracture Elongation (%)
380-196	22	L	66.2	31.8	31.7
380-197	22	L	66.7	31.1	33.3
380-198	-46	L	70.5	30.4	35.5
380-199	-46	L	71.9	31.7	34.0
380-200	-101	L	79.3	46.4	34.3
380-202	-101	L	80.2	46.0	34.7

Table 7.4.2.3.1-2: A105 Nozzle Tensile Data V0348

Specimen ID	Test Temp. (°C)	ASTM Orientation	Tensile Stress (ksi)	Yield Stress (ksi)	Fracture Elongation (%)
483-63	21	L	76.0	49.0	22.7
483-64	21	L	75.5	48.5	27.0
483-65	-46	L	84.7	60.9	13.7
483-66	-46	L	81.7	48.0	33.2
483-67	-101	L	90.5	64.9	20.6
483-68	-101	L	90.3	62.3	25.8

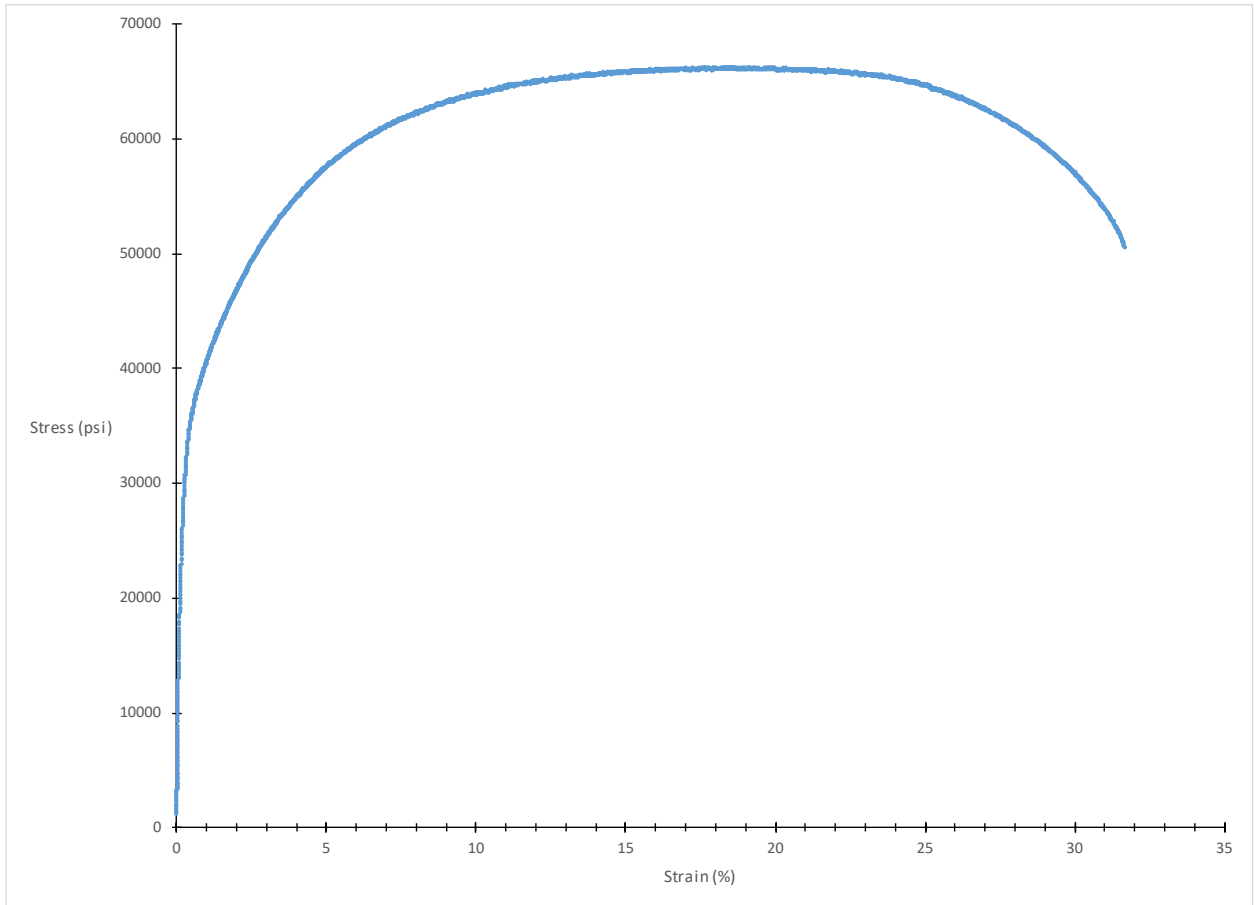


Figure 7.4.2.3.1-1: A105 Smooth Specimen Tensile Plot for Sample 380-196

7.4.2.3.2 Notch Tensile Tests

Notch tensile tests were not performed on this material.

7.4.2.3.3 Fracture Properties

All room temperature testing was performed per ASTM E1820 (10). All other temperatures were tested per ASTM E1921 (7). Testing for both standards use specimen design S-226 Rev B. All A105 fracture tests came from vessels V0032 and V0348 and were tested with the crack plane in the C-R orientation as defined by ASTM. The specimens used were ASTM E1820 compact specimens (C(T)) with $W = 1.0$ inches and $B = 0.375$ inch, $a/W = 0.5$. All specimens were side-grooved to a total thickness reduction of 20%. The cutting diagram used to remove the C(T) specimens from the V0032 nozzle is shown in Figure 7.4.2.3.3-1.

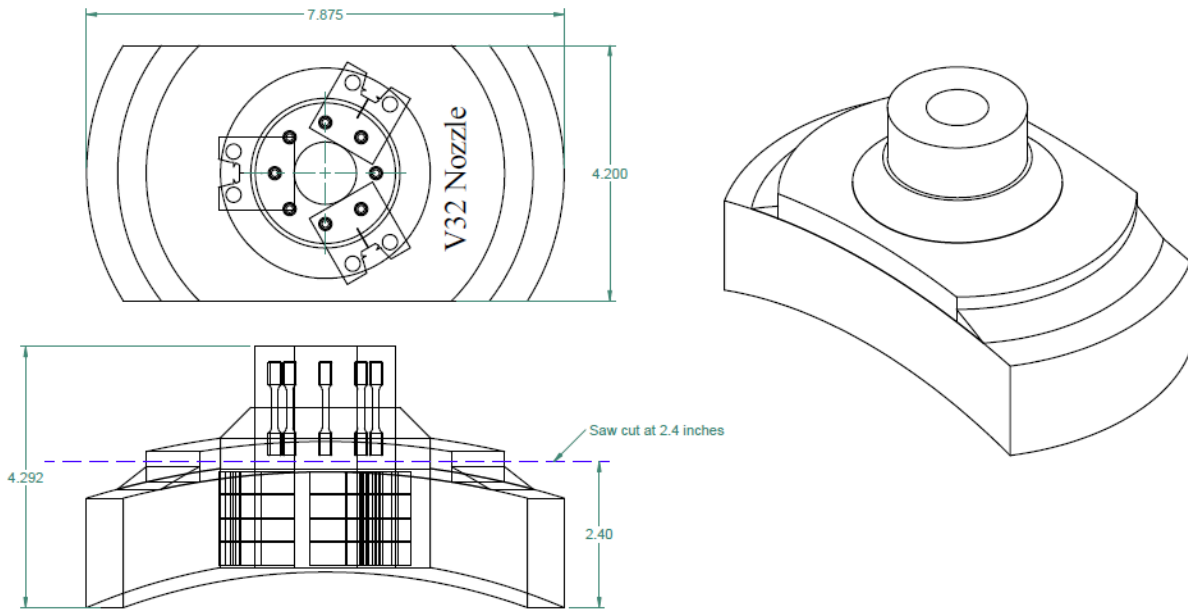


Figure 7.4.2.3.3-1: Cut Plan for V0032 Nozzle Specimens

Figure 7.4.2.3.3-2 shows a typical load versus crack opening displacement record for an A105 nozzle test. The resulting J integral resistance curve (J-R curve) is presented in Figure 7.4.2.3.3-3 which shows the evaluation of J_Q according to E1820.

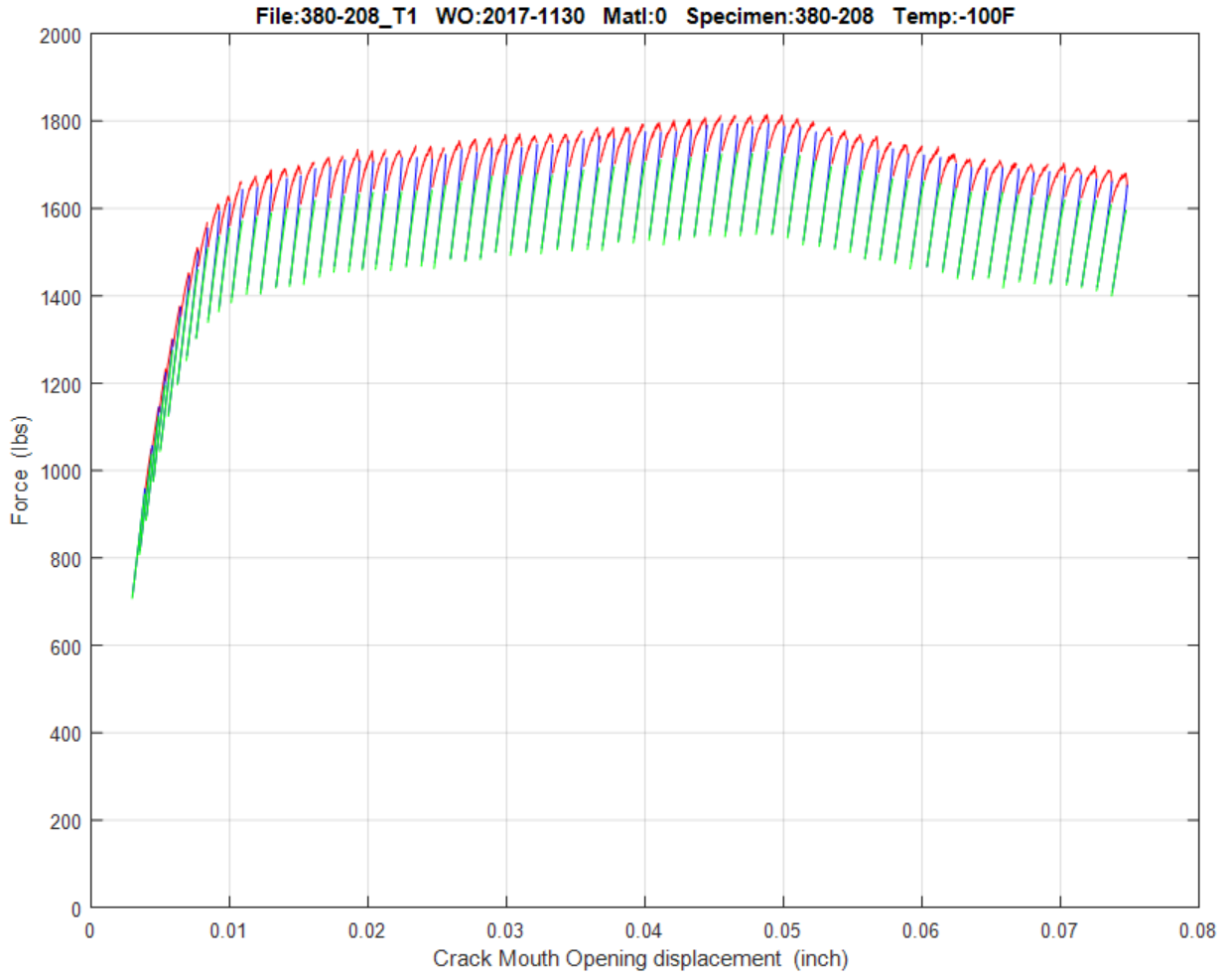


Figure 7.4.2.3.3-2: A105 Load Versus COD Plot, Sample 380-208

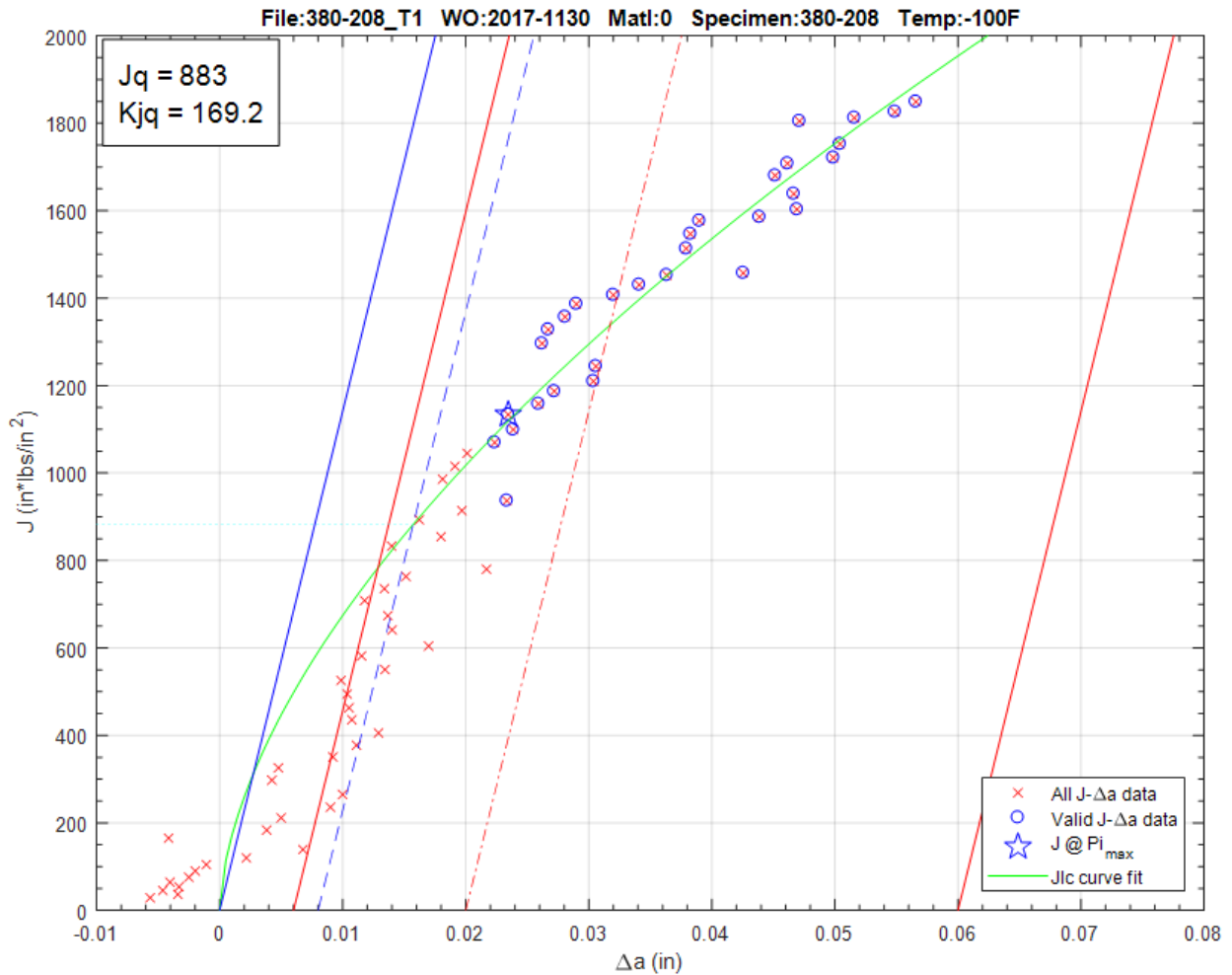


Figure 7.4.2.3.3-3: A105 J_q Versus Δa Plot, Sample 380-208

The test data shown in Table 7.4.2.3.3-1 are raw values obtained from fracture tests conducted on V0032 A105 nozzle material. Test results that are considered upper shelf are listed under ASTM E1820, while transition temperature test results are listed under E1921. Tests that meet the complete validity requirements for $J_q = J_{1c}$ and $K_{Jq} = K_{1c}$ are denoted with an asterisk. Despite invalidities, J_q and K_{Jq} convey valuable fracture toughness information, especially when the test results are applied directly to the sample material source. Specimen 380-208 demonstrated some characteristics of an upper shelf test, however it was within the temperature window and has been used as a censored data point for E1921 evaluation.

Table 7.4.2.3.3-1: A105 Nozzle Fracture Data V0032

Specimen ID	Test Temp. (°C)	ASTM Crack Plane Orientation	W (in)	a ₀ (in)	a _f (in)	B ₀ (in)	B _N (in)	J _q (kJ/m ²)	K _{Jq} (MPa √m)	K _{JCLT} (MPa √m)	ASTM Standard
380-208	-73	C-R	0.9991	0.5065	0.5732	0.3494	0.2857	155	186	148	E1921
380-207	-101	C-R	0.9996	0.5316	0.5318	0.3495	0.2813	26	76	63	E1921
380-209	-101	C-R	0.9986	0.5023	0.5070	0.3500	0.2801	75	129	104	E1921
380-210	-101	C-R	0.9997	0.5086	0.5135	0.3495	0.2784	52	108	88	E1921
380-211	-101	C-R	0.9991	0.5040	0.5103	0.3501	0.2828	72	127	102	E1921

Results from the five E1921 tests are presented in Table 7.4.2.3.3-2 and Table 7.4.2.3.3-3. These results were obtained using the T₀TEM Code described in Section 4.2. The T₀ reference temperature for this data set was evaluated as -92°C using the E1921 master curve shown in Figure 7.4.2.3.3-4.

Table 7.4.2.3.3-2: T₀ Individual Specimen Results V0032 A105 Nozzle

Specimen Name	Temperature (°C)	K _{JcRaw} (MPa*m ^{0.5})	1T Data (MPa*m ^{0.5})	Uncensored Data	Test Temp -T ₀ (°C)
380-207	-101	76.2	63.2	1	-10
380-208	-73	185.9	103.9	0	18
380-209	-101	129.1	103.9	1	-10
380-210	-101	108.3	87.9	1	-10
380-211	-101	126.9	102.2	1	-10

Table 7.4.2.3.3-3: T₀ Calculation Results V0032 A105 Nozzle

Initial T ₀ (°C)	-92
Total Samples	5
Samples within T ₀ ± 50°C (N)	5
Number of Uncensored Data (r)	4
Poisson's Ratio	0.3
Σ(r _i n _i)	0.67
Samples Between T _i - T ₀ 50 to -14 °C	4
Samples Between T _i - T ₀ -15 to -35 °C	0
Samples Between T _i - T ₀ -36 to -50 °C	0
T ₀ scrn (°C)	-88
Homogenous or Inhomogeneous	Homogenous

The results of the E1921 analysis show that the A105 material removed from the V0032 nozzle is macroscopically homogenous, indicating consistent properties throughout the sampled material. For this data set, the ductile-brittle transition temperature was found to be -92°C. This does not meet the E1921 validity criteria for a sufficient number of samples tested in an appropriate temperature range with Σ(r_i n_i) < 1.0. However, the results are still considered useful as they are consistent and in family.

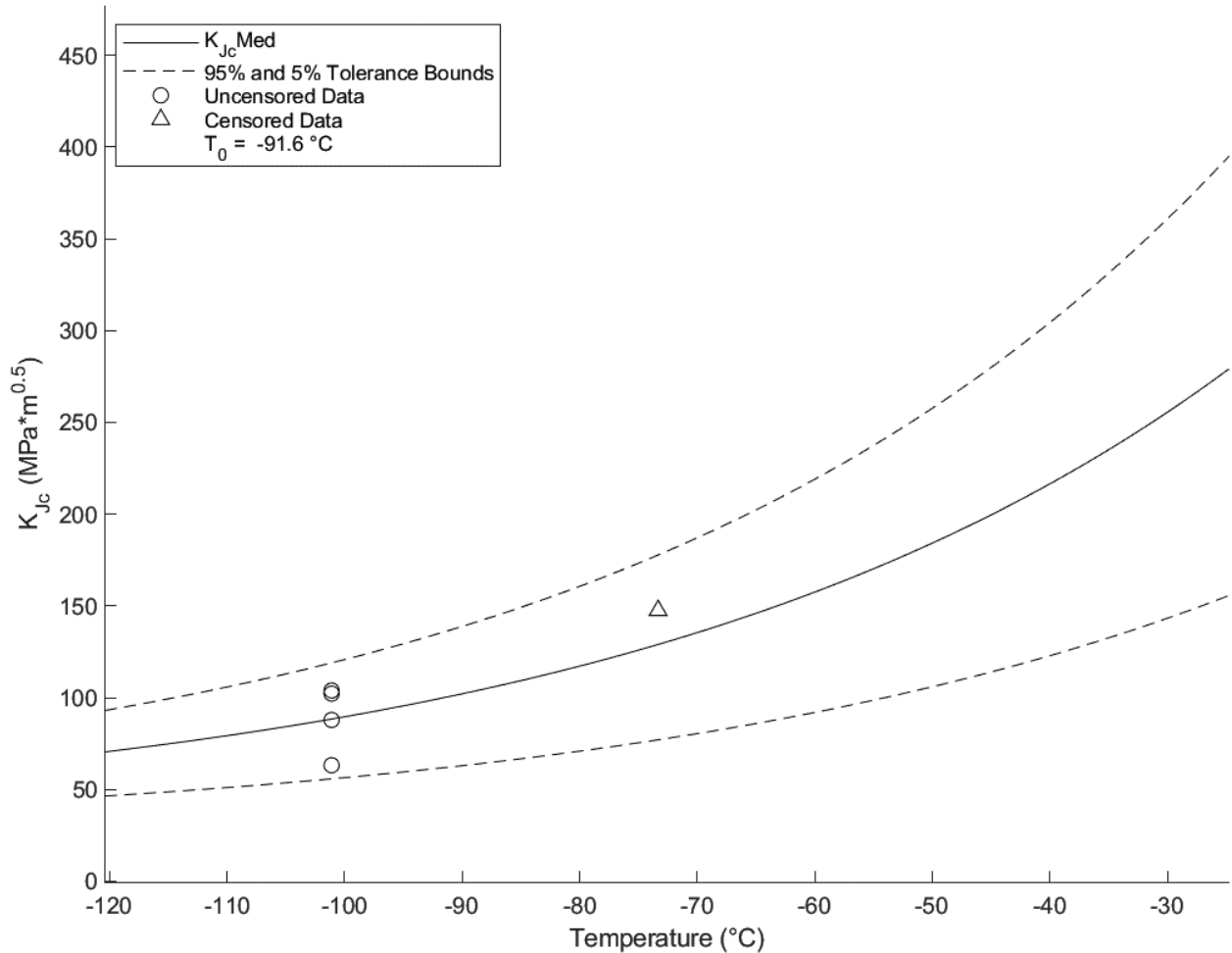


Figure 7.4.2.3.3-4: V0032 A105 Nozzle T_0 Plot ($T_0 = -92^\circ\text{C}$)

Table 7.4.2.3.3-4 provides raw test data values obtained from fracture tests conducted on V0348 A105 nozzle material. Test results that are considered upper shelf are listed under ASTM E1820, while transition temperature test results are listed under E1921. Tests that meet the complete validity requirements for $J_q = J_{1C}$ and $K_{Jq} = K_{J1C}$ are denoted with an asterisk. Despite invalidities, J_q and K_{Jq} convey valuable fracture toughness information, especially when the test results are applied directly to the sample material source. Specimens 483-52 and 483-53 demonstrated some characteristics of an upper shelf test, however they were within the temperature window and have been used as censored data points for E1921 evaluation.

Table 7.4.2.3.3-4: A105 Nozzle Fracture Data V0348

Specimen ID	Test Temp. (°C)	ASTM Crack Plane Orientation	W (in)	a ₀ (in)	a _f (in)	B ₀ (in)	B _N (in)	J _q (kJ/m ²)	K _{Jq} (MPa √m)	K _{JCLT} (MPa √m)	ASTM Standard
483-51	-101	C-R	1.0030	0.5097	0.5177	0.3791	0.3017	35	89	74	E1921
483-52	-101	C-R	1.0029	0.5245	0.5245	0.3772	0.3005	120	164	133	E1921
483-53	-101	C-R	1.0020	0.5424	0.5424	0.3761	0.3056	204	214	172	E1921
483-54	-129	C-R	1.0031	0.5188	0.5271	0.3748	0.3093	44	99	82	E1921
483-56	-129	C-R	1.0033	0.5182	0.5223	0.3747	0.3103	53	109	90	E1921
483-57	-129	C-R	1.0018	0.5474	0.5500	0.3759	0.3090	20	67	57	E1921
483-58	-129	C-R	1.0040	0.5349	0.5349	0.3773	0.3047	12	52	45	E1921
483-60	-129	C-R	1.0012	0.5190	0.5216	0.3752	0.3039	31	84	70	E1921

Results from the eight E1921 tests are presented in Table 7.4.2.3.3-5 and Table 7.4.2.3.3-6. These results were obtained using the T₀TEM Code described in Section 4.2. The T₀ reference temperature for this data set was evaluated as -111°C using the E1921 Master Curve shown in Figure 7.4.2.3.3-5.

Table 7.4.2.3.3-5 T₀ Individual Specimen Results V0348 A105 Nozzle

Specimen Name	Temperature (°C)	K _{JcRaw} (MPa*m ^{0.5})	1T Data (MPa*m ^{0.5})	Uncensored Data	Test Temp -T ₀ (°C)
483-51	-101	88.9	73.9	1	10
483-52	-101	163.8	132.7	1	10
483-53	-101	213.6	157.1	0	10
483-54	-129	99.3	82.1	1	-18
483-56	-129	109.1	89.7	1	-18
483-57	-129	66.9	56.7	1	-18
483-58	-129	52.0	45.1	1	-18
483-60	-129	83.9	70.0	1	-18

Table 7.4.2.3.3-6 T₀ Calculation Results V0348 A105 Nozzle

Initial T ₀ (°C)	-111
Total Samples	8
Samples within T ₀ ± 50°C (N)	8
Number of Uncensored Data (r)	7
Poisson's Ratio	0.3
Σ(ri ni)	1.05
Samples Between T _i - T ₀ 50 to -14 °C	2
Samples Between T _i - T ₀ -15 to -35 °C	5
Samples Between T _i - T ₀ -36 to -50 °C	0
T ₀ scrn (°C)	-99
Homogenous or Inhomogeneous	Inhomogeneous

The results of the E1921 analysis show that the A105 material removed from the V0348 nozzle is macroscopically inhomogeneous, however there are not enough data points to sufficiently qualify the inhomogeneity characterization. For this data set, the ductile-brittle transition temperature was found to be -111°C. This data set meets the E1921 validity criteria for a sufficient number of samples tested in

an appropriate temperature range with $\sum(r_i n_i) \geq 1.0$. Given the consistency of the data with other tested A105 lots, it is safe to conclude that the standard Master Curve gives a good characterization of the material.

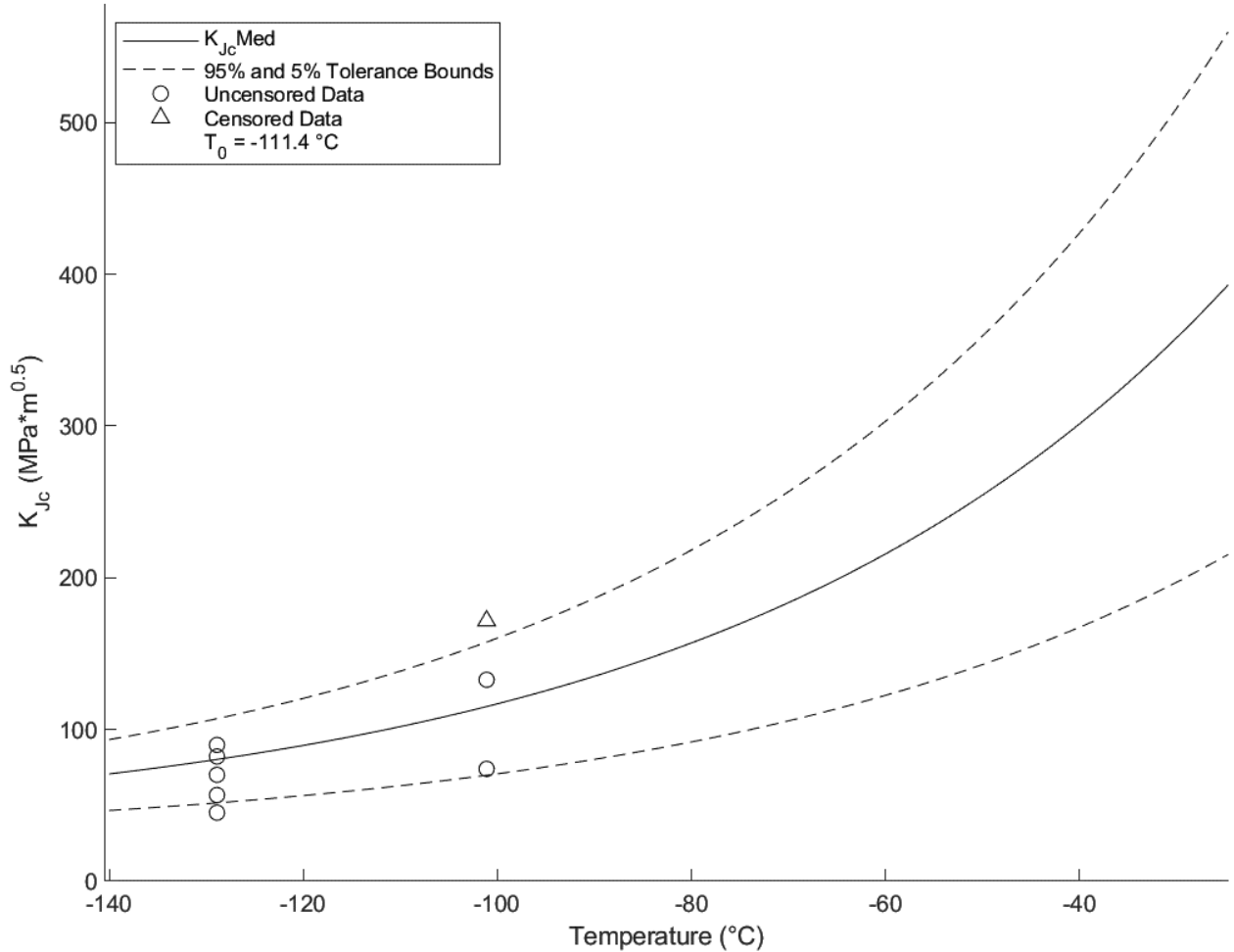


Figure 7.4.2.3.3-5: V0348 A105 Nozzle T_0 Plot ($T_0 = -111\text{C}$)

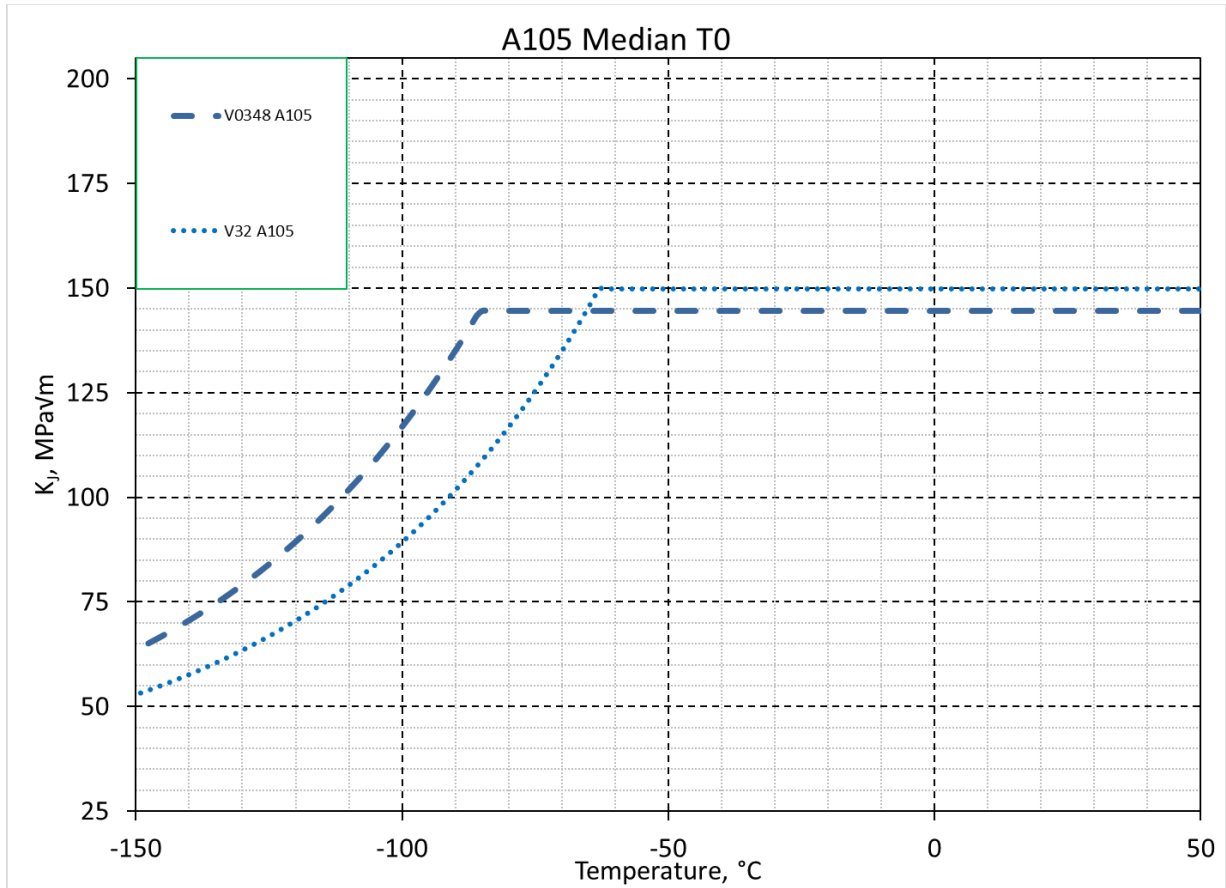


Figure 7.4.2.3.3-6: A105 Nozzle T₀ Combined Master Curve Plot

7.4.2.3.4 Fatigue Crack Growth

Fatigue crack growth tests were not performed on this material.

7.4.2.3.5 Charpy Impact

Charpy impact tests were not performed on this material.

7.5 Weld Materials

LPVs contain many different types of welds in various locations. These welds are the most common location of flaws found in vessels and, as such, are the most likely failure points. A number of weld processes were used. Shielded Metal Arc Welding (SMAW) (commonly referred to as stick welding), Gas Metal Arc Welding (GMAW) (also referred to Metal Inert Gas, or MIG, Submerged Arc Welding (SAW) (abbreviated in general shop conversation as “sub-arc”) welds), and possibly Gas Tungsten Arc Welding (GTAW) (also referred to as Tungsten Inert Gas (TIG), or Heli-arc) are found throughout the LPV fleet. Very few of these welds were inspected with modern non-destructive evaluation (NDE) techniques and, therefore, are more subject to multiple types of manufacturing defects. Also, the material characteristics of the weld metal deposits are not well documented, and even when documented, mechanical properties are subject to the individual weld application and any stress relief or post weld heat treatment. In addition, the welding process produces HAZ in the surrounding parent material. The weld types investigated in this project are longitudinal wrapper welds, inner layer welds, circumferential through-thickness welds, and nozzle welds.

7.5.1 Longitudinal Wrapper Weld

Longitudinal wrapper welds are welds along the length of the vessel and join wrapper plate edges to each other to create cylinders. In the case that there is only one plate per layer, the weld joins the wrapper back to itself. If there are multiple plates per layer, then the weld joins the edge of one plate to the next. These welds also join the current wrap to the previous wrap such that each subsequent layer is unable to twist or slide out of position. Longitudinal wrapper welds are offset from layer to layer around the vessel so that no adjacent layers have welds on top of each other (see Figure 7.5.1-1). In some instances, it was observed that the weld produced significant over-burn through the backer layer, enough that three layers were joined. Wrapper layer welds are “green” welds. They received no post-weld inspection, stress relief, or heat treatment. In some cases, the welds were ground smooth to allow for a closer fit of the following layer.

Testing performed during this project was conducted on the weld nugget located in the joined plate of any investigated layer weld, so that only the weld metal would be tested. Tests were also conducted in the HAZ produced by the weld and in the parent plate material. Wrapper layers are typically 0.25 inches nominal thickness. Weld deposit material varies by manufacturer.

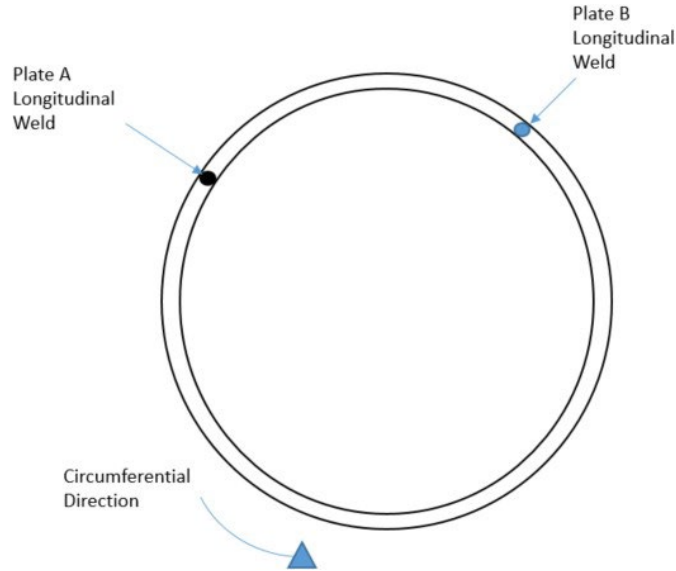


Figure 7.5.1-1: Weld Offset Diagram

7.5.1.1 Chemical Composition

Weld material specifications are not typically available or verifiable, therefore the chemical composition reported is only of the collected data. Data shown in Table 7.5.1.1-1 is only from the weld center, collected from Arc Spark OEM analyses of vessels at MSFC. HAZ chemistry is that of the parent plate material and is therefore not dealt with in this section.

Table 7.5.1.1-1: Longitudinal Weld Collected Chemistry Data

Vessel	C	Si	Mn	P	S	Cr	Mo	Ni	Cu	V
V0023	0.081	0.28	0.75	0.014	0.021	0.05	0.39	1.65	0.027	0.16
V32	0.12	0.4	1.5	0.017	0.022	0.15	0.22	1.19	0.038	0.066
V0348	0.14	0.16	0.73	0.012	0.019	0.04	0.16	0.039	0.075	0.066
V0125	0.088	0.41	1.52	0.014	0.025	0.22	0.28	1.4	0.086	0.048
MV50466-8	0.13	0.39	1.52	0.014	0.02	0.14	0.18	1.04	0.036	0.078

7.5.1.2 Metallography

The only metallographic study performed on longitudinal seam welds was a grain orientation study involving LPVs V0125 and MV50466-8. No grain size, grain size through thickness, or carburization layer thickness studies were performed, and no macro cubes were produced.

Grain Orientation Study

The grain orientation study is a polish and etch of a seam weld cross section. Its purpose is to confirm the correct orientation for fracture testing. In this case, the P orientation, parallel to the weld path, was found to be the most realistic and proper orientation for further tests.

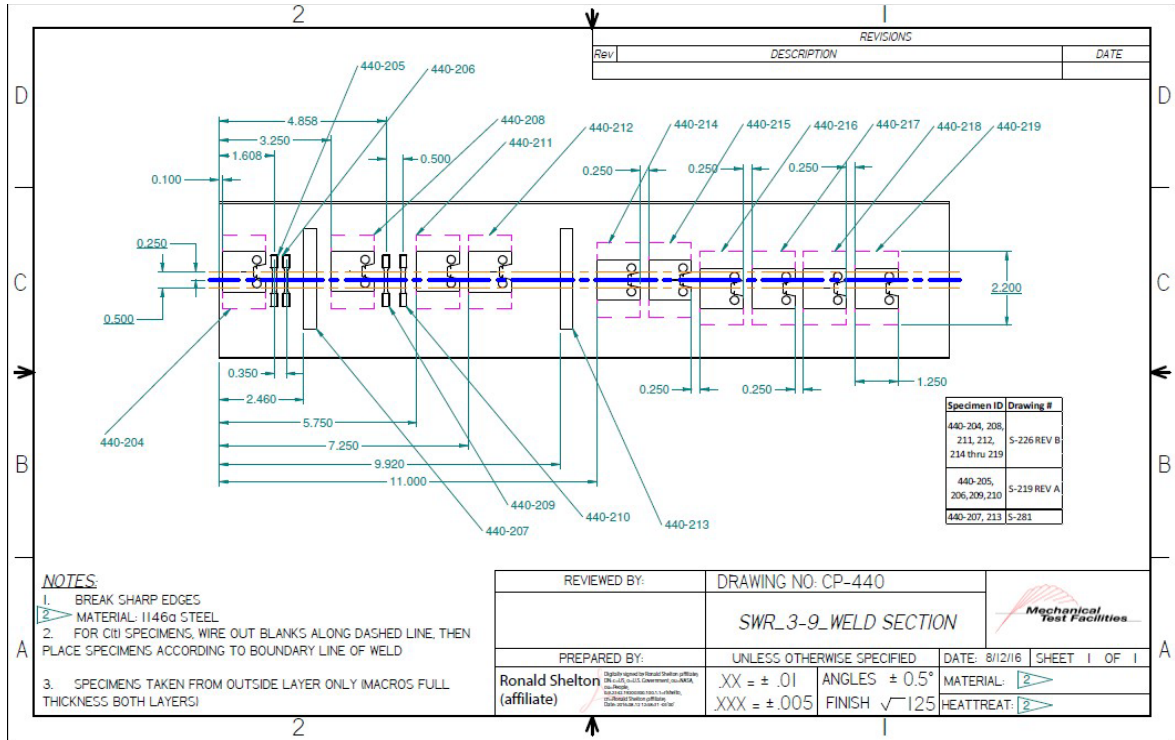


Figure 7.5.1.2-1: Cut Plan for Macros from MV50466-8 Seam Weld

The macros shown in Figure 7.5.1.2-2, Figure 7.5.1.2-3, and Figure 7.5.1.2-4 were extracted from the cross-section of V0125 and MV50466-8 seam welds, near the location of tensile and fracture test specimens.

Cross-section micrograph of multi-pass axial shell weld

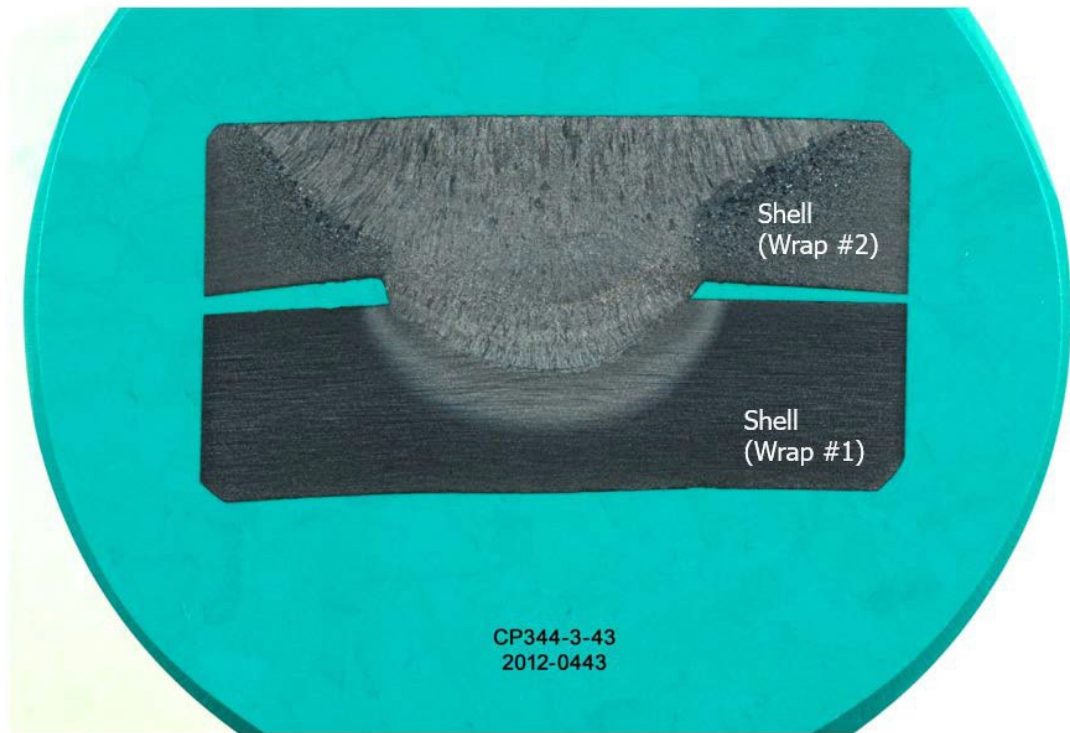


Figure 7.5.1.2-2: V0125 Seam Weld Macro



440-224 (160788003)

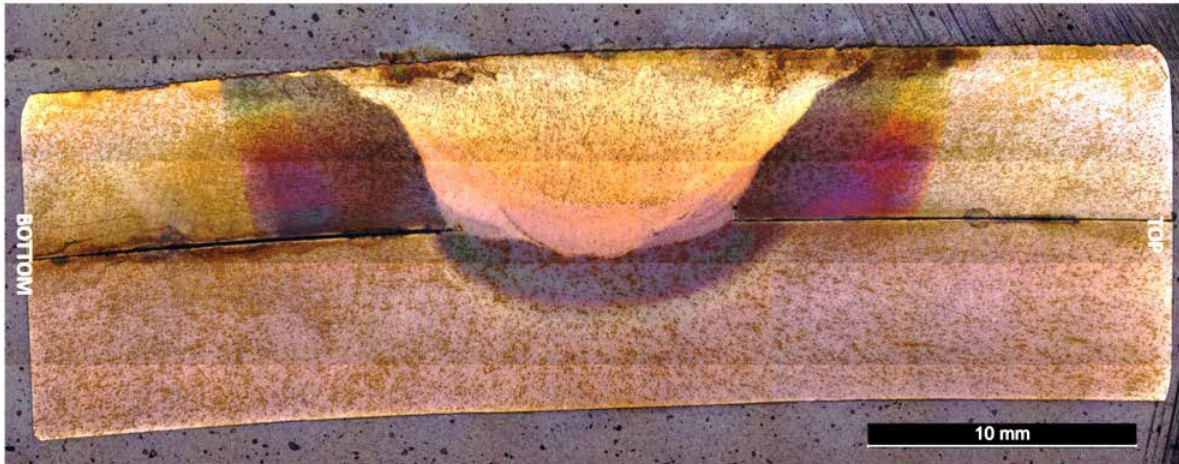


Figure 7.5.1.2-3: MV50466-8 Seam Weld Macro (Edge of wrapper plate unfused)



440-231 (160788004)

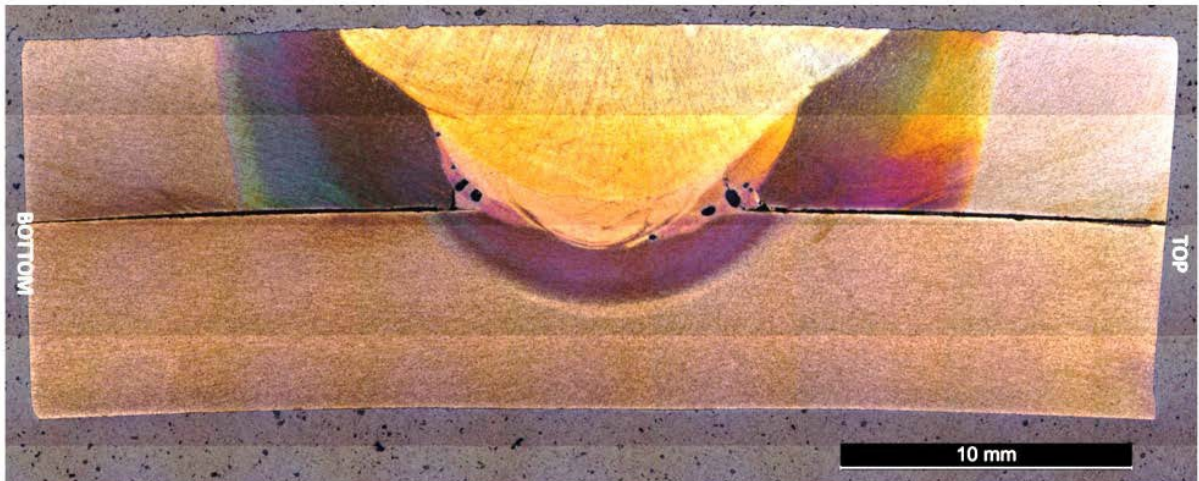


Figure 7.5.1.2-4: MV50466-8 Seam Weld Macro (Significant porosity)

Hardness

Vickers Hardness (VHN) traces were conducted on some longitudinal wrapper welds to help identify the degree of variance in material properties and stress concentrations across the parent-weld-parent span. These were used to identify areas of concern and direct testing towards less favorable material conditions which would indicate worst case crack scenarios.



Figure 7.5.1.2-5: MV50466-8 Seam Weld 440-163 Indent Locations

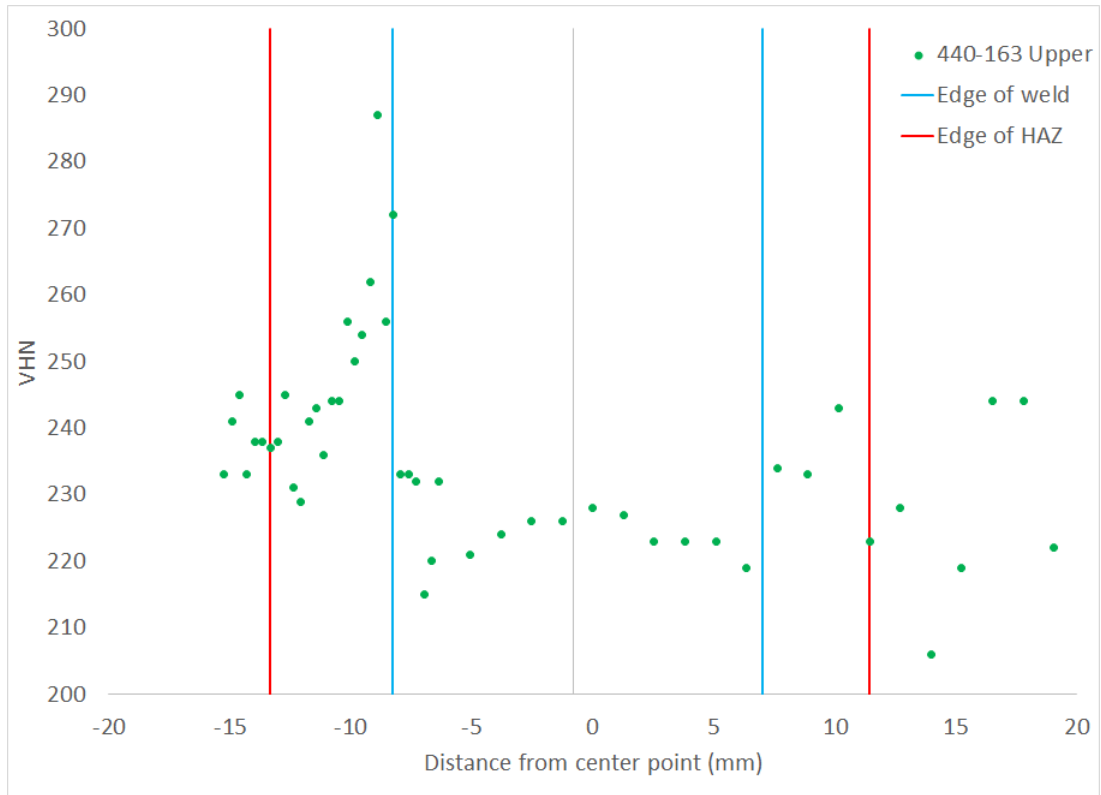


Figure 7.5.1.2-6: MV50466-8 Seam Weld 440-163 Hardness Trace



Figure 7.5.1.2-7: MV50466-8 Seam Weld 440-173 Indent Locations

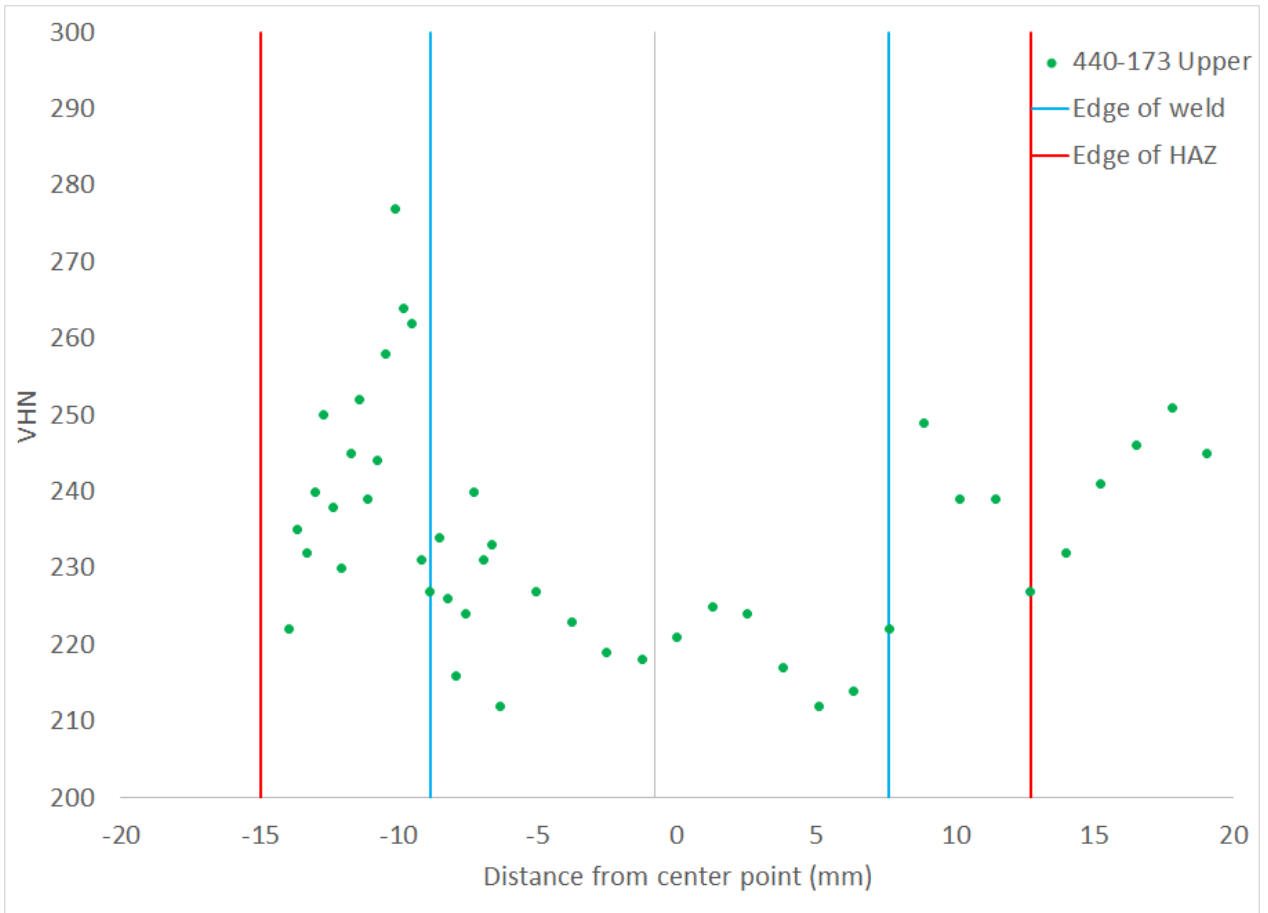


Figure 7.5.1.2-8: MV50466-8 Seam Weld 440-173 Hardness Trace

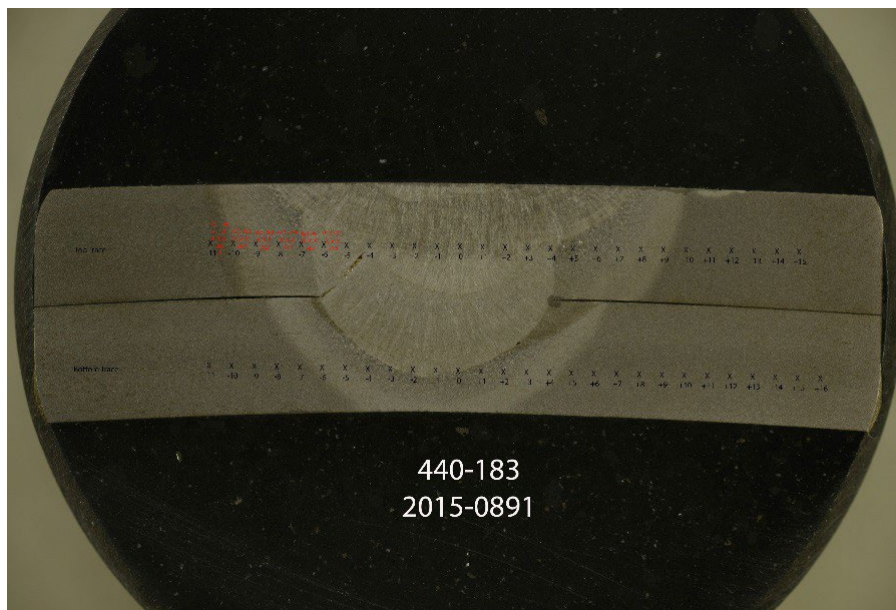


Figure 7.5.1.2-9: MV50466-8 Seam Weld 440-183 Indent Locations

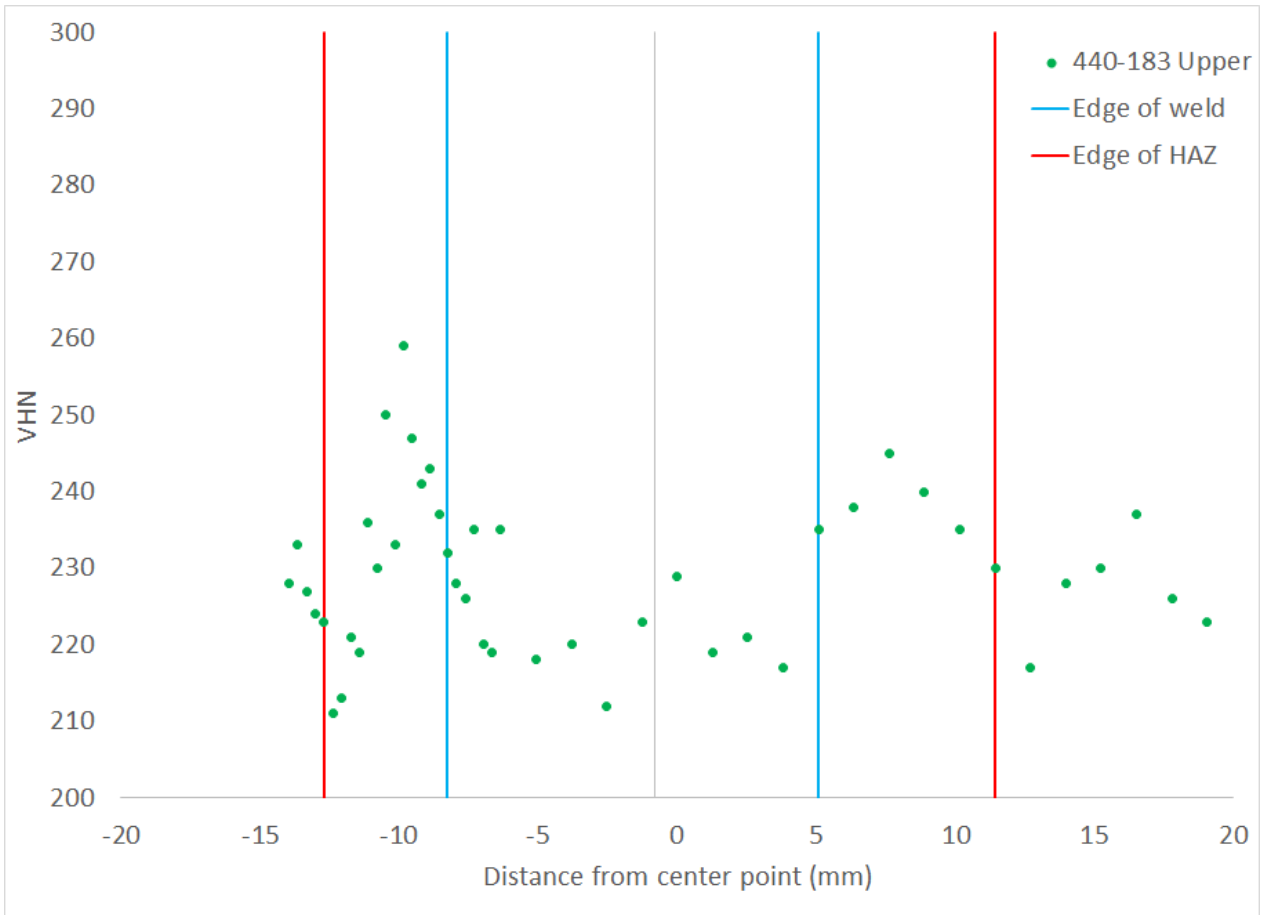


Figure 7.5.1.2-10: MV50466-8 Seam Weld 440-183 Hardness Trace

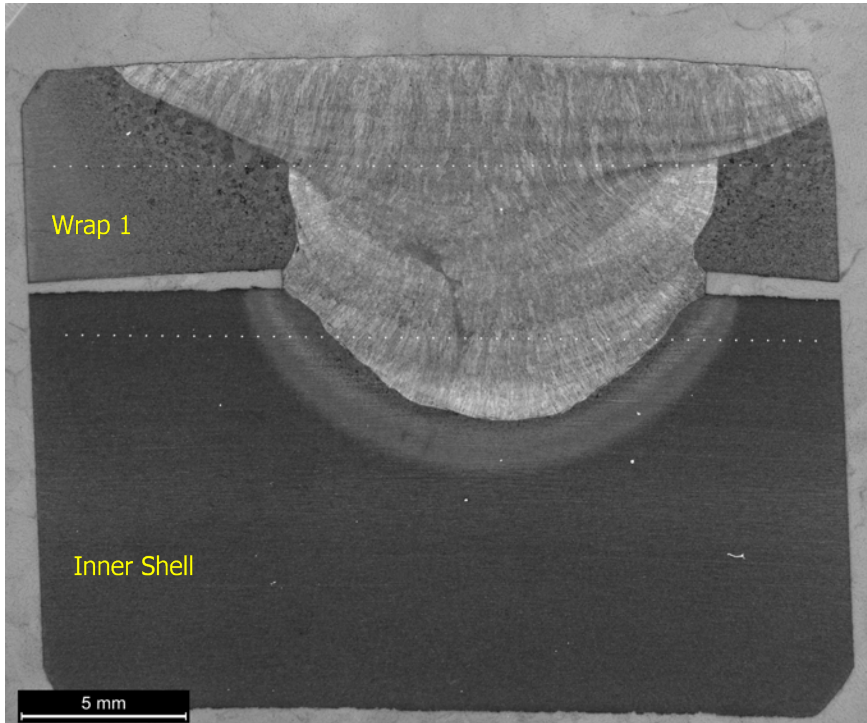


Figure 7.5.1.2-11: V0125 Seam Weld CP344-3-30 Indent Locations

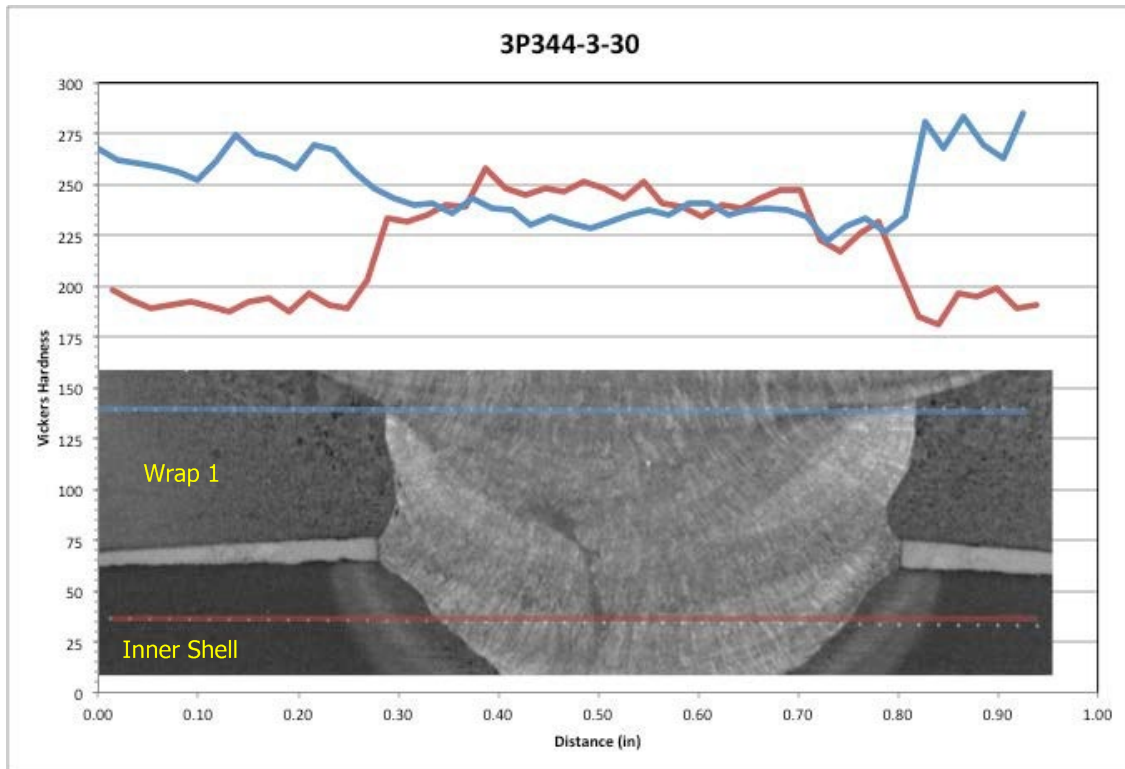


Figure 7.5.1.2-12: V0125 Seam Weld CP344-3-30 Hardness Trace

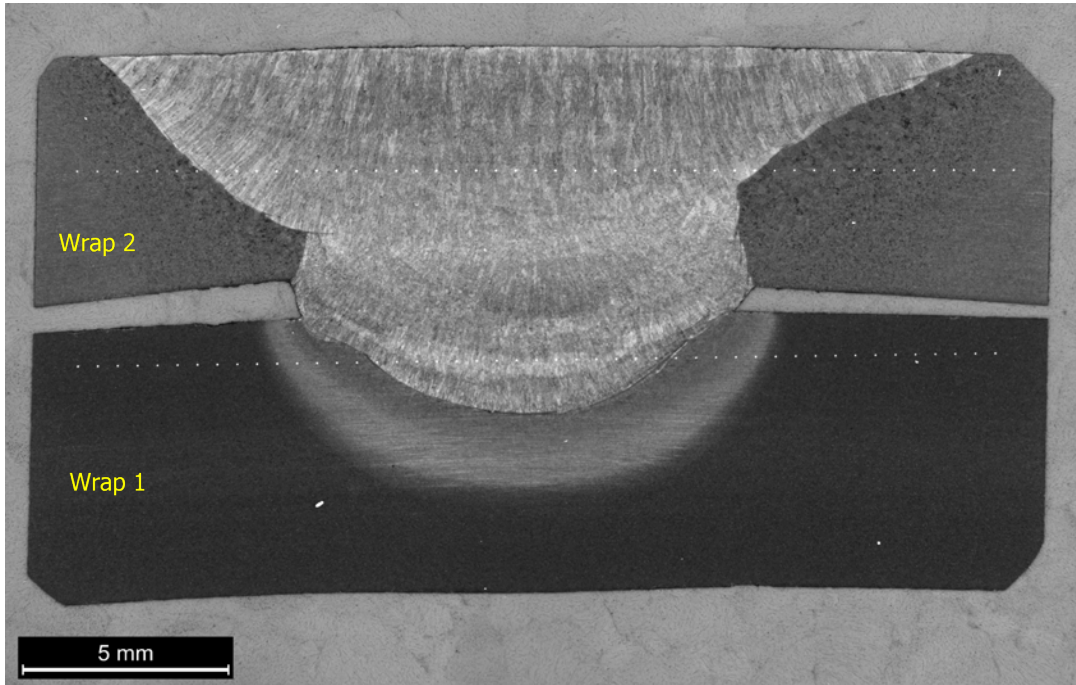


Figure 7.5.1.2-13: V0125 Seam Weld CP344-3-43 Indent Locations

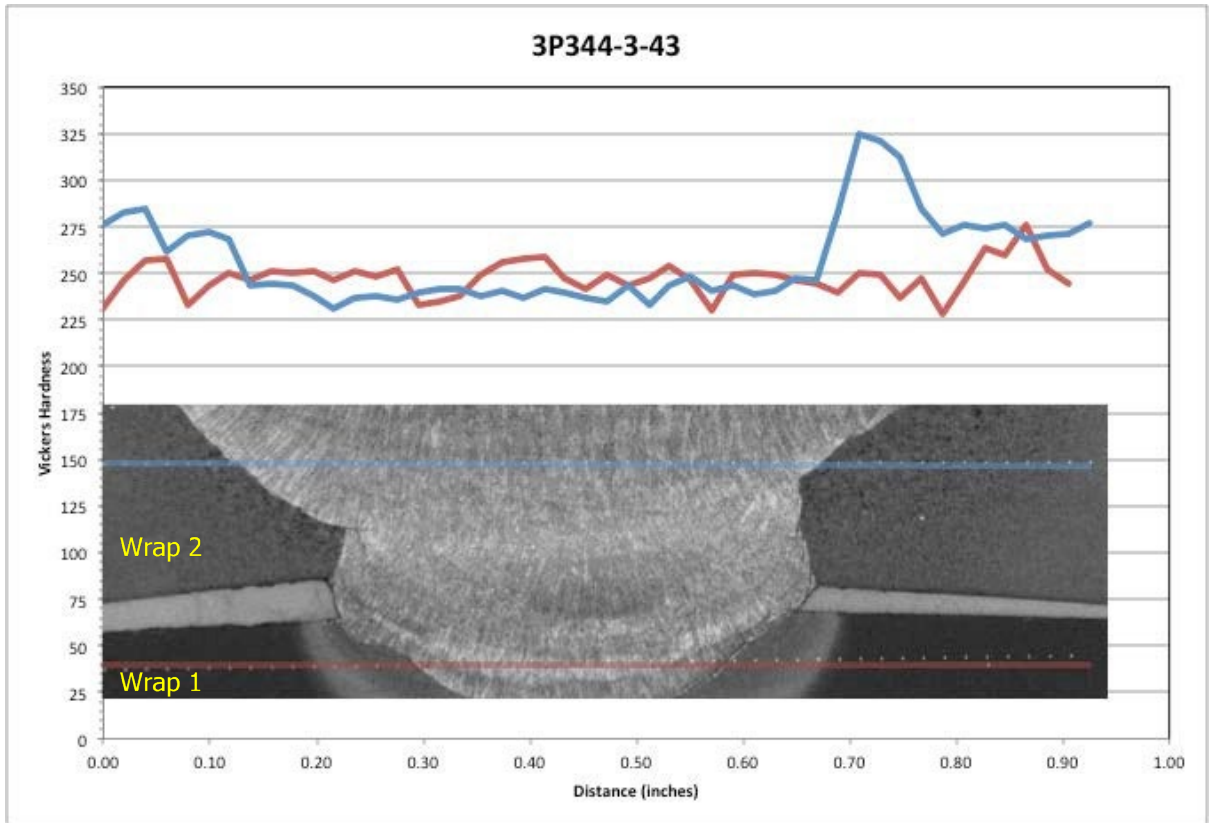


Figure 7.5.1.2-14: V0125 Seam Weld CP344-3-43 Hardness Trace

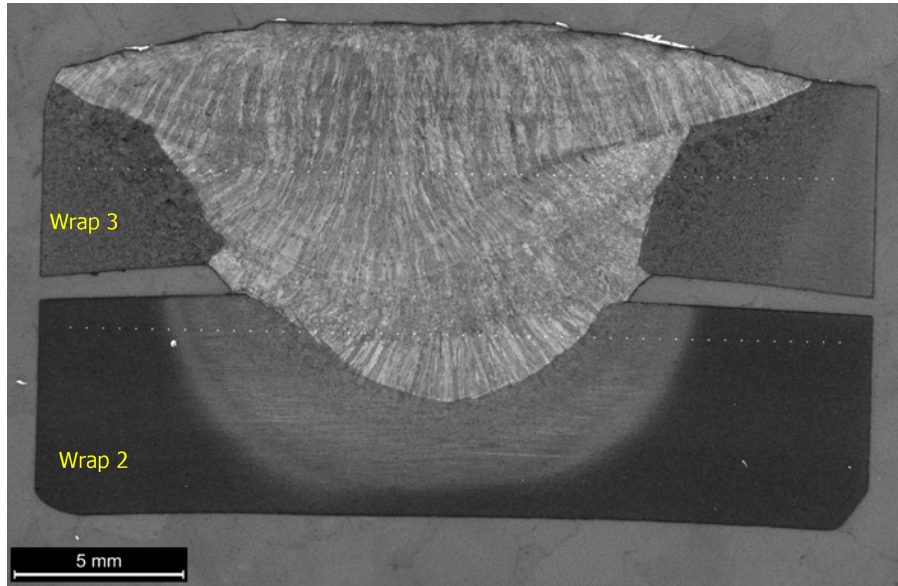


Figure 7.5.1.2-15: V0125 Seam Weld CP344-3-54 Indent Locations

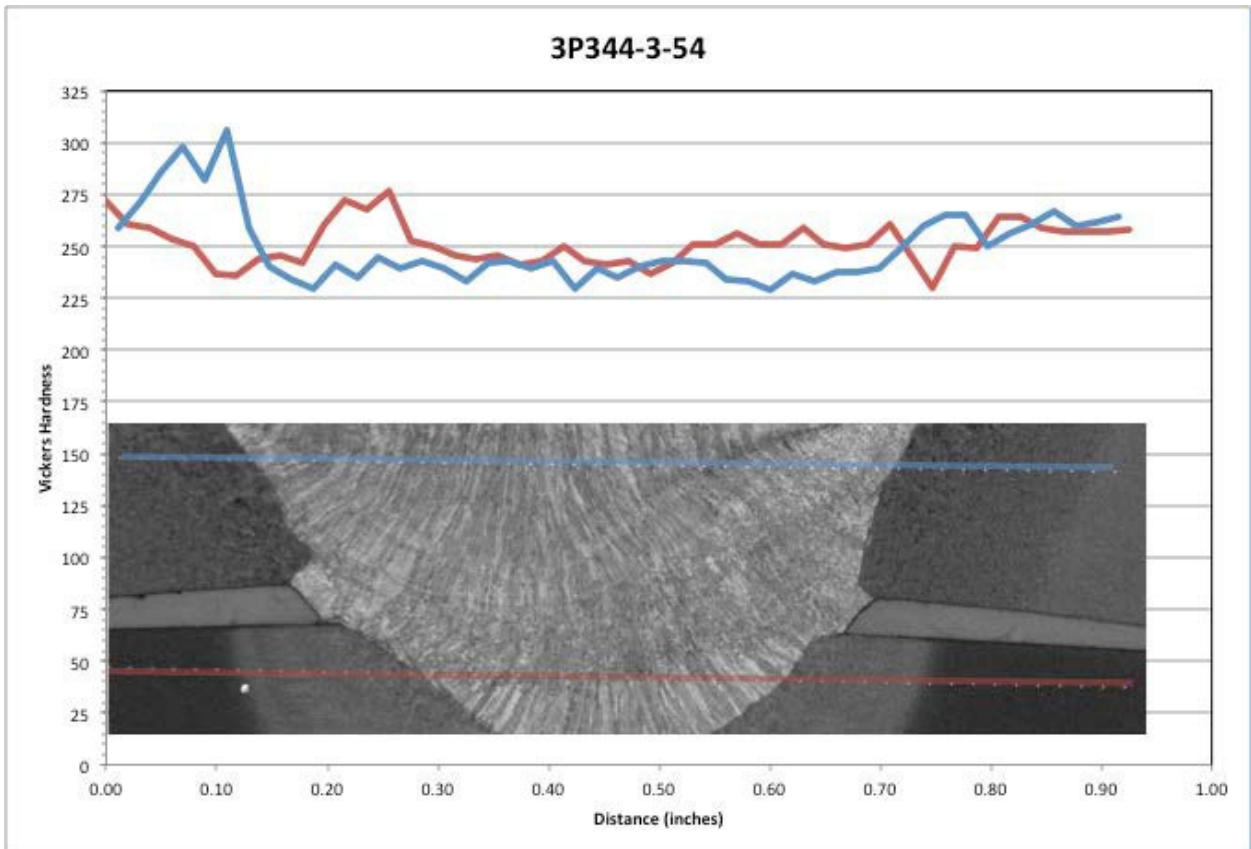


Figure 7.5.1.2-16: V0125 Seam Weld CP344-3-54 Hardness Trace

7.5.1.3 Mechanical Properties

Mechanical properties for the weld metal vary by manufacturer and application parameters and are only characterized by the tests documented in the following sections.

7.5.1.3.1 Smooth Tensile Tests

Smooth tensile tests were conducted at MSFC on round specimens according to ASTM E8, “Standard Test Methods for Tension Testing of Metallic Materials” (51) using specimen design S-219 Rev A. The mechanical test frame consisted of a servo-hydraulic actuator and reaction frame. The frame used an LVDT for displacement feedback. Stress measurements were derived from load measurements and the initial specimen measurements. Strain measurements were derived from an extensometer and the initial specimen measurements.

The results obtained from testing of longitudinal wrapper welds from vessels MV50466-8, V0023, V0032 and V0125 are presented in Table 7.5.1.3.1-1, Table 7.5.1.3.1-2, Table 7.5.1.3.1-3, and Table 7.5.1.3.1-4. A typical engineering stress-strain curve is shown in Figure 7.5.1.3.1-1.

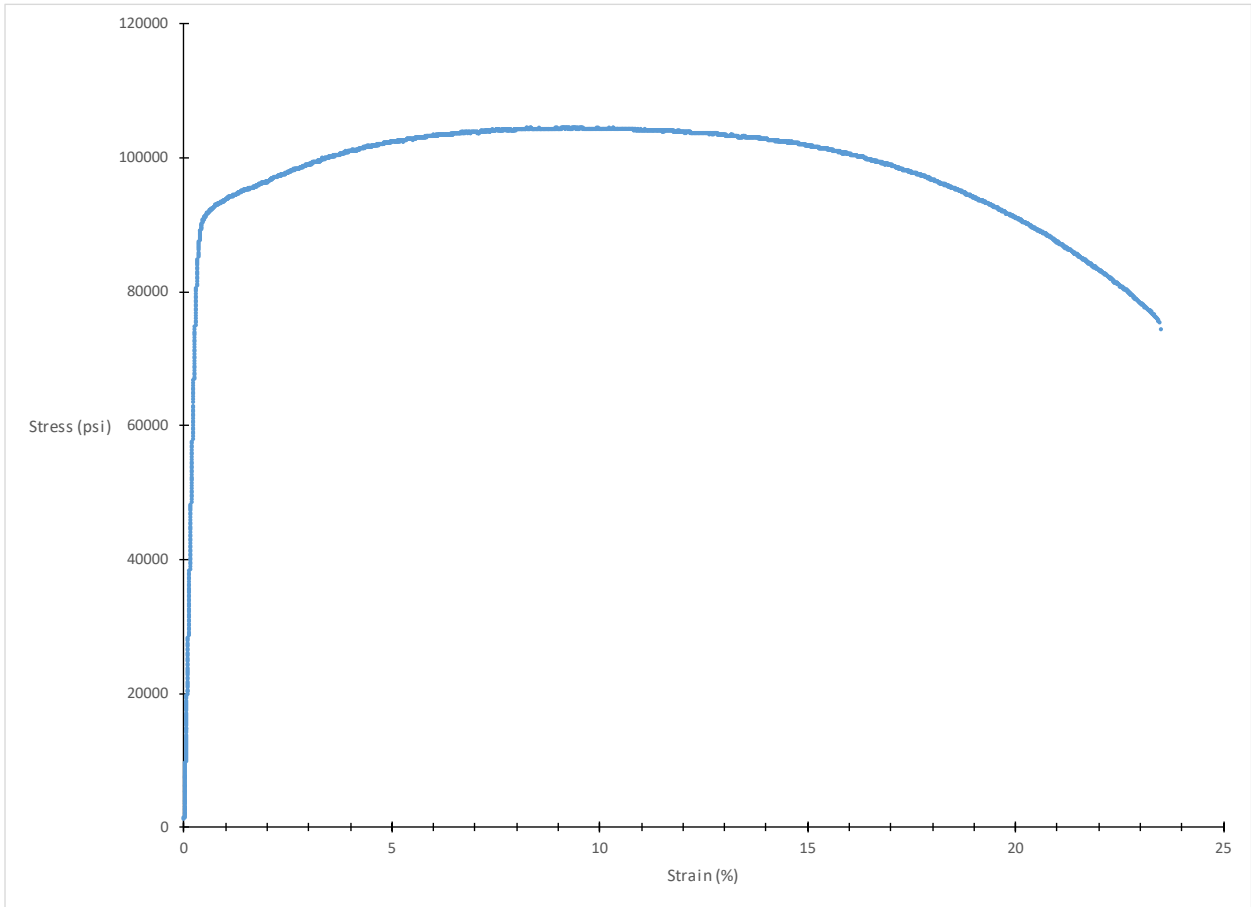


Figure 7.5.1.3.1-1: Longitudinal Seam Weld Smooth Tensile Plot Sample 519-53

Table 7.5.1.3.1-1: Longitudinal Weld Smooth Tensile Data MV50466-8

Specimen ID	Test Temp. (°C)	ASTM Orientation	Tensile Stress (ksi)	Yield Stress (ksi)	Fracture Elongation (%)
440-164	21	P	112.7	98.7	19.8
440-172	21	N	110.0	90.9	19.4
440-174	21	P	112.0	91.0	19.3
440-182	21	N	111.0	91.5	19.4
440-205	-29	N	121.8	99.8	19.8
440-221	-29	N	125.0	108.8	9.9
440-223	-29	N	138.9	104.1	9.7
440-220	-46	N	115.6	99.0	19.5
440-222	-46	N	119.3	99.5	20.9
440-206	-73	N	124.1	98.9	21.7

Table 7.5.1.3.1-2 Longitudinal Weld Smooth Tensile Data V0023

Specimen ID	Test Temp. (°C)	ASTM Orientation	Tensile Stress (ksi)	Yield Stress (ksi)	Fracture Elongation (%)
519-53	21	N	104.5	91.4	23.5
519-54	21	N	105.5	91.4	21.3
519-55	-46	N	115.6	95.3	22.2
519-56	-46	N	116.2	98.5	20.8
519-57	-101	N	130.0	97.7	23.6
519-58	-101	N	131.1	99.7	23.3

Table 7.5.1.3.1-3: Longitudinal Weld Smooth Tensile Data V0032

Specimen ID	Test Temp. (°C)	ASTM Orientation	Tensile Stress (ksi)	Yield Stress (ksi)	Fracture Elongation (%)
380-145	21	N	115.0	94.7	24.0
380-147	-29	N	121.8	94.8	24.3
380-148	-73	N	129.2	93.5	24.0
380-159	21	N	111.6	90.9	24.4
380-160	-29	N	119.3	92.1	22.0
380-161	-73	N	127.1	93.4	23.5
380-162	21	N	116.7	93.7	22.1
380-172	21	N	114.9	94.4	21.0
380-173	-29	N	124.2	96.3	24.0
380-174	-73	N	131.0	96.6	25.1
380-175	21	N	114.9	94.0	23.6
380-181	21	N	107.7	88.3	21.5
380-182	-29	N	115.2	89.7	23.2
380-183	-73	N	125.2	92.3	21.9
380-184	21	N	109.3	88.3	23.3

Table 7.5.1.3.1-4: Longitudinal Weld Smooth Tensile Data V0125

Specimen ID	Test Temp. (°C)	ASTM Orientation	Tensile Stress (ksi)	Yield Stress (ksi)	Fracture Elongation (%)
CP344-3-41	26	N	117.5	94.4	16.6
CP344-3-28	25	N	108.1	89.5	16.7
CP344-3-40	25	N	117.0	94.8	17.5
CP344-3-27	24	N	110.2	92.3	13.9
CP344-3-52	24	N	115.7	92.9	16.6
CP344-3-51	24	N	112.4	90.5	16.7
CP344-3-29	-46	N	141.2	109.2	16.5
CP344-3-42	-46	N	152.4	114.7	20.6
CP344-3-53	-46	N	180.2	145.6	20.1

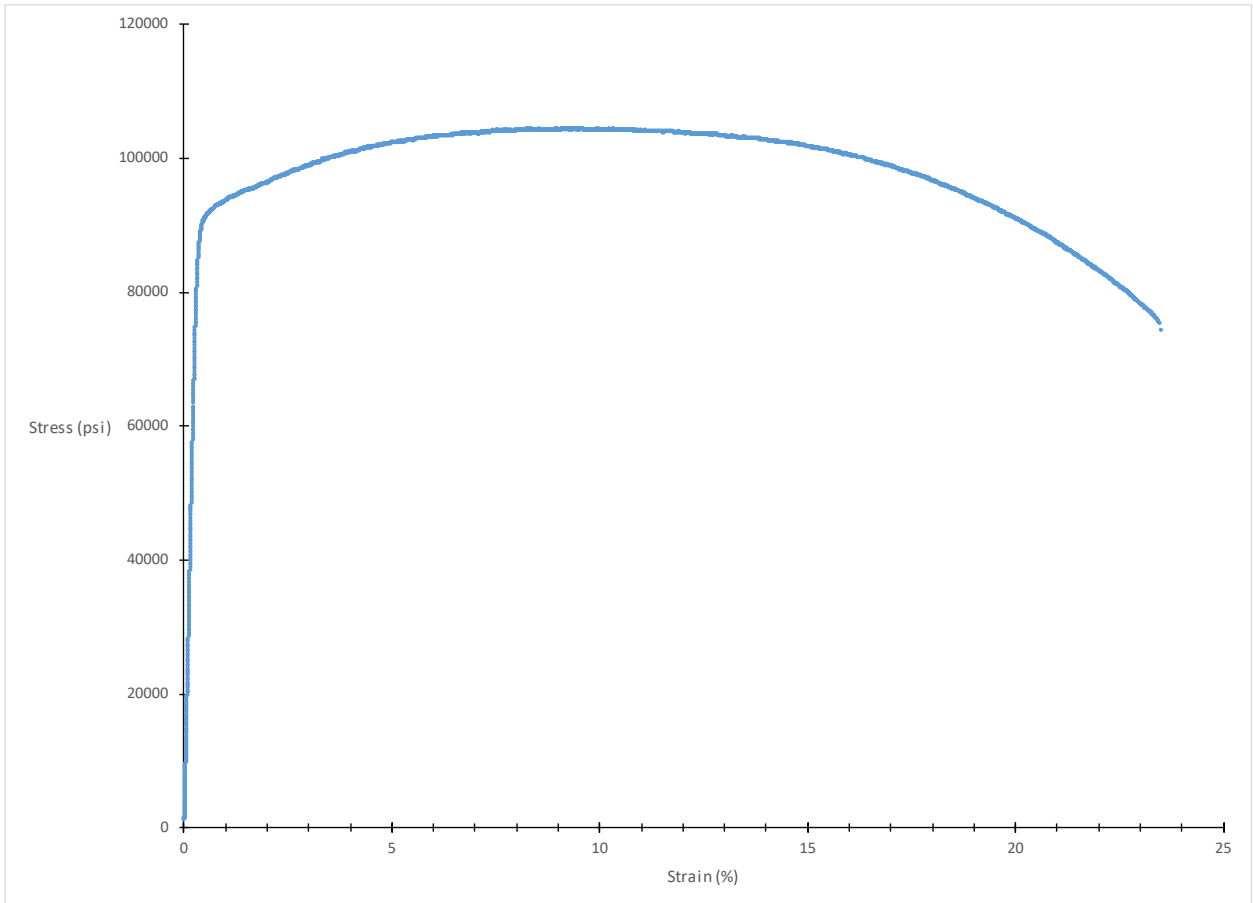


Figure 7.5.1.3.1-1: Longitudinal Seam Weld Smooth Tensile Plot Sample 519-53

7.5.1.3.2 Notch Tensile

Notch tensile tests were not performed on this material.

7.5.1.3.3 Fracture Properties

All room temperature testing was performed in accordance with ASTM E1820 (10). All other temperatures were tested in accordance with ASTM E1921 (7). Testing for both standards use specimen design S-226 Rev B with the thickness machined to maximum allowable thickness. All longitudinal seam weld fracture tests came from vessels V0125, V0032, MV50466-8, and V0023 and were tested with the crack plane in the N-P orientation as defined by ASTM. The specimens used were ASTM E1820 compact specimens (C(T)) with $W = 1.0$ inches and $0.2 \text{ inches} \leq B \leq 0.375 \text{ inches}$, $a/W = 2.0$. All specimens were side-grooved to a total thickness reduction of 20%. The cutting diagram used to remove the C(T) specimens from the MV50466-8 wrapper is shown in Figure 7.5.1.3.3-3. Examples of Load Versus COD and J_q Versus Δa plots are shown in Figure 7.5.1.3.3-1 and Figure 7.5.1.3.3-2.

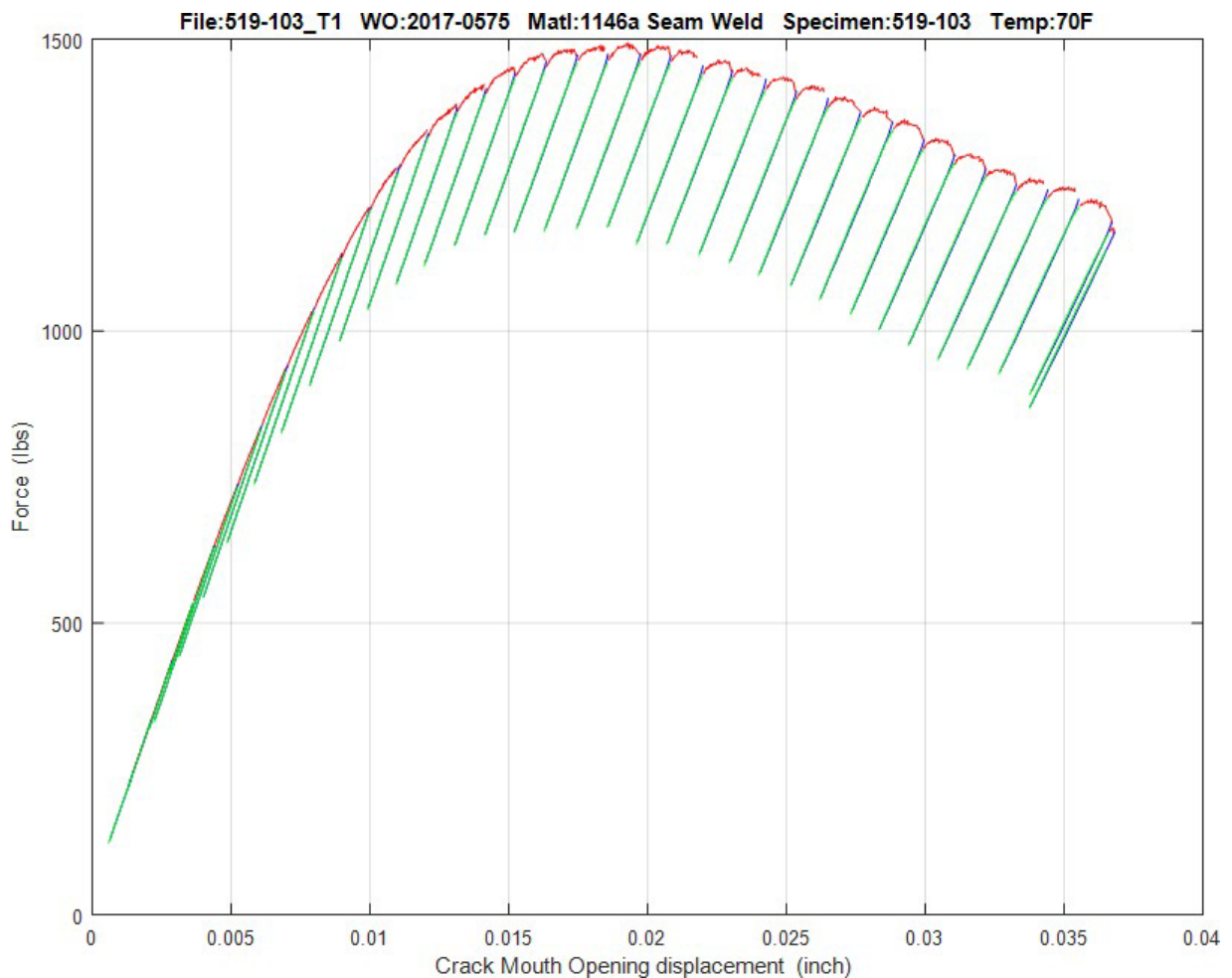


Figure 7.5.1.3.3-1: Longitudinal Seam Weld Load Versus COD Plot, Sample 519-103

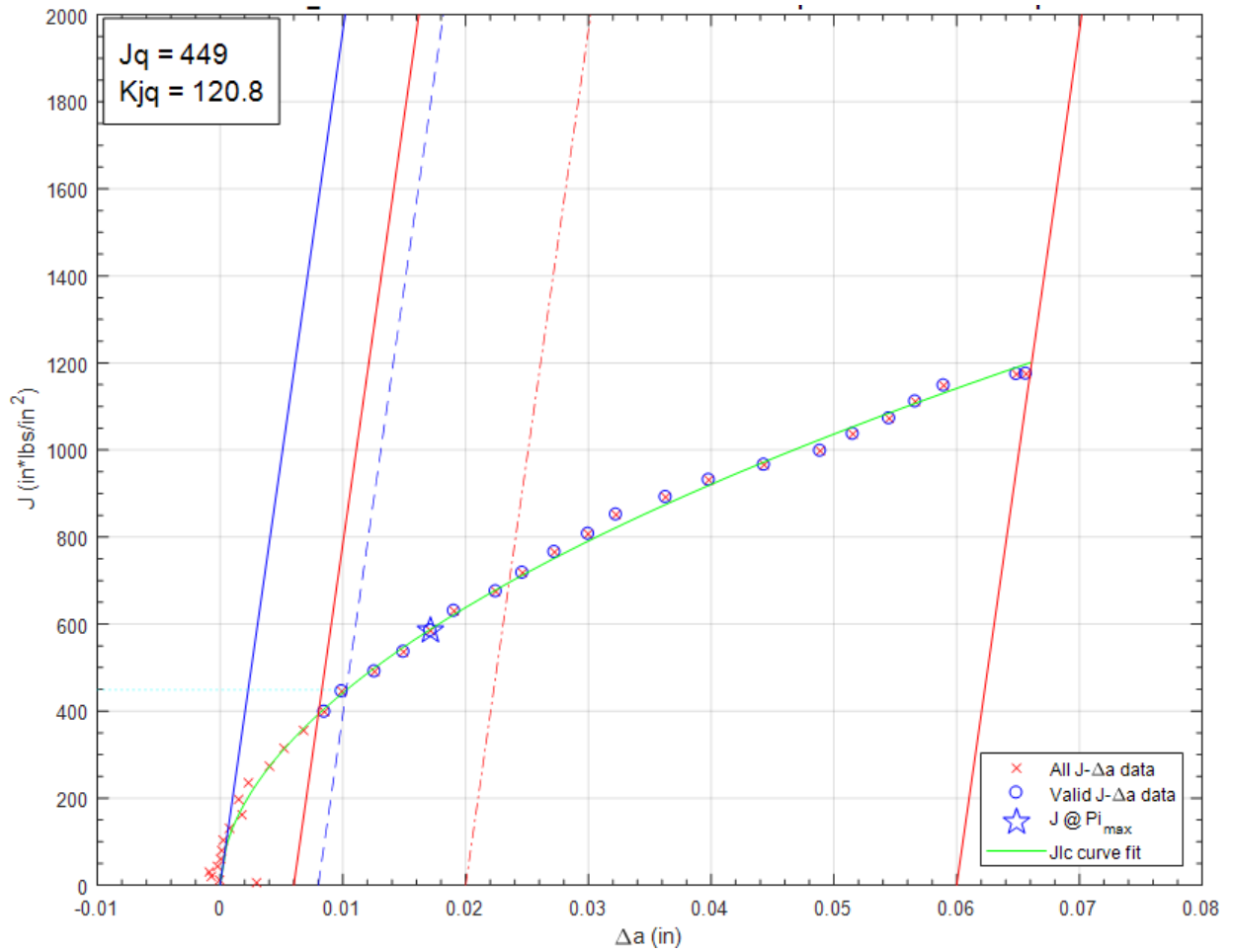


Figure 7.5.1.3.3-2: Longitudinal Seam Weld J_q Versus Δa Plot, Sample 519-103

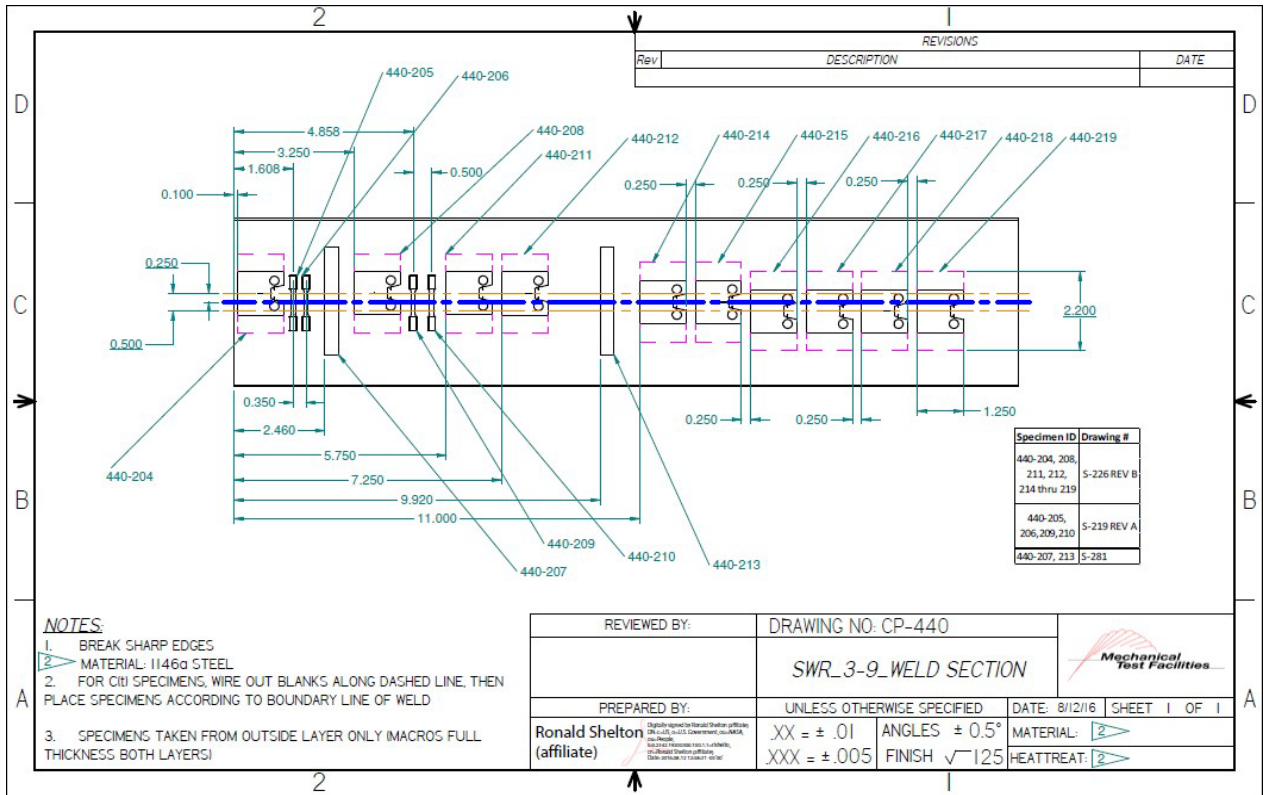


Figure 7.5.1.3.3-3: Cut Plan for Fracture Specimens from MV50466-8 Seam Weld

The test data in Table 7.5.1.3.3-1 are raw values obtained from fracture tests conducted on V0125 longitudinal seam weld material. Test results that are considered upper shelf are listed under ASTM E1820, while transition temperature test results are listed under E1921. Tests that meet the complete validity requirements for $J_q = J_{1C}$ and $K_{Jq} = K_{J1C}$ are denoted with an asterisk. Despite invalidities, J_q and K_{Jq} convey valuable fracture toughness information, especially when the test results are applied directly to the sample material source. Material from the V0125 seam weld was tested as low as -46°C , however a cleavage failure was not seen. Therefore, no T_0 Master Curve can be produced. However, it can be assumed that the transition temperature will be at a temperature below -46°C .

Table 7.5.1.3.3-1: Seam Weld Fracture Data V0125

Specimen ID	Test Temp. ($^\circ\text{C}$)	ASTM Crack Plane Orientation	W (in)	a_0 (in)	a_f (in)	B_0 (in)	B_N (in)	J_q (kJ/m^2)	K_{Jq} ($\text{MPa}\sqrt{\text{m}}$)	K_{J1C} ($\text{MPa}\sqrt{\text{m}}$)	ASTM Standard
CP-344-3-34	23	N-P	0.9979	0.6019	0.6555	0.1885	0.1530	96	146	---	E1820
CP-344-3-21	22	N-P	0.9977	0.5987	0.6677	0.1882	0.1450	169	194	---	E1820
CP-344-3-46	21	N-P	0.9970	0.6293	0.6696	0.1891	0.1430	135	174	---	E1820
CP-344-3-47	21	N-P	0.9993	0.5985	0.6396	0.1898	0.1440	108	155	---	E1820
CP-344-3-23	-46	N-P	0.9983	0.6197	0.6623	0.1898	0.0154	124	166	---	E1820
CP-344-3-36	-46	N-P	0.9990	0.5987	0.6506	0.1880	0.1500	80	134	---	E1820
CP-344-3-48	-46	N-P	1.0012	0.6044	0.7928	0.1883	0.1568	63	118	---	E1820

The test data in Table 7.5.1.3.3-2 are raw values obtained from fracture tests conducted on MV50466-8 longitudinal seam weld material. Test results that are considered upper shelf are listed under ASTM E1820, while transition temperature test results are listed under E1921. Tests that meet the complete validity requirements for $J_q = J_{1C}$ and $K_{Jq} = K_{J1C}$ are denoted with an asterisk. Despite invalidities, J_q and K_{Jq} convey valuable fracture toughness information, especially when the test results are applied directly to the sample material source.

Table 7.5.1.3.3-2: Seam Weld Fracture Data MV50466-8

Specimen ID	Test Temp. (°C)	ASTM Crack Plane Orientation	W (in)	a ₀ (in)	a _f (in)	B ₀ (in)	B _N (in)	J _q (kJ/m ²)	K _{Jq} (MPa√m)	K _{JC1T} (MPa√m)	ASTM Standard
440-167	21	N-P	0.9995	0.5048	0.5953	0.1951	0.1463	63	119	---	E1820
440-177	21	N-P	0.9986	0.5019	0.5894	0.1961	0.1540	50	106	---	E1820
440-230	-29	N-P	1.0011	0.5086	0.5802	0.1987	0.1618	63*	118	---	E1820
440-232	-29	N-P	1.0000	0.5050	0.5611	0.1996	0.1628	79	133	---	E1820
440-233	-46	N-P	1.0000	0.5052	0.5651	0.1946	0.1600	94*	145	---	E1820
440-234	-46	N-P	1.0000	0.5074	0.5751	0.1956	0.1630	98	148	---	E1820
440-214	-73	N-P	1.0006	0.5089	0.5162	0.1965	0.1607	26	76	57	E1921
440-215	-73	N-P	1.0000	0.5132	0.5170	0.1968	0.1573	31	84	62	E1921
440-235	-73	N-P	0.9999	0.5084	0.5184	0.1929	0.1558	67	122	88	E1921

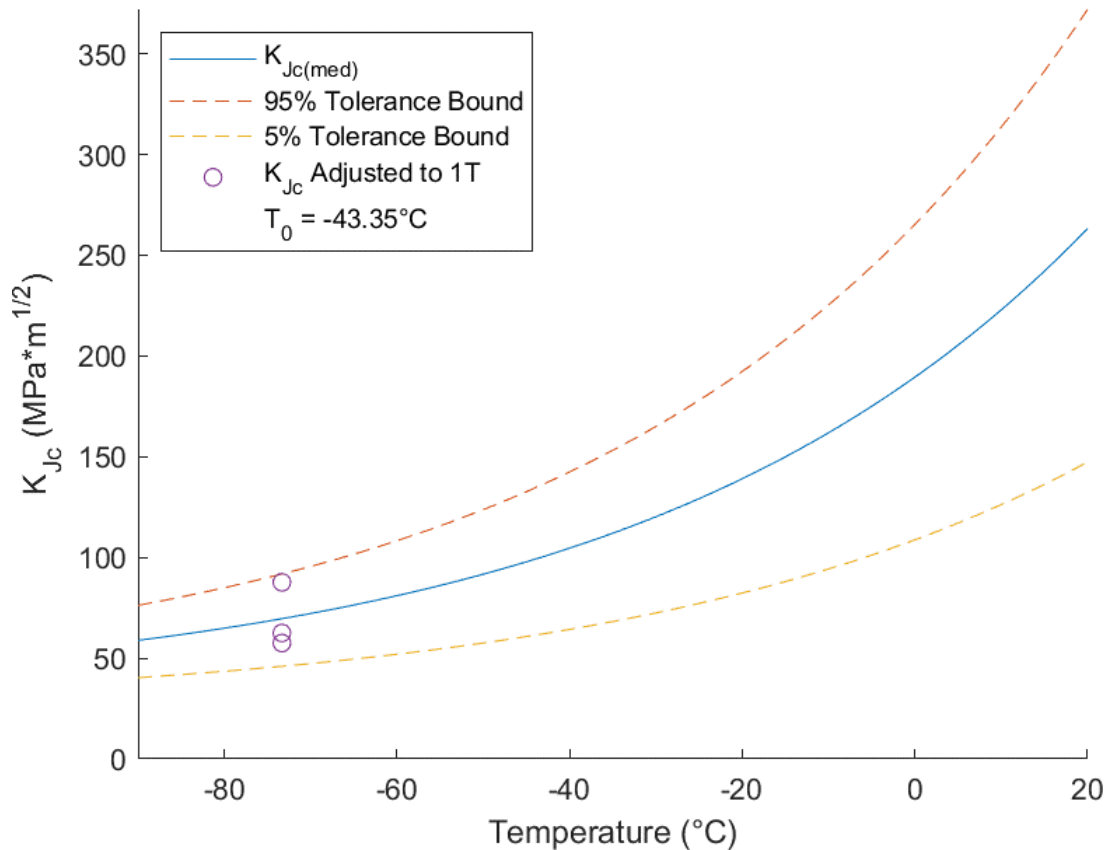


Figure 7.5.1.3.3-4: MV50466-8 Seam Weld Center T_0 Plot

Results from the three E1921 tests are presented in Table 7.5.1.3.3-3 and Table 7.5.1.3.3-4. These results were obtained using the T_0 TEM Code described in Section 4.2. The T_0 reference temperature for this data set was evaluated as -43°C using the E1921 Master Curve shown in Figure 7.5.1.3.3-4.

Table 7.5.1.3.3-3: Seam Weld Center T_0 Individual Specimen Results, MV50466-8

Specimen Name	Temperature ($^\circ\text{C}$)	KjcRaw (MPa*m ^{0.5})	1T Data (MPa*m ^{0.5})	Uncensored Data	Test Temp - T_0 ($^\circ\text{C}$)
440-214	-73	76.3	57.5	1	-30
440-215	-73	83.8	62.5	1	-30
440-235	-73	122.1	87.7	1	-30

Table 7.5.1.3.3-4: MV50466-8 Seam Weld Center T_0 Calculation Results

Initial T_0 ($^\circ\text{C}$)	-43
Total Samples	3
Samples within $T_0 \pm 50^\circ\text{C}$ (N)	3
Number of Uncensored Data (r)	3
Poisson's Ratio	0.3
$\Sigma(r_i n_i)$	0.43
Samples Between $T_i - T_0$ 50 to -14°C	0
Samples Between $T_i - T_0$ -15 to -35°C	3
Samples Between $T_i - T_0$ -36 to -50°C	0
$T_{0\text{scrn}}$ ($^\circ\text{C}$)	-32
Homogenous or Inhomogeneous	Homogenous

The results of the E1921 analysis show that the seam weld material removed from the MV50466-8 wrapper layer is macroscopically homogeneous. For this data set, the ductile-brittle transition temperature was found to be -43°C . This data set does not meet the E1921 validity criteria for a sufficient number of samples tested in an appropriate temperature range with $\Sigma(r_i n_i) < 1.0$. However, the tests conducted are consistent enough to consider the result useful.

The test data in Table 7.5.1.3.3-5 are raw values obtained from fracture tests conducted on MV50466-8 longitudinal seam weld HAZ material. Test results that are considered upper shelf are listed under ASTM E1820, while transition temperature test results are listed under E1921. Tests that meet the complete validity requirements for $J_q = J_{1C}$ and $K_{Jq} = K_{J1C}$ are denoted with an asterisk. Despite invalidities, J_q and K_{Jq} convey valuable fracture toughness information, especially when the test results are applied directly to the sample material source.

Table 7.5.1.3.3-5: Seam Weld HAZ Fracture Data MV50466-8

Specimen ID	Test Temp. (°C)	ASTM Crack Plane Orientation	W (in)	a ₀ (in)	a _f (in)	B ₀ (in)	B _N (in)	J _q (kJ/m ²)	K _{Jq} (MPa √m)	K _{JClT} (MPa √m)	ASTM Standard
440-169	23	N-P	1.0027	0.5072	0.5741	0.1992	0.1590	50*	106	---	E1820
440-168	21	N-P	0.9983	0.5059	0.5621	0.2008	0.1580	36	90	---	E1820
440-178	21	N-P	0.9994	0.5034	0.5676	0.2032	0.1550	75	129	---	E1820
440-179	21	N-P	0.9979	0.5059	0.5865	0.2000	0.1575	26	76	---	E1820
440-225	-29	N-P	1.0006	0.5358	0.5669	0.1967	0.1606	41	96	71	E1921
440-226	-29	N-P	1.0000	0.5073	0.5653	0.1942	0.1600	92	143	---	E1820
440-203	-46	N-P	0.9999	0.5113	0.5779	0.1932	0.1566	34	87	---	E1820
440-204	-46	N-P	1.0004	0.5057	0.6104	0.1965	0.1585	83	136	---	E1820
440-208	-73	N-P	1.0003	0.5054	0.5164	0.1927	0.1533	46	102	74	E1921
440-211	-73	N-P	1.0003	0.5105	0.5193	0.1970	0.1656	31	83	62	E1921
440-212	-73	N-P	1.0005	0.5097	0.5708	0.1895	0.1488	76	131	93	E1921
440-216	-73	N-P	1.0002	0.5112	0.5160	0.1968	0.1586	34	88	65	E1921
440-217	-73	N-P	1.0003	0.5106	0.5121	0.1933	0.1569	22	70	53	E1921
440-218	-73	N-P	1.0001	0.5090	0.5317	0.1810	0.1430	15	58	45	E1921
440-219	-73	N-P	1.0002	0.5082	0.5111	0.1907	0.1568	14	55	43	E1921
440-227	-73	N-P	1.0006	0.5108	0.5252	0.1964	0.1594	18	64	49	E1921
440-228	-73	N-P	0.9994	0.5224	0.5414	0.1898	0.1517	83	136	97	E1921
440-229	-73	N-P	1.0000	0.5104	0.5146	0.1980	0.1576	12	51	41	E1921

Results from the ten E1921 tests is presented in Table 7.5.1.3.3-6 and Table 7.5.1.3.3-7. These results were obtained using the T₀TEM Code described in Section 4.2. The T₀ reference temperature for this data set was evaluated as -44°C using the E1921 Master Curve shown in Figure 7.2.1.3.3-5.

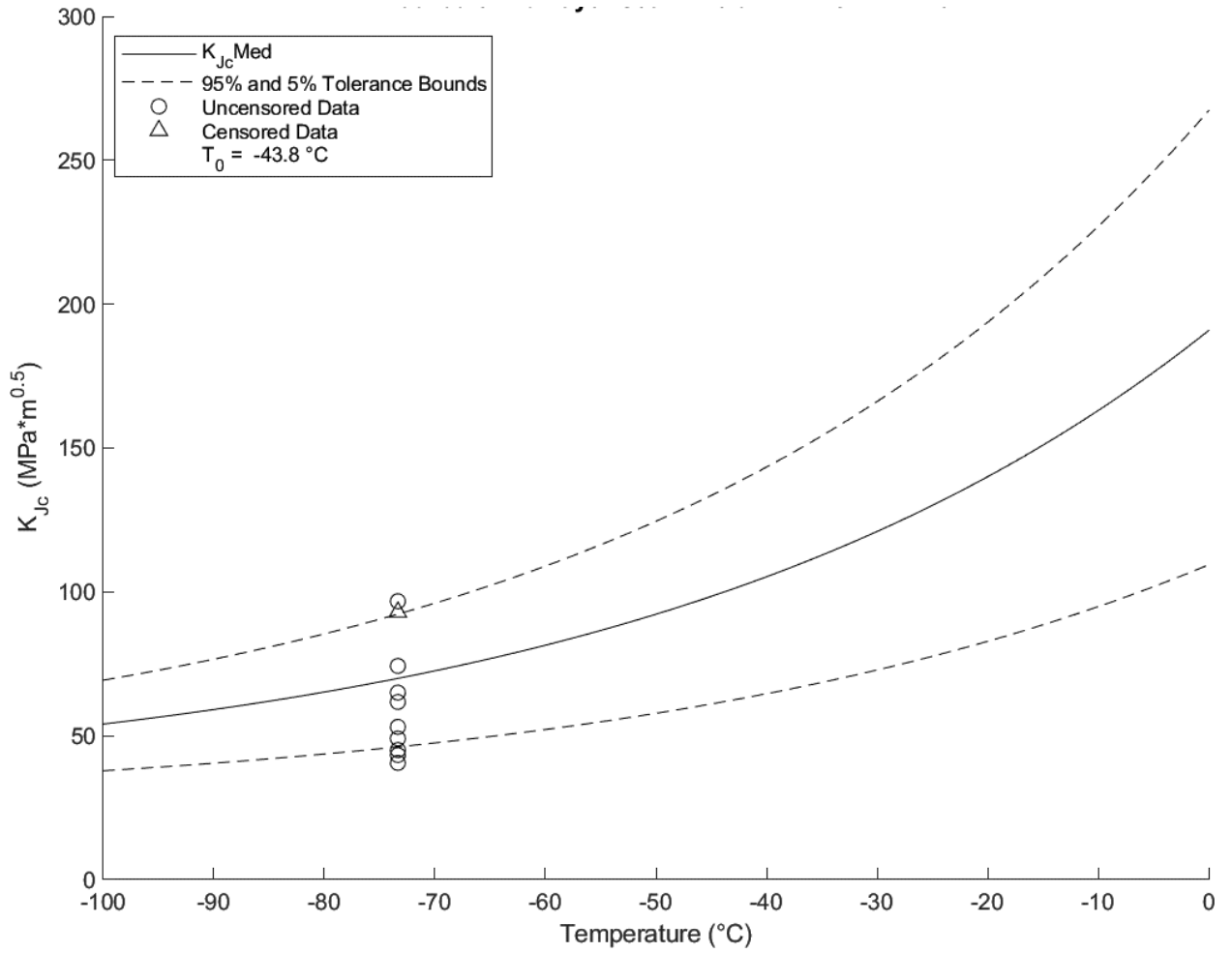


Figure 7.5.1.3.3-5: MV50466-8 Seam Weld HAZ T_0 Plot

Table 7.5.1.3.3-6: MV50466-8 Seam Weld HAZ T₀ Individual Specimen Results

Specimen Name	Temperature (°C)	K _{Jc} Raw (MPa*m ^{0.5})	1T Data (MPa*m ^{0.5})	Uncensored Data	Test Temp -T ₀ (°C)
440-208	-73	101.9	74.3	1	-29
440-211	-73	82.7	61.8	1	-29
440-212	-73	130.7	93.0	0	-29
440-216	-73	87.6	65.0	1	-29
440-217	-73	69.9	53.1	1	-29
440-218	-73	58.4	45.1	1	-29
440-219	-73	55.3	43.3	1	-29
440-227	-73	63.7	49.1	1	-29
440-228	-73	136.3	96.8	1	-29
440-229	-73	50.9	40.6	1	-29

Table 7.5.1.3.3-7: MV50466-8 Seam Weld HAZ T₀ Calculation Results

Initial T ₀ (°C)	-44
Total Samples	10
Samples within T ₀ ± 50°C (N)	10
Number of Uncensored Data (r)	9
Poisson's Ratio	0.3
Σ(r _i n _i)	1.29
Samples Between T _i - T ₀ 50 to -14 °C	0
Samples Between T _i - T ₀ -15 to -35 °C	9
Samples Between T _i - T ₀ -36 to -50 °C	0
T _{0scrn} (°C)	-17
Homogenous or Inhomogeneous	Inhomogeneous

The results of the E1921 analysis show that the seam weld HAZ material removed from the MV50466-8 wrapper layer is macroscopically inhomogeneous. For this data set, the ductile-brittle transition temperature was found to be -44°C. This data set meets the E1921 validity criteria for a sufficient number of samples tested in an appropriate temperature range with $\Sigma(r_i n_i) \geq 1.0$. From examination of the fracture surfaces, there is reason to believe some samples may have tested closer to weld material than HAZ. The data set presents as multimodal inhomogeneous due to the difference in T_{0scrn} and the initial T₀. However, there are not enough samples to accurately characterize the likelihood of inhomogeneity. Therefore, the original T₀ will be used.

The test data in Table 7.5.1.3.3-8 are raw values obtained from fracture tests conducted on V0032 longitudinal seam weld material. Test results that are considered upper shelf are listed under ASTM E1820, while transition temperature test results are listed under E1921. Tests that meet the complete validity requirements for $J_q = J_{1C}$ and $K_{Jq} = K_{J1C}$ are denoted with an asterisk. Despite invalidities, J_q and K_{Jq} convey valuable fracture toughness information, especially when the test results are applied directly to the sample material source.

Table 7.5.1.3.3-8: Seam Weld Fracture Data V0032

Specimen ID	Test Temp. (°C)	ASTM Crack Plane Orientation	W (in)	a ₀ (in)	a _f (in)	B ₀ (in)	B _N (in)	J _q (kJ/m ²)	K _{Jq} (MPa √m)	K _{JCI,T} (MPa √m)	ASTM Standard
380-176	23	N-P	1.0011	0.5160	0.5687	0.1990	0.1596	127	169	---	E1820
380-177	23	N-P	1.0018	0.5093	0.5683	0.1996	0.1604	121	165	---	E1820
380-143	-29	N-P	0.9998	0.4942	0.5712	0.1912	0.1517	75	130	---	E1820
380-144	-46	N-P	1.0006	0.5088	0.5708	0.1984	0.1593	72	127	92	E1921
380-149	-73	N-P	1.0004	0.5045	0.5164	0.2007	0.1588	83	136	98	E1921
380-153	-73	N-P	0.9998	0.5279	0.5588	0.1996	0.1554	122	165	---	E1820
380-154	-73	N-P	1.0015	0.5096	0.5697	0.2003	0.1601	195	209	---	E1820
380-155	-84	N-P	1.0008	0.5084	0.5122	0.1996	0.1614	81	134	96	E1921
380-156	-84	N-P	1.0014	0.5339	0.5533	0.2005	0.1556	169	194	137	E1921
380-157	-84	N-P	1.0013	0.5228	0.5360	0.1998	0.1587	122	165	117	E1921
380-171	-84	N-P	1.0003	0.5033	0.5117	0.1999	0.1628	51	107	78	E1921
380-178	-107	N-P	1.0013	0.5066	0.5202	0.1995	0.1561	39	93	69	E1921
380-187	-107	N-P	1.0004	0.5080	0.5139	0.1986	0.1583	41	96	71	E1921
380-188	-107	N-P	1.0002	0.5065	0.5079	0.1981	0.1584	45	100	73	E1921
380-189	-107	N-P	0.9994	0.5030	0.5135	0.1997	0.1583	27	78	59	E1921
380-190	-107	N-P	1.0009	0.5035	0.5090	0.1991	0.1619	41	96	71	E1921
380-191	-107	N-P	1.0013	0.5074	0.5113	0.1982	0.1585	38	93	68	E1921

Results from the 14 E1921 tests are presented in Table 7.5.1.3.3-9 and Table 7.5.1.3.3-10. These results were obtained using the T₀TEM Code described in Section 4.2. The T₀ reference temperature for this data set was evaluated as -84°C using the E1921 Master Curve shown in Figure 7.5.1.3.3-6.

Table 7.5.1.3.3-10: V0032 Seam Weld T_0 Calculation Results

Initial T_0 (°C)	-84
Total Samples	14
Samples within $T_0 \pm 50^\circ\text{C}$ (N)	14
Number of Uncensored Data (r)	11
Poisson's Ratio	0.3
$\Sigma(r_i n_i)$	1.69
Samples Between $T_i - T_0$ 50 to -14 °C	5
Samples Between $T_i - T_0$ -15 to -35 °C	6
Samples Between $T_i - T_0$ -36 to -50 °C	0
$T_{0\text{scrn}}$ (°C)	-77
Homogenous or Inhomogeneous	Homogenous

The results of the E1921 analysis show that the seam weld material removed from the V0032 wrapper layer is macroscopically homogeneous. For this data set, the ductile-brittle transition temperature was found to be -84°C . This data set meets the E1921 validity criteria for a sufficient number of samples tested in an appropriate temperature range with $\Sigma(r_i n_i) \geq 1.0$.

The test data in Table 7.5.1.3.3-11 are raw values obtained from fracture tests conducted on V0032 longitudinal seam weld HAZ material. Test results that are considered upper shelf are listed under ASTM E1820, while transition temperature test results are listed under E1921. Tests that meet the complete validity requirements for $J_q = J_{1C}$ and $K_{Jq} = K_{J1C}$ are denoted with an asterisk. Despite invalidities, J_q and K_{Jq} convey valuable fracture toughness information, especially when the test results are applied directly to the sample material source.

Table 7.5.1.3.3-11: Seam Weld HAZ Fracture Data V0032

Specimen Name	Temperature (°C)	KjcRaw (MPa*m ^{0.5})	1T Data (MPa*m ^{0.5})	Uncensored Data	Test Temp -T0 (°C)
380-150	-73	70.7	53.9	1	-47
380-151	-73	50.7	40.5	1	-47
380-152	-73	96.6	71.3	1	-47
380-158	-62	72.4	54.9	0	-36
380-163	-62	84.0	62.8	1	-36
380-165	-62	65.5	50.4	1	-36
380-166	-51	85.5	63.8	1	-25
380-167	-51	179.4	101.6	0	-25
380-168	-51	101.1	74.1	1	-25
380-169	-51	66.0	50.7	1	-25
380-170	-51	89.5	66.4	1	-25
380-179	-51	90.9	67.4	1	-25
380-180	-51	75.1	56.8	1	-25
380-185	-51	142.0	101.6	1	-25
380-186	-51	68.2	52.3	1	-25

Results from the 15 E1921 tests are presented in Table 7.5.1.3.3-12 and Table 7.5.1.3.3-13. These results were obtained using the T₀TEM Code described in Section 4.2. The T₀ reference temperature for this data set was evaluated as -26°C using the E1921 Master Curve shown in Figure 7.5.1.3.3-7.

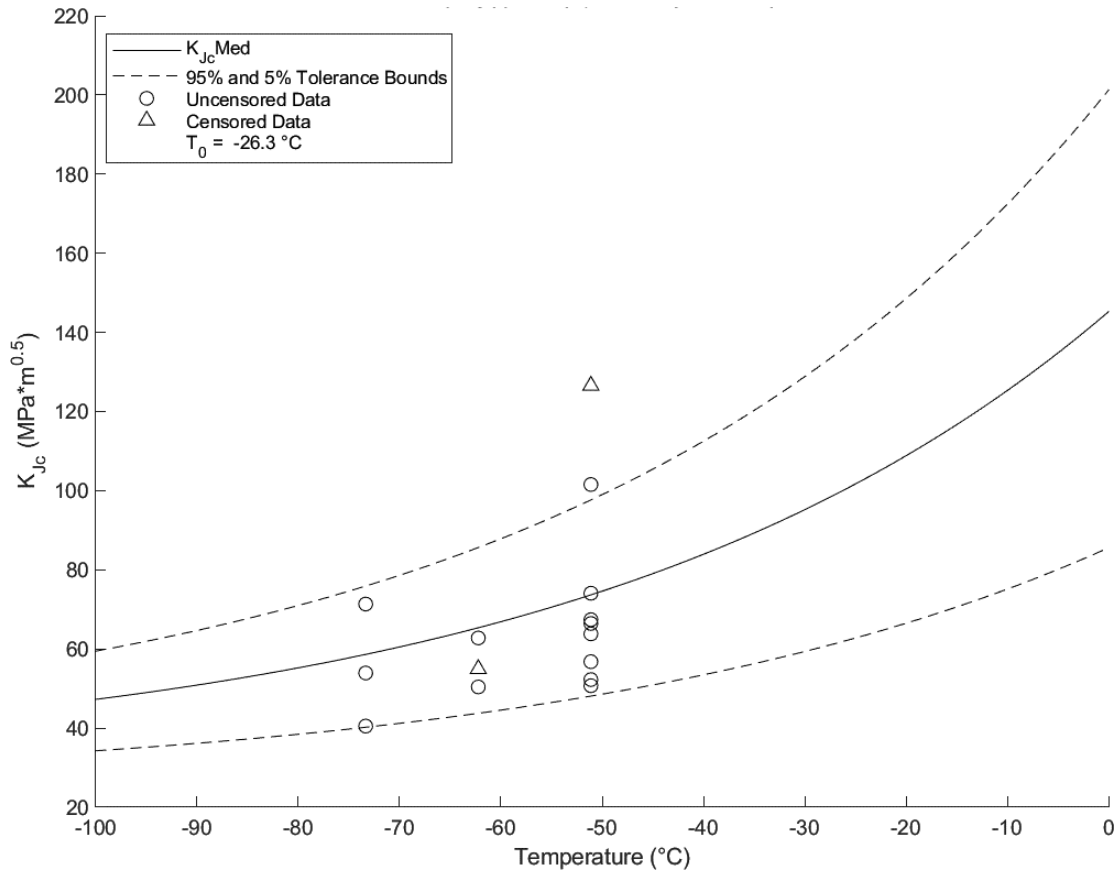


Figure 7.5.1.3.3-7: V0032 Seam Weld HAZ T₀ Plot

Table 7.5.1.3.3-12: V0032 Seam Weld HAZ T₀ Individual Specimen Results

Specimen Name	Temperature (°C)	KjcRaw (MPa*m ^{0.5})	1T Data (MPa*m ^{0.5})	Uncensored Data	Test Temp -T ₀ (°C)
380-150	-73	70.7	53.9	1	-47
380-151	-73	50.7	40.5	1	-47
380-152	-73	96.6	71.3	1	-47
380-158	-62	72.4	54.9	0	-36
380-163	-62	84.0	62.8	1	-36
380-165	-62	65.5	50.4	1	-36
380-166	-51	85.5	63.8	1	-25
380-167	-51	179.4	101.6	0	-25
380-168	-51	101.1	74.1	1	-25
380-169	-51	66.0	50.7	1	-25
380-170	-51	89.5	66.4	1	-25
380-179	-51	90.9	67.4	1	-25
380-180	-51	75.1	56.8	1	-25
380-185	-51	142.0	101.6	1	-25
380-186	-51	68.2	52.3	1	-25

Table 7.5.1.3.3-13 V0032 Seam Weld HAZ T_0 Calculation Results

Initial T_0 (°C)	-26
Total Samples	15
Samples within $T_0 \pm 50^\circ\text{C}$ (N)	15
Number of Uncensored Data (r)	13
Poisson's Ratio	0.3
$\Sigma(r_i n_i)$	1.77
Samples Between $T_i - T_0$ 50 to -14 °C	0
Samples Between $T_i - T_0$ -15 to -35 °C	8
Samples Between $T_i - T_0$ -36 to -50 °C	5
$T_{0\text{scrn}}$ (°C)	-15
Homogenous or Inhomogeneous	Inhomogeneous

The results of the E1921 analysis show that the seam weld HAZ material removed from the V0032 wrapper layer is macroscopically inhomogeneous. For this data set, the ductile-brittle transition temperature was found to be -26°C. This data set meets the E1921 validity criteria for a sufficient number of samples tested in an appropriate temperature range with $\Sigma(r_i n_i) \geq 1.0$. From examination of the fracture surfaces, there is reason to believe some samples may have tested closer to weld material than HAZ. The data set presents as multimodal inhomogeneous due to the difference in $T_{0\text{scrn}}$ and the initial T_0 .

However, there are not enough samples to accurately characterize the likelihood of inhomogeneity. Therefore, the original T_0 will be used.

The test data in Table 7.5.1.3.3-14 are raw values obtained from fracture tests conducted on V0023 longitudinal seam weld material. Test results that are considered upper shelf are listed under ASTM E1820, while transition temperature test results are listed under E1921. Tests that meet the complete validity requirements for $J_q = J_{1C}$ and $K_{Jq} = K_{J1C}$ are denoted with an asterisk. Despite invalidities, J_q and K_{Jq} convey valuable fracture toughness information, especially when the test results are applied directly to the sample material source.

Table 7.5.1.3.3-14: Seam Weld Fracture Data V0023

Specimen ID	Test Temp. (°C)	ASTM Crack Plane Orientation	W (in)	a ₀ (in)	a _f (in)	B ₀ (in)	B _N (in)	J _q (kJ/m ²)	K _{Jq} (MPa √m)	K _{JCIT} (MPa √m)	ASTM Standard
519-103	21	N-P	0.9991	0.5199	0.5979	0.2009	0.1579	79	133	---	E1820
519-104	21	N-P	0.9996	0.5208	0.5866	0.2016	0.1595	76	130	---	E1820
519-72	20	N-P	0.9997	0.5177	0.5849	0.1843	0.1467	88*	140	---	E1820
519-43	-84	N-P	0.9992	0.5162	0.5459	0.1984	0.1570	128	169	119	E1921
519-44	-84	N-P	1.0005	0.5193	0.5253	0.1999	0.1599	51	107	78	E1921
519-46	-84	N-P	1.0004	0.5255	0.5409	0.2015	0.1597	30	82	62	E1921
519-47	-84	N-P	1.0002	0.5155	0.5245	0.2016	0.1605	58	114	83	E1921
519-67	-96	N-P	1.0000	0.5212	0.5235	0.1892	0.1465	30	81	60	E1921
519-68	-96	N-P	0.9998	0.5140	0.5243	0.1998	0.1590	59	115	83	E1921
519-69	-96	N-P	0.9996	0.5289	0.5304	0.1909	0.1494	40	95	70	E1921
519-70	-96	N-P	0.9999	0.5128	0.5170	0.2019	0.1598	26	76	58	E1921
519-71	-96	N-P	0.9995	0.5097	0.5191	0.2016	0.1592	56	112	82	E1921
519-48	-96	N-P	0.9997	0.5232	0.5296	0.2003	0.1587	51	107	78	E1921

Results from the 10 E1921 tests are presented in Table 7.5.1.3.3-15 and Table 7.5.1.3.3-16. These results were obtained using the T₀TEM Code described in Section 4.2. The T₀ reference temperature for this data set was evaluated as -65°C using the E1921 Master Curve shown in Figure 7.5.1.3.3-8.

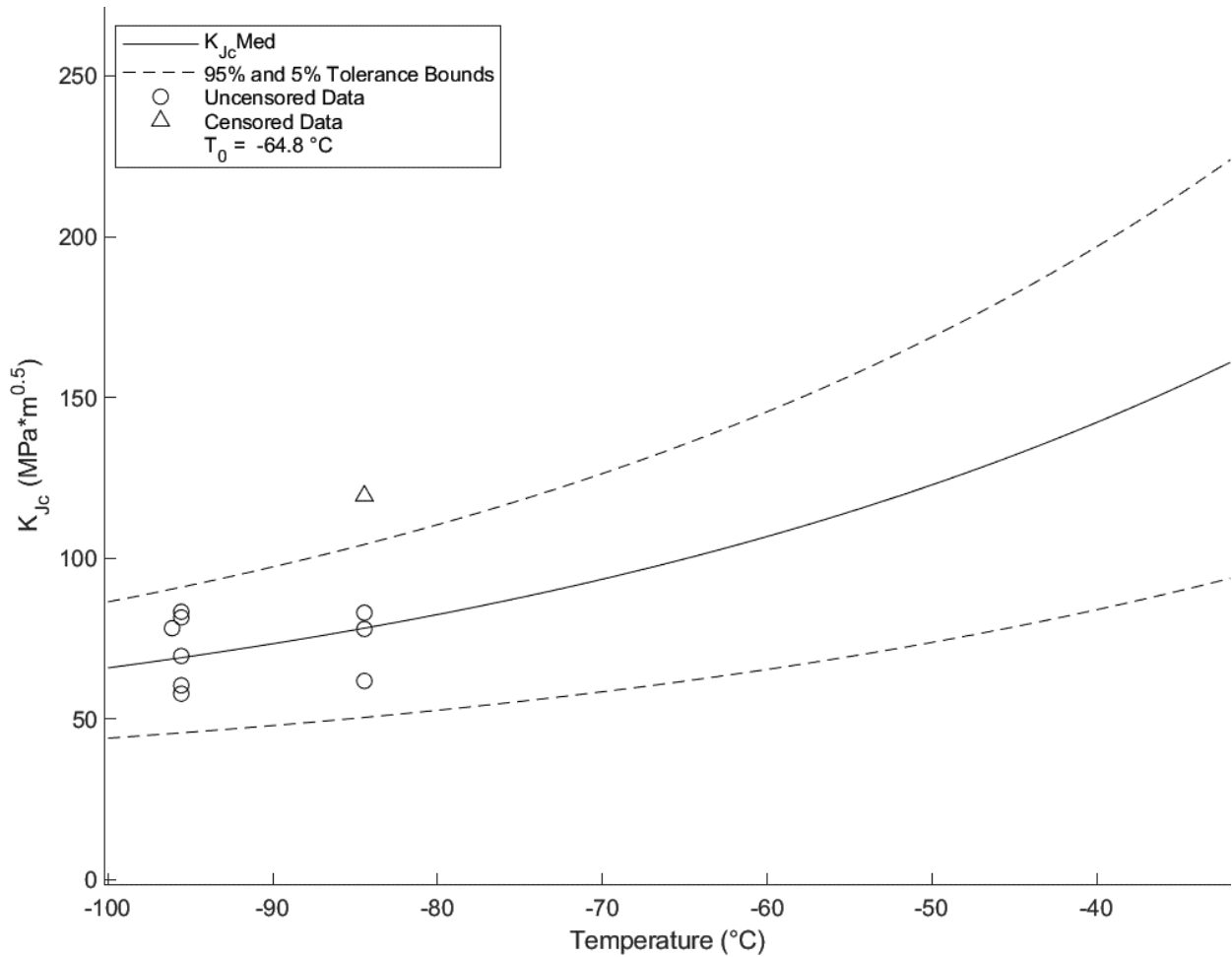


Figure 7.5.1.3.3-8: V0023 Seam Weld T_0 Plot

Table 7.5.1.3.3-15: V0023 Seam Weld T₀ Individual Specimen Results

Specimen Name	Temperature (°C)	KjcRaw (MPa*m ^{0.5})	1T Data (MPa*m ^{0.5})	Uncensored Data	Test Temp -T ₀ (°C)
519-43	-84	168.9	83.3	0	-20
519-44	-84	106.7	78.0	1	-20
519-46	-84	82.4	61.8	1	-20
519-47	-84	114.1	83.0	1	-20
519-48	-96	107.0	78.2	1	-31
519-67	-96	81.3	60.5	1	-31
519-68	-96	114.7	83.3	1	-31
519-69	-96	95.0	69.6	1	-31
519-70	-96	76.5	57.9	1	-31
519-71	-96	111.9	81.6	1	-31

Table 7.5.1.3.3-16: V0023 Seam Weld T₀ Calculation Results

Initial T ₀ (°C)	-65
Total Samples	10
Samples within T ₀ ± 50°C (N)	10
Number of Uncensored Data (r)	9
Poisson's Ratio	0.3
Σ(r _i n _i)	1.29
Samples Between T _i - T ₀ 50 to -14 °C	0
Samples Between T _i - T ₀ -15 to -35 °C	9
Samples Between T _i - T ₀ -36 to -50 °C	0
T ₀ scrn (°C)	-65
Homogenous or Inhomogeneous	Homogenous

The results of the E1921 analysis show that the seam weld material removed from the V0023 wrapper layer is macroscopically homogeneous. For this data set, the ductile-brittle transition temperature was found to be -65°C. This data set meets the E1921 validity criteria for a sufficient number of samples tested in an appropriate temperature range with $\Sigma(r_i n_i) \geq 1.0$.

The test data in Table 7.5.1.3.3-17 are raw values obtained from fracture tests conducted on V0023 longitudinal seam weld HAZ material. Tests that are considered upper shelf are listed under ASTM E1820, while transition temperature tests are listed under E1921. Tests that meet the complete validity requirements for $J_q = J_{1C}$ and $K_{Jq} = K_{J1C}$ are denoted with an asterisk. Despite invalidities, J_q and K_{Jq} convey valuable fracture toughness information, especially when the test results are applied directly to the sample material source. Specimen 519-87 was machined to be a HAZ specimen, however the fracture surface indicates that it may have transitioned to mostly weld material during the test and therefore did not cleave. Because of this, it is listed as an E1820 test.

Table 7.5.1.3.3-17 Seam Weld HAZ Fracture Data V0023

Specimen ID	Test Temp. (°C)	ASTM Crack Plane Orientation	W (in)	a ₀ (in)	a _r (in)	B ₀ (in)	B _N (in)	J _q (kJ/m ²)	K _{Iq} (MPa√m)	K _{JCIT} (MPa√m)	ASTM Standard
519-90	-23	N-P	0.9998	0.5358	0.6204	0.1964	0.1582	40	94	---	E1820
519-95	-23	N-P	0.9992	0.5269	0.5310	0.2021	0.1592	35	88	---	E1820
519-93	-23	N-P	1.0000	0.5291	0.5734	0.2022	0.1546	80	134	96	E1921
519-94	-23	N-P	0.9999	0.5250	0.5628	0.2015	0.1617	70	125	90	E1921
519-98	-23	N-P	0.9998	0.6845	0.7652	0.1854	0.1514	42	97	70	E1921
519-92	-23	N-P	1.0004	0.5211	0.5294	0.2019	0.1616	35	88	65	E1921
519-97	-23	N-P	1.0008	0.5202	0.5312	0.2024	0.1582	30	82	62	E1921
519-91	-23	N-P	0.9991	0.5225	0.5247	0.1960	0.1597	29	81	60	E1921
519-96	-23	N-P	0.9999	0.5213	0.5213	0.2015	0.1612	27	78	59	E1921
519-87	-40	N-P	0.9998	0.5163	0.5823	0.2018	0.1640	63	118	---	E1820
519-89	-40	N-P	1.0006	0.5603	0.5641	0.2028	0.1626	29	81	61	E1921
519-88	-40	N-P	1.0008	0.5144	0.5183	0.2040	0.1659	27	78	59	E1921
519-65	-57	N-P	1.0001	0.5218	0.5346	0.1960	0.1583	50	105	77	E1921
519-64	-57	N-P	1.0000	0.5192	0.5252	0.1924	0.1539	28	80	59	E1921
519-66	-57	N-P	1.0003	0.5167	0.5213	0.2049	0.1632	21	69	53	E1921
519-63	-73	N-P	1.0000	0.5257	0.5351	0.2038	0.1641	42	97	72	E1921
519-62	-73	N-P	1.0000	0.5242	0.5283	0.2024	0.1636	17	62	48	E1921
519-61	-73	N-P	0.9999	0.5204	0.5215	0.2028	0.1630	14	57	45	E1921

Results from the 12 E1921 tests are presented in Table 7.5.1.3.3-18 and Table 7.5.1.3.3-19. These results were obtained using the T₀TEM Code described in Section 4.2. The T₀ reference temperature for this data set was evaluated as 8°C using the E1921 Master Curve shown in Figure 7.5.1.3.3-9.

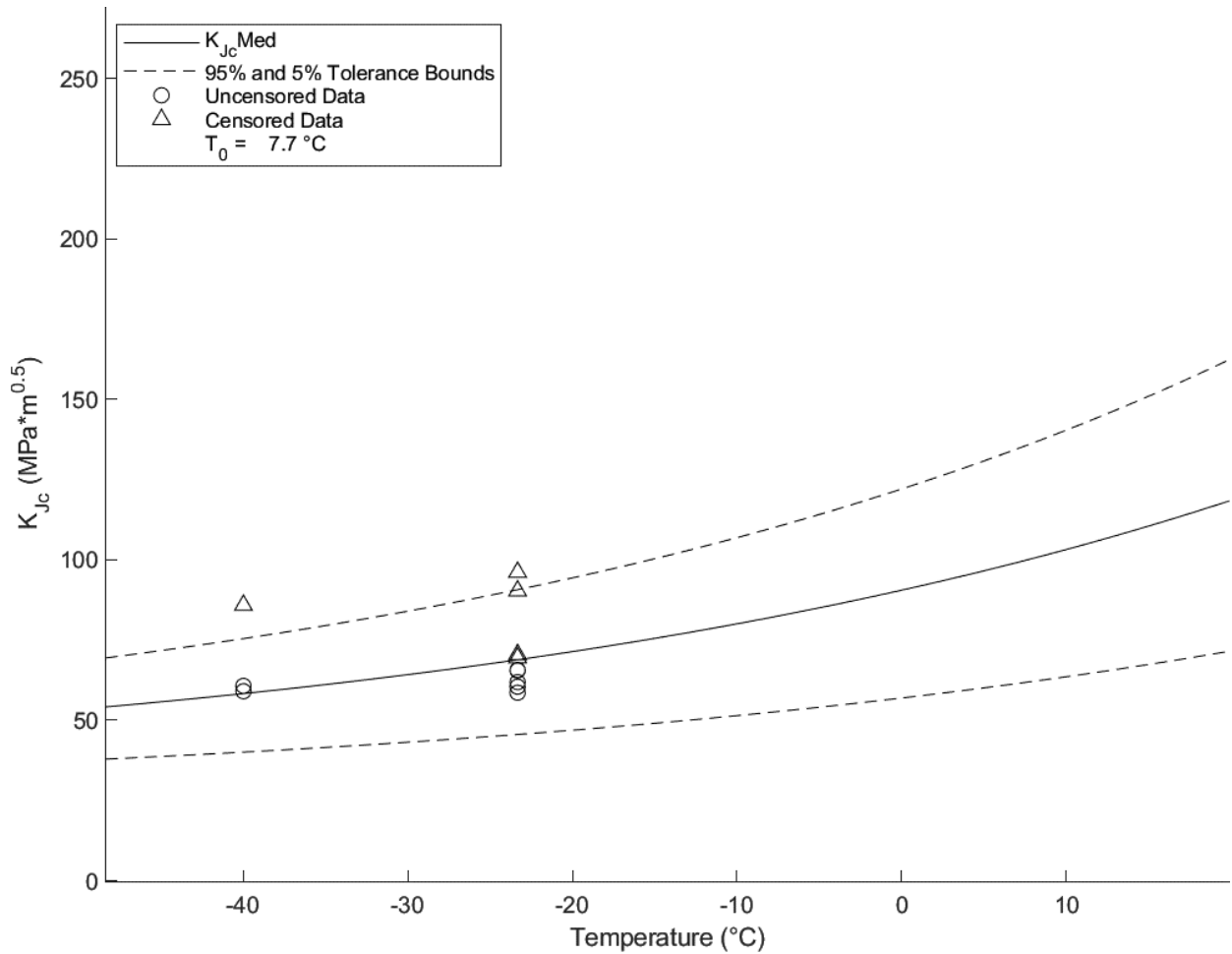


Figure 7.5.1.3.3-9: V0023 Seam Weld HAZ T_0 Plot

Table 7.5.1.3.3-18: : V0023 Seam Weld HAZ T_0 Individual Specimen Results

Specimen Name	Temperature (°C)	KjcRaw (MPa*m ^{0.5})	1T Data (MPa*m ^{0.5})	Uncensored Data	Test Temp -T0 (°C)
519-87	-40	118.2	65.7	0	-48
519-88	-40	78.1	59.0	1	-48
519-89	-40	80.6	60.7	1	-48
519-90	-23	94.3	65.7	0	-31
519-91	-23	80.8	60.5	1	-31
519-92	-23	87.9	65.5	1	-31
519-93	-23	133.5	65.7	0	-31
519-94	-23	124.9	65.7	0	-31
519-95	-23	88.1	65.7	1	-31
519-96	-23	77.6	58.6	1	-31
519-97	-23	82.4	61.9	1	-31
519-98	-23	96.9	65.7	0	-31

Table 7.5.1.3.3-19: V0023 Seam Weld HAZ T₀ Calculation Results

Initial T₀ (°C)	8
Total Samples	12
Samples within T₀ ± 50°C (N)	12
Number of Uncensored Data (r)	7
Poisson's Ratio	0.3
Σ(r_i n_i)	0.96
Samples Between T_i - T₀ 50 to -14 °C	0
Samples Between T_i - T₀ -15 to -35 °C	5
Samples Between T_i - T₀ -36 to -50 °C	2
T₀scrn (°C)	15
Homogenous or Inhomogeneous	Homogenous

The results of the E1921 analysis show that the seam weld HAZ material removed from the V0023 wrapper layer is macroscopically homogeneous. For this data set, the ductile-brittle transition temperature was found to be 8°C. This data set meets the E1921 validity criteria for a sufficient number of samples tested in an appropriate temperature range with $\Sigma(r_i n_i) \geq 1.0$.

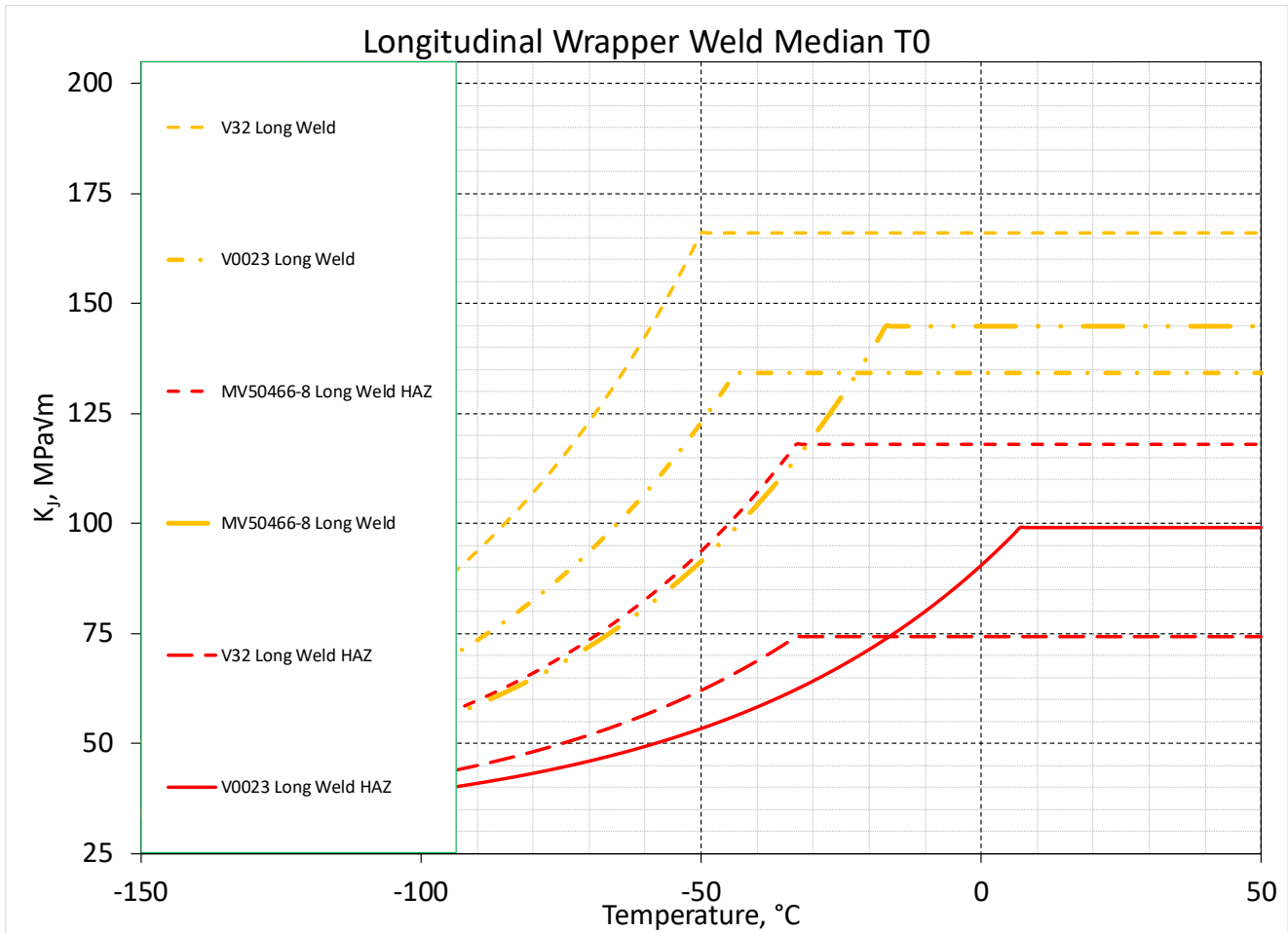


Figure 7.5.1.3.3-10: Longitudinal Wrapper Weld and HAZ T_0 Plot Combined

7.5.1.3.4 Fatigue Crack Growth

Sections of V0023 were tested to determine the fatigue crack growth rates according to ASTM E647 (11). Load ratios of $R = 0.1$ and $R = 0.7$ were chosen corresponding to load cycles, slight pressure variations, and nearly full pressure releases of the LPVs. These tests were conducted on the center of the longitudinal seam weld found in the second wrapper layer as seen in Figure 7.5.1.3.4-1 and Figure 7.5.1.3.4-2. Table 7.5.1.3.4-1 and Table 7.5.1.3.4-2 show the test matrix and threshold result of each E647 test conducted. The individual fatigue growth curves are shown in Figure 7.5.1.3.4-3 through Figure 7.5.1.3.4-6. These curves are input into NASGRO to create material data packages used for structural analysis and crack growth prediction.



Figure 7.5.1.3.4-1: Specimen Cut Plan da/dN V0023 Seam Weld

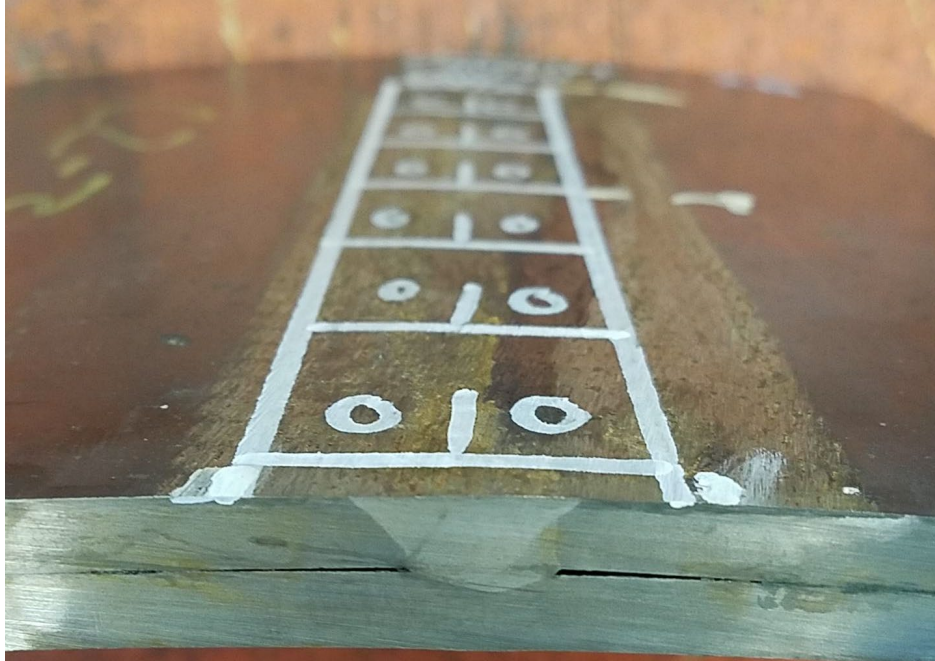


Figure 7.5.1.3.4-2: Specimen Cut Plan da/dN V0023 Seam Weld (Continued)

Table 7.5.1.3.4-1: V0023 Seam Weld da/dN Test Matrix

Lot	Material	Orientation	Stock Thickness	Specimen Thickness	Machine	R=0.1	R=0.7	Spares
V23 2AB LW	Weld	NP	0.5	0.2	6	2	2	2

Table 7.5.1.3.4-2: V0023 Seam Weld da/dN Results

Specimen ID	Temperature (°F)	R-Ratio	Segment	C (1/in)	Frequency (Hz)	Threshold (□K) (KSI√in)	Location
V23-2AB-LW-1	75	0.1	A	-20	30	4.595	Wrapper Weld
			B	6	30		
V23-2AB-LW-2	75	0.1	A	-20	30	3.778	Wrapper Weld
			B	6	30		
V23-2AB-LW-3	75	0.7	A	-20	30	2.828	Wrapper Weld
			B	6	30		
V23-2AB-LW-4	75	0.7	A	-20	30	2.804	Wrapper Weld
			B	6	30		

ASTM E647

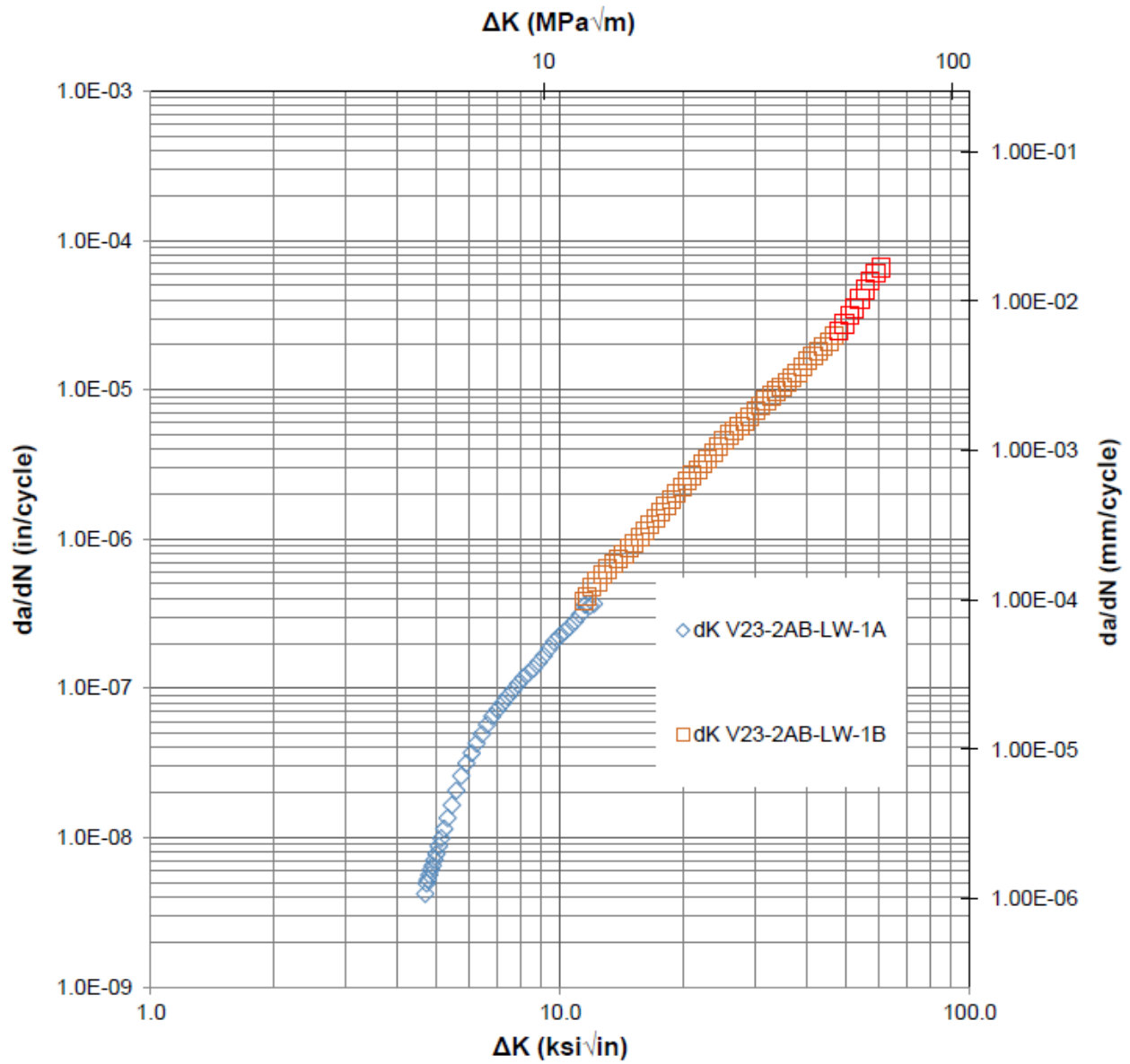


Figure 7.5.1.3.4-3: V0023-2AB-LW-1 Plot R = 0.1

ASTM E647

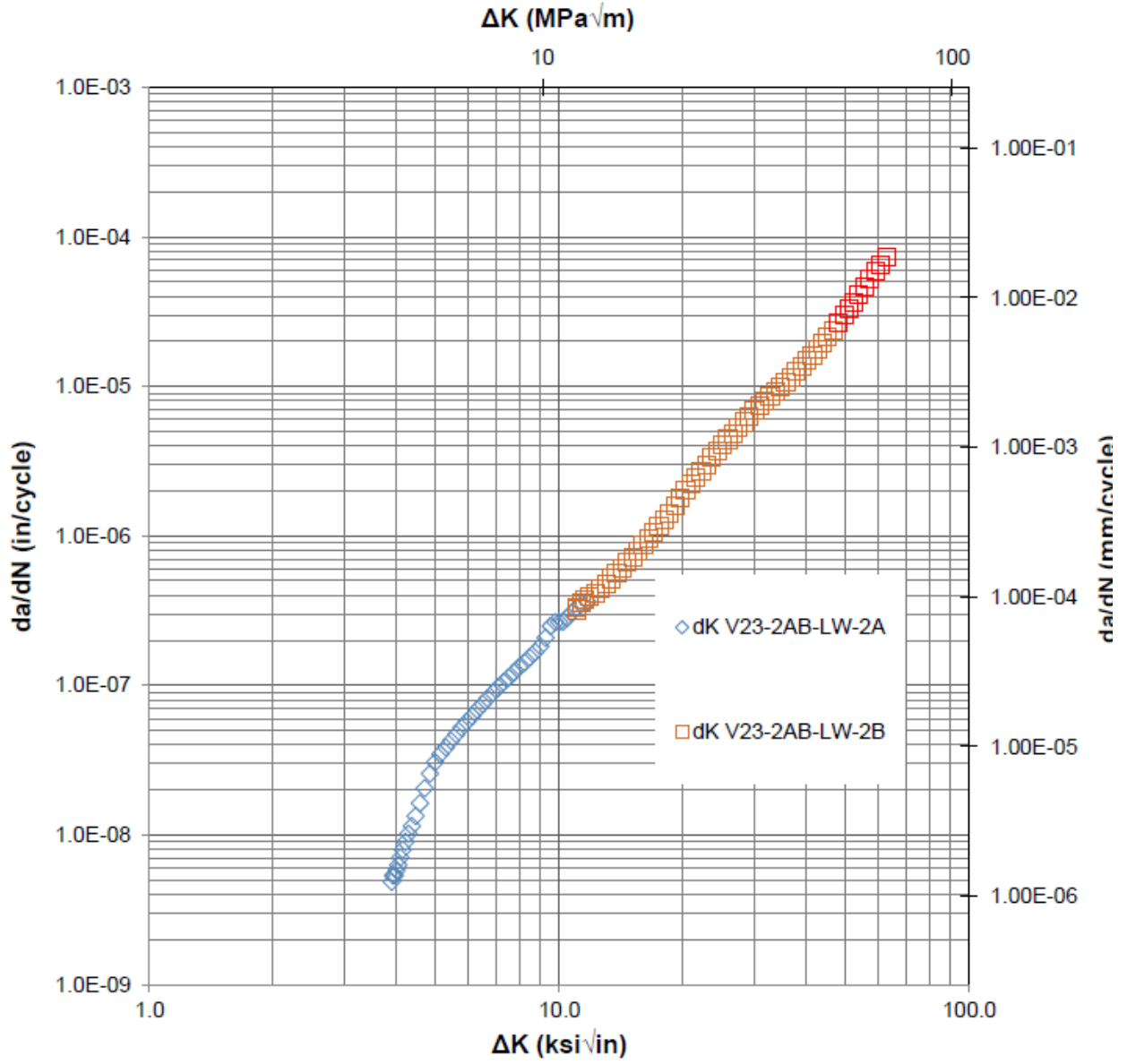


Figure 7.5.1.3.4-4: V0023-2AB-LW-2 Plot R = 0.1

ASTM E647

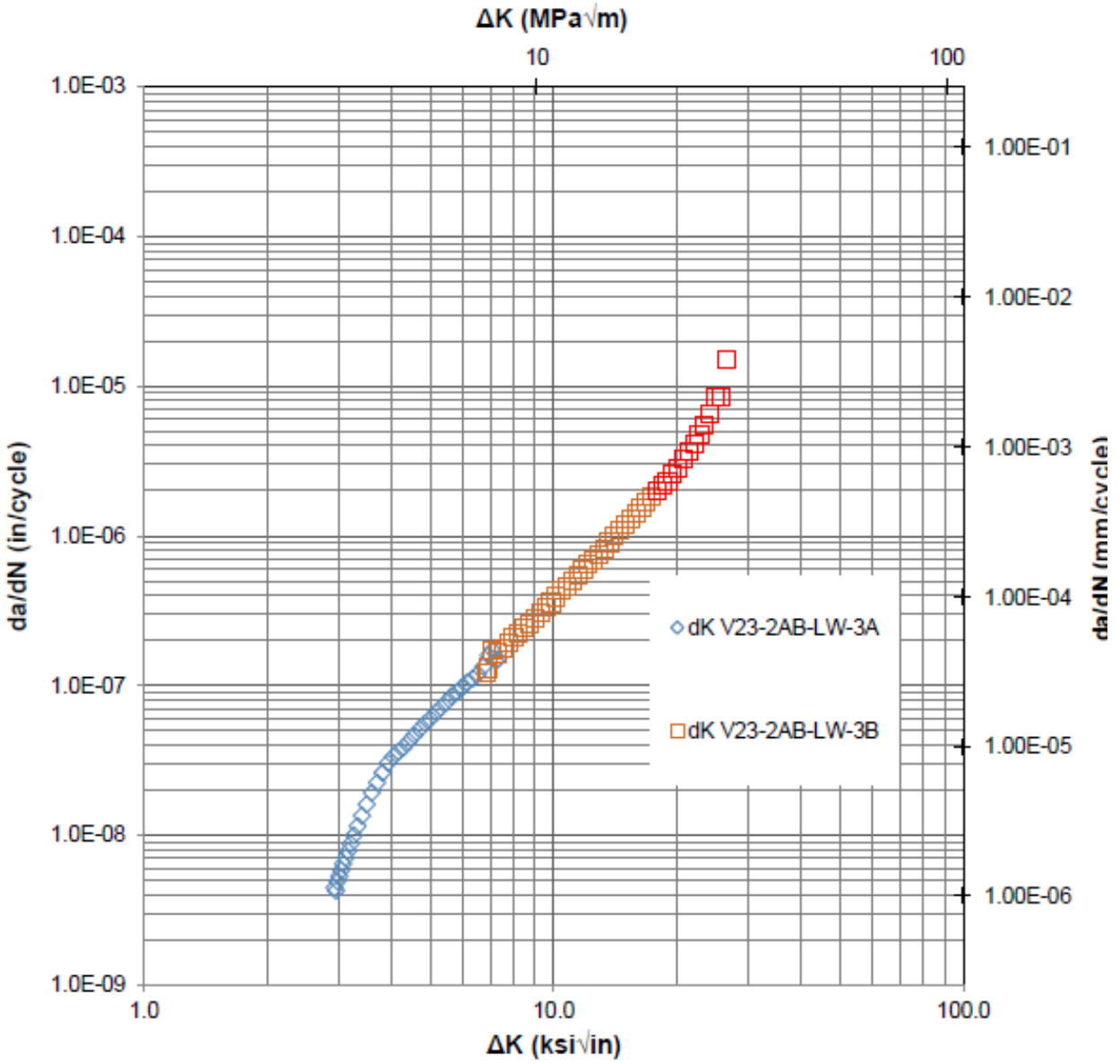


Figure 7.5.1.3.4-5: V0023-2AB-LW-3 Plot R = 0.7

7.5.2 Inner Layer Weld

Inner layer welds are welds used to join the inner layer of a LPV to itself or to another course of inner layer material. During manufacturing, inner layers were assembled first to create the base of the vessel, and the intermediate and outer layers were wrapped around after. During to this process, inner layer welds were fully inspected and given post weld heat treatment. Inner layer welds do not typically suffer from porosity, lack of fusion, or significant residual weld stresses. Inner layers are usually thicker than the wrapper layers, typically measuring 0.375 inches to 0.5 inches. When the first wrapper layer is applied, the inner layer is used as a backer and becomes fixed to the first wrapper. Longitudinal welds are offset in the circumferential direction around the LPV so as not to overlap directly, however, circumferential inner welds do cross wrapper longitudinal welds. This is due to the mismatch in material length, inner shell courses being generally shorter and require more circumferential welds to achieve the desired overall length. Overall, inner layer welds are of higher quality, with less residual stress than the shell layer welds.

7.5.2.1 Chemical Composition

Weld material specifications are not typically available or verifiable, therefore the chemical composition reported is only of the collected test data. Data is only from the weld center, HAZ chemistry is that of the parent plate material. Table 7.5.2.1-1 presents data collected from inner welds of dissected vessels.

Table 7.5.2.1-1: Collected Chemistry Data

Vessel	Location	C	Si	Mn	P	S	Cr	Mo	Ni	Cu	V
V0023	Inner Circ	0.08	0.82	1.77	0.019	0.019	0.078	0.350	0.150	0.110	0.030
V32	Inner Seam	0.09	0.77	1.52	0.019	0.020	0.080	0.340	0.240	0.220	0.048
V0348	Inner Seam	0.14	0.39	0.91	0.016	0.031	0.048	0.057	0.024	0.092	0.061
V125	Inner Seam	0.15	0.60	1.61	0.020	0.023	0.091	0.290	0.410	0.099	0.068
MV50466-8	Inner Seam	0.11	0.19	1.15	0.017	0.018	0.110	0.390	2.370	0.085	0.062

7.5.2.2 Metallography

Metallography tests were performed on this material to observe number of weld passes and basic orientation of microstructure. This was done in order to confirm the tested orientation as the weakest and to identify weld order, HAZ location and size, and grain structure. Thus, grain orientation studies were performed, but grain size, grain size through thickness, and carburization layer thickness studies were not, and no macro cubes were produced.

Grain Orientation Study

The grain orientation study is a polish and etch of a weld cross section. Its purpose is to confirm the correct orientation for fracture testing. In this case, the P orientation, parallel to the weld path, was found to be the most realistic and proper orientation for further tests.

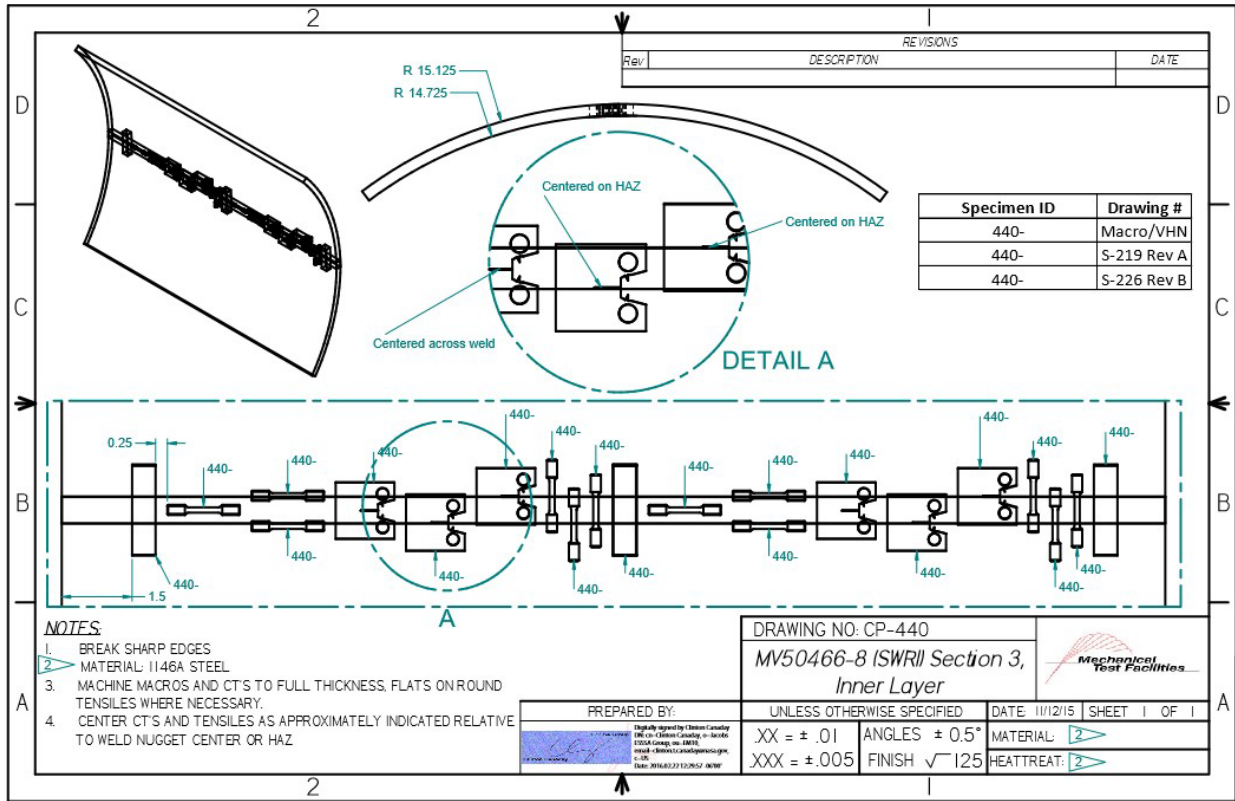


Figure 7.5.2.2-1: Cut Plan for Macros from MV50466-8 Seam Weld

The macros shown in figures Figure 7.5.2.2-2, Figure 7.5.2.2-3, Figure 7.5.2.2-4, and Figure 7.5.2.2-5 were extracted from the cross-sections of MV50466-8, V0032, V0023, and V0125 inner layer welds, near the location of tensile and fracture test specimens.



Figure 7.5.2.2-2: MV50466-8 Inner Weld Macro



Figure 7.5.2.2-3: V0032 Inner Weld Macro



Figure 7.5.2.2-4: V0032 Inner Weld Macro

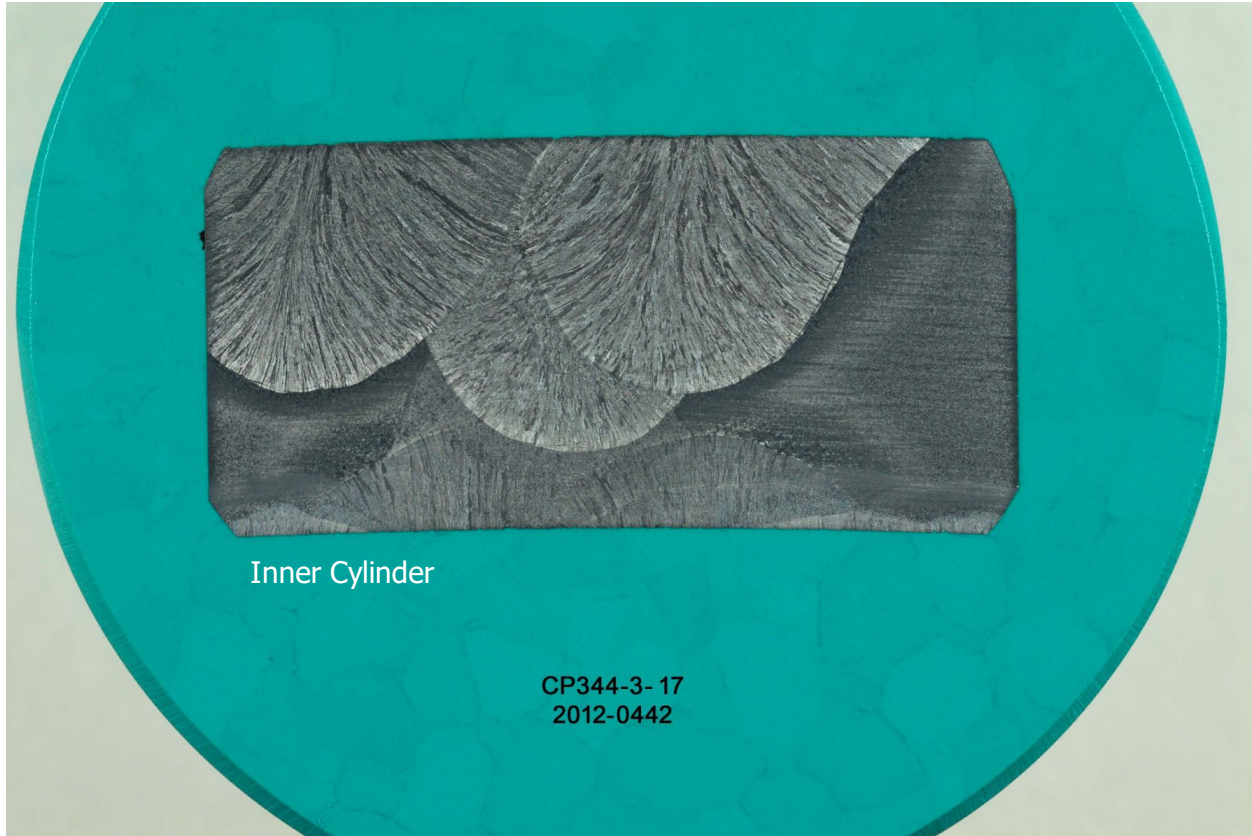


Figure 7.5.2.2-5: V0125 Inner Weld Macro

Hardness

Hardness traces were conducted on some inner layer welds to help identify the degree of variance in material properties and stress concentrations across the parent-weld-parent span. These were used to identify areas of concern and direct testing towards less favorable material conditions which would indicate worst-case crack scenarios.

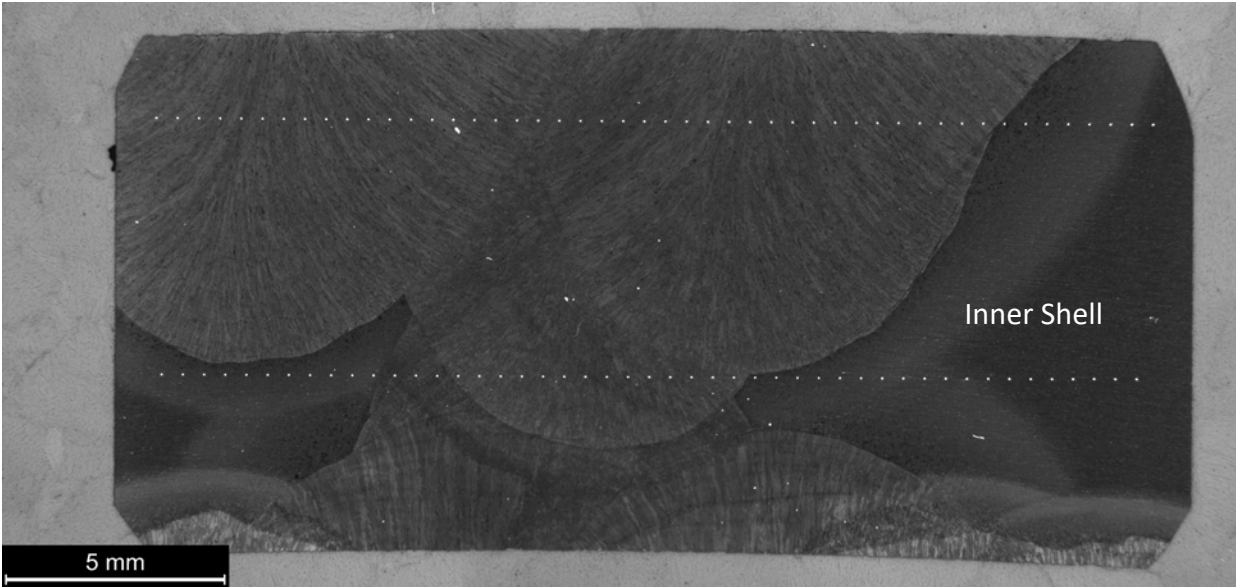


Figure 7.5.2.2-6: V0125 Inner Weld Indent Locations

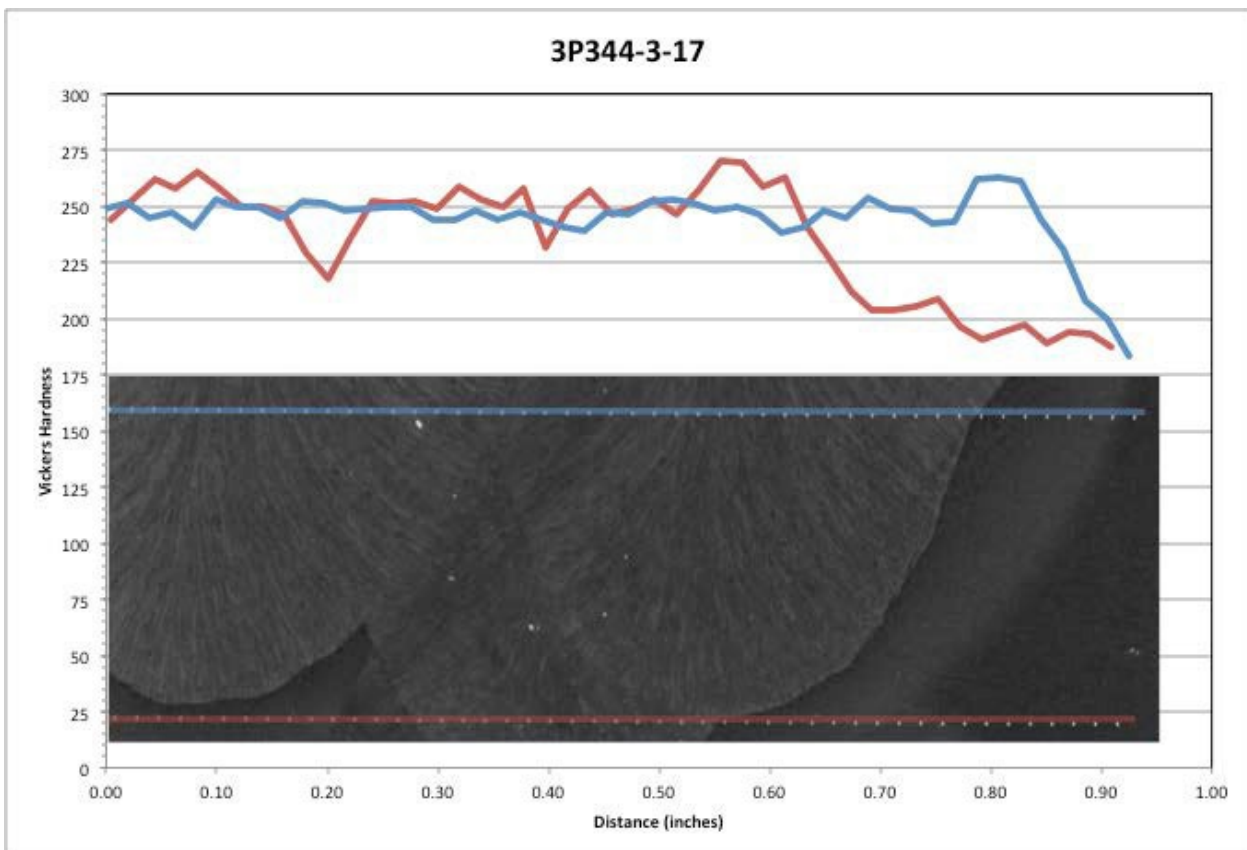


Figure 7.5.2.2-7: V0125 Inner Weld Hardness Trace

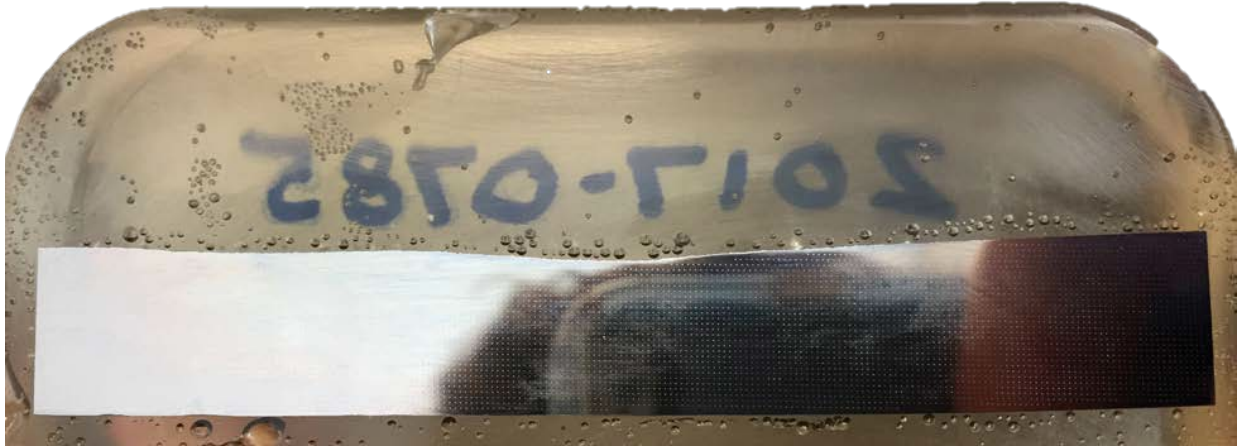


Figure 7.5.2.2-8: V0023 Inner Weld Indent Locations

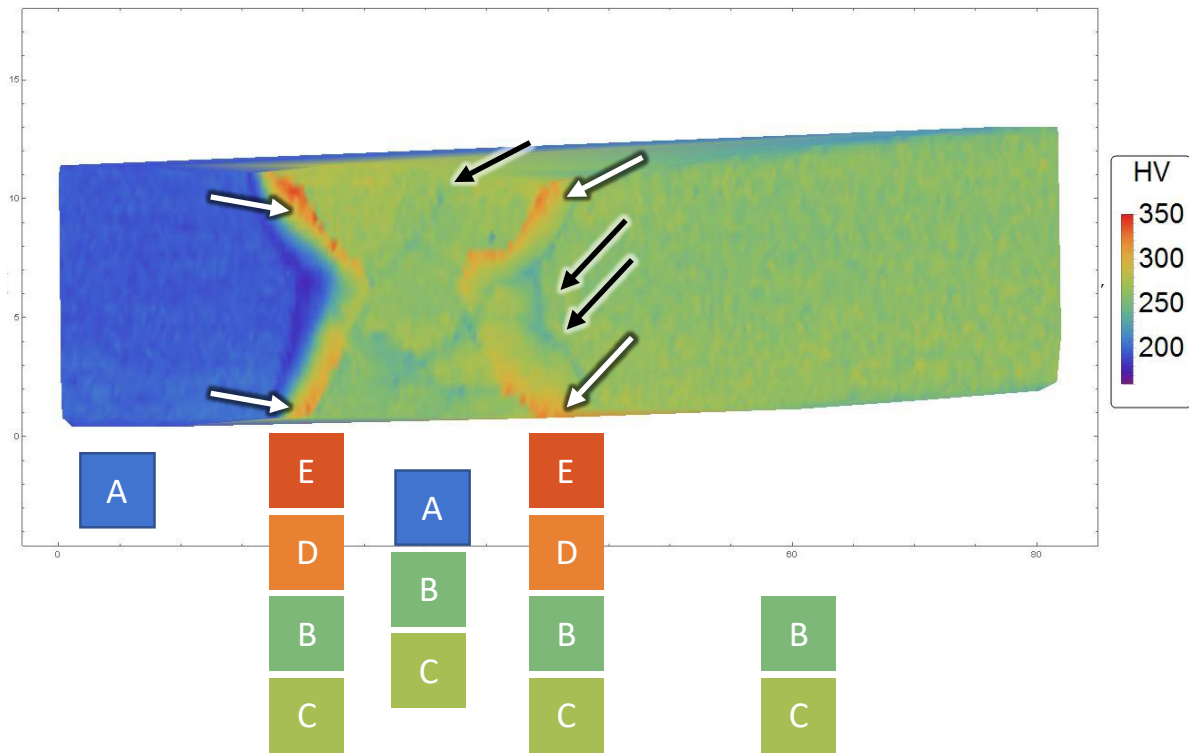


Figure 7.5.2.2-9: V0023 Inner Weld Hardness Map

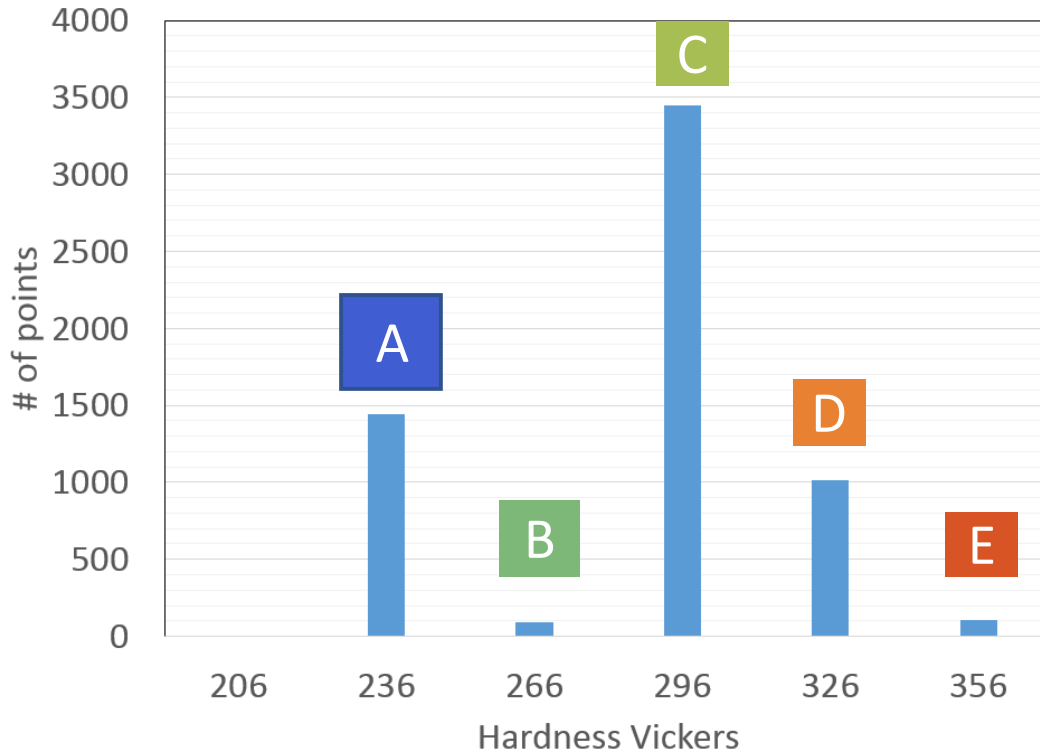


Figure 7.5.2.2-10: V0023 Inner Weld Hardness Distribution

7.5.2.3 Mechanical Properties

Mechanical properties for the weld metal vary by manufacturer and application parameters and are only characterized by the tests documented in this section.

7.5.2.3.1 Smooth Tensile Tests

Smooth tensile tests were conducted on round specimens at MSFC according to ASTM E8, “Standard Test Methods for Tension Testing of Metallic Materials” (51) using specimen design S-219 Rev A. The mechanical test frame consisted of a servo-hydraulic actuator and reaction frame. The frame used an LVDT for displacement feedback. Stress measurements were derived from load measurements and the initial specimen measurements. Strain measurements were derived from an extensometer and the initial specimen measurements.

Attempts to run tensile tests on HAZ material were inconclusive as properties either matched weld material or parent material. Many tests had extensometer slippage or breakage outside of the gauge section, rendering the fracture elongation values suspect.

The results obtained from testing of inner layer welds from vessels MV50466-8, V0125, V0032, and V0023 are presented in Table 7.5.2.3.1-1 through Table 7.5.2.3.1-4. Figure 7.5.2.3.1-1 shows a typical engineering stress-strain curve.

Table 7.5.2.3.1-1: Inner Weld Smooth Tensile Data, MV50466-8

Specimen ID	Test Temp. (°C)	ASTM Orientation	Tensile Stress (ksi)	Yield Stress (ksi)	Fracture Elongation (%)
440-325	21	N	104.1	85.1	6.3
440-326	21	N	103.7	86.9	2.7

Table 7.5.2.3.1-2: Inner Weld Smooth Tensile Data, V0023

Specimen ID	Test Temp. (°C)	ASTM Orientation	Tensile Stress (ksi)	Yield Stress (ksi)	Fracture Elongation (%)
519-195	21	N	103.1	92.2	3.3
519-196	21	N	105.0	97.9	2.5
519-197	21	N	107.9	96.2	4.7
519-205	21	N	119.1	101.5	9.0
519-206	21	N	116.9	100.9	6.1
519-207	21	N	116.6	105.3	4.6
519-208	21	N	120.7	104.1	8.7
519-209	21	N	119.2	102.8	18.5

Table 7.5.2.3.1-3: Inner Weld Smooth Tensile Data, V0032

Specimen ID	Test Temp. (°C)	ASTM Orientation	Tensile Stress (ksi)	Yield Stress (ksi)	Fracture Elongation (%)
380-122	21	N	102.7	88.3	21.9
380-125	21	N	102.5	87.9	21.4
380-123	-46	N	107.4	90.5	17.3
380-124	-101	N	112.9	95.9	23.8

Table 7.5.2.3.1-4: Inner Weld Smooth Tensile Data, V0125

Specimen ID	Test Temp. (°C)	ASTM Orientation	Tensile Stress (ksi)	Yield Stress (ksi)	Fracture Elongation (%)
CP-344-3-10	21	N	101.9	83.8	5.0
CP-344-3-11	21	N	101.6	88.8	4.0

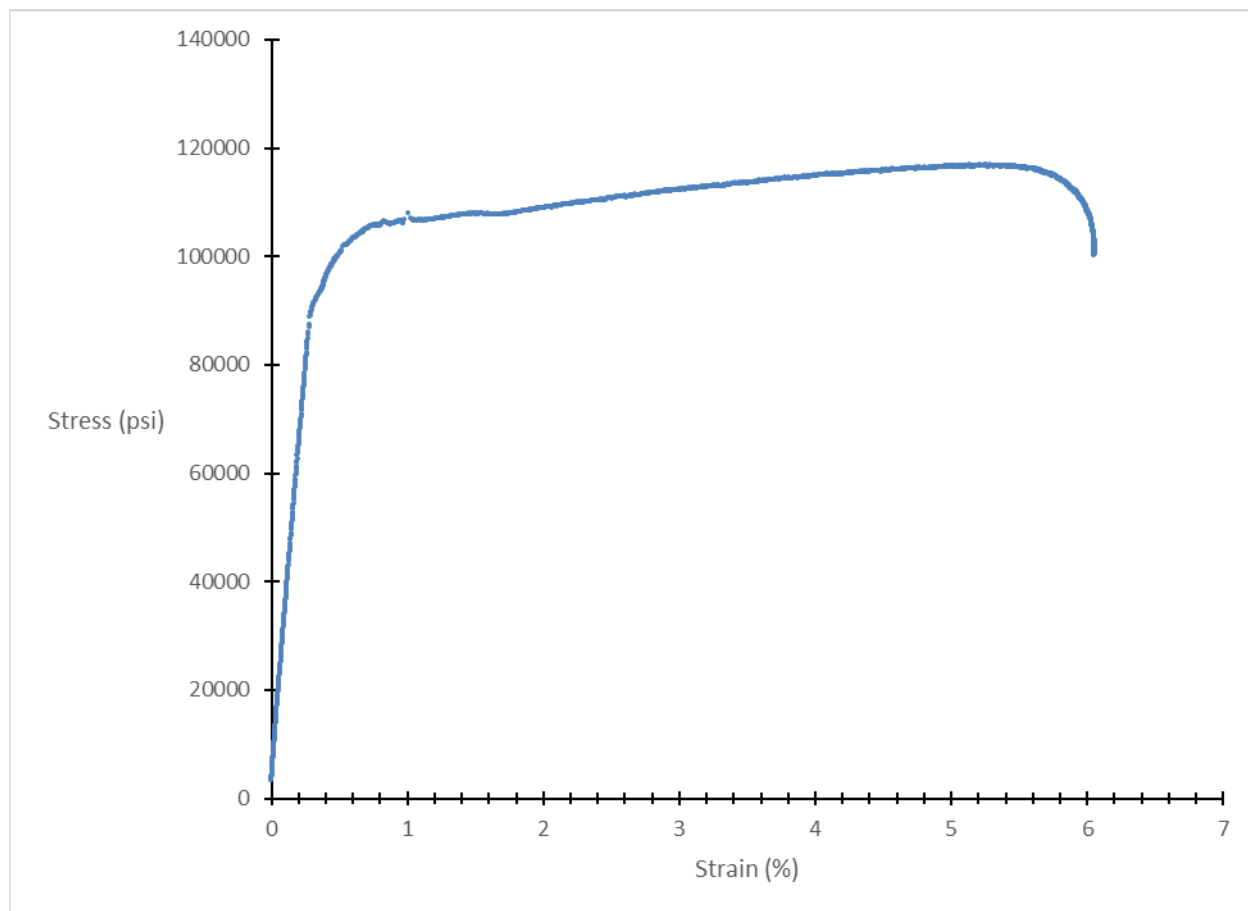


Figure 7.5.2.3.1-1: Inner Layer Weld Smooth Tensile Plot for Sample 519-206

Inner layer weld tensile tests can be difficult to interpret due to the sample passing through multiple weld passes, usually including backfill passes. The multiple weld boundaries, HAZ, and even different weld metals can produce inconsistent failure modes and elongations. Therefore, the main purpose of these tests is to roughly estimate mechanical properties for application to actual fracture toughness tests. No conclusions should be drawn from the fracture elongation or curve shape.

7.5.2.3.2 Notch Tensile

Notch tensile tests were not performed on this material.

7.5.2.3.3 Fracture Properties

All room temperature testing was performed in accordance with ASTM E1820 (10). All other temperatures were tested in accordance with ASTM E1921 (7). Testing for both standards use specimen design S-226 Rev B. Inner layer weld fracture tests came from vessels MV50466-8, V0023, V0032, and V0125. The samples tested had the crack plane in the N-P orientation as defined by ASTM. The HAZ was tested for V0023 only. All specimens were side-

grooved to a total thickness reduction of 20%. The cutting diagram used to remove the C(T) specimens from the V0023 head-to-shell weld is shown in Figure 7.5.2.3.3-3. Examples of Load Versus COD and J_q Versus Δa plots are shown in Figure 7.5.2.3.3-1 and Figure 7.5.2.3.3-2.

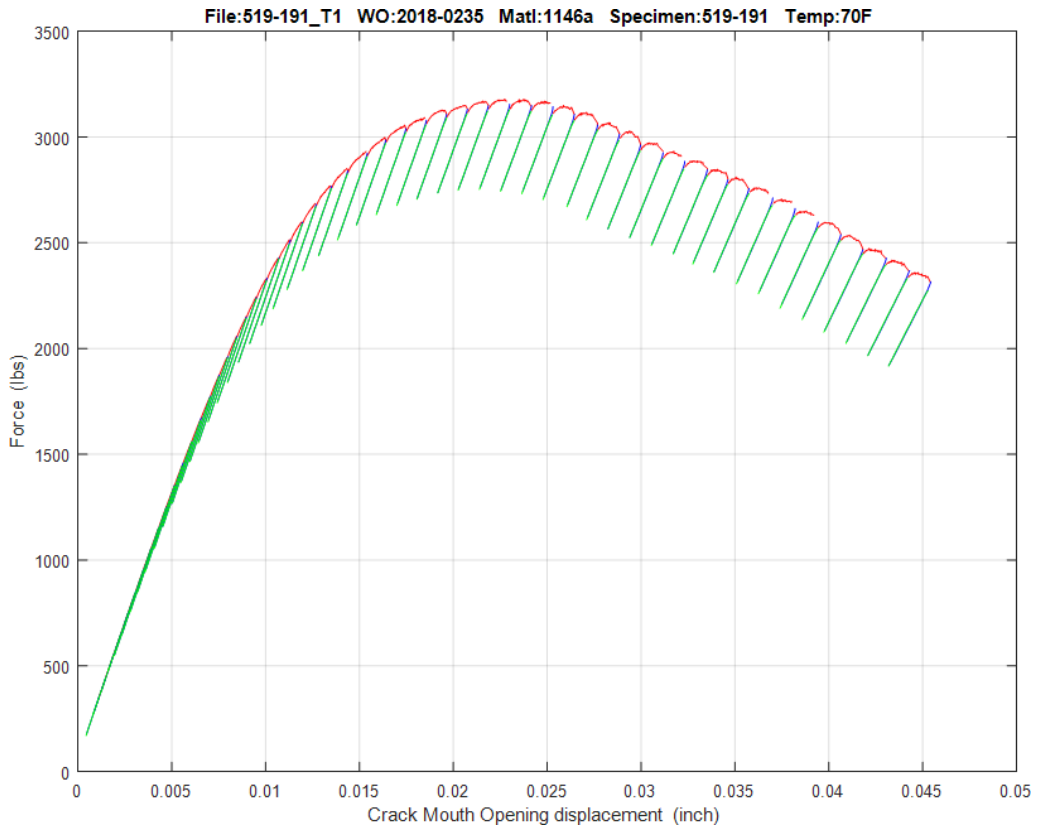


Figure 7.5.2.3.3-1: Inner Layer Weld Load Versus COD Plot, Sample 519-191

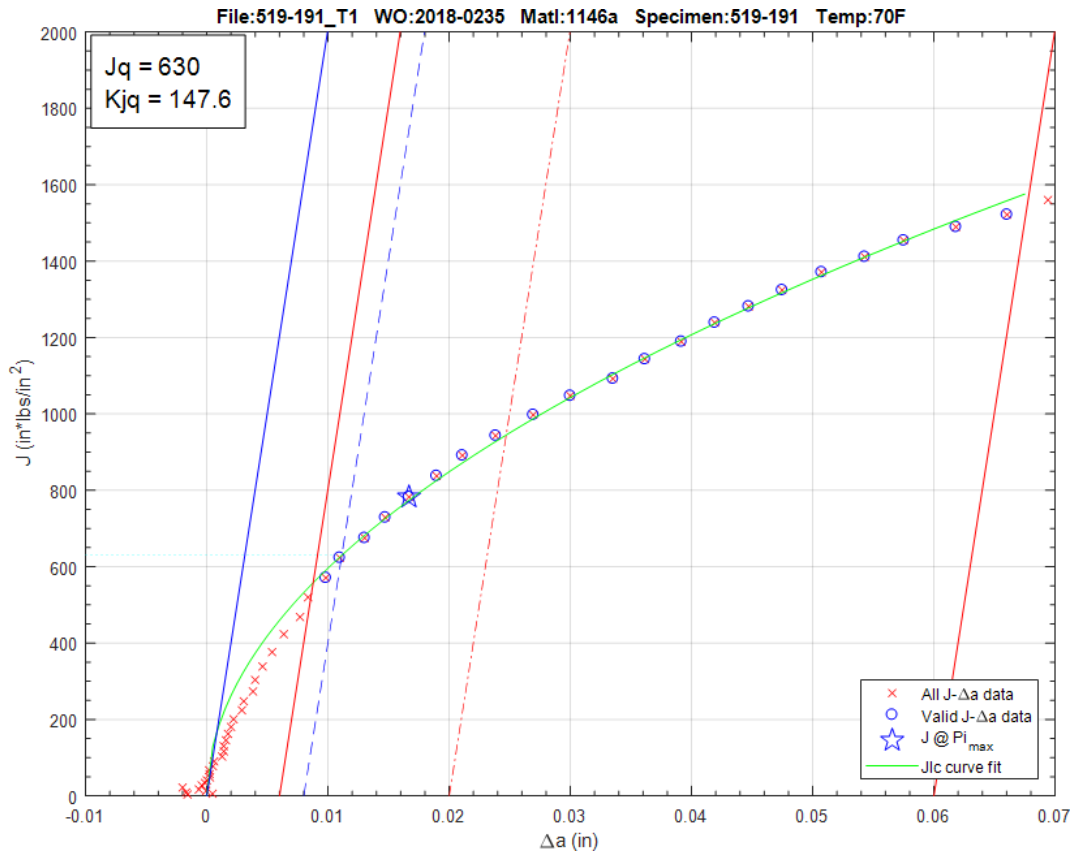


Figure 7.5.2.3.3-2: Inner Layer Weld J_q Versus Δa Plot, Sample 519-191

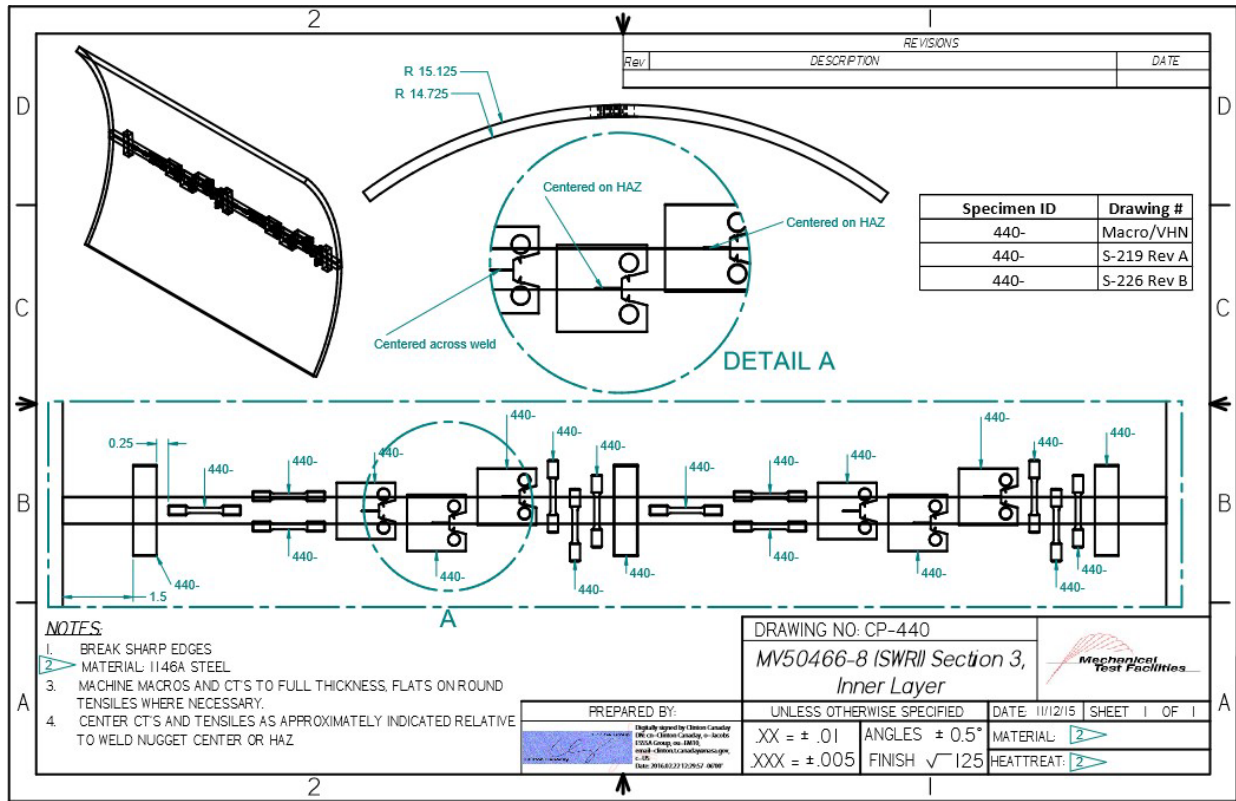


Figure 7.5.2.3.3-3: Cut Plan for Fracture Specimens from MV50466-8 Inner Weld

The test data in Table 7.5.2.3.3-1 are raw values obtained from fracture tests conducted on V0125 inner layer weld material. Test results that are considered upper shelf are listed under ASTM E1820, while transition temperature test results are listed under E1921. Tests that meet the complete validity requirements for $J_q = J_{1C}$ and $K_{Jq} = K_{J1C}$ are denoted with an asterisk. Despite invalidities, J_q and K_{Jq} convey valuable fracture toughness information, especially when the test results are applied directly to the sample material source.

Table 7.5.2.3.3-1: Inner Layer Weld Fracture Toughness Data, V0125

Specimen ID	Test Temp. (°C)	ASTM Crack Plane Orientation	W (in)	a_0 (in)	a_f (in)	B_0 (in)	B_N (in)	J_q (kJ/m ²)	K_{Jq} (MPa √m)	K_{Jc1T} (MPa √m)	ASTM Standard
CP-344-3-4	26	N-P	1.0010	0.6063	0.6787	0.3770	0.3000	100	150	---	E1820
CP-344-3-5	23	N-P	1.0007	0.6266	0.6876	0.3779	0.3000	90	142	---	E1820
CP-344-3-6	-46	N-P	1.0002	0.6719	0.6832	0.3780	0.3040	38	92	---	E1820

Results from the single E1921 test are presented in Table 7.5.2.3.3-2 and Table 7.5.2.3.3-3. These results were obtained using the T_0 TEM Code described in Section 4.2. The T_0 reference temperature for this data set was evaluated as -19°C using the E1921 Master Curve shown in Figure 7.5.2.3.3-4.

Table 7.5.2.3.3-2: Inner Layer Weld T₀ Individual Specimen Results, V0125

Specimen Name	Temperature (°C)	KjcRaw (MPa*m ^{0.5})	1T Data (MPa*m ^{0.5})	Uncensored Data	Test Temp -T ₀ (°C)
CP-344-3-6	-46	92.3	76.7	1	-27

Table 7.5.2.3.3-3: Inner Layer Weld T₀ Calculation Results, V0125

Initial T ₀ (°C)	-19
Total Samples	1
Samples within T ₀ ± 50°C (N)	1
Number of Uncensored Data (r)	1
Poisson's Ratio	0.3
Σ(r _i n _i)	0.14
Samples Between T _i - T ₀ 50 to -14 °C	0
Samples Between T _i - T ₀ -15 to -35 °C	1
Samples Between T _i - T ₀ -36 to -50 °C	0
T ₀ scrn (°C)	-19
Homogenous or Inhomogeneous	Homogenous

The results of the E1921 analysis show that the weld material removed from the inner layer weld is macroscopically homogenous, indicating consistent properties throughout the sampled material. For this data set, the ductile-brittle transition temperature was found to be 19°C. This result does not meet the E1921 validity criteria for a sufficient number of samples tested in an appropriate temperature range with $\Sigma(r_i n_i) < 1.0$. Since there was only one sample tested close enough to T₀ to be used in a Master Curve, the results of this analysis should be taken with extreme caution.

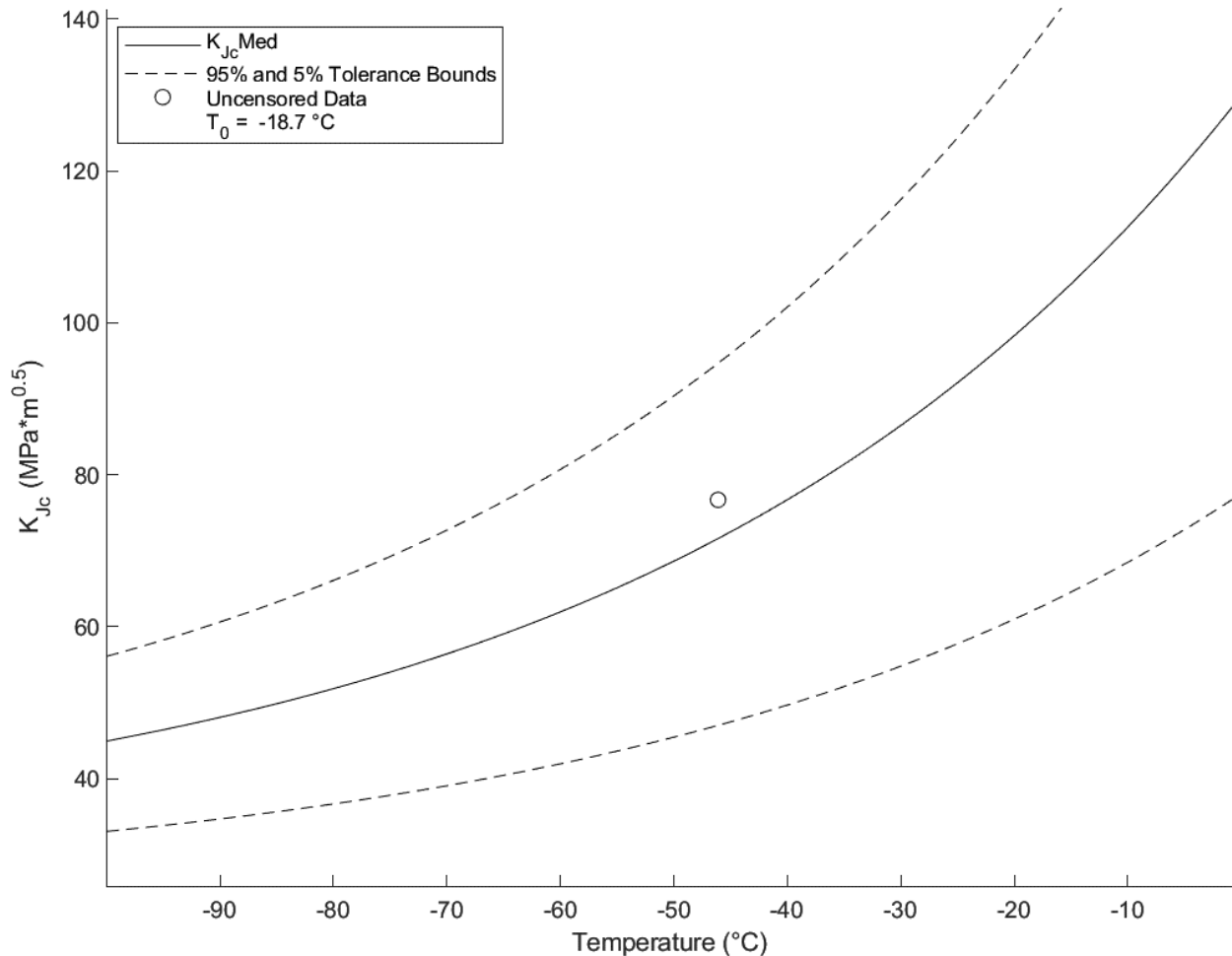


Figure 7.5.2.3.3-4: Inner Layer Weld T_0 Plot, V0125

The following test data are raw values obtained from fracture tests conducted on MV50466-8 inner layer weld material. Test results that are considered upper shelf are listed under ASTM E1820, while transition temperature test results are listed under E1921. Tests that meet the complete validity requirements for $J_q = J_{1C}$ and $K_{Jq} = K_{J1C}$ are denoted with an asterisk. Despite invalidities, J_q and K_{Jq} convey valuable fracture toughness information, especially when the test results are applied directly to the sample material source.

Table 7.5.2.3.3-4 presents raw test data obtained from fracture tests conducted on V0032 inner layer weld material. Test results that are considered upper shelf are listed under ASTM E1820, while transition temperature test results are listed under E1921. Tests that meet the complete validity requirements for $J_q = J_{1C}$ and $K_{Jq} = K_{J1C}$ are denoted with an asterisk. Despite invalidities, J_q and K_{Jq} convey valuable fracture toughness information, especially when the test results are applied directly to the sample material source.

Table 7.5.2.3.3-4: Inner Layer Weld Fracture Toughness Data, V0032

Specimen ID	Test Temp. (°C)	ASTM Crack Plane Orientation	W (in)	a ₀ (in)	a _r (in)	B ₀ (in)	B _N (in)	J _q (kJ/m ²)	K _{Jq} (MPa√m)	K _{JC1T} (MPa√m)	ASTM Standard
380-121	22	N-P	0.9971	0.5423	0.6324	0.3729	0.3073	87	140	---	E1820
380-120	0	N-P	0.9988	0.5764	0.5868	0.3735	0.3128	68	123	101	E1921
380-126	0	N-P	0.9979	0.5382	0.5519	0.3726	0.3098	50	105	87	E1921
380-127	0	N-P	0.9959	0.5404	0.5425	0.3732	0.3092	25	75	63	E1921
380-118	-12	N-P	0.9979	0.5440	0.5532	0.3745	0.3122	43	98	81	E1921
380-119	-12	N-P	0.9991	0.5286	0.5286	0.3740	0.3115	21	68	58	E1921
380-117	-46	N-P	0.9965	0.5318	0.5366	0.3722	0.3093	25	75	63	E1921
380-116	-73	N-P	0.9968	0.5189	0.5192	0.3739	0.3098	7	41	36	E1921

Results from the five E1921 tests are presented in Table 7.5.2.3.3-5 and Table 7.5.3.3.3-6. These results were obtained using the T₀TEM Code described in Section 4.2. The T₀ reference temperature for this data set was evaluated as 17°C using the E1921 Master Curve shown in Figure 7.5.2.3.3-5.

Table 7.5.2.3.3-5: Inner Layer Weld T₀ Individual Specimen Results, V0032

Specimen Name	Temperature (°C)	K _{JcRaw} (MPa*m ^{0.5})	1T Data (MPa*m ^{0.5})	Uncensored Data	Test Temp -T ₀ (°C)
380-118	-12	97.7	80.8	1	-29
380-119	-12	68.3	57.8	1	-29
380-120	0	123.0	100.5	1	-17
380-126	0	105.5	86.8	1	-17
380-127	0	75.1	63.1	1	-17

Table 7.5.2.3.3-6: Inner Layer Weld T₀ Calculation Results, V0032

Initial T ₀ (°C)	17
Total Samples	5
Samples within T ₀ ± 50°C (N)	5
Number of Uncensored Data (r)	5
Poisson's Ratio	0.3
Σ(r _i n _i)	0.71
Samples Between T _i - T ₀ 50 to -14 °C	0
Samples Between T _i - T ₀ -15 to -35 °C	5
Samples Between T _i - T ₀ -36 to -50 °C	0
T ₀ scrn (°C)	17
Homogenous or Inhomogeneous	Homogenous

The results of the E1921 analysis show that the weld material removed from the inner layer weld is macroscopically homogeneous, indicating consistent properties throughout. For this data set, the ductile-brittle transition temperature was found to be 17°C. This result does not meet the E1921 validity criteria for a sufficient number of samples tested in an appropriate temperature range with Σ(r_i n_i) < 1.0. However, because the results are consistent and the tests

were only two samples short of validity, the Master Curve can be considered sufficiently accurate to use for evaluation.

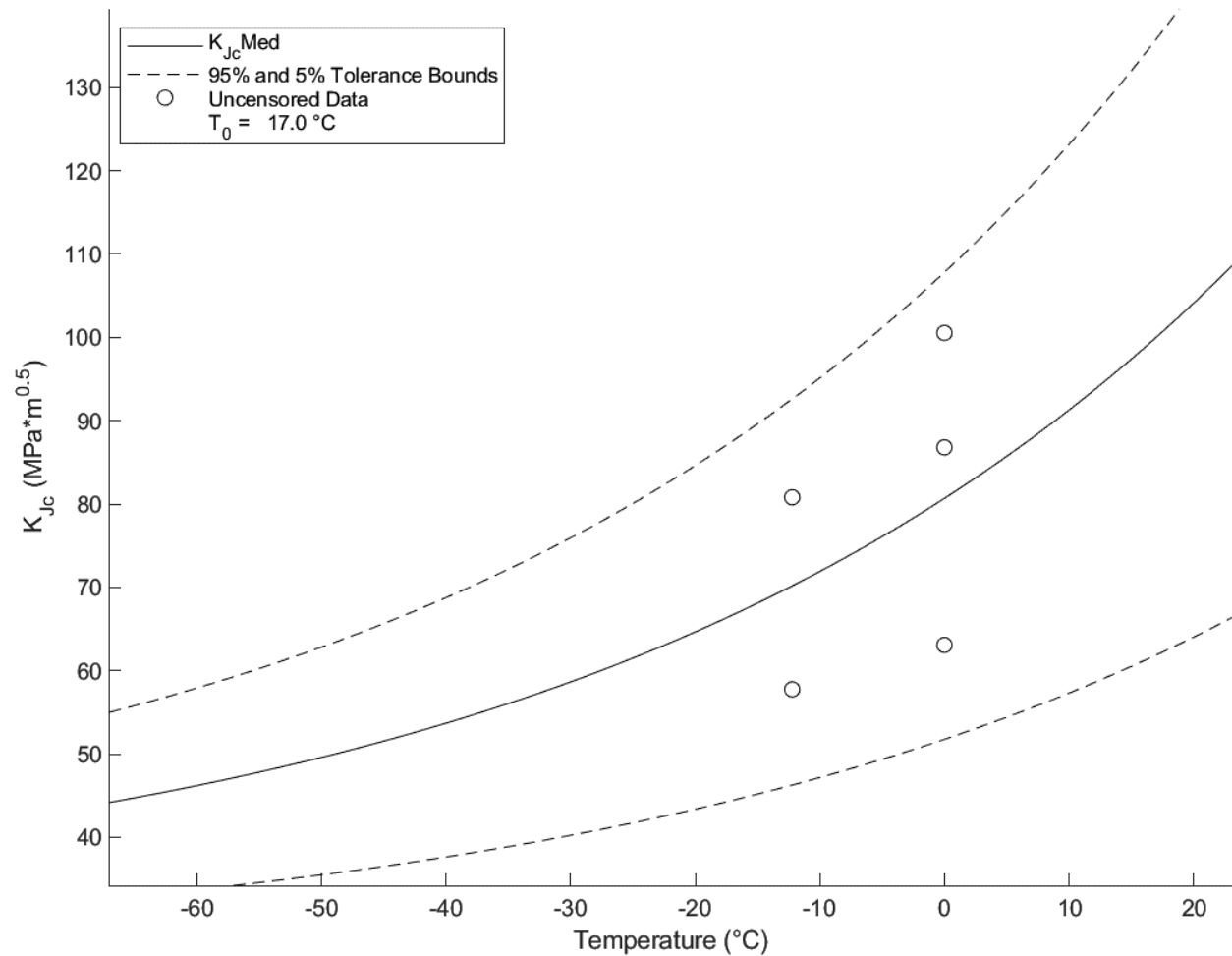


Figure 7.5.2.3.3-5: Inner Layer Weld T_0 Plot, V0032

The test data in Table 7.5.2.3.3-7 are raw values obtained from fracture tests conducted on V0023 inner layer weld material. Test results that are considered upper shelf are listed under ASTM E1820, while transition temperature test results are listed under E1921. Tests that meet the complete validity requirements for $J_q = J_{1C}$ and $K_{Jq} = K_{J1C}$ are denoted with an asterisk. Despite invalidities, J_q and K_{Jq} convey valuable fracture toughness information, especially when the test results are applied directly to the sample material source.

Table 7.5.2.3.3-7: Inner Layer Weld Fracture Toughness Data, V0023

Specimen ID	Test Temp. (°C)	ASTM Crack Plane Orientation	W (in)	a_0 (in)	a_f (in)	B_0 (in)	B_N (in)	J_q (kJ/m ²)	K_{Jq} (MPa√m)	K_{JCT} (MPa√m)	ASTM Standard
519-191	21	T-L	0.9995	0.5175	0.6082	0.3776	0.2977	118	162	131	E1921
519-194	0	T-L	0.9996	0.5189	0.5269	0.3749	0.3024	59	115	94	E1921
519-200	0	T-L	0.9999	0.5395	0.5450	0.3749	0.2960	39	93	77	E1921
519-204	0	T-L	0.9999	0.5191	0.5354	0.3396	0.2617	111	158	125	E1921

Results from the four E1921 tests are presented in Table 7.5.2.3.3-8 and Table 7.5.2.3.3-9. These results were obtained using the T_0 TEM Code described in Section 4.2. The T_0 reference temperature for this data set was evaluated as -1°C using the E1921 master curve shown in Figure 7.5.2.3.3-6.

Table 7.5.2.3.3-8: Inner Layer Weld T_0 Individual Specimen Results, V0023

Specimen Name	Temperature ($^\circ\text{C}$)	KjcRaw ($\text{MPa}\cdot\text{m}^{0.5}$)	1T Data ($\text{MPa}\cdot\text{m}^{0.5}$)	Uncensored Data	Test Temp - T_0 ($^\circ\text{C}$)
519-191	21	162.2	125.1	0	22
519-194	0	115.1	94.4	1	1
519-200	0	93.0	77.1	1	1
519-204	0	157.7	125.1	1	1

Table 7.5.2.3.3-9: Inner Layer Weld T_0 Calculation Results, V0023

Initial T_0 ($^\circ\text{C}$)	-1
Total Samples	4
Samples within $T_0 \pm 50^\circ\text{C}$ (N)	4
Number of Uncensored Data (r)	3
Poisson's Ratio	0.3
$\Sigma(r_i n_i)$	0.5
Samples Between $T_i - T_0$ 50 to -14°C	3
Samples Between $T_i - T_0$ -15 to -35°C	0
Samples Between $T_i - T_0$ -36 to -50°C	0
$T_{0\text{scrn}}$ ($^\circ\text{C}$)	7
Homogenous or Inhomogeneous	Homogenous

The results of the E1921 analysis show that the weld material removed from the inner layer weld is macroscopically homogeneous, indicating consistent properties throughout. For this data set, the ductile-brittle transition temperature was found to be -1°C . This result does not meet the E1921 validity criteria for a sufficient number of samples tested in an appropriate temperature range with $\Sigma(r_i n_i) < 1.0$. However, due to the consistency of the results, the Master Curve can be considered a reasonably accurate description of the transition temperature.

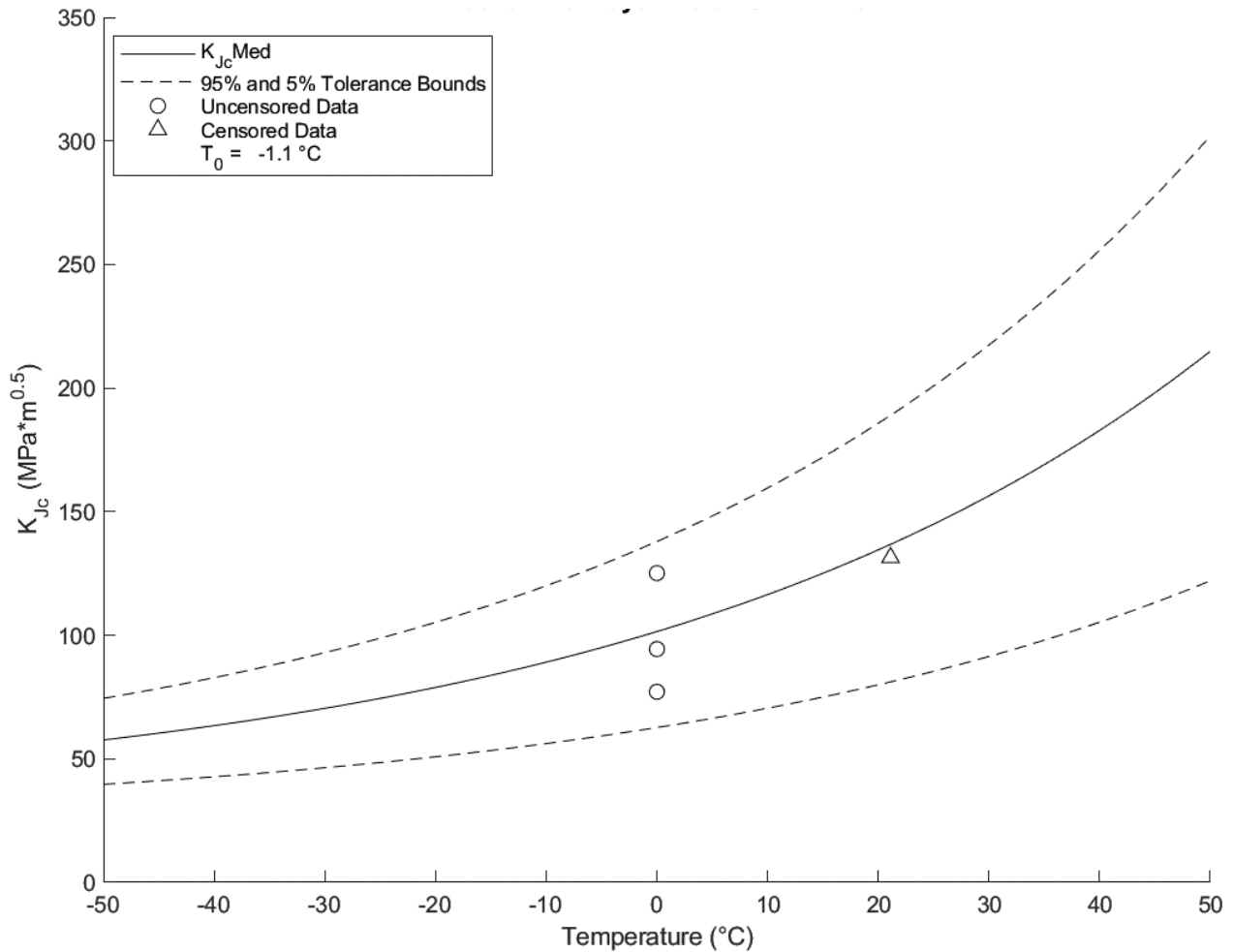


Figure 7.5.2.3.3-6: Inner Layer Weld T_0 Plot, V0023

The test data in Table 7.5.2.3.3-10 are raw values obtained from fracture tests conducted on V0023 inner layer weld HAZ material. Test results that are considered upper shelf are listed under ASTM E1820, while transition temperature test results are listed under E1921. Tests that meet the complete validity requirements for $J_q = J_{1C}$ and $K_{Jq} = K_{J1C}$ are denoted with an asterisk. Despite invalidities, J_q and K_{Jq} convey valuable fracture toughness information, especially when the test results are applied directly to the sample material source.

Table 7.5.2.3.3-10: Inner Layer Weld HAZ Fracture Toughness Data, V0023

Specimen ID	Test Temp. (°C)	ASTM Crack Plane Orientation	W (in)	a_0 (in)	a_f (in)	B_0 (in)	B_N (in)	J_q (kJ/m ²)	K_{Jq} (MPa \sqrt{m})	K_{JcIT} (MPa \sqrt{m})	ASTM Standard
519-192	21	T-L	0.9999	0.5164	0.5257	0.3529	0.2827	63	118	96	E1921
519-193	21	T-L	0.9997	0.5099	0.6403	0.3522	0.2788	58	114	92	E1921
519-201	21	T-L	0.9988	0.5216	0.6134	0.3013	0.2399	55	111	88	E1921
519-202	21	T-L	0.9993	0.5330	0.6897	0.3503	0.2792	50	105	86	E1921
519-203	22	T-L	0.9995	0.5445	0.6695	0.3457	0.2730	44	99	81	E1921

Results from the five E1921 tests is presented in Table 7.5.2.3.3-11 and Table 7.5.2.3.3-12. These results were obtained using the T_0 TEM Code described in Section 4.2. The T_0 reference temperature for this data set was evaluated as -27°C using the E1921 Master Curve shown in Figure 7.5.2.3.3-7.

Table 7.5.2.3.3-11: Inner Layer Weld HAZ T_0 Individual Specimen Results, V0023

Specimen Name	Temperature ($^{\circ}\text{C}$)	KjcRaw (MPa*m ^{0.5})	1T Data (MPa*m ^{0.5})	Uncensored Data	Test Temp - T_0 ($^{\circ}\text{C}$)
519-192	-18	118.3	95.8	1	10
519-193	-18	113.5	92.0	0	10
519-201	-18	111.2	87.6	0	10
519-202	-18	105.4	85.7	0	10
519-203	-18	99.2	80.7	0	10

Table 7.5.2.3.3-12: Inner Layer Weld HAZ T_0 Calculation Results, V0023

Initial T_0 ($^{\circ}\text{C}$)	-27
Total Samples	5
Samples within $T_0 \pm 50^{\circ}\text{C}$ (N)	5
Number of Uncensored Data (r)	1
Poisson's Ratio	0.3
$\Sigma(r_i n_i)$	0.17
Samples Between $T_i - T_0$ 50 to -14°C	1
Samples Between $T_i - T_0$ -15 to -35°C	0
Samples Between $T_i - T_0$ -36 to -50°C	0
$T_{0\text{scrn}}$ ($^{\circ}\text{C}$)	-3
Homogenous or Inhomogeneous	Homogenous

The results of the E1921 analysis show that the HAZ material removed from the inner layer weld HAZ is macroscopically homogeneous, indicating consistent properties throughout. For this data set, the ductile-brittle transition temperature was found to be -27°C . This result does not meet the E1921 validity criteria for a sufficient number of samples tested in an appropriate temperature range with $\Sigma(r_i n_i) < 1.0$. The properties of the HAZ are similar to that of parent plate material and show significant ductile instability at low K values, resulting in violations of the crack extension censoring without reaching the target $KJ = 100 \text{ MPa}\sqrt{\text{m}}$ for Master Curve calculation.

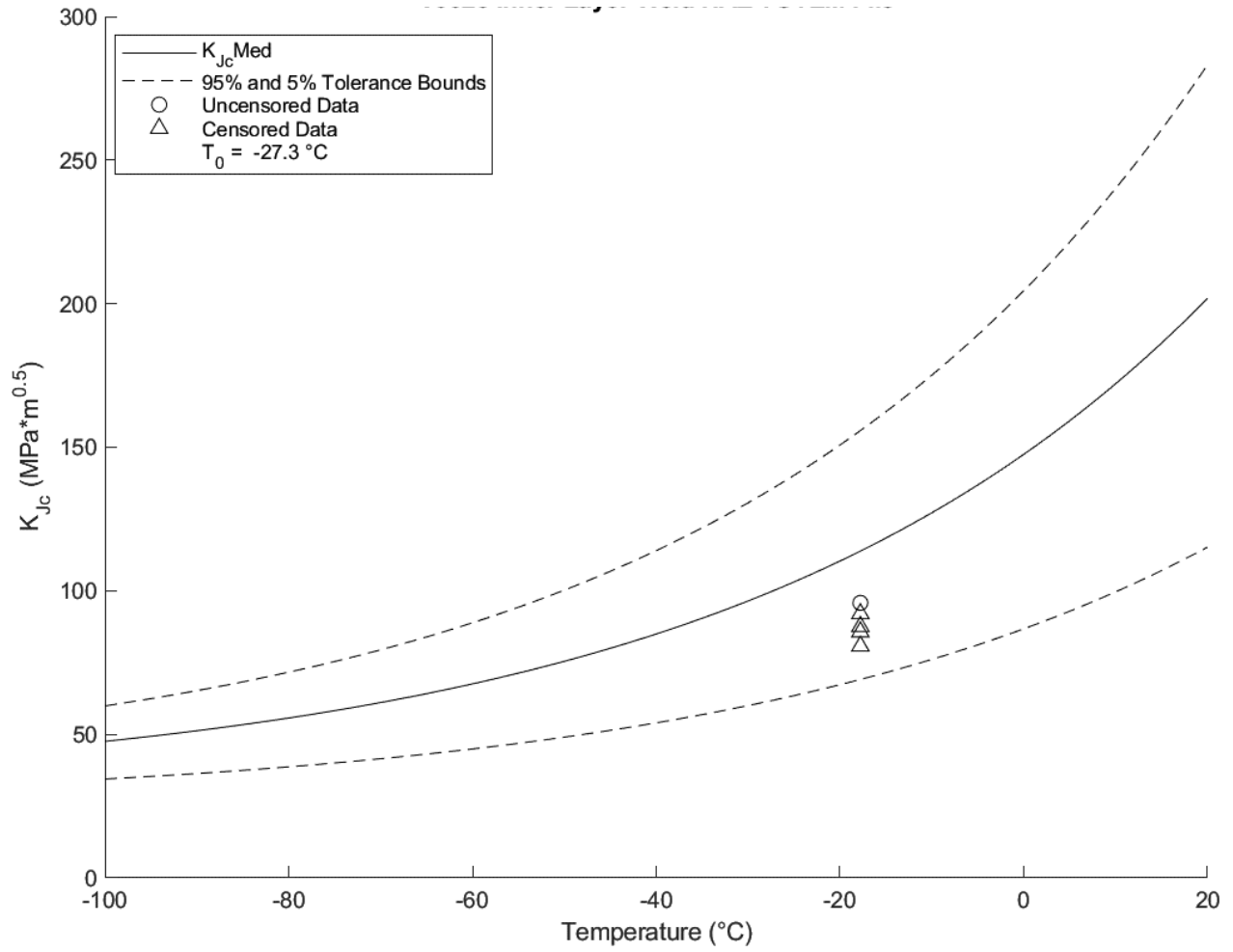


Figure 7.5.2.3.3-7: Inner Layer Weld HAZ T_0 Plot, V0023

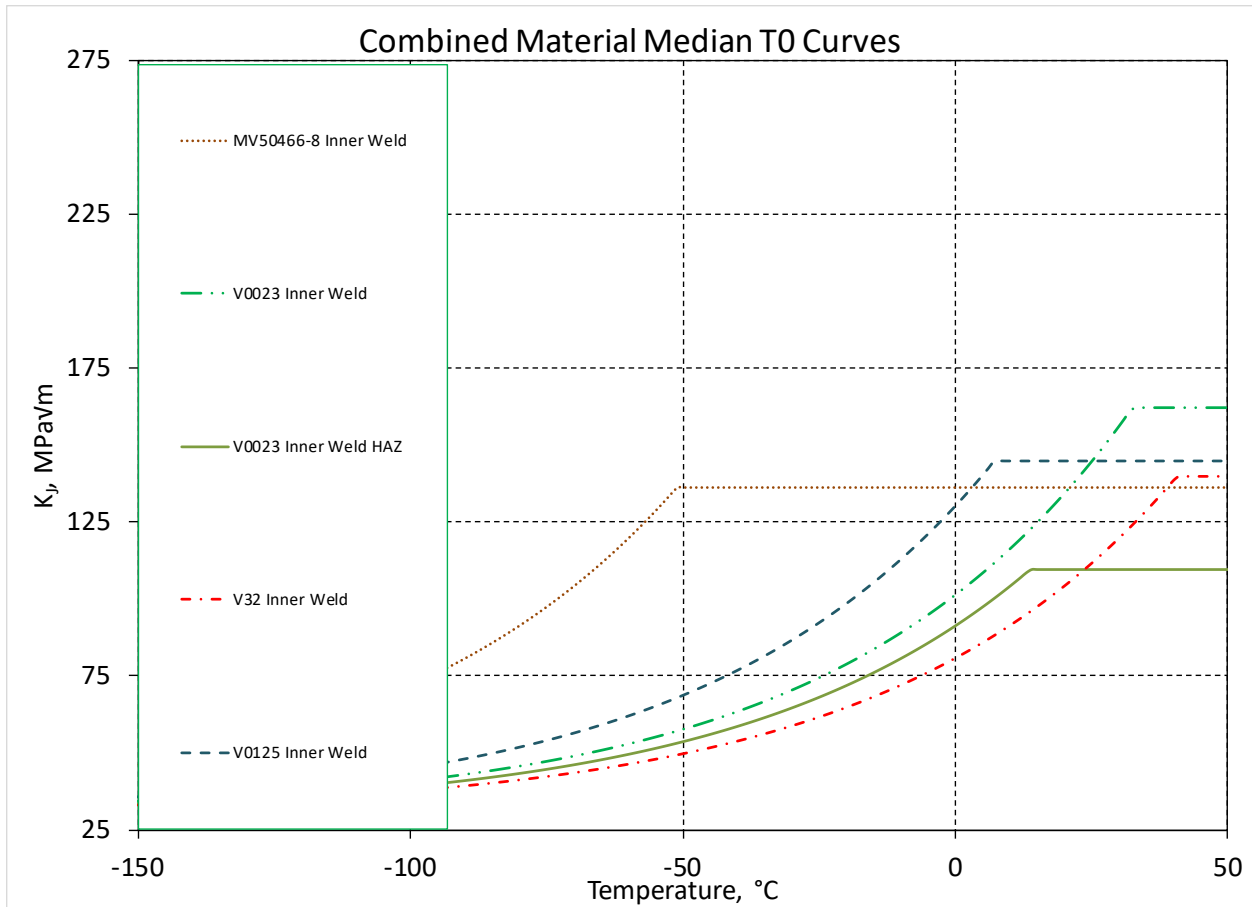


Figure 7.5.2.3.3-8: Inner Weld Combined T₀ Plot

7.5.2.3.4 Fatigue Crack Growth

Sections of V0023 were tested to determine the fatigue crack growth rates according to ASTM E647 (11). Load ratios of $R = 0.1$ and $R = 0.7$ were chosen corresponding to load cycles resulting from slight pressure variations and nearly full pressure releases of the LPVs. These tests were conducted on the center of the circumferential seam weld found in the second wrapper layer as seen in Figure 7.5.2.3.4-1 and Figure 7.5.2.3.4-2. Table 7.5.2.3.4-1 and Table 7.5.2.3.4-2 show the test matrix and threshold result of each E647 test conducted. The individual fatigue growth curves are shown in Figure 7.5.2.3.4-3 through Figure 7.5.2.3.4-6. These curves are input into NASGRO to create material data packages used for structural analysis and crack growth prediction.

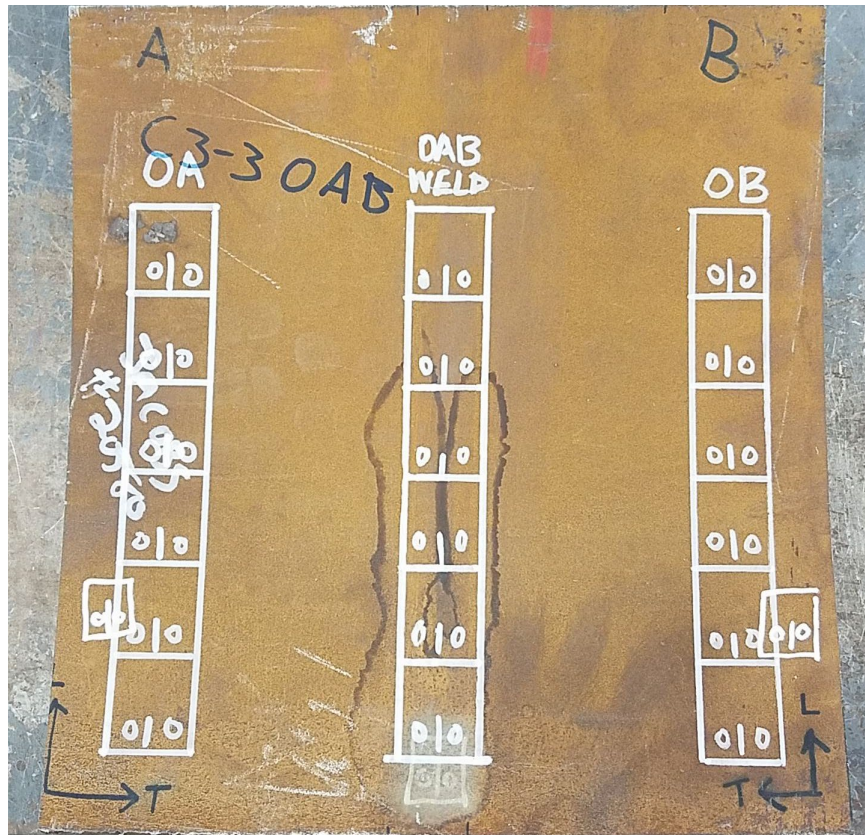


Figure 7.5.2.3.4-1: Specimen Cut Plan da/dN V0023 Inner Layer Weld



Figure 7.5.2.3.4-2: Specimen Cut Plan da/dN V0023 Inner Layer Weld (Continued)

Table 7.5.2.3.4-1: V0023 Inner Layer Weld da/dN Test Matrix

Lot	Material	Orientation	Stock Thickness	Specimen Thickness	Machine	R=0.1	R=0.7	Spares
V23 0AB Inner LW	Weld	NP	0.5	0.375	6	2	2	2

Table 7.5.2.3.4-2: V0023 Inner Layer Weld da/dN Results

Specimen ID	Temperature (°F)	R-Ratio	Segment	C (1/in)	Frequency (Hz)	Threshold (□K) (KSI√in)	Location
V23-0AB-LW-1	75	0.1	A	-20	30	5.193	Inner Weld
			B	6	30		
V23-0AB-LW-2	75	0.1	A	-20	20	4.182	Inner Weld
			B	6	20		
V23-0AB-LW-3	75	0.7	A	-20	20	2.579	Inner Weld
			B	6	20		
V23-0AB-LW-4	75	0.7	A	-20	20	2.692	Inner Weld
			B	6	20		

ASTM E647

ΔK (MPa \sqrt{m})

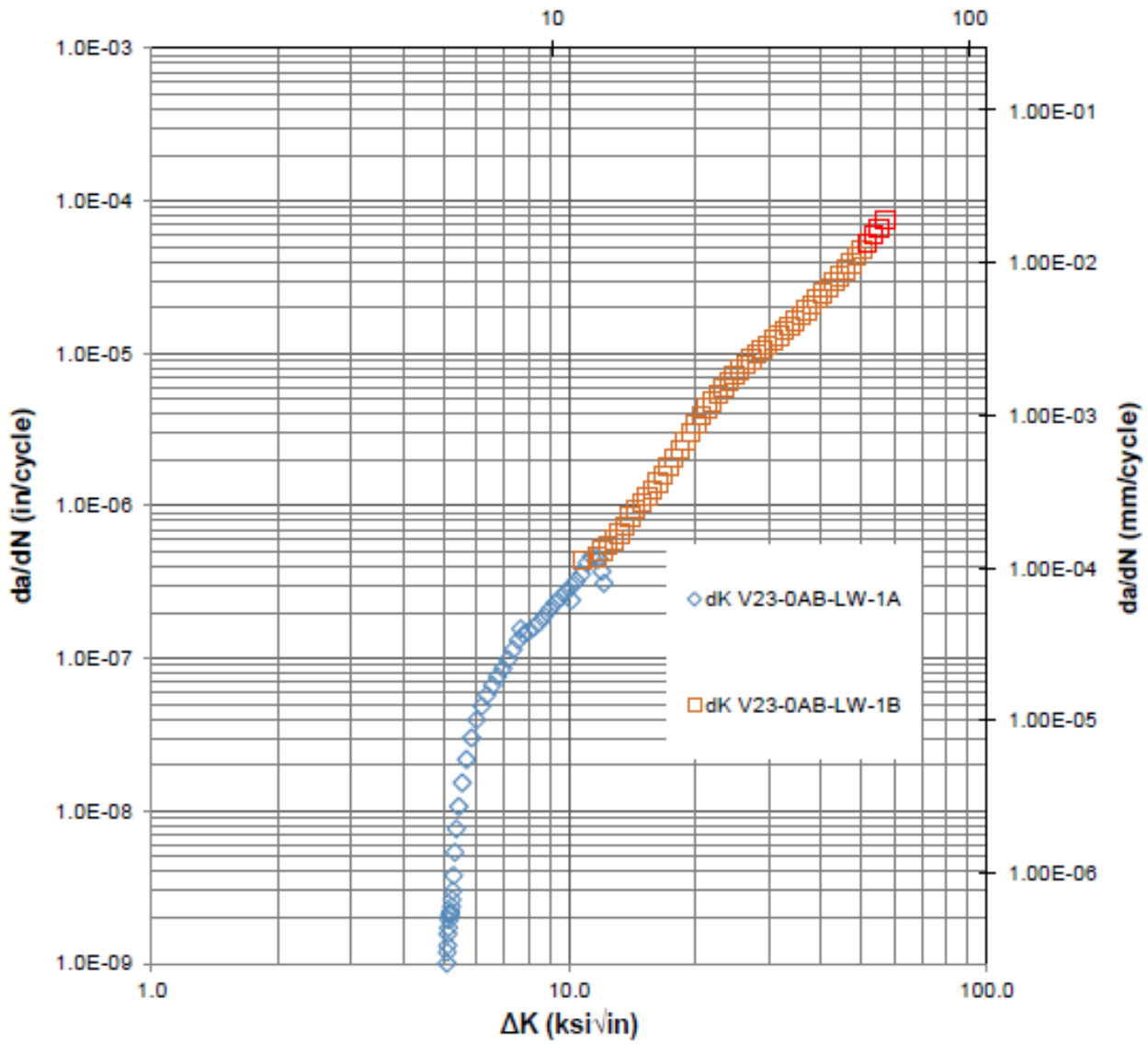


Figure 7.5.2.3.4-3: V0023-0AB-LW-1 Plot R = 0.1

ASTM E647

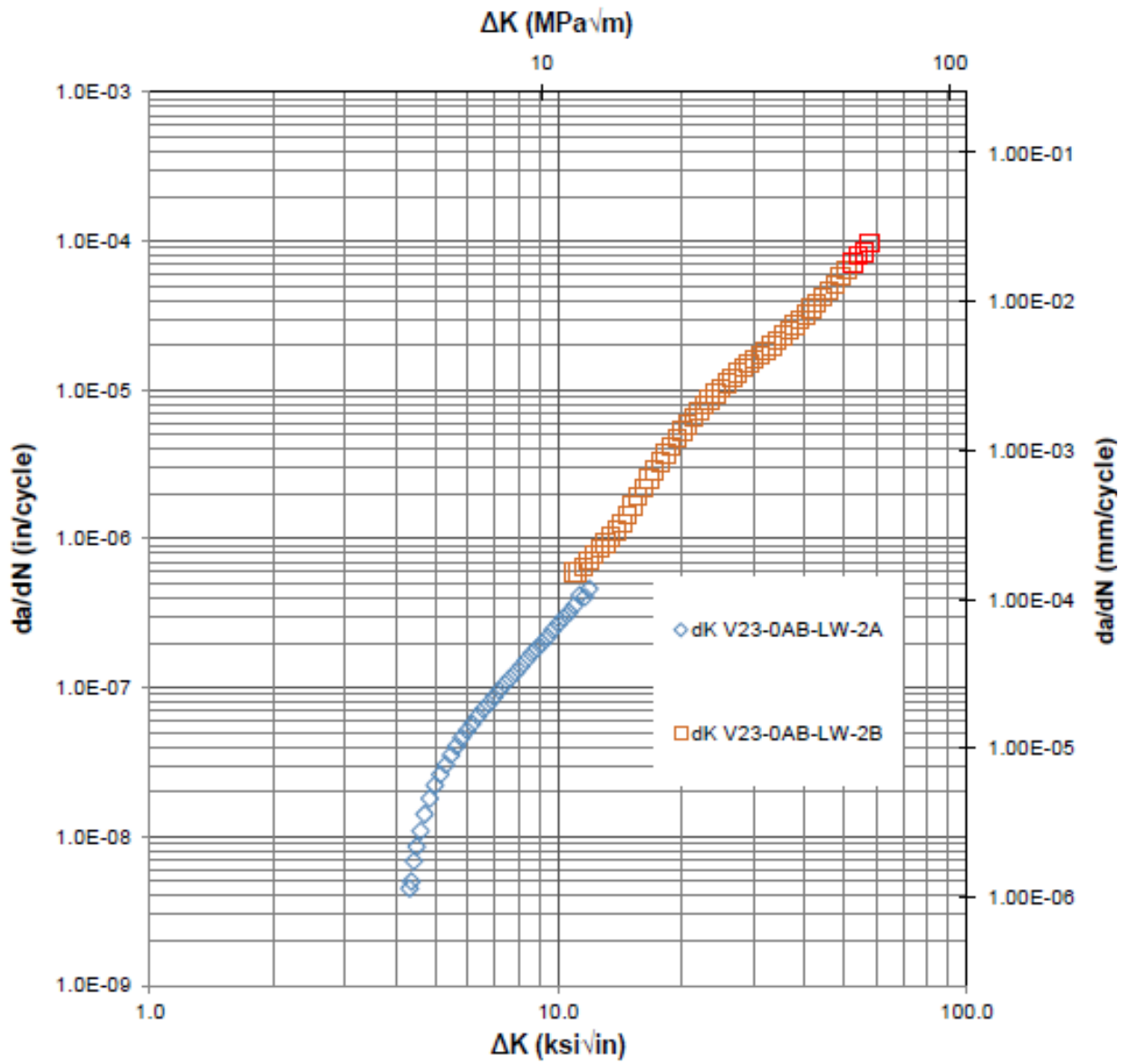


Figure 7.5.2.3.4-4: V0023-0AB-LW-2 Plot R = 0.1

ASTM E647

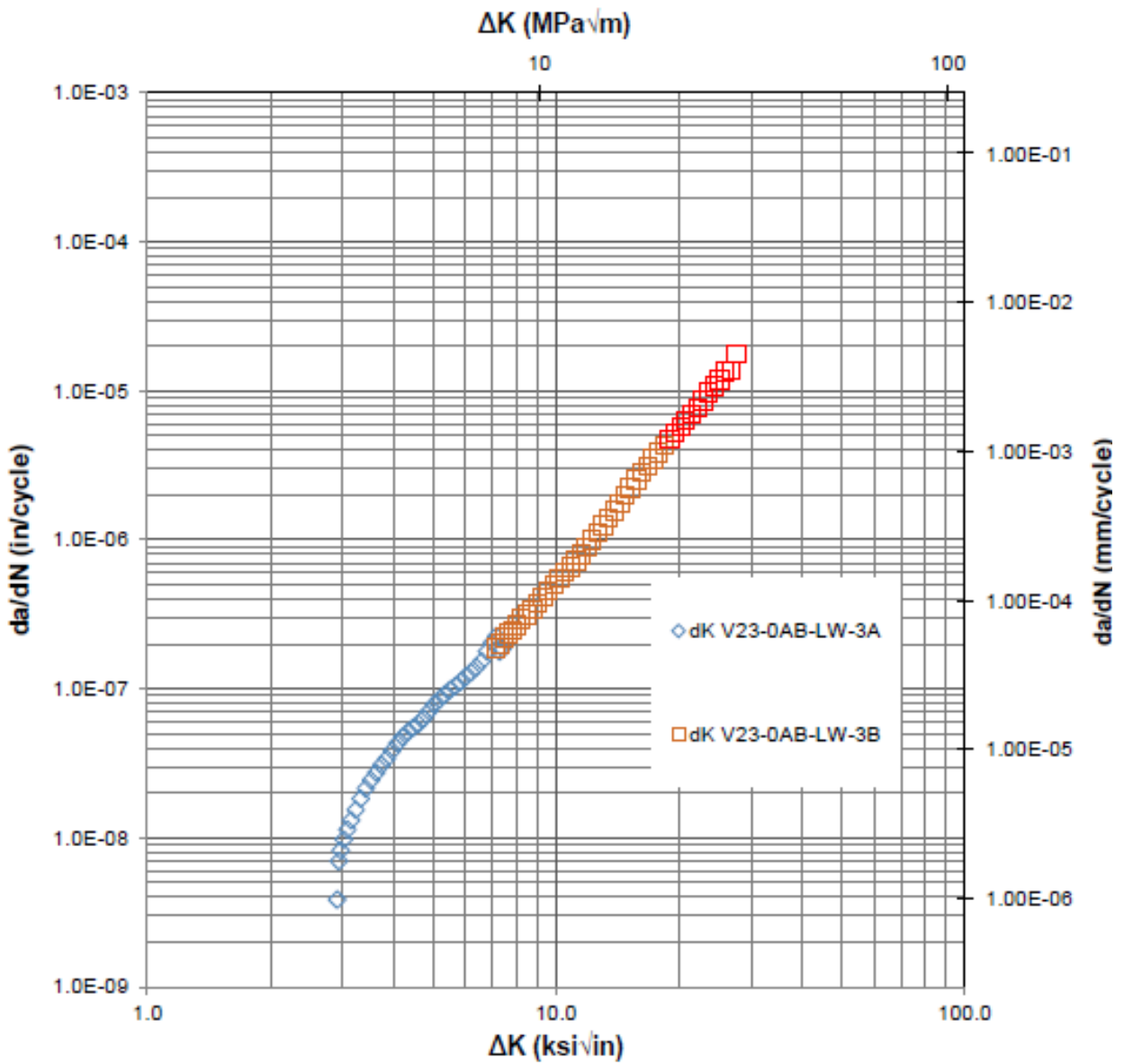


Figure 7.5.2.3.4-5: V0023-0AB-LW-3 Plot R = 0.7

7.5.3 Full Thickness Circumferential Welds

Full thickness circumferential welds are welds that penetrate the full thickness of the vessel from the inner to the outer surface. Their purpose is to connect major sections of the vessel together. These welds are found in two common locations: at the head-to-shell interface and the shell-to-shell interface. Head-to-shell welds connect the layered shell courses to the monolithic vessel heads at each end of the LPV. Shell-to-shell welds connect layered full thickness shell courses to each other. Not all vessels contain shell-to-shell welds, typically these welds are found only in vessels that exceed the length of standard plate materials. However, all vessels contain head-to-shell welds. There are many different aspects that affect the structural properties of these welds, primarily the joining of different steel types and material thicknesses at the head-to-shell interface. These tests cited within this section characterize the weld deposit material, as well as the HAZ on the head side of head-to-shell welds. The HAZ on the layer side of the weld is impossible to test due to material constraints but is considered to be characterized by shell parent and longitudinal weld HAZ material tests.

7.5.3.1 Chemical Composition

Weld material specifications are not typically available or verifiable, therefore the chemical composition reported is only of the collected data. Data is only from the weld center. The HAZ chemistry is that of the parent plate material. Table 7.5.3.1-1 provides data collected from vessel welds in dissected vessels.

Table 7.5.3.1-1: Collected Chemistry Data

Vessel	Location	C	Si	Mn	P	S	Cr	Mo	Ni	Cu	V
MV50466-8	Head to Shell Inner Layer	0.072	0.29	0.73	0.015	0.017	0.03	0.47	1.84	0.06	0.18
MV50466-8	Head to Shell Wrap Layer	0.073	0.3	0.76	0.013	0.026	0.031	0.48	1.88	0.11	0.17
V0023	Head to Shell Inner Layer	0.077	0.28	0.74	0.019	0.023	0.032	0.48	1.86	0.051	0.19
V0023	Head to Shell Wrap Layer	0.08	0.31	0.78	0.012	0.025	0.048	0.44	1.75	0.088	0.17
V0023	Shell to Shell Inner Layer	0.11	0.27	0.84	0.022	0.042	0.058	0.52	1.85	0.11	0.22
V0023	Shell to Shell Wrap Layer	0.1	0.28	0.81	0.017	0.04	0.052	0.49	1.83	0.1	0.2
V32	Head to Shell Inner Layer	0.052	0.41	1.71	0.015	0.018	0.16	0.32	1.55	0.09	0.022
V32	Head to Shell Wrap Layer	0.08	0.29	0.74	0.016	0.026	0.051	0.48	1.99	0.12	0.2
V125	Head to Shell Inner Layer	0.054	0.47	1.71	0.013	0.019	0.12	0.27	1.01	0.065	0.029
V125	Head to Shell Wrap Layer	0.062	0.29	1.44	0.011	0.022	0.23	0.37	1.47	0.079	0.028
V066	Head to Shell Wrap Layer	0.07	0.4	1.31	0.012	0.011	0.3	0.52	2.37	0.49	0.008

7.5.3.2 Metallography

Metallography tests were performed on this material to observe number of weld passes and basic orientation of the microstructure. This was done in order to confirm the tested orientation as the weakest and to identify weld order, HAZ location and size, and grain structure. Only grain orientation studies were performed. No grain size, grain size through thickness, or carburization layer thickness studies were done, and no macro cubes were produced.

Grain Orientation Study

The grain orientation study is a polish and etch of a weld cross section. Its purpose is to confirm the correct orientation for fracture testing. In this case, the P orientation, parallel to the weld path, is found to be the most realistic and proper orientation for further tests.

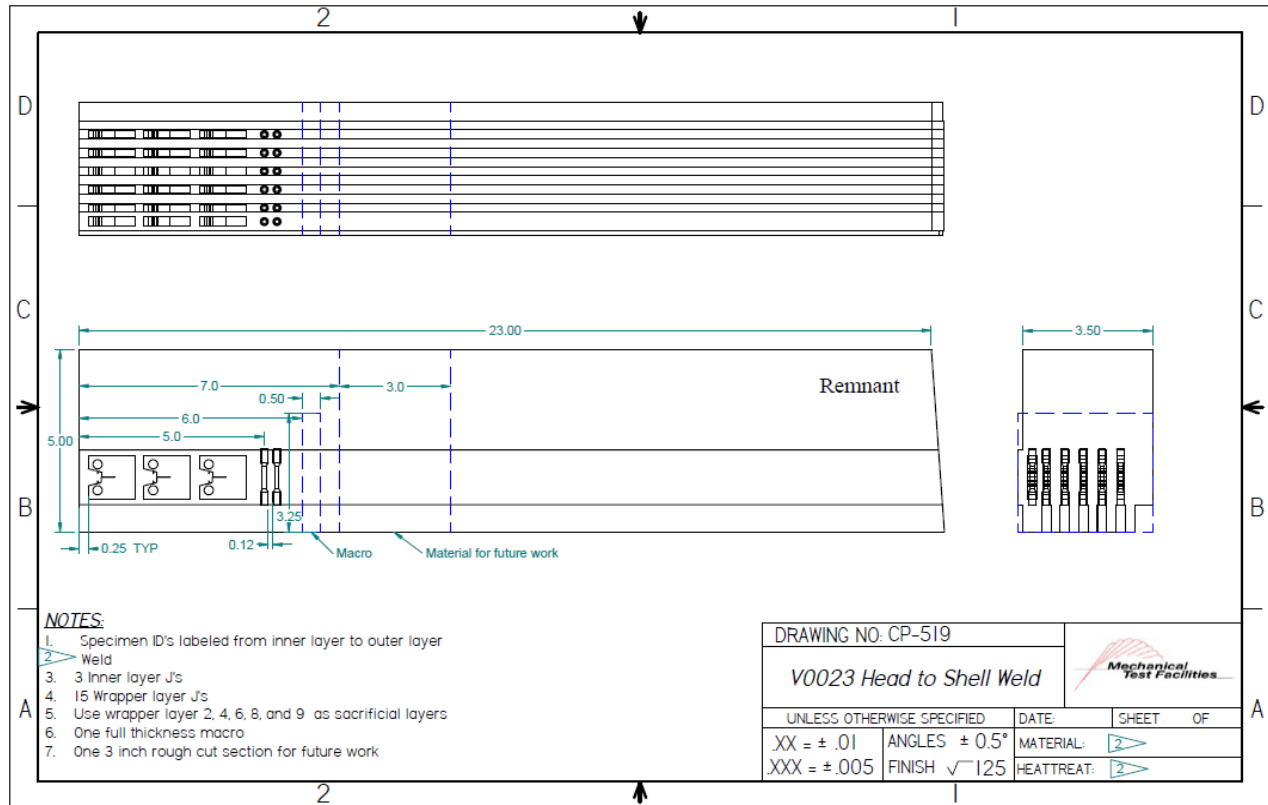


Figure 7.5.3.2-1: Cut Plan for Macros from V0023 Head-to-Shell Weld

The following macros were extracted from the cross-section of LPVs V0125, V0032, MV50466-8, and V0023 near the location of tensile and fracture test specimens.

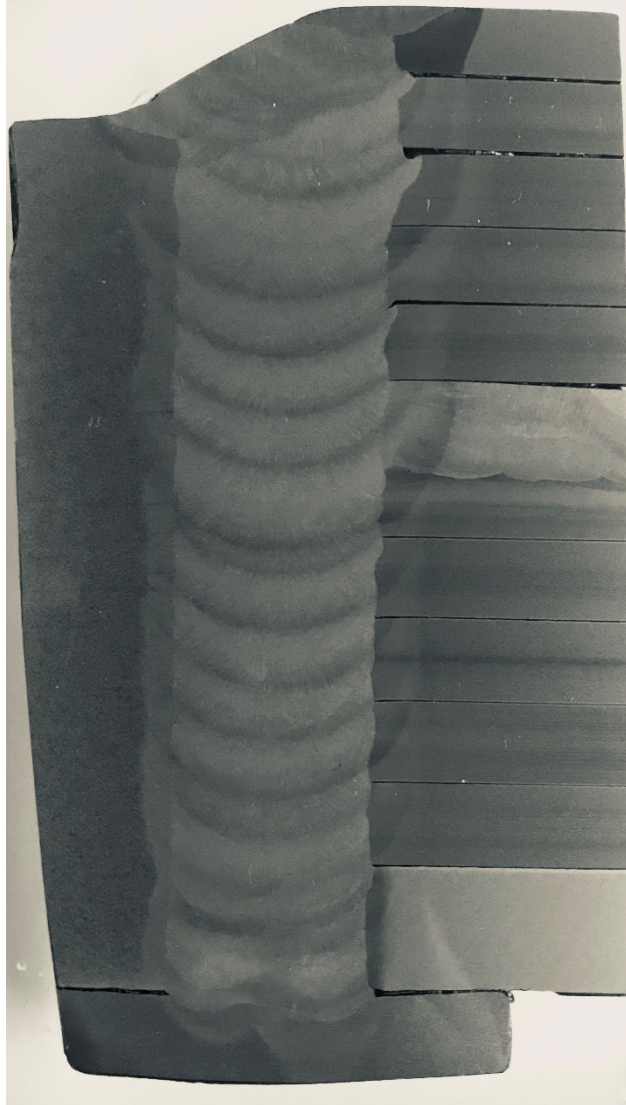


Figure 7.5.3.2-2 MV50466-8 Head-to-Shell Weld Macro (with Longitudinal Weld Intersection)

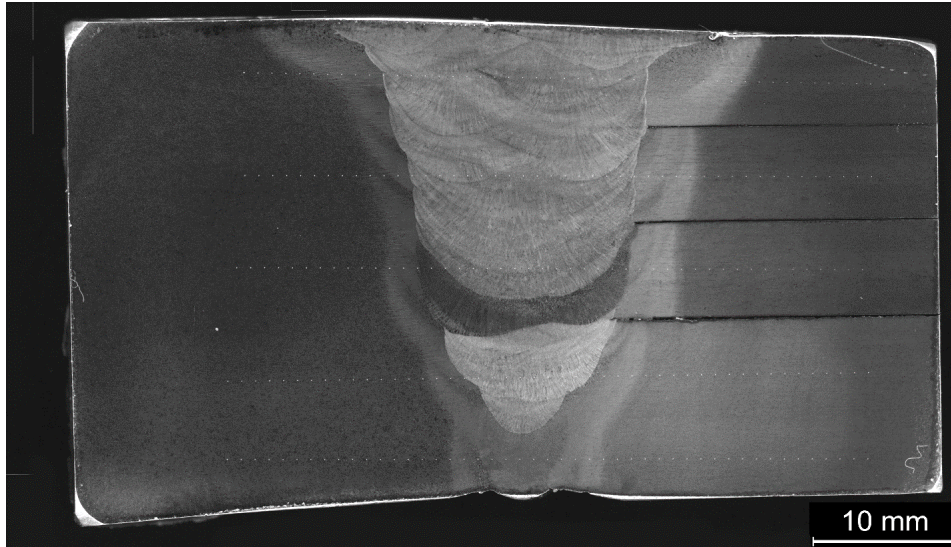


Figure 7.5.3.2-3: V0125 Head-to-Shell Weld Macro



Figure 7.5.3.2-4: V0032 Head-to-Shell Weld Macro

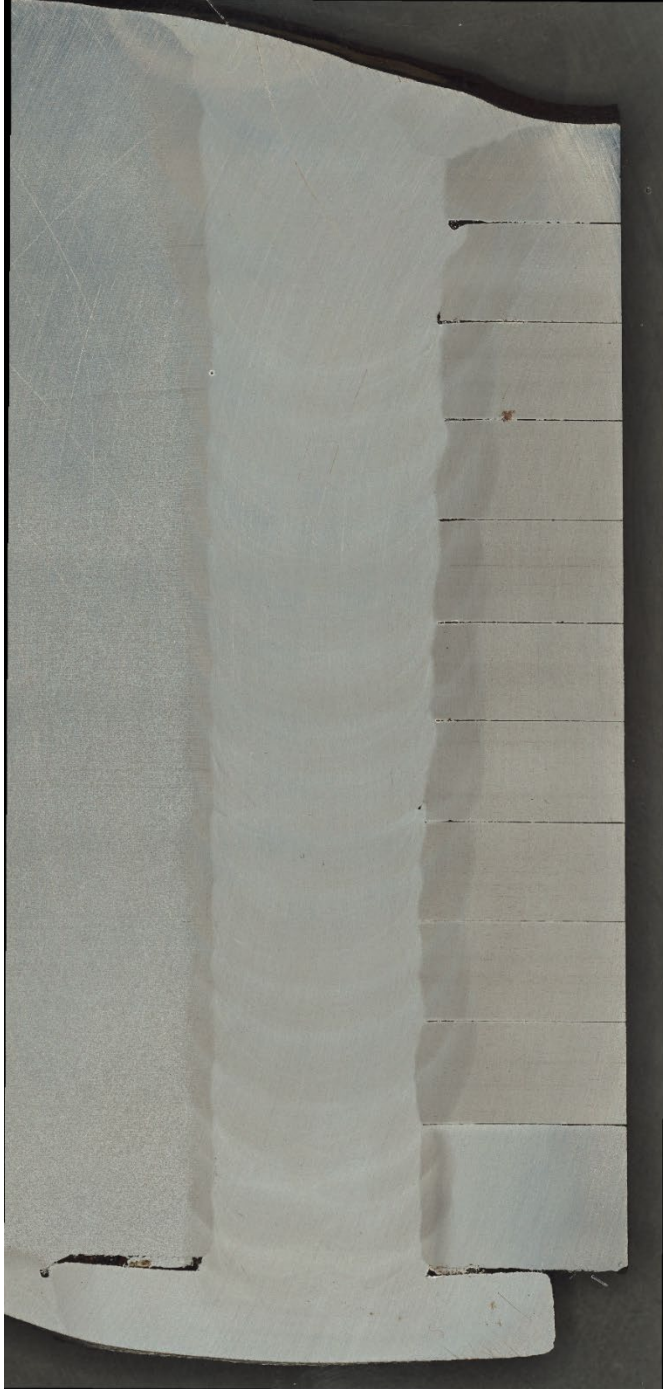


Figure 7.5.3.2-5: V0023 Head-to-Shell Weld Macro

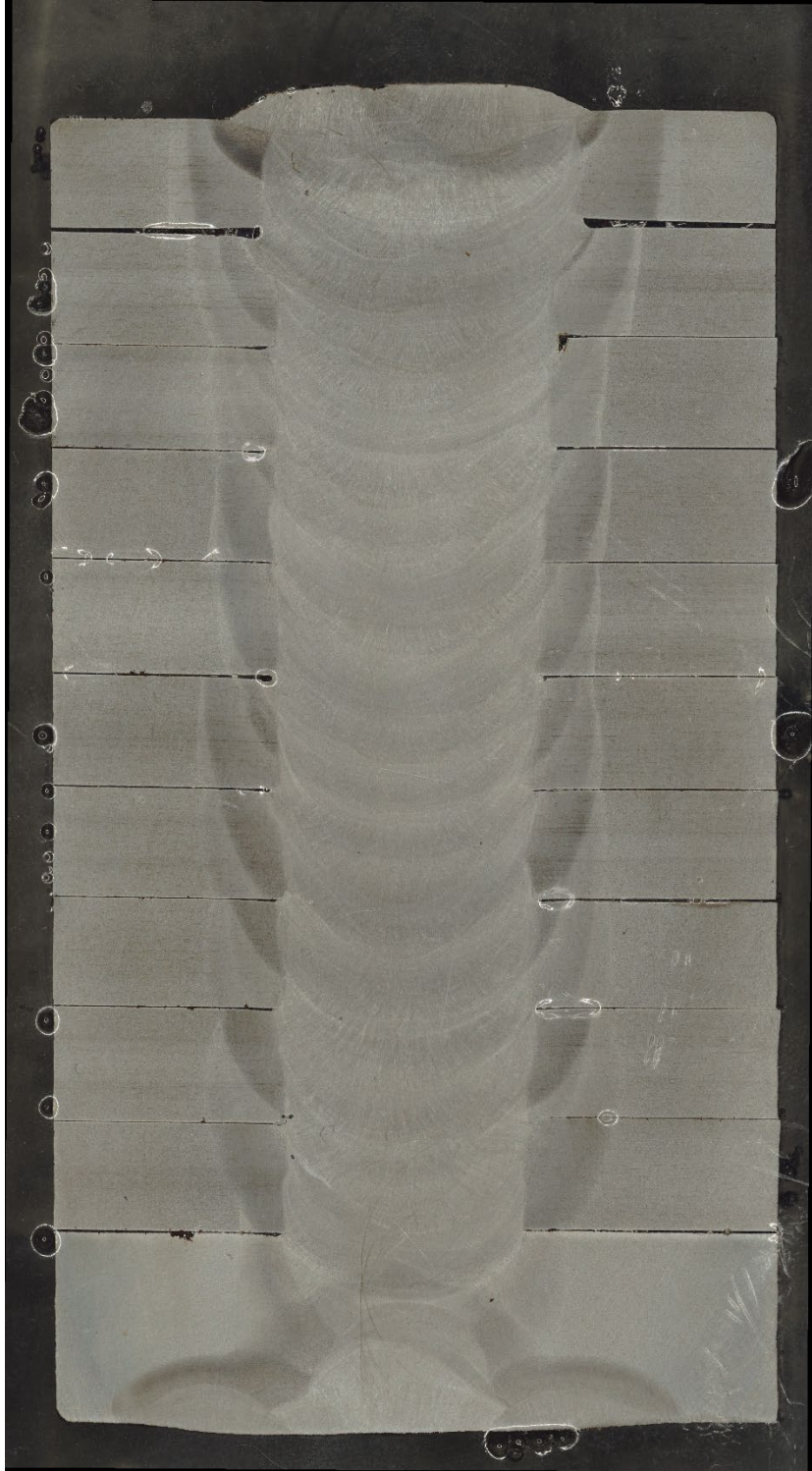


Figure 7.5.3.2-6: V0023 Shell-to-Shell Weld Macro

Hardness

Hardness traces were conducted on some full thickness welds to help identify the degree of variance in material properties and stress concentrations across the parent-weld-parent span. These were used to identify areas of concern and direct testing towards less favorable material conditions that would indicate worst-case crack scenarios.

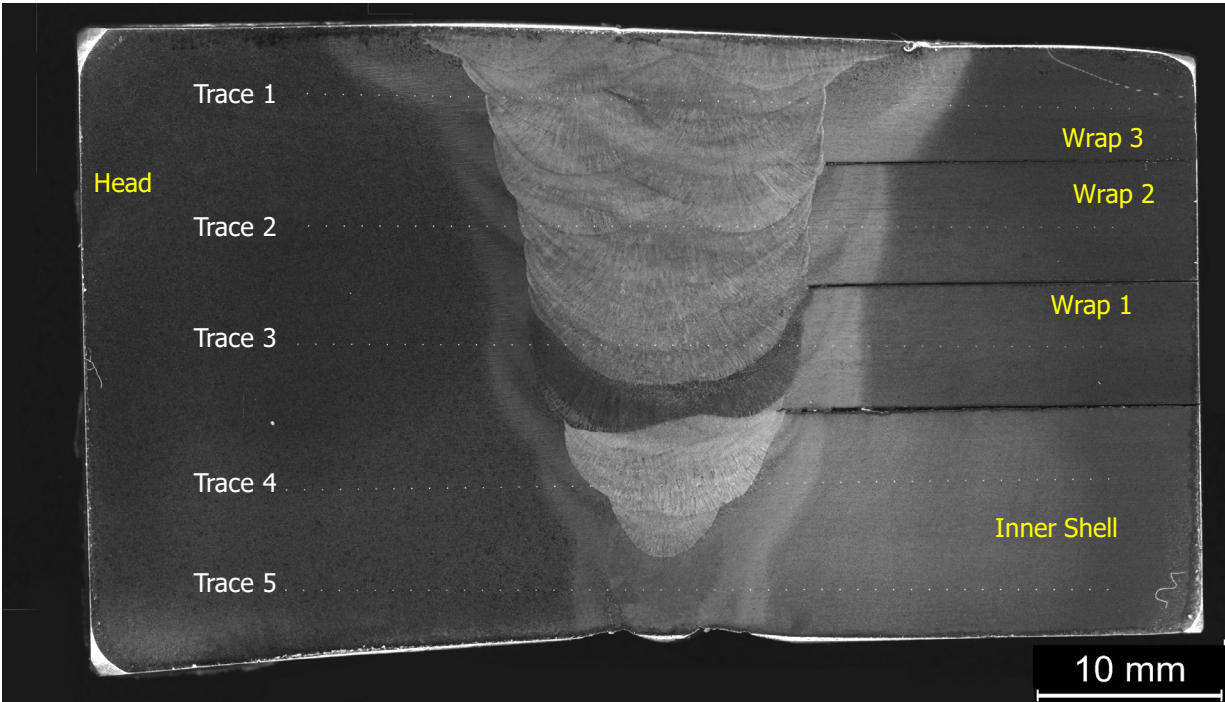


Figure 7.5.3.2-7: V0125 Head-to-Shell Weld Indent Locations

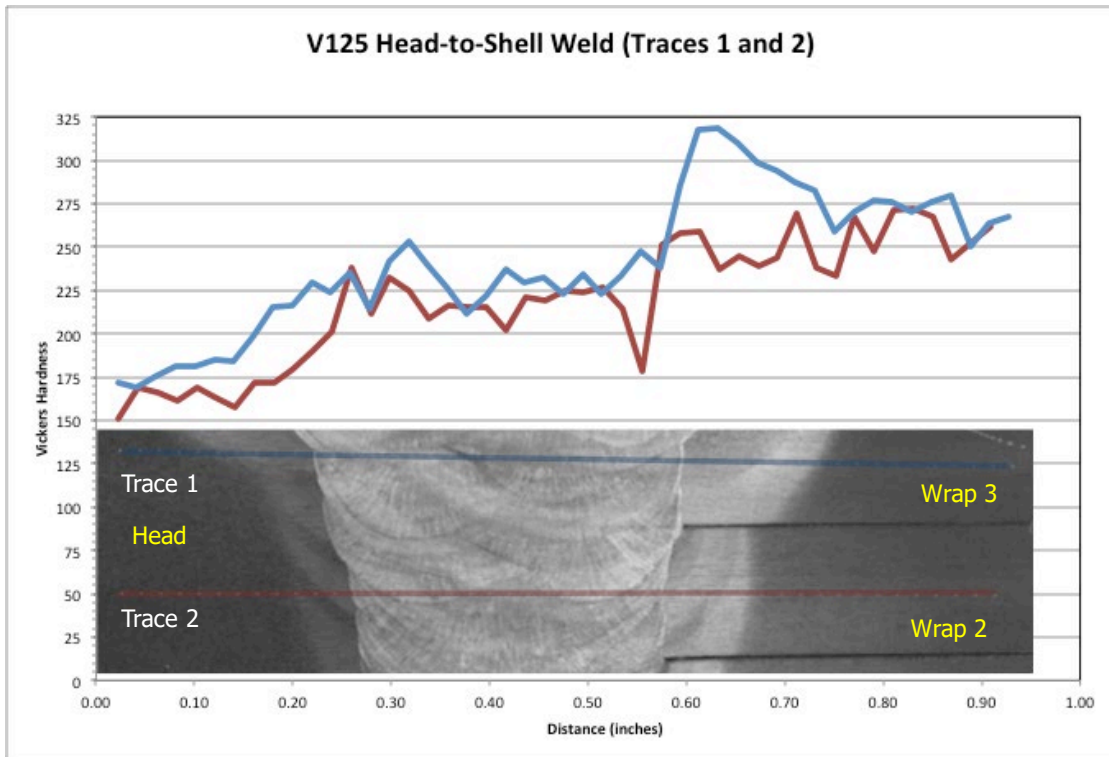


Figure 7.5.3.2-8: V0125 Head-to-Shell Weld Traces 1 and 2

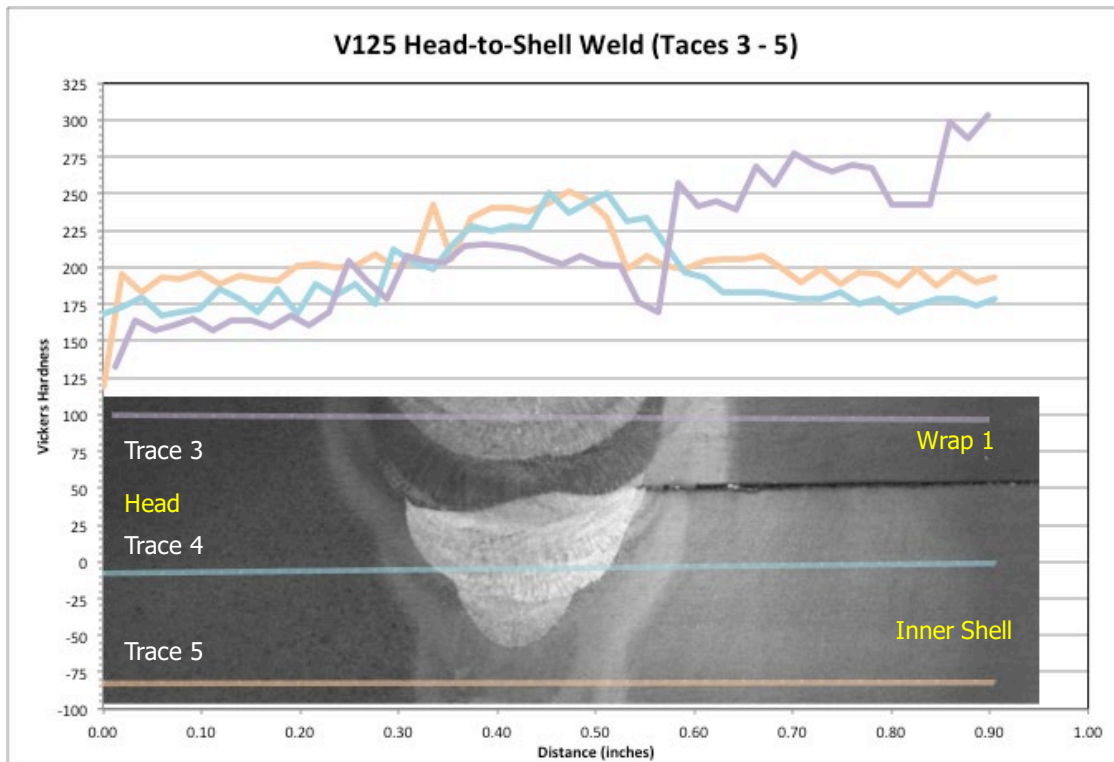


Figure 7.5.3.2-9: V0125 Head-to-Shell Weld Traces 3,4, and 5

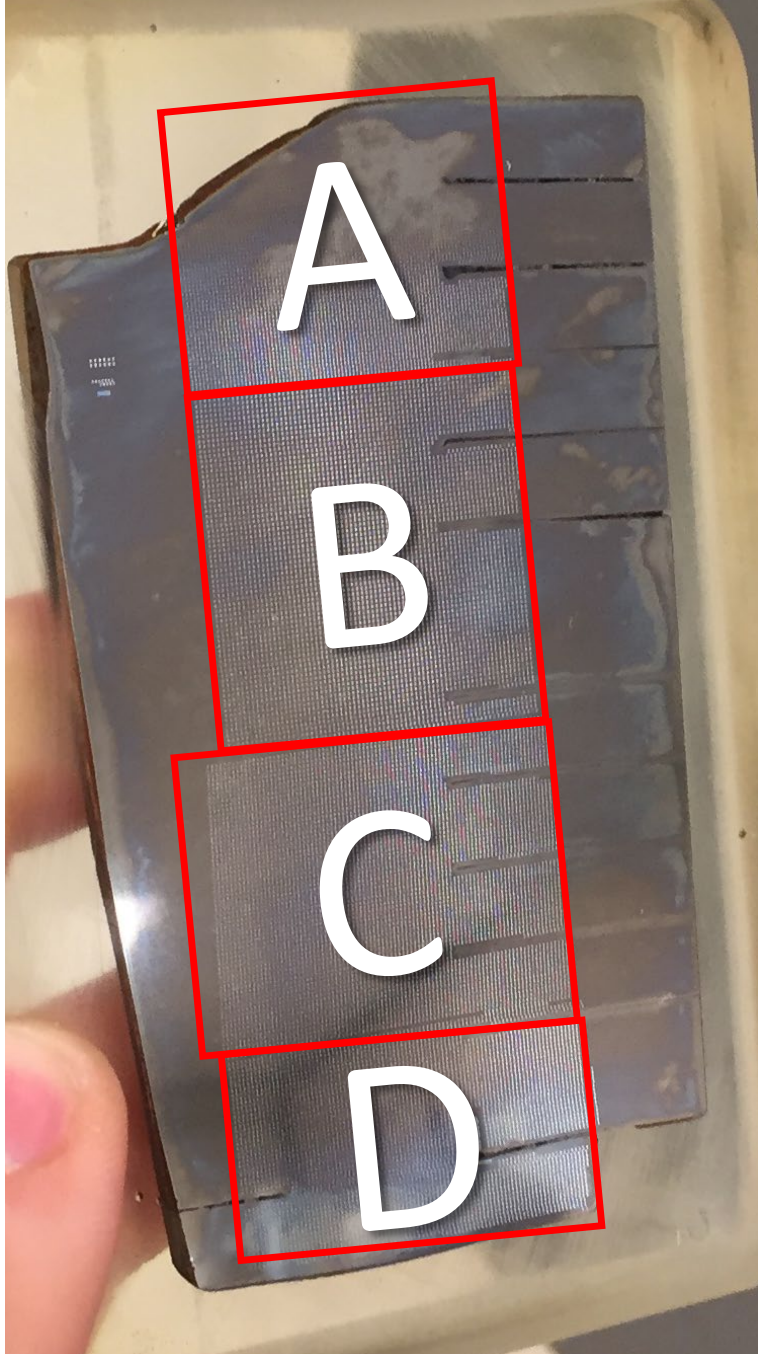


Figure 7.5.3.2-10: MV50466-8 Head-to-Shell Weld Indent Location

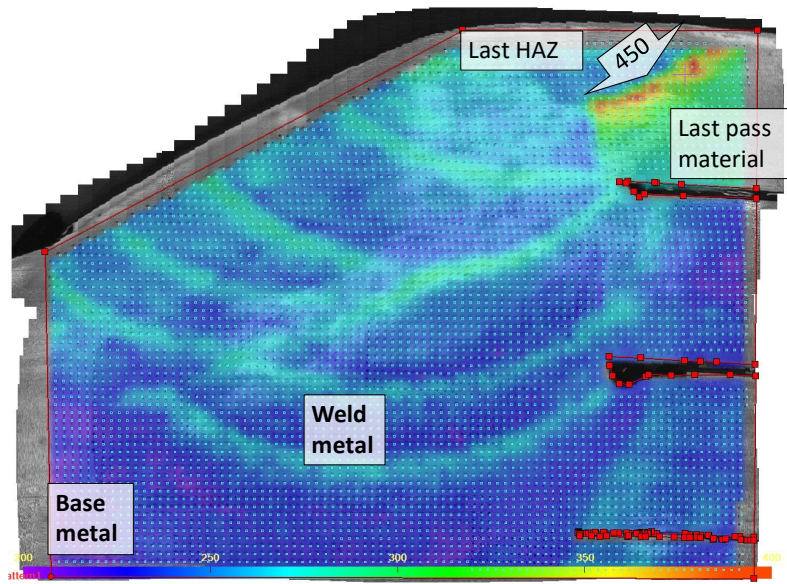


Figure 7.5.3.2-11: MV50466-8 Head-to-Shell Weld Section A
 *Note: Scale: 200-400 HV, Spacing: 0.3 mm

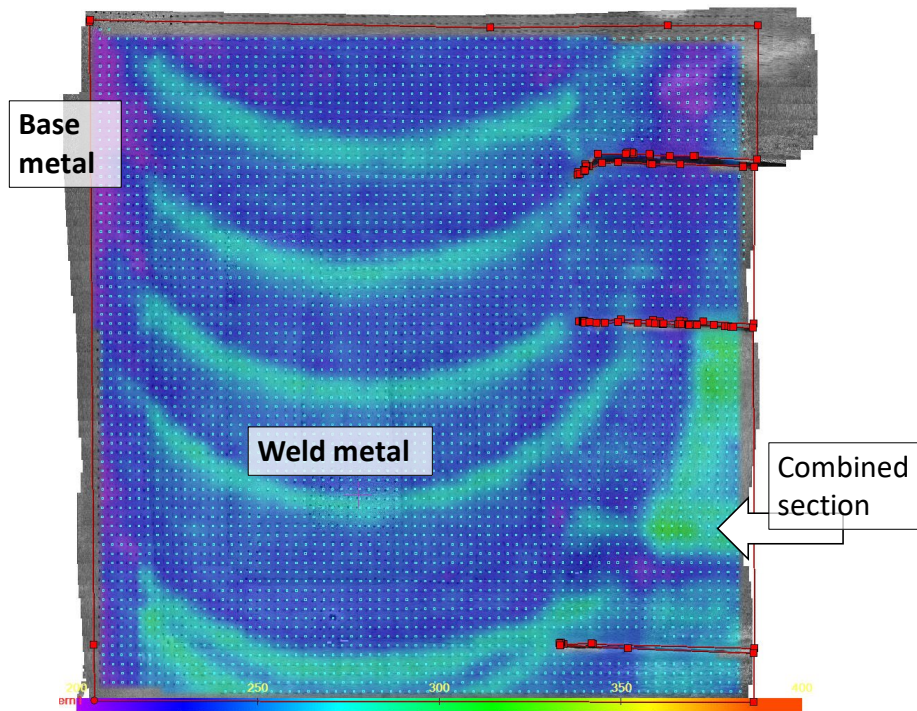


Figure 7.5.3.2-12: MV50466-8 Head-to-Shell Weld Section B
 *Note: Scale: 200-400 HV, Spacing: 0.3mm

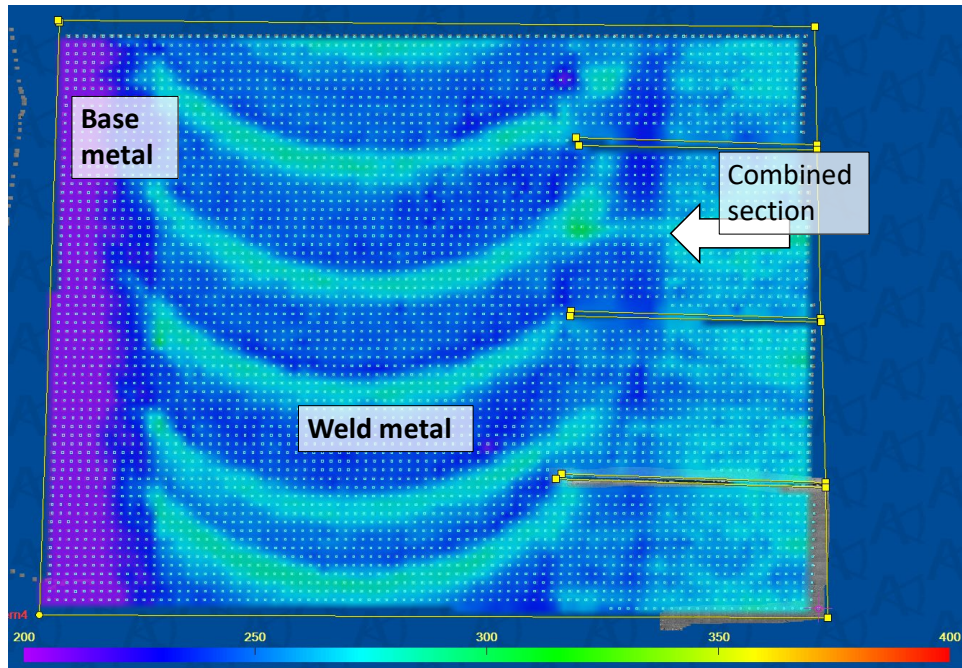


Figure 7.5.3.2-13: MV50466-8 Head-to-Shell Weld Section
Note: Scale: 200-400 HV, spacing 0.3 mm

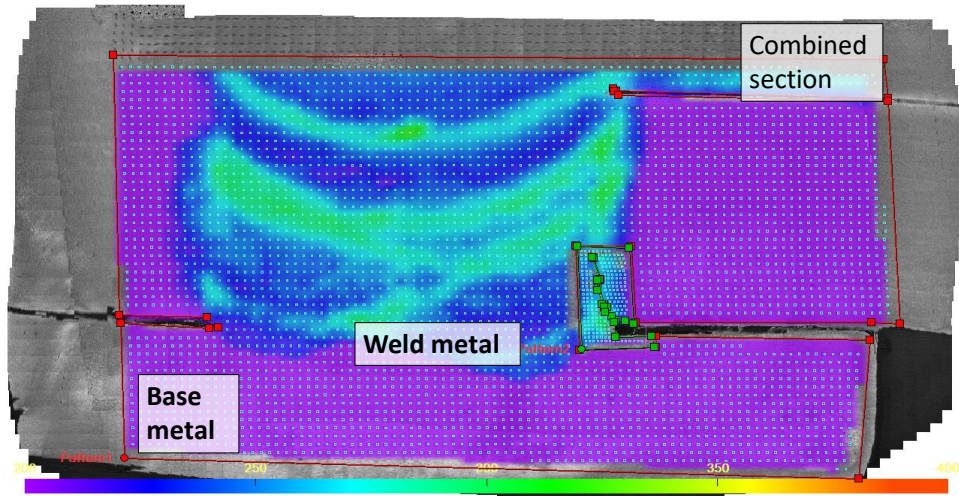


Figure 7.5.3.2-14: MV50466-8 Head-to-Shell Weld Section D
 Note: Scale: 200-400 HV, Spacing: 0.3mm (0.15 mm around crack)

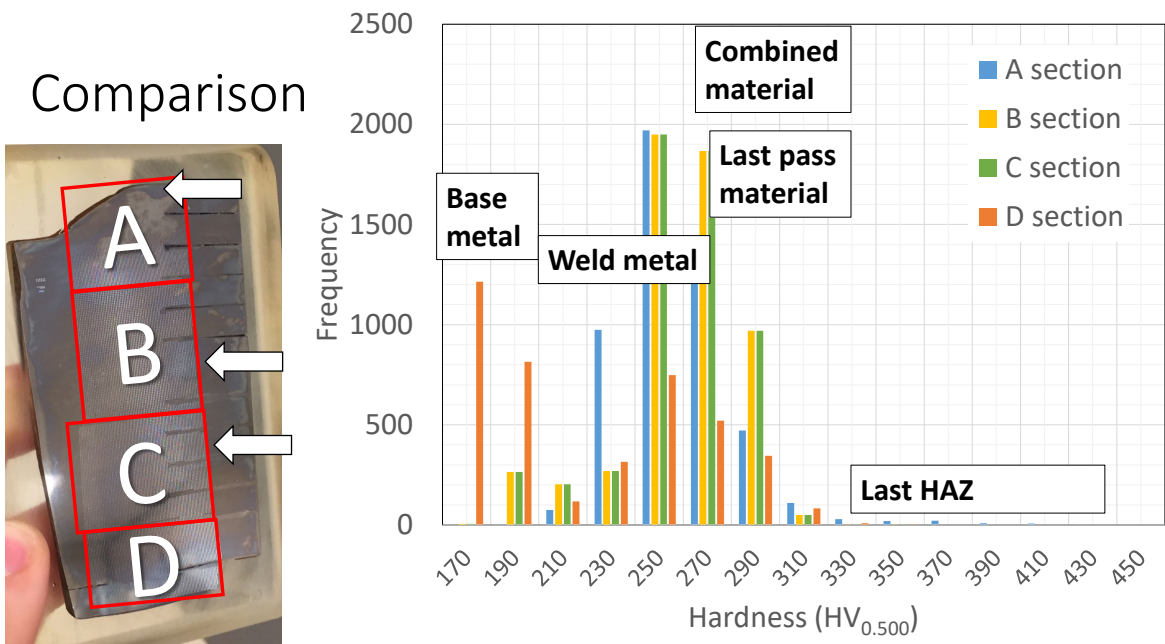


Figure 7.5.3.2-15: MV50466-8 Head-to-Shell Weld Hardness Frequency Comparison

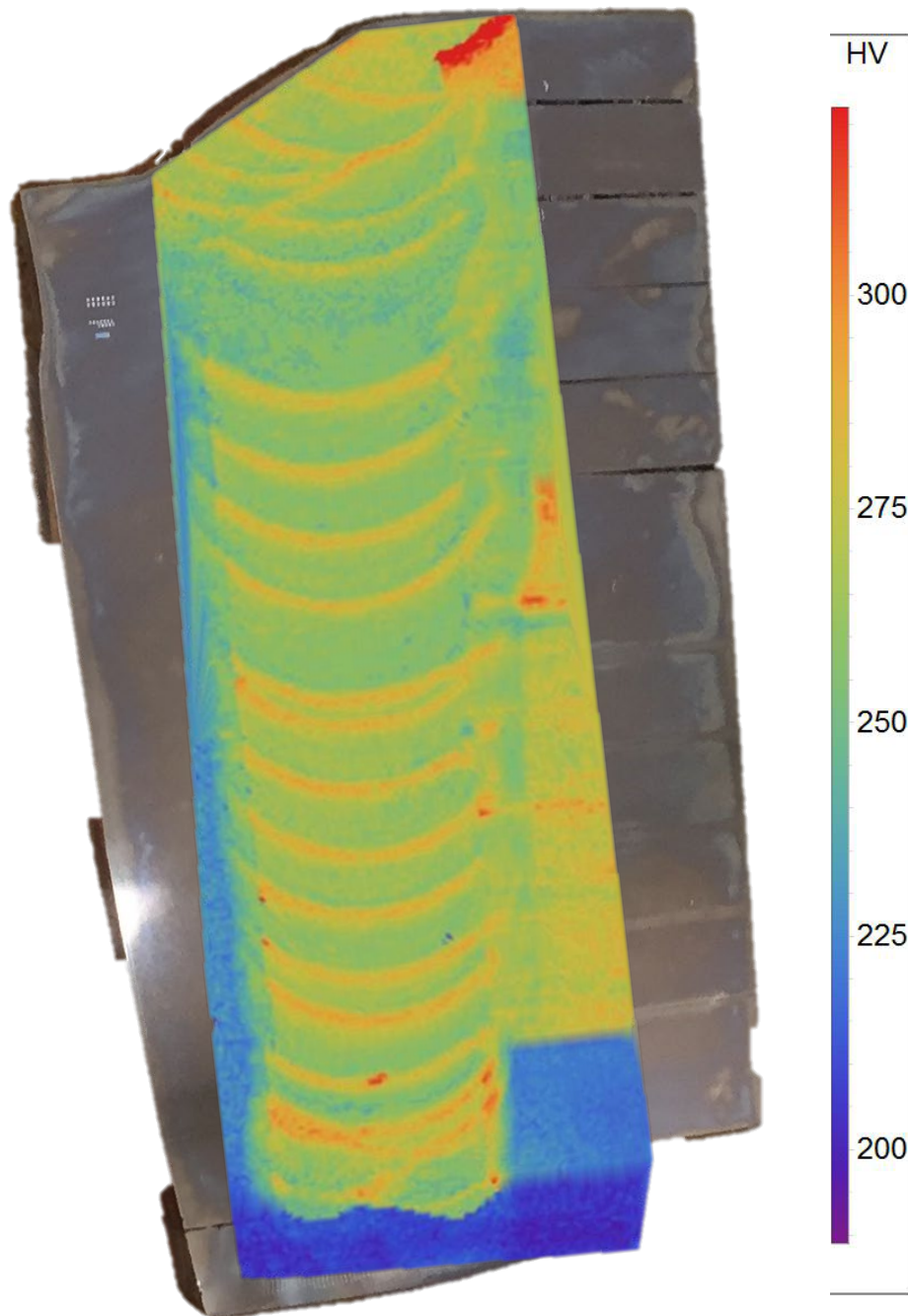


Figure 7.5.3.2-16: MV50466-8 Head-to-Shell Weld Full Hardness Map

7.5.3.3 Mechanical Properties

Mechanical properties for the weld metal vary by manufacturer and application parameters and are only characterized by the tests documented in the following sections.

7.5.3.3.1 Smooth Tensile Tests

Smooth tensile tests were conducted at MSFC on round specimens in accordance with ASTM E8, "Standard Test Methods for Tension Testing of Metallic Materials" (51) using specimen design S-219 Rev A. The mechanical test frame consisted of a servo-hydraulic actuator and reaction frame. The frame used an LVDT for displacement feedback. Stress measurements were derived from load measurements and the initial specimen measurements. Strain measurements were derived from an extensometer and the initial specimen measurements.

Attempts to run tensile tests on HAZ material were inconclusive as properties either matched weld material or parent material. Many weld tests also had extensometer slippage or broke outside of the gauge section. Therefore, the fracture elongation values are considered suspect.

The results obtained from testing of full thickness welds from vessels MV50466-8, V0125, V0032, V0023, and V0066 are presented in Table 7.5.3.3.1-1 through Table 7.5.3.3.1-5. A typical engineering stress-strain curve is shown in Figure 7.5.3.3.1-1.

Table 7.5.3.3.1-1: Head-to-Shell Weld Smooth Tensile Data MV50466-8

Specimen ID	Test Temp. (°C)	ASTM Orientation	Tensile Stress (ksi)	Yield Stress (ksi)	Fracture Elongation (%)
440-315	21	P	117.8	112.5	12.0
440-316	21	P	128.5	120.7	20.0
440-317	300	P	116.0	103.6	18.0
440-318	300	P	116.5	103.8	17.0
440-319	500	P	92.5	83.2	19.0
440-320	500	P	90.9	83.5	16.0
440-321	700	P	41.7	39.5	12.0
440-322	700	P	41.4	36.9	19.0

Table 7.5.3.3.1-2: Head-to-Shell Weld Smooth Tensile Data V0125

Specimen ID	Test Temp. (°C)	ASTM Orientation	Tensile Stress (ksi)	Yield Stress (ksi)	Fracture Elongation (%)
CP-344-8-3	21	P	132.4	116.2	14.8
CP-344-8-10	21	N	109.5	97.2	19.6
CP-344-8-11	21	N	100.2	90.2	1.9
CP-344-8-14	21	N	107.5	95.1	19.1
CP-344-8-15	21	N	95.4	79.8	3.4
CP-344-8-16	21	N	108.1	96.1	20.2
CP-344-8-17	21	N	95.4	81.1	8.8
CP-344-8-26	21	P	111.5	100.3	25.2
CP-344-8-8	21	N	108.5	97.3	20.4
CP-344-8-9	21	N	99.7	91.8	1.2

Table 7.5.3.3.1-3: Head-to-Shell Weld Smooth Tensile Data V0032

Specimen ID	Test Temp. (°C)	ASTM Orientation	Tensile Stress (ksi)	Yield Stress (ksi)	Fracture Elongation (%)
380-234	21	N	107.8	92.9	19.7
380-235	21	N	110.5	94.9	19.7
380-240	21	N	116.4	104.3	12.1
380-241	21	N	115.3	103.2	17.6
380-236	-46	N	119.7	95.6	9.9
380-242	-46	N	120.4	105.4	15.2
380-237	-101	N	127.6	98.8	9.9
380-238	-101	N	125.9	99.3	10.9
380-243	-101	N	126.3	108.9	20.6
380-244	-101	N	123.2	105.6	23.7

Table 7.5.3.3.1-4: Head-to-Shell Weld Smooth Tensile Data V0023

Specimen ID	Test Temp. (°C)	ASTM Orientation	Tensile Stress (ksi)	Yield Stress (ksi)	Fracture Elongation (%)
519-310	21	N	115.2	107.0	10.0
519-314	21	N	121.1	104.8	23.5
519-315	21	N	105.9	94.4	17.8
519-318	21	N	112.2	101.4	16.4
519-320	21	N	109.9	97.7	19.6
519-311	-46	N	107.4	95.2	20.1
519-312	-46	N	123.1	108.5	24.6
519-313	-101	N	116.6	103.2	21.9
519-317	-101	N	126.5	108.0	23.9

Table 7.5.3.3.1-5: Shell-to-Shell Weld Smooth Tensile Data V0066

Specimen ID	Test Temp. (°C)	ASTM Orientation	Tensile Stress (ksi)	Yield Stress (ksi)	Fracture Elongation (%)
629-28	21	N	114.5	102.8	12.4
629-32	21	N	115.2	105.7	16.6
629-36	21	N	121.0	106.3	7.1
629-29	-46	N	126.9	110.6	22.0
629-33	-46	N	125.1	110.8	22.1
629-37	-46	N	124.8	105.7	14.9
629-30	-101	N	132.1	109.8	22.2
629-34	-101	N	131.2	110.9	18.3
629-38	-101	N	140.7	120.5	13.0

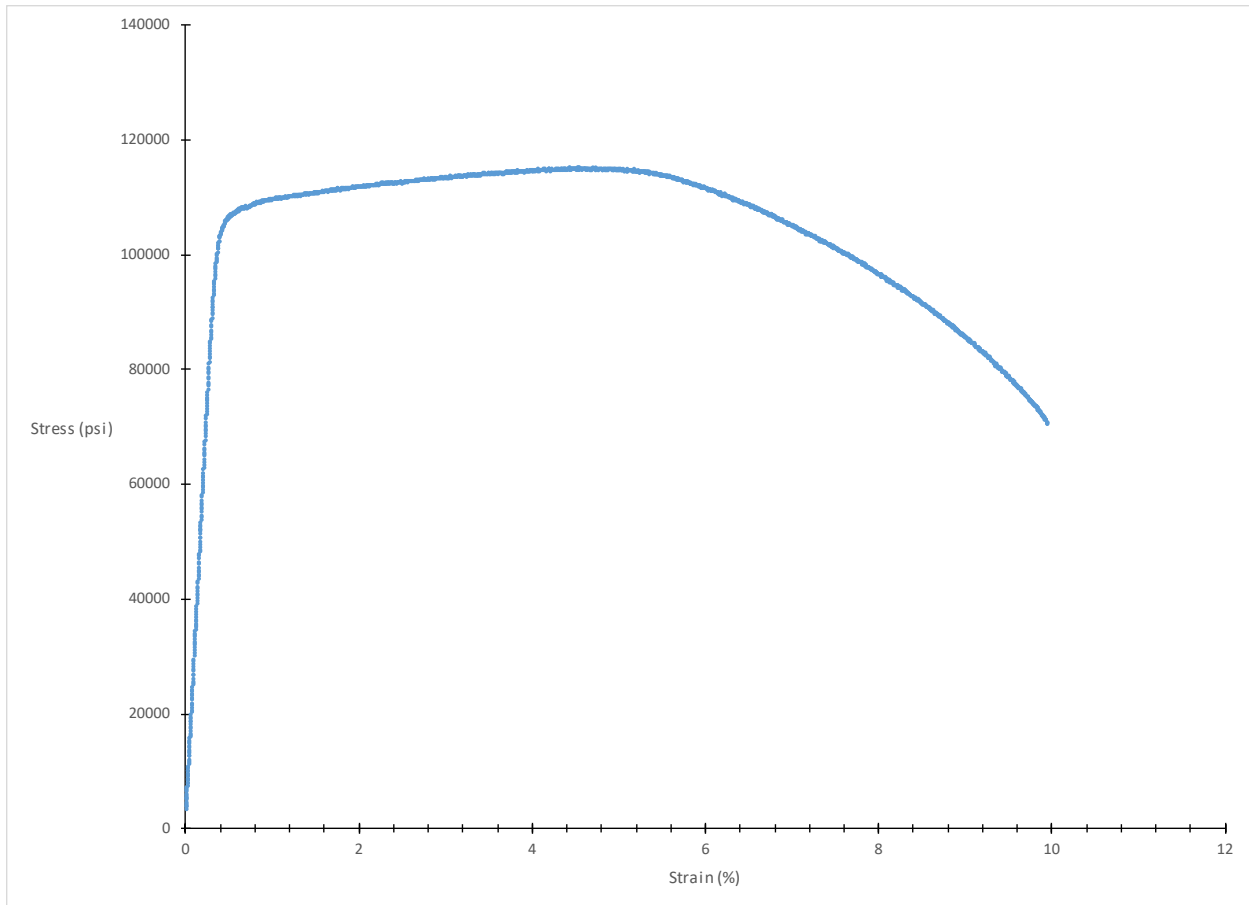


Figure 7.5.3.3.1-1: Full Thickness Weld Smooth Tensile Plot for Sample 519-310

Full thickness weld tensile tests can be difficult to interpret due to the sample passing through multiple weld passes layered on top of each other. The multiple weld boundaries, HAZ, and even different weld metals can produce inconsistent failure modes and elongations. Therefore, the main purpose of these tests is to roughly estimate mechanical properties for application to actual fracture toughness tests. No conclusions should be drawn from the fracture elongation or curve shape.

7.5.3.3.2 Notch Tensile

Notch tensile tests were not performed on this material.

7.5.3.3.3 Fracture Properties

All room temperature testing was performed in accordance with ASTM E1820 (10). All other temperatures were tested in accordance with ASTM E1921 (7). Testing for both standards use specimen design S-226 Rev B for the head-to-shell welds and S-318 Rev A for the shell-to-shell welds. Head-to-shell weld fracture tests came from vessels V0125, V0032, and V0023 and were tested with the crack plane in the N-P orientation as defined by ASTM. The head HAZ was tested for V0125 only. The shell-to-shell weld was tested for V0066 only, in the N-P orientation

as defined by ASTM. All specimens were side-grooved to a total thickness reduction of 20%. The cutting diagram used to remove the C(T) specimens from the V0023 head-to-shell weld is shown in Figure 7.5.3.3.3-3. Examples of Load Versus COD and J_q Versus Δa plots are shown in Figure 7.5.3.3.3-1 and Figure 7.5.3.3.3-2.

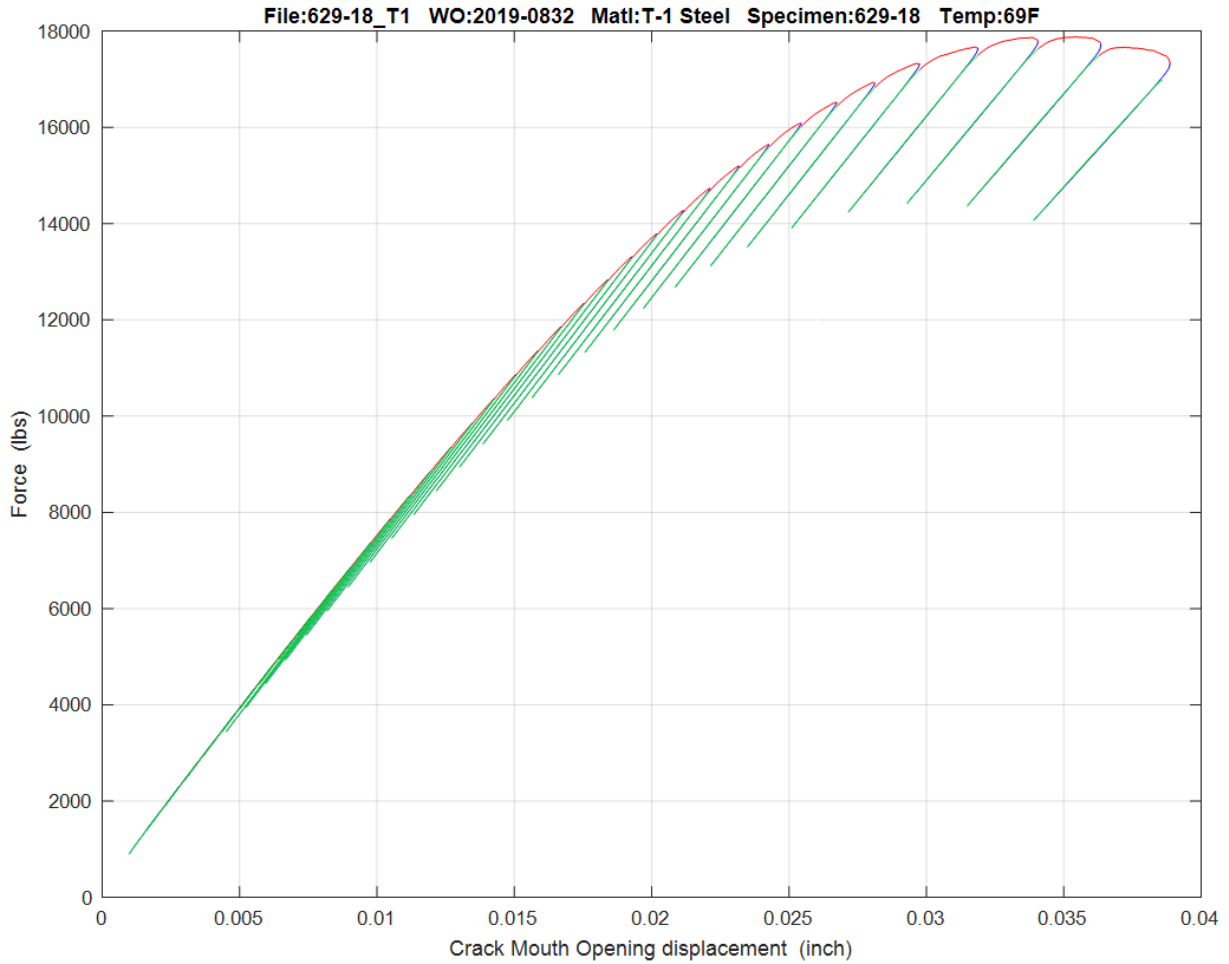


Figure 7.5.3.3.3-1: Shell-to-Shell Weld Load Versus COD Plot, Sample 629-18

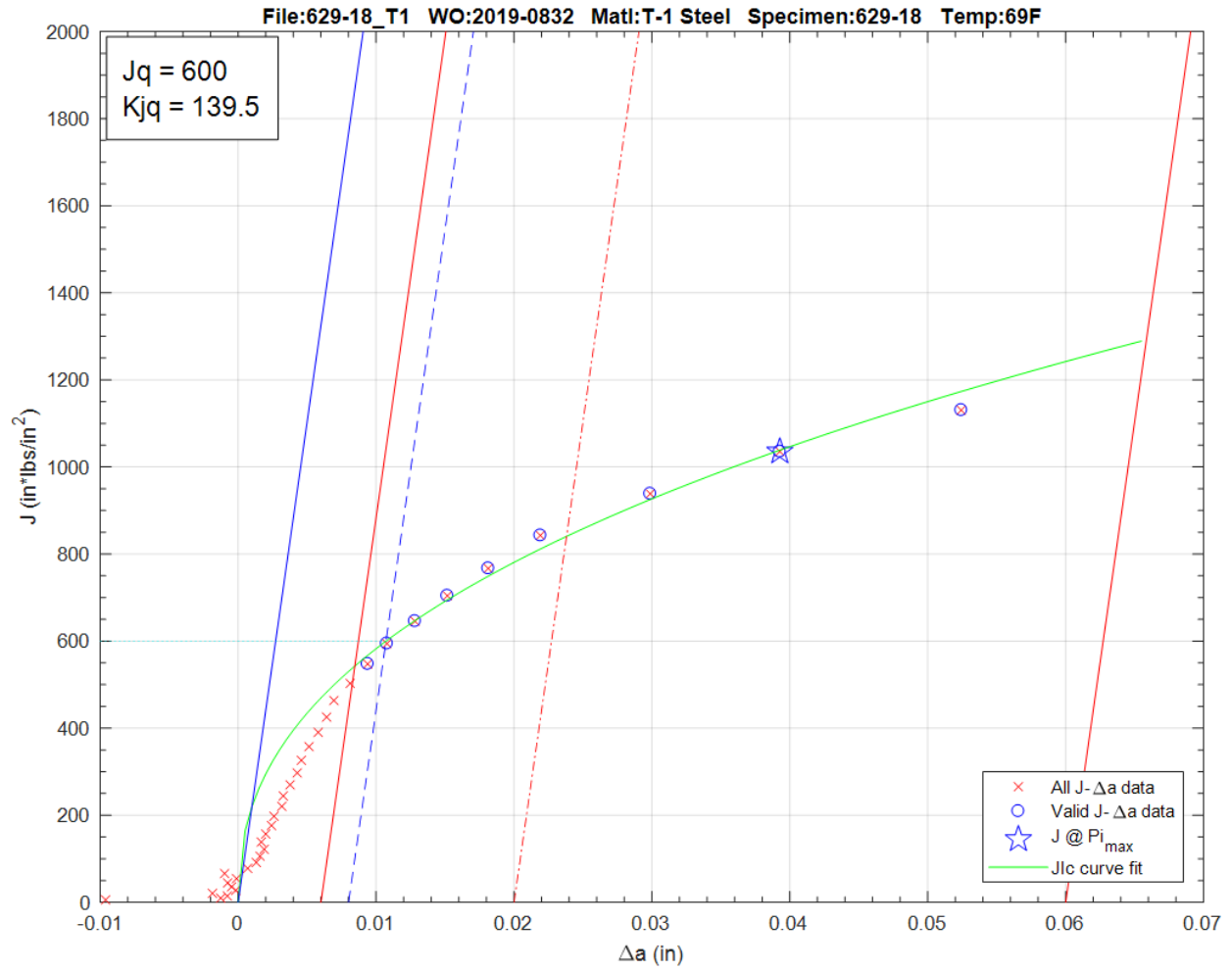


Figure 7.5.3.3-2: Shell-to-Shell Weld J_q Versus Δa Plot, Sample 629-18

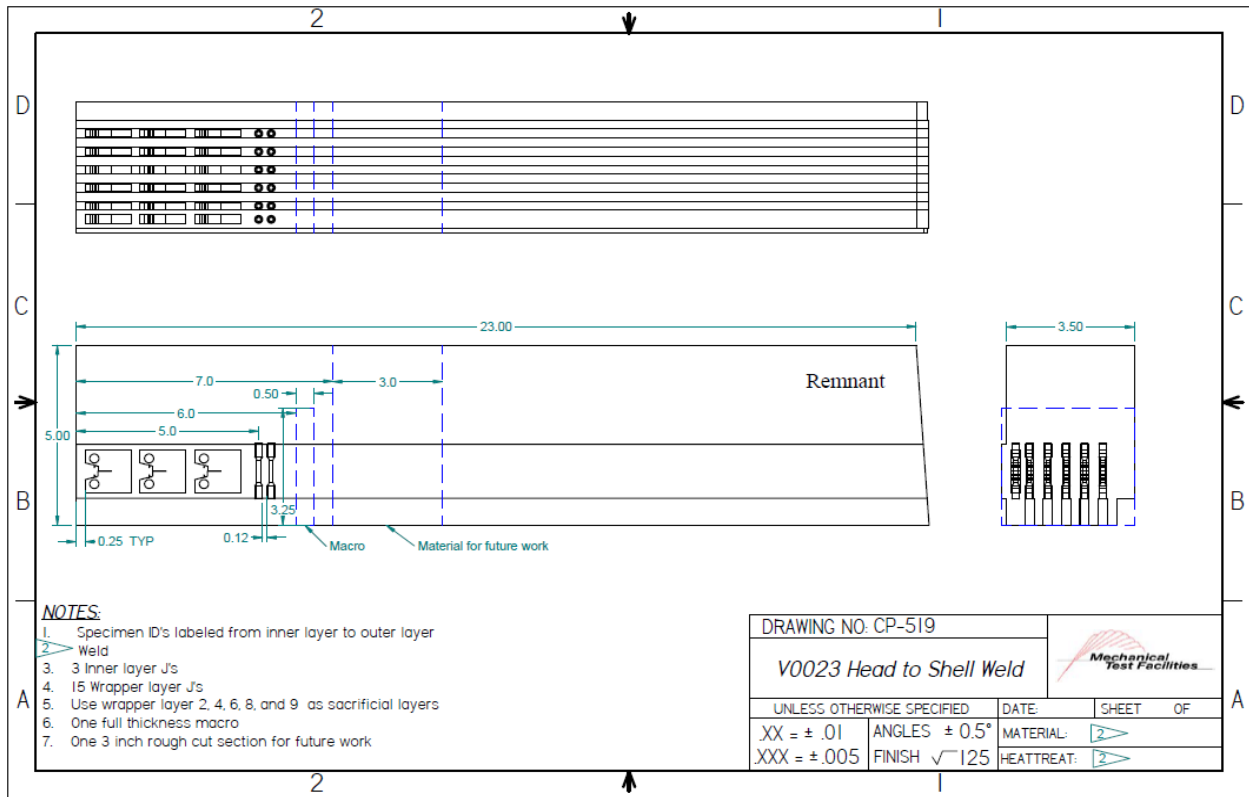


Figure 7.5.3.3.3-3: Cut Plan for Fracture Specimens from V0023 Head-to-Shell Weld

The test data in Table 7.5.3.3.3-1 are raw values obtained from fracture tests conducted on V0125 head-to-shell weld material. Table 7.5.3.3.3-2 contains raw values from V0125 head HAZ. Test results that are considered upper shelf are listed under ASTM E1820, while transition temperature test results are listed under E1921. Tests that meet the complete validity requirements for $J_q = J_{1C}$ and $K_{Jq} = K_{J1C}$ are denoted with an asterisk. Despite invalidities, J_q and K_{Jq} convey valuable fracture toughness information, especially when the test results are applied directly to the sample material source.

Table 7.5.3.3.3-1: Head-to-Shell Weld Fracture Data, V0125

Specimen ID	Test Temp. (°C)	ASTM Crack Plane Orientation	W (in)	a ₀ (in)	a _r (in)	B ₀ (in)	B _N (in)	J _q (kJ/m ²)	K _{Jq} (MPa √m)	K _{JCIT} (MPa √m)	ASTM Standard
CP-344-5-2	23	N-P	0.9982	0.4911	0.5767	0.1858	0.1438	43	98	---	E1820
CP-344-5-3	23	N-P	0.9923	0.4956	0.6171	0.1862	0.1439	143	179	---	E1820
CP-344-5-4	23	N-P	0.9965	0.5321	0.5793	0.1879	0.1436	106	154	---	E1820
CP-344-8-7	22	N-P	1.0001	0.5220	0.5930	0.3764	0.3010	214	219	---	E1820
CP-344-8-13	22	N-P	1.0038	0.5422	0.6129	0.3779	0.3038	320	267	---	E1820

Table 7.5.3.3.3-2 Head-to-shell Weld HAZ (Head Side) Fracture Data, V0125

Specimen ID	Test Temp. (°C)	ASTM Crack Plane Orientation	W (in)	a ₀ (in)	a _r (in)	B ₀ (in)	B _N (in)	J _q (kJ/m ²)	K _{Jq} (MPa √m)	K _{JCIT} (MPa √m)	ASTM Standard
CP-344-8-12	23	N-Q	0.9999	0.5202	0.5818	0.3765	0.3012	142	178	0	E1820
CP-344-8-19	23	N-P	0.9997	0.5158	0.5500	0.3598	0.2863	95	146	0	E1820
CP-344-8-21	23	N-P	0.9994	0.5176	0.5946	0.3595	0.2872	99	148	0	E1820
CP-344-8-6	22	N-Q	1.0011	0.5111	0.5531	0.3770	0.3031	173	197	0	E1820
CP-344-8-18	22	N-P	0.9998	0.5917	0.6558	0.3773	0.3000	131	171	0	E1820

No E1921 tests were conducted on V0125 head-to-shell weld or HAZ. The results of the HAZ tests show toughness that is between the weld material and A225 head. Therefore, it can be assumed that the HAZ will be bounded by the two lots.

The following test data provided in Table 7.5.3.3.3-3 are raw values obtained from fracture tests conducted on V0032 head-to-shell weld material. These tests were taken only from the intersection of the inner wrap layer and the head-to-shell weld. Test results that are considered upper shelf are listed under ASTM E1820, while transition temperature test results are listed under E1921. Tests that meet the complete validity requirements for $J_q = J_{1C}$ and $K_{Jq} = K_{1C}$ are denoted with an asterisk. Despite invalidities, J_q and K_{Jq} convey valuable fracture toughness information, especially when the test results are applied directly to the sample material source.

Table 7.5.3.3.3-3: Head-to-shell Weld Inner Shell V0032

Specimen ID	Test Temp. (°C)	ASTM Crack Plane Orientation	W (in)	a ₀ (in)	a _r (in)	B ₀ (in)	B _N (in)	J _q (kJ/m ²)	K _{Jq} (MPa √m)	K _{JCIT} (MPa √m)	ASTM Standard
380-216	-18	N-P	1.0011	0.5126	0.6035	0.2515	0.2012	147	182	---	E1820
380-221	-51	N-P	0.9998	0.5355	0.5408	0.2493	0.2001	45	101	77	E1921
380-217	-73	N-P	1.0009	0.5218	0.5309	0.2517	0.2016	48	103	79	E1921
380-218	-73	N-P	1.0075	0.5205	0.5237	0.2512	0.2045	29	81	63	E1921
380-219	-73	N-P	0.9995	0.5187	0.5241	0.2512	0.2037	41	96	74	E1921
380-220	-73	N-P	1.0006	0.5393	0.5437	0.2513	0.2001	55	110	84	E1921

Results from the five E1921 tests are presented in Table 7.5.3.3.3-4 and Table 7.5.3.3.3-5. These results were obtained using the T₀TEM Code described in Section 4.2. The T₀ reference temperature for this data set was evaluated as -43°C using the E1921 Master Curve shown in Figure 7.5.3.3.3-4.

Table 7.5.3.3.3-4: Head-to-shell Weld (Inner Layer) T₀ Individual Specimen Results, V0032

Specimen Name	Temperature (°C)	KjcRaw (MPa*m ^{0.5})	1T Data (MPa*m ^{0.5})	Uncensored Data	Test Temp -T ₀ (°C)
380-217	-73	103.4	79.1	1	-31
380-218	-73	80.5	62.9	1	-31
380-219	-73	95.9	73.7	1	-31
380-220	-73	110.5	84.1	1	-31
380-221	-51	100.7	77.0	1	-8

Table 7.5.3.3.3-5 Head-to-shell Weld (Inner Layer) T₀ Calculation Results, V0032

Initial T₀ (°C)	-43
Total Samples	5
Samples within T₀ ± 50°C (N)	5
Number of Uncensored Data (r)	5
Poisson's Ratio	0.3
Σ(r_i n_i)	0.74
Samples Between T_i - T₀ 50 to -14 °C	1
Samples Between T_i - T₀ -15 to -35 °C	4
Samples Between T_i - T₀ -36 to -50 °C	0
T₀scrn (°C)	-43
Homogenous or Inhomogeneous	Homogenous

The results of the E1921 analysis show that the weld material removed from the head-to-shell inner layer weld is macroscopically homogenous, indicating consistent properties throughout the sampled material. For this data set, the ductile-brittle transition temperature was found to be -43°C. This result does not meet the E1921 validity criteria for a sufficient number of samples tested in an appropriate temperature range with $\Sigma(r_i n_i) < 1.0$. However, the consistency of the samples and goodness of fit gives reason to use the T₀ with confidence. It is important to note that the V0032 head-to-shell weld is the only through thickness weld in which the weld properties differed significantly between the inner layer and wrapper layers. In most cases, the through thickness weld was consistent enough throughout to be considered one data set.

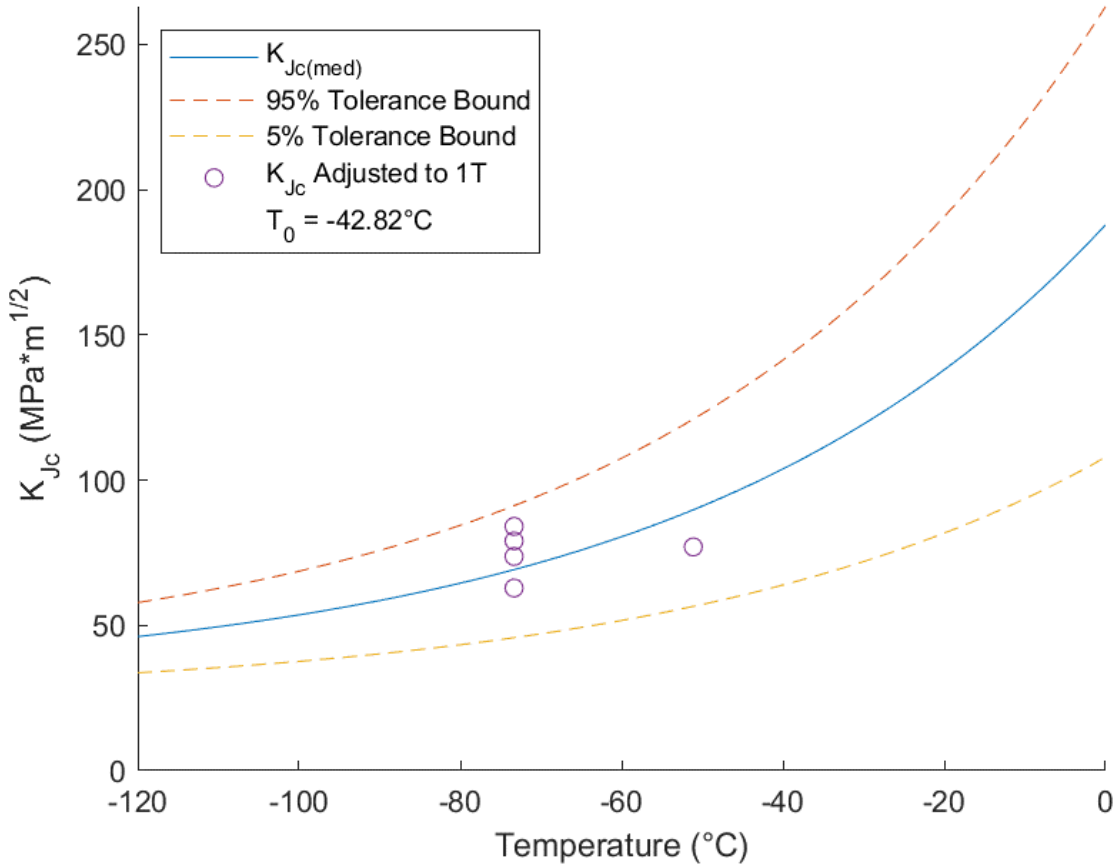


Figure 7.5.3.3.3-4: Head-to-Shell Weld (Inner Layer) T_0 Plot, V0032

The following test data are raw values obtained from fracture tests conducted on V0032 head-to-shell weld material. These tests were taken only from the intersection of the outer wrap layers and the head-to-shell weld. Test results that are considered upper shelf are listed under ASTM E1820, while transition temperature test results are listed under E1921. Tests that meet the complete validity requirements for $J_q = J_{1C}$ and $K_{Jq} = K_{J1C}$ are denoted with an asterisk. Despite invalidities, J_q and K_{Jq} convey valuable fracture toughness information, especially when the test results are applied directly to the sample material source.

Table 7.5.3.3.3-6: Head-to-Shell Weld Wrapper Layer V0032

Specimen ID	Test Temp. (°C)	ASTM Crack Plane Orientation	W (in)	a ₀ (in)	a _r (in)	B ₀ (in)	B _N (in)	J _q (kJ/m ²)	K _{Jq} (MPa√m)	K _{JCIT} (MPa√m)	ASTM Standard
380-233	22	N-P	1.0015	0.5135	0.6947	0.2002	0.1625	63	119	---	E1820
380-232	22	N-P	1.0012	0.5081	0.5850	0.2000	0.1600	68	123	---	E1820
380-226	-7	N-P	1.0015	0.5262	0.5366	0.1985	0.1581	66	121	88	E1921
380-227	-7	N-P	1.0005	0.5228	0.6060	0.2008	0.1641	50	106	78	E1921
380-228	-7	N-P	1.0014	0.5251	0.5329	0.1978	0.1629	59	115	83	E1921
380-225	-18	N-P	1.0016	0.5221	0.5302	0.1982	0.1575	48	104	76	E1921
380-229	-18	N-P	1.0011	0.5201	0.5217	0.1987	0.1610	34	87	65	E1921
380-230	-18	N-P	1.0000	0.5139	0.5166	0.2012	0.1619	42	97	72	E1921
380-231	-18	N-P	0.9993	0.5151	0.6047	0.2012	0.1637	54	109	80	E1921
380-223	-46	N-P	1.0003	0.5209	0.5270	0.1992	0.1606	43	98	72	E1921
380-224	-46	N-P	1.0008	0.5221	0.5314	0.2013	0.1600	27	77	58	E1921
380-222	-73	N-P	1.0014	0.5199	0.5205	0.1995	0.1597	19	65	50	E1921

Results from the 10 E1921 tests is presented in Table 7.5.3.3.3-7 and Table 7.5.3.3.3-8. These results were obtained using the T₀TEM Code described in Section 4.2. The T₀ reference temperature for this data set was evaluated as 3 °C using the E1921 Master Curve shown in Figure 7.5.3.3.3-5.

Table 7.5.3.3.3-7: Head-to-Shell Weld (Wrapper Layer) T₀ Individual Specimen Results, V0032

Specimen Name	Temperature (°C)	K _{JcRaw} (MPa*m ^{0.5})	1T Data (MPa*m ^{0.5})	Uncensored Data	Test Temp -T ₀ (°C)
380-223	-46	97.9	72.0	1	-49
380-224	-46	77.1	58.2	1	-49
380-225	-18	103.6	75.8	1	-21
380-226	-7	121.2	87.5	1	-10
380-227	-7	106.0	77.6	0	-10
380-228	-7	114.9	83.3	1	-10
380-229	-18	86.7	64.5	1	-21
380-230	-18	97.4	71.8	1	-21
380-231	-18	109.4	79.9	0	-21
380-232	22	123.1	87.5	0	18
380-233	22	118.9	86.2	0	19

Table 7.5.3.3.3-8: Head-to-Shell Weld (Wrapper Layer) T_0 Calculation Results, V0032

Initial T_0 (°C)	3
Total Samples	11
Samples within $T_0 \pm 50^\circ\text{C}$ (N)	11
Number of Uncensored Data (r)	7
Poisson's Ratio	0.3
$\Sigma(r_i n_i)$	1.01
Samples Between $T_i - T_0$ 50 to -14 °C	2
Samples Between $T_i - T_0$ -15 to -35 °C	3
Samples Between $T_i - T_0$ -36 to -50 °C	2
$T_{0\text{scrn}}$ (°C)	12
Homogenous or Inhomogeneous	Homogenous

The results of the E1921 analysis show that the weld material removed from the head-to-shell inner layer weld is macroscopically homogenous, indicating consistent properties throughout the sampled material. For this data set, the ductile-brittle transition temperature was found to be 3°C. This result meets the E1921 validity criteria for a sufficient number of samples tested in an appropriate temperature range with $\Sigma(r_i n_i) \geq 1.0$. It is important to note that the V0032 head-to-shell weld is the only through thickness weld in which the weld properties differed significantly between the inner layer and wrapper layers. In most cases, the through thickness weld was consistent enough throughout to be considered one data set. It is impossible to trace back the reason for the differences in the properties of what seems to be the same weld. It is likely that the initial weld of the inner layer to the head was done with a different filler that is tougher and more resistant to embrittlement from the contents of the vessel, since it is the only part of the head-to-shell weld exposed.

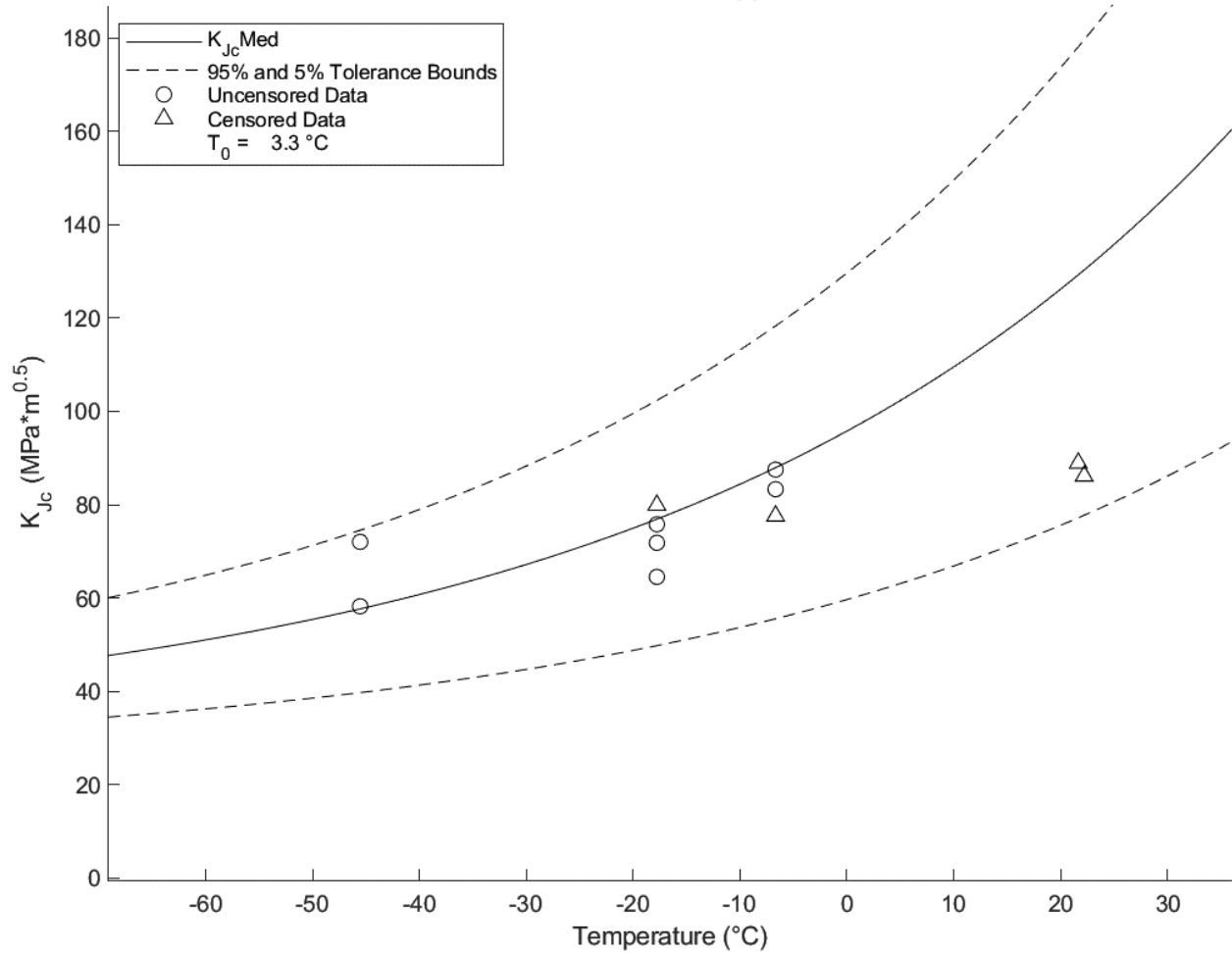


Figure 7.5.3.3.3-5: Head-to-Shell Weld (Wrapper Layer) T_0 Plot, V0032

The test data presented in Table 7.5.3.3.3-9 are raw values obtained from fracture tests conducted on V0023 head-to-shell weld material. Test results that are considered upper shelf are listed under ASTM E1820, while transition temperature test results are listed under E1921. Tests that meet the complete validity requirements for $J_q = J_{1C}$ and $K_{Jq} = K_{J1C}$ are denoted with an asterisk. Despite invalidities, J_q and K_{Jq} convey valuable fracture toughness information, especially when the test results are applied directly to the sample material source.

Table 7.5.3.3.3-9: Head-to-Shell Weld V0023

Specimen ID	Test Temp. (°C)	ASTM Crack Plane Orientation	W (in)	a ₀ (in)	a _r (in)	B ₀ (in)	B _N (in)	J _q (kJ/m ²)	K _{Iq} (MPa√m)	K _{JCIT} (MPa√m)	ASTM Standard
519-301	23	N-P	0.9986	0.5055	0.6065	0.2020	0.1580	84	137	---	E1820
519-294	21	N-P	0.9985	0.5598	0.6457	0.2019	0.1588	86	138	---	E1820
519-298	21	N-P	0.9979	0.5121	0.5844	0.2495	0.1977	106	154	---	E1820
519-300	-25	N-P	0.9985	0.5184	0.6074	0.2029	0.1637	106	154	110	E1921
519-302	-25	N-P	0.9990	0.5064	0.6727	0.2015	0.1596	126	168	119	E1921
519-293	-46	N-P	0.9977	0.5137	0.5216	0.2012	0.1571	54	110	80	E1921
519-295	-46	N-P	0.9984	0.5094	0.5434	0.2008	0.1588	135	173	123	E1921
519-296	-46	N-P	0.9980	0.5188	0.5240	0.2011	0.1590	58	114	83	E1921
519-303	-46	N-P	0.9976	0.5169	0.5303	0.2006	0.1598	50	106	77	E1921
519-304	-46	N-P	0.9975	0.5206	0.5241	0.2514	0.1965	41	96	74	E1921
519-305	-46	N-P	0.9990	0.5067	0.5905	0.2026	0.1597	108	156	111	E1921
519-299	-59	N-P	0.9994	0.5140	0.5195	0.2005	0.1596	119	163	116	E1921
519-306	-59	N-P	0.9990	0.5078	0.5101	0.2015	0.1603	49	105	77	E1921
519-307	-59	N-P	0.9991	0.5217	0.5306	0.2012	0.1597	65	120	87	E1921
519-308	-59	N-P	0.9990	0.5203	0.5251	0.2007	0.1594	79	133	96	E1921
519-309	-61	N-P	0.9976	0.5230	0.5456	0.2008	0.1590	48	103	76	E1921
519-292	-73	N-P	0.9978	0.5201	0.5242	0.2507	0.1976	34	87	67	E1921
519-297	-73	N-P	0.9980	0.5227	0.5282	0.2031	0.1597	22	71	54	E1921

Results from the 15 E1921 tests is presented in Table 7.5.3.3.3-10 and Table 7.5.3.3.3-11. These results were obtained using the T₀TEM Code described in Section 4.2. The T₀ reference temperature for this data set was evaluated as -46°C using the E1921 Master Curve shown in Figure 7.5.3.3.3-6.

Table 7.5.3.3.3-10 Head-to-Shell Weld T₀ Individual Specimen Results, V0023

Specimen Name	Temperature (°C)	K _{JcRaw} (MPa√m ^{0.5})	1T Data (MPa√m ^{0.5})	Uncensored Data	Test Temp -T ₀ (°C)
519-292	-73	86.5	67.1	1	-27
519-293	-46	110.3	80.5	1	0
519-295	-46	173.4	115.8	0	0
519-296	-46	113.7	82.7	1	0
519-297	-73	70.8	54.1	1	-27
519-299	-59	163.2	115.8	1	-14
519-300	-25	154.1	110.0	0	21
519-302	-25	167.8	115.8	0	21
519-303	-46	105.9	77.5	1	0
519-304	-46	96.3	74.0	1	0
519-305	-46	155.6	111.0	0	0
519-306	-59	105.1	77.0	1	-14
519-307	-59	120.5	87.3	1	-14
519-308	-59	133.1	95.7	1	-14
519-309	-61	103.1	75.6	1	-15

Table 7.5.3.3.3-11 Head-to-shell Weld T₀ Calculation Results, V0023

Initial T₀ (°C)	-46
Total Samples	15
Samples within T₀ ± 50°C (N)	15
Number of Uncensored Data (r)	11
Poisson's Ratio	0.3
Σ(r_i n_i)	1.76
Samples Between T_i - T₀ 50 to -14 °C	8
Samples Between T_i - T₀ -15 to -35 °C	3
Samples Between T_i - T₀ -36 to -50 °C	0
T₀scrn (°C)	-38
Homogenous or Inhomogeneous	Homogenous

The results of the E1921 analysis show that the weld material removed from the head-to-shell weld is macroscopically homogenous, indicating consistent properties throughout the sampled material. For this data set, the ductile-brittle transition temperature was found to be -46°C. This result meets the E1921 validity criteria for a sufficient number of samples tested in an appropriate temperature range with $\Sigma(r_i n_i) \geq 1.0$.

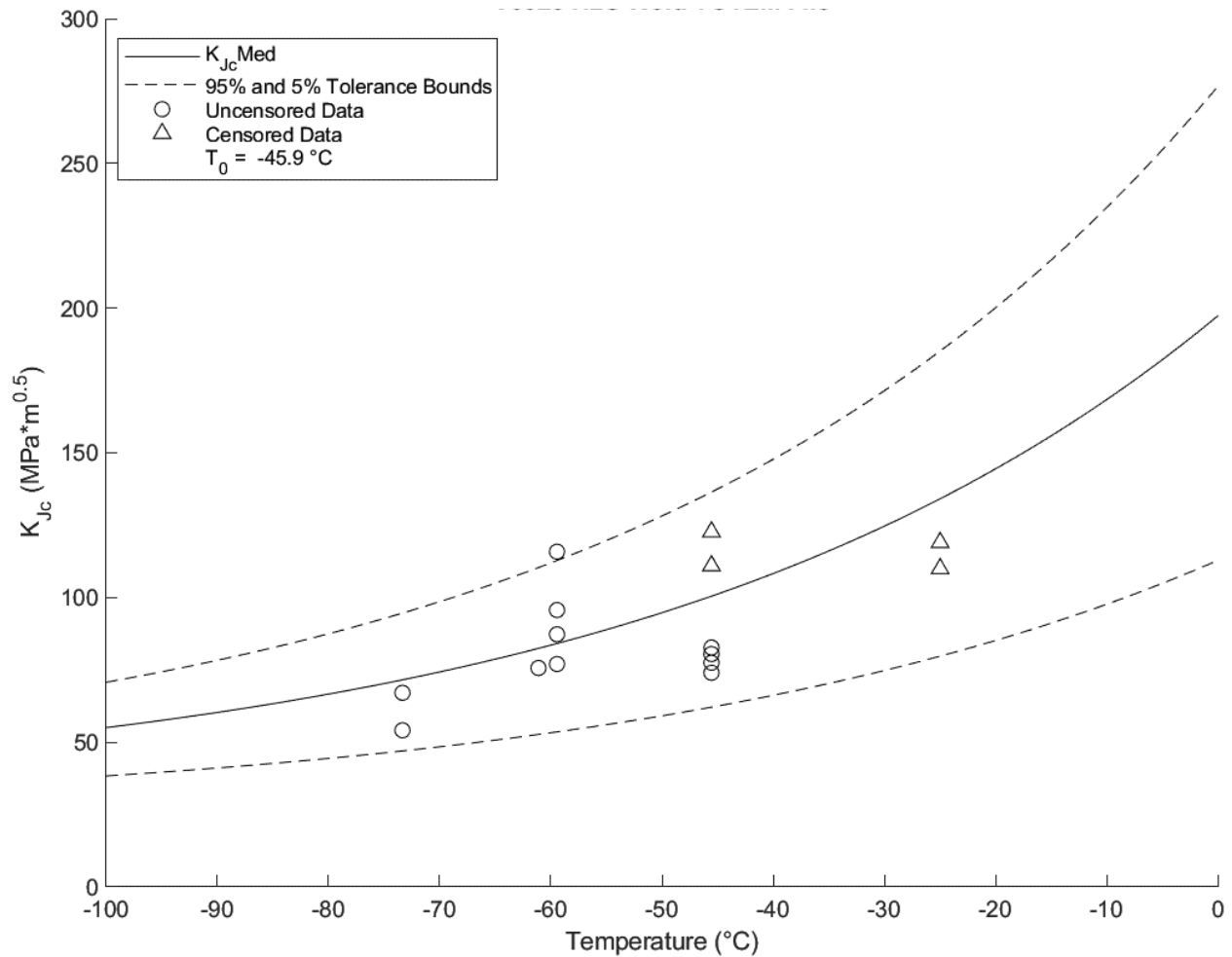


Figure 7.5.3.3.3-6: Head-to-shell Weld T_0 Plot, V0023

The test data provided in Table 7.5.3.3.3-12 are raw values obtained from fracture tests conducted on V0066 shell-to-shell weld material. Test results that are considered upper shelf are listed under ASTM E1820, while transition temperature test results are listed under E1921. Tests that meet the complete validity requirements for $J_q = J_{1C}$ and $K_{Jq} = K_{J1C}$ are denoted with an asterisk. Despite invalidities, J_q and K_{Jq} convey valuable fracture toughness information, especially when the test results are applied directly to the sample material source.

Table 7.5.3.3-12: Head-to-Shell Weld V0023

Specimen ID	Test Temp. (°C)	ASTM Crack Plane Orientation	W (in)	a ₀ (in)	a _r (in)	B ₀ (in)	B _N (in)	J _q (kJ/m ²)	K _{Jq} (MPa√m)	K _{JCIT} (MPa√m)	ASTM Standard
629-18	21	N-P	2.0041	1.0230	1.1011	1.0045	0.8075	105	153	---	E1820
629-24	21	N-P	2.0010	1.0268	1.1150	0.9998	0.8062	104	153	---	E1820
629-19	-73	N-P	2.0021	1.0330	1.1005	0.9973	0.8005	116	161	161	E1921
629-25	-73	N-P	2.0012	1.0341	1.0459	1.0027	0.8126	68	123	123	E1921
629-20	-101	N-P	2.0022	1.0206	1.1510	1.0004	0.8046	114	160	160	E1921
629-21	-101	N-P	2.0003	1.0298	1.0423	1.0030	0.8041	102	151	151	E1921
629-22	-101	N-P	1.9936	1.0193	1.0514	1.0031	0.7875	57	113	113	E1921
629-26	-101	N-P	1.9996	1.0351	1.0473	1.0037	0.8062	65	121	121	E1921
629-27	-101	N-P	2.0020	1.0372	1.0508	1.0033	0.8091	51	107	107	E1921

Results from the seven E1921 tests is presented in Table 7.5.3.3-13 and Table 7.5.3.3-14. These results were obtained using the T₀TEM code described in Section 4.2. The T₀ reference temperature for this data set was evaluated as -116°C using the E1921 Master Curve shown in Figure 7.5.3.3-7.

Table 7.5.3.3-13: Head-to-Shell Weld T₀ Individual Specimen Results, V0023

Specimen Name	Temperature (°C)	K _{JcRaw} (MPa*m ^{0.5})	1T Data (MPa*m ^{0.5})	Uncensored Data	Test Temp -T ₀ (°C)
629-19	-73	161.1	159.9	0	43
629-20	-101	159.9	159.9	1	15
629-21	-101	151.3	151.4	1	15
629-25	-73	123.4	123.4	1	43
629-26	-101	120.8	120.9	1	15
629-27	-101	106.7	106.8	1	15
629-22	-101	112.6	112.6	1	15

Table 7.5.3.3-14: Head-to-Shell Weld T₀ Calculation Results, V0023

Initial T ₀ (°C)	-116
Total Samples	7
Samples within T ₀ ± 50°C (N)	7
Number of Uncensored Data (r)	6
Poisson's Ratio	0.3
Σ(r _i n _i)	1
Samples Between T _i - T ₀ 50 to -14 °C	6
Samples Between T _i - T ₀ -15 to -35 °C	0
Samples Between T _i - T ₀ -36 to -50 °C	0
T ₀ scrn (°C)	-109
Homogenous or Inhomogeneous	Homogenous

The results of the E1921 analysis show that the weld material removed from the head-to-shell weld is macroscopically homogenous, indicating consistent properties throughout the

sampled material. For this data set, the ductile-brittle transition temperature was found to be 116°C. This result meets the E1921 validity criteria for a sufficient number of samples tested in an appropriate temperature range with $\sum(r_i n_i) \geq 1.0$.

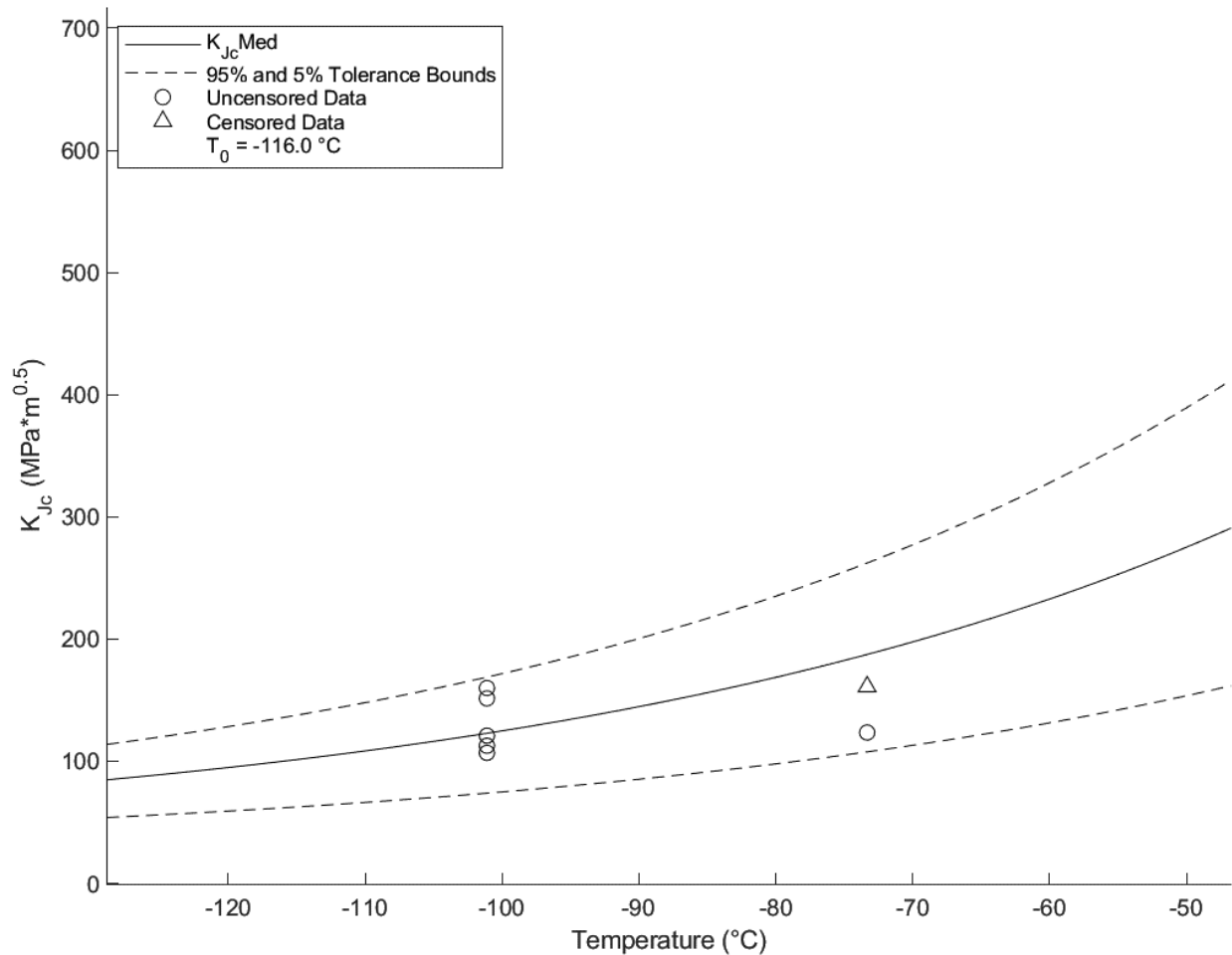


Figure 7.5.3.3.3-7: Head-to-Shell Weld T_0 Plot, V0023

7.5.3.3.4 Fatigue Crack Growth

Sections of V0023 head-to-shell weld and head side HAZ were tested to determine the fatigue crack growth rates according to ASTM E647 (11). Load ratios of $R = 0.1$ and $R = 0.7$ were chosen to reflect load cycles corresponding to slight pressure variations and nearly full pressure releases of the LPVs, respectively. These tests were conducted on material taken from a single stack of specimens placed one layer apart to encompass a full thickness profile as shown in Figure 7.5.3.3.4-1. Figure 7.5.3.3.4-2 shows the combined fatigue crack growth curves for the head-to-shell weld and HAZ material from vessel V0023. These curves are input into NASGRO to create material data packages used for structural analysis and crack growth prediction.

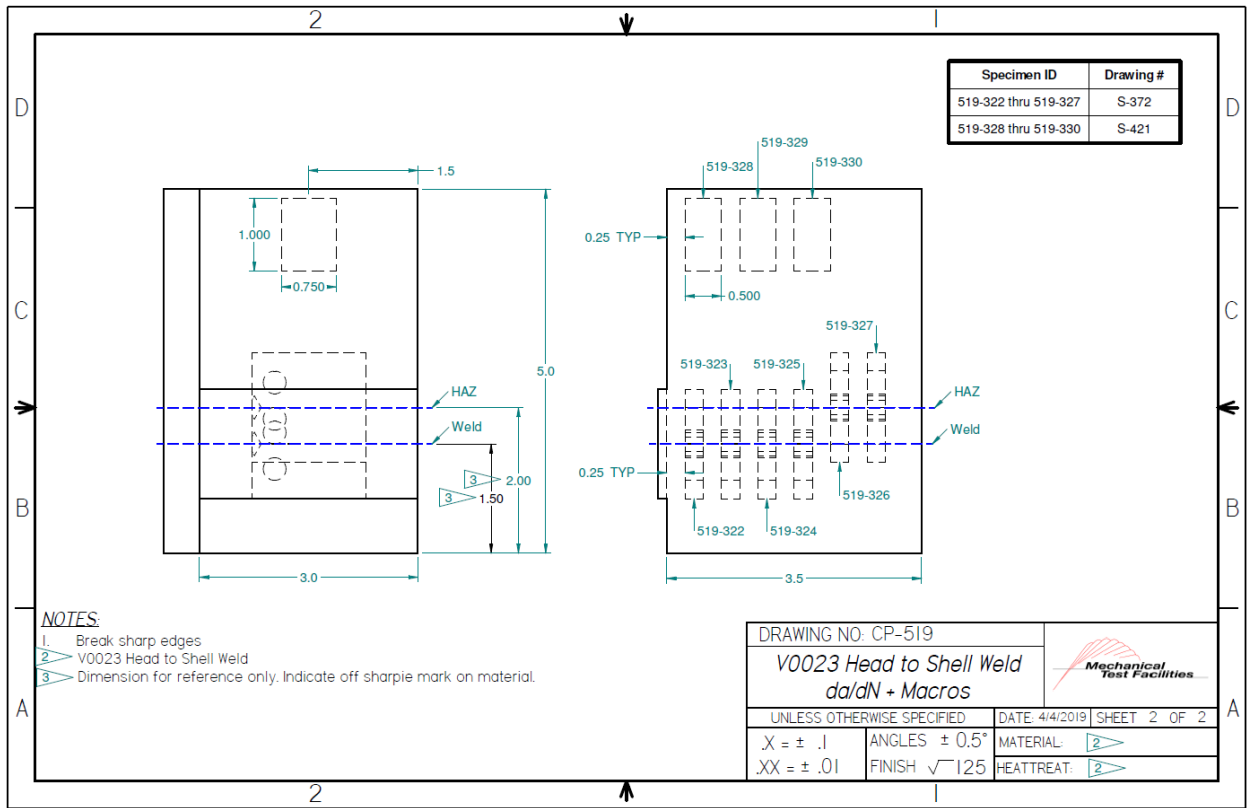


Figure 7.5.3.3.4-1: Cut Plan for Fatigue Specimens from V0023 Head-to-Shell Weld

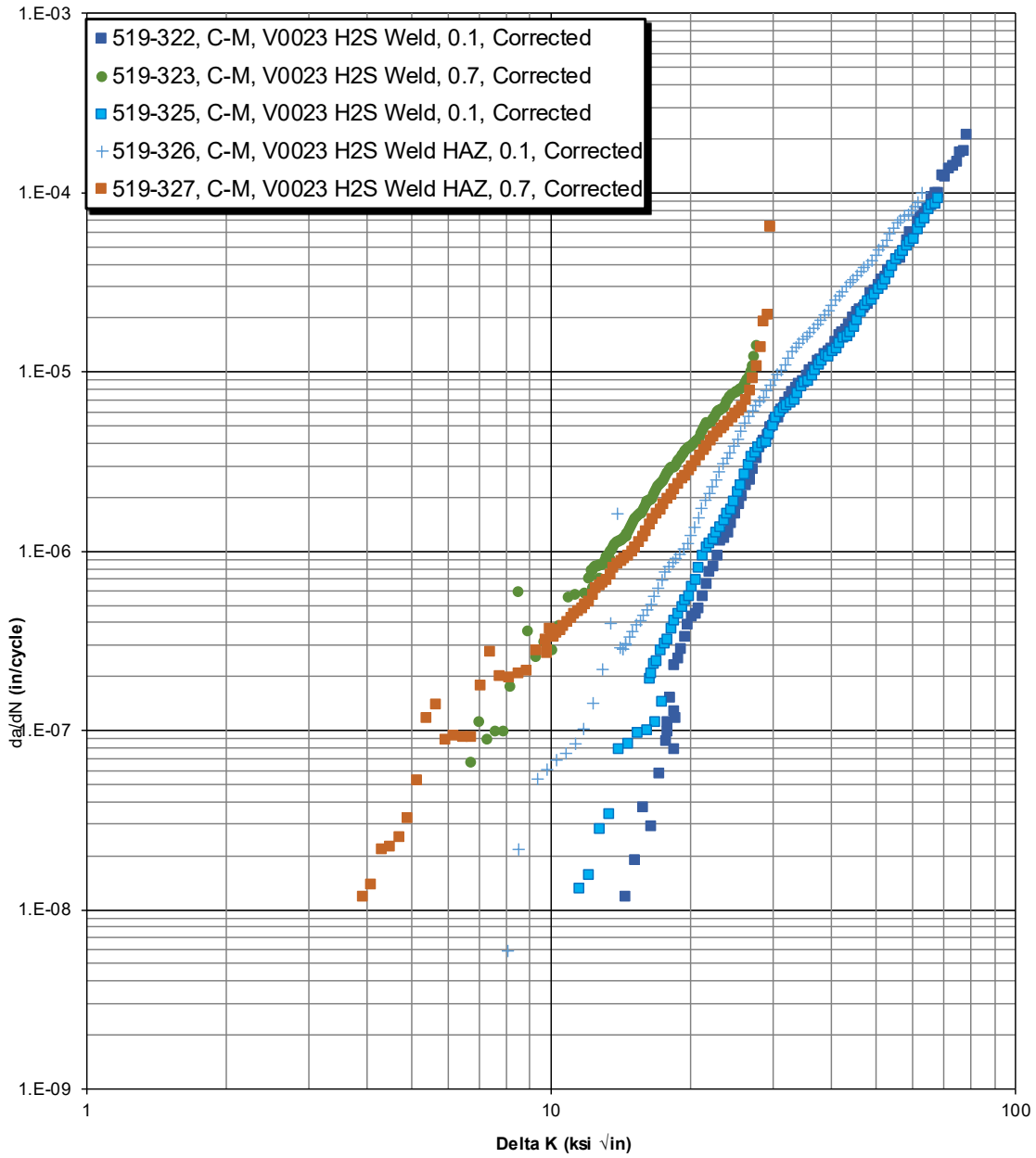


Figure 7.5.3.3.4-2: Fatigue Crack Growth Curves, V0023 Head-to-Shell Weld and HAZ

7.5.3.3.5 Charpy Impact

Charpy impact tests were not performed on this material.

7.5.4 Nozzle Welds

Nozzle welds in LPVs are most commonly found in the monolithic heads. The material investigated here comes from MV50466-8, a 5002 nozzle welded into an A225 head. Tests were conducted on the weld metal itself as well as the HAZ on the head side of the weld.

7.5.4.1 Chemical Composition

The chemical composition of the weld filler used is unknown, therefore only the data in Table 7.5.4.1-1 Inner Layer Weld Fracture Toughness Data, V0023, collected from Arc Spark analyses of vessels at MSFC, are available. HAZ data was not collected as it is nominally the same as the head material. Weld chemistry was tested on PV0296, but no mechanical testing was conducted.

Table 7.5.4.1-1: Collected Nozzle Weld Chemistry

Vessel	C	Si	Mn	P	S	Cr	Mo	Ni	Cu	V
MV50466-8	0.07	0.65	0.77	0.013	0.016	0.039	0.010	0.076	0.090	0.024
PV0296	0.10	0.13	0.55	0.011	0.021	0.029	0.370	1.460	0.110	0.130

7.5.4.2 Metallography

Only a hardness study was performed on this material. No grain orientation, grain size, grain size through thickness, or carburization layer thickness studies were performed, and no macro cubes were produced.

Hardness Study

A section of nozzle-to-head weld was examined for hardness characteristics.

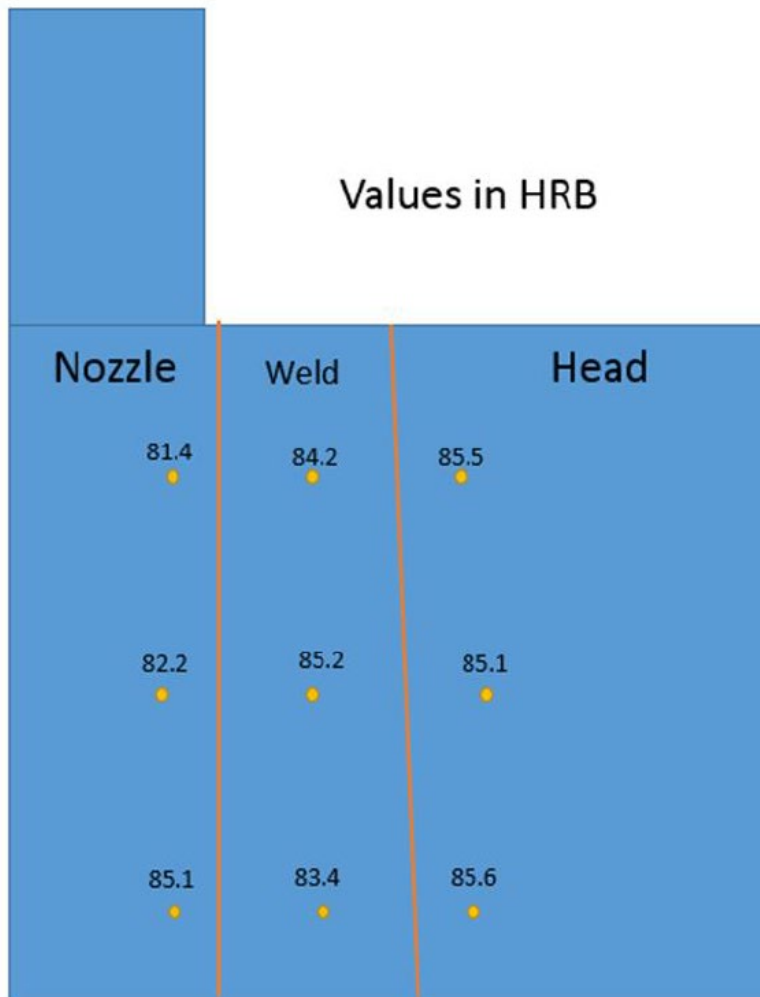


Figure 7.5.4.2-1: MV50466-8 Nozzle Weld Hardness Map

Summary

The weld metal displays similar hardness characteristics to the surrounding materials. As hardness in steels is typically correlated strongly with strength, it is likely that the nozzle-to-head weld matches well with its surrounding components.

7.5.4.3 Mechanical Properties

Since the exact weld filler used is not known, precise expectations cannot be found for strength or other mechanical properties. It can be assumed that the weld center properties are not exceptionally grain-dependent and test results in any orientation will be reasonably close to target orientation. Tensile properties were tested in the N orientation (normal to weld path) due to material constraints.

7.5.4.3.1 Smooth Tensile Tests

Smooth tensile tests were conducted at MSFC on round specimens according to ASTM E8, "Standard Test Methods for Tension Testing of Metallic Materials" (51) using specimen design S-219 Rev A. The mechanical test frame consisted of a servo-hydraulic actuator and reaction frame. The frame used an LVDT for displacement feedback. Stress measurements were derived from load measurements and the initial specimen measurements. Strain measurements were derived from an extensometer and the initial specimen measurements.

Table 7.5.4.3.1-1: MV50466-8 Nozzle Weld Tensile Data

Specimen ID	Test Temp. (°C)	ASTM Orientation	Tensile Stress (ksi)	Yield Stress (ksi)	Fracture Elongation (%)
440-297	27	N	80.9	61.9	24.4
440-298	27	N	80.9	62.9	25.4
440-299	-46	N	87.2	69.3	28.2
440-300	-46	N	90.2	72.7	N/A
440-301	-101	N	96.2	78.3	N/A
440-302	-101	N	94.4	76.7	29.6

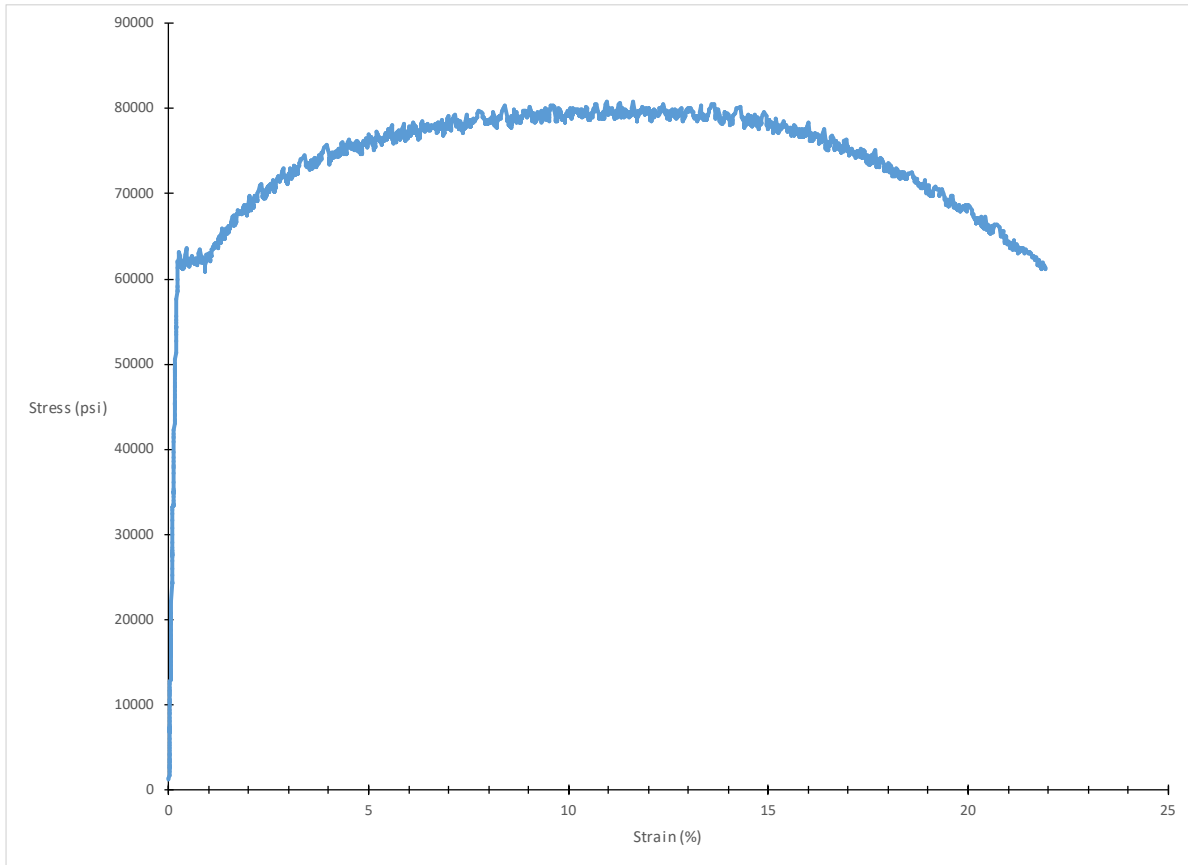


Figure 7.5.4.3.1-1: Nozzle Weld Smooth Tensile Plot Sample 440-298

7.5.4.3.2 Notch Tensile

Notch tensile tests were not performed on this material.

7.5.4.3.3 Fracture Properties

All room temperature testing was performed per ASTM E1820 (10). All other temperatures were tested per ASTM E1921 (7). All nozzle weld fracture tests came from MV50466-8 and were tested in the N-Q orientation. Tests were conducted on Charpy sized SE(B) specimens in order to fit within material constraints. All fracture tests and individual data

are fully documented in “Determination of the Reference Temperature, T_0 , for Nozzle Weld and HAZ of Vessel MV50466-8” by Richard E. Link (65).

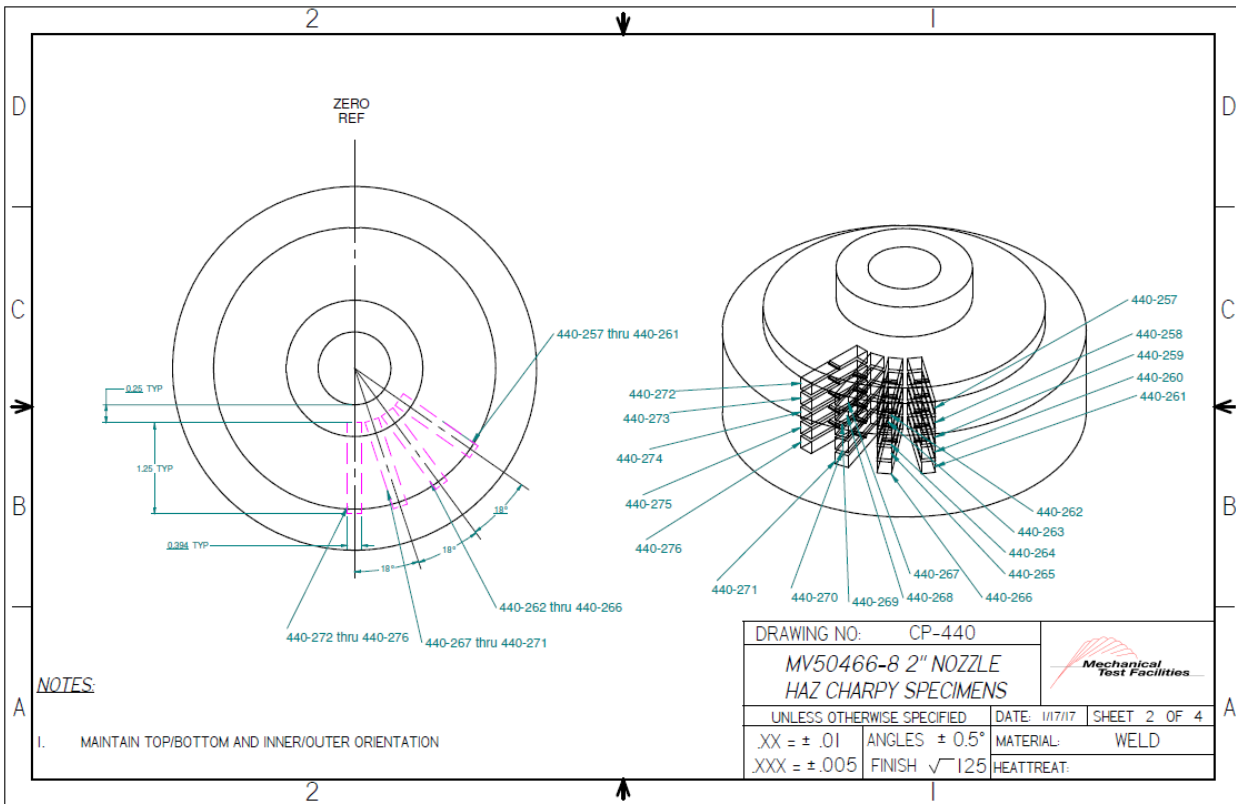


Figure 7.5.4.3.3-1: MV50466-8 Example Fracture Cut Plan

The test data in Table 7.5.4.3.3-1 are raw values obtained from fracture tests conducted on MV50466-8 nozzle to head weld HAZ (62). Test results that are considered upper shelf are listed under ASTM E1820, while transition temperature test results are listed under E1921. Tests that meet the complete validity requirements for $J_q = J_{1C}$ and $K_{Jq} = K_{J1C}$ are denoted with an asterisk. Despite invalidities, J_q and K_{Jq} convey valuable fracture toughness information, especially when the test results are applied directly to the sample material source.

Table 7.5.4.3.3-1: MV50466-8 Nozzle-to-Head Weld HAZ Fracture Data

Specimen ID	Test Temp. (°C)	ASTM Crack Plane Orientation	W (in)	a ₀ (in)	a _r (in)	B ₀ (in)	B _N (in)	J _q (kJ/m ²)	K _{Iq} (MPa√m)	K _{JC1T} (MPa√m)	ASTM Standard
440-257	-66	N-Q	0.3980	0.2080	0.2080	0.3960	0.3960	171	196	159	E1921
440-259	-78	N-Q	0.3980	0.2080	0.2080	0.3950	0.3950	22	70	60	E1921
440-260	-78	N-Q	0.3980	0.2050	0.2050	0.3950	0.3950	142	178	145	E1921
440-261	-78	N-Q	0.3930	0.2060	0.2060	0.3950	0.3950	162	190	155	E1921
440-262	-78	N-Q	0.3980	0.2030	0.2030	0.3950	0.3950	21	69	59	E1921
440-263	-78	N-Q	0.3980	0.2040	0.2040	0.3960	0.3960	106	154	126	E1921
440-264	-78	N-Q	0.3980	0.2060	0.2060	0.3960	0.3960	135	174	142	E1921
440-258	-84	N-Q	0.3970	0.2050	0.2050	0.3970	0.3970	5	33	30	E1921
440-265	-85	N-Q	0.3980	0.2060	0.2060	0.3960	0.3960	179	200	163	E1921
440-266	-85	N-Q	0.3930	0.2020	0.2020	0.3930	0.3930	53	109	90	E1921
440-267	-85	N-Q	0.3980	0.2100	0.2100	0.3930	0.3930	160	189	154	E1921
440-268	-85	N-Q	0.3980	0.2140	0.2140	0.3920	0.3920	223	223	181	E1921
440-269	-90	N-Q	0.3980	0.2100	0.2100	0.3960	0.3960	42	97	81	E1921
440-270	-90	N-Q	0.3980	0.2090	0.2090	0.3920	0.3920	100	149	122	E1921
440-271	-90	N-Q	0.3970	0.2140	0.2140	0.3920	0.3920	151	184	149	E1921
440-272	-95	N-Q	0.3980	0.2090	0.2090	0.3930	0.3930	19	66	56	E1921
440-273	-95	N-Q	0.3980	0.2120	0.2120	0.3920	0.3920	83	136	112	E1921
440-274	-95	N-Q	0.3980	0.2060	0.2060	0.3920	0.3920	15	57	49	E1921
440-275	-95	N-Q	0.3980	0.2120	0.2120	0.3900	0.3900	38	92	77	E1921
440-276	-95	N-Q	0.3930	0.2090	0.2090	0.3920	0.3920	20	67	57	E1921

Results from the 20 E1921 tests are presented in Table 7.5.4.3.3-2 and Table 7.5.4.3.3-3. These results were obtained using the T₀TEM Code described in Section 4.2. The T₀ reference temperature for this data set was evaluated as -90°C using the E1921 Master Curve shown in Figure 7.5.4.3.3-2. Given the number of specimens tested, the material was able to be properly characterized as macroscopically inhomogeneous with a 97% confidence in multimodal inhomogeneity. This gives a multimodal transition temperature of T_m = -95°C. The multimodal Master Curve and confidence bounds are shown in Figure 7.5.4.3.3-3.

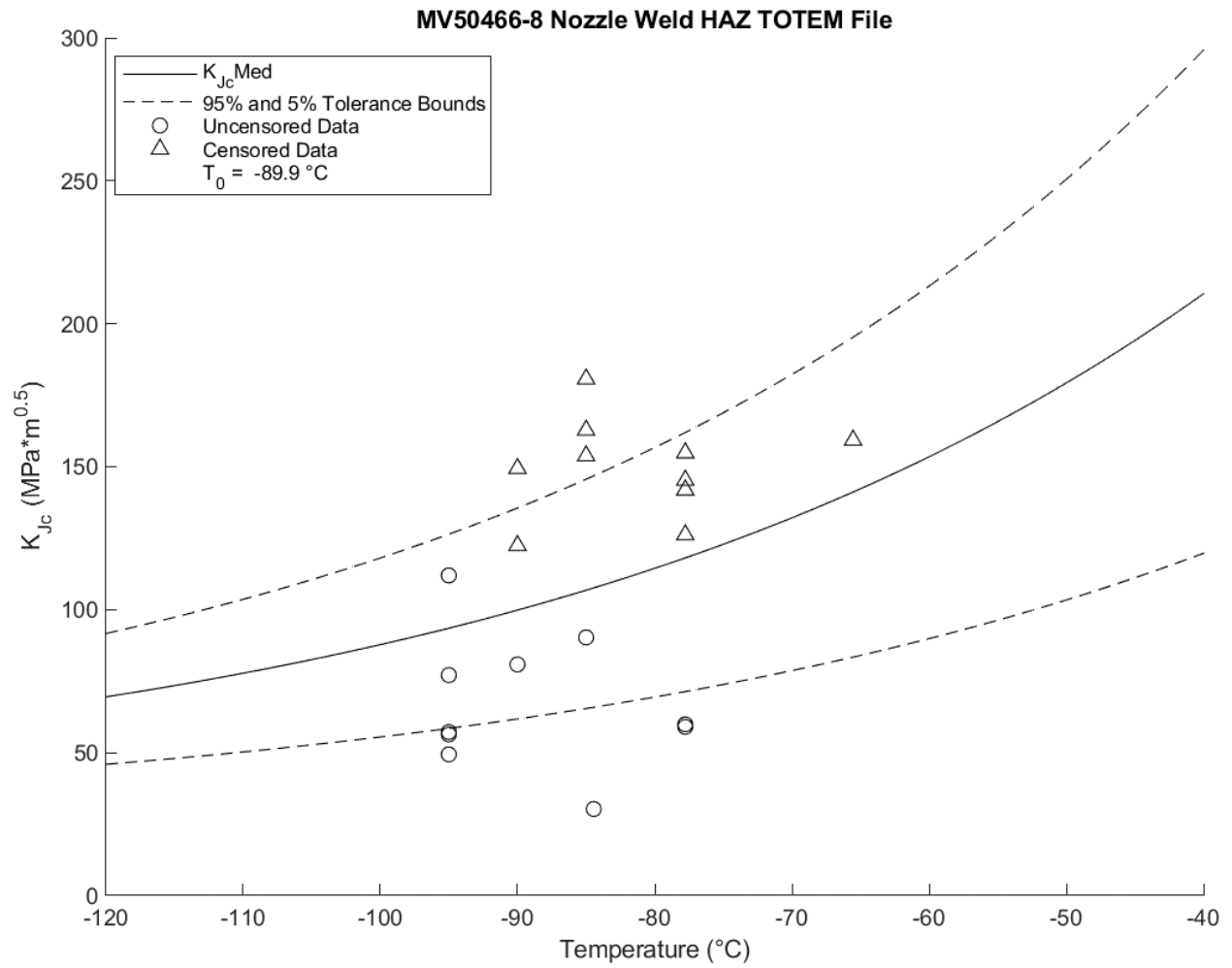


Figure 7.5.4.3.3-2: MV50466-8 Nozzle-to-Head Weld HAZ T_0 Plot ($T_0 = -90^\circ\text{C}$)

Table 7.5.4.3.3-2: MV50466-8 Nozzle-to-Head Weld HAZ T₀ Individual Specimen Results

Specimen Name	Temperature (°C)	KjcRaw (MPa*m ^{0.5})	1T Data (MPa*m ^{0.5})	δ _i	Test Temp -T ₀ (°C)
440-257	-66	195.6	110.6	0	24
440-258	-84	33.0	30.3	1	5
440-259	-78	70.3	59.9	1	12
440-260	-78	178.0	113.0	0	12
440-261	-78	190.1	111.2	0	12
440-262	-78	69.2	59.0	1	12
440-263	-78	153.8	113.3	0	12
440-264	-78	173.6	112.7	0	12
440-265	-85	200.0	113.3	0	5
440-266	-85	108.8	90.3	1	5
440-267	-85	189.0	112.0	0	5
440-268	-85	223.1	110.8	0	5
440-269	-90	96.7	80.8	1	0
440-270	-90	149.4	112.6	0	0
440-271	-90	183.5	110.9	0	0
440-272	-95	65.9	56.4	1	-5
440-273	-95	136.3	112.0	1	-5
440-274	-95	57.1	49.4	1	-5
440-275	-95	92.3	77.1	1	-5
440-276	-95	67.0	57.2	1	-5

Table 7.5.4.3.3-3: MV50466-8 Nozzle-to-Head Weld HAZ T₀ Calculation Results

Initial T ₀ (°C)	-90
Total Samples	20
Number of Samples Between +50/-50°C (N)	20
Number of Uncensored Data (r)	10
Poisson's Ratio	0.3
Σ(r _i n _i)	1.67
Samples Between T _i - T ₀ 50 to -14 °C	10
Samples Between T _i - T ₀ -15 to -35 °C	0
Samples Between T _i - T ₀ -36 to -50 °C	0
T ₀ scrn (°C)	-77
Homogenous or Inhomogeneous	Inhomogeneous

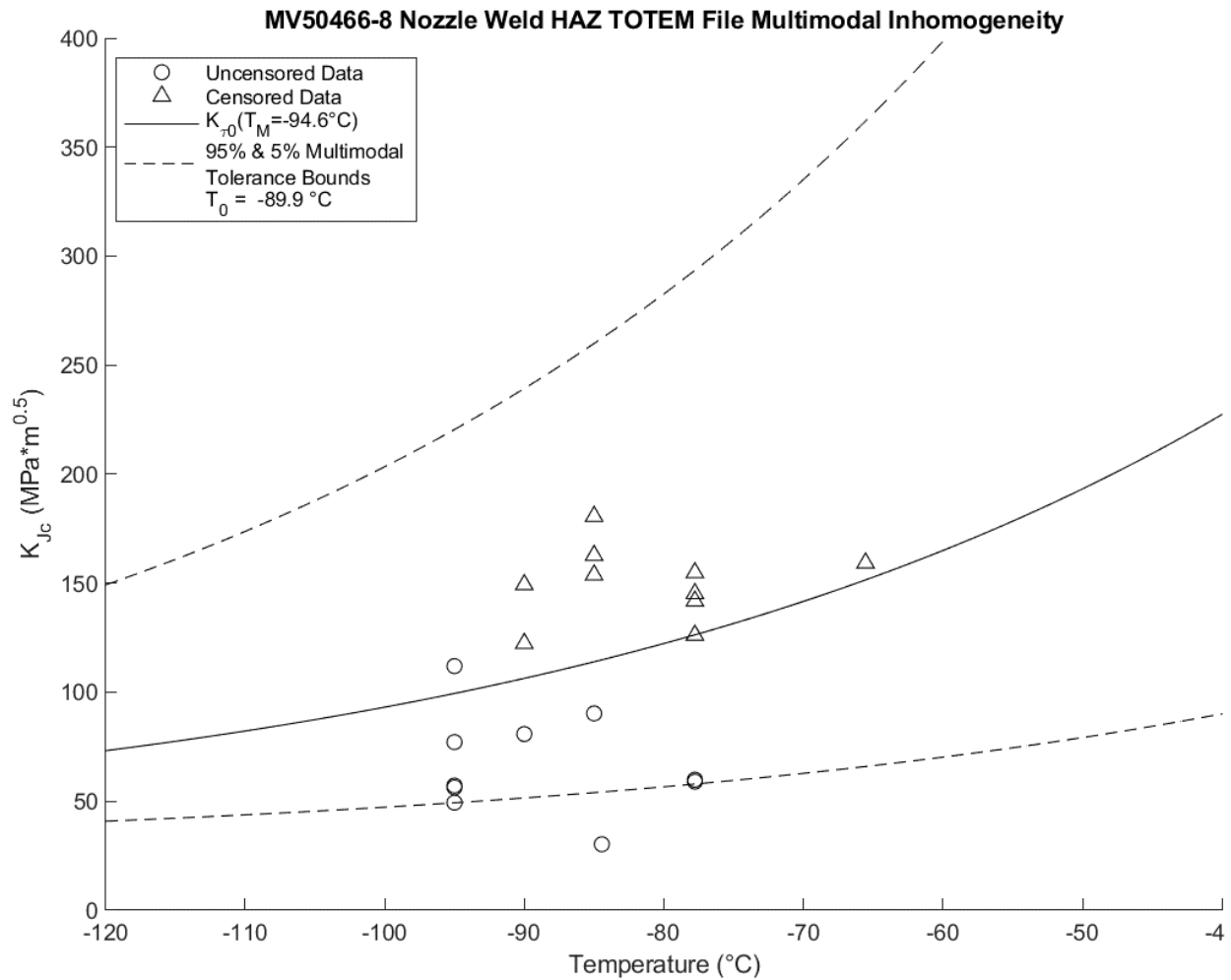


Figure 7.5.4.3.3-3: MV50466-8 Nozzle to Head Weld HAZ Multimodal T_m Plot ($T_m = -95^\circ\text{C}$)

Table 7.5.4.3.3-4: MV50466-8 Nozzle-to-Head Weld HAZ Multimodal T_m Calculation Results 7

T_m (°C)	-95
Sigma T_m (°C)	55
Multimodal Max ln(L)	57.61
MLNH Criterion	2
MLNH from Multimodal	4.31
Multimodal Homogeneity?	Inhomogeneous
Multimodal Confidence (%)	97

The multimodal T_m value moves the transition temperature 5°C lower and expands the confidence bounds to more accurately reflect the composition of the data set.

The test data Table 7.5.4.3.3-5 are raw values obtained from fracture tests conducted on MV50466-8 nozzle to head weld (62). Test results that are considered upper shelf are listed under ASTM E1820, while transition temperature test results are listed under E1921. Tests that

meet the complete validity requirements for $J_q = J_{1C}$ and $K_{Jq} = K_{J1C}$ are denoted with an asterisk. Despite invalidities, J_q and K_{Jq} convey valuable fracture toughness information, especially when the test results are applied directly to the sample material source.

Table 7.5.4.3.3-5 MV50466-8 Nozzle-to-Head Weld Fracture Data

Specimen ID	Test Temp. (°C)	ASTM Crack Plane Orientation	W (in)	a ₀ (in)	a _f (in)	B ₀ (in)	B _N (in)	J _q (kJ/m ²)	K _{Jq} (MPa√m)	K _{JC1T} (MPa√m)	ASTM Standard
440-277	-80	N-Q	0.3980	0.2030	0.2030	0.3930	0.3930	40	95	79	E1921
440-278	-80	N-Q	0.3980	0.2080	0.2080	0.3920	0.3920	42	97	81	E1921
440-279	-80	N-Q	0.3940	0.2090	0.2090	0.3940	0.3940	44	99	83	E1921
440-280	-80	N-Q	0.3960	0.2060	0.2100	0.3930	0.3930	189	205	167	E1921
440-281	-80	N-Q	0.3900	0.2060	0.2100	0.3930	0.3930	203	213	173	E1921
440-282	-90	N-Q	0.3980	0.2110	0.2150	0.3930	0.3930	201	212	172	E1921
440-283	-95	N-Q	0.3980	0.2100	0.2100	0.3940	0.3940	84	137	113	E1921
440-284	-95	N-Q	0.3970	0.2100	0.2100	0.3930	0.3930	64	120	99	E1921
440-285	-95	N-Q	0.3980	0.2070	0.2070	0.3920	0.3920	12	52	45	E1921
440-286	-95	N-Q	0.3980	0.2080	0.2080	0.3930	0.3930	29	80	68	E1921
440-287	-95	N-Q	0.3980	0.2090	0.2090	0.3920	0.3920	37	91	76	E1921
440-288	-95	N-Q	0.3980	0.2000	0.2000	0.3930	0.3930	10	46	41	E1921
440-289	-90	N-Q	0.3980	0.2000	0.2000	0.3930	0.3930	67	122	101	E1921
440-290	-90	N-Q	0.3980	0.1990	0.1990	0.3920	0.3920	65	121	100	E1921
440-291	-90	N-Q	0.3980	0.2000	0.2000	0.3920	0.3920	43	98	82	E1921
440-292	-90	N-Q	0.0000	0.0000	0.0000	0.0000	0.0000	0	0	0	E1921
440-293	-90	N-Q	0.3980	0.1990	0.1990	0.3930	0.3930	69	124	102	E1921
440-294	-90	N-Q	0.3970	0.2010	0.2010	0.3920	0.3920	131	171	140	E1921
440-295	-90	N-Q	0.3980	0.2010	0.2010	0.3930	0.3930	14	55	48	E1921
440-296	-90	N-Q	0.3980	0.2000	0.2000	0.3930	0.3930	17	62	53	E1921

Results from the 19 E1921 tests are presented in Table 7.5.4.3.3-6 and Table 7.5.4.3.3-7. These results were obtained using the T₀TEM Code described in Section 4.2. The T₀ reference temperature for this data set was evaluated as -83°C using the E1921 Master Curve shown in Figure 7.5.4.3.3-4. Given the number of specimens tested, the material was able to be properly characterized as macroscopically inhomogeneous with a 95% confidence in multimodal inhomogeneity. This gives a multimodal transition temperature of T_m = -78°C. The multimodal master curve and confidence bounds are shown in Figure 7.5.4.3.3-5.

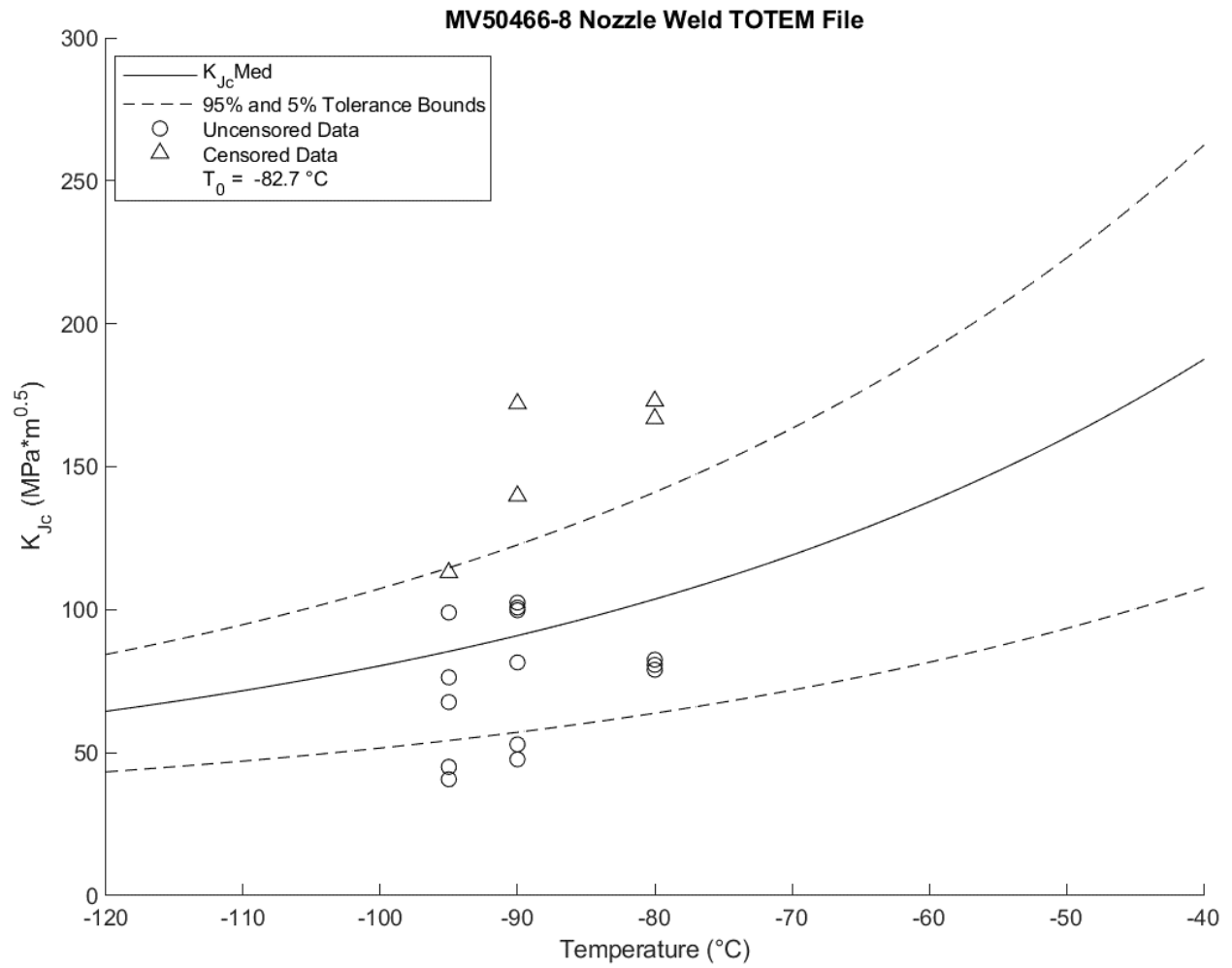


Figure 7.5.4.3.3-4: MV50466-8 Nozzle-to-Head Weld T_0 Plot ($T_0 = -83^\circ\text{C}$)

Table 7.5.4.3.3-6: MV50466-8 Nozzle-to-Head Weld T₀ Individual Specimen Results

Specimen Name	Temperature (°C)	K _{jc} Raw (MPa*m ^{0.5})	1T Data (MPa*m ^{0.5})	δ _i	Test Temp -T ₀ (°C)
440-277	-80	94.5	79.0	1	3
440-278	-80	96.7	80.7	1	3
440-279	-80	98.9	82.5	1	3
440-280	-80	205.5	102.5	0	3
440-281	-80	213.2	102.5	0	3
440-282	-90	212.1	102.5	0	-7
440-283	-95	137.4	112.9	0	-12
440-284	-95	119.8	99.0	1	-12
440-285	-95	51.6	45.0	1	-12
440-286	-95	80.2	67.7	1	-12
440-287	-95	91.2	76.3	1	-12
440-288	-95	46.2	40.7	1	-12
440-289	-90	122.0	100.7	1	-7
440-290	-90	120.9	99.8	1	-7
440-291	-90	97.8	81.6	1	-7
440-293	-90	124.2	102.5	1	-7
440-294	-90	171.4	114.7	0	-7
440-295	-90	54.9	47.7	1	-7
440-296	-90	61.5	52.9	1	-7

Table 7.5.4.3.3-7: MV50466-8 Nozzle-to-Head Weld T₀ Calculation Results

Initial T ₀ (°C)	-83
Total Samples	19
Number of Samples Between +50/-50°C (N)	19
Number of Uncensored Data (r)	14
Poisson's Ratio	0.3
Σ(r _i n _i)	2.33
Samples Between T _i - T ₀ 50 to -14 °C	14
Samples Between T _i - T ₀ -15 to -35 °C	0
Samples Between T _i - T ₀ -36 to -50 °C	0
T ₀ scrn (°C)	-73
Homogenous or Inhomogeneous	Inhomogeneous

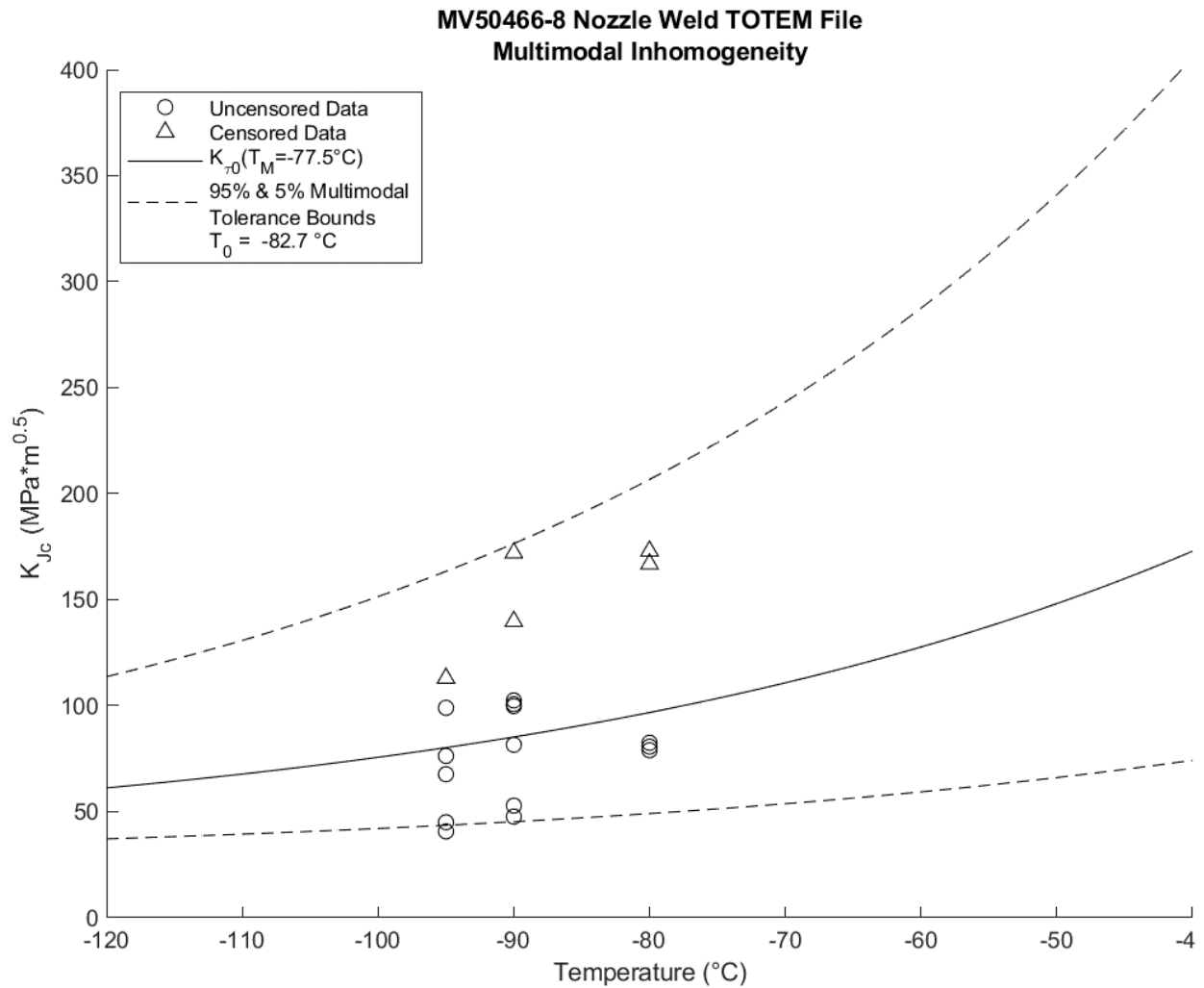


Figure 7.5.4.3.3-5: MV50466-8 Nozzle-to-Head Weld Multimodal T_m Plot ($T_m = -78^\circ\text{C}$)

Table 7.5.4.3.3-8: MV50466-8 Nozzle to Head Weld Multimodal T_m Calculation Results

T_m ($^\circ\text{C}$)	-78
Sigma T_m ($^\circ\text{C}$)	29
Multimodal Max $\ln(L)$	71.1
MLNH Criterion	2
MLNH from Multimodal	4.6
Multimodal Homogeneity?	Inhomogeneous
Multimodal Confidence (%)	94.7

The multimodal T_m value moves the transition temperature 5°C higher and expands the confidence bounds to more accurately reflect the composition of the data set.

7.5.4.3.4 Fatigue Crack Growth

Fatigue crack growth tests were not performed on this material.

7.5.4.3.5 Charpy Impact

Charpy impact tests were not performed on this material.

8 CONCLUSIONS

The following section covers observations and conclusions made by the materials team during the course of the materials test program. These cover not only basic data summaries, but observations related to the testing of LPV materials, as well as application of material data to the overall LPV certification and characterization effort.

One of the key observations of the LPV materials effort is the inability to use proof test logic as a flaw screening method for LPVs in service. Proof test logic is one of the simplest and most straightforward methods that can be used to verify the safety of a pressure vessel. By pressurizing the vessel to a proof factor above what would cause a critical flaw to fail, the entire vessel can be screened at once for critical flaw sizes. When working with vessel materials that have severe temperature dependence, and ECF (environmental correction factor) must be applied. The ECF takes into account the difference in fracture toughness between the as-tested temperature and the expected critical operation temperature. This factor is multiplied by the required proof factor to find the pressure at which the vessel would be considered to be adequately screened. For almost all LPV materials, the ECF adjusted proof factor would be so high that it would require testing at pressures that would yield the vessel materials, and in many cases exceed the rated burst pressure of the vessel. Charts detailing the relationship between temperature and ECF, as well as the ECF at example temperature of -20F, can be found for each common vessel component and material in Section 9.1.

Another observation from this testing effort is the substantial variability between, and within, material lots. As detailed in Section 7, many of these legacy materials vary significantly from lot to lot despite having the same material designation. More concerning is the tendency of some materials to vary within a single lot. This provides little confidence that the characterization of some of the most common materials in the fleet can be applied to the safety assurance of the fleet. This Technical Memorandum provides the results of a significant materials testing program run for the purpose of allowing validation of LPVs in the NASA fleet. It is not exhaustive, leaving certain material combinations and locations untested. However, it is intended that in conjunction with analytical work documented in NASA/TM-20210020972 *NASA Ground-based Layered Pressure Vessels Structural Analysis Report* and NDE development documented in NASA/TM-20210020973 *NASA Ground-based Layered Pressure Vessels NDE Report*, the information presented herein will facilitate validation of the vast majority of NASA LPVs.

Also, while the work documented here was funded by NASA with the intent of permitting continued safe operation of NASA assets, much of the material data presented herein will be applicable to LPVs owned by other Governmental entities as well as the private sector.

8.1 Summary Charts

8.1.1 Head Data Summary

Table 8.1.1-1: Head Material Hardness and Chemistry Data Summary

Head			Chemistry (%)											
Material	Vessel	Hardness (HRB)	C	Si	Mn	P	S	Cr	Mo	Ni	Cu	Nb	V	B
A212	V0348	78	0.26	0.26	0.82	0.019	0.03	0.021	0.005	0.007	0.024	0.003	0.002	0.001
A225	MV50466-8	84	0.19	0.21	1.46	0.032	0.063	0.19	0.028	0.21	0.024	0.003	0.11	0.002
A225	PV0296	81	0.1505	0.2345	1.311	0.0123	0.0133	0.0191	0.00685	0.0076	0.0194	0.0031	0.1035	0.000545
A225	V0023	91	0.21	0.2	1.43	0.025	0.023	0.25	0.056	0.35	0.04	0.003	0.098	0.0006
A225	V32	82	0.26	0.23	1.38	0.032	0.048	0.21	0.062	0.027	0.027	0.003	0.091	0.0008
A302	V071	83	0.19	0.22	1.34	0.008	0.02	0.14	0.45	0.51	0.22	0.003	0.003	0.0006
T-1	V066	94	0.15	0.25	0.84	0.014	0.027	0.41	0.48	0.9	0.26	0.003	0.035	0.006

Table 8.1.1-2: Head Material Mechanical Data Summary

Head			To			Upper Shelf		
Material	Vessel	Orientation	σ_{YS} (ksi)	UTS (ksi)	Elong. (%)	°C	°F	KJ, MPa \sqrt{m}
A225	MV50466-8	C-M	50-51	76-77	31-32	-43	-45	171
A225	V32	C-M	55-58	77-81	34-37	-105	-157	193
A225	PV0296	C-M	51	82-85	21-22	-75	-103	287
A225	V0023	C-M	62	91	24	-2	28	197
A212	V0348	C-M	40-44	75-80	34-36	-58	-72	153
A302	V071	C-M	68-70	90-92	25-28	-93	-135	226

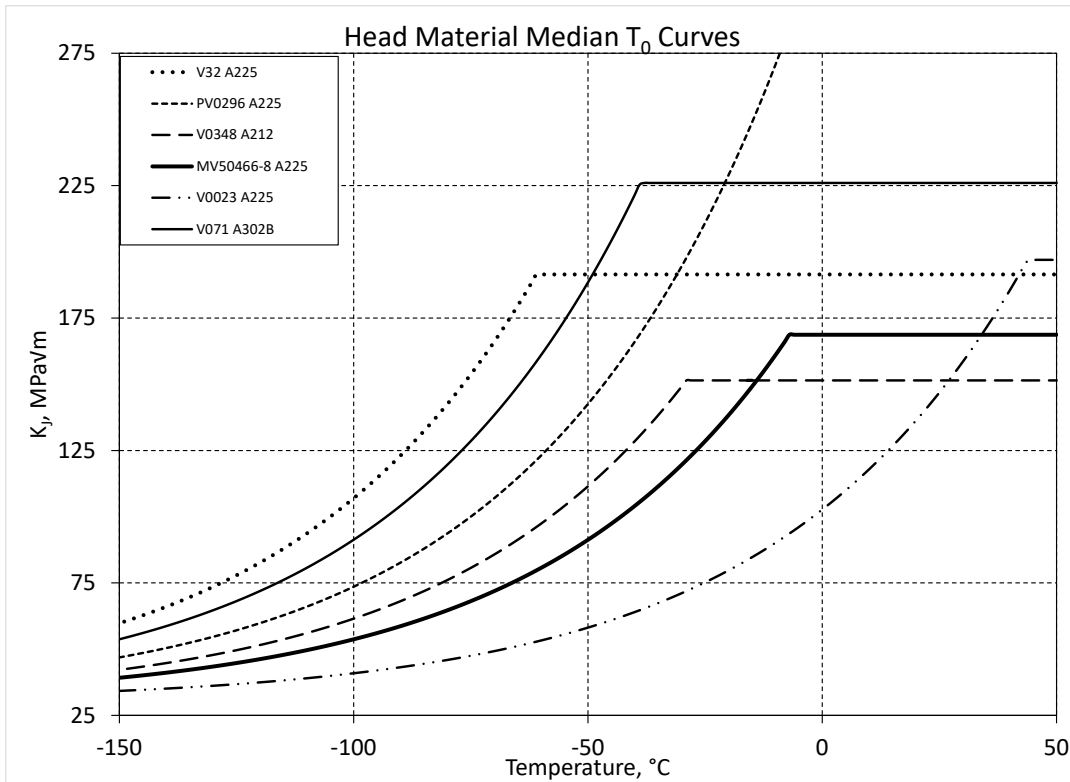


Figure 8.1.1-1: Head Material Median T_0 Curves

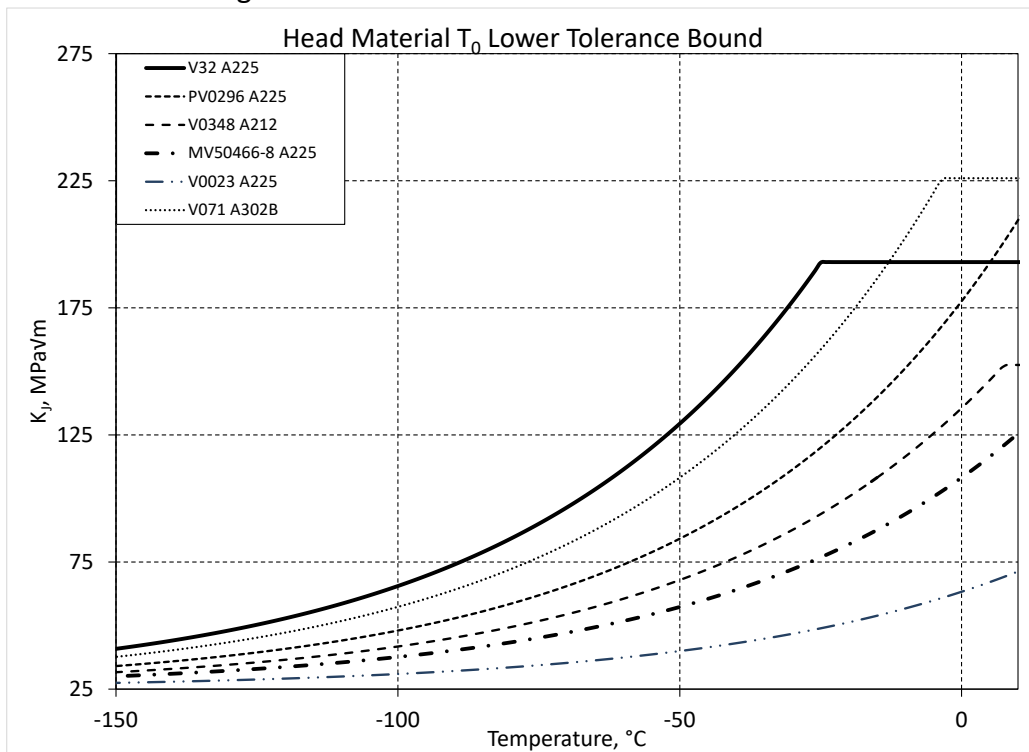


Figure 8.1.1-2: Head Material T_0 Lower Tolerance Bound

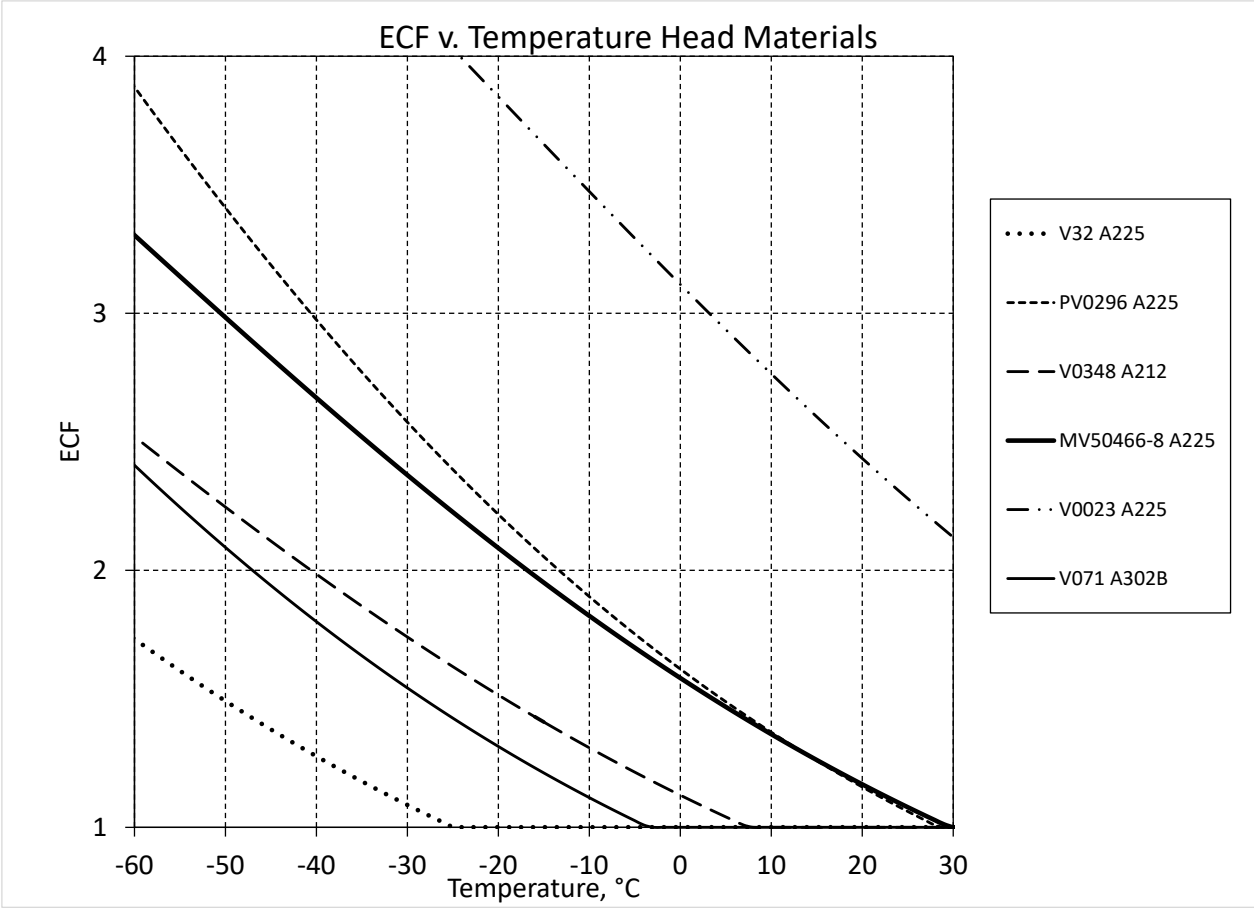


Figure 8.1.1-3: Head Material ECF v. Temperature

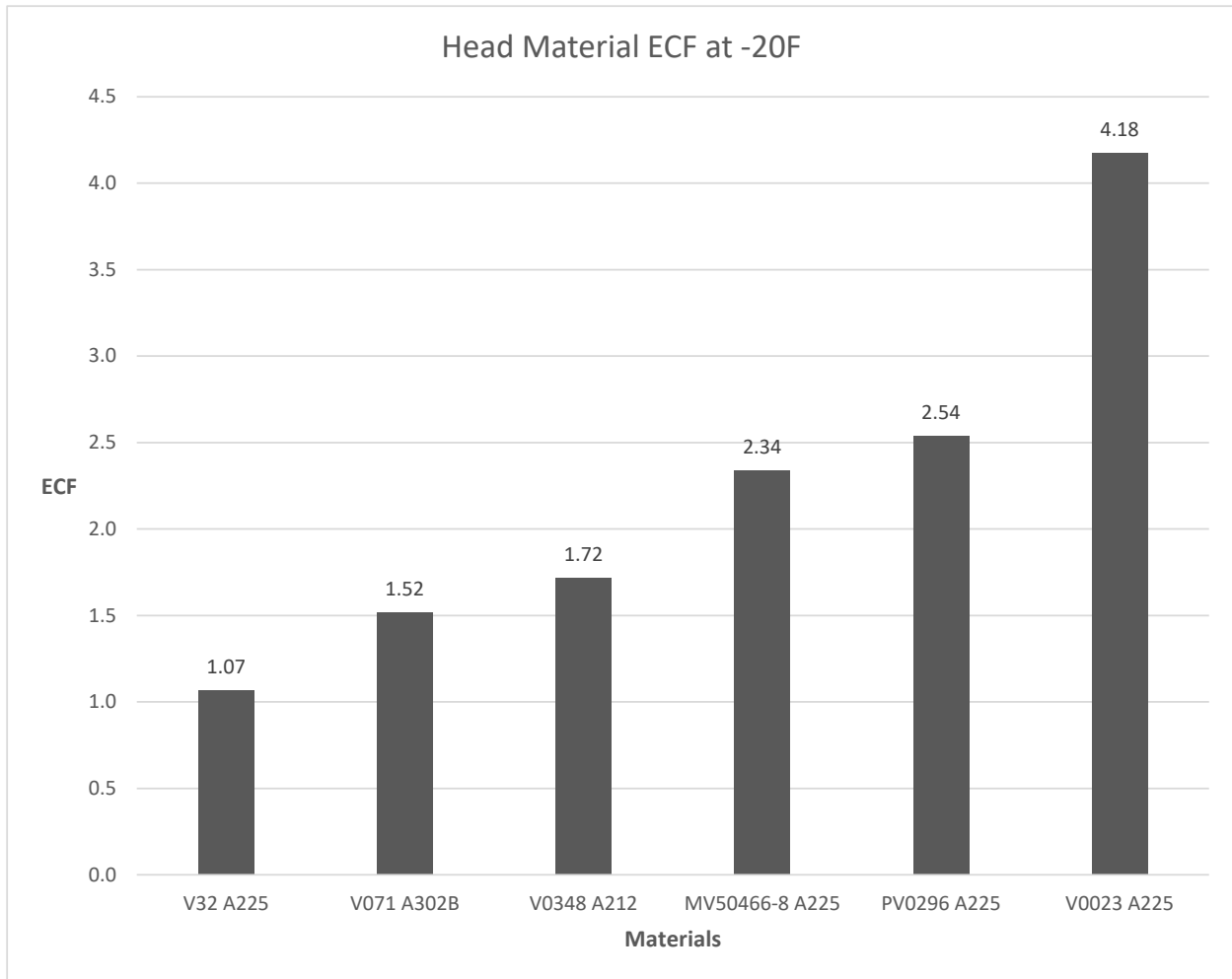


Figure 8.1.1-4: Head Material ECF at -20F

8.1.2 Nozzle Data Summary

Table 8.1.2-1: Nozzle Material Hardness and Chemistry Data Summary

Nozzle			Chemistry (%)											
Material	Vessel	Hardness (HRB)	C	Si	Mn	P	S	Cr	Mo	Ni	Cu	Nb	V	B
5002 Mod.	MV50466-8	83	0.25	0.27	1.34	0.011	0.019	0.071	0.035	0.66	0.095	0.003	0.12	0.0005
5002 Mod.	V125	83	0.28	0.25	1.61	0.02	0.14	0.095	0.044	0.56	0.075	0.003	0.13	0.002
A105 Gr. II	V32	73	0.26	0.22	0.66	0.006	0.015	0.025	0.01	0.038	0.048	0.003	0.002	0.0005
A105 Gr. II	V0348	79	0.27	0.2	0.76	0.012	0.031	0.081	0.036	0.1	0.24	0.003	0.002	0.0006

Table 8.1.2-2: Nozzle Material Mechanical Data Summary

Nozzle						To		Upper Shelf
Material	Vessel	Orientation	σ_{YS} (ksi)	UTS (ksi)	Elong. (%)	°C	°F	KJ, MPa \sqrt{m}
5002 Mod.	MV50466-8	C-R	---	---	---	-55	-67	180
5002 Mod.	V125	L	61	91	---	---	---	---
A105 Gr. II	V32	C-R	31-32	66-67	32-33	-91	-132	151
A105 Gr. II	V0348	C-R	48-49	75-76	23-27	-111	-168	145

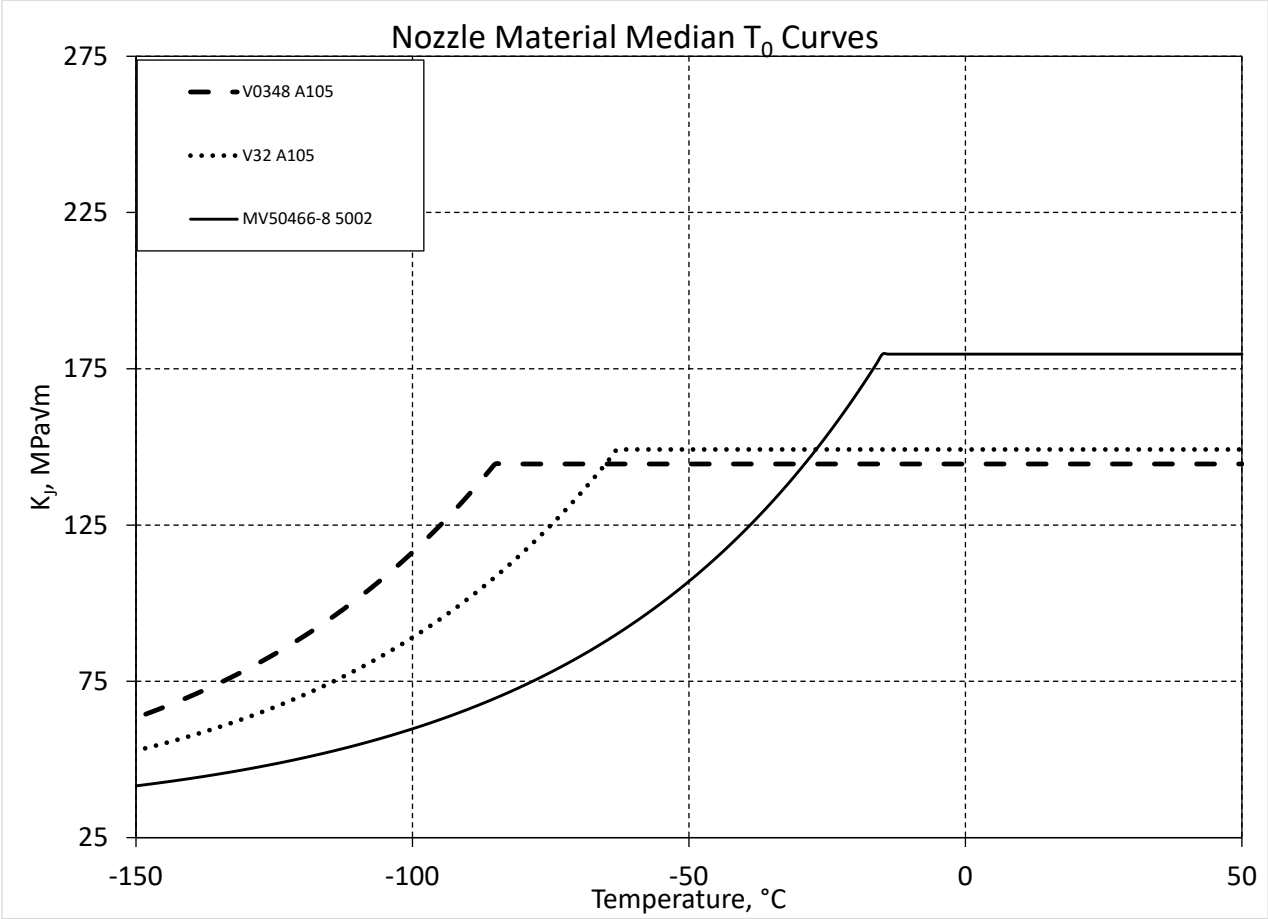


Figure 8.1.2-1: Nozzle Material Median T_0 Curves

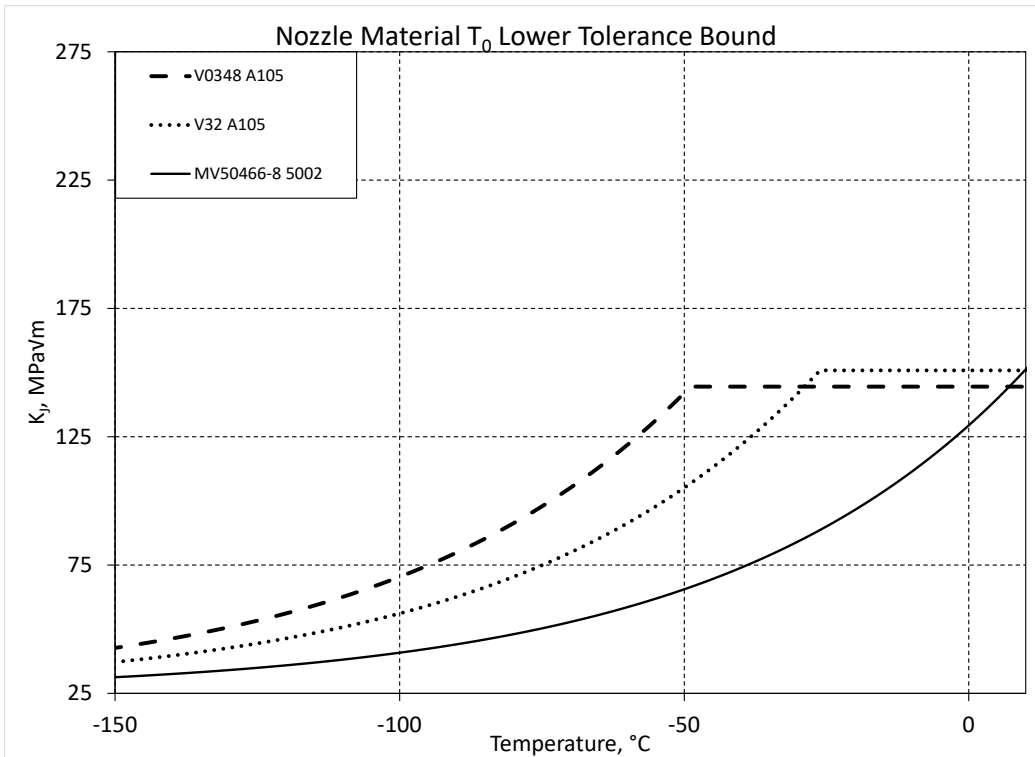


Figure 8.1.2-2: Nozzle Material ECF v. Temperature

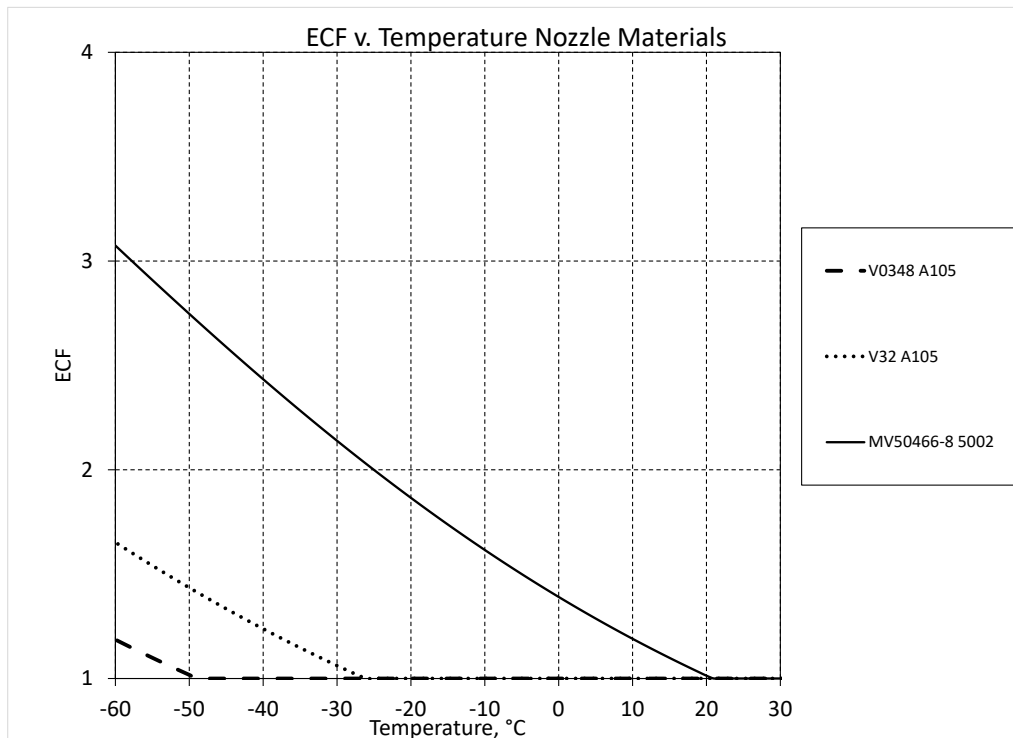


Figure 8.1.2-3: Nozzle Material ECF at -20F

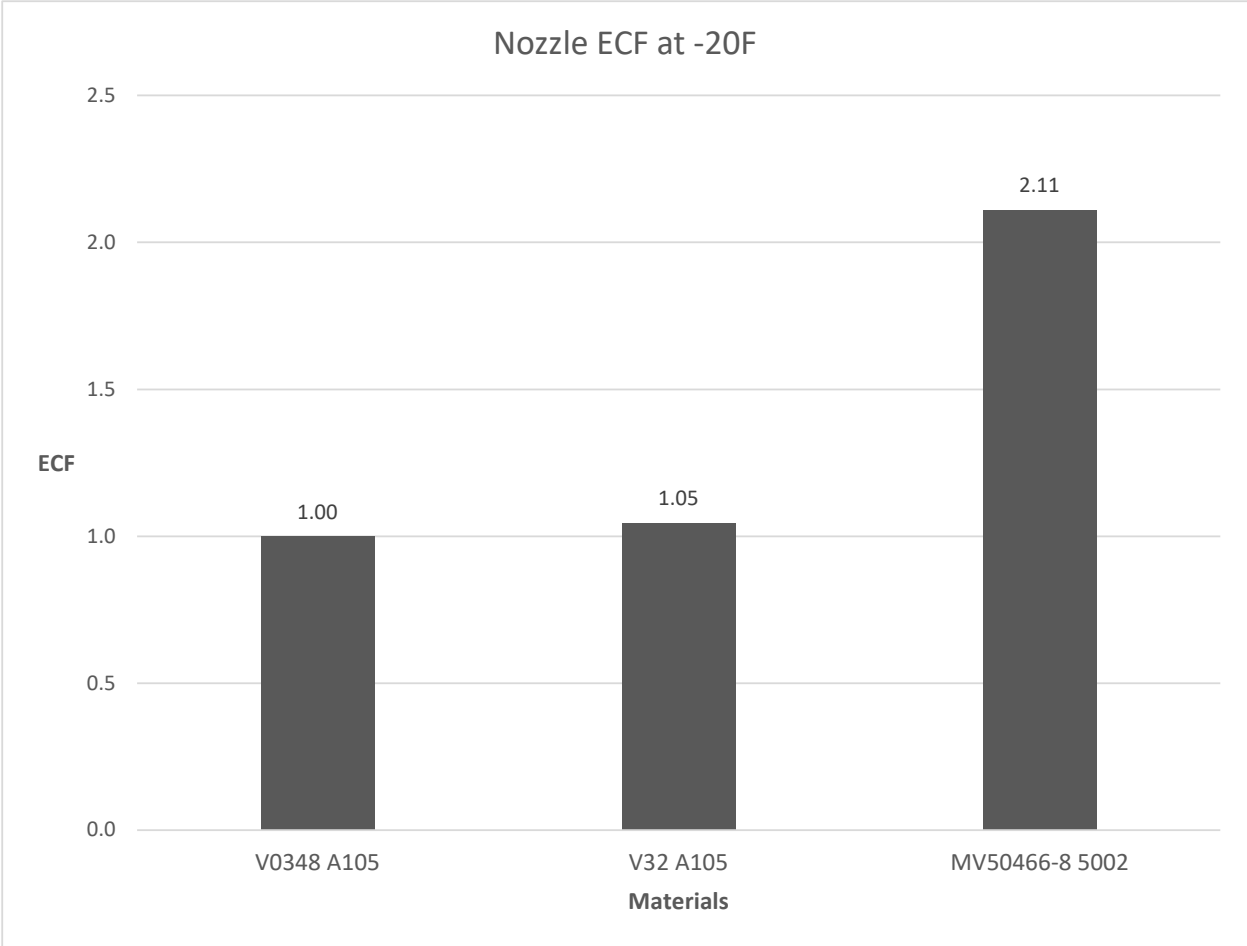


Figure 8.1.2-4: Nozzle Material ECF at -20F

8.1.3 Wrapper Data Summary

Table 8.1.3-1: Wrapper Material Hardness and Chemistry Data Summary

Wrapper			Chemistry (%)											
Material	Vessel	Hardness (HRB)	C	Si	Mn	P	S	Cr	Mo	Ni	Cu	Nb	V	B
1143 Inner	V125	90	0.26	0.28	1.35	0.025	0.028	0.071	0.013	0.5	0.026	0.003	0.13	0.0005
1146 Inner	MV50466-8	92	0.17	0.25	1.41	0.027	0.029	0.18	0.01	0.56	0.05	0.007	0.15	0.0005
1146 Inner	V32	81	0.18	0.22	1.19	0.016	0.017	0.064	0.017	0.51	0.028	0.003	0.14	0.0005
1146 Inner C3-1 0B	V0023	91	0.24	0.32	1.59	0.021	0.035	0.11	0.034	0.58	0.041	0.003	0.15	0.0006
1146 Inner C4-2 0B	V0023	99	0.25	0.32	1.58	0.021	0.035	0.11	0.034	0.57	0.04	0.003	0.15	0.001
1146 Inner C4-2 0B	V0023	99	0.25	0.32	1.58	0.021	0.035	0.11	0.034	0.57	0.04	0.003	0.15	0.001
1146 Wrapper	MV50466-8	103	0.22	0.24	1.33	0.02	0.017	0.066	0.014	0.5	0.036	0.003	0.13	0.0005
1146 Wrapper	V125	101	0.25	0.27	1.39	0.015	0.03	0.044	0.01	0.52	0.03	0.003	0.15	0.0005
1146 Wrapper	V0023	99	0.23	0.24	1.37	0.03	0.018	0.088	0.022	0.52	0.045	0.004	0.14	0.0006
1146 Wrapper	V32	101	0.25	0.27	1.28	0.014	0.02	0.039	0.009	0.5	0.026	0.003	0.14	0.0005
T-1 Wrapper	V066	96	0.15	0.25	0.88	0.014	0.025	0.68	0.46	0.82	0.27	0.004	0.034	0.005

Table 8.1.3-2: Wrapper Material Mechanical Data Summary

Material	Wrapper					To		Upper Shelf
	Vessel	Orientation	σ_{YS} (ksi)	UTS (ksi)	Elong. (%)	°C	°F	KJ, MPavm
1146 Wrapper	MV50466-8	T-L	86-88	119-120	17	-7.3	19	73
1146 Wrapper	V125	T-L	98-101	132-134	14-15	-13	9	70
1146 Wrapper	V0023	T-L	91-92	121	18-20	---	---	102
1146 Inner C4-2 OB	V0023	T-L	99	133	17	61	142	81
1146 Inner C3-1 OB	V0023	T-L	68	97	29	-99	-146	120
1146 Inner C4-2 OB	V0023	L-T	98-100	131-133	19-20	32	90	98
1146 Inner	MV50466-8	T-L	70-71	94-95	17-19	-54	-65	116
1143 Inner	V125	T-L	69-73	93-95	>20	-71	-96	100
1146 Wrapper	V32	T-L	74	99.5	---	---	---	81
T-1 Wrapper	V066	T-L	107	118	20	-123	-189	149
1146 Inner	V32	T-L	45-54	76-82	29-38	-52	-62	140

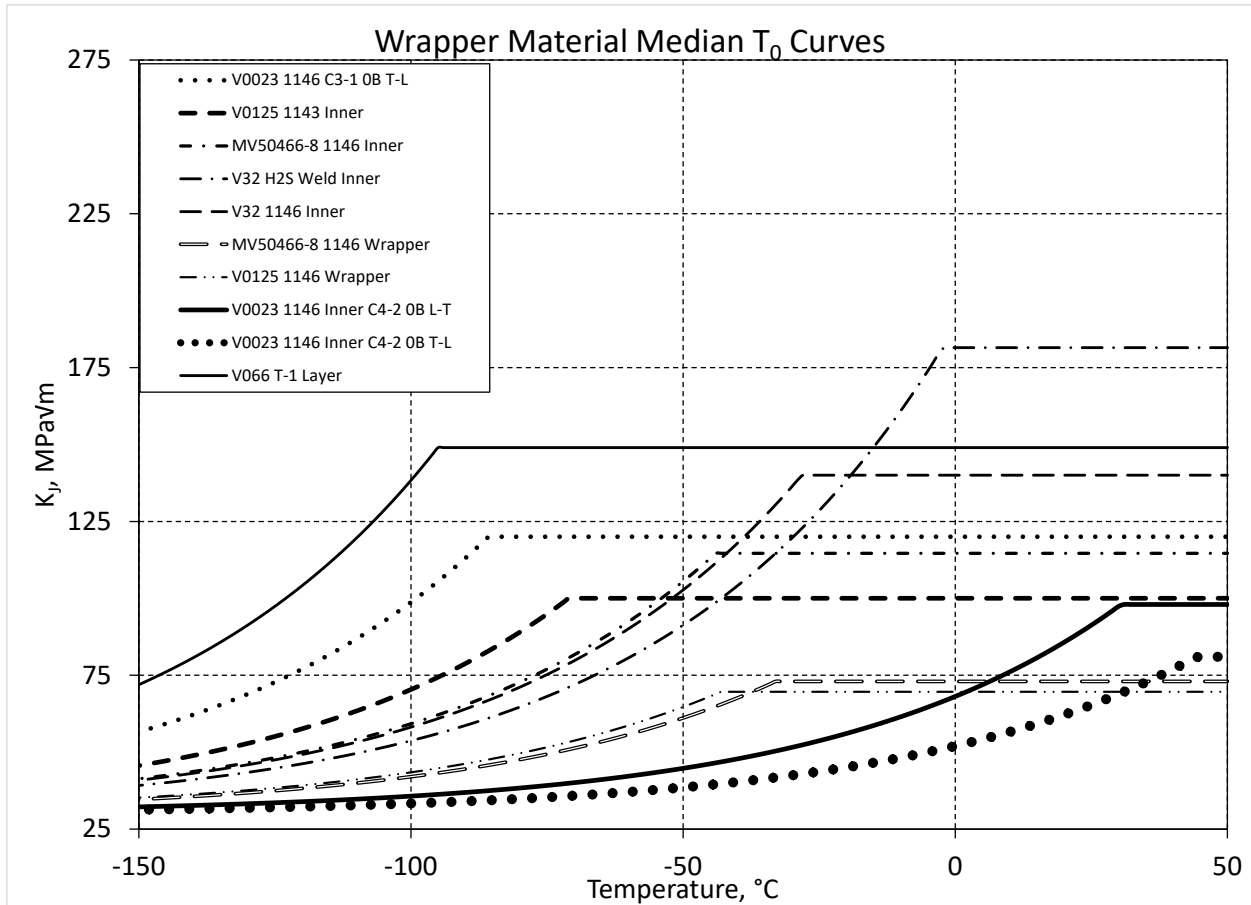


Figure 8.1.3-1: Wrapper Material Median T_0 Curves

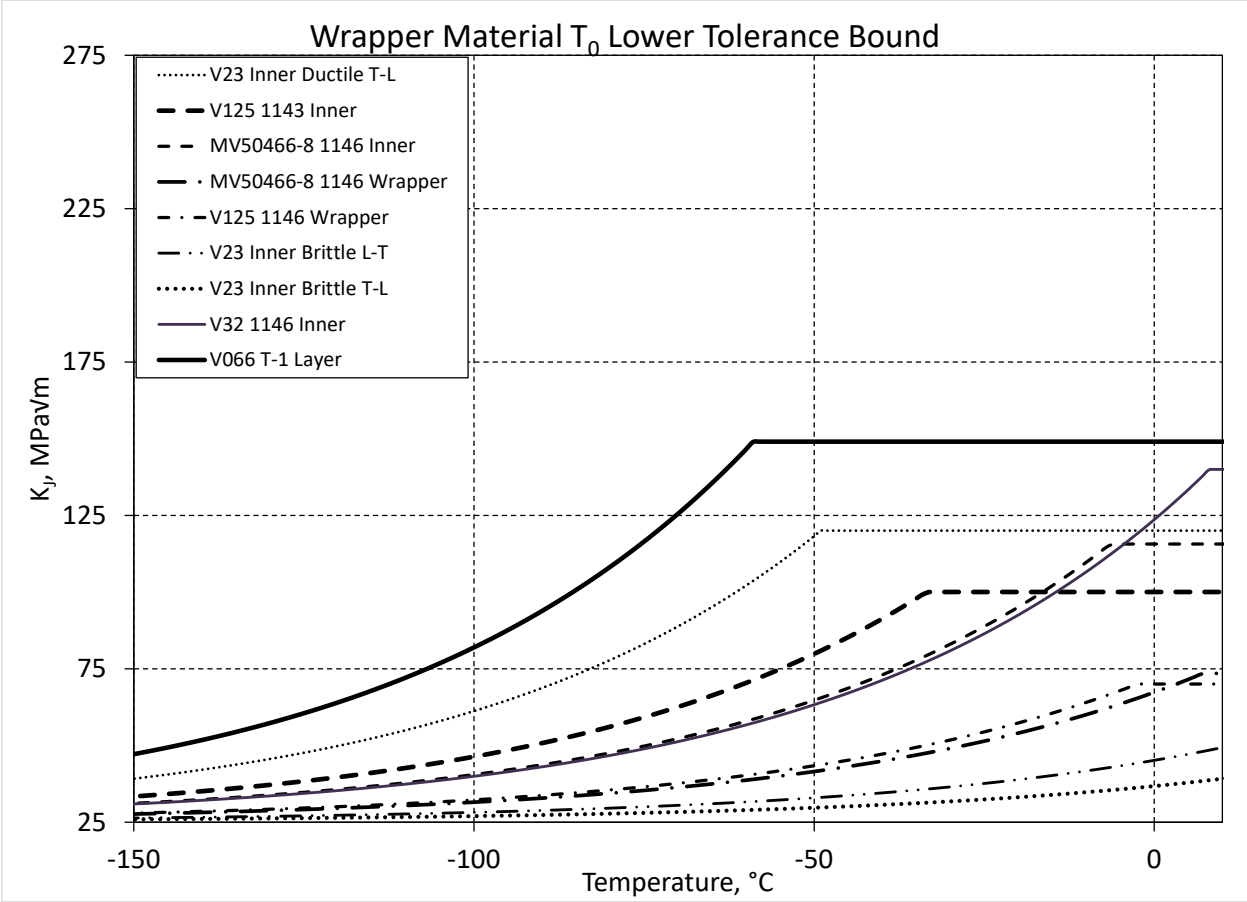


Figure 8.1.3-2: Wrapper Material T_0 Lower Tolerance Bound

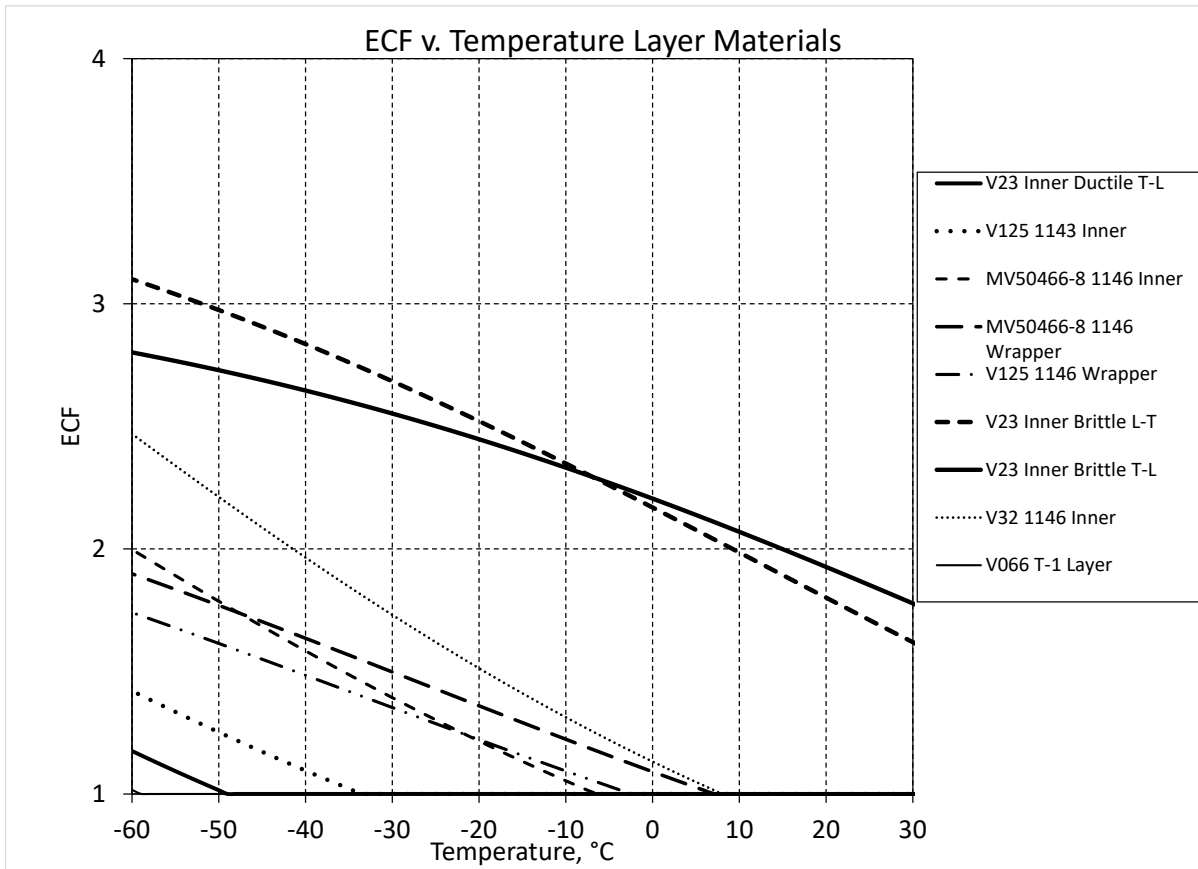


Figure 8.1.3-3: Wrapper Material ECF v. Temperature

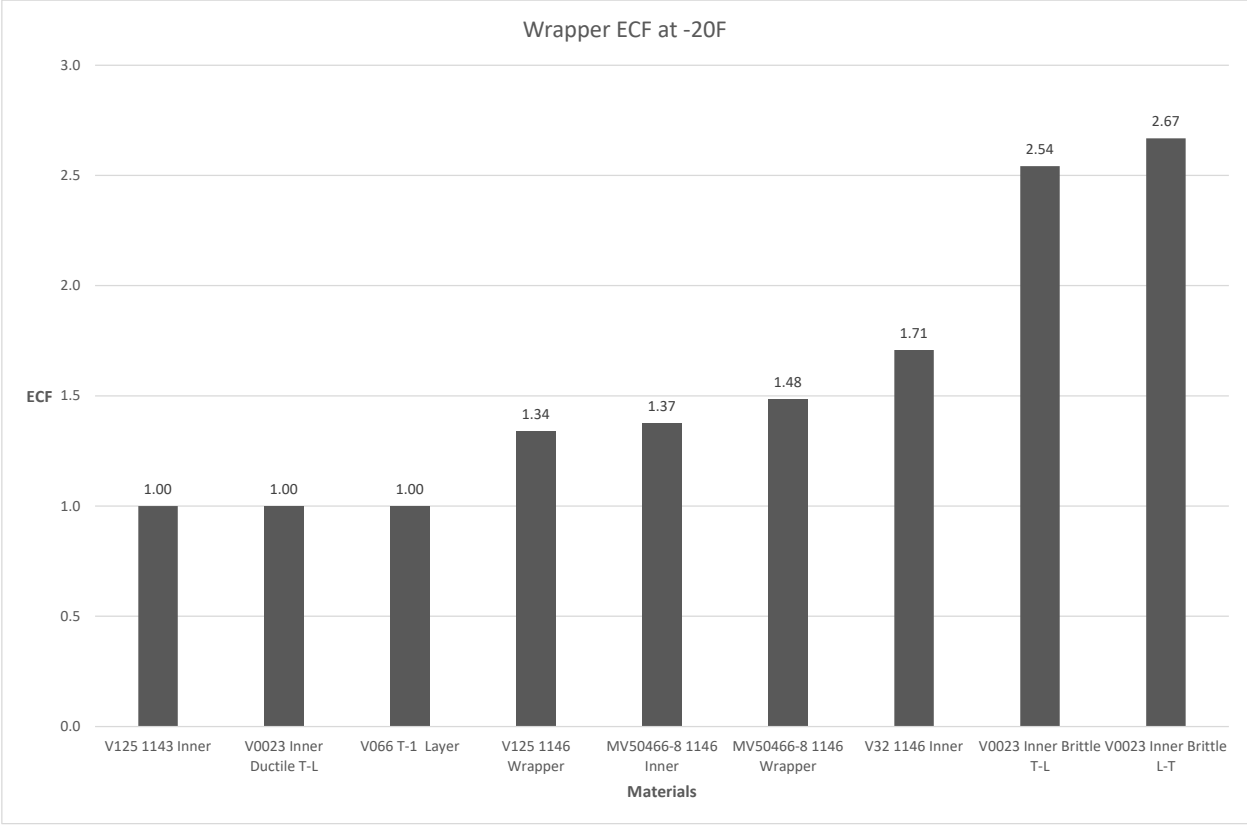


Figure 8.1.3-4: Wrapper Material ECF at -20F

8.1.4 Weld Data Summary

Table 8.1.4-1: Weld Material Hardness and Chemistry Data Summary

Weld			Chemistry (%)											
Material	Vessel	Hardness (HRB)	C	Si	Mn	P	S	Cr	Mo	Ni	Cu	Nb	V	B
Head to Shell Weld	V0023	---	0.08	0.31	0.78	0.012	0.025	0.048	0.44	1.75	0.088	0.003	0.17	0.0005
Head to Shell Weld	V125	93	0.062	0.29	1.44	0.011	0.022	0.23	0.37	1.47	0.079	0.006	0.028	0.0005
Head to Shell Weld	MV50466-8	---	0.073	0.3	0.76	0.013	0.026	0.031	0.48	1.88	0.11	0.003	0.17	0.0005
Head to Shell Weld Inner	V32	---	0.052	0.41	1.71	0.015	0.018	0.16	0.32	1.55	0.09	0.003	0.022	0.0005
Head to Shell Weld Wrapper	V32	---	0.08	0.29	0.74	0.016	0.026	0.051	0.48	1.99	0.12	0.003	0.2	0.0005
Head to Shell Weld, Head HAZ	V125	---	---	---	---	---	---	---	---	---	---	---	---	---
Head to Shell Weld, Head HAZ	MV50466-8	---	---	---	---	---	---	---	---	---	---	---	---	---
Inner HAZ	V0023	---	---	---	---	---	---	---	---	---	---	---	---	---
Inner Weld	V0023	---	0.081	0.82	1.77	0.019	0.019	0.078	0.35	0.15	0.11	0.003	0.03	0.0005
Inner Weld	V32	---	0.087	0.77	1.52	0.019	0.02	0.08	0.34	0.24	0.22	0.004	0.048	0.0005
Inner Weld	V125	---	0.15	0.6	1.61	0.02	0.023	0.091	0.29	0.41	0.099	0.008	0.068	0.0005
Inner Weld	MV50466-8	---	0.11	0.19	1.15	0.017	0.018	0.11	0.39	2.37	0.085	0.003	0.062	0.0005
Longitudinal Weld	MV50466-8	---	0.13	0.39	1.52	0.014	0.02	0.14	0.18	1.04	0.036	0.006	0.078	0.0005
Longitudinal Weld	V32	---	0.12	0.4	1.5	0.017	0.022	0.15	0.22	1.19	0.038	0.004	0.066	0.0005
Longitudinal Weld	V0023	---	0.081	0.28	0.75	0.014	0.021	0.05	0.39	1.65	0.027	0.003	0.16	0.0005
Longitudinal Weld HAZ	MV50466-8	---	---	---	---	---	---	---	---	---	---	---	---	---
Longitudinal Weld HAZ	V32	---	---	---	---	---	---	---	---	---	---	---	---	---
Longitudinal Weld HAZ	V0023	---	---	---	---	---	---	---	---	---	---	---	---	---
Nozzle HAZ	MV50466-8	---	---	---	---	---	---	---	---	---	---	---	---	---
Nozzle Weld	MV50466-8	84	0.074	0.65	0.77	0.013	0.016	0.039	0.01	0.076	0.09	0.003	0.024	0.0005
Shell to Shell Weld	V066	94	0.07	0.4	1.31	0.012	0.011	0.3	0.52	2.37	0.49	0.003	0.008	0.0005

Table 8.1.4-2: Weld Material Mechanical Data Summary

Weld						To		Upper Shelf
Material	Vessel	Orientation	σ_{YS} (ksi)	UTS (ksi)	Elong. (%)	°C	°F	KJ, MPavm
Nozzle Weld	MV50466-8	NQ	62-63	81	24-25	-91	-132	175
Nozzle HAZ	MV50466-8	NQ	---	---	---	-96	-141	175
Longitudinal Weld	MV50466-8	NP	86-92	109-112	9-19	-43	-45	146
Longitudinal Weld	V32	NP	88-95	108-117	21-24	-85	-121	167
Longitudinal Weld	V0023	NP	91	105	21-23	-65	-85	135
Longitudinal Weld HAZ	MV50466-8	NP	97-100	120-129	16-18	-45	-49	120
Longitudinal Weld HAZ	V32	NP	---	---	---	-9	16	75
Longitudinal Weld HAZ	V0023	NP	---	---	---	8	46	100
Head to Shell Weld Wrapper	V32	NP	104	116	12-18	3	37	121
Head to Shell Weld Inner	V32	NP	93-95	108-111	19-20	-43	-45	182
Head to Shell Weld	V125	NP	100-116	112-132	15-25	---	---	243
Head to Shell Weld, Head HAZ	V125	NP	59-60	82-90	27-29	---	---	144
Inner Weld	V0023	NP	92-105	103-120	18-19	-1	30	162
Inner HAZ	V0023	NP	---	---	---	7	45	110
Inner Weld	V32	NP	88	103	21-22	17	63	140
Head to Shell Weld	MV50466-8	NP	53	79	---	---	---	132
Head to Shell Weld, Head HAZ	MV50466-8	NP	59	84	---	---	---	216
Shell to Shell Weld	V066	NP	104	116	14	-116	-177	153
Inner Weld	V125	NP	85	102	---	-19	-2	145
Inner Weld	MV50466-8	NP	85	104	---	-73	-99	136
Head to Shell Weld	V0023	NP	94-107	105-121	17-20	-46	-51	143

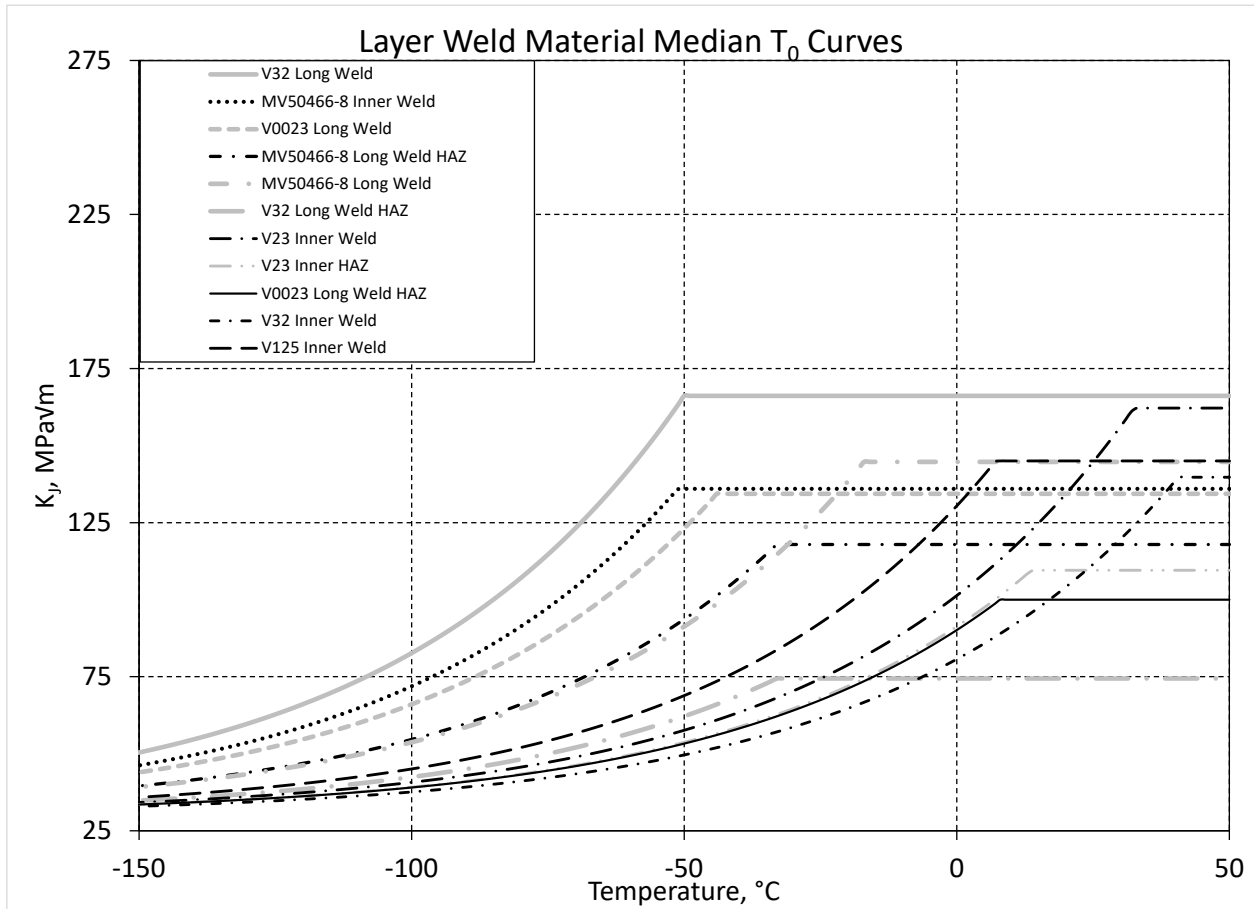


Figure 8.1.4-1: Layer Weld Material Median T_0 Curves

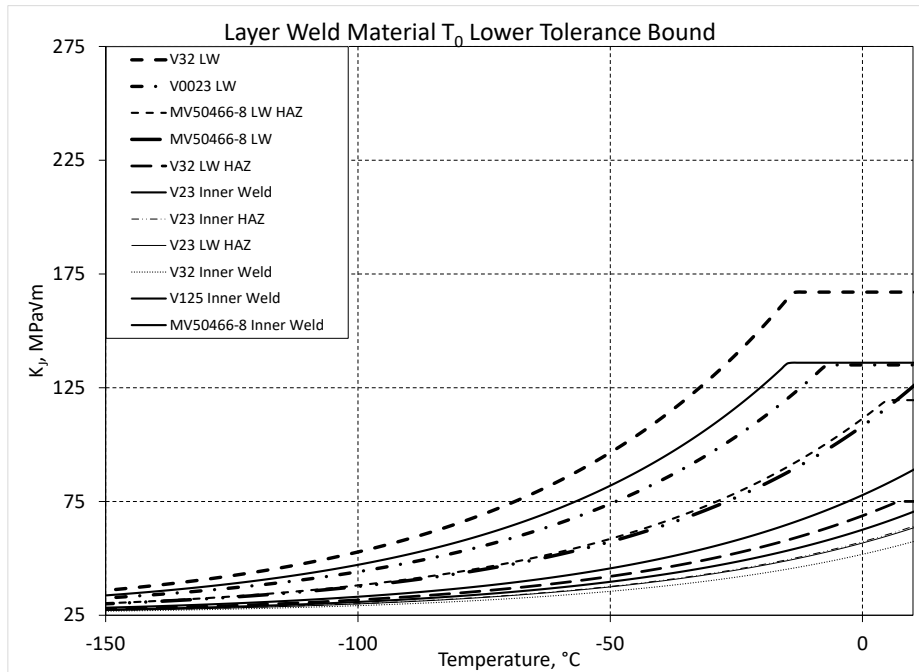


Figure 8.1.4-2: Layer Weld Material T_0 Lower Tolerance Bound

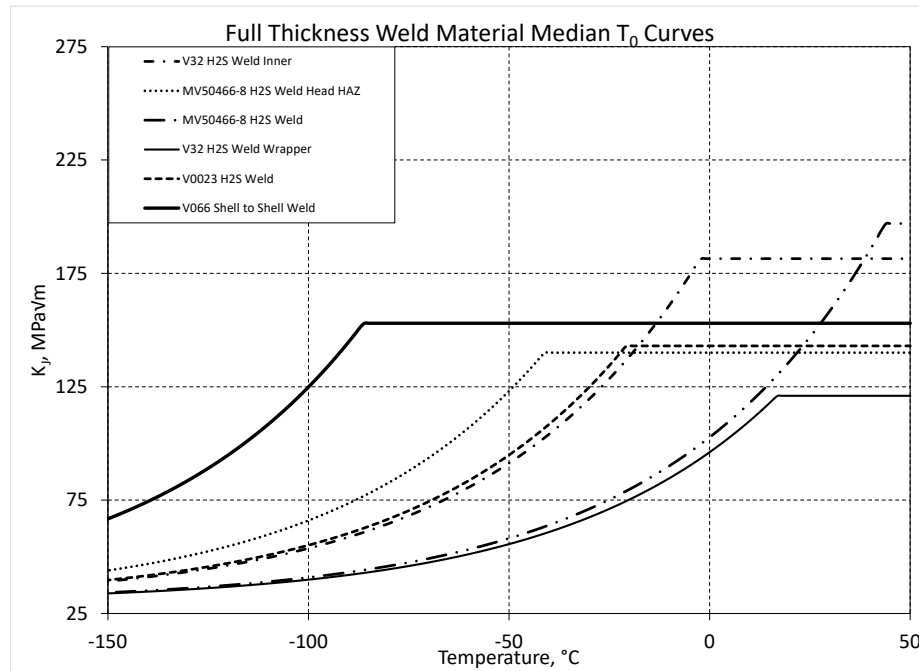


Figure 8.1.4-3: Full Thickness Weld Material Median T_0 Curves

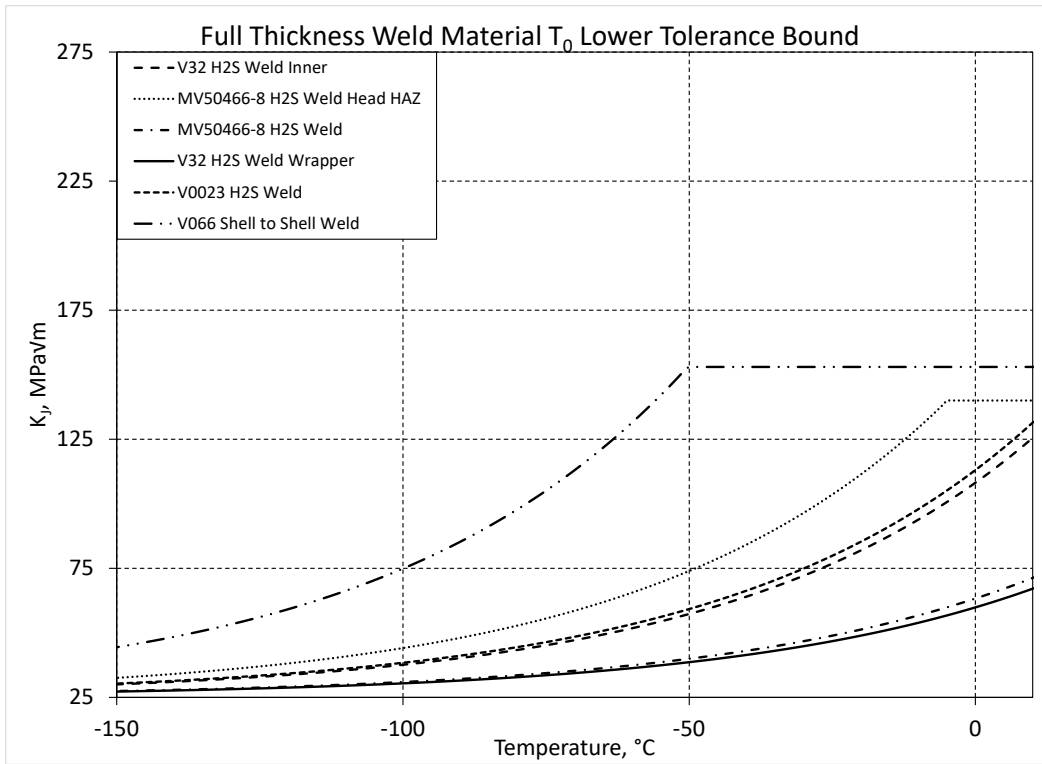


Figure 8.1.4-4: Full Thickness Weld Material T_0 Lower Tolerance Bound

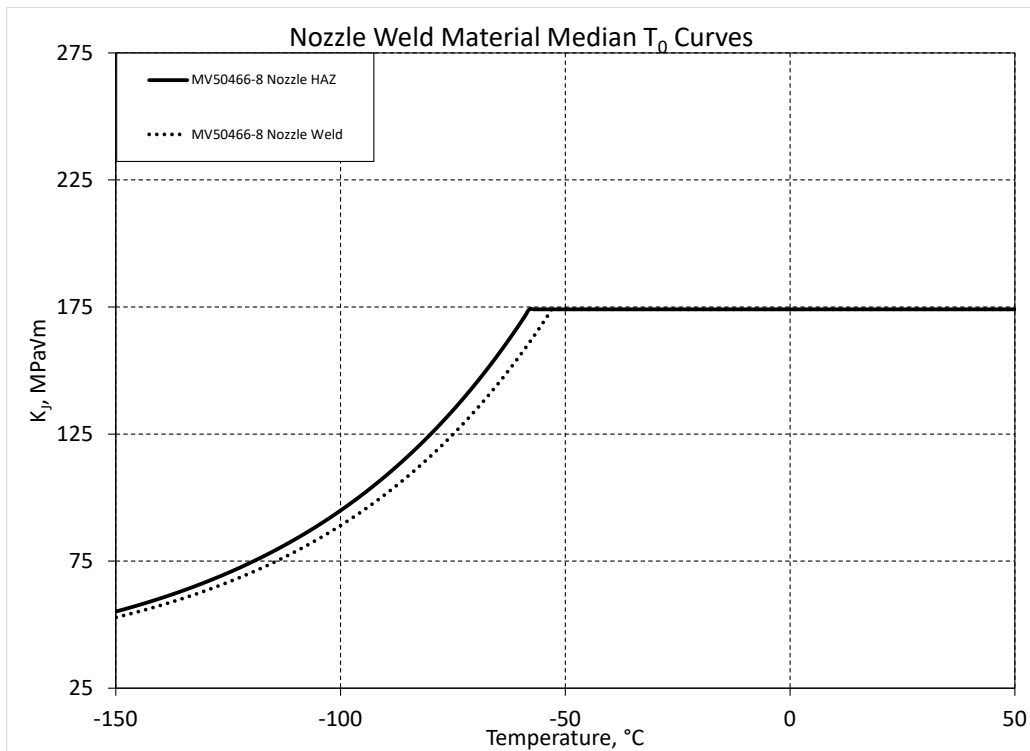


Figure 8.1.4-5: Nozzle Weld Material Median T_0 Curves

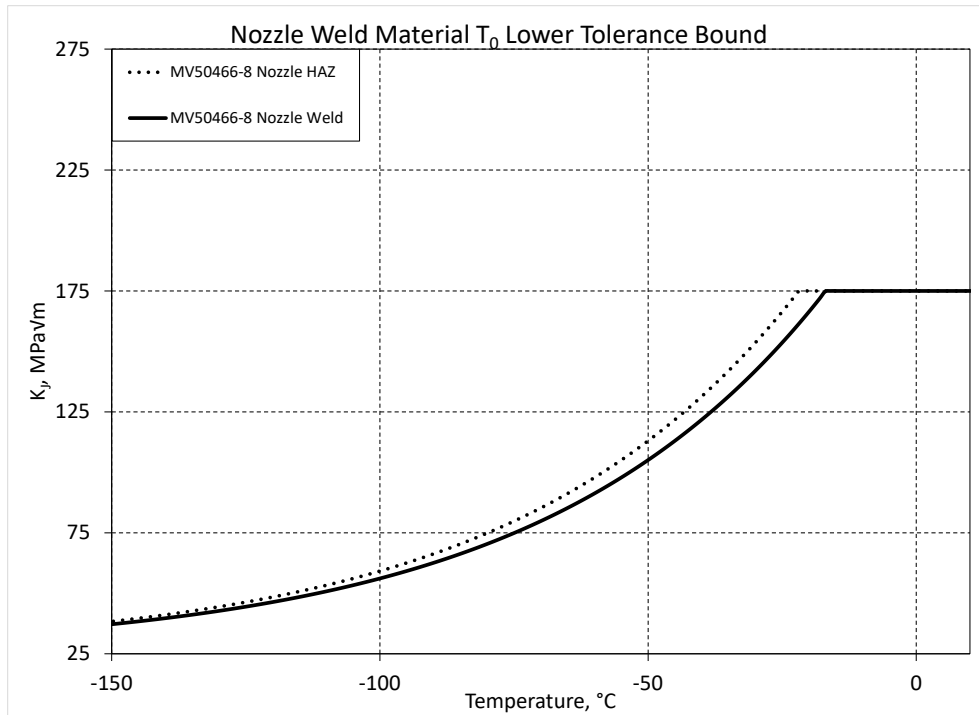


Figure 8.1.4-6: Nozzle Weld Material T_0 Lower Tolerance Bound

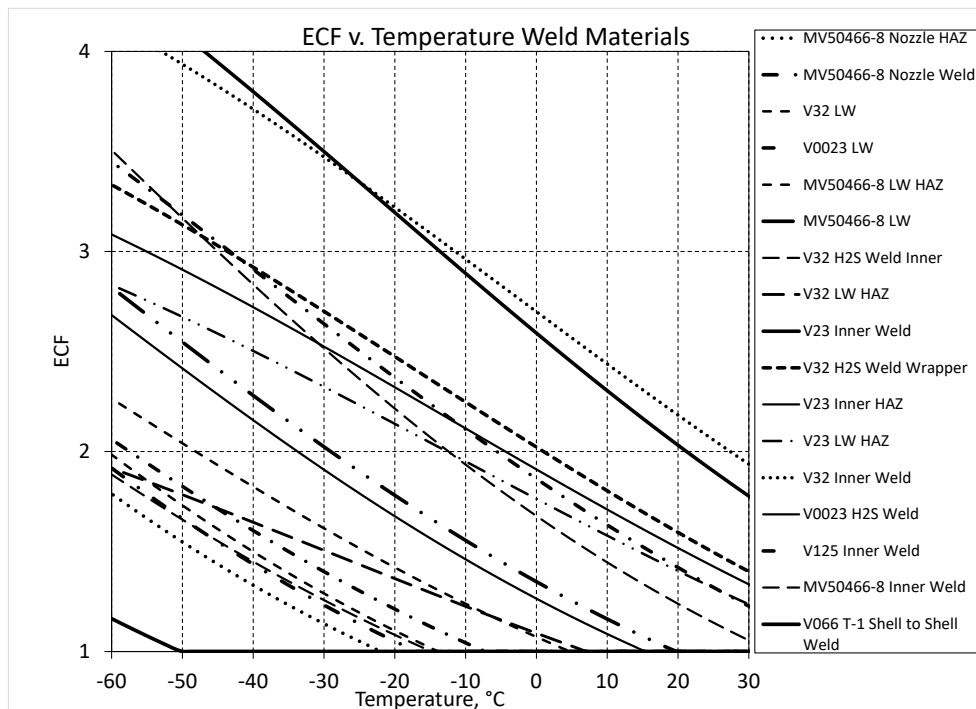


Figure 8.1.4-7: Weld Material ECF v. Temperature

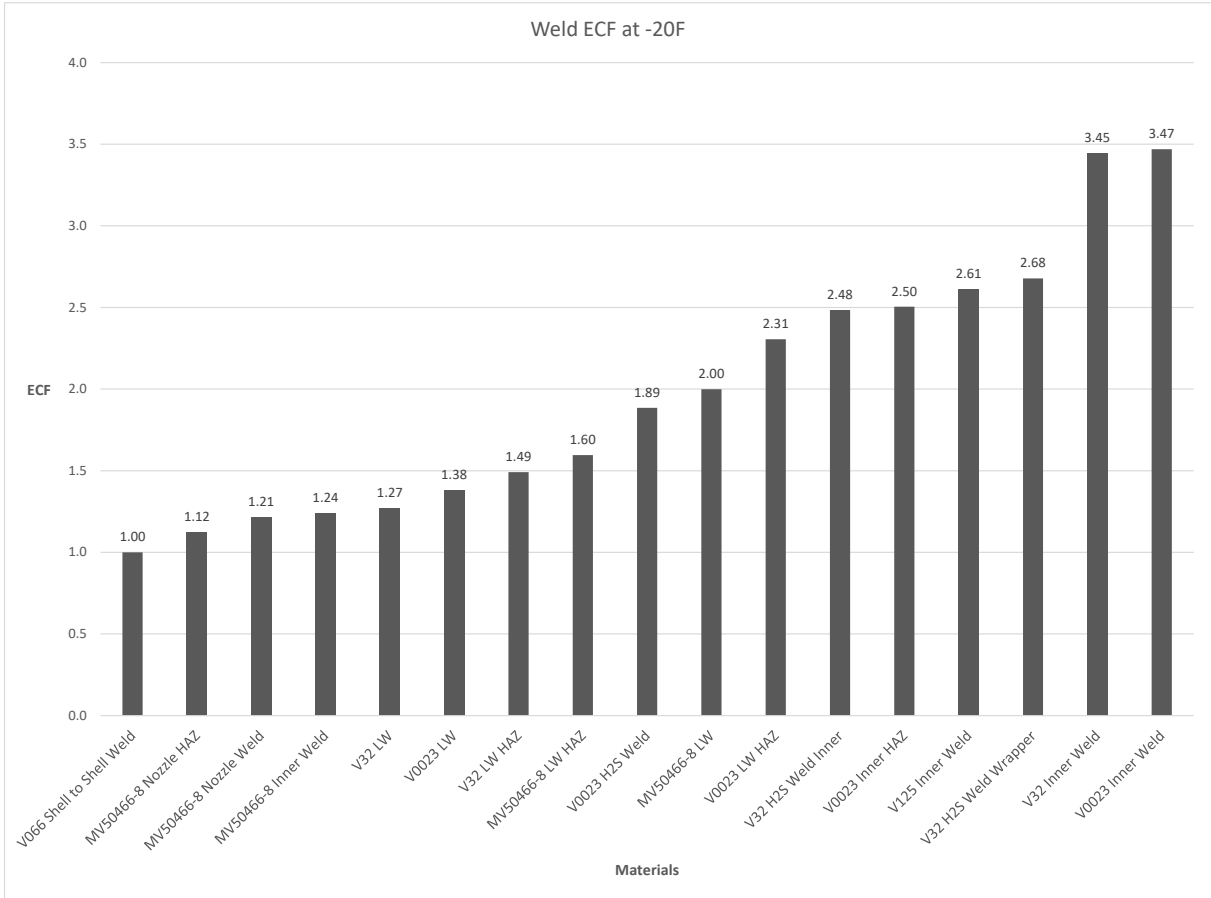


Figure 8.1.4-8: Weld Material ECF at -20F

BIBLIOGRAPHY

1. **NASA Engineering Safety Center.** Evaluation of Agency Non-code Layered Pressure Vessels (LPVs) Volume I (corrected copy) and Volume II. s.l. : NASA, 2014. Vol. I (corrected copy) and II. NASA-TM-2014-218505.
2. **ASME.** Section VIII Rules for Construction of Pressure Vessels Division 2 Alternative Rules. *ASME Boiler & Pressure Vessel Code, An International Code 2010*. New York, NY : The American Society of Mechanical Engineers, 2011.
3. —. *1987 Addenda - BPVC Section VIII Rules for Construction of Pressure Vessels Division 1*. 1987.
4. **Gross, J.H.** The Effect of Strength and Thickness on Notch Ductility. Atlantic City, NJ : ASTM Symposium on Testing by Impact, 1969.
5. **ASME.** Summer 1979 Addenda to the 1977 Section VIII. s.l. : American Society of Mechanical Engineers, 1979.
6. —. Section II - Materials. *ASME Boiler and Pressure Vessel Code, An International Code*. New York, NY : The American Society of Mechanical Engineers, 2019.
7. **ASTM.** E1921-19 Standard Test Method for Determination of Reference Temperature, T₀, for Ferritic Steels in the Transition Range. *E1921-19*. s.l. : American Society for Testing Materials, 2019.
8. —. E2298-13 Standard Test Method for Instrumented Impact Testing of Metallic Materials. West Conshocken, PA : American Society for Testing Materials, 2013.
9. **Cardinal, J.W. and Popelar, C.F.** *Multilayer Pressure Vessel Materials Testing and Analysis (Phase 2) NASA/CR-2014-218158*. s.l. : NASA, 2014.
10. **ASTM.** E1820 Standard Test Method for Measurement of Fracture Toughness. *E1820-19*. West Conshocken, PA : American Society of Testing Materials, 2019.
11. —. *E647 Standard Test Method for Measurement of Fatigue Crack Growth Rates*. s.l. : American Society for Testing Materials, 2015. E647-15.
12. **Battelle Memorial Institute.** *Metallic Materials Property Development and Standardization (MMPDS-16)*. Columbus, OH : s.n., 2021. MMPDS-16.
13. **SAE.** *Composite Materials Handbook CMH-17*. s.l. : SAE International, 2017. CMH-17.
14. **ASME.** *ASME Boiler and Pressure Vessel Code VIII*. New York, NY : American Society of Mechanical Engineers, 2019.
15. —. Section III - Division 1 NB Class 1 Nuclear Components. *Boiler and Pressure Vessel Code*. s.l. : American Society of Mechanical Engineers, 2019.

16. **ASTM.** *E208 Standard Test Method for Conducting Drop-Weight Test to Determine Nil-Ductility Transition Temperature of Ferritic Steels.* s.l. : American Society of Testing Materials, 2019. E208.
17. —. *E23 Standard Test Methods for Notched Bar Impact Testing of Metallic Materials.* s.l. : American Society of Testing Materials, 2018. E23.
18. —. *Use of Fracture Toughness Test Data to Establish Reference Temperature for Pressure Retaining Materials.* New York : ASTM, 1999. Section XI, Division 1.
19. **ASME.** *Use of Fracture Toughness Test Data to Establish Reference Temperature for Pressure Retaining Materials Other than Bolting for Class 1 Vessels, Section III, Division 1.* New York : ASME, 1999. ASME Boiler and Pressure Vessel Code: An American National Standard, Code Case N-631.
20. **Pressure Vessel Research Committee.** *WRC - Bulletin 175 PVRC Recommendations on Toughness Requirements for Ferritic Materials.* s.l. : Welding Research Council, 1972.
21. **Wallin, K.** *Fracture Toughness of Engineering Materials, Estimation and Application.* s.l. : EMAS Publishing, 2011.
22. **ASTM.** *A350/A350M-14 Standard Specification for Carbon and Low-Alloy Steel Forgings, Requiring Notch Toughness Testing for Piping Components.* s.l. : ASTM, 2014. A350/A350M-14.
23. **Haggag, F.M.** *In-Situ Automated Ball Indentation (ABI) Testing of A350 Steel Flanges at Ambient Temperature for Offshore Qualifications at -46°C(-50°F).* Oak Ridge, TN : ABI Services LLC, 2016.
24. **ASTM.** *A517 Standard Specification for Pressure Vessel plates, Alloy Steel, High-Strength, Quenched and Tempered.* s.l. : ASTM, 1984. A517-84.
25. **Barsom, J.M. and Rolfe, S.T.** KIC Transition-Temperature Behaviour of A517-F Steel. Monroevill, PA : Engineering Fracture Mechanics, 1971, Vol. 2, pp. 341-357.
26. **ASTM.** *A724 Standard Specification for Pressure Vessel Plates, Carbon-Manganese-Silicon Steel, Quenched and Tempered, for Welded Layered Pressure Vessels.* 1999. A 724/A 724M -- 99.
27. —. *A387 Standard Specification for Pressure Vessel Plates, Alloy Steel, Chromium-Molybdenum.* s.l. : ASTM, 1999. A 387/A 387M -- 99.
28. **Pense, Alan W.** 1980 Adams Lecture: Twenty Years of Pressure Vessel Steel Research. s.l. : American Welding Society and the Welding Research Council, Supplement 311-s, 1980.
29. **Mielcarek, Justin MARS123.** *ASME Boiler Pressure Vessel Code Design Analysis for MARS 1, 2 and 3.* 2010. 289661.

30. **ASTM.** *A182 Standard Specification for Forged or Rolled Alloy and Stainless Steel Pipe Flanges, Forged Fittings, and Valves and Parts for High-Temperature Service.* 2020. A 182/A182M -- 20.
31. —. *A312 Standard Specification for Seamless and Welded Austenitic Stainless Steel Pipes.* 1995. A 312/A 312M -- 95a.
32. —. *A516 Standard Specification for CARBON STEEL PLATES OF INTERMEDIATE TENSILE STRENGTH FOR FUSION-WELDED PRESSURE VESSELS FOR ATHERMOSPHERIC AND LOW TEMPERATURE SERVICE.* 1964. A 516 -- 64.
33. —. *A302 Standard Specification for Pressure Vessel Plates, Alloy Steel, Manganese-Molybdenum and Manganese-Molybdenum-Nickel.* *Annual Book of ASTM Standards.* Philadelphia : ASTM, 1983. A302.
34. **NUREG6426 McCabe, D.E., Manneschildt, E.L., and Swain, R.L.** *Ductile fracture Toughness of Modified A302 Grade B Plate Materials, Data Analysis.* s.l. : ORNL for the U.S. Nuclear Regulatory Commission, 1997. NUREG/CR-6426.
35. **Hiser, A.L. and Terrell, J.B.** *Size Effects on J-R Curves for a A302B Plate.* Washington DC : U.S. Nuclear Regulatory Commission, 1989. NUREG/CR-5265.
36. **ASTM.** *A533 Specification for Pressure Vessel Plates, Alloy Steel, Quenched and Tempered, Manganese-Molybdenum and Manganese-Molybdenum-Nickel.* s.l. : American Society for Testing and Materials, 1993. SA-533/SA-533M.
37. **Chaouadi, R., Fabry, A., van Walle, E., and Van de Velde, J.** *Fracture Toughness of the Ni-Modified A302-B Plate of the BR3 Reactor Pressure Vessel.* *Effects of Radiation on Materials: 19th International Symposium.* West Conshohocken, PA : ASTM, 2000. Vol. STP 1366.
38. **A52 McCabe, D.E., Merkle, J.G., and Kim Wallin.** *An Introduction to the Development and Use of the Master Curve Method.* West Conshohocken : ASTM, 2005. ASTM Manual 52.
39. **Pellini, W.S. and Puzak, P.P.** *Practical Considerations in Applying Laboratory Fracture Test Criteria to the Fracture-safe Design of Pressure Vessels.* s.l. : Naval Research Laboratory, 1963. NRL Report 6030.
40. **Wang, J.A.** *Analysis of the Irradiation Data for A302B and A533B Correlation Monitor Materials.* s.l. : ORNL for the U.S. Nuclear Regulatory Commission, 1996. NUREG/CR-6413.
41. **Stofanak, R.J., Poskie, T.J., Li, Y.Y., and Wire, G.L.** *Irradiation Damage Behaviour of Low Alloy Steel Wrought and Weld Materials.* West Mifflin, PA : Westinghouse Electric Corporation Bettis Laboratory, 1992.
42. *A simple theoretical Charpy-V - KIC correlation for irradiation embrittlement.* **Wallin, K.** *Innovative Approaches to Irradiation Damage and Fracture Analysis,* New York : American Society of Mechanical Engineers, 1989, Vols. PVP-170.

43. *Comparison of irradiation-induced shifts of KJC and Charpy impact toughness for reactor pressure vessel steels.* **Sokolov, M. and Nanstad, R.K.** Effects of Radiation on Materials: 18th International Symposium, West Conshohocken, PA : ASTM, 1999, Vol. STP 1325.
44. **Iradj, Sattari-Far and Wallin, Kim.** *Application of Master Curve Methodology for Structural Integrity Assessments of Nuclear Components.* s.l. : Swedish Nuclear Power Inspectorate, 2005.
45. **Otte, Karl H. and Widera, Otto E.** *Design and Fabrication of a Seawater Test Chamber at Chicago Bridge and Iron Company.* s.l. : Summer Institute on Case Methods, 1967. ECL 92A.
46. **Jawad, Maan. A.O.** *SMITH MATERIAL CROSS-REFERENCE.* s.l. : GLOBAL ENGINEERING & TECHNOLOGY, LLC, 2017.
47. **ASTM.** *A225 Standard Specification for Pressure Vessel Plates, Alloy Steel, Manganese-Vanadium-Nickel.* s.l. : American Society for Testing Materials, 2017. A225.
48. **A.O. SMITH CORPORATION.** *V108 DATA PACKAGE INDEX PRESSURE VESSEL 3500 PSIG -120 FT^3 A.O. SMITH CORPORATION VESSEL NO. MV50223-3.*
49. **STRUTHERS WELLS CORPORATION.** *V106 Data Package Index Pressure Vessel.* Vessel No. 48-2172-1.
50. **Board of Contract Appeals.** *Board of Contract Appeals Decisions.* s.l. : Commerce Clearing House, 1963. Volume 63.
51. **ASTM.** *E8 Standard Test Methods for Tension Testing of Metallic Materials.* s.l. : American Society for Testing Materials, 2016. E8.
52. —. *G142 Standard Method for Determination of Susceptibility of Metals to Embrittlement in Hydrogen Containing Environments at High Pressure, High Temperature, or Both.* s.l. : American Society for Testing Materials, 2016. G142.
53. —. *A212 High Tensile Strength Carbon-Silicon Steel Plates for Boilers and Other Pressure Vessels.* s.l. : American Society for Testing Materials, 1964. A212.
54. —. *E112 Standard Test Methods for Determining Average Grain Size.* s.l. : American Society of Testing Materials, 2013. E112.
55. **AOS1146A.O. Smith.** *Material Specification: 1146-a High Tensile Strength-Low Alloy Steel Flange Quality Plates.* Milwaukee : A.O. Smith Corporation Production Laboratory, 1956. 1146-a.
56. **NUREG5265 Hiser A.L. and Terrell, J.B.** *Size Effects on J-R Curves for a A302B Plate.* Washington DC : U.S. Nuclear Regulatory Commission, 1989. NUREG/CR-5265.
57. **CBI1146Chicago Bridge & Iron.** *Specification for High Strength Low-Alloy Steel Plates (1146).* s.l. : CB&I Standard, 1963. 1146.

58. **CBI1143CBI**. *Specification for HIGH STRENGTH LOW-ALLOY STEEL PLATES (1143)*. Oak Brook : CBI Standard, 1963. 626-1143.

59. **Westmoreland Mechanical Testing and Research, Inc.** *WMT&R Report No. 3-55107*. 2013. E23-12c.

60. **AOS5002A.O. Smith**. *5002-a High Tensile Strength, Low Alloy Steel Forgings for Fusion Welded Pressure Vessels (ASTM-A336, Modified)*. Milwaukee : Central Material and Process Control, A.O. Smith Corporation, 1961. 5002-a.

61. **ASTM**. *A105 Standard Specifications for Forged or Rolled Steel Pipe Flanges, Forged Fittings, and Valves and Parts for High-Temperature Service*. Philadelphia : American Society for Testing and Materials, 1965. A105.

62. **LINK Link, Richard E.** *Determination of the Reference Temperature, T_0 , for Nozzle Weld and HAZ of Vessel MV50466-8*. USNA Engineering and Weapons Division Report. Annapolis : United States Naval Academy, 2018. EW Report 01-18.